Durham E-Theses

Elemental and isotopic geochemistry of kimberlites from the Lac de Gras field, northwest territories, Canada.

Dowall, David Phillip
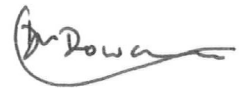
How to cite:

Use policy

Abstract

Detailed major/trace element and high-precision Hf-Nd-Sr isotope data has been acquired for 86 samples of kimberlites from the recently discovered Lac de Gras kimberlite field in the Northwest Territories, Canada, plus 23 samples from other Canadian kimberlite occurrences. This constitutes the most comprehensive geochemical database available for kimberlites at the present time, and allows detailed comparisons to be made with the well-documented kimberlites of the Kaapvaal craton, southern Africa. Major and trace element data shows that some Lac de Gras kimberlites have interacted extensively with continental crust, whereas others are minimally contaminated with crust but have physically incorporated large quantities (>30%) of lithospheric mantle peridotite.

Fresh, minimally-contaminated kimberlites from Lac de Gras have both elemental and isotopic characteristics that are transitional relative to those typical of southern African Group I and II kimberlites. The Hf-Nd isotope variations of these samples also define a linear array that strongly suggests mixing of two or more components/reservoirs within the mantle. Isotopic mixing models and mass balance considerations constrain the most likely candidate components/reservoirs to be depleted sub-continental lithospheric mantle and a component with an isotopically-enriched, negative $\Delta\varepsilon_{Hf}$ signature that is derived from beneath the lithosphere. Such a component has previously been identified in southern African kimberlites, indicating that it is globally extensive within the mantle. Its restriction to magmas generated at great depths, and its unusual Hf isotope signature also suggest that it may reside in isolation at some mantle boundary layer. Ancient oceanic crust, generated by melting in the presence of garnet and subsequently subducted and stored below the lithosphere, could evolve to negative $\Delta\varepsilon_{Hf}$ compositions. Melts of this material, variably recombined with the depleted, garnet-rich melting residua that constitute the lithosphere, can then account for the Hf-Nd kimberlite isotopic array. Trace element characteristics, such as K and Sr anomalies, are consistent with those of OIB-like magmas derived from within the convecting mantle.

Declaration

I declare that this thesis, which I submit for the degree of Doctor of Philosophy at the University of Durham, is my own work and not substantially the same as any which has previously been submitted at this or any other university.

David Philip Dowall

University of Durham
August 2004

Acknowledgements

Elemental and isotopic geochemistry of kimberlites from the Lac de Gras field, Northwest Territories, Canada.

David Philip Dowall
BA, Hons (Oxford)
MSc (Imperial College)

A thesis submitted in partial fulfilment of the requirements
for the degree of Doctor of Philosophy
at the University of Durham.

Department of Earth Sciences
University of Durham

August 2004

Contents

Chapter 1

Introduction

1.1 STUDY OBJECTIVES

Most studies of the geochemistry and petrogenesis of kimberlites during the last four decades have been based upon the numerous well-documented occurrences of these rocks in southern Africa. The discovery, from 1991 onwards, of a large kimberlite province in the Northwest Territories-Nunavut region of northern Canada (Carlson *et al.*, 1999; Nowicki *et al.*, 2003), has provided the ideal opportunity to test and expand the petrological understanding of kimberlites developed from southern African samples.

This study is based on comprehensive major/trace element and high-precision isotopic analyses of 98 samples from the newly discovered Slave kimberlite province, plus several samples from other, recently discovered kimberlite fields elsewhere in Canada. This new dataset enables a detailed geochemical comparison to be made between suites of kimberlites that have been emplaced within different cratonic regions. Further to this, a principal aim of the study has been to use this detailed data to investigate more thoroughly the processes that act to modify the geochemistry of kimberlite magmas as they ascend from their mantle source region through the sub-continental lithosphere and crust. By improving our understanding of these processes, it is possible to place better constraints on the elemental and isotopic character of the primary kimberlite magma. This in turn assists in constraining the location of the kimberlite source region within the mantle.

The analysis of the isotope geochemistry of Slave kimberlites presented here builds upon recent studies of Hf-Nd-Sr isotope variations in South African kimberlites (Nowell *et al.*, 1999; in press). These studies identify an unusual Hf isotope signature in the South African samples, which only appears to be observed in magmas that originate from the extreme depth within the mantle (e.g. diamond-bearing rocks such as kimberlites and lamproites). The second main aim of this study has been to investigate whether or not this Hf isotope signature exists within kimberlites from the Slave province, and if it does, to obtain further insight into its origin. This may also have implications for identifying the location of the kimberlite source region.

A subsidiary objective of this study has been to expand the isotopic database on kimberlites, and to broaden its scope given the predominance of samples from southern Africa. The solution chemistry of Hf presents a variety of analytical challenges to obtaining high and reliable yields from high Mg/Si and Ca/Si matrices, such as those of kimberlites. There is clearly a need for these challenges to be addressed if determinations of the Hf isotope geochemistry of these rocks are to become routine, thus enabling the isotopic database for kimberlites to expand further to other, so far less well-characterised provinces (e.g. Siberia, Brazil, Australia, Inida, Finland, China).

1.2 ASPECTS OF KIMBERLITE PETROLOGY

Due to the many unusual characteristics of kimberlites, literature relating to them is particularly rich in descriptive terminology, much of which is not normally applied to other kinds of igneous rocks. A summary of the key characteristics of kimberlites is therefore provided below.

1.2.1 Occurrence

Kimberlites occur in small (typically <1km diameter), volcanic pipe-like structures and associated networks of hypabyssal dykes and, more rarely, sills. They are found only in continental settings and are typically situated within or marginal to cratonic areas. Almost all diamondiferous kimberlites are found within cratons, and consequently the 'on-craton' or 'off-craton' distinction is an important characteristic of a kimberlite body. The level of exposure within the pipe varies, depending on the erosion history of the area. In southern Africa preservation of the crater region, which marks the palaeosurface at the time of eruption, is rarely observed. Crater facies deposits are more commonly found among Canadian occurrences. The only suggested occurrence of kimberlite lava to date is from the Igwisi Hills, Tanzania (e.g. Bassett, 1954), although this interpretation is controversial.

1.2.2 The facies concept

The petrography of kimberlite specimens is very variable within a kimberlite body. The relationship between the petrography of a specimen and its location within a body is described by the 'textural genetic classification' system (Clement and Skinner, 1979; Mitchell, 1986). In this framework, based on observations made on southern African kimberlites, three distinct zones, or facies, of kimberlite are recognised as resulting from different magmatic processes acting upon a single magmatic entity (Hawthorne, 1975; Clement and Skinner, 1979). The interrelation of these three facies is shown in Figure 1.1.

CRATER FACIES

DIATREME FACIES

HYPABYSSAL FACIES
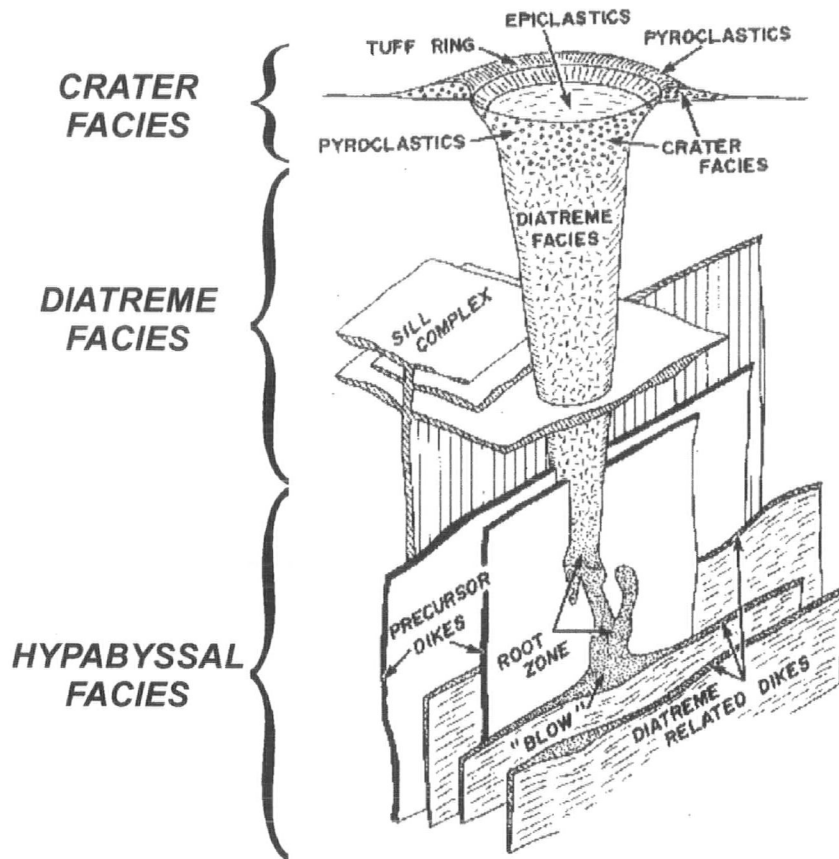
Figure 1.1 Location of different textural-genetic kimberlite facies within an idealised pipe structure. After Hawthorne (1975) and Mitchell (1986).

The *crater facies*, where preserved, consists primarily of pyroclastic and reworked epiclastic rocks. These are dominated by variably well to poorly bedded tuffs and tuff breccias. Epiclastic shales and mudstones typically take the form of lacustrine deposits and are probably associated with the development of crater lakes or maars above the kimberlite body. Crater facies rocks are rarely found at Southern African kimberlite localities, but do appear to be very common, especially in western Canadian occurrences.

4

The *diatreme facies* occupies the steep-sided, 'inverted cone'-shaped pipe that is characteristic of many kimberlite bodies. The rocks found in this zone are termed tuffisitic kimberlites and tuffisitic kimberlite breccias (Clement, 1979; Clement and Skinner, 1979) and are composed of clasts of xenolithic and autolithic material set in a fine-grained matrix that is dominated by serpentine. Mitchell (1986) points out the term 'tuffisitic' has genetic implications, which may not be applicable to the formation of the diatreme itself, and hence proposes 'volcaniclastic' (Fisher, 1961) as a more appropriate, non-genetic term.

Hypabyssal facies kimberlites are found in the 'root zone' of the intrusion below the base of the diatreme, and consist mainly of dykes and occasional sills, which act as feeder structures to the diatreme and crater. Dykes at high structural levels are rarely observed to cross-cut diatreme zone rocks. At many localities the crater and diatreme have been completely removed by erosion, and only the hypabyssal intrusive rocks remain. Hypabyssal kimberlites are massive, crystalline rocks that tend to be less altered and contain significantly lower levels of xenolithic contamination than the rocks of the diatreme and crater facies. Consequently, they are the most appropriate rocks to choose for geochemical analysis in any study of the chemistry of the kimberlite magma. Hypabyssal kimberlites usually contain abundant olivine macrocrysts, which may be either cognate (i.e. phenocrysts), or xenocrysts derived from disaggregated peridotites. Rare examples of hypabyssal kimberlite are devoid of phenocrysts or xenocrysts and are consequently described as 'aphanitic'. In the absence of genuinely glassy kimberlites, aphanitic material that is free of any visible contamination may be most representative of the parental magmatic liquid, if it can be ascertained that these samples are not flow-differentiated.

It is clear, from studies during the past decade in Canada, that many of the kimberlites in western Canada (e.g. Lac de Gras occurrences) bear no resemblance to the classic southern African model of a kimberlite pipe (Figure 1.2). This is especially relevant in the Lac de Gras area, where a number of kimberlite pipes (e.g. Grizzly, Leslie, Arnie, Aaron) are comprised solely of or are dominated by hypabyssal material. Estimates based on sedimentological reconstructions of the Lac de Gras area (e.g. Stasiuk *et al.*, 2003; Sweet *et al.*, 2003; Hamblin *et al.*, 2003) indicate that there has been only ~200m of erosion since the time of kimberlite formation, implying that large volumes of kimberlite magma were emplaced as hypabyssal intrusions very close to the palaeosurface. Morphological differences between kimberlites from southern Africa and Lac de Gras are likely to primarily reflect differences in the lithological and structural character of the rocks into which they are emplaced (Field and Scott-Smith, 1999; Kjarsgaard, 2003).

1.2.3 Composition

Kimberlites are notoriously difficult to classify petrologically (Mitchell, 1986; 1995) because of their highly complex and variable chemical and mineralogical composition. They are hybrid magmatic rocks, composed partially of xenolithic and xenocrystal material incorporated into the magma as it ascends from its source region to the surface. Kimberlites typically have a highly inequigranular texture ranging from a very fine-grained groundmass up to xenoliths or xenocrysts that are several tens of centimetres in diameter.

Southern Africa   # Lac de Gras

PRESENT EROSION SURFACE

CRATER FACIES	☐ Pyroclastic kimberlite
	▨ Epiclastic (resedimented) kimberlite
DIATREME FACIES	▨ Tuffisitic kimberlite breccia
HYPABYSSAL FACIES	■ Massive kimberlite

500m

1000m
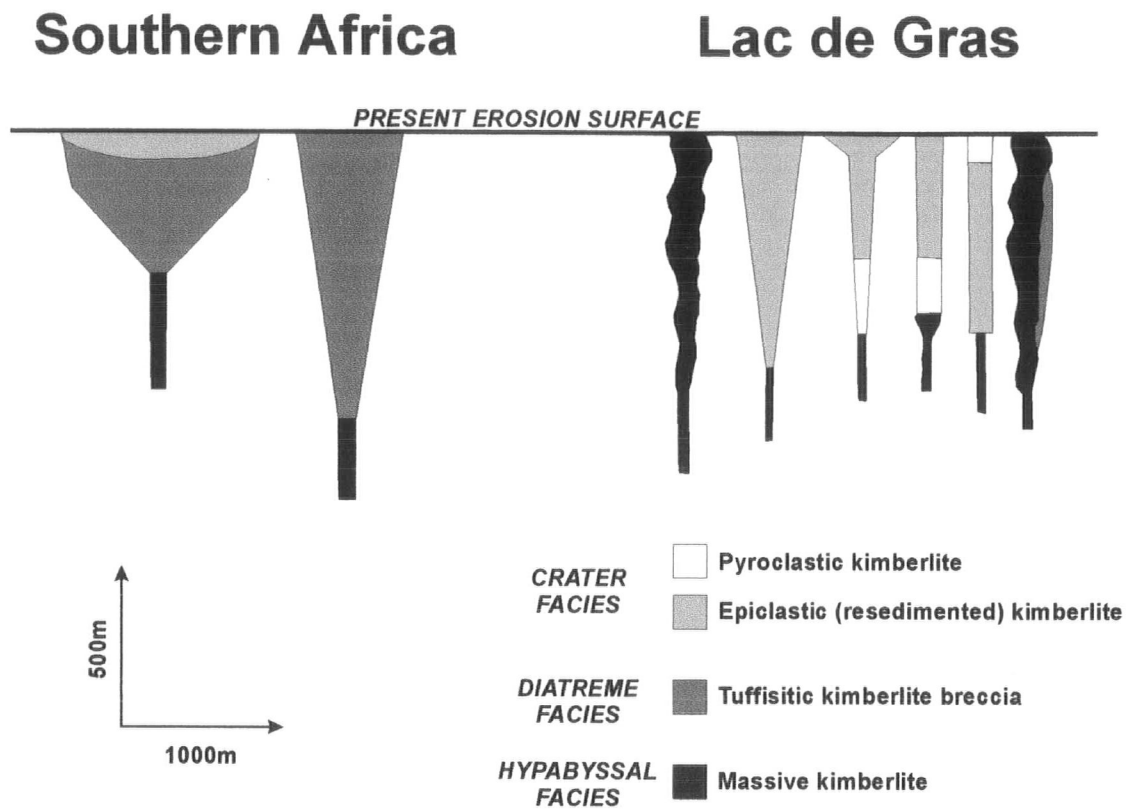
Figure 1.2 Cartoons to illustrate differences in style and variety of pipe morphologies in southern Africa and Lac de Gras. After Kjarsgaard (2003).

The extremely fine-grained groundmass and microphenocrystic phases typical of most hypabyssal kimberlites are considered to be most representative of the parental magma. These constituents are typical silica-poor and ultrabasic in nature, with an unusually high content of volatile components (dominantly H_2O and CO_2). Unlike most igneous rocks, archetypal kimberlites are typically richer in K_2O than Na_2O. They are often classified as ultrapotassic rocks, but this is misleading, because their high K_2O/Na_2O ratios derive from having very low Na_2O, rather than very high K_2O. Principal groundmass minerals include olivine, spinel, monticellite, phlogopite, perovskite, primary carbonates and apatite. One or two of these phases are typically dominant in any given specimen, and this forms the basis of the classification scheme proposed by

Skinner and Clement (1979), which is widely used. A much greater mineralogical diversity is imposed on the kimberlite by its compliment of xenoliths and megacrysts, including olivine, garnet, ilmenite, phlogopite, orthopyroxene, clinopyroxene and spinel. The provenance of the megacryst suite (i.e. cognate versus xenocrystal origins) is as yet unresolved. In addition to these relatively common phases, kimberlites may also contain rutile, brucite, various clay minerals, sulphides and other, more exotic phases in small quantities. Mitchell (1986; 1995; 1997) provides a comprehensive coverage of the complex petrography of these rocks.

1.2.4 Group I and Group II kimberlites

The study of Nd and Sr isotopic variation in South African kimberlites by Smith (1983) demonstrated that there are two distinct groups of kimberlites that occur within the Kaapvaal craton. Group I kimberlites have an isotopic signature that is indicative of derivation from a source that is near chondritic and similar to that seen in ocean island basalts (OIBs), whereas Group II kimberlites have a more enriched isotopic signature, which may relate to derivation from an EM II-type (Zindler and Hart, 1986) source within the lithosphere (Smith, 1983). These two groupings correspond broadly to the 'basaltic' (~Group I) and 'micaceous' (~Group II) kimberlites defined by Wagner (1914). To date Group II kimberlites have only been identified within the Kaapvaal craton of South Africa, where they tend to pre-date the majority of Group I bodies in the region (Gurney et al. 1991). Skinner et al. (1994) have also identified a small number of kimberlites from the NW edge of the Kaapvaal craton that have isotopic signatures that are transitional between Group I and Group II. This kind of signature is similar to those seen in the few isotopic analyses of kimberlites from Brazil (Bizzi et al., 1994), Finland (O'Brien and Tyni, 1999) and China (Tompkins et al., 1999).

1.3 REGIONAL GEOLOGY

The majority of samples analysed in this study (Appendix A) are drawn from the Lac de Gras field of the Archaean Slave province, Northwest Territories, Canada. Consequently this section focuses on the geology of the Slave craton and the immediate area around Lac de Gras. A small number of samples have been analysed from Somerset Island, in the Churchill province of northern Canada, and several localities in the Superior province of south-central Canada. The regional geology of these areas is not reviewed here, but key references suitable for gaining a geological overview are provided in Table 1.1.

1.3.1 Slave province

The Slave province (Figure 1.3) is an Archaean cratonic region covering approximately 210,000km^2 of the Northwest Territories and Nunavut, northern Canada (Pell, 1997). Like other Archaean cratons, exposed rocks consist of basement gneiss complexes, intruded by granitic plutons and overlain by various supracrustal rocks, i.e. granite-greenstone terranes. Unlike most cratonic regions, the greenstone belts of the Yellowknife Supergroup (YKSG), which dominate the supracrustal sequences of the Slave craton, are dominated by metasedimentary, rather than metavolcanic, units (Padgham and Fyson, 1992). Granitoid plutons, which were emplaced in several episodes both contemporaneous to and postdating the Yellownife Supergroup, account for ~65% of current exposure in the Slave province (King *et al.*, 1992; Padgham and Fyson, 1992; van Breeman *et al.*, 1992; Davis *et al.*, 1994). Four major swarms of Proterozoic diabase dykes were emplaced after stabilisation of the craton. These are dominated by the 1.27Ga Mackenzie swarm (LeCheminant and Heaman, 1989), but also include the older (2.02-2.23Ga) Lac de Gras, Mackay and Malley swarms

(LeCheminant and van Breeman, 1994). The orientation of these dyke swarms is indicative of dominant structural grains within the crust, which may also be exploited by kimberlites as they ascend to the surface.

Events	References
Churchill province (Somerset Island and Rankin Inlet kimberlites)	
Pre- and syn-orogenic (3.0-2.0Ga) igneous activity (komatiites, basalts and granites),	Bickford *et al.* (1994); Percival (1996)
Continental collision	Hoffman (1988, 1990)
Post-orogenic igneous activity	Peterson *et al.* (1994)
Somerset Island	
Development of Archaean basement	Frisch *et al.* (1987); Frisch and Sandeman (1991)
Proterozoic igneous and sedimentary events	Blackadar (1967); Okulitch *et al.* (1986); Fahrig (1987)
Phanerozoic sedimentary events	Okulitch *et al.* (1986); Stewart (1987)
Superior province (Attawapiskat, Kirkland Lake and Timiskaming kimberlites)	
Geological overview	Card (1990)
Gneisses	e.g. Wooden *et al.* (1982); Moser (1988); Moser *et al.* (1991)
Plutonic rocks	e.g. T. E. Smith *et al.* (1985); Beakhouse *et al.* (1988); Corfu *et al.* (1989)
Supracrustal rocks	e.g. Turner and Walker (1973); Dimroth *et al.* (1982); Sylvester *et al.* (1987)
Tectonic assembly	Langford and Morin (1976); Ludden *et al.* (1986); Hoffman (1988)

Table 1.1 Papers summarising the geology of the Churchill Province (including Somerset Island) and the Superior Province.

Some insight into the large-scale tectonic structure of the craton is provided by isotopic studies, which appear to broadly divide the Slave province into western and eastern domains. Thorpe et al. (1992) reported high $^{207}Pb/^{204}Pb$ ratios in crustal rocks from the western Slave, and low $^{207}Pb/^{204}Pb$ from the east. This was interpreted in terms of lead being derived from an ancient, enriched upper crustal source in the west, and from a more juvenile, mantle source in the east. The boundary line between the two domains passes to the west of the Lac de Gras kimberlite field; the kimberlites thus appear to be located within relatively juvenile neo-Archaean crust. Although this boundary line is based on relatively few isotopic analyses, it is supported by Nd isotope evidence (Davis and Hegner, 1992), which also indicates that granitic crust from the central and eastern parts of the province is derived from more juvenile sources, whereas granitoids from the western side of the craton preserve an older crustal signature. The Nd isotope boundary is oriented more NE-SW than the Pb isotope line, and passes slightly further to the east. Despite this, crustal xenoliths from the Grizzly and Torrie kimberlites are meso-Archaean in age, suggesting that in the Lac de Gras area, juvenile neo-Archaean crust overlies older meso-Archaean basement (Bleeker et al., 1999a; Kjarsgaard, 2001).

The isotopic subdivision defined by Thorpe et al. (1992) and Davis and Hegner (1992) is broadly consistent with the tectonic structure of the craton envisaged by Kusky (1989), whereby high-strain zones representing orogenic sutures separate four discrete crustal terranes. From west to east, these tectonic blocks are the Anton terrane, the Contwoyto terrane and the Hackett River terrane. The Sleepy Dragon terrane is also included as an easterly extension of the Anton terrane. The current assembly of these terranes is interpreted (Kusky, 1989) as an Archean analogue of collision between a micro-continent (Anton-Sleepy Dragon) and an island arc and associated accretionary

prism (Hackett River). The location of the Hackett River terrane thus represents the position of an ancient subduction zone, with the Contwoyto terrane representing the fold-thrust orogenic belt produced by the collision of continent and arc. The Lac de Gras kimberlites are all located within the metasedimentary rocks and associated granitoid plutons of the Contwoyto terrane.

1.3.2 Vicinity of Lac de Gras

Table 1.2 provides a summary of the bedrock geology of the area around the Lac de Gras kimberlite field, which is described in detail by Kjarsgaard et al. (2002) and references therein. The geology of the area (Figure 1.4) is dominated by the greywackes of the Yellowknife Supergroup (YKSG) and the granitoid plutons that intruded during and after formation of these metasedimentary units. Metavolcanic elements are not common in the area, as is typical of the Slave province in general. The structural grain of the central part of the area, where most of the Lac de Gras kimberlites are situated, is NW-SE trending, which again is characteristic of the eastern Slave province (Henderson et al., 1999). Direct evidence for faulting is limited (Kjarsgaard et al., 2002) but up to four main trends are evident from joint set measurements (Wright, 1998). These structural elements may play a role in controlling the distribution of kimberlites in the upper crust within the Slave province and the Lac de Gras field. The bedrock lithologies intruded by each kimberlite at the present exposure level is also shown in Figure 1.4. The majority of kimberlites investigated from the BHP claim block on the north side of Lac de Gras are emplaced within syn-YKSG granitoids, while most of those from Kennecott claims to the south and south-east are situated within YKSG metasediments and post-YKSG granitoids at the present-day erosion level.
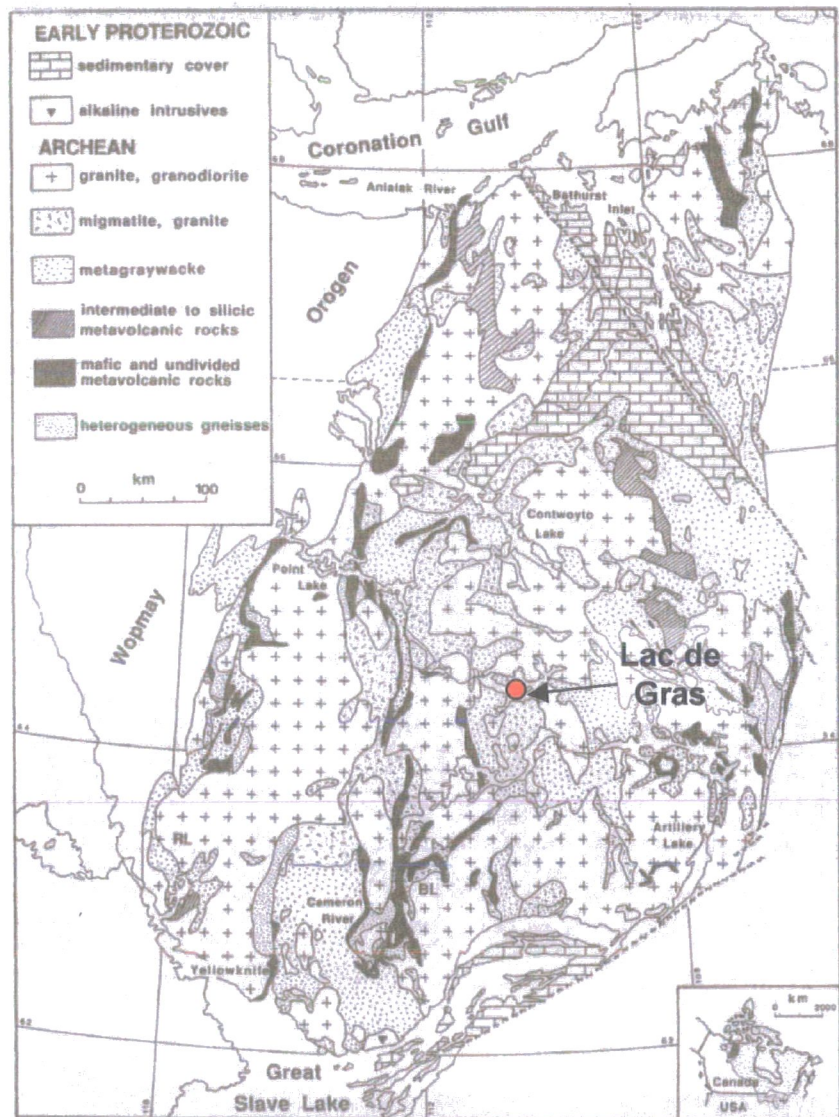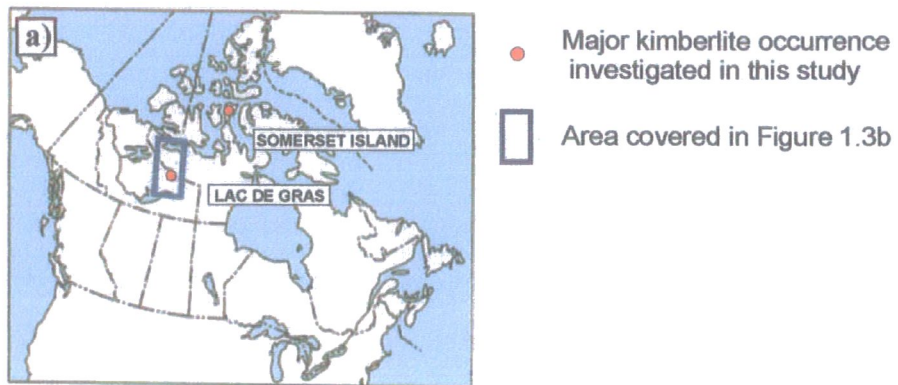
Figure 1.3 a) Location of the Lac de Gras and Somerset Island kimberlite occurrences in continental North America (modified from Kjarsgaard, 2003); b) Generalised geology of the Slave craton, showing distribution of basement gneisses and metasedimentary and metavolcanic rocks of the Yellowknife Supergroup (modified from Kusky, 1989).

Bedrock elements	References
a) Pre- and syn-YKSG basement	
Quartzofeldspathic gneisses, granitoid migmatites and meta-granite/tonalite, e.g. Jolly Lake Complex	McGlynn (1977); Thompson *et al.* (1993; 1994; 1995); Thompson and Kerswill (1994)
Migmatitic gneiss from SW shore of MacKay Lake has zircon U-Pb age of 3325±8Ma	Bleeker *et al.* (1999a)
Central Slave Basement Complex (CSBC), consisting of Jolly Lake and similar meta-granitoid/gneiss complexes (e.g. Big Lake, Anton, Sleepy Dragon)	Bleeker *et al.* (1999a)
Central Slave Cover Group (~2.9-2.8Ga) overlies BSBC in Jolly Lake area; small exposures of quartzites and banded iron formations (BIF)	Bleeker *et al.* (1999b)
b) YKSG volcanics and syn-YKSG felsic/mafic intrusives	
Courageous Lake greenstone belt: ~2700Ma mafic-dominated west side and ~2670Ma felsic-dominated east side. Basalts, breccias, agglomerates, rhyolites, felsic porphyries	Folinsbee (1949); Moore (1956); Villeneuve (1993); Thompson and Kerswill (1994); Villeneuve *et al.* (1997)
Central Volcanic Belt: ~2670Ma intermediate volcaniclastics and tuffs, plus minor mafic and felsic lavas	Bostock (1980), King *et al.* (1988); Mortenson *et al.* (1988)
Back River Complex: stratovolcanic succession composed of andesitic-rhyolitic lavas, tuffs and volcaniclastics; oldest rocks ~2710Ma, end of activity ~2690Ma	Lambert (1982; 1996); van Breeman *et al.* (1987); Villeneuve *et al.* (2001)
Aylmer Lake volcanic dome: mafic to felsic volcanics and volcaniclastics of ~2680Ma	Renaud *et al.* (2001); MacLachlan *et al.* (2002)
c) YKSG sediments	
Extensive meta-greywacke turbiditic mudstones, divided into Contwoyto (+ BIF) and Itchen (- BIF) formations. BIFs common at interface between sediments and volcanics	Bostock (1980); King *et al.* (1991)

(continued)

Bedrock elements	References
d) Syn- and post-YKSG granitoids	
~2650Ma biotite tonalities/granodiorites, intruding metasedimentary turbidites	van Breeman *et al.* (1990); King *et al.* (1991)
~2625-2608Ma trondhjemites, diorites, quartz diorites, hornblende-biotite tonalities and biotite granodiorites; often found as composite intrusions	van Breeman *et al.* (1990; 1992); Villeneuve (1993)
~2599-2588Ma muscovite-biotite granites and biotite granites	van Breeman *et al.* (1992); Thompson and Kerswill (1994)
e) Proterozoic intrusions	
Dominantly diabase/dolerite dykes divided into 5 groups on basis of orientation and age: Palaeoproterozoic Malley, Mackay and Lac de Gras swarms; Mesoproterozoic Mackenzie and '305' swarms	LeCheminant and van Breeman (1994); Wilkinson *et al.* (2001)

Table 1.2 Bedrock lithological elements in the vicinity of the Lac de Gras kimberlite field (summarised from Kjarsgaard *et al.*, 2002).

1.3.3 Location of kimberlite pipes

Stubley (2003) presents a geometric analysis of the distribution of kimberlites within the Slave province, which indicates that occurrences may be preferentially concentrated along two 'corridors'. The 'western corridor' is aligned NNE-SSW and encompasses the kimberlites of the south-west and far northern Slave, which are not represented in this study. The remainder of the Slave occurrences, including those from the vicinity of Lac de Gras, Contwoyto Lake, Kennady Lake and Snap Lake (see Appendix A), are accommodated within a 'central corridor' that is oriented broadly NW-SE. Stubley (2003) suggests that the orientation of these trends correspond to structural controls operating at lower crustal to mantle depths. Structural elements are clearly important

controls on kimberlite emplacement, although as Helmstaedt and Gurney (1997) point out, there may be little or no connection between the tectonic controls on emplacement within the upper crust, and those that initially trigger melting within kimberlite source regions.
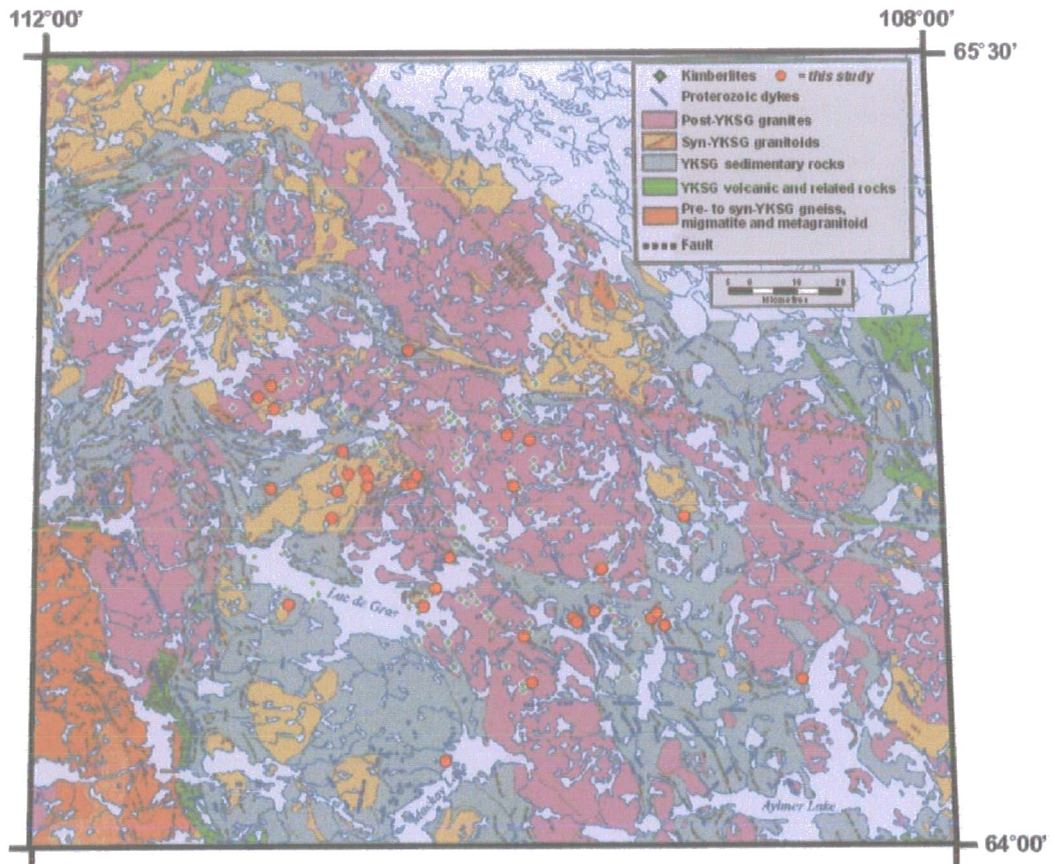
Figure 1.4 Bedrock geology of the area around the Lac de Gras kimberlite field (from Kjarsgaard *et al.*, 2002), showing locations of known kimberlites, including those investigated in this study.

The locations of all Lac de Gras kimberlite bodies investigated in this study are shown in Figures 1.5 and 1.6. These samples account for 70 of the 80 Slave kimberlite analyses produced for this study; a more detailed regional breakdown of all samples analysed is given in section 4.3.2. For convenience of statistical analysis in Chapters

4-6, the hypabyssal kimberlites are divided into a number of groups, on the basis of mutual proximity, as indicated in the legend to Figure 1.5. The focus of these groups is the Grizzly kimberlite (group A1), for which analyses of 14 separate samples have been obtained. These samples are subsequently considered together with a further eight hypabyssal kimberlites from 'central north Lac de Gras' (group A2). The remaining six hypabyssal bodies situated north of Lac de Gras constitute group B. The kimberlites located on or south of Lac de Gras are contained within groups C and D: the two close clusters of three bodies between Lac de Gras and Aylmer Lake (T-34, T-35, T-36 and T-19, T-21, T-237) constitute group C, while the remainder of the more southerly bodies are contained in group D. The grouping of the kimberlites in this way is primarily an aid to data representation and does not directly imply any petrological or petrogenetic association. The positions of all Lac de Gras kimberlites included in this study are identified by name in Figure 1.6.

As indicated in Appendix A, the published ages of kimberlites studied from Lac de Gras range from 45.2 ± 1.3Ma (for Aaron: Creaser et al., 2003) to 73.7 ± 3.2Ma (for C13: Heaman et al., 2003). All kimberlites from the BHP Billiton claim that feature in this study and have published ages, fall within a range of 45.2 ± 1.3Ma to 59.7 ± 1.5Ma (Creaser et al., 2003). In contrast, the kimberlites from the De Beers claim south of Hardy Lake have been dated at 72 ± 2Ma (Scott-Smith and McKinlay, 2002), and the T-series kimberlites from the Kennecott claim area around the northern edge of Afridi Lake are inferred to be of a similar age (B. A. Kjarsgaard, pers. comm.). Where published ages are not available for bodies analysed in this study, an age estimate is provided by the average age of dated kimberlites in their vicinity (53Ma for those in the immediate vicinity of Lac de Gras; 72Ma for those around Hardy Lake and Afridi

Lake). In practice, changing the age of any given kimberlite by up to 10Ma only produces a shift in the calculated initial ratio of 2-3 in the sixth decimal place, or <<1 epsilon unit (see Chapter 6 and Appendix F). It should be noted that while kimberlite ages are very similar in groups A1, A2 and C (as defined above), groups B and D include bodies from both the 45.2-59.7Ma age range and the ~72Ma kimberlites more typical of the Hardy Lake and Afridi Lake areas. Groupings of kimberlites from beyond the Lac de Gras field (see Chapter 4) also include bodies with a wider range on ages; these ages are tabulated in Appendix A.

The kimberlites from the Contwoyto (Jericho, Muskox) and South-East Slave fields (Snap Lake, Kennady Lake) are located just beyond the extent of the map shown in Figure 1.4, to the north and south respectively. All of these kimberlites intrude Archaean granitoids (Price *et al.*, 2000; Mogg *et al.*, 2003; Hetman *et al.*, 2003); the Snap Lake dyke is also known to intrude metavolcanics of the YKSG (Mogg *et al.*, 2003) and the Jericho and Muskox pipes commonly contain xenoliths of limestone derived from sedimentary cover that is now completely eroded (Cookenboo and Daoud, 1996).

1.4 PETROGRAPHY

Detailed petrographic studies of the kimberlites from Lac de Gras, which are the focus of this investigation, have been undertaken by Armstrong *et al.* (in press) and B. A. Kjarsgaard (unpublished). The mineralogy of selected kimberlites studied by these and other workers is summarised in Appendix B. No significant additional petrography was undertaken during this project, because the majority of samples were received as powders; exceptions to this are listed in Appendix C.
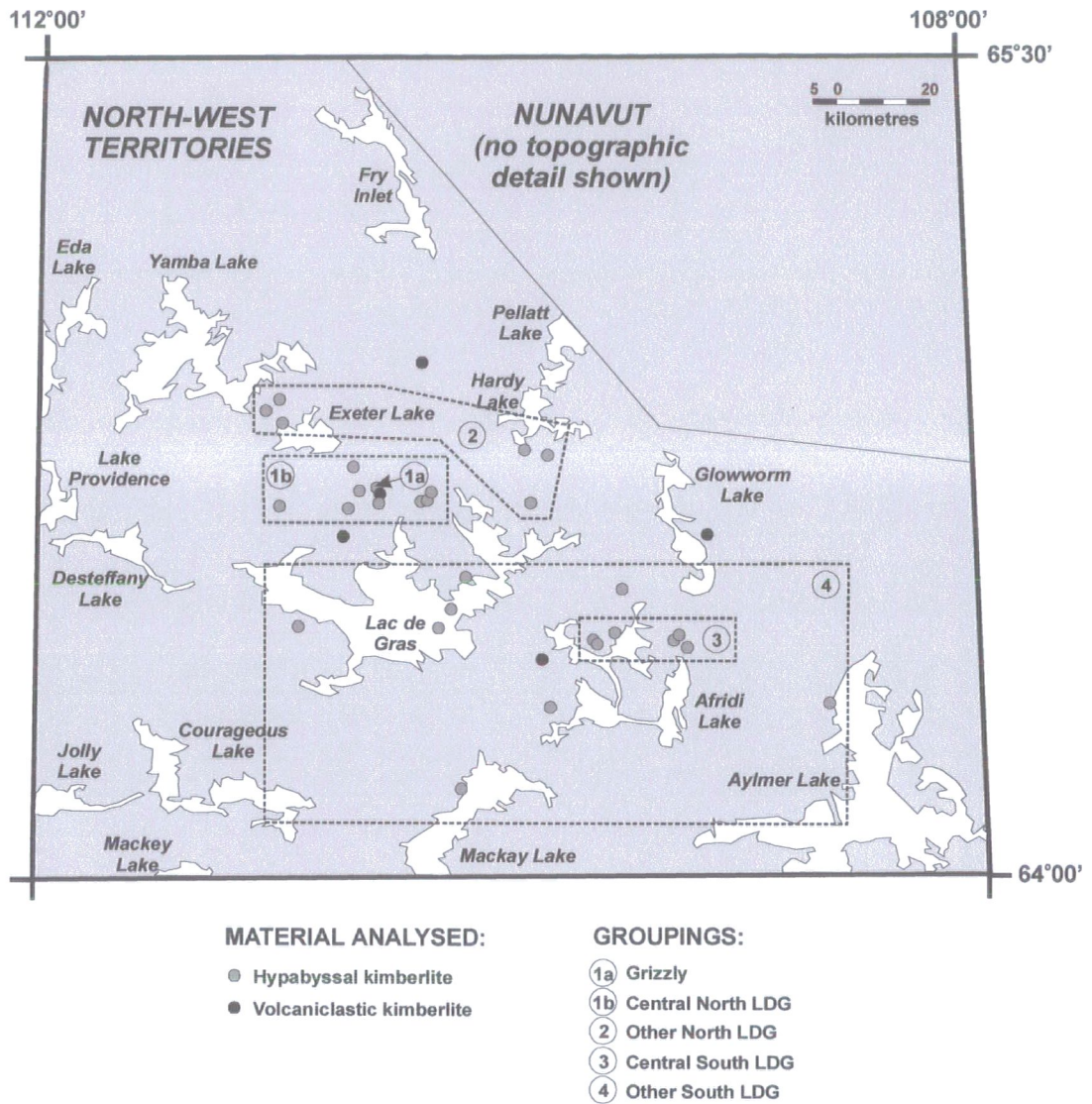
Figure 1.5 Sketch map of area around the Lac de Gras kimberlite field showing locations of hypabyssal and volcaniclastic kimberlite bodies investigated during this study. Positions are shown relative to major lakes in the area, and groupings of kimberlites adopted in Chapters 4 and 5 are indicated. Map based on Kjarsgaard *et al.* (2002).

Hypabyssal kimberlites from the Slave craton, and the Lac de Gras field in particular, are noted for their freshness relative to samples from southern Africa. In many cases, such as those illustrated in Figure 1.7, there is minimal evidence of alteration in these kimberlites, with olivine macrocrysts and microphenocrysts remaining largely unserpentinised, and low proportions of clay minerals and secondary calcite in the groundmass. Geochemical measures of alteration are discussed further in section 5.2.

The apparent absence of alteration in these samples makes them preferable for petrogenetic studies in comparison to less fresh alternatives. The main petrographic characteristics of Lac de Gras kimberlites are summarised below.

1.4.1 Silicate and oxide phases

Olivine is ubiquitous in Lac de Gras kimberlites, both as macrocrysts derived from diaggregated peridotite, and as phenocrysts that have crystallised directly from the kimberlite magma. Macrocrysts are discriminated from phenocrysts primarily on the basis of grain size and shape. Macrocrysts are typically anhedral and larger than 1mm, whereas phenocrysts are typically euhedral to subhedral and smaller than 0.4mm (Armstrong *et al.*, in press). Although there is some overlap in the Mg number of both olivine populations, macrocrysts are on average more magnesian than phenocrysts (Armstrong *et al.*, in press).

Phlogopite macrocrysts are rarely observed in the kimberlites studied, but phlogopite and kinoshitalite are common microphenocryst and groundmass phases. Koala West and Porpoise are particularly phlogopite-rich bodies. The majority of phlogopite from Lac de Gras kimberlites appear to follow Type 1 and Type 3 TiO_2-Al_2O_3 compositional trends as identified by Mitchell (1986). An exception to this is the phlogopite from the Porpoise body, which follows the Type 2 TiO_2-Al_2O_3 trend of Mitchell (1986) towards tetraferriphlogopite; this trend is more characteristic of the micas in Group II, rather than Group I, kimberlites (Mitchell, 1995).
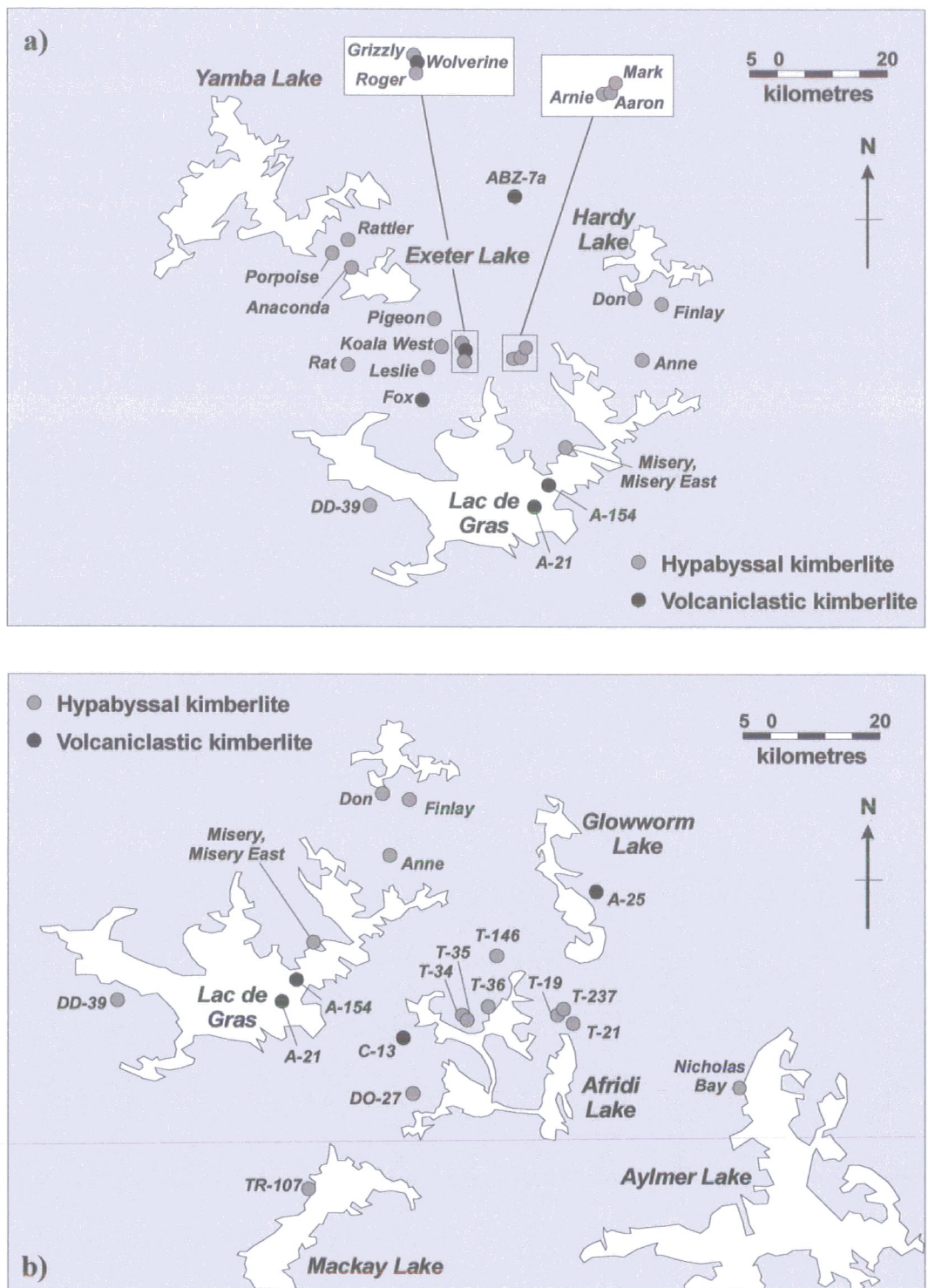
Figure 1.6 Sketch map of area around the Lac de Gras kimberlite field showing locations of individual kimberlite bodies investigated during this study: a) north and central Lac de Gras; b) central and south Lac de Gras. Positions are shown relative to major lakes in the area. Map based on Kjarsgaard *et al.* (2002).

21

The modal abundance of spinel varies between Lac de Gras kimberlites, but is present in greater than accessory quantities in some bodies (Grizzly, Misery East, Rattler) and is abundant in others (Anaconda, Koala West). Resorbed spinels with 'atoll' morphologies (Mitchell and Clarke, 1976) are observed in many bodies (e.g. Anaconda, Koala West, Porpoise, Rattler) and these are found to be consistently more TiO_2-rich and Cr_2O_3-poor than non-atoll spinels from other Lac de Gras kimberlites (Armstrong et al., in press).

Monticellite is present in variable amounts in the Lac de Gras kimberlites studied, and is quite abundant in the Leslie and Rat kimberlites. Monticellite is easily altered to calcite (Mitchell, 1986); the presence of fresh monticellite in many bodies is thus indicative of the exceptional freshness of many Lac de Gras kimberlites. The low Fe content of monticellite from kimberlites of the BHP claim block distinguishes them from the majority of other published monticellite analyses (Armstrong et al., in press), including those from kimberlites of the Diavik property, located just a few kilometres further south (Masun, 1999).

Perovskite and apatite are present as accessory phases in most of the Lac de Gras kimberlites; perovskite is particularly common in the Leslie, Porpoise and Rattler bodies, and apatite is most common in Koala West and Porpoise. These minerals are important geochemical repositories for elements such as the REEs and U.

Modal abundance of primary groundmass serpentine in the Lac de Gras kimberlites is very variable, being of minor importance in bodies such as Anaconda, Leslie and Rattler, more common in Grizzly, Koala West and Misery East, and abundant in

Porpoise. The abundance levels reported in Appendix B do not include secondary serpentine introduced by alteration of olivine, monticellite, etc.
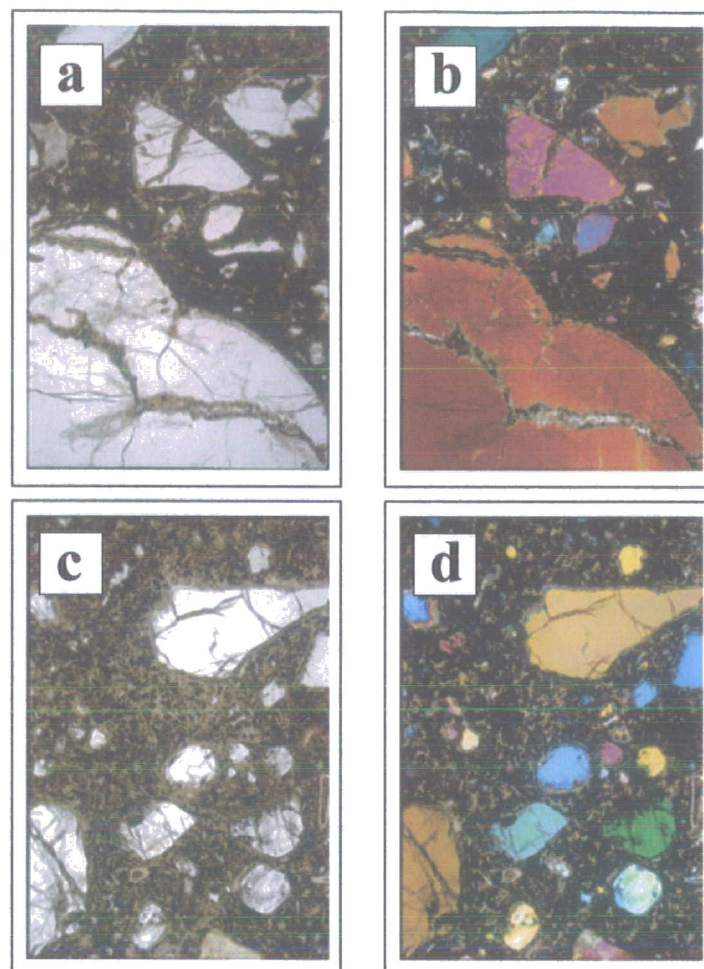
Figure 1.7 Photomicrographs showing typical fresh, largely unaltered appearance of Slave hypabyssal kimberlite in thin section: a) Leslie (Lac de Gras field), x2.5, PPL; b) Leslie, x2.5, XPL; c) Muskox (Contwoyto field), x2.5, PPL; d) Muskox, x2.5, XPL. Courtesy of Dr. B. A. Kjarsgaard.

1.4.2 Carbonate phases

Carbonates occur in kimberlites as either primary, magmatic phases, or as secondary phases introduced by alteration of minerals such as olivine, monticellite and phlogopite. Careful examination of textures for the presence of pseudomorphs can help to

determine which carbonates are the result of alteration, but more recently stable isotope studies have been used to distinguish primary and secondary carbonate. Preliminary carbon and oxygen isotope data indicate that the majority of carbonates in the Lac de Gras kimberlites studied have mantle-type signatures, and are thus primary crystallisation products from a CO_2-rich magma (B. A. Kjarsgaard, pers. comm.). This again demonstrates the freshness of many of these kimberlites.

Four separate parageneses of carbonate mineralisation in the Lac de Gras kimberlites are listed in Appendix B. The most commonly observed is that of non-segregational accumulations throughout the groundmass. Sr-Ba calcite is particularly ubiquitous among carbonate phases from Lac de Gras kimberlites, with the cores of calcite grains typically more enriched in Sr and Ba than the rims (Armstrong et al., in press).

Carbonate of intermediate calcite-dolomite composition is observed in the Anaconda, Misery East, Rat and Rattler bodies; in these instances discrete domains of calcite-dolomite and dolomite-magnesite solid solution exist within carbonate grains (Armstrong et al., in press). End-member compositions of dolomite or magnesite are rarely observed. Armstrong et al. (in press) divide the eight kimberlites in their study into two groups that are, respectively, predominantly calcite-bearing and dolomite-bearing. The calcite-bearing group commonly exhibit strongly serpentinised olivine phenocrysts, abundant groundmass monticellite that is unaltered, or pseduomorphed by calcite, and a serpentine-rich groundmass. Conversely, the dolomite-bearing group display fresh olivine phenocrysts, and a groundmass that contains an abundance of monticellite that is pseduomorphed by serpentine, but is otherwise serpentine-poor. Armstrong et al. (in press) interpret these relationships as evidence of the Lac de Gras

kimberlites being derived from magmas that have variable CO_2/H_2O contents, with high CO_2/H_2O magmas crystallising dolomite-rich carbonate paragenesis, and low CO_2/H_2O magmas producing calcite-rich parageneses. Kimberlite carbonates may therefore contain a great deal of information regarding the relative abundance of volatile components within the parent magma.

Chapter 2

Pre-concentration of Hf, Nd and Sr from the kimberlite matrix

2.1 CHAPTER OVERVIEW

During the course of this project it has been necessary to develop a new pre-concentration chemistry procedure to address the difficulties associated with obtaining consistently high yields of Hf from kimberlites. The new technique incorporates modifications to a number of existing, published methodologies, and has the advantage of enabling time- and cost-efficient separation of Hf, Nd and Sr from a wide variety of geological samples prior to isotopic analysis by PIMMS. This chapter presents the rationale for this new technique, describes the methodology and provides a discussion of associated issues regarding the analysis of samples prepared in this manner, with particular reference to applying corrections for isobaric interferences.

A previous version of this chapter has been published as Dowall *et al.* (2003).

2.2 INTRODUCTION

Ultramafic rocks and their constituent minerals pose a particular problem in Hf isotope geochemistry, as they are one of the few groups of geological materials that cannot be routinely analysed for Hf isotope composition using procedures based on established chemical pre-concentration techniques. This is principally due to the fact that these materials contain very high levels of Mg and Ca in relation to their Si content.

The technique presented here was developed initially as a means of obtaining improved yields of Hf from kimberlites, which typically have some of the highest Mg/Si and Ca/Si ratios encountered in silicate rocks. It can, however, be successfully applied to a wide range of whole rock and mineral separate samples to perform the necessary pre-concentration chemistry for Hf, Sr and Nd isotopic analysis from a single dissolution. The combined chemistry and mass spectrometry technique also offers significant benefits in terms of cost and time efficiency in comparison to other published procedures.

One of the major benefits of performing isotopic analyses by plasma ionisation multi-collector mass spectrometry (PIMMS, *aka* MC-ICP-MS) is that large numbers of samples can be analysed very quickly in comparison to thermal ionisation mass spectrometry (TIMS). Consequently, it is now usually the case that pre-concentration chemistry, not mass spectrometry, is the rate-determining step in obtaining an analysis. The rapidity of this procedure is therefore well suited to studies requiring large throughputs of samples for Hf-Sr-Nd isotopic characterisation.

2.3 PRE-CONCENTRATION OF TRACE ELEMENTS FROM GEOLOGICAL MATERIALS

2.3.1 The role of chemical pre-concentration in isotope geology

Studies of the isotopic character of geological materials require that the element, or elements, of interest (e.g. Sr, Nd, Hf, Pb, Os and their respective radioactive parents) are efficiently separated from the bulk matrix of the sample.

This process, commonly known as pre-concentration, is essential when employing TIMS techniques, because the presence of impurities on the filament can seriously inhibit ionisation of the analyte and may also lead to severe isobaric interferences. The advent of PIMMS during the last decade has effectively eliminated the problem of ionisation suppression due to the very high temperatures attainable within the plasma. Recent associated developments such as dynamic reaction cells have, for some applications, also reduced the need for pre-concentration as spectral overlaps can be resolved within the instrument.

However, to achieve the extremely high levels of analytical precision required in isotope geochemistry (e.g. <20ppm accuracy and 10-20ppm internal precision) it is desirable to separate the analyte as fully as possible from other elements that may cause atomic (e.g. ^{87}Rb on ^{87}Sr) or polyatomic/molecular (e.g. BaO on Nd) isobaric interferences, or matrix effects. This is achieved typically by dissolution of a powdered rock sample in an appropriate combination of acids, and subsequently isolation of the analyte by utilisation of the selective retention and release of different elements on ion-exchange resins in the presence of acid solutions.

2.3.2 Limitations of silicate digestion techniques

Conventional procedures for the dissolution of silicate rocks are all based around attack by hydrofluoric acid (HF), usually in combination with another mineral acid. HF is the only acid that can readily dissolve silicates, due to the solubility of the SiF_6^{2-} ion in acid solution. A review of the rationale for mixed-acid digestion of silicates is given in Potts (1987). Once digested, the sample is dissolved in a dilute acid appropriate for the ion-exchange technique being employed.

Not all fluorides are highly soluble. Magnesium and calcium in particular have been shown to form a variety of insoluble fluoride compounds on digestion of silicate minerals with concentrated HF (Langmyhr and Kringstad, 1966; Croudace, 1980). These compounds incorporate, or co-precipitate, a wide range of trace elements within their structures (Yokoyama et al., 1999), directly affecting the yields. This process can have disastrous consequences for elemental abundance determinations and inter-element fractionation (Boer et al., 1993). Although 100% yields during dissolution are not essential for heavy (high mass number) isotope ratio measurements, low yields translate directly into smaller signals, and consequently less precise analyses, according to counting statistics.

The solution chemistry of Hf is particularly sensitive to co-precipitation by insoluble Ca-Mg fluorides. Consequently, a key objective of obtaining consistently high Hf yields during sample dissolution is to avoid or limit the formation of these compounds. One solution to this problem is the addition of perchloric acid ($HClO_4$) during or after the initial HF digestion step (Walsh, 1980; Patchett and Tatsumoto, 1980; Blichert-Toft et al., 1997), to drive off residual HF on evaporation. XRD characterisation of precipitates formed by $HClO_4$ addition (Yokoyama et al., 1999) appears to confirm that HF is completely expelled from the solution, suppressing fluoride formation. Unfortunately, these studies also report formation of oxide precipitates during evaporation of $HClO_4$. XRD analysis indicates that these oxides also contain high field strength elements (HFSE) such as Hf (Yokoyama et al., 1999).

David *et al.* (1999; 2001) suggest that the co-precipitation of Hf into insoluble fluorides is a function of the silica content of the sample, with low-silica materials being more likely to be associated with poor yields of tetravalent ions. Consequently, Hf extraction when using HF-based digestion procedures might be expected to be most problematic from materials with high Mg/Si and Ca/Si ratios.

Mg/Si and Ca/Si ratios vary widely in igneous rocks (Figure 2.1). Sub-alkaline and alkaline non-potassic basic to acidic rocks are all located within a region bounded by Mg/Si <0.3 and and Ca/Si <0.35. Few problems with Hf yield are encountered when using HF to digest such rock types.

Ultrabasic rocks have higher Mg/Si in the range 0.5-1.5 and Ca/Mg below 0.4. Common mineral separates such as garnet, orthopyroxene and clinopyroxene similarly have Mg/Si between 0.5-1.0 and Ca/Si of less than 0.5. With the exception of clinopyroxene, which has the highest Ca/Si ratio, these sample types also tend not to pose particular problems regarding extraction of trace elements when using conventional HF-based chemistry.

In contrast to most types of igneous rocks, Mg/Si and Ca/Si ratios in kimberlites are both elevated and highly variable. This is due largely to the fact that kimberlites are crystallisation products of complex, hybrid magmas that are naturally lower in silica (typically 20-40%, average ~32% SiO_2) than most igneous rocks. This suggests that severe problems with fluoride formation and co-precipitation of trace elements should beset dissolution of kimberlites, and in practice this is generally the case. Hf yields

Figure 2.1 Variation in average Mg/Si and Ca/Si ratios for some common geological materials. Based on data from Le Maitre (1976).

vary widely (from 90% to almost zero) in an unpredictable manner, reducing systematic analysis of suites of kimberlites virtually to a process of 'trial and error'.

2.3.3 Existing procedures for dissolution and separation of Hf, Sr and Nd from geological materials

Table 2.1 provides a comparison of the modified procedure presented here with some widely adopted published procedures for separation of Hf, Sr and Nd. All of these techniques involve a HF-based digestion of the silicate rock matrix, followed by isolation of the elements of interest from solution using ion-exchange columns. Variations between techniques arise mainly from differences in the target element and the method of analysis, i.e. TIMS versus PIMMS. Most procedures in the literature tend to be specific to a single element and, as a result, multi-element isotope studies require multiple dissolutions of a sample, increasing the amount of time and resources expended on acquiring data for a single sample.

The simplest kind of scheme is that reported by Fraser (1987) for Sr and Nd separation. After a mixed HF and HNO_3 digestion, followed by treatment with HNO_3 and dilute HCl, the sample is ready for the ion-exchange process. The separation of Hf requires additional steps. The majority of recent techniques for Hf separation are based on anion-exchange chemistry (Blichert-Toft *et al.*, 1997; David *et al.*, 1999, 2001; Salters and Hart, 1991; Nowell *et al.*, 1998a). In this approach the sample is loaded on to the column in dilute hydrofluoric acid solution, with Hf present as an anion complex. This requires a time consuming series of acid leaching and decanting steps with dilute HF to extract Hf from the fluoride precipitate formed during digestion. In our cation-exchange chemistry this leaching step is unnecessary and excellent Hf yields can be obtained using a standard dissolution procedure similar to that used by Fraser (1987) for Sr and Nd.

Reference	Analysis method	Dissolution			Ion-exchange separation			Elements obtained
		Type	Reagent volume (mL)	Time taken	Number of column stages	Reagent volume (mL)	Time taken	
Fraser (1985)	TIMS	HF, HNO$_3$	18	2-3 days	2	~55 for Sr; ~115 for Sr + Nd	1 day for Sr; 2 days for Sr + Nd	Sr, Nd
Patchett and Tatsumoto (1980)	TIMS	HF, HClO$_4$, HNO$_3$	~60	4-5 days (bomb dissolution)	3	~50	1-2 days	Hf, (Lu)
Salters and Hart (1991)	TIMS	HF, HNO$_3$	~25	2-3 days	3	~350	1-2 days	Hf
Blichert-Toft et al. (1997)	PIMMS	HF, HClO$_4$, HNO$_3$	Not specified	3 days	2	~40	1 day	Hf, (Lu)
Nowell et al. (1998a)	TIMS	HF, HNO$_3$	38	4-5 days (bomb dissolution)	3	~350	1-2 days	Hf
This study	PIMMS	HF, HNO$_3$	12	3 days (longer if using bombs)	2	Hf: 14 Hf + Sr: 30 Hf, Sr + Nd: 55	1 day	Hf, Sr, Nd

Table 2.1 Comparison of chemical pre-concentration procedures from a selection of widely adopted published methods with this study.

The length of time required for the dissolution stage depends, to a large extent, on the nature of the sample. Samples containing refractory accessory phases such as zircon ideally require a high-pressure bomb dissolution or fusion technique to ensure that all silicates are fully decomposed, and this can take several days. Otherwise, a duration of 2-3 days is typical of most techniques, including that proposed here.

The quantity of acid used during the digestion is more variable and is broadly dependent on the amount of rock powder being digested. This has been reduced over the years as advances in analytical instrumentation have permitted high-precision analyses to be obtained from progressively smaller amounts of analyte. The volume of acid used in our procedure is minimal compared to most published techniques, which assists in reducing associated blank levels.

In previous integrated Hf-Nd-Sr isotopic studies of rock suites it has been common practice to perform one dissolution for Sr and Nd and a second dissolution on a separate aliquot of powder for Hf. A sufficiently pure Sr fraction can then be obtained from a single cation-exchange column, with the Nd fraction obtained requiring a further purification step on a subsequent column. Separation of Hf is a more involved process, typically requiring 3 columns to fully isolate Hf from Ti and Zr (Patchett and Tatsumoto, 1980; Salters and Hart, 1991; Nowell *et al.*, 1998a). This is an essential requirement for TIMS analysis but for analysis of Hf by PIMMS the Zr removal step is unnecessary (Blichert-Toft *et al.*, 1997). Using the modified technique presented here it can be demonstrated that, contrary to Blichert-Toft *et al.* (1997), only partial removal

of Ti is necessary to ensure a high-precision Hf analysis (section 2.4.4), simplifying the chemistry further.

Because our procedure enables Hf, Nd and Sr fractions to be collected from a single cation-exchange column, the amount of dissolution and column chemistry required for a batch of samples is significantly reduced. The effect this has in terms of reduction in column stages, resin, reagents and time is evident from Table 2.1.

2.4 A MODIFIED PROCEDURE FOR DISSOLUTION AND CHEMICAL SEPARATION OF Hf-Sr-Nd FROM GEOLOGICAL MATERIALS

2.4.1 Dissolution of the silicate matrix

The sample dissolution scheme is shown in Table 2.2. Whole rock digestions are carried out in 15mL Savillex teflon beakers using approximately 100mg of sample powder. All dry-downs for isotopic work at Durham University are conducted using infrared lamps in a HEPA filtered clean air environment to minimise the likelihood of fall-in blank during the evaporation.

2.4.2 Stage I ion-exchange column

The purpose of this step is to produce separate Hf-, Sr-, and Nd-bearing fractions that are, as far as possible, free of elements which may cause isobaric or matrix interferences (e.g. ^{176}Lu on ^{176}Hf, ^{87}Rb on ^{87}Sr). 1.5mL of Bio-Rad AG50W-X8 200-400 mesh cation-exchange resin is loaded into an 8 × 40mm Bio-Rad polypropylene column. Before sample loading the resin is cleaned and pre-conditioned according to the scheme outlined in Table 2.3. After each use the resin may be cleaned and reused without any loss in functionality.

The elution scheme for this chromatography column (Table 2.4) is based on a measured calibration profile (Figure 2.2) produced by collecting successive 1mL fractions of a dissolved kimberlite sample and analysing them using the PerkinElmer ELAN 6000 quadrupole ICP-MS at Durham University. Table 2.4 also indicates which other elements are collected along with Hf, Sr and Nd. The Nd cut, for example, is a general rare earth element (REE) fraction, containing the elements La through to Lu. It is essential to include the Ba removal step indicated in Table 2.4 for any samples with high Ba concentrations, such as kimberlites. This is because BaO^+ formed in the plasma causes several isobaric interferences on Sm and Nd isotopes, which cannot be corrected for with sufficient accuracy. This has a detrimental effect on the corrections made for mass bias and interfering elements (section 2.6.4).

Overlap between Hf, Sr and Nd peaks on this column is effectively zero (Figure 2.2), and the narrowness of each peak permits virtually the entire fraction of each element to be collected in a small volume of acid, which promotes excellent column yields and low blanks. Furthermore, it is evident from Figures 2.3a and 2.3b that almost complete separation of Hf from Lu and Sr from Rb can also be achieved. In practice the Sr cut contains a small amount of Rb for which an interference correction must be made (section 2.6.4). The small spike in Lu present within the Hf-bearing fraction is probably due to breakthrough of cations that are only loosely bound to the resin; this is a common phenomenon at the beginning of an elution.

Nd and Sm are both rare earth elements and therefore have very similar chemical properties. As a result it is not possible to separate them using this chemistry (Figure

2.3c). Fortunately, one of the major advantages of PIMMS techniques in comparison to TIMS is the ability to ionise and monitor element pairs like Sm and Nd or Rb and Sr

Reagent	Action	Purpose
1 mL 16N HNO$_3$ + 4 mL 29N HF	Seal, 24-48 hrs at 120°C	Conversion of silicates to H$_2$SiF$_6$
	Dry down	Decomposition of H$_2$SiF$_6$ to SiF$_4$; volatilisation of SiF$_4$ and excess HF
2 mL 16N HNO$_3$	Seal, 24 hrs at 120°C	Residual HF removed; sample in soluble nitrate form
	Dry down	
5 mL 12N HCl	Seal, 24 hrs at 120°C	Solution in chloride form
	Dry down	
1 mL 1N HCl	Warm	Sample in same medium as conditioned columns

Table 2.2 Procedure for dissolution of silicate geological materials.

Reagent	Volume (mL)	Purpose
4N HF	10	Removes residual Hf
18.2MΩ H$_2$O	10	Washes off HF
6N HCl	10	Removes residual Nd and Sr; converts resin to chloride form
18.2MΩ H$_2$O	10	Washes off HCl
1N HCl	10	Conditions column in loading acid

Table 2.3 Procedure for cleaning and pre-conditioning of Bio-Rad AG50W-X8 cation-exchange resin.

Reagent	Volume (mL)	Action	Fraction contents
1N HCl	1	Load and collect	Hf + other HFSE and 1st period transition elements
1N HF – 1N HCl	3	Collect	Hf + other HFSE and 1st period transition elements
1N HF – 1N HCl	13	Elute	Bulk sample including Rb
2.5N HCl	14	Collect	Sr + other alkaline earths
2N HNO$_3$	10	Elute	Ba
6N HCl	12	Collect	Nd + other REE

Table 2.4 Procedure for separation of Hf-, Sr- and Nd-bearing fractions from the Stage I column.
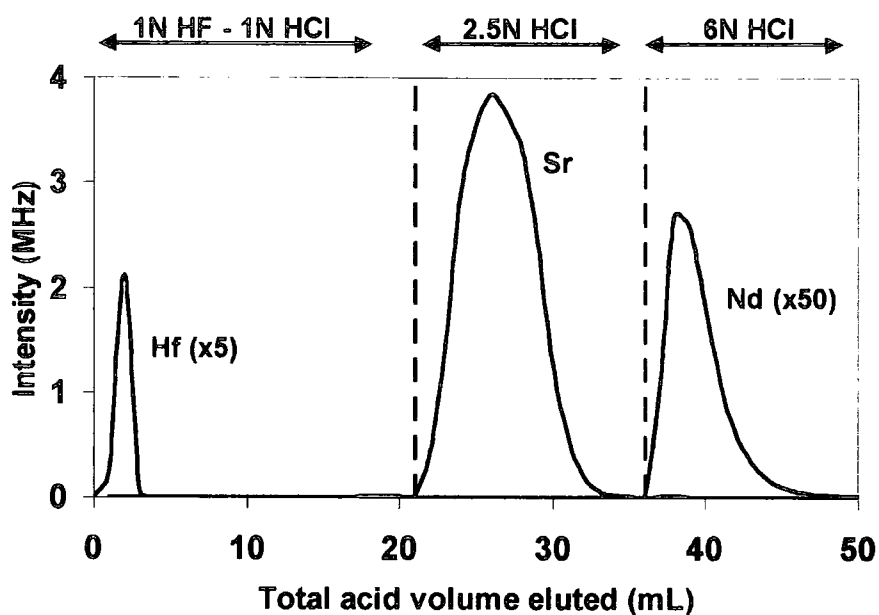
Figure 2.2 Calibration curve for elution of Hf, Sr and Nd from Bio-Rad AG50W-X8 200-400 mesh cation-exchange resin. 'Intensity' scale represents recorded signal intensity in millions of counts per second.

simultaneously and then make a mathematical correction for any spectral overlaps (section 2.6.4). Consequently, the Sr- and Nd-bearing fractions obtained from this column require no further processing and once diluted in 3% HNO_3 are ready to be analysed.

2.4.3 Stage II ion-exchange column

This column stage consists of a 8 × 40mm Bio-Rad polypropylene column containing 1mL of Bio-Rad AG1-X8 200-400 mesh anion-exchange resin, cleaned and pre-conditioned before sample loading according to the scheme outlined in Table 2.5. As with the stage I columns, the anion-exchange resin may be cleaned and re-used without compromising the chemistry in any way.

38
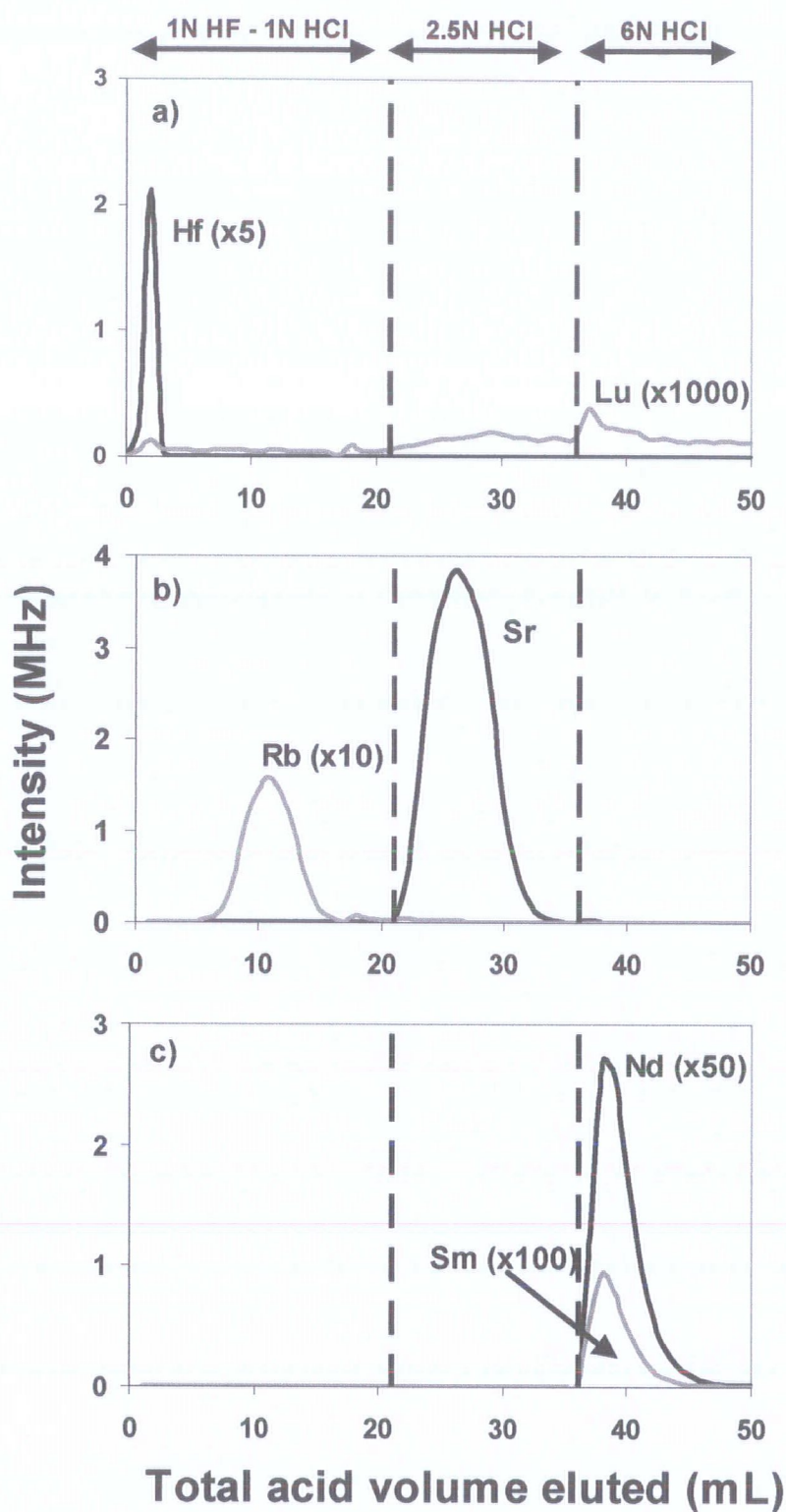
Figure 2.3 Calibrated degrees of separation of: a) Hf from Lu; b) Sr from Rb; c) Nd from Sm, during mixed acid elution from Bio-Rad AG50W-X8 200-400 mesh cation-exchange resin. 'Intensity' scale represents recorded signal intensity in millions of counts per second.

Reagent	Volume (mL)	Purpose
29N HF	10	Removes residual Hf
18.2MΩ H_2O	10	Washes off HF
12N H_2SO_4	10	Converts resin to sulphate form
18.2MΩ H_2O	10	Washes off H_2SO_4
0.52N H_2SO_4 – 5% H_2O_2	10	Conditions column in loading acid

Table 2.5 Procedure for cleaning and pre-conditioning of Bio-Rad AG1-X8 anion-exchange resin.

Reagent	Volume (mL)	Action	Contents
0.52N H_2SO_4 – 5% H_2O_2	1	Load and elute	Ti and other 1st period transition elements
0.52N H_2SO_4 – 5% H_2O_2	4	Elute	Ti and other 1st period transition elements
1N HF – 2N HCl	5	Collect	Hf, Zr + other HFSE

Table 2.6 Procedure for separation of Hf and Zr from Ti on the Stage II column.

The purpose of the second stage column is to remove Ti, which according to Blichert-Toft *et al.* (1997) can reduce the transmission of Hf within the PIMMS instrument. This is supposedly due largely to deposition of titanium oxide around the aperture of the skimmer cone, although space-charge effects in the ion beam may also be a factor.

The procedure for separating Ti from Zr and Hf (Table 2.6), is a modified and miniaturised version of the widely adopted technique presented by Barovich *et al.* (1995). The elution profile shown in Figure 2.4 demonstrates that for low-Ti samples, such as many kimberlites, 5mL of 0.52N H_2SO_4 – 5% H_2O_2 is sufficient to remove almost all Ti from the resin, and significantly reduce the Ti/Hf ratio in the collected

fraction. Even in the case of samples with higher Ti content, such as basalts, 5mL of
$0.52N\ H_2SO_4 - 5\%\ H_2O_2$ removes enough Ti to ensure that transmission of Hf in the
PIMMS instrument is not inhibited.
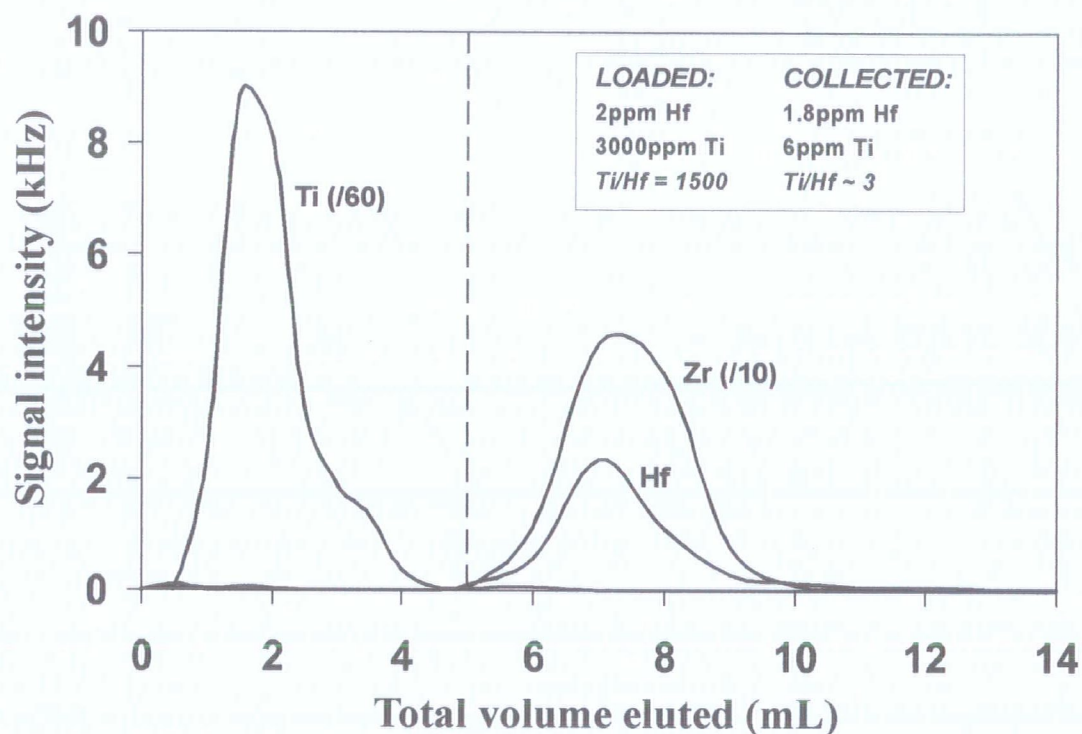
Figure 2.4 Calibration curve for elution of Ti, Hf and Zr in a synthetic kimberlite matrix from Bio-
Rad AG1-X8 200-400 mesh anion-exchange resin. Dashed line indicates change of eluant from
$0.52N\ H_2SO_4 - 5\%\ H_2O_2$, to $1N\ HF - 2N\ HCl$.

2.4.4 Testing the criticality of Ti removal for Hf isotope ratio determination

To ensure that miniaturisation of the Ti removal chemistry was justifiable and that data
quality was not being compromised, a separate experiment was conducted to
investigate the sensitivity of Hf to the presence of Ti in solution. A series of 50ppb and
200ppb Hf standard solutions (made from 1000ppm Johnson Matthey ICP standard)
doped with progressively larger amounts of Ti were analysed on the ThermoFinnigan
Neptune PIMMS instrument at Durham University. The analysis method was identical

41

to that used for samples (see section 2.6) and the average ^{180}Hf intensity and measured ^{176}Hf/^{177}Hf ratio were recorded for each solution.

It is evident that the presence of Ti up to concentrations of 100ppm in either a 50ppb or 200ppb Hf solution has very little effect on the intensity of the ^{180}Hf beam (Figure 2.5a). At concentrations in excess of ~500ppm, the ^{180}Hf intensity begins to diminish exponentially. This critical value appears to be similar for both the 50ppb and 200ppb Hf solutions, which suggests that it is the absolute abundance of Ti in solution, rather than the Ti/Hf ratio, that controls the measured Hf intensity. After running solutions containing in excess of 1000ppm Ti, the undoped Hf solutions were re-analysed. In both cases it was found that the ^{180}Hf signal only recovered to about 60% of its initial intensity. This suggests that the effect of large amounts of Ti in a solution is not transient, as would be expected if Ti were simply causing ionisation suppression of Hf in solution.

A critical part of an ICP-MS instrument is the low vacuum interface region, which enables transmission of ions from the plasma source, at atmospheric pressure, to the focussing and mass analysis systems, which are kept at moderate and high vacuum, respectively. The interface region consists of two nickel cones, known as the sampler and skimmer cones. These are arranged co-axially, allowing ions to pass through the apertures at their vertices into the instrument, while deflecting away other, uncharged particles in the ion beam. After running the series of Ti-doped solutions through the instrument, these cones were found to be coated with white deposits of titanium oxide, reducing the size of the aperture. Consequently, the efficiency of ion transmission across the instrument interface had been reduced.
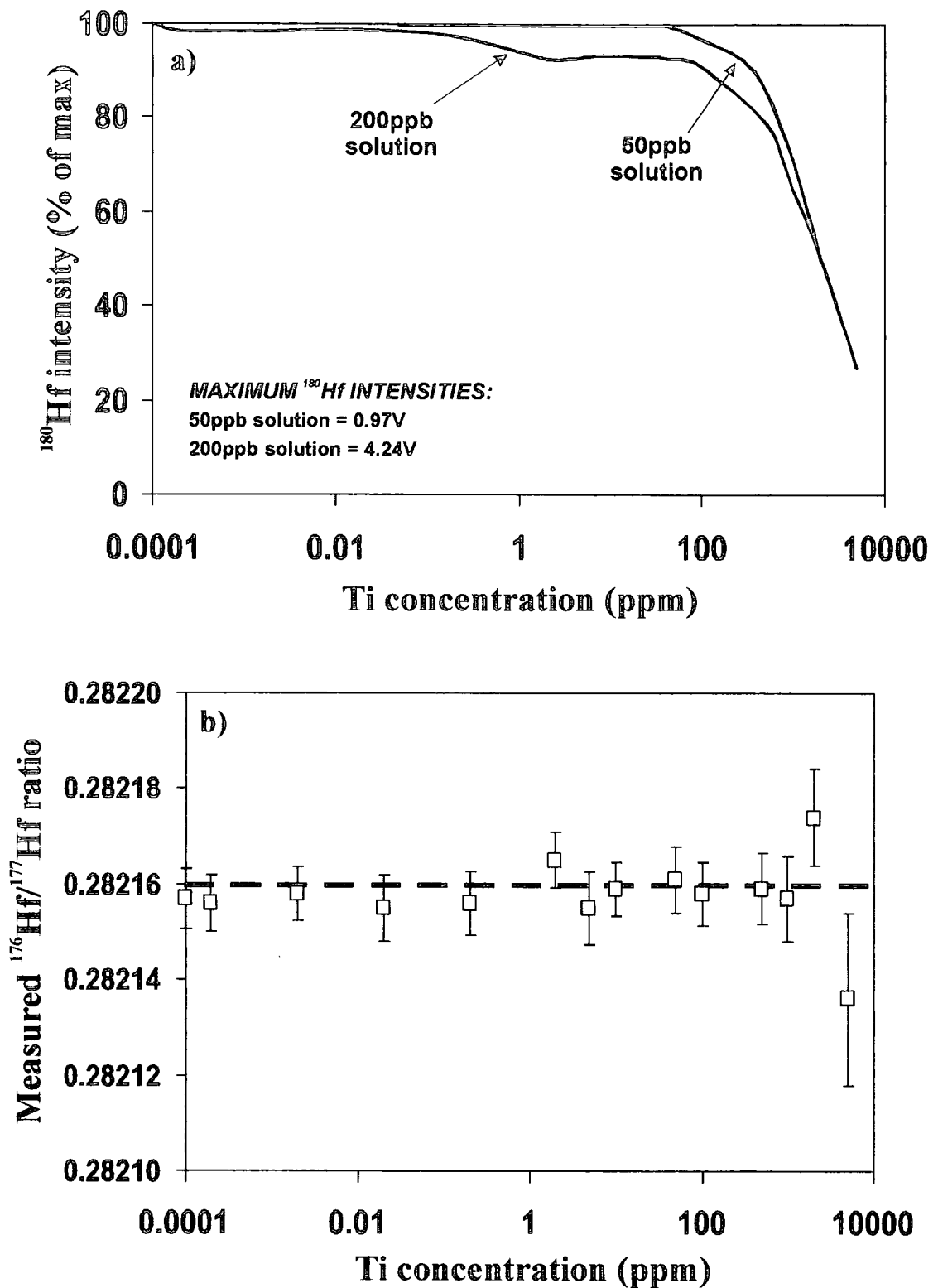
Figure 2.5 Variation in: a) measured ¹⁸⁰Hf intensity; b) measured ¹⁷⁶Hf/¹⁷⁷Hf isotope ratio, with different levels of Ti doping in Johnson Matthey Hf ICP standard solution. Dashed line in (b) represents accepted value for JMC 475 Hf isotopic standard (0.28216, Nowell *et al.*, 1998). This standard is considered to be isotopically indistinguishable from the JM Hf ICP standard (Blichert-Toft *et al.*, 1997).

The ^{176}Hf/^{177}Hf ratio measured for each doped 200ppb Hf solution is shown in Figure 2.5b. The Johnson Matthey Hf ICP standard is considered to be isotopically indistinguishable from the JMC 475 international Hf isotope solution standard (Blichert-Toft et al., 1997), for which the established ^{176}Hf/^{177}Hf ratio is 0.282160 (Nowell et al., 1998a). The measured value in the Ti-doped solution does not deviate from within error of this accepted value until the Ti concentration is raised to in excess of 1000ppm. The associated internal precision, in terms of the standard error of the mean, only begins to deteriorate significantly at these levels. This effect is not directly due to any molecular interaction between Ti and Hf in solution, but is predominantly the result of the decrease in instrumental sensitivity. There is thus little evidence that the presence of Ti in the sample solution at concentrations below 1000ppm is responsible for reduction in accuracy or precision of isotopic measurements, such as the 'systematic drift' in measured Hf isotopic ratios reported by Blichert-Toft et al. (1997).

This observation supports our approach of not fully removing Ti from samples prior to Hf isotopic analysis, which would require a particularly time-consuming elution and subsequent fuming of H_2SO_4 (Barovich et al., 1995) for samples containing several weight percent TiO_2, e.g. basalts or ilmenite. While we do not advocate the routine analysis of sample solutions containing several hundred parts per million Ti, as this will result in cones regularly becoming encrusted with Ti deposits, our observations introduce the possibility of reducing the amount of elution required on the second stage column. Reduction in the elution volume can contribute towards minimising blank levels, and is both more time- and cost-efficient.

2.5 BLANKS AND YIELDS

Blank levels for Hf, Nd and Sr measured in both the dissolution and column stages of the chemistry are reported in Table 2.7. The total procedural blank (TPB) is considered to be the sum of the blank contributions from these two stages.

Analyte	Dissolution blank (pg)	Stage I column blank (pg)	Stage II column blank (pg)
Hf	30	30	70
Nd	20	50	—
Sr	200	300	—

Table 2.7 Measured Hf, Nd and Sr blanks measured from the dissolution and column stages.

The respective TPBs of 130pg and 70pg for Hf and Nd are negligible in comparison to the amount of Hf and Nd in a kimberlite dissolution, which is typically in the order of 100ng of Hf and 1000ng of Nd. For 100mg kimberlite dissolutions the high levels of Sr and Nd in these rocks meant that ultra-pure acids were not considered necessary. This resulted in a Sr blank of ~500pg. This value is unusually high, and may also reflect the presence of residual Sr, not fully removed by the Teflon cleaning procedure, in the beakers used for preparing the Sr blank analyses. In the case of samples with low (sub-μg levels) of Sr, blanks can be further reduced by use of commercial ultra-pure grade or Teflon re-distilled acids, and more stringent Teflon cleaning protocols. Microchemistry techniques have recently been developed at Durham University, which offer Sr blanks of ~10-15pg.

Typical yields of Hf, Sr and Nd using this modified chemistry are reported for three different sample types in Table 2.8. All of these recoveries compare favourably with

those quoted for similar pre-concentration techniques and ensure sufficient quantities of analyte are present to obtain a high-precision isotopic analysis.

Sample type	Hf yield (%)	Nd yield (%)	Sr yield (%)
Alkali basalt	>85	>90	>70
Lamproite	>80	>75	>70
Kimberlite	>80	>75	>70

Table 2.8 Typical recoveries of Hf, Nd and Sr from different geological materials.

2.6 MASS SPECTROMETRY

2.6.1 General

All isotopic measurements on samples processed using this modified chemistry have been made using the ThermoFinnigan Neptune PIMMS instrument at Durham University. This represents the majority of all Hf, Nd and Sr isotopic analyses within the dataset for this study. The remainder of the Hf analyses were performed by PIMMS on a VG Elemental Plasma 54, and some of the Nd and Sr analyses were acquired by TIMS using a Finnigan MAT 262, at the NERC Isotope Geosciences Laboratory (NIGL), Keyworth. All sample preparation for these analyses was based on prototype versions of the chemistry described in the previous sections, and is not discussed separately here. The operating conditions described below are those used routinely on the Neptune instrument at Durham; these do not differ significantly from those used with the Plasma 54 at NIGL.

2.6.2 Sample introduction

Once collected from the ion-exchange columns, the Hf, Sr and Nd fractions are evaporated to dryness and taken up in 1mL 3% HNO_3 solution. Sample solutions are

introduced into the plasma using an Elemental Scientific Inc. (ESI) PFA-50 microflow nebuliser and an ESI dual cyclonic Scott double pass (CSDP) quartz spray chamber. For lower concentration samples a Cetac Aridus desolvating nebuliser is used for sample introduction. Typical sample uptake rates were 70-100μl/min. Each analysis is based on the average of 90 measurement cycles with an integration time of 4.1 seconds per cycle.

2.6.3 Cup configurations

The Durham Neptune is equipped with nine Faraday cup detectors. The standard cup configurations employed for each element are shown in Table 2.9a-c. Hf, Nd and Sr all have isotopes that are subject to isobaric interferences, which are also shown in Table 2.9.

	L4	L3	L2	L1	Axial	H1	H2	H3	H4
a) Hf	^{172}Yb	^{173}Yb	^{175}Lu	^{176}Hf ^{176}Lu ^{176}Yb	^{177}Hf	^{178}Hf	^{179}Hf	^{180}Hf $^{180}Ta*$ $^{180}W*$	
b) Nd	^{142}Nd ^{142}Ce	^{143}Nd	^{144}Nd ^{144}Sm	^{145}Nd	^{146}Nd	^{147}Sm	^{148}Nd ^{148}Sm	^{149}Sm	^{150}Nd ^{150}Sm
c) Sr	^{82}Kr	^{83}Kr	^{84}Sr ^{84}Kr	^{85}Rb	^{86}Sr ^{86}Kr	^{87}Sr ^{87}Rb	^{88}Sr		

Table 2.9 Standard cup configurations for isotopic analysis of: a) Hf; b) Nd; c) Sr, on the Thermo-Finnigan MAT Neptune at Durham University. Isobaric interferences on specific isotopes are shown in italics. * = interference not corrected for.

2.6.4 Interference corrections

One of the main sources of isobaric interference during isotopic analysis of Hf, Nd and Sr arises from spectral overlaps from the parent elements of the analyte, i.e. Lu on Hf,

Sm on Nd and Rb on Sr. There are also other isobaric overlaps to account for, namely Yb on Hf, Ce on Nd and Kr on Sr. The correction for ^{86}Kr is particularly critical because instrumental mass bias during Sr analyses is measured using the ^{86}Sr/^{88}Sr ratio.

The separation of Hf from Lu and Yb provided by the modified chemical procedure presented above is such that corrections to the ^{176}Hf/^{177}Hf ratio are in fact minor and can be performed during data acquisition by applying established (Nowell and Parrish, 2001) values for the natural ^{176}Lu/^{175}Lu and ^{176}Yb/^{173}Yb ratios. Since Rb is not completely separated from Sr, and Sm and Nd are not resolved at all by the chemistry, larger corrections are required on measured ^{87}Sr/^{86}Sr and ^{143}Nd/^{144}Nd ratios. At present these are performed externally to the data acquisition routine. Detailed descriptions of the correction procedures adopted for isobaric interferences on Hf, Nd and Sr are given in Nowell and Parrish (2001) and Nowell et al. (2003). To provide an example of the general principles of the correction routines, an outline of the procedure for Nd is given below.

Nd is subject to isobaric interferences from Sm and Ce on four of its seven isotopes (Table 2.9). The objective of the correction procedure is to determine how much of the signal intensity measured at a particular mass is due to the appropriate Nd isotope, and how much is due to the interfering element. One approach is to peak-strip measured ^{142}Nd, ^{144}Nd, ^{148}Nd and ^{150}Nd away from the interfering Sm and Ce isotopes. This is possible because the Sm and Ce interferences are all on stable Nd isotopes and the ratios of these isotopes to the stable, interference-free ^{145}Nd and ^{146}Nd isotopes are well established (Wasserburg et al., 1981).

The alternative approach, which is currently in use at Durham, is to peak-strip Sm from Nd. Unfortunately, the cup configuration used (Table 2.9b) does not permit stripping of ^{142}Ce from ^{142}Nd, as it does not include an interference-free Ce monitor peak (e.g. ^{140}Ce). However, measurements of four stable Nd isotope ratios (^{145}Nd/^{144}Nd, ^{146}Nd/^{144}Nd, ^{148}Nd/^{144}Nd and ^{150}Nd/^{144}Nd) are made in each analysis to ensure that the ^{143}Nd/^{144}Nd ratio obtained is reliable and the Sm correction is accurate.

The correction for the presence of ^{144}Sm, ^{148}Sm and ^{150}Sm is made by monitoring the intensity of the interference-free ^{147}Sm and ^{149}Sm isotopes in the H1 and H3 cups. The ^{147}Sm/^{149}Sm ratio is used to derive the instrumental mass bias for each sample by comparison to the accepted value of 0.9216 (Wasserburg et al., 1981). Application of this mass bias coefficient to the accepted values of ^{144}Sm/^{147}Sm, ^{148}Sm/^{147}Sm and ^{150}Sm/^{147}Sm (Wasserburg et al., 1981; Table 2.10) enables the 'measured' values of these ratios to be calculated for each sample. Since the measured intensity of ^{147}Sm is known, the 'measured' ^{144}Sm, ^{148}Sm and ^{150}Sm intensities can then be determined. Subtracting these values from the measured intensities at masses 144, 148 and 150 gives the true intensities for ^{144}Nd, ^{148}Nd and ^{150}Nd, from which the 'measured', interference-free ^{143}Nd/^{144}Nd, ^{148}Nd/^{144}Nd and ^{150}Nd/^{144}Nd ratios can be obtained.

^{144}Sm/^{147}Sm	^{148}Sm/^{147}Sm	^{150}Sm/^{147}Sm
0.20504	0.74970	0.49213

Table 2.10 Natural Sm isotope ratios (from Wasserburg et al., 1981) used for correction of isobaric interferences of Sm on Nd.

Although the same principles can be used to correct for the interferences of ^{86}Kr and ^{87}Rb on ^{86}Sr and ^{87}Sr, the situation is more complicated (Nowell et al., 2003). Kr is an

inherent impurity in the argon supply, and consequently, the $^{86}Sr/^{88}Sr$ ratio, which is used in TIMS analysis to determine the Sr mass bias of the instrument, is not interference-free in a PIMMS analysis due to the presence of ^{86}Kr. A correction for the presence of ^{86}Kr must be applied before a mass bias measurement can be made. The difficulties associated with making accurate corrections for interference of Kr and Rb on Sr, and approaches for resolving these problems, are discussed in detail in Nowell *et al.* (2003).

2.6.5 Accuracy, precision, reproducibility and repeatability of corrected data

To ensure that sample data is of consistently high quality during isotope ratio measurement it is essential to regularly monitor the accuracy and reproducibility of isotopic values in a standard reference material. The long-term reproducibility of the $^{176}Hf/^{177}Hf$, $^{143}Nd/^{144}Nd$ and $^{87}Sr/^{86}Sr$ ratios for appropriate standard solutions during the first two years of operation of the Durham Neptune is shown in Table 2.11. Average measured values for these ratios are within error of the accepted values. Further details of the long-term performance of the Durham Neptune and reproducibility of other Hf, Nd and Sr isotope ratios are presented in Nowell *et al.* (2003).

It is also important to ensure that the interference corrections applied to the data, such as for Sm on Nd, are accurate and consistent over time. To achieve this it is common practice at intervals during Nd analytical sessions at Durham to run both a pure J&M Nd isotopic standard solution and the same solution doped with Sm to give a Sm/Nd ratio of 0.2 or 0.4. Table 2.11 shows the close agreement between the mean measured $^{143}Nd/^{144}Nd$ ratio in doped and undoped solutions of the J&M Nd standard. The

variation in measured $^{143}Nd/^{144}Nd$, $^{148}Nd/^{144}Nd$ and $^{150}Nd/^{144}Nd$ ratios for both doped and undoped J&M over time (Nowell *et al.*, 2003) indicates that the interference correction routine produces values that are both accurate and reproducible.

Element and Standard	Ratio	Accepted value (with refs)	Number of standards run	Mean measured value	Error (± 2SD abs)	Error (± 2SD ppm)
Hf (JMC 475)	$^{176}Hf/^{177}Hf$	0.282160[1]	237	0.282156	11	39
Nd (J&M - pure)	$^{143}Nd/^{144}Nd$	0.51111[2]	258	0.511101	17	33
Nd (J&M – Sm doped)	$^{143}Nd/^{144}Nd$	0.51111[2]	136	0.511105	18	35
Nd (J&M – all)	$^{143}Nd/^{144}Nd$	0.51111[2]	394	0.511103	18	34
Sr (NBS 987)	$^{87}Sr/^{86}Sr$	0.71024[3]	274	0.710264	26	37

Table 2.11 Reproducibility of measured Hf, Nd and Sr isotope ratios for standard solutions. Based on all analytical sessions conducted during first year of operation of the Durham Neptune. References: 1 = Nowell *et al.* (1998a); 2 = Royse *et al.* (1998); 3 = Thirlwall (1991).

A further check on the effectiveness of the interference corrections is provided by a comparison of Nd data for clinopyroxenes run by PIMMS with values for the same samples previously determined by TIMS (Figure 2 in Nowell *et al.*, 2003). The close agreement between the two data sets suggests that use of the chemical pre-concentration procedure proposed here, in conjunction with PIMMS techniques and appropriate mathematical corrections for residual isobaric overlaps, can produce data of comparable accuracy and precision to that obtained by TIMS.

The repeatability of isotope ratio measurements between replicate analyses of a single sample, such as for the kimberlite shown in Figure 2.6, is also excellent. GRZ-1/1,
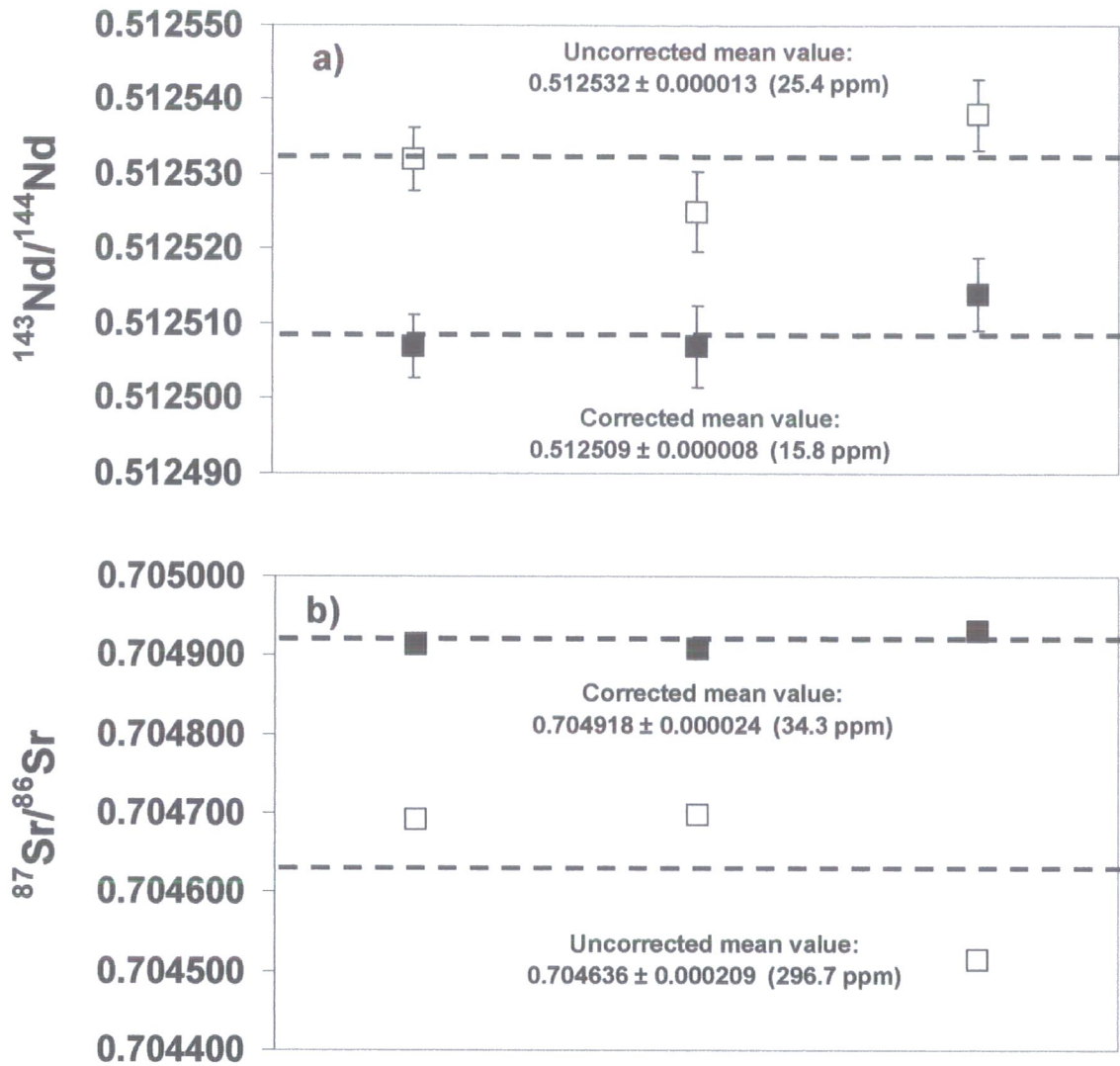
Figure 2.6 Effect of applying interference corrections to: a) Nd isotopic ratios; b) Sr isotopic ratios, for three replicates of the kimberlite GRZ-1. Open symbols are uncorrected data; closed symbols are corrected data. Dashed lines denote mean values. All errors are ± 2 standard deviations from the mean. Error bars in (b) are smaller than the data points at scale of the diagram.

GRZ-1/2 and GRZ-1/3 are separate dissolutions of the same whole rock kimberlite powder, processed using the modified pre-concentration chemistry and analysed by PIMMS with appropriate interference corrections for Nd and Sr. The repeatability of the $^{143}Nd/^{144}Nd$ and $^{87}Sr/^{86}Sr$ ratios is represented by the magnitude of the deviation of each replicate analysis from the mean (Figure 2.6). It is evident that the repeatability of the $^{143}Nd/^{144}Nd$ ratio and, in particular, the $^{87}Sr/^{86}Sr$ ratio is greatly improved by applying appropriate corrections to the data.

The magnitude of the discrepancy between mean corrected and uncorrected values for the Sr data emphasises the importance of these corrections in obtaining accurate and repeatable isotope ratio measurements. Nowell *et al.* (2003) provide a detailed discussion of this with reference to correcting Sr isotope data for six replicate analyses of a whole rock powder based on separate dissolutions, and analysed at a range of beam intensities.

2.7 SUMMARY

A modified dissolution and pre-concentration technique has been developed that is widely applicable to non-ore lithologies and provides a rapid and efficient means of separating Hf, Sr and Nd for isotopic analysis by PIMMS. The technique offers the following major advantages:

1. Genuine savings in laboratory time, resources and cost relative to most currently available techniques.

2. Methodology suited to high throughput of samples. At present 60 isotopic measurements (20 × Hf, Sr, Nd) can be obtained within a week, from powder to data. This could easily be scaled up further.

3. Recovery of separate Hf-, Nd- and Sr-bearing fractions from a single ion-exchange column, with minimal requirement for further purification.

4. Miniaturised Hf-Ti separation chemistry simplifies overall procedure, reduces blank levels and further increases sample throughput. For low-Ti samples it is possible to omit the Hf-Ti separation step altogether.

5. Reliable recovery of Hf and high Hf, Sr and Nd yields are obtained for a wide variety of rock types, including high-Mg and high-Ca materials.

6. Low blanks are easily achieved due to the low reagent and resin volumes required.

Chapter 3

Statistical treatment of geochemical data

3.1 INTRODUCTION

This chapter outlines and provides a rationale for certain aspects of the treatment applied to the major and trace element data in Chapter 4. It should be emphasised at the outset that the ideas presented in this chapter are not new. They are simply a restatement of statistical principles and methods that have been advocated by many members of the mathematical geology community (most notably Chayes, 1960, 1971; Butler, 1981; Aitchison, 1986) for several decades as a means of avoiding erroneous statistical treatment and consequent misinterpretation of geological data. The uptake of these ideas into the geochemical literature has in general been extremely slow and, as a result, some of the approaches adopted in this study differ from the more conventional approach taken in previous similar investigations of variations in whole-rock kimberlite geochemistry, e.g. Fraser (1985), Spriggs (1988), Tainton (1992). A further reason for applying these principles in this study is because they offer a solution to the particular problem posed by the large variations in volatile content that is characteristic of kimberlites, and which makes comparison of kimberlite analyses very difficult.

Three main data processing issues are addressed. Firstly, and most fundamentally, the nature of compositional data and its special characteristics are reviewed, and a method for statistical manipulation of the data is presented. Secondly, the effects of widely variable volatile contents in elemental datasets, which is of particular relevance to kimberlites, is discussed. Thirdly, the usage and limitations of ratio correlation in

petrogenesis is reassessed. Points one and three are the subject of comprehensive works by Aitchison (1986) and Chayes (1971) respectively, and extensive mathematical proofs for the arguments outlined below can be found in these references. More accessible summaries of these arguments, with a minimum of supporting mathematics, can be found in Rollinson (1992; 1993), Reyment and Savazzi (1999) and Davis (2002).

3.2 ANALYSIS OF COMPOSITIONAL DATA

3.2.1 Nature of compositional data

Major and trace element analyses together with many other kinds of geological measurements are examples of compositional data. The defining characteristic of such datasets is that the values are reported in proportional, rather than absolute, terms. In geochemistry, for example, major element concentrations are quoted in parts per hundred, i.e. percentages, and trace elements in parts per million, billion or trillion. Whichever of these units is in use, the quantity being expressed is effectively a ratio, the denominator of which is a function of all the other variables being measured.

A fundamental property of compositional data is that the sum of all components (i.e. each quantity analysed for) in any sample must equal 100%, or unity. In reality a geochemical analysis rarely, if ever, sums to exactly 100% but this is due to either omissions (i.e. elements not detected or not looked for) or analytical errors, which are unavoidable. The fact that the original sample is the sum of its component parts remains incontrovertible. Major and trace element data are consequently examples of constrained data, because they are not free to take any value but instead must range between zero and 100%.

3.2.2 Consequences of closure in compositional datasets

The property of summing to unity is often referred to as 'closure' or the 'constant-sum effect'. A number of problems arise from the effects of closure in a dataset. Firstly, constrained data can never consist of mutually independent variables. Any change in the value of any variable may potentially produce a change in any other variable, because the sum of all variables must always equal unity. This negates the usual null hypothesis of correlation between two variables, which states that there is no interdependence between the variables.

Major and trace element data is necessarily expressed relative to the sum of all components, so this data will always be auto-correlated to some extent, regardless of whether any correlation between the variables really exists: correlation is induced by the constant-sum constraint. Standard statistical tests of correlation such as Pearson's product-moment coefficient cannot therefore produce a meaningful result with compositional data, because the conventional null hypothesis is not valid.

A second, related problem is the existence of negative bias in the data. This arises because an increase in any component must result in a decrease in at least one of the other components, to preserve the constant sum condition. Conversely, a decrease in any given component implies that at least one of the other components must increase in magnitude. In statistical terms, this means that the covariance of at least one pair of variables within a composition *must* be negative. In geochemical analyses this effect is most obvious when the control variable is an abundant oxide. Kimberlite analyses are dominated by MgO, SiO_2 and volatile content, which together typically constitute

60-85% of the analysis by weight. This inevitable tendency towards negative bias is a common feature in sets of major element binary variation diagrams based on any geochemical dataset. An excellent example of enforced negative bias is shown by the data of Bhatia (1983).

The third major difficulty encountered with compositional data concerns the generation of subcompositions from the original data array. A subcomposition is simply a subset of components from within a set of several components. In geochemistry, this is a convenient means of reducing the dimensionality of the dataset from 10 or more, to 2 or 3, which can easily be represented on a flat sheet of paper. A common occurrence of this is the recalculation of oxide data to produce plotting parameters for AFM diagrams. Unfortunately, unpredictable variations in the covariance between pairs of variables occur between the full composition and the subcomposition, i.e. the correlation coefficient between any two variables will differ between the subcomposition (e.g. the AFM) and the parent data set. In addition, the rank order of variances of each variable is liable to change between the subcomposition and the initial dataset. Consequently, inferences made about the correlation of variables and the relative strength of correlations in a small number of compositional dimensions, are unlikely to be true for the parent dataset as a whole.

The unfortunate consequence of these simple properties of compositional data is that any analysis and interpretation based upon the covariance of raw major or trace element data is fundamentally unsound. This extends from the simple correlation of two variables, such as Harker diagrams of major element oxides, to complex multivariate analytical techniques, such as principal components or cluster analysis. Clearly, a very

large proportion of published interpretations of geochemical data are subject to these limitations, and some attempt must be made to address the extent of this problem, at least for the purposes of this study, to ensure that inferences made from the data are statistically meaningful.

3.2.3 Methods for removing compositional interdependence

The properties of compositional datasets outlined above appear to invalidate many of the constructions commonly used for statistical analysis of geochemical data. At the very least, it is implicit that many of the correlations observed between 'raw' variables are spurious and thus inferences based upon such observations may be erroneous. If we are to make the most informed use of the data, in the collection of which so much time and care is invested, then we require statistical procedures that are conceptually robust to distinguish real variations from those that are induced within the data.

Aitchison (1986) presents a set of mathematical transformations that can be applied to compositional data to remove the effects of interdependence. The details of these functions and their application are beyond the scope of this thesis, but the fundamental principle that underlies them forms the basis of the approach adopted in this study. Aitchison (1986) observes that compositional data is a measure of proportionality rather than an absolute quantity, and consequently any analysis of compositional data should be concerned with the relative magnitudes of components, rather than their absolute magnitudes. Ratios of components are thus a more appropriate means than absolute values for representing the variation within compositional datasets.

Aitchison (1986) goes on to state that, because the computation of the variance and covariance of ratios is complex, a more convenient means of manipulating the data is to work in terms of log-ratios. The logarithmic transformation used is normally the natural logarithm, $\log_e(x)$, or ln (x). In this study, the term 'log-ratio' implies 'the natural logarithm of a ratio'. A component X, such as SiO_2 in a major element analysis, is thus represented by the natural logarithm of the ratio X/Y, where Y is another component within the composition. The variable *ln (X/Y)* is completely unconstrained and thus is not subject to constant-sum restriction. The choice of the component Y does not affect the covariance structure of the data, but Y must be common to all components within any single composition. For the purposes of this study it is sufficient to work in terms of simple ratios, although in some instances use of log-ratios enable scales to be compressed for convenient graphical representation. Use of log-ratios is also consistent with the approach of Aitchison (1986) in the full construction of covariance matrices, which can be used as a basis for more complex, multivariate analysis of compositional data. This kind of analysis is not performed here, but would be a useful extension of this project.

In some sections of Chapter 4 data analyses are presented in terms of raw, rather than ratio data. The reason for this is usually to maintain consistency with the approach taken by previous studies when comparing other datasets with that presented here. Wherever possible in these cases, analyses have been performed in terms of both raw and ratio data as a means of assessing the magnitude of any spurious relationships within the raw data. Any correlations based on 'raw data' that are presented have thus been compared with equivalent 'log-ratio' plots to ensure that observed trends are not a function of closure and auto-correlation.

3.3 VOLATILE CONTENT IN WHOLE-ROCK ANALYSES

3.3.1 Volatile components in kimberlites

Kimberlites are characterised by very high contents of volatile components in comparison to most other mantle-derived rocks. The average volatile content of the hypabyssal Lac de Gras kimberlites is ~12 wt%, and in some cases is in excess of 20 wt%. This volatile fraction is composed mostly of H_2O and CO_2, with lesser amounts of sulphur. Chlorine and fluorine may also be present in trace quantities. In Appendix D volatile data is reported either on the basis of individual components or collectively as a 'loss on ignition' (LOI).

Volatiles may be cognate to the magma, or introduced by alteration processes after emplacement of the body within the crust. Mitchell (1986) has suggested that the presence of magmatic volatiles in high concentrations can promote the development of localised textural and compositional heterogeneities, which if sampled may yield analyses far removed from the 'true' magmatic composition. A thorough petrographic examination of samples prior to selection for analysis is therefore essential. Given the high probability of depletion and re-enrichment of volatiles taking place during eruption of the kimberlite and subsequent near-surface alteration, it seems unlikely that the eventual concentration of volatiles determined in a sample can ever be truly representative of the parental magma. Hypabyssal kimberlites are presumably less susceptible to these processes than volcaniclastic kimberlites, which have almost certainly been partially devolatilised. Nevertheless, the variability of volatile content on both an inter- and intra-kimberlite scale (Appendix D), even within hypabyssal facies rocks, suggests that caution should be adopted if making inferences about

magma composition on the basis of volatile content. This is a problem of less consequence when dealing with more common, volatile-poor rocks such as basalts, granites, etc.

3.3.2 Statistical effect of volatile content on compositions

As a component of a whole-rock composition, which is subject to the constant sum constraint, the magnitude and variability of volatile content in kimberlites directly affects the magnitide of other major and trace element components within the analysis. Due to the negative bias effect, the magnitude of components such as MgO and SiO_2 are likely to be lower in kimberlites with high volatile contents. It is clear, therefore, that the abundance of MgO, or any other component, in kimberlites with very different volatile contents cannot be directly compared; some kind of normalisation process is required to account for the variation in volatile content between samples.

Fortunately, using ratios rather than raw data removes the problem of variable volatile content as well as solving the problem of closure. This is because the ratio of any two components within a composition is not dependent on the magnitude of any other component (Table 3.1). In scenario 1, the five components, A-E, sum to 100% with $A/B = 0.5$ and $C/D = 0.25$. In scenario 2, the abundance of component B has doubled to 40%. The entire composition must still sum to 100%, so components A, B, C and D must decrease proportionately in magnitude. In scenario 3 component E is not detected, so the other components proportionately increase to satisfy the constant-sum constraint. If we assume that component E represents a volatile component, and is thus not necessarily truly representative of the sample, then there is also a problem in determining the 'true' representative values of components A-D. In which scenario is

component E representative of the initial magma conditions? The simplest solution is to work in terms of ratios of components, rather than their absolute values, because these ratios do not change as absolute magnitudes vary. This is demonstrated for the ratios A/B and C/D in Table 3.1. For the purposes of this study, the complicating effects of high and variable volatile contents can be 'normalised out' by forming a subcomposition that excludes the volatile components, and then working in terms of ratios.

Scenario	A	B	C	D	E	A/B	C/D
1	10	20	10	40	20	0.5	0.25
2	7.5	15	7.5	30	40	0.5	0.25
3	12.5	25	12.5	50	-	0.5	0.25

Table 3.1 Demonstration of the invariance of component ratios, as individual components vary to satisfy the constant-sum constraint.

3.4 RATIO CORRELATION

The correlation of ratios is commonly employed in the analysis of geochemical data, with strong positive or negative correlations typically being interpreted as evidence of petrogenetic processes such as mixing, or fractionation during melting or crystallisation. The use of ratios, rather than absolute values of elemental abundances, as advocated in the preceding sections, might appear to increase the importance of ratio correlation as an analytical tool still further.

If ratio correlation is to be used in geochemical data analysis, then the variables used as numerators and denominators in the ratios must be selected with great care. This is because the use of numerators or denominators that are common to both ratios can

produce large amounts of auto-correlation, which may easily and erroneously be interpreted as indicating systematic trends in the data. Pearson (1896) initially showed that, given a set of uncorrelated variables A, B and C, ratios formed from these variables, such as A/C vs B/C, A/B vs A/C, A vs A/B, or B vs A/B, will always demonstrate some degree of correlation. Chayes (1949, 1971), Butler (1986) and Rollinson and Roberts (1986) all present examples of the detrimental effects this can have on analysis and interpretation of geochemical data.

Since meaningful interpretations cannot be made of trends in variables that are auto-correlated to some extent, it is advisable to avoid using these kinds of ratios in the first place. Sometimes, however, there are only a limited number of elements available to use in forming ratios, and common numerators or denominators may become necessary. In these instances binary variation diagrams of ratios with common elements may be used for visual classification of samples into groupings, but any interpretation of apparent systematic variation within the data should be strictly avoided. Wherever possible in the analyses of Chapters 4 and 5, ratio pairs of the form A/B vs C/D are used, so there are no common numerator or common denominator effects.

Chapter 4

Variation of major and trace element abundances in Lac de Gras kimberlites

4.1 CHAPTER OVERVIEW

Kimberlites are hybrid rocks and as a result characteristically display a large degree of compositional variation both within and between provinces, fields and even individual intrusions. It is well known that most kimberlites incorporate variable amounts of different mantle and crustal materials *en route* to the surface, and these processes can be a major control on the eventual whole-rock chemistry of the sample.

This chapter provides a brief summary of previous influential studies of the major and trace element geochemistry of kimberlites, and discusses some of the problems inherent in the investigation of these unusual rocks. The variability of key major and trace element abundances in the Canadian kimberlites is described and illustrated, and comparisons are made with other well-characterised suites of kimberlites from southern Africa and elsewhere. This forms the basis for the detailed analysis of processes responsible for producing these elemental variations, as presented in Chapter 5.

4.2 INTRODUCTION

4.2.1 Previous studies of kimberlite major/trace element geochemistry

For a hundred years following the 1870s discovery of primary (i.e. non-alluvial) diamond deposits in South Africa the majority of kimberlite research was concerned with the more easily accessible questions of petrography, mineralogy, diamond content, and structure and emplacement of pipes. Some of this early work is summarised in the

classic monographs by Wagner (1914) and Williams (1932). These works also contain a small number of good quality whole rock major element analyses, performed by classical wet chemistry techniques. Advances in analytical technology and the discovery of the Siberian kimberlite province in the 1950s precipitated an escalation in investigations of the chemical composition of kimberlites. Large volumes of compositional data for Siberian kimberlites were generated, although Mitchell (1986) points out that much of this data was semi-quantitative and cannot be used in comparison to more recent data. A useful distillation of some of the Soviet work is given in Frantsesson (1968, and 1970 in translation).

The 'modern era' of kimberlite geochemical studies dates from the early 1970s, with the influential compilation of work on kimberlites from Lesotho by Nixon (1973) and the inception of the First International Kimberlite Conference. The publication of the proceedings of this meeting marked the beginning of a large increase in the number of well-documented investigations of kimberlite petrography, mineralogy and geochemistry. The monographs of Dawson (1980), Mitchell (1986) and Mitchell (1995) provide comprehensive reviews of this body of kimberlite literature.

Some of the earliest high quality major and trace element analyses of whole-rock kimberlites during this period were acquired by Gurney and Ebrahim (1973), Fesq *et al.* (1975), Kable *et al.* (1975) and Mitchell and Brunfelt (1975). These studies helped to identify some of the fundamental geochemical characteristics of these rocks, such as their potassic nature and extreme enrichment in both compatible and incompatible elements. They also provided some of the first chemical evidence to support the

distinction between the 'basaltic' and 'micaceous' types identified by Wagner (1914) on a petrographic basis.

These foundations were built upon by the work of Smith *et al.* (1985a), who presented a comprehensive set of trace element data obtained on hypabyssal samples carefully selected in order to minimise the input from alteration and contamination. This data, used in association with the isotopic data of Smith (1983) and by application of multivariate statistical analysis, more firmly established the key elemental distinctions between kimberlite groups. Smith (1983) introduced the concept of Group I and II kimberlites, which is broadly synonymous with the basaltic/micaceous petrographic classification of Wagner (1914), but defines these two groups entirely on the basis of isotopic character. Smith *et al.* (1985a) showed that Group II kimberlites – *orangeites* in the terminology of Mitchell (1995) – are enriched in SiO_2, K_2O, Pb, Rb, Ba and LREEs and depleted in TiO_2 and Nb in relation to Group I – or *archetypal* (Mitchell, 1995) – kimberlites.

With the advent of plasma source techniques in mass spectrometry it has now become relatively routine to acquire large volumes of accurate and precise trace element data. For this study new major and trace element determinations have been made on 123 whole rock kimberlite samples, including 86 from the Lac de Gras kimberlite field, North West Territories. These analyses form part of a comparative database of 388 kimberlite analyses, incorporating data from southern Africa (Smith *et al.*, 1985a; Fraser, 1987; Spriggs, 1988; Tainton, 1992; Nowell, unpublished), West Africa (Taylor *et al.*, 1994), Finland (O'Brien and Tyni, 1998) and China (Tompkins *et al.*, 1998). Samples from Sisimiut area of Greenland (Scott, 1979) have subsequently been shown

not strictly to be archetypal kimberlites, as in some cases they contain melilite (Mitchell *et al.*, 1999). These rocks are better classified as ultramafic lamprophyres, but are included here to extend comparisons of elemental characteristics in alkaline ultramafic rocks on a global scale.

4.2.2 Problems inherent in comparison of kimberlite compositional data

A number of problems exist when attempting to draw comparisons between geochemical data acquired in different kimberlite studies. Firstly, there is the issue of differential data quality between studies. Inevitably, the accuracy and precision of trace element data in particular has improved steadily since the 1970s as analytical methods and instrumentation have evolved. Associated errors are not always fully quoted in the literature, making it difficult to assess the relative quality of datasets and the extent of coherence between them. Wherever possible in this study, trace element data acquired by ICP-MS methods is used for comparative purposes.

Secondly, due to the hybrid nature of kimberlites, samples of whole rocks will commonly contain material contributions from the lithospheric mantle and crust through which the magma has passed. Kimberlite is also extremely susceptible to secondary alteration processes, which also act to modify the original magma chemistry. The effects of these processes are in general much more pronounced in the volcaniclastic portions of the intrusion (i.e. the diatreme and crater facies). It is therefore of great importance to select only samples known to be from the hypabyssal facies if any meaningful interpretation of the data regarding parental magma characteristics is to be made. This has not always been the case in a number of studies

68

of kimberlite geochemistry. In this work only data from hypabyssal facies rocks are used, unless otherwise stated (e.g. for comparative purposes).

Thirdly, even within hypabyssal samples it is common to see evidence of small fragments of xenolithic material. In this study attempts have been made to extract by hand any such crustal material from the coarse crush, but it is impossible to remove all crustal contamination in this way. Furthermore, finely comminuted crustal material can be disseminated throughout a sample that appears 'uncontaminated' to the naked eye. Contamination by lithospheric mantle material (e.g. olivine, spinel, phlogopite) is also extremely difficult to remove by hand-picking, as these phases also occur as phenocrysts and microphenocrysts in the kimberlite. This leads to issues such as the 'olivine macrocryst problem' discussed by Mitchell (1986). It is not always stipulated in the literature to what extent, if any, xenolithic material has been screened out from samples. If samples are not handled in the same manner there will certainly be compositional inconsistencies between them.

Lastly, there is a danger in kimberlite studies of introducing a sampling bias into the data. The kimberlites that have been most extensively studied, and from which most samples are made available, tend to be those where mining operations have taken place. This is partly because better quality samples for geochemical purposes are usually found at some depth below the erosion level in an intrusion (i.e. hypabyssal facies rocks from below the surficial weathering profile), but also because there is naturally more interest in richly diamondiferous bodies than those that are barren or uneconomic. The average geochemistry of kimberlites represented in a database could, therefore, be biased towards components that may be linked to diamond content. Elevated content

of lithospheric mantle might be an example of such a component. In the Lac de Gras dataset there is a representative range of kimberlites from economic, through marginal to barren, with regard to diamond content, so any 'mine bias' effects should be minimal.

4.3   DATA REPRESENTATION

4.3.1   General major/trace element characteristics

4.3.1.1   Comparison of elemental distribution patterns

All major and trace element data acquired during this study is tabulated in Appendix D. The extent of compositional variation observed in selected hypabyssal kimberlites from around the world is shown in Figures 4.1 to 4.3. The set of hypabyssal kimberlites from Canada is composed mostly (80 of 94; 85%) of samples from the Slave craton, and of these 70 (87%) are from the Lac de Gras field. In this thesis, the term 'southern Africa' covers South Africa, Namibia, Lesotho and Botswana.

Figures 4.1 to 4.3 compare, for selected elements, key descriptive statistics between regions hosting major kimberlite provinces. Similar diagrams for other elements of interest can be found in Appendix E. Note that Figure 4.1 is merely an annotated key to assist interpretation of these diagrams. The *magnitude* and *dispersion* (range and variability) of each element is represented by means of box-plots, which display the mean, median, range, inter-quartile range and 5th and 95th percentiles of each dataset. Comparison is made between several global provinces for which reliable compositional data exist. A further analysis of the *distribution* of data between samples from North America and Southern Africa is also provided in the form of histograms. These help to

visualise the shape of the data and in particular indicate whether a dataset has a
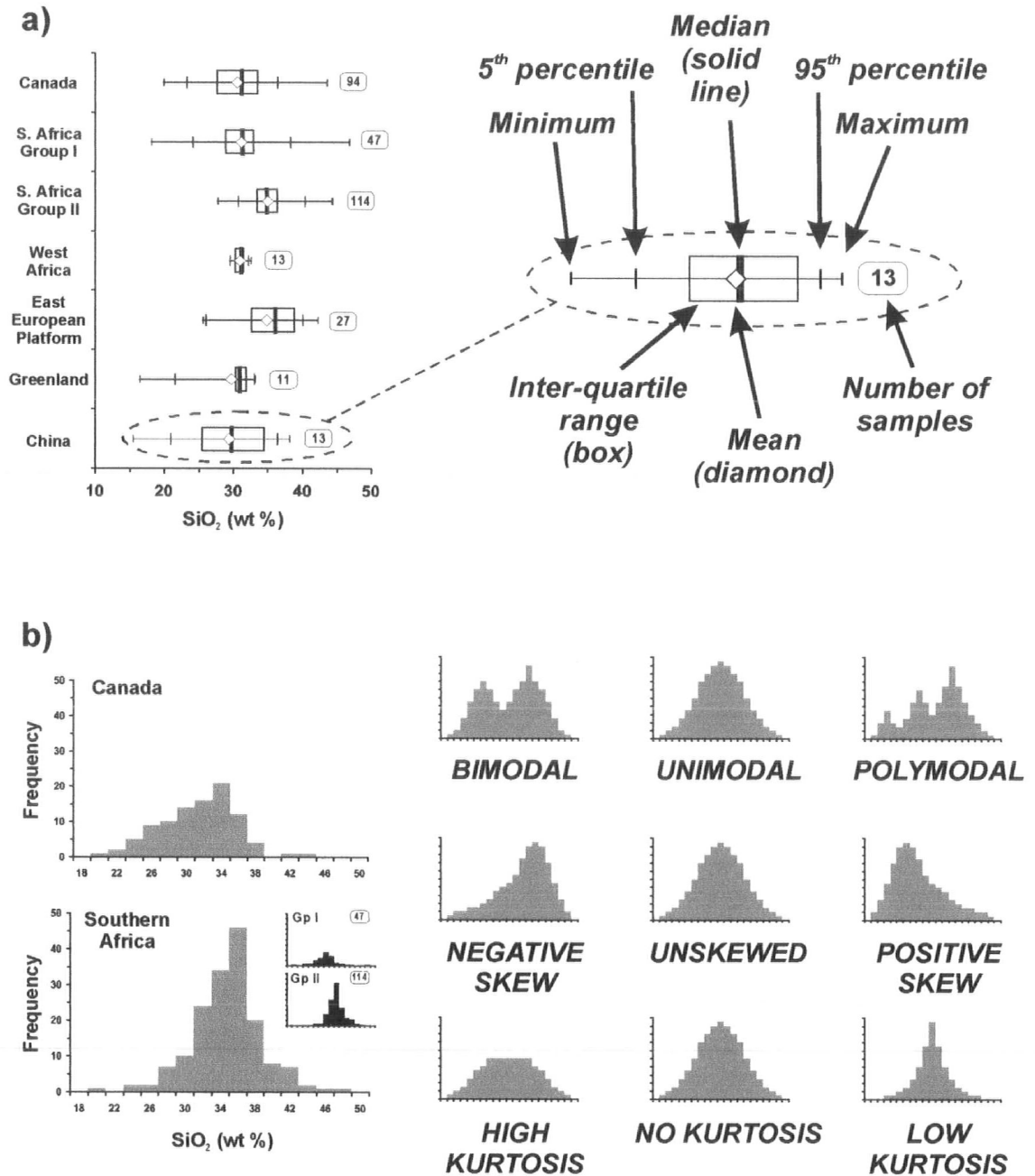
Figure 4.1 Interpretation of major and trace element dispersion and distribution diagrams: **a)** measures of magnitude and dispersion; **b)** measures of the shape of the distribution.

Gaussian distribution, the extent of any skewness or kurtosis, and the number of apparent modes within a dataset.
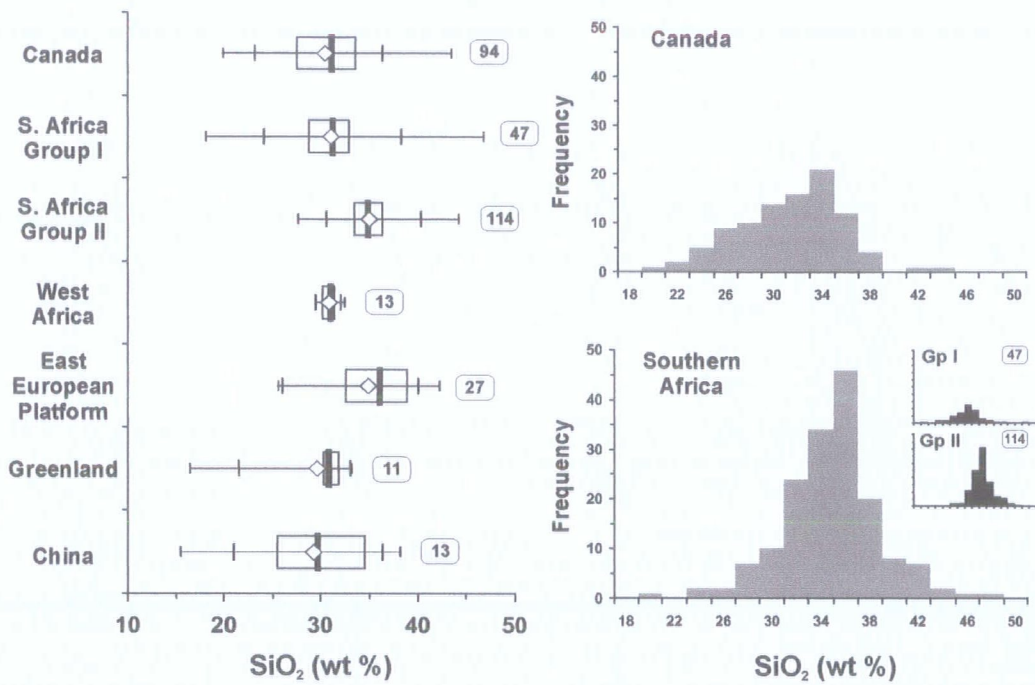
Figure 4.2a Dispersion and distribution of SiO_2 in selected global hypabyssal kimberlite occurrences.
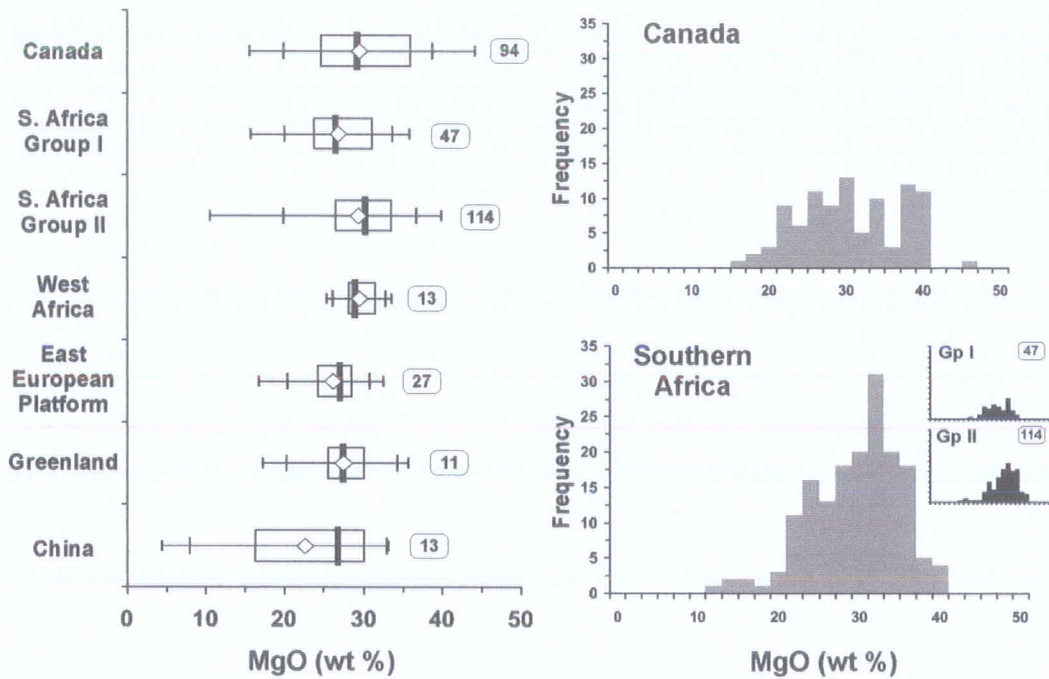
Figure 4.2b Dispersion and distribution of MgO in selected global hypabyssal kimberlite occurrences.
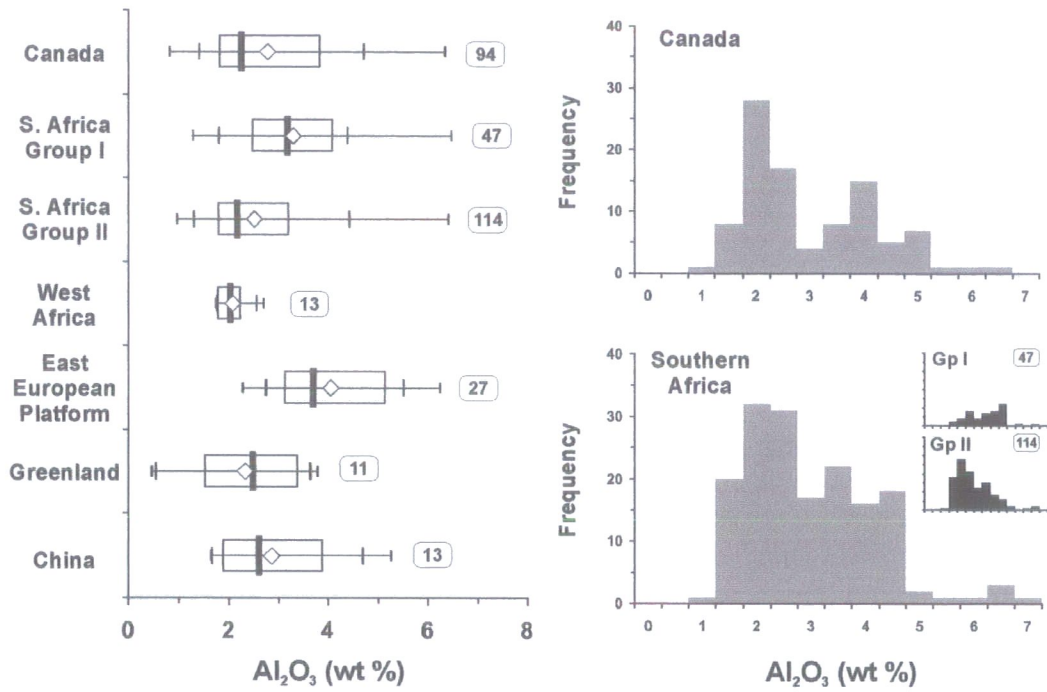
Figure 4.2c Dispersion and distribution of Al_2O_3 in selected global hypabyssal kimberlite occurrences.
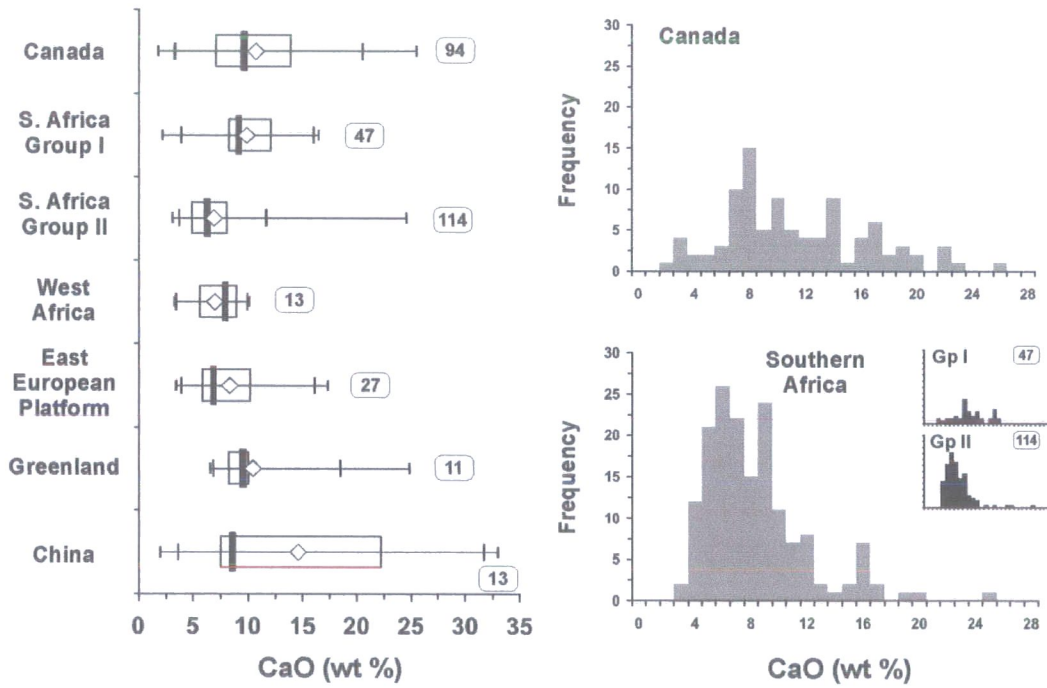
Figure 4.2d Dispersion and distribution of CaO in selected global hypabyssal kimberlite occurrences.

4.3.1.2 Major elements

The oxides of Si, Mg, Al and Ca (Figure 4.2a-d) together constitute over 70% by weight of most kimberlites and thus exert the greatest influence on the bulk chemistry of these rocks. Processes of alteration, crustal contamination, and olivine accumulation and removal also affect the relative abundance of these elements in a sample. The dispersion of SiO_2, Al_2O_3 and CaO in Canadian kimberlites is very similar to that observed in Group I kimberlites from Southern Africa. The ranges of SiO_2 and CaO are distinct between southern African Group I and Group II samples. There is some overlap in the ranges of Al_2O_3 in Canadian and Southern African kimberlites, but the median of the southern African Group I samples is much higher than that of the Canadian and southern African Group II kimberlites. The inter-quartile range of MgO in the Canadian dataset is slightly elevated relative to southern African Group I samples, and encompasses the inter-quartile range in MgO of Group II kimberlites. The median MgO of the Canadian data is intermediate to that of southern African Group I and Group II.

The distribution of SiO_2 in both Canadian and southern African samples approximates to a normal or Gaussian model, with a degree of negative and positive skew, respectively. In the Canadian samples MgO, Al_2O_3 and CaO clearly have distributions with more than a single mode, and this is also apparent in the southern African data. This could indicate that more than one process may be controlling the abundance of these oxides in kimberlite magmas. The bimodal distribution of MgO in southern Africa appears to correspond to the modes of the individual Group I and Group II populations, but the position of modes in the Canadian MgO data is much more

variable. This suggests that the extent to which processes controlling composition operate may be very variable, even within a single province or field.

The variability of Fe_2O_3 $_T$, TiO_2, Na_2O and K_2O in these samples is illustrated in Appendix E.

The main sinks for Ti in kimberlites are ilmenite, a ubiquitous member of the low-Cr megacryst suite, perovskite, a common accessory mineral that is also the principal carrier of REEs in kimberlites, phlogopite and late-stage groundmass spinel (Ti-magnetite), which can be abundant in some occurrences. Canadian and southern African samples are TiO_2-poor relative to most of the other regions represented. The TiO_2 content of Canadian kimberlites is very similar to that of southern Africa Group II, rather than Group I. The distribution of TiO_2 in Canada and southern Africa approximates to a unimodal Gaussian model with a prominent positive skew.

Kimberlites are potassic rocks and typically have $K_2O/Na_2O > 1$, due primarily to low abundances of Na_2O. Elevated levels of Na_2O in kimberlites are generally considered to represent input from crustal contamination. Many of the hypabyssal samples from Lac de Gras analysed in this study have Na_2O abundances below the XRF detection limit of 0.05-0.1%. As a result the lower end of the inter-quartile range for Na in the Canadian data is effectively zero, and the distribution inevitably has a strong positive skew. Even in the most Na-rich hypabyssal kimberlites from Lac de Gras, the Na_2O content rarely exceeds 0.5%. Volcaniclastic kimberlites from the diatreme or crater facies routinely have in excess of 0.5% Na_2O, which is typically inferred to be due to

contamination and alteration. The median and inter-quartile range of Na_2O in Canadian hypabyssal samples is more similar to southern African Group II kimberlites.

Levels of K_2O in kimberlites are closely linked to the modal abundance of phlogopite. Consequently, Group II kimberlites from southern Africa tend to be richer in K_2O than Group I rocks. The distribution of K_2O in Southern African kimberlites is polymodal with a large positive skew. The two most prominent modes are likely to correspond to the discrete populations of Group I and II kimberlites. The Canadian K_2O distribution also has a large positive skew, but is not unequivocally polymodal. The median and inter-quartile range of K_2O abundance in Canadian kimberlites is clearly more similar to southern African Group I samples.

4.3.1.3 Trace elements I: compatible elements

The compatible elements of greatest importance in kimberlite studies are Ni and Cr, as these elements are highly representative of the modal abundance of olivine in a sample (Mitchell, 1986). The regional variability of Sc and V abundance in kimberlites is shown in Appendix E.

The magnitude and dispersion of Ni content (Figure 4.3a) is quite variable on a regional scale. The median Ni content of the Canadian data (1100ppm) is intermediate to that of southern African Group I (930ppm) and Group II (1340ppm). The inter-quartile range of Group II kimberlites has the greatest offset to high Ni in the entire database. The median Ni content in West African samples (1270ppm) is also high, but in China, Greenland and the East European Platform median Ni levels are much lower (<1000ppm in each case). The distribution of Ni in both the Canadian and southern
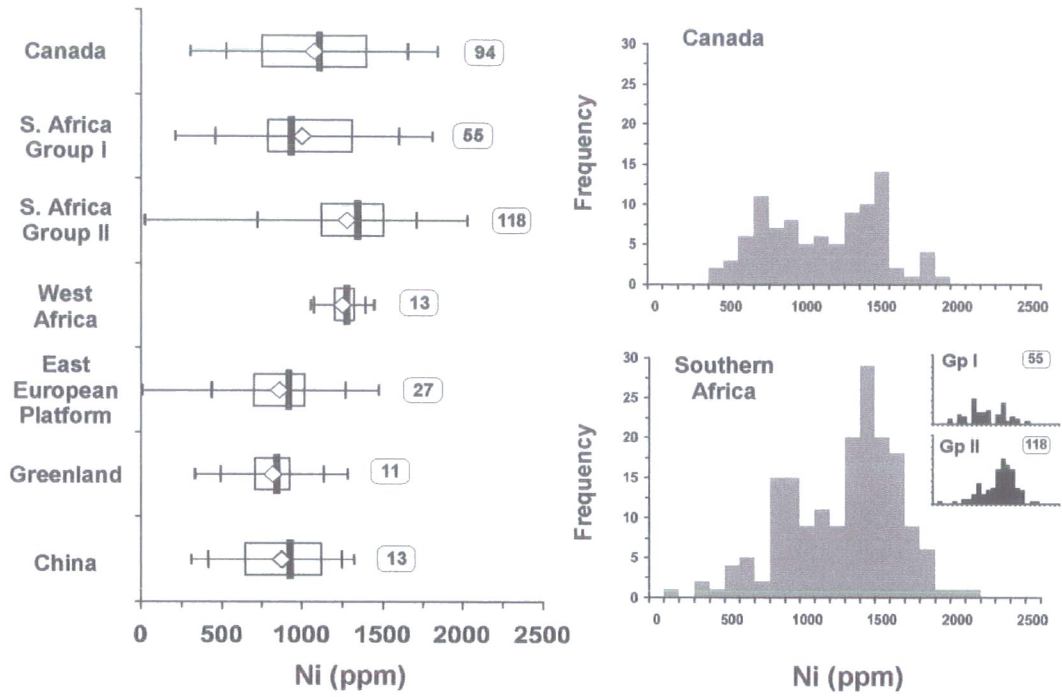
Figure 4.3a Dispersion and distribution of Ni in selected global hypabyssal kimberlite occurrences.
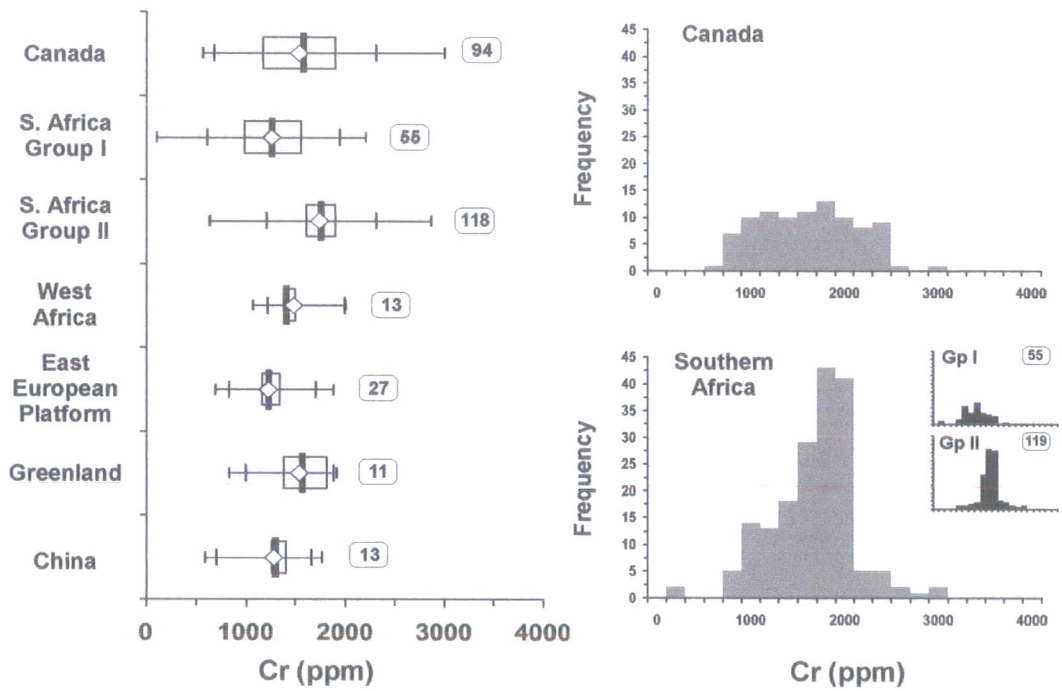
Figure 4.3b Dispersion and distribution of Cr in selected global hypabyssal kimberlite occurrences.
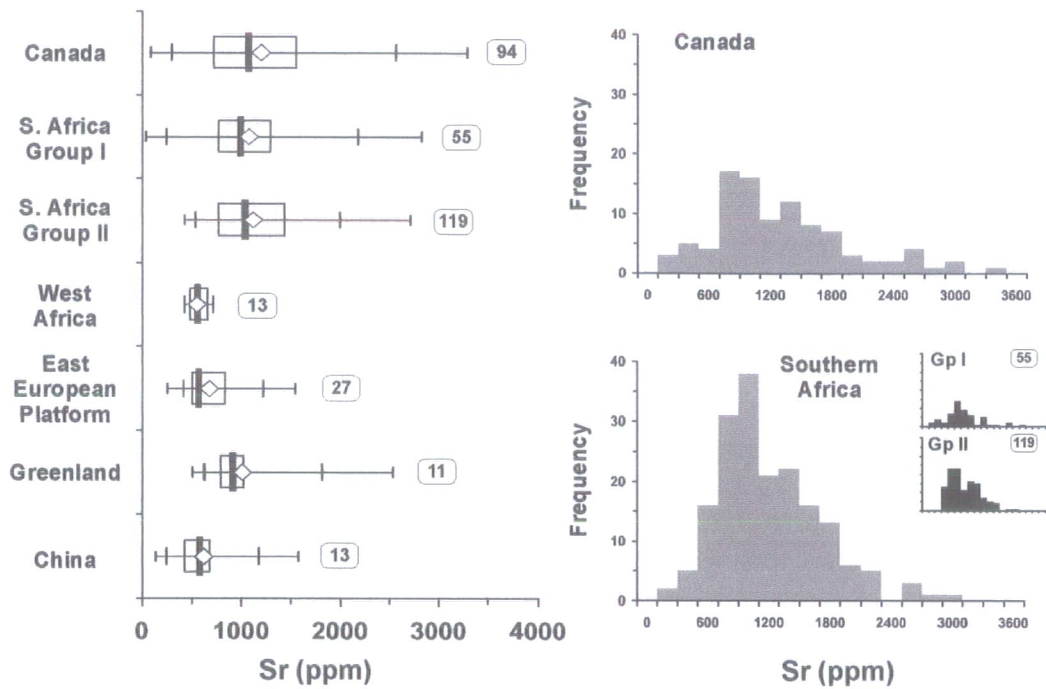
Figure 4.3c Dispersion and distribution of Sr in selected global hypabyssal kimberlite occurrences.
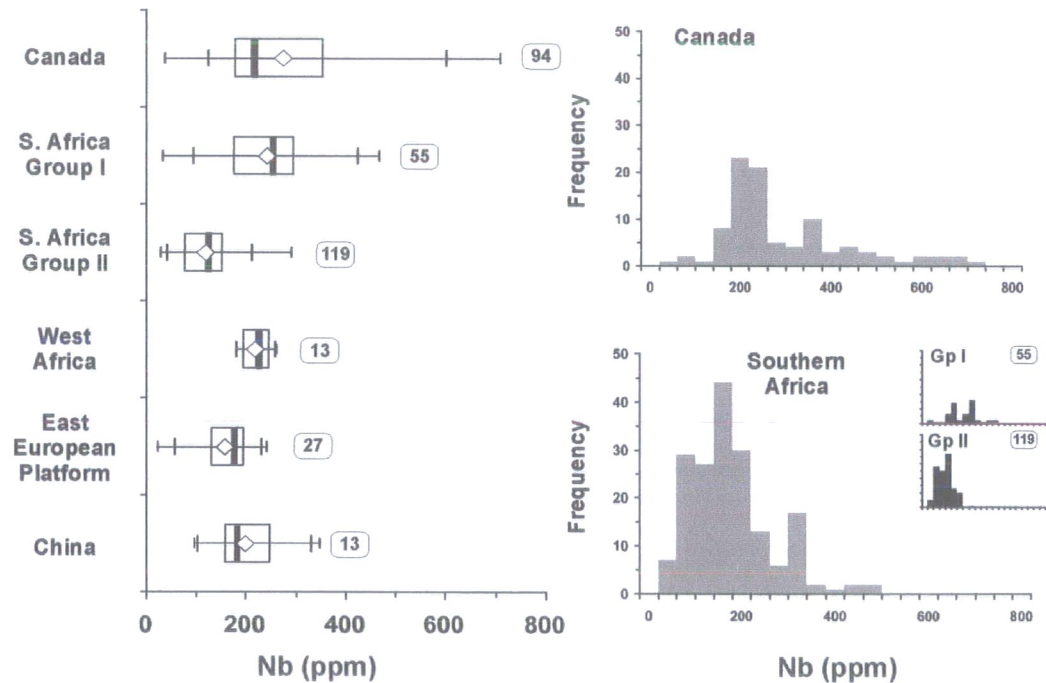
Figure 4.3d Dispersion and distribution of Nb in selected global hypabyssal kimberlite occurrences.

African data is clearly bimodal. There are obvious peaks at 700-900ppm in both

datasets, which is close to the median value observed in China, Greenland and the East

78

European Platform kimberlites. In addition there is a second peak in the southern African data at 1300-1500ppm, which corresponds to the Group II samples. The second peak in the Canadian data is at approximately 1500ppm Ni.

In addition to olivine, Cr is often hosted within chromite (Cr-spinel xenocrysts and early phenocrysts) in kimberlites. This refractory phase is difficult to dissolve for analytical purposes, and comparisons of Cr abundance data obtained by XRF and solution–based methods should be approached with caution. The trace element data table in Appendix D indicates which method was used for each sample. The median Cr content of the Canadian data (1590ppm) is again intermediate to the medians of southern Africa Group I (1260ppm) and Group II (1750ppm). Polymodality in the southern African data is controlled by the differential Cr content of Group I and Group II samples. The distribution is essentially unimodal, with a negative skew corresponding to input from Group I samples. The Canadian data has an extremely high kurtosis, but it is not clear whether there is more than a single mode.

4.3.1.4 Trace elements II: large ion lithophile elements (LILEs)

LILEs (or low field strength elements, LFSE) are distinguished from other incompatible trace elements on the basis of having an ionic potential greater than 2.0 (Rollinson, 1993). This group thus consists of elements with an ionic charge of +1 or +2 and large ionic radii. Rb, Sr, Cs, Ba and Pb are the LILEs of particular geological interest. The principal carrier of Rb, Ba, Cs and Pb in kimberlites is phlogopite, and so Group II and other mica-rich samples might be expected to have greater abundances of these elements. Perovskite may also be a carrier for Pb. Sr substitutes primarily for Ca in apatite, carbonate phases and perovskite. Ba also substitutes for Ca in carbonates

(Armstrong *et al.*, in press). LILEs tend to be amongst the most chemically mobile elements, and may be leached from kimberlite by near-surface syn- and post-emplacement alteration processes, although the effects of this are rarely seen in fresh hypabyssal facies samples. The regional variation in abundance of Rb, Ba and Pb is shown in Appendix E.

Variation in Sr content (Figure 4.3c) is very similar in Canadian and southern African Group I and Group II kimberlites. The Rb and Pb content of Canadian samples are more akin to southern African Group I kimberlites, whereas their Ba content is more similar to southern African Group II samples. The distribution of Pb and Ba in both regions is unimodal with a positive skew, while the distribution of Rb in Canada and southern Africa is more bimodal in character.

4.3.1.5   Trace elements III: high field strength elements (HFSEs)

The HFSEs are here considered to include Nb, Ta, Hf, Zr, Y, U and Th. With the exception of Y, all of these elements are hosted in kimberlites primarily by perovskite. Other accessory phases are more selective hosts, e.g. ilmenite (Nb, Hf and Ta), zircon (Hf and Zr), and apatite (U and Th). Nb is a particularly immobile element that is frequently used in geochemical models as a benchmark against which to measure the variable mobility of other elements.

The dispersion and distribution of Nb content (Figure 4.3d) in Canadian kimberlites is most similar to Group I kimberlites from southern Africa, although the median of the Canadian data is slightly lower and its inter-quartile range is broader. In both regions there appear to be multiple modes in the data distribution. South African Group I

kimberlites show two peaks in Nb abundance at approximately 150 and 350ppm, the first of which corresponds to the mode of the Group II samples. The Canadian data has a principal mode at around 200-250ppm, with a secondary peak at 350-400ppm and a long positive skew up to 700ppm.

The regional variability of Hf, Zr and Y is shown in Appendix E. All of these elements are considerably less abundant in Canadian kimberlites than in those from southern Africa. There is little difference in their median and inter-quartile range between southern African Group I and Group II samples.

4.3.1.6 Trace elements IV: rare earth elements (REEs)

Kimberlites are more enriched in the larger radius light REEs (LREEs) than smaller radius heavy REEs (HREEs), and consequently form characteristic sloping patterns on chondrite-normalised rare earth diagrams. This distribution pattern is very similar to that observed in kimberlite perovskite (Jones and Wyllie, 1984), which is a typical groundmass phase and not commonly encountered as a xenocryst. This phase is thus the major sink for REEs in kimberlites. Very similar patterns of REE distribution, at lower abundances, are also observed in apatite and carbonate minerals in carbonatites (Hornig-Kjarsgaard, 1998); thus these minerals are the most likely hosts for the REEs in kimberlites that have little or no modal perovskite.

The dispersion and distribution of La, Nd, Sm and Lu (Appendix E) are broadly similar with only small variations between regions. The abundance of any given REE tends to be greater in the southern African data than in the Canadian samples. There is no evidence of bimodality in the Canadian data. There are multiple peaks in the southern

African La and Nd data, but this does not persist in the mid- and heavy-REEs. This observation may also be related to the effects of crustal contamination on the HREE in some southern African samples.

4.3.1.7 Distribution of log-ratio data

Figures 4.2-4.3 are constructed from 'raw' elemental data, which is subject to the limitations of closure and differential volatile content discussed in Chapter 3. It is important to know how the translated log-ratio data proposed as a solution to this problem is distributed in relation to the raw data. As noted in Chapter 3, the 'log-ratio' transformation employs the natural logarithms ($\log_e[x]$ or $\ln[x]$) rather than logarithms to base 10 ($\log_{10}[x]$).

Figure 4.4 compares the distribution of raw and log-ratio data for a selection of major and minor elements. Nb has been selected as the denominator for ratio construction because of its immobile nature, and because its abundance changes little in relation to many other elements during processes such as alteration, crustal and lithospheric contamination, and fractionation. The conversion from oxide (wt%) data to elemental (ppm) data for the major elements (e.g. Si instead of SiO_2) does not affect the shape of the distribution (Figure 4.4).

In each case shown in Figure 4.4 the log-ratio translation process does not affect the overall shape of the distribution. For example, the distribution of SiO_2 and ln (Si/Nb) are both unimodal and skewed; Ni and ln (Ni/Nb) are both bimodal. In the case of Mg,
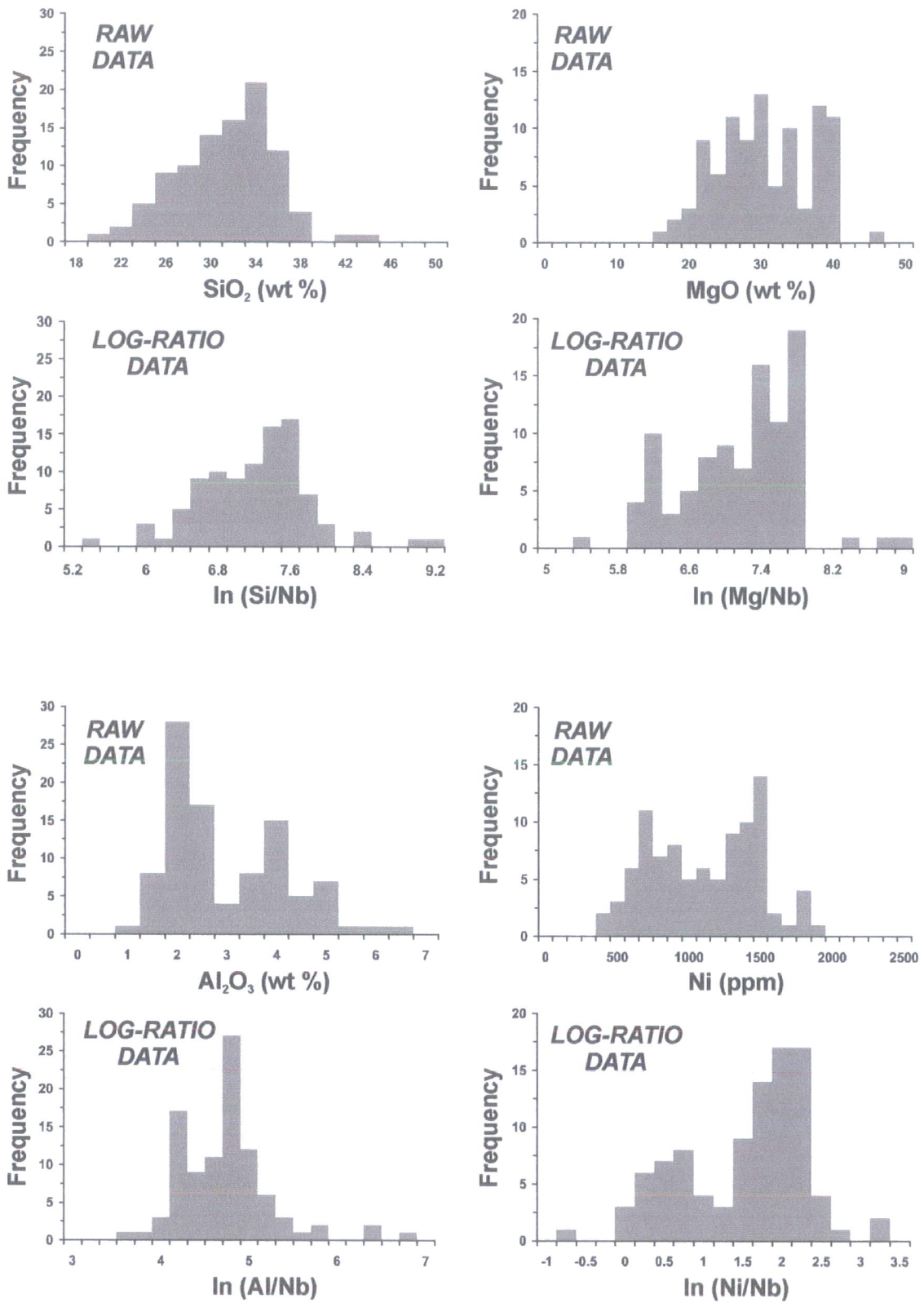
Figure 4.4 Comparison of distribution of selected raw and log-ratio major and minor element data from Canadian hypabyssal kimberlites.

the log-ratio conversion also appears to remove some of the 'noise' of the raw data distribution, although in both instances the overall distribution is polymodal. In all cases the variation structure of each element is preserved between the raw data and the log-ratio data. While the log-ratio format is preferable for maintaining statistical integrity during modelling, it is conceptually more abstract and thus less easy to interpret directly than the raw data format. For this reason, having observed that there are no artificial correlations resulting from closure, the raw data format is retained in this chapter for the purposes of visual representation of the data.

4.3.1.8 Comparison with southern African Group I and Group II kimberlites

Although the Group I/II classification system for kimberlites from Southern Africa was originally based on isotopic criteria (Smith, 1983), distinctions can also be made between the groups using major and trace element characteristics (Smith *et al.*, 1985a). Group I kimberlites tend to have higher TiO_2, Fe_2O_3 T, CaO and Na_2O, and lower SiO_2 and K_2O than Group II kimberlites. The variation of major element abundance with MgO content in hypabyssal kimberlites from Canada is compared to that of Southern African Group I and II samples in Figure 4.5. The variation of SiO_2, CaO, K_2O and P_2O_5 with MgO in the Canadian samples is most similar to Southern African Group I, whereas the variation of TiO_2, Fe_2O_3 T and Na_2O with MgO is more similar to Group II kimberlites.

The levels of Ti present in Canadian kimberlites are similar to those of Southern African Group II kimberlites on a chondrite-normalised distribution diagram of the compatible elements (Figure 4.6a-b). The Ni content of Southern African Group I

kimberlites provides the best fit to the Canadian data, while Group II kimberlites have
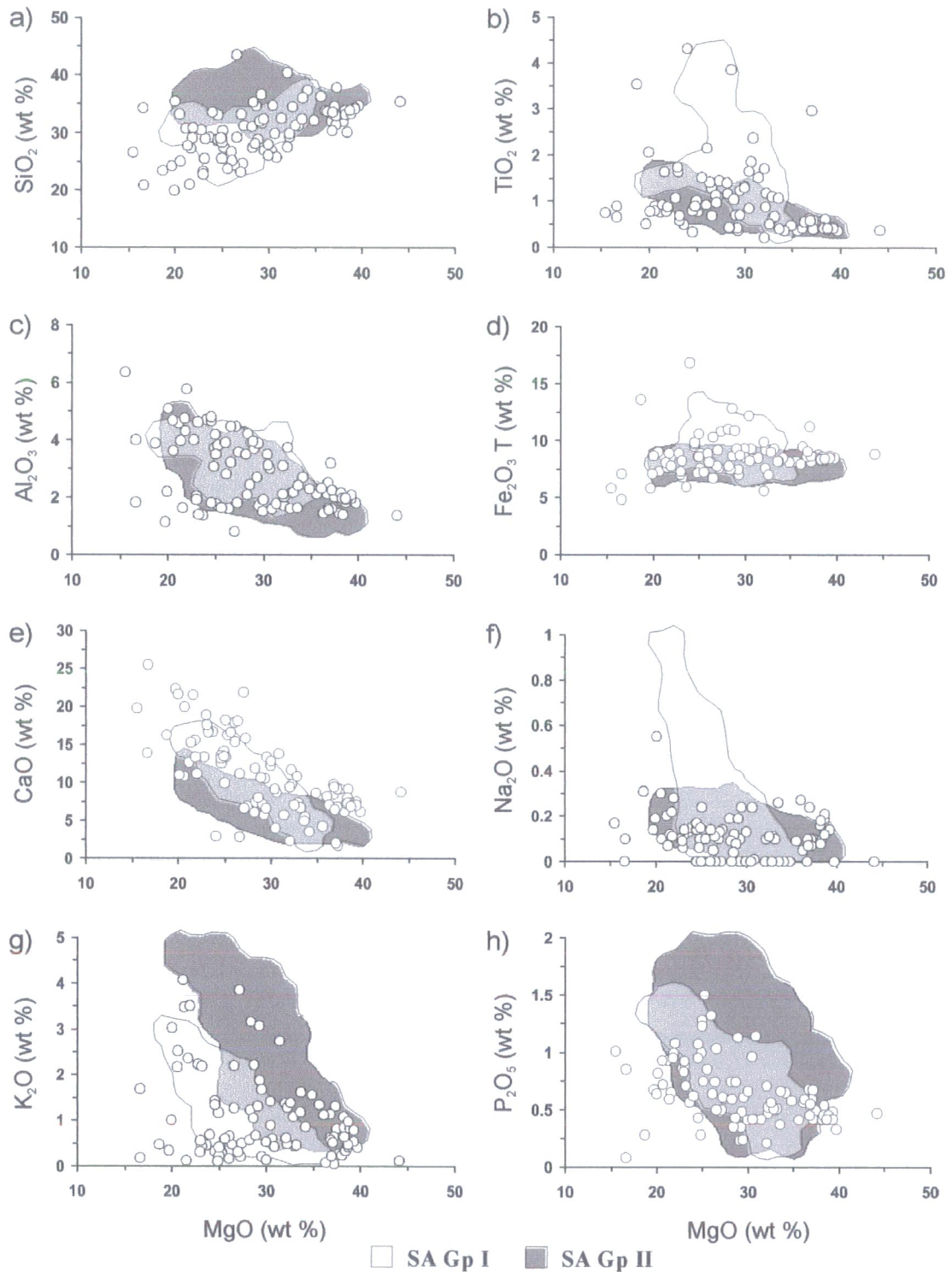
Figure 4.5 Major element compositional variation of Canadian hypabyssal kimberlites, and comparison to compositional range of Southern African Group I and II kimberlites. SA data from Smith *et al.* (1985a), Fraser (1987), Spriggs (1988), Tainton (1992), Nowell *et al.* (1999; in press), and this study.
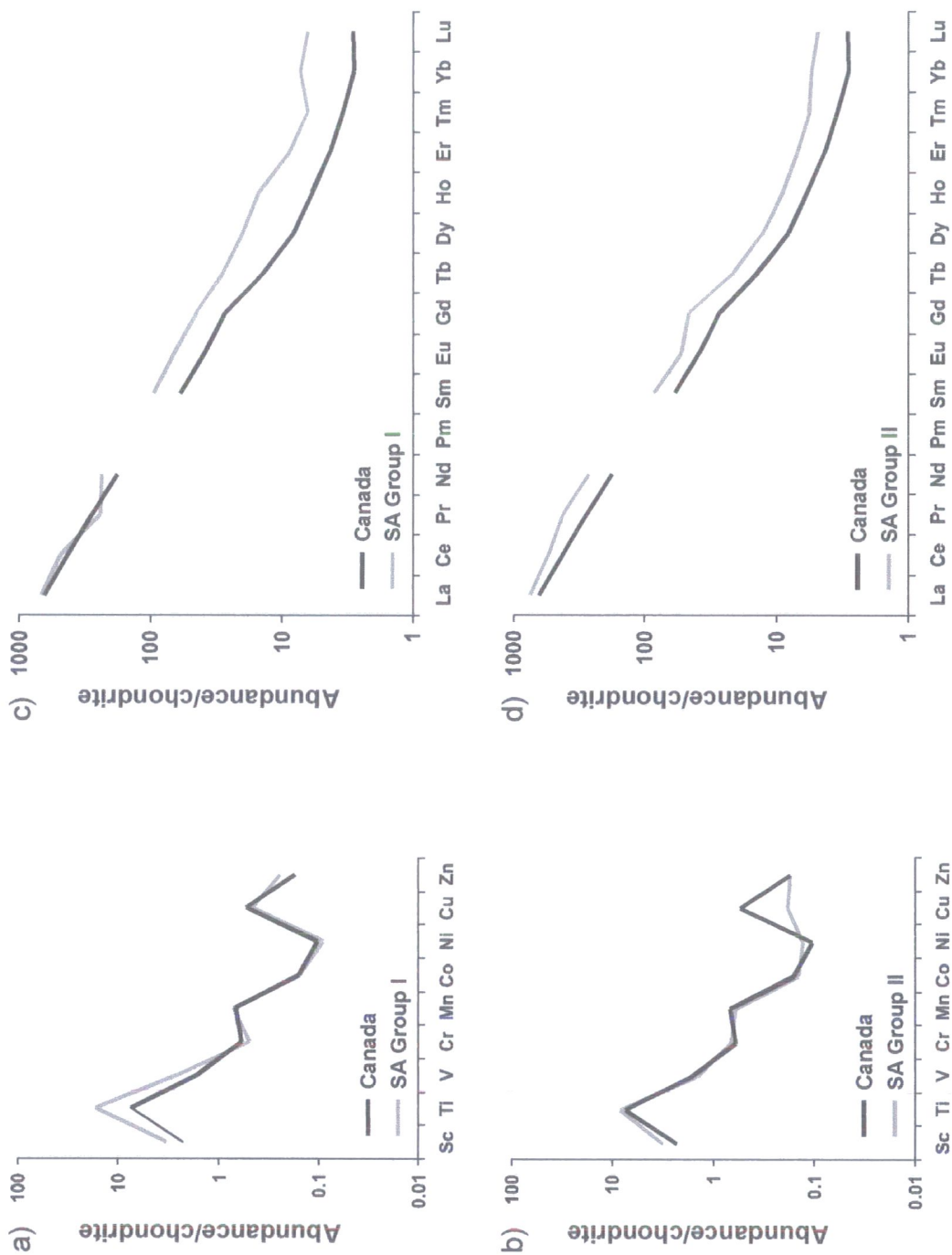
Figure 4.6 Continued overleaf.
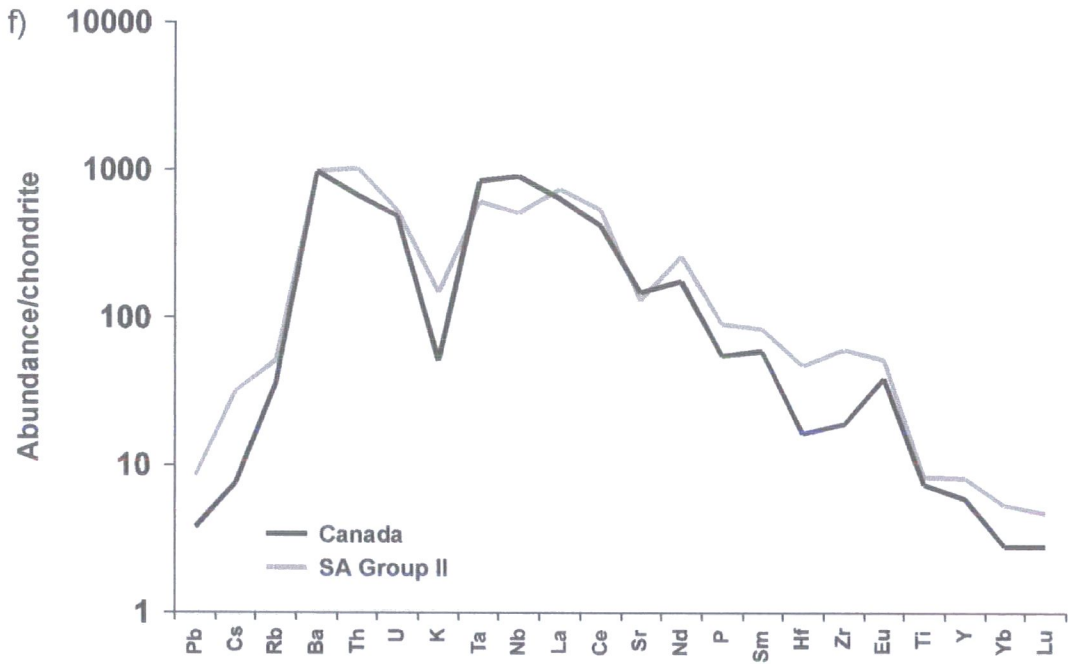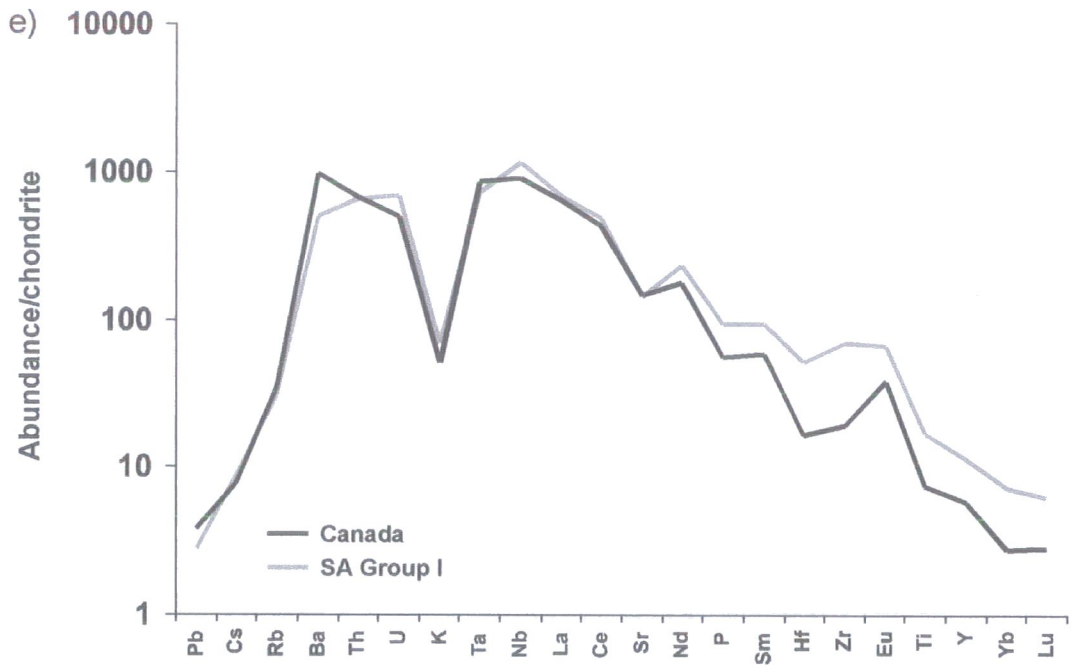
Figure 4.6 Chondrite-normalised element distribution patterns for Canadian hypabyssal kimberlites and Southern African Group I and Group II hypabyssal kimberlites: (a-b) compatible elements; (c-d) rare earth elements; (e-f) extended incompatible element series. All data normalised to chondritic values of McDonough and Sun (1995).

more similar abundances of Cr and Co. The LREE content of Canadian kimberlites is similar to that of Group I samples from southern Africa (Figure 4.6c-d), but their MREE-HREE content is lower than observed in both Group I and Group II samples. The abundance of some of the most incompatible elements (e.g. Pb, Cs, Rb: Figure 4.6e-f) is most like that of Group I kimberlites. Only the abundance of Ba and U is more akin to Group II kimberlites.

Figure 4.7 illustrates selected geochemical characteristics of Canadian hypabyssal kimberlite samples on a series of variation diagrams originally devised to demonstrate compositional differences between Group I and II kimberlites (Smith *et al.*, 1985a; Le Roex, 1986). The bivariate plots of K_2O-TiO_2 and SiO_2-Pb (Figure 4.7a-d) were found by Smith *et al.* (1985a) on the basis of multivariate discriminant analysis to be the most efficient two-component classifiers of kimberlites into their correct isotopically-defined groups. In both plots, the data from Canadian kimberlites do not fall exclusively into either grouping, although in SiO_2-Pb space there appears to be a greater affinity for Group I, with some samples having anomalously high Pb content. By contrast, data from other Group I kimberlites outside southern Africa (Siberia, West Africa, Greenland, Finland and China) are mostly located in the southern African Group I fields. Le Roex (1986) put forward a discrimination scheme based on the variation of La, Ba and Zr with Nb content (Figure 4.7e-h). The location of the Canadian samples in these projections indicates that they have a character intermediate to Group I and Group II in terms of La-Ba-Nb, but more similar to Group I kimberlites in terms of Ba-Zr-Nb variation. In these instances the data from other non-southern African Group I occurrences behaves in the same manner as the Canadian samples.
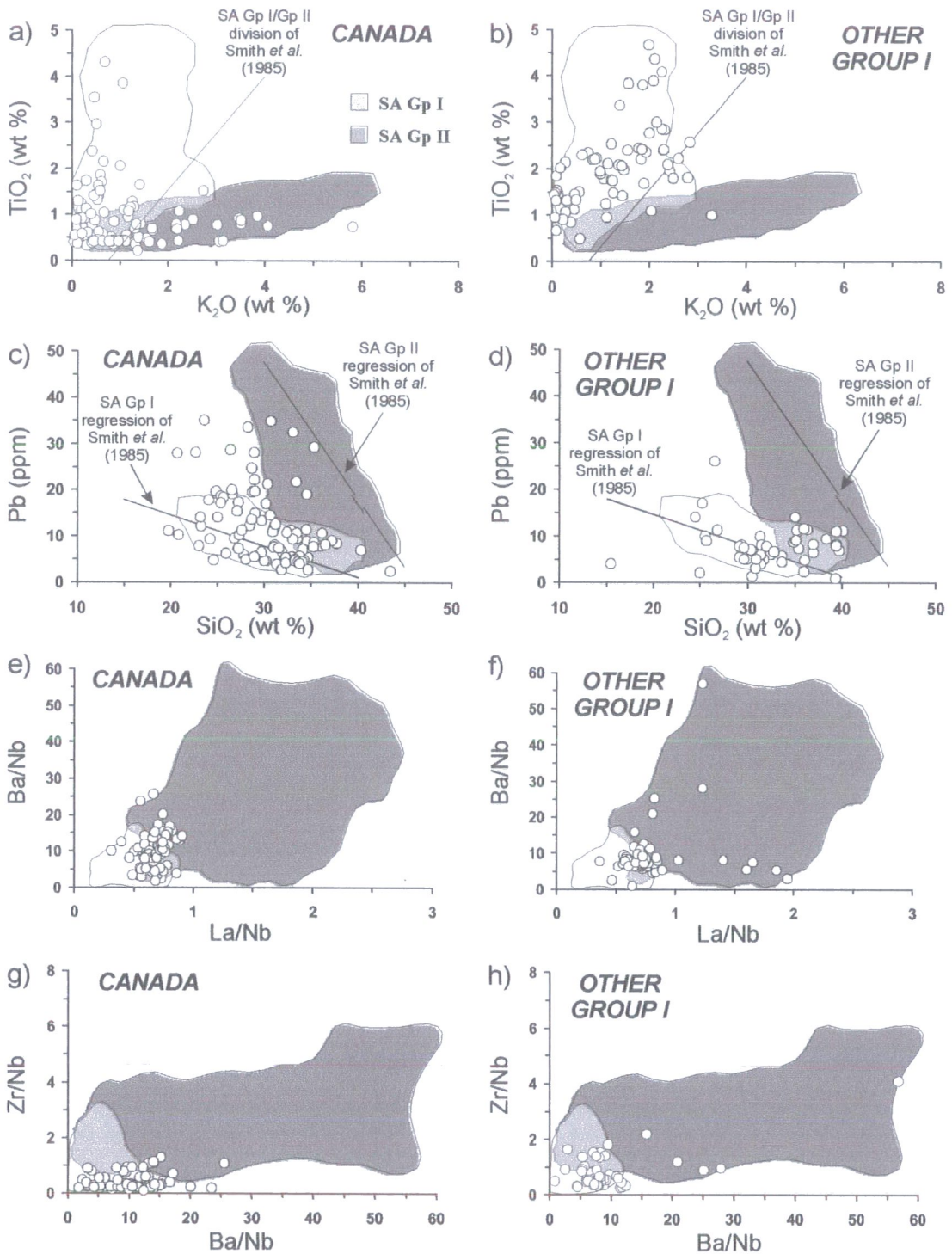
Figure 4.7 Distribution of Canadian hypabyssal kimberlites and other 'Group I' hypabyssal samples from Siberia (this study), West Africa (Taylor *et al.*, 1994), Greenland (Scott, 1979), Finland (O'Brien and Tyni, 1999) and China (Tompkins *et al.*, 1999). All relative to location of Southern African Group I and Group II samples in: (a-b) K_2O-TiO_2 space; (c-d) SiO_2-Pb space; (e-f) La/Nb-Ba/Nb space; (g-h) Ba/Nb-Zr/Nb space.

These simple comparisons between the elemental signatures of southern African Group I/II kimberlites and the data from Canadian hypabyssal samples indicates that the latter have characteristics of both Group I and Group II. In some cases the signature of the Canadian samples is transitional between the two Southern African groupings. Table 4.1 summarises some of these similarities and differences. It is often argued that kimberlites inherit their trace element character almost exclusively from their mantle sources, because their abundances of compatible and incompatible elements are too high to be modified significantly by contamination. If this is the case, then the Canadian kimberlites do not appear to be derived exclusively from either a southern African Group I-like or Group II-like source. The effects of crustal contamination on the Canadian kimberlites are discussed further in Chapter 5.

Affinity of Canadian kimberlites	Elements
Southern African Group I	SiO_2, CaO, K_2O, Rb, Pb
Southern African Group II	Al_2O_3, Fe_2O_3, TiO_2, Na_2O, V, Ba
Intermediate	MgO, Ni, Cr, Nb
Both	Sr, La, Nd
Neither	Sc, Hf, Zr, Y, Sm, Lu

Table 4.1 Apparent similarities and differences between variation in abundance of selected major and trace elements within hypabyssal kimberlites from Canada and southern Africa. Based on data dispersion and distribution patterns shown in **Figures 4.2-4.3** and **Appendix E**.

4.3.2 Compositional variation in Canadian kimberlites

4.3.2.1 Introduction

This section investigates the detailed variations in chemical composition between and within selected Canadian kimberlite occurrences. A total of 94 new major and trace

element analyses have been acquired for hypabyssal facies samples from Canada. 80 of these are samples from the Slave craton, 70 of which are drawn from intrusions within the Lac de Gras kimberlite field. The kimberlites have been grouped for comparative purposes on a broadly geographical basis (Figure 1.5). The 14 samples from the Grizzly pipe are considered as an individual group to investigate the extent of any compositional heterogeneity within a single intrusion. Two additional groups incorporate the intrusions immediately adjacent to and outlying from Grizzly. Similarly, two groups cover the small clusters and more widely dispersed kimberlites around and to the south-east of Lac de Gras.

A further two groups encompass analyses from beyond the Lac de Gras field. One consists of all other hypabyssal samples from the Slave craton (Contwoyto Lake and South-East Slave), while the other contains all other hypabyssal samples from outside the Slave (Churchill and Superior provinces). No analyses of volcaniclastic kimberlite are included in these groupings.

4.3.2.2 Variation between Canadian kimberlite fields

88 of the Canadian hypabyssal samples analysed are drawn from just three individual kimberlite fields. This subset of the data is dominated by the 70 samples from Lac de Gras, but in addition there are 8 analyses from the Contwoyto field, which is located approximately 100km north of Lac de Gras, 9 analyses from the Somerset Island field (1200km NE of Lac de Gras) and one sample from Rankin Inlet in the Churchill province, approximately 1200km east of Lac de Gras. The range of variation in key major and trace element abundances for each of these fields is shown in Figure 4.8.
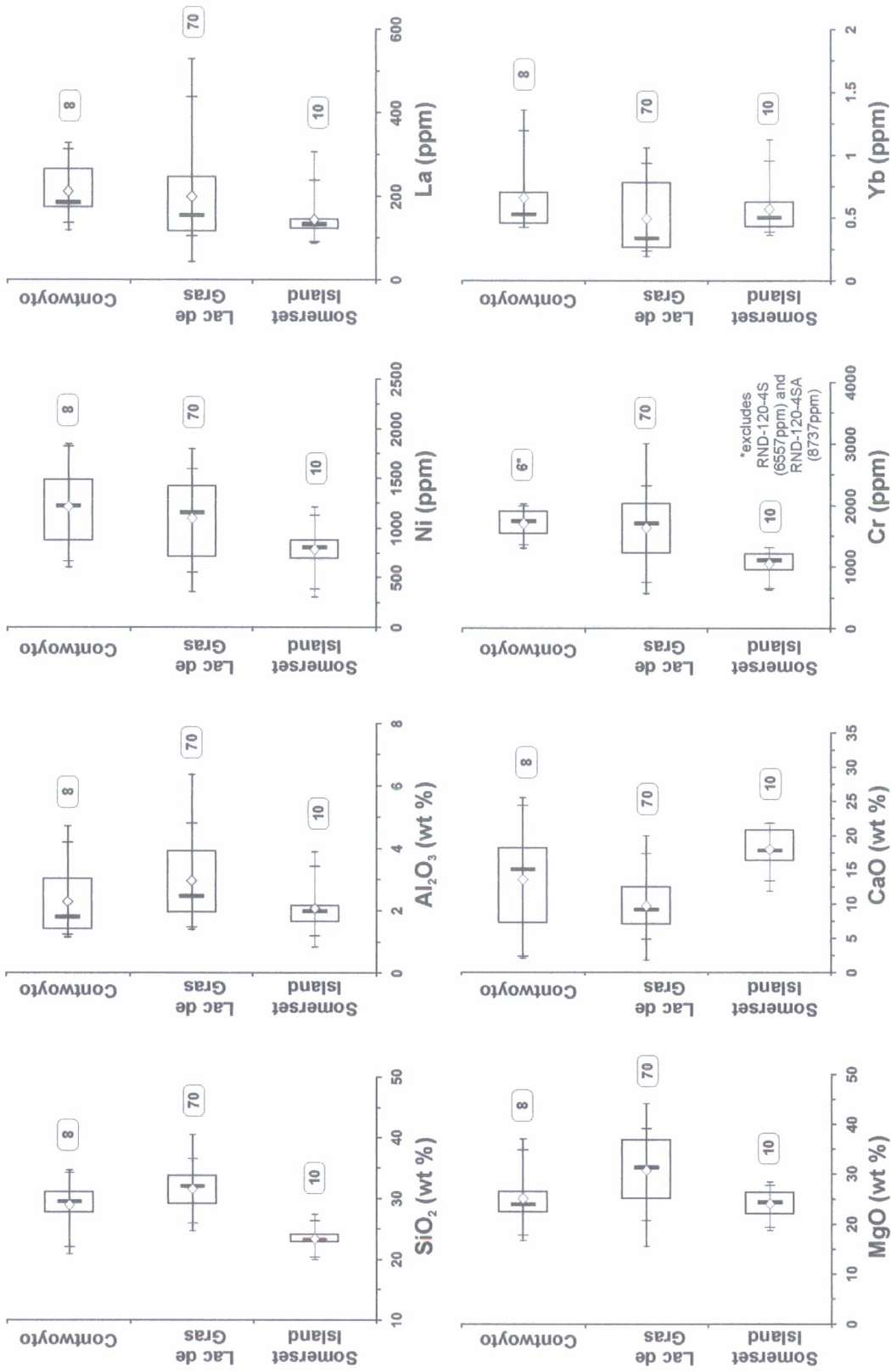
Figure 4.8 Dispersion of selected major and trace element data in hypabyssal kimberlites from the Contwoyto, Lac de Gras and Somerset Island fields. Legend as in **Figure 4.1**.

92

The Lac de Gras kimberlites have, on average, the greatest abundance of SiO_2, MgO and Al_2O_3, and the lowest abundance of CaO. The kimberlites from Somerset Island have the greatest CaO content, but these intrusions are emplaced into Palaeozoic platform carbonate sequences (e.g. Mitchell and Fritz, 1973). The median Ni and Cr content of the Lac de Gras and Contwoyto fields are very similar and greater than in Somerset Island kimberlites. This is quite surprising because the MgO content of the Contwoyto samples is considerably lower than that of Lac de Gras, and is more closely comparable to Somerset Island. While both Lac de Gras and Contwoyto host diamondiferous kimberlites with economic potential the Somerset Island kimberlites are very low grade or barren. The Somerset Island samples have lower La and higher Yb levels than the Lac de Gras average, and hence have flatter normalised rare earth patterns, which could be indicative of greater crustal contamination. The Contwoyto samples have both greater La and Yb than the Lac de Gras average, and have similar normalised La/Yb ratios to those in kimberlites from Lac de Gras. Since differential contamination would be expected to produce a range of La/Yb (see Chapter 5), the difference in REE content between Contwoyto and Lac de Gras kimberlites is most likely inherent to the magmas from these different regions, possibly generated by different amounts of melting in a common deep mantle source.

4.3.2.3 Group A1: Intra-kimberlite variation in Grizzly

Grizzly (Figure 1.5-1.6) is part of a large cluster of kimberlite bodies situated between Lac de Gras and Exeter Lake (see also Group B below). Most of these bodies have been emplaced within a syn-Yellowknife Supergroup composite intrusion of hornblende-biotite tonalite, biotite granodiorite and quartz diorite. The country rock to Grizzly at the present erosion level is quartz diorite (Kjarsgaard et al., 2002). The 14

Grizzly samples have been obtained from various depths within a single diamond drill-core. Most of the pipes owned and studied by BHP Billiton appear to contain more than one intrusive phase of kimberlite magma (D. Dyck, *pers. comm.*). It is impossible to be certain, therefore, that each Grizzly sample is representative of the same individual magmatic injection; the only assumption made for the purposes of this exercise is that all of the samples are derived from magmas that share a common source and have experienced very similar petrogenetic histories culminating in emplacement in extremely close proximity within a single kimberlite pipe. Nevertheless, some inherent variability in mineralogy (e.g. modal olivine content) between samples is an inherent feature of kimberlites and may contribute to any observed compositional variation.

The MgO contents of the Grizzly samples are among the highest of all from Lac de Gras (Figure 4.9), consistent with petrographic observations that these samples contain high modal abundances of olivine (Appendix B). The variation in MgO between the Grizzly samples could be generated by either addition (e.g. through contamination by lithospheric mantle) or removal (e.g. by fractionation) of olivine. This is investigated further in sections 5.3 and 5.5. The variation in MgO content cannot be attributable merely to differential volatile content and associated constant-sum effects, because recalculating the analysis on a volatile-free basis does not remove this observed variation. In addition, the samples from Grizzly have some of the lowest volatile (CO_2 + H_2O) contents of all the Canadian kimberlites analysed.
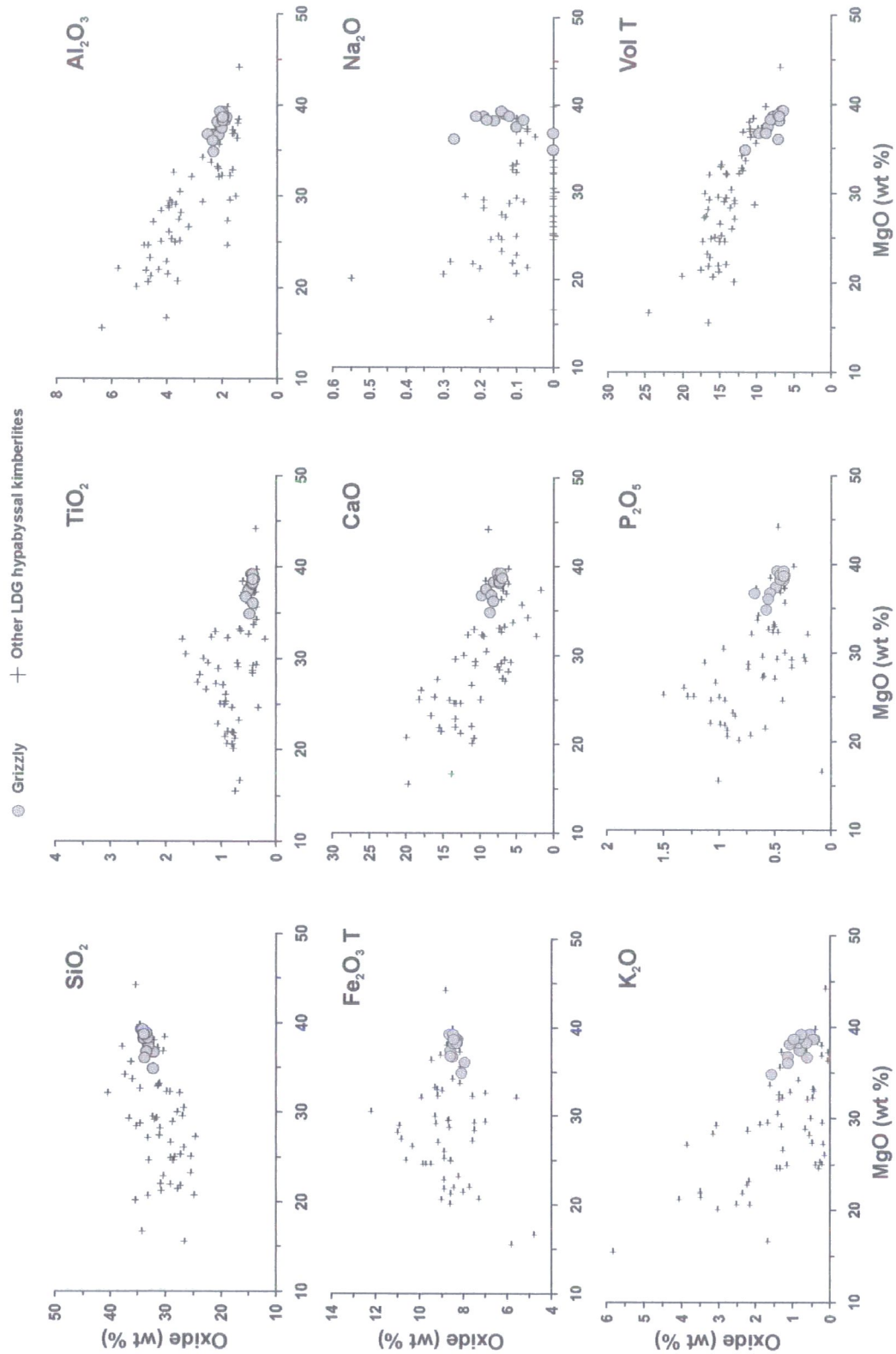
Figure 4.9 Major element compositional variation of hypabyssal samples from Grizzly, relative to other Lac de Gras kimberlites.

95

Increasing MgO content is associated with increases in abundance of SiO_2 and Fe_2O_3 T, and decreases in abundance of Al_2O_3, CaO, K_2O and P_2O_5. The abundances of the three major components of olivine are thus positively correlated, while most other major elements show negative correlations with MgO. The most notable major element variations within Grizzly are those of Na_2O and K_2O. Higher contents of these elements may indicate a greater contribution from crustal contamination or alteration processes, although variation in K_2O could also be controlled by differential content of phlogopite, or a variable dilution effect by differential olivine addition/removal. There is, however, no correlation between SiO_2 and K_2O content in these samples, which does not support phlogopite control. The general increase in SiO_2 and decrease in K_2O with increasing MgO is consistent with olivine control. Olivine and phlogopite addition/removal, and crustal contamination are discussed in detail in sections 5.3-5.5.

Trends in variation of trace element content in Grizzly are broadly consistent to those observed in the Lac de Gras kimberlites as a whole (Figure 4.10). The Grizzly samples are notably some of the least REE-enriched of all. The chondrite-normalised rare earth distribution pattern (Figure 4.10a) for Grizzly is parallel to the median distribution for Lac de Gras. Abundances of compatible elements (Figure 4.10b) are also close to the values of Lac de Gras, with the exception of Grizzly having slight relative depletions in Sc, Ti, V and Cu, and enrichment in Ni.
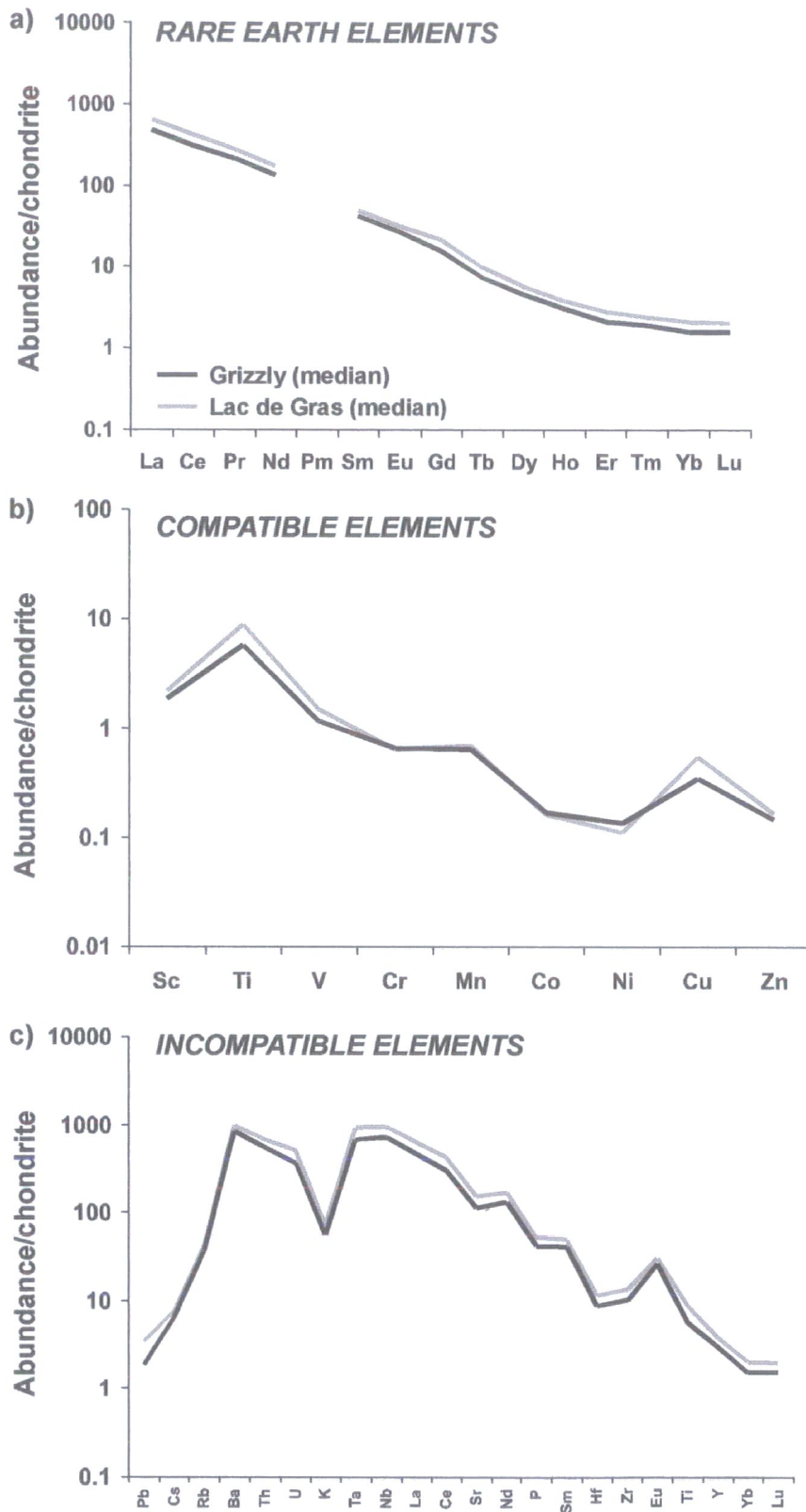
Figure 4.10 Variation in trace element composition in hypabyssal facies samples from Grizzly, relative to other Lac de Gras kimberlites.

On an extended incompatible element distribution diagram (Figure 4.10c), Grizzly has slightly lower Cs, Rb, Ba and K compared to the Lac de Gras median; otherwise the other elements are of similar abundance. The pronounced negative anomaly at K is a striking feature of this pattern that is commonly observed in both Group I and Group II kimberlites.

The number of separate samples analysed from Grizzly enables a comparison of intra-kimberlite compositional variation to be made against the Finsch kimberlite of South Africa, from which multiple samples have also been analysed (Fraser, 1987). Finsch is a group II kimberlite and is known to consist of several separate phases of intrusion (Fraser, 1987) corresponding to different textural-genetic facies and mineralogies. Consequently, some differences in the magnitude of major and trace element abundances in comparison to Grizzly are to be expected. Consistent with this hypothesis, Figure 4.11a-b clearly shows that the extent of variation in each oxide is much greater in Finsch than in Grizzly. At least three of these intrusive phases, plus internal and external dykes are represented in the 15 samples considered here, and this appears to account for much of the major element variation.

It is not known to what extent, if any, there are discrete intrusive phases at Grizzly, but the limited major element variation suggests that the body as sampled is relatively homogeneous. Sampling at Grizzly does not cover the entire extent of the kimberlite
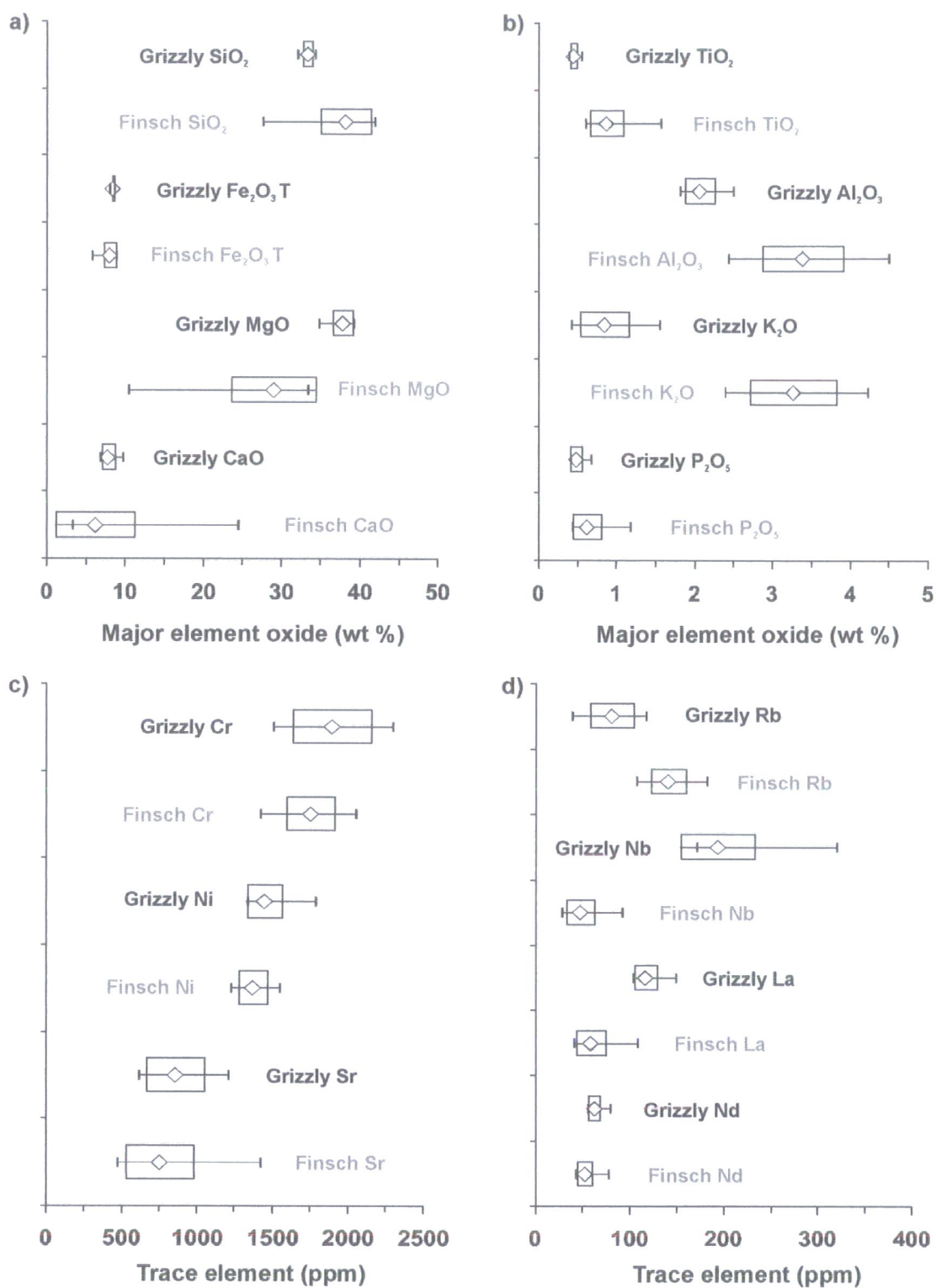
Figure 4.11 Relative variation of selected major and trace elements between samples from the Grizzly and Finsch kimberlites. Data for Finsch from Fraser (1987). Analysis based on 14 samples from Grizzly and 15 samples from Finsch.

body, as is the case at Finsch. The extent of trace element variations in Grizzly is similar to that observed in Finsch for Ni, Cr, Sr and Nd, but is more variable for Nb, La and Rb (Figure 4.11c-d).

4.3.2.4   Group A2: Neighbouring kimberlites to Grizzly

This group is composed of the other kimberlites situated between Lac de Gras and Exeter Lake (Figure 1.5). With the exception of Rat, all of these bodies are located within a 20km radius of Grizzly. Three kimberlites – Mark, Aaron and Arnie – form a tight cluster within just 2-3km of each other, and are all situated within a narrow outcrop of Itchen Formation metaturbidites of the Yellowknife Supergroup. Further to the west, the Rat and Pigeon bodies are also emplaced into metaturbidites at the present erosion level. The remainder of the kimberlites in this group (Roger, Koala West, and Leslie) intrude through a pluton of biotite granodiorite and hornblende-biotite tonalite (Kjarsgaard *et al.*, 2002).

Major and trace element variations within and between kimberlites in this group are illustrated in Appendix E. There is a large degree of major element variation between the individual kimberlites in the group. Intra-kimberlite variation is very limited in some kimberlites (e.g. Leslie, Roger, Pigeon) but is substantial in others (e.g. Rat, Aaron, Koala West). Leslie, Mark, Arnie and one sample from Aaron all have MgO contents in excess of 35 wt %, similar to that observed in Grizzly. Roger and Koala West have lower MgO and SiO_2 than Grizzly, but higher Al_2O_3 and P_2O_5. Pigeon also has in excess of 3 wt% Al_2O_3. Roger is the most Ca-rich of this group, while Pigeon and Koala West have similar CaO abundances to Leslie, Mark and Arnie.

Intra-kimberlite variations in trace element abundance are small in Roger, Koala West, Leslie and Pigeon, but are considerably greater in Rat and Aaron. Roger and Koala West tend to have the highest trace element abundances in this group, while Mark, Leslie and Pigeon have lower concentrations of trace elements, more akin to Grizzly. The chondrite-normalised rare earth distribution patterns of most of these kimberlites are parallel to each other and the trends observed in Lac de Gras as a whole. Aaron and Rat are the exception to this: in each of these bodies the sample with the lowest MgO has lower LREE-MREE and higher HREE concentrations than the other. This produces a flattening of the distribution pattern in the Eu-Lu range. The samples from Pigeon also display this MREE-HREE flattening, which is characteristic of crustal contamination.

Arnie, Mark and Leslie have some of the highest abundances of Ni and Cr in this group, while Roger and Koala West have some of the lowest. By contrast, Roger and Koala West contain high concentrations of Sc and Ti. The transition element signature of Pigeon is similar to that of Mark and Arnie, except for a notable depletion in Cr. The most anomalous transition element patterns are again displayed by low-MgO samples from Rat and Aaron.

All of the kimberlites in this group display a negative K anomaly on a normalised incompatible element distribution diagram. This anomaly is most pronounced in Arnie, Mark, Leslie and Roger, and least pronounced in Pigeon. The low-MgO 'anomalous' samples from Aaron and Rat tend to be less enriched in LILE and HFSE than the more MgO-rich samples from the same intrusions.

4.3.2.5 Group B: Other kimberlites north of Lac de Gras

The group is composed of two kimberlite clusters (Figure 1.5). The first is situated between Yamba Lake and Exeter Lake, and consists of the Porpoise and Rattler bodies, which are emplaced into biotite monzogranite, and the Anaconda body, which intrudes through biotite granodiorite and hornblende-biotite tonalite (Kjarsgaard *et al.*, 2002). The second cluster, consisting of the Cretaceous Anne (HL-10), Finlay (HL-11) and Don (HL-12) intrusions, is located a few kilometres south of Hardy Lake, north-east of Lac de Gras. These kimberlites have also been emplaced into biotite monzogranite at the current erosion level (Kjarsgaard *et al.*, 2002). There is a distance of approximately 50km between the two clusters, although within each cluster only 5-10km separates the individual kimberlites.

Major and trace element variations within and between kimberlites in this group are illustrated in Appendix E. The extent of major element variation between these kimberlites is very similar to that observed in the bodies adjacent to Grizzly. The Don kimberlite has the closest major element composition to Grizzly, although its SiO_2 and K_2O contents are slightly higher and its CaO content is lower. The other kimberlites in this group have MgO contents below 35 wt%. Anaconda and Porpoise are the only two bodies to display intra-kimberlite variations; they have a range of MgO and most other major oxides. Finlay and Porpoise have significantly higher Al_2O_3 than the other bodies in these two clusters. Anaconda, Rattler and Porpoise all have CaO contents in excess of those in the kimberlites from the Hardy Lake area.

All six kimberlites in this group have typical normalised rare earth patterns parallel to the overall Lac de Gras trend. Finlay has the highest abundance of REEs, while Anne,

Don and Anaconda are the most deficient in these elements. Rattler and Porpoise show a small range of intra-kimberlite variation in the REEs and some compatible elements. Porpoise is notably depleted in Ni, Cr and V relative to the Lac de Gras median; this kimberlite has the lowest MgO in this group. Don also has lower Ni than is typical among the Lac de Gras kimberlites. None of these bodies display any significant intra-kimberlite variation across the other incompatible elements, with the exception of an anomalous U spike in one of the samples from Anne. The negative K anomaly is present in all of these samples to varying degrees and is most pronounced in the Anaconda and Don kimberlites.

4.3.2.6   Group C: Kimberlites south and east of Lac de Gras

This group of six kimberlites again consists of two clusters of three bodies, separated by about 15km (Figure 1.5). The first cluster consists of T-34, T-35 and T-36, while to the east lie T-19, T-21 and T-237. All of these kimberlites intrude through metasedimentary rocks of the Yellowknife Supergroup (Kjarsgaard et al., 2002).

Major and trace element variations within and between kimberlites in this group are illustrated in Appendix E. All of these samples have significantly lower MgO (<30 wt%) and higher Al_2O_3 (>3 wt%) contents than those of Grizzly. The T-36 and T-237 kimberlites show some intra-kimberlite variation in MgO and other major oxides. Major element variation within the other kimberlites in this group is minimal.

Intra-kimberlite trace element variations are also rare amongst these six kimberlites. In each case the normalised REE patterns are mutually parallel, but all show a tendency towards flattening out in the MREE-HREE range. The REE contents of all these

samples are higher than the median value for Lac de Gras. Similarly, the Ni and Cr abundance in all of these samples is lower than typical for the Lac de Gras suite as a whole. Together with the lower MgO and higher Al_2O_3 contents, and higher MREE and HREE, this could be evidence of dilution of a typical 'olivine' signature with crustally derived material (see Chapter 5). Incompatible element abundances are similar to or greater than the Lac de Gras median value. K anomalies are generally smaller than those observed in the kimberlites situated on the north side of Lac de Gras. This is most pronounced in this group in the T-237 body, and is again consistent with addition of crust (Chapter 5).

4.3.2.7 Group D: Other Lac de Gras kimberlites

This group covers the remainder of the hypabyssal samples drawn from seven widely spaced intrusions around the immediate area of, and to the south and far east of Lac de Gras (Figure 1.5). The easternmost extent of the study area is marked by the kimberlite at Nicholas Bay, on the northern shore of Aylmer Lake. Nicholas Bay, TR-107 and DD-39 are emplaced within Yellowknife Supergroup metasediments, while the other kimberlites of this group intrude muscovite-biotite monzogranites (Kjarsgaard et al., 2002).

Major and trace element variations within and between kimberlites in this group are illustrated in Appendix E. The inter-kimberlite major element variation observed between these seven bodies is very large, encompassing almost the entire range seen in the Lac de Gras field. Intra-kimberlite variation is again limited, with only Misery, Misery East and T-146 showing any significant differences between samples from a single body. DD-39 has the highest MgO content, comparable to that of Grizzly, while

TR-107 and T-146 are the most MgO-poor. These two samples also have high Al_2O_3, K_2O, Na_2O and P_2O_5. Only DD-39, Misery and Misery East contain less than 3 wt% Al_2O_3 in this sample group.

The general lack of intra-kimberlite variation is again also reflected in the trace element compositons of these kimberlites. All have mutually parallel normalised REE patterns. The greatest abundance of REEs is found in T-146 and TR-107, while all the other bodies have REE contents typical of the Lac de Gras median.

The MgO-poor kimberlites from T-146 and TR-107 are depleted in Ni and Cr relative to the Lac de Gras median. These kimberlites also have a commensurate excess of Sc, V and Ti relative to the more MgO-rich bodies in this group. T-146 and TR-107 are also significantly enriched in incompatible elements relative to the other kimberlites in this group and the Lac de Gras median. DD-39 appears to be depleted in Cs and Rb relative to Lac de Gras as a whole, and with Misery is the one of only two kimberlites to display a negative K anomaly of a comparable magnitude to those observed in the more northerly groups. Petrographically, these two kimberlites are more similar to the intrusions on the northern side of Lac de Gras (groups 1 and 2).

4.3.2.8 Group E: Slave kimberlites outside the Lac de Gras area

This group includes kimberlites from the Contwoyto field (Jericho and Muskox), and from the South-East Slave field (Kennady Lake and Snap Lake). Sample JD-51 from Jericho has been proposed by Price *et al.* (2000) to be a compositional proxy for a primary kimberlite liquid, on the basis of an absence of any evident macrocrystal olivine.

Major and trace element variations within and between kimberlites in this group are illustrated in Appendix E. The extent of intra-kimberlite major element variation appears to be greater in these kimberlites than that typical of Lac de Gras intrusions. Unfortunately only single samples of hypabyssal material were obtained from the South-East Slave bodies, so intra-kimberlite variations in this area cannot be assessed. The two samples from RND-120 (Jericho) have very disparate MgO contents, potentially indicating a large amount of differential olivine addition/subtraction. This is also observed to a lesser extent in JD-69. Only a single sample from RND-120 has an MgO content similar to that of Grizzly. JD-51 has very low MgO, in accordance with its olivine-poor nature. The Jericho samples are also notable for displaying a wide range in CaO from one intrusion to another. JD-69 and JD-82 are the only kimberlites in this group to have Al_2O_3 contents below 3 wt%.

RND-120 is highly enriched in trace elements relative to the other kimberlites in this group and those from Lac de Gras. The MREE-HREE abundances in JD-51, JD-69 and JD-82 are also elevated relative to the Lac de Gras median. The negative K anomalies are more accentuated in the kimberlites from the Contwoyto field.

4.3.2.9 Group F: Canadian kimberlites beyond the Slave Province

Analyses have been obtained on a further nine samples from kimberlites located outside the Slave craton. Four samples analysed for this study are from separate kimberlites (Batty Bay, Elwin Bay, Jos and JP South) from Somerset Island, which is located at the northern end of the Gulf of Boothia and is part of the Churchill Province. For comparison, a further four analyses of a Somerset Island kimberlite (Nikos) from

the study of Schmidberger *et al.* (2002) are included. An additional sample from the Churchill Province is also included from the kimberlite at Rankin Inlet. Four samples are also taken from the Attawapiskat, Kirkland Lake and Timiskaming fields of the Superior Province. The two samples from the Timiskaming field are taken from different kimberlites (Guigues and Peddie).

Major and trace element variations within and between kimberlites in this group are illustrated in Appendix E. The four samples from Nikos (Schmidberger *et al.*, 2002) on Somerset Island do not provide strong evidence for intra-kimberlite homogeneity in this body. As in the other kimberlite groups investigated, there is a considerable range of major element compositions between different kimberlites. The samples from Kirkland Lake and Timiskaming have the highest MgO contents, although these are still lower (<35 wt%) than the values typical of Grizzly. The Churchill Province samples are notable for their high TiO_2 and CaO, and low SiO_2 and Fe_2O_3 T relative to Lac de Gras kimberlites. High CaO contents in the Somerset Island kimberlites may be related to the carbonate sedimentary cover through which the bodies intrude in this area (Mitchell and Fritz, 1973). Alternatively, this could be due to higher modal proportions of primary magmatic carbonates.

All the kimberlites from the Churchill and Superior provinces show considerable trace element deviations from the median of the Lac de Gras dataset. The Churchill province kimberlites are variably enriched in REEs relative to those from Lac de Gras. The samples from the Superior province display a range of REE enrichment and depletion relative to Lac de Gras, and the REE patterns from Attawapiskat and Kirkland Lake are noticeably flattened in the MREE-HREE.

The Churchill province kimberlites analysed in this study are variably depleted in Cr and Ni, and enriched in Ti, relative to Lac de Gras. Only partial compatible element data is reported by Schmidberger *et al.* (2002), so this data is not included here. The Superior province kimberlites are also Cr-poor and Ti-rich relative to Lac de Gras. The patterns of variable enrichment and depletion in REEs relative to Lac de Gras also apply broadly for other incompatible elements. All the kimberlites from both the Superior and Churchill provinces have a negative K anomaly.

4.3.2.10 Summary

Although a large range in major and trace element abundances is evident between kimberlites on both a local and regional scale, there is a striking degree of intra-kimberlite homogeneity in many intrusions. This is exemplified by the limited variation observed between the multiple analyses of hypabyssal kimberlite from the Grizzly pipe. Many of the most MgO-rich kimberlites analysed, including Grizzly, are found within 20km of each other between Lac de Gras and Exeter Lake. Similarly, the majority of kimberlites from south and east of Lac de Gras have Al_2O_3 and HREE contents indicating more extensive contamination by crustal material.

Where intra- and inter-kimberlite geochemical variations do occur, they tend to be coupled across the major and trace element chemistry of the kimberlite (e.g. variations in MgO are coupled with those in Ni and Cr; adding olivine to a magma may concentrate these elements and 'dilute' others, such as the HREEs). Certain element distribution patterns are characteristic of kimberlites, such as high LREE/HREE ratios and negative anomalies in K relative to other LILE and HFSE elements. Variations in

the magnitude of these characteristics may also be diagnostic of variable addition and subtraction of material derived from the mantle and crust. The effect of processes such as contamination, alteration and fractionation on the elemental geochemistry of kimberlites is investigated in detail in the next chapter.

Chapter 5

Major and trace element geochemistry – processes

5.1 CHAPTER OVERVIEW

In this chapter, the detailed major and trace element data presented in Chapter 4 are used to investigate the processes responsible for modifying the chemistry of a kimberlite melt subsequent to separation from its mantle source region. There are four main controls which may operate to varying degrees: contamination of the magma by physical incorporation of lithospheric mantle xenoliths, contamination of the magma by continental crust, fractionation of early crystallising phases from the magma, and post-emplacement alteration. Each of these processes and their effects on kimberlite geochemistry is discussed.

5.2 ALTERATION

5.2.1 Nature and extent of alteration processes

Mineral assemblages typical of kimberlite are very susceptible to alteration, which proceeds by a range of processes, often in discrete stages. There are two main phases of alteration. The first is a deuteric process, whereby late-stage fluids cognate to the intrusion interact with the kimberlite mineralogy. Subsequently, post-emplacement weathering processes can produce alteration and leaching of the kimberlite by groundwater in the near-surface environment.

Deuteric alteration occurs during and immediately after emplacement of the kimberlite and may be promoted by high volatile contents in the magma, which exsolve during the eruptive phase. This process can result in partial to complete replacement of olivine macrocrysts by pseudomorphs of fine-grained serpentine and redistribution of primary carbonate within the groundmass (Spriggs, 1988; Tainton, 1992). The subsequent alteration of serpentine to other low-temperature hydrated magnesium silicates such as vermiculite and saponite (Kresten, 1973) are an extension of these deuteric processes, rather than weathering effects. Spriggs (1988) maintains that the bulk composition of the system remains unchanged by deuteric alteration, although Kresten (1973) argues that some material will be lost in solution, such as brucite, which is a common by-product of the breakdown of olivine to serpentine. The resulting low activity of Mg^{2+} in the system is the driving force for subsequent formation of vermiculite and saponite (Kresten, 1973).

Weathering processes may occur at any time after emplacement of the kimberlite and result in the breakdown of phlogopite and serpentine to chlorite, a variety of clay minerals including illite, kaolinite and montmorillonite, calcite and calc-silicates such as members of the epidote group (Kresten, 1973; Deer, et al., 1992). Secondary serpentine may be formed as fibrous overgrowths on olivine pseudomorphs which are distinct from deuteric serpentine (Spriggs, 1988). Removal of material from the system, in particular leaching of mobile elements in solution, is common during weathering (Fesq, 1975; Spriggs, 1988; Tainton, 1992). Calcretes and lateritic assemblages often develop at the near-surface (Kresten, 1973; Tainton, 1992), particularly in tropical latitudes (Fairbairn and Robertson, 1966).

All kimberlites that ascend fully through the crust and become emplaced in a surficial environment are likely to be affected to some degree by circulating groundwater fluids, or by exposure to subaerial weathering processes. Crater and diatreme facies rocks are thus more likely to be immediately subject to near surface alteration, but erosion could subsequently bring any level of the kimberlite intrusion into the near surface alteration zone. Tainton (1992) describes how alteration in dykes of hypabyssal facies kimberlite from South Africa tends to decrease from the margins to the centre of the feature, suggesting ingress of fluids along the contact between the dyke and the country rock, whereas in the diatreme environment alteration is more evenly distributed throughout the pipe. This is probably due to the inherent high porosity of crater and diatreme facies kimberlite. It is conceivable that fluids responsible for alteration could exploit fractures and other structures to reach any part of a kimberlite body.

In general, massive hypabyssal facies kimberlite has low porosity and should be less altered than the kimberlite breccias of the diatreme facies. Consequently hypabyssal facies rocks are the preferred focus of the current study. Petrographic examination of the LDG samples indicates that they have experienced variable, but limited post-emplacement alteration (Armstrong et al., in press), particularly in relation to many hypabyssal kimberlites from southern Africa (B. A. Kjarsgaard, pers. comm.). Mitchell (1986) suggests that in many studies of South African kimberlites, samples categorised as 'fresh' are in fact altered to some extent.

5.2.2 Mineralogical and chemical effects of alteration processes

Modification of the whole-rock chemistry by weathering and other near-surface alteration processes is a complex function of the specific mineralogy of the kimberlite,

the chemistry of the fluids involved and the amount of alteration that takes place. The pre-alteration bulk chemistry of the rock is already a function of the initial primary magma composition, the amount of mantle and crustal material assimilated by the kimberlite magma during ascent, and crystal fractionation processes. The rate and extent of alteration may be controlled by proximity to the surface, and thus indirectly by the ambient rate of erosion, together with other structural characteristics of the local geology and prevailing conditions of subsequent hydrothermal systems. Despite the complex nature of the problem, it is possible to make some observations about the probable effects of alteration based on the few studies that have actively included these rocks (e.g. Fesq *et al.*, 1975; Taylor *et al.*, 1994).

Alteration processes do not affect all the mineralogical constituents of a kimberlite equally, although the phases that are typically altered often tend to be some of the most modally abundant. These include olivine, which becomes partially or fully serpentinised, phlogopite, which is degraded to chlorite and other clay minerals, and carbonates such as calcite and dolomite (Fairbairn and Robertson, 1966; Tainton, 1992; Taylor *et al.*, 1994). Primary carbonates are leached from kimberlite by some fluids, and reintroduced as secondary carbonates by others (e.g. formation of magnesite during serpentinisation; re-precipitation of calcite from solution, e.g. Armstrong *et al.*, in press). These different phases of carbonate can be difficult to resolve chemically, although detailed studies of mineral chemistry are currently being conducted to assess their relative contributions (e.g. Armstrong *et al.*, in press).

The replacement of olivine by serpentine and, subsequently, other minerals proceeds by several chemical reactions, examples of which are given in Deer *et al.* (1992). Further

decomposition of serpentine to talc, chlorite, other clays and carbonates such as calcite and magnesite is dependent on the H_2O and CO_2 content of the ambient pore fluids (Deer *et al.*, 1992). The net flux of elements during these processes tends to lead to a decrease in the Mg, Fe^{2+} and Si content of the rock and an increase in the Al, Fe^{3+} and Ca content. Serpentinisation also produces a large net decrease in the density of the rock, and thus there is a large volume expansion for a given mass of material.

Phlogopite is a major constituent of Group II kimberlites but is also often found as a groundmass phase in Group I intrusions, and more rarely as a phenocryst phase. During alteration it degrades to sericite, chlorite and a range of other clays, as well as calcite and epidote group minerals (Deer *et al*, 1992). These reactions lead to a decrease in Mg and K coupled with an increase in Al and Ca.

The clay minerals introduced by alteration of both olivine and phlogopite are capable of hosting a variety of trace elements. The more mobile incompatible elements in these systems tend to be those with large ion lithophile tendencies, such as the alkaline (e.g. Rb, Cs) and alkaline-earth metals (e.g. Sr, Ba) and the lightest rare earth elements (La, Ce). Other incompatible elements, such as the high field strength elements (e.g. Nb, Ta, Hf, Zr) are considered to be relatively immobile during alteration. Taylor *et al.* (1994) suggested the following order of mobility on the basis of analyses of altered kimberlites from Liberia:

MOBILE   Sr $\approx$ Rb > Ba > La $\approx$ Ce > P $\approx$ Zr > Nb   IMMOBILE

This is consistent with the study of Nesbitt *et al.* (1980), which found that alkaline and alkaline-earth elements with smaller ionic radii (e.g. Na, Ca, Sr) are preferentially removed in solution during weathering while those with larger ionic radii (e.g. Rb, Cs, Ba) are mobilised but become adsorbed onto clays and so remain within the weathering profile unless mass wasting processes (e.g. erosion) are active.

Aside from major and trace element, it seems probable that there is some relationship between volatile content and the degree of alteration of a sample. The role of H_2O and CO_2 in serpentinisation and carbonation of the rock has already been noted. Unfortunately, the pattern is complicated due to the naturally high and variable volatile content of kimberlite magmas. There is also a lack of information regarding the extent to which the magma devolatilises during emplacement and to which volatiles (particularly CO_2) are lost from the system during alteration. Given the number of unconstrained factors influencing volatile content it seems unwise to use this in isolation as a measure of alteration.

5.2.3 Identifying major and trace element indicators of alteration

Identifying major and trace element variations that are characteristic of alteration is not straightforward. The effects of alteration can be difficult to distinguish from the effects of crustal contamination. In addition, most studies (including this one) have deliberately avoided analysing altered material. Well-characterised altered kimberlites are therefore scarce. Gurney and Ebrahim (1973) reported major element analyses of 25 kimberlites from Lesotho, subsets of which constitute suites of fresh to altered material from individual localities, e.g. Lemphane. Fesq *et al.* (1975) presented major and average trace element data for a selection of South African kimberlites, including

the contaminated and altered Koffiefontein and Ebenhaezer intrusions. They noted relative depletion of Cs > Rb > K in the vicinity of contacts between kimberlite dykes and country rock, and suggested the use of the ratios K/Rb, K/Cs and Th/U as tracers of alteration.

More recently, Spriggs (1988) attempted a more detailed major and trace element comparison of fresh and altered kimberlites from Namibia. A number of trends can be identified relative to Nb content on binary variation diagrams that appear to discriminate the effects of alteration from those of fractionation and crustal contamination. The main observations of this study were that alteration, or some combination of alteration and contamination, causes depletion of alkali and alkaline-earth elements along with P and Pb. Taylor et al. (1994) also presented major and trace element data for two suites of kimberlites: a set of variably contaminated hypabyssal and volcaniclastic samples from the Koidu area of Sierra Leone, and a set of altered but apparently uncontaminated kimberlites from just below the weathering profile at Sample Creek, Liberia. They concluded that high total H_2O content together with depletion in CO_2 and mobile incompatible elements are the most diagnostic geochemical signatures of alteration in these rocks.

Although the binary variation alteration vectors of Spriggs (1988) provide a reasonable fit to the few Namibian data, it is difficult to apply these same vectors successfully to other similar datasets, such as that of Taylor et al. (1994). The main reason for this is that Spriggs (1998) expresses the alteration vectors in terms of concentrations, which tend to be specific to a particular suite of related rocks. Given the large scope for relative enrichment and depletion in many elements between kimberlites from different

fields, or even neighbouring intrusions, it is more appropriate to work in terms of elemental ratios if we want to develop a more general scheme for recognising signatures of alteration.

A possible approach to identifying trends of progressive alteration in kimberlites is to attempt to quantify the development of clay minerals within the bulk rock as a result of post-emplacement weathering-related processes. This will, on average, lead to an increase in the abundance of SiO_2 and Al_2O_3, with a decrease in MgO. The Na_2O/K_2O ratio is also likely to increase. Unfortunately, these are also the trends produced by crustal contamination of a kimberlite (Section 5.4), making it highly problematic to assess the relative contributions of alteration and contamination.

An alternative approach is to utilise the differential mobility of minor and trace elements released from minerals during weathering. A wide variety of minerals are found in kimberlites (Mitchell, 1986; 1995), but by far the most abundant of those phases susceptible to alteration are olivine and phlogopite. Primary groundmass calcite, the content of which is very variable between kimberlites, and apatite are also commonly re-precipitated or replaced as a result of interaction with groundwater.

Although the majority of olivine serpentinisation is thought to occur as an isochemical, deuteric process, in reality some Mg is likely to be lost from the system during serpentinisation as a result of formation and subsequent dissolution of brucite (Kresten, 1973). The principal trace elements hosted by olivine are compatible elements such as Ni and Cr, which are not considered to be particularly mobile. Using Mg or elements such as Ni and Cr as tracers of alteration within a suite of rocks would be complicated

by the hybrid nature of kimberlite, which results in samples having very variable olivine contents that differ from those of the primary magma.

The decomposition of phlogopite to a succession of clay minerals during weathering is potentially a better approach to identifying alteration effects, since phlogopite is the main host for a variety of alkaline and alkaline-earth elements such as K, Na, Ca, Ba, Rb and Cs (Deer et al., 1992). Sr is also present as an interlayer cation in phlogopite, but is mainly hosted within carbonate phases. It may be mobilised as a result of groundwater dissolution and re-precipitation of primary carbonate. The most leachable of these cations tend to be those with low ionic charge (i.e. 1+ or 2+) and small ionic radius. These are easily mobilised by exchange with H^+ ions in acidic groundwater fluids and are less readily adsorbed into exchange sites in clay minerals than larger radius cations (Nesbitt et al., 1980). Na, Ca and Sr are thus more extensively removed in solution while Rb, Cs and Ba will tend to remain to some extent in the clay-rich, weathered portion of the kimberlite.

Apatite has been observed to be pseudomorphed by late-stage calcite in some kimberlites (Mitchell, 1986). Weathering of apatite may also release other elements that substitute for Ca in the apatite structure, such as Sr and LREEs.

In contrast to these easily weathered phases, some trace elements are primarily hosted in more refractory oxide minerals such as perovskite. Nb is particularly abundant as a substitute for Ti in the dysanalyte variety of this mineral, along with lesser amounts of Ta; REEs are enriched in the knopite and loparite varieties (Boctor and Boyd, 1979; Deer et al., 1992). Abundances of these relatively immobile elements should therefore

remain virtually constant throughout weathering processes. This is borne out by the choice of Nb as an immobile reference element by Spriggs (1988) in his bivariate 'alteration vector' diagrams and by its common utilisation in geochemical classification schemes. Nevertheless, under some weathering conditions refractory phases like perovskite and ilmenite can break down to products such as leucoxene (Mitchell, 1986; Heaman and Kjarsgaard, 2000). Thus, no element is entirely resistant to the effects of alteration.

5.2.4 Quantifying alteration

Compositional datasets for kimberlites from Namibia (Spriggs, 1988) and West Africa (Taylor *et al.*, 1994) contain both fresh and altered samples and provide the best opportunity within the literature to investigate the effect of alteration on selected elemental abundances. If parameters capable of charcterising alteration in these kimberlites can be identified, they may be applicable to identifying alteration in the Canadian kimberlites. In the case of the Gibeon kimberlites, both fresh and altered samples are from the same kimberlite field, all samples are hypabyssal and there is good evidence that all the rocks are genetically related (Spriggs, 1988). This not the case for the West African samples, which are drawn from different fields in Sierra Leone (fresh samples) and Liberia (altered samples). It cannot be assumed that there is any genetic link between the magmas that were emplaced in these two areas. Consequently, while there is considerable variation in the abundance of some elements between the populations of 'fresh' and 'altered' kimberlites (Figure 5.1) in West Africa, these variations cannot exclusively be attributed to alteration, and this data should be treated with caution. It is included in Figures 5.1 and 5.2 for comparison purposes only.
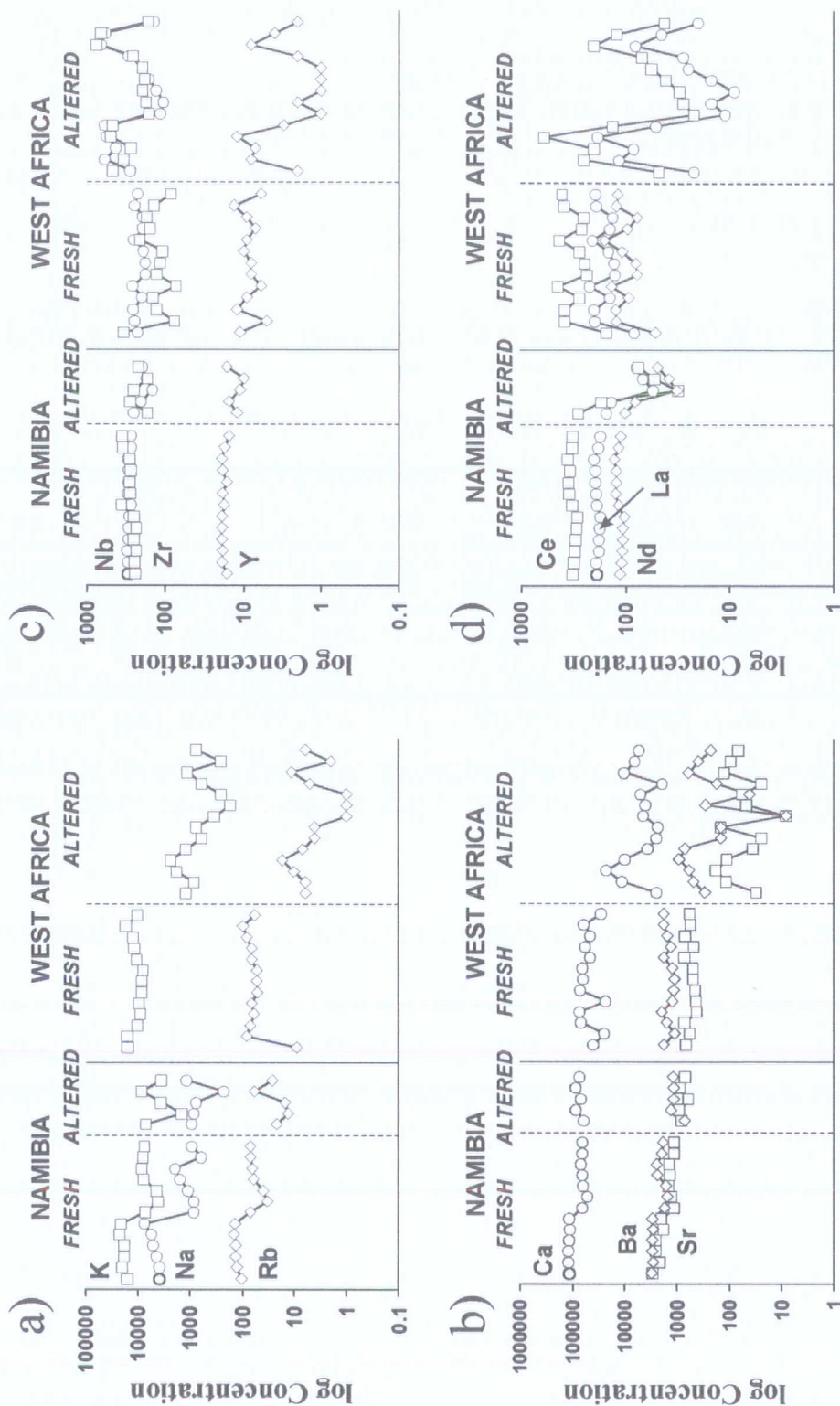
Figure 5.1 Variation of elemental abundance in kimberlites from Namibia (Spriggs, 1988) and West Africa (Taylor *et al.*, 1994). a) Alkaline elements; b) Alkaline-earth elements; c) High field strength elements; d) Light rare earth elements. All Namibian kimberlites are from the Gibeon province. Unaltered West African kimberlites are from the Koidu field, Sierra Leone; altered West African kimberlites are from the Sample Creek field, Liberia.

The greatest difference between elemental abundances in fresh and altered kimberlites from Gibeon is seen in the LILEs and LREEs (e.g. Na, K, Rb, Ce), with more moderate variation in elements such as Ba and Sr, and very little variation in Nb (Figure 5.1). Some of the reduction in abundances, particularly of less mobile elements, may be due to volume expansion in the rock as a result of serpentinisation. This will reduce elemental abundances on a weight-for-weight basis. These observations are broadly supported by the West African data, and are reasonably consistent with the arguments concerning relative element mobility developed above.

The differential mobility of elements can be used as a basis for discriminating between chemically altered and fresh material, and to provide some indication of the extent to which the alteration has proceeded. The theoretical considerations and practical examples presented above suggest that the most effective indicators of alteration should take the form:

[Alkaline *or* Alkaline-earth element] / [HFSE]

Suitable choices of element would include Na, Rb, Ca, Sr for the numerator and Nb, Ta, Hf, Zr, Y for the denominator. In practice there are some limitations on these selections. For instance, the use of Ca is questionable given the extreme variability in abundance of this element between kimberlites. Also, high quality Ta and Hf data for altered kimberlites in the literature is very limited.

Examination of various trace element log-ratio pairs indicates that few are able to discriminate fully between samples known to be altered, and those considered

relatively fresh. Despite Na being supposedly one of the most mobile elements, Na/HFSE ratios cannot distinguish between fresh and altered samples. This may be due to opposing effects of Na being removed by leaching, but introduced by crustal contamination. Ratios involving K, Rb or Ba are sensitive to the presence of phlogopite in the sample. Consequently, the field of fresh mica-rich (principally South African Group II intrusions) and mica-poor kimberlites are offset in K-Ba-HFSE or K-Rb-HFSE space.

Ratios involving Ce, Ba and Sr in association with HFSEs appear to be most effective at discriminating between fresh and altered material in African kimberlite datasets (Figure 5.2). These ratios are not sensitive to variable volatile content between samples. Both the change in magnitude of the ratio (Figure 5.2a-c) and the change in relative abundance of numerator and denominator (Figure 5.2d-f) are illustrated. The relative change in elemental abundance between Ce-Nb, Ba-Nb and Sr-Nb in fresh and altered samples is quite clear, even when there appears to be little change in the ln (Ba/Nb) or ln (Sr/Nb) ratios. The trends observed are consistent with progressive removal of Sr, Ba and Ce from less refractory phases like phlogopite, apatite and calcite. Crustal contamination is likely to lead to rapid reduction in the Nb concentration in any mixture with a typical kimberlite composition, relative to reduction in Ce, Ba or Sr. Consequently, it should be possible to discriminate crustal contamination trends from alteration trends using these parameters.
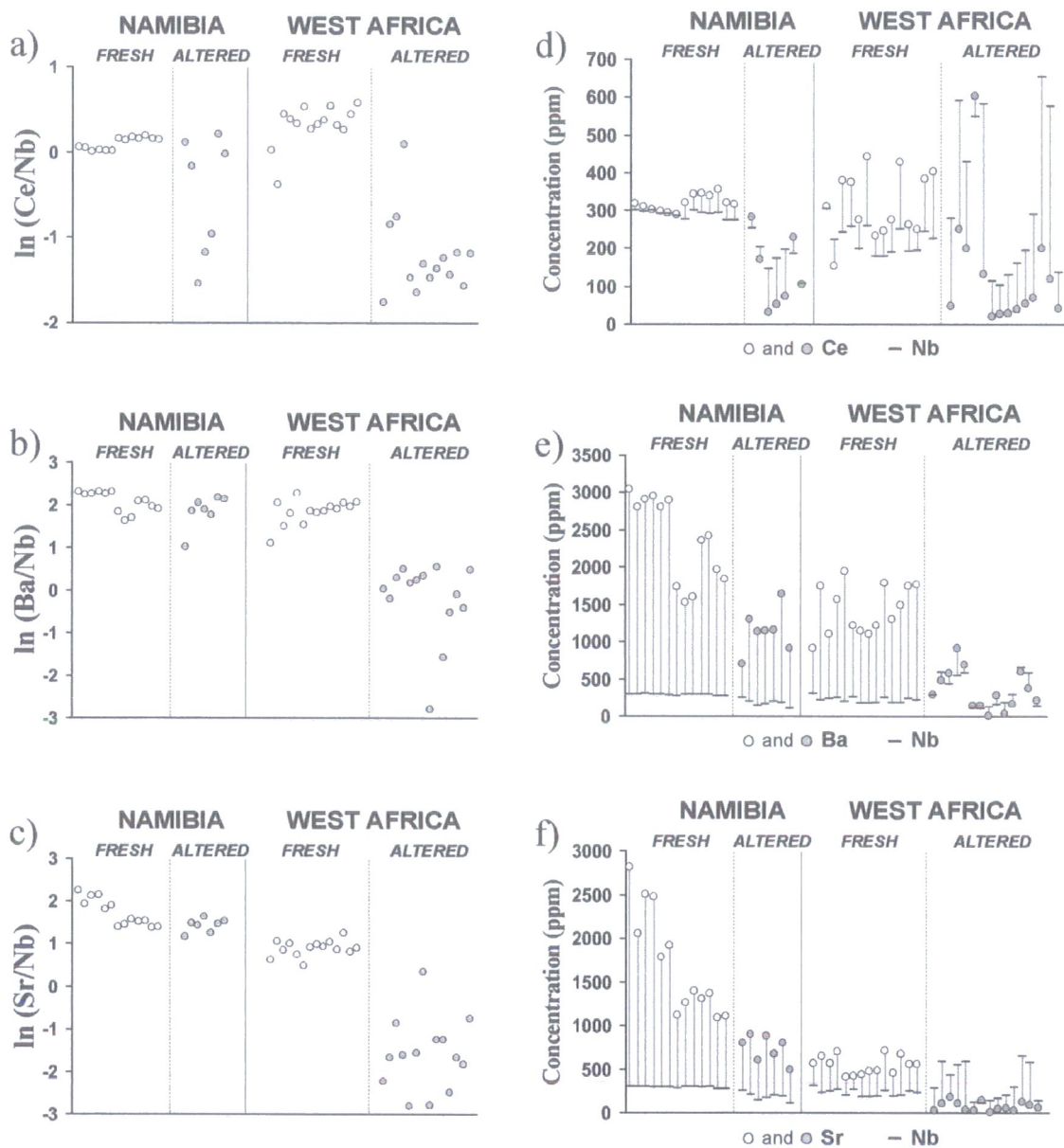
Figure 5.2 Variation of log-ratios and abundances of selected elements that demonstrate differential mobility during alteration in kimberlites from Namibia (Spriggs, 1988) and West Africa (Taylor *et al.*, 1994).

5.2.5 Alteration in the LDG and other Canadian kimberlites

Hypabyssal samples from LDG are recognised as being generally less altered than those from many African kimberlites, but the 16 volcanilcastic samples analysed from LDG might be expected to show some chemical effects of alteration. There is in fact very little offset towards low Ce/Nb, Ba/Nb and Sr/Nb apparent in either the hypabyssal or volcaniclastic kimberlites from LDG (Figure 5.3). In the case of all three parameters the LDG data display limited scatter around a median value ($\sim$0.1 for ln [Ce/Nb]; $\sim$2.3 for ln [Ba/Nb]; $\sim$1.5 for ln [Sr/Nb]). Although some samples plot well below the median value for a particular log-ratio parameters (Figure 5.3a-c), none do so consistently for all three parameters. It is difficult to rule out the inherent compositional variability of kimberlites as being the possible cause of these variations. There is very little variation evident in the volcaniclastic kimberlites relative to the hypabyssal samples, suggesting that any additional alteration in the volcaniclastic rocks is not detectable on the basis of log-ratios alone.

An analysis of the relative abundance of Ce, Ba, Sr and Nb in the LDG samples (Figure 5.3d-f) indicates that two samples, from Aaron (AAR-2) and Rat (RAT-4), have very low abundances of all these elements. These trends are not, however, well correlated with low ln (Ce, Ba, Sr/Nb) and consequently could be recording crustal contamination, or a combination of crustal contamination and alteration. Several of the volcaniclastic kimberlites from LDG have similar low Ce, Ba, Sr and Nb abundances, and low Ce/Nb, Ba/Nb and Sr/Nb; these rocks might be expected to contain signatures of both alteration and crustal contamination.
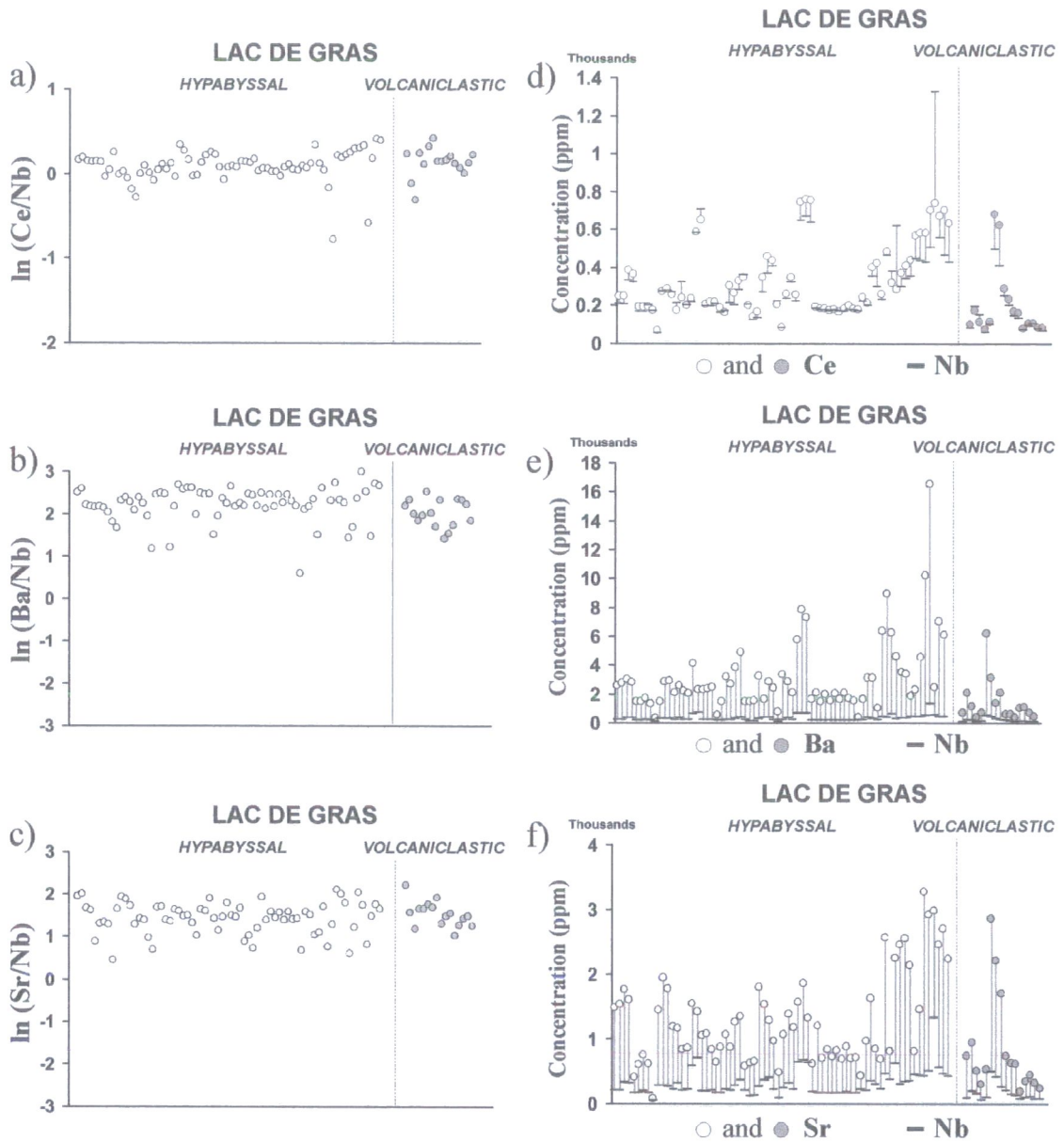
Figure 5.3 Variation of log-ratios and abundances of selected elements that demonstrate differential mobility during alteration in kimberlites from Lac de Gras.

Among Canadian kimberlites analysed from fields and provinces beyond LDG and the Slave craton, the four volcaniclastic samples from the South-West Slave, South-East Slave and Fort à la Corne fields all have low abundances of Ce, Ba and Sr and low Ce/Nb, Ba/Nb and Sr/Nb. None of the hypabyssal samples from outside the Slave province have clear signatures of alteration in terms of Ce-Nb, Ba-Nb and Sr-Nb variations. The two samples from the RND-120 intrusion at Jericho in the Contwoyto field do have ln (Sr/Nb) that is negative and much lower than any of the other kimberlites analysed from Jericho. This is partly due to the Nb content of these samples, which is higher than any of the other Jericho samples, but RND-120 also has very low (<200ppm) Sr abundances.

5.2.6 Summary

Syn- and post-emplacement alteration processes are capable of leaching substantial amounts of mobile trace elements from kimberlite matrices. Ratios such as Ce/Nb, Ba/Nb and Sr/Nb, in conjunction with elemental abundances of Ce, Ba, Sr and Nb, may offer some insight into which kimberlites have experienced measurable amounts of alteration. Despite this, the hypabyssal kimberlites from LDG appear to be very fresh, with none having clear Ce-Ba-Sr-Nb signatures of alteration comparable to those observed in some southern African kimberlites. This supports field and petrographic observations regarding the general freshness of hypabyssal kimberlites from LDG. Only two hypabyssal samples from LDG have low Ce, Ba, and Sr abundances, with variable Ce/Nb, Ba/Nb, Sr/Nb ratios. Low abundances of Nb associated with these samples suggest that the observed chemical trends may reflect a combination of

alteration and crustal contamination. Several of the volcaniclastic samples analysed from LDG have these kinds of signatures.

5.3 FRACTIONATION OF KIMBERLITE MAGMAS

5.3.1 Evidence for fractionation in kimberlites

No clear consensus exists on the extent, if any, to which primary kimberlite magmas undergo crystal fractionation. One of the largest barriers to resolving this issue is the complicating effects of other processes, namely contamination by mantle and crustal material and post-emplacement secondary alteration that act to modify the primary composition of kimberlite magmas. Entrainment and assimilation of olivine derived from the lithospheric mantle in particular masks the effects of possible olivine fractionation. An additional constraint is that few detailed studies have been conducted on sets of kimberlite samples that can be regarded with confidence as being genetically related, e.g. studies of intra-kimberlite compositional variations. Exceptions to this are the studies of South African Group II kimberlites of Fraser (1985) and Tainton (1992). Scott (1979) and Spriggs (1988) have investigated geochemical variations in suites of ultramafic lamprophyres and Group I kimberlites, respectively, that are likely to be related on a local geographical scale. The conclusions of these studies with regard to the effects of fractionation are summarised in Table 5.1.

5.3.2 Fractionation mechanisms

The fractionation of kimberlite magmas cannot be considered in isolation from other processes of magmatic evolution such as contamination by the crust and lithospheric mantle, which can and probably do affect kimberlite magmas (see sections 5.4 and 5.5). A kimberlite magma can start fractionating as soon as it is separated from its source

region and begins ascending. This is an important consideration, because assimilation of mantle peridotite and crust will alter the composition of the magma, i.e. pre-, syn- and post-contamination fractionation will commence from different initial bulk chemistries. This is, of course, dependent on the extent to which any entrained mantle or crustal material actually dissolves in the kimberlite magma. A considerable proportion of any macrocrystal olivine that is separated out from the evolving magma could, in fact, be xenocrystal in origin. Equally, olivine macrocrysts can also be high-pressure phenocrysts; careful petrography is required to determine the relative modal abundance of xenocrysts and phenocrysts.

Incorporation of crustal material into the kimberlite magma (see section 5.4) can lead to significant reductions in the bulk MgO content of a sample. Differential amounts of crustal contamination in a suite of samples may produce a range of MgO and other major element compositions that superficially resemble fractionation trends. Careful examination of major and trace element data should enable the effects of fractionation to be resolved from those of contamination by crustal and also mantle material.

The two most likely mechanisms for removing early-forming phases from the kimberlite magma are gravitational separation during ascent and flow differentiation during ascent and emplacement. Several workers have observed flow differentiation phenomena in dykes and sills from South Africa (Dawson and Hawthorne, 1973; Clement, 1982; Mitchell, 1986). Hand specimens from the Jagersfontein kimberlite clearly show development of olivine-rich and olivine-poor layers on a centimetre scale, producing extreme chemical heterogeneity on a local scale. There is also evidence on a thin-section scale of flow banding in samples from the dykes of the Jericho intrusion.

Reference	Evidence for olivine fractionation	Evidence against olivine fractionation	Evidence for phlogopite fractionation	Evidence against phlogopite fractionation
Fraser (1987)		1) High magnesium number of samples indicates olivine removal not occurred. 2) Most samples do not show positive correlation between SiO_2 and Ni.		1) Abundance of late-crystallising phlogopite in groundmass suggests no previous K depletion. 2) Cores of groundmass phlogopites are more Ti-rich than phenocrysts.
Spriggs (1988)	Major elements consistent with derivation of most evolved sample by fractionation of olivine + Cr-spinel.	Trace elements not consistent with other Gibeon kimberlites being parental to most evolved sample.		
Tainton (1992)		Elevated Ni and Cr rules out olivine fractionation as means of generating high observed levels of incompatible elements.		Variation of SiO_2 and incompatible elements does not support genesis of associated lamproites by fractionation of olivine + phlogopite ± Cr-spinel from kimberlite magmas.

Table 5.1   Literature evidence for and against operation of olivine and/or phlogopite fractionation in kimberlite magmas.

Arndt (2003) envisages a process operating in South African Group II kimberlites whereby the ascending magma interacts with the lithospheric mantle, entraining peridotitic olivine as xenocrysts and chemically assimilating orthopyroxene and other less refractory phases. This increases the SiO_2 content of the magma and adjusts its Mg/Fe ratio such that olivine crystallising from it has a forsterite content like that of the assimilated material. Although it is not stipulated to what extent, if any, the crystallising olivine is fractionated from the magma, this is essentially an assimilation-fractional crystallisation (AFC)-type process, where latent heat of crystallisation drives the assimilation of material into the magma (DePaolo, 1981). Arndt (2003) suggests that this process does not operate to the same extent in Group I magmas, which pass upwards through the mantle more rapidly, entraining but not resorbing lithospheric material and thus retaining an isotopic signature characteristic of the sub-lithopsheric convecting mantle. Differential volatile content is proposed as a possible means of varying the speed of ascent and degree of lithospheric interaction between Group I and Group II magmas.

5.3.3 Fractionating phases in LDG kimberlites

The phases most commonly considered on the basis of textural evidence to represent phenocrysts in kimberlites are olivine and phlogopite (Mitchell, 1986). Together with spinel, these are the earliest crystallising phases within kimberlite magmas. Phlogopite is not, however, commonly observed as a phenocryst phase in the LDG kimberlites; instead it occurs mainly as microphenocrysts or as a groundmass phase (Armstrong *et al.*, in press). In addition, the experiments of Edgar *et al.* (1988) on phase relations in the aphanitic Wesselton kimberlite from South Africa at 10-50kbar, show that above 1200°C, the only phases that crystallise are olivine and spinel. Phlogopite phenocrysts

130

are only likely to form in the rare cases when the K_2O content of the magma is >2wt% (B. A. Kjarsgaard, pers. comm.). In the following analysis ilmenite and perovskite are also included because they are ubiquitous phases and exert important controls on the budget of elements such as the HFSEs and REEs.

The 14 analyses of samples from the Grizzly kimberlite are used to investigate in detail fractionation trends within the LDG dataset. These samples can reasonably be assumed to be cogenetic, and thus be derived from a magma with a common initial bulk chemistry and evolutionary history. Observations made on this well constrained group can then be extended to the dataset at large.

5.3.4 Major and trace element models of fractionation

Plotting the major and minor element variations of LDG hypabyssal kimberlites with respect to vectors describing the evolution of residual liquids during fractional crystallisation of phenocryst phases (Figure 5.4), allows general trends in compositional control by those phases to be identified. Any correspondence with trends evident in the kimberlite data can then be identified. Vectors representing addition of typical crustal compositions are included on these diagrams for comparative purposes. The effects of crustal admixing with kimberlite magmas are discussed further in section 5.4.

Any analysis of fractionation or contamination of magma must take into consideration the initial composition upon which these processes operate. In this case, the models presented in Figure 5.4 require specification of the initial kimberlite magma composition, from which phenocryst phases may crystallise. Identification of such a

'primary' composition is usually complicated by the large and variable amounts of contamination by crust and lithospheric mantle typically experienced by kimberlites.

In previous work on kimberlites (e.g. Edgar *et al.*, 1988; Price *et al.*, 2000), samples of aphanitic kimberlite, which contain virtually no discernable olivine macrocrysts, have been used as the closest available proxy for a 'primary' kimberlite liquid. Aphanitic kimberlites are, however, very rare, and it is also difficult to be certain that these rocks are not macrocryst-free due to efficient fractionation having taken place. The study of Price *et al.* (2000), for example, identifies 'aphanitic' compositions with a wide range of MgO contents.

Graphical methods have also been used to estimate possible primary compositions. Arndt (2003) uses MgO and FeO variations in South African kimberlites to constrain the MgO content of the primary magma to 18-22wt%. Le Roex *et al.* (2003) use inflections in compositional trends between macrocrystal and aphanitic kimberlites from South Africa to obtain a value of 28-29 wt% for the primary magma. The samples analysed for this study span a continuous range of MgO from 15-45wt%. Within this range, samples known from petrography to have large modal proportions of olivine (including xenocrysts) typically have MgO in excess of ~34wt%, e.g. Grizzly, Mark, Arnie. Samples known to contain significant contributions from crustal contamination generally have MgO of less than ~25wt% (e.g. Fox). Clear petrographic evidence of fractionation in the Lac de Gras samples has been harder to identify (Appendix B), but any fractionation of olivine will also reduce MgO content.

As an initial estimate for this model, the 'primary' magma prior to fractionation is assumed to have 30wt% MgO. This approximately corresponds with samples that have minimal evident contributions from crustal or lithospheric contamination (e.g. Anaconda, Rattler), and is also in broad agreement with the estimates of Le Roex *et al.* (2003). Plotting regression lines through the LDG data for MgO vs other elements provides estimates of other 'primary' abundances, corresponding to 30wt% MgO. These are, 30wt% SiO_2, 8.5wt% Fe_2O_3 T, 0.8wt% TiO_2, 2.5wt% Al_2O_3, 1200ppm Ni and 1500ppm Cr. The identification and interpretation of fractionation trends in the LDG kimberlites is clearly highly dependent on the values chosen to represent the compositions of both the parental magma and the end-member fractionating phases. The discussion that follows is based on the values selected above.

Figure 5.4 indicates that olivine fractionation provides the best fit to the compositional variation observed in the LDG kimberlites. Despite this, the substantial MgO contents (34.9 to 39.3 wt%) of samples from Grizzly and several other kimberlites from LDG strongly implies that compositional variation in these samples cannot be the product of fractionation alone, as the parental magma would require an MgO content in excess of 40 wt% to yield appropriate residual liquid compositions during olivine fractionation. The high MgO of these samples is almost certainly due to the addition of xenocrystal olivine into the magma. This process increases the abundance of elements such as Mg, Fe, Si, Ni and Cr in the magma, whereas olivine fractionation will deplete the residual liquid of these elements. The effects of assimilation of lithospheric mantle into kimberlite magmas are discussed in more detail in section 5.5. In both high and low MgO samples, contamination by crust may also be responsible for some of the observed variation towards higher SiO_2 and Al_2O_3, and lower Fe_2O_3 T, TiO_2, Cr and Ni.
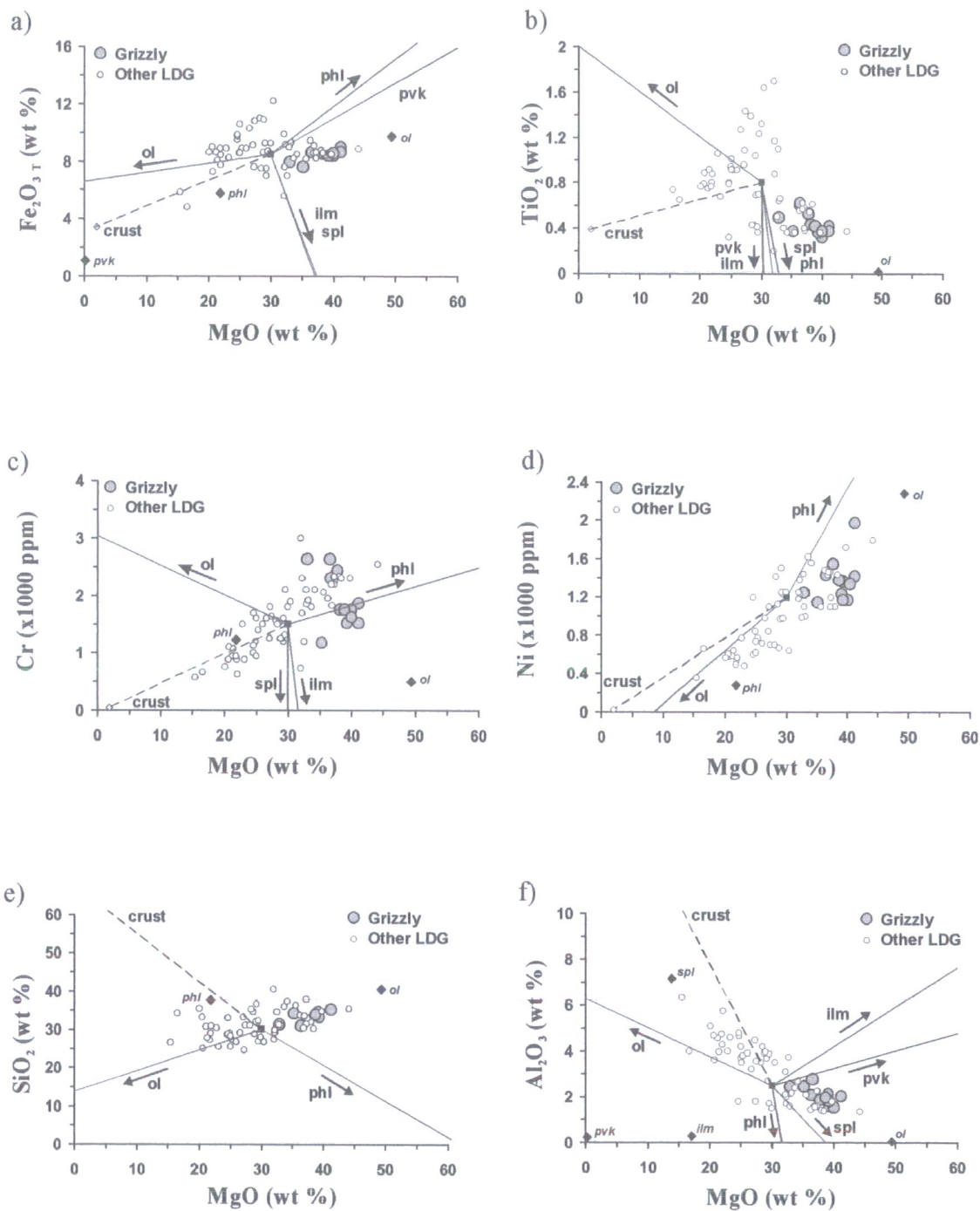
Figure 5.4 LDG hypabyssal kimberlite variation in selected major and trace elements and compositional control lines indicating evolution of residual liquid during fractional crystallisation of olivine, phlogopite, Cr-spinel, perovskite and ilmenite from a 'primary' kimberlite magma with 30wt% MgO, 30wt% SiO_2, 8.5wt% $Fe_2O_{3\,T}$, 2.5wt% Al_2O_3, 0.8wt% TiO_2, 1500ppm Cr, 1200ppm Ni. Representative phenocryst compositions from Mitchell (1986).

For samples with <30wt% MgO, fractionation of olivine is able to account for some of the variation in all elements shown in Figure 5.4, with the exception of Cr. Fe_2O_3 T, Cr and Ni variations are broadly consistent with some degree of compositional control by phlogopite, but this is not the case for TiO_2 and Al_2O_3. Phlogopite is rich in both of these components relative to kimberlites, so fractionation of phlogopite from a magma should result in obvious TiO_2 and Al_2O_3 compositional trends in the residual liquid. Since this is not observed in the LDG kimberlites analysed, it seems unlikely that phlogopite fractionation can have been an important process in the evolution of these rocks. This is consistent with the generally phlogopite-poor nature of the LDG kimberlites.

The greater scatter of data around the olivine fractionation vector in samples with <30wt% MgO could be explained by small amounts of fractionation of any of the other phases under consideration. Cr-spinel in particular could account for some of the limited observed variation in Fe_2O_3 T, TiO_2 and Al_2O_3. As previously noted, there is little petrographic evidence for the presence of ilmenite or perovskite as phenocryst phases in the rocks studied. Cr-spinel is thus the most likely phase to influence the kimberlite compositions by early-stage crystallisation, in association with olivine, from the magma.

5.3.5 Summary

There is no consistent evidence in the major or trace element data from LDG kimberlites to support fractionation of phlogopite from a parental magma as a principal means of generating observed chemical variations. Olivine or olivine + Cr-spinel

control lines do appear capable of reproducing the broadly linear major and trace element compositional trends observed in kimberlites with MgO contents lower than that of the parental magma (here assumed to be 30wt%). Clearly, if the magma originally has a lower MgO content (e.g. 20wt%) then the same trends could be explained by olivine or olivine + Cr-spinel addition. Removal of olivine ± Cr-spinel by fractionation can also occur in more MgO-rich (>30wt%) magmas, but these have almost certainly experienced assimilation of olivine from lithospheric peridotites, which tends to obscure trends in olivine fractionation.

5.4 CONTAMINATION BY CRUSTAL MATERIAL

5.4.1 Nature of crustal contamination

Xenoliths of continental crust are routinely entrained by kimberlites during their ascent and emplacement. All levels of the crust through which the kimberlite passes may be sampled in this way, rather than just the country rocks in immediate contact with the kimberlite diatreme. This is borne out by the presence of both lower and upper crustal xenoliths in kimberlites (Nixon, 1973).

The quantity and type of material incorporated by the kimberlite can vary widely both between and within intrusions. The hypabyssal facies typically contains few crustal xenoliths (Mitchell, 1986), but diatreme facies rocks may contain large proportions of visible, macroscopic crustal fragments, e.g. the Premier and Koffiefontein-Ebenhaezer intrusions of South Africa studied by Fesq *et al.* (1975). The Koffiefontein diatreme contains mostly xenoliths of shale, whereas at Bellsbank the principal crustal contaminant is sedimentary carbonate (Kable *et al.*, 1975). The Premier kimberlite is composed of multiple intrusive bodies with very variable bulk chemistries: the heavily

contaminated Premier Grey body contains 43% crustal material, which is dominantly quartzite, whereas the Premier Brown intrusion contains 28% crust, most of which is basic igneous material derived from the Bushveld intrusion into which the kimberlite was emplaced (Fesq *et al.*, 1975).

A similar range of contamination types and extents could be present in the LDG kimberlites, which intrude through a variety of basement gneisses, metasedimentary rocks and associated granitoids. Any effect that crustal contamination has on the bulk geochemistry of the kimberlite, and comparisons between contaminated kimberlites, are likely to be influenced by this variability in quantity and nature of the contaminants.

5.4.2 Existing methods for quantifying crustal contamination

Various attempts have been made to quantify the extent of crustal contamination within kimberlites. These schemes are based mostly around the concept that crustal rocks generally have higher SiO_2 and lower MgO contents than kimberlites. In their extensive major element study of over 600 Siberian kimberlites Ilupin and Lutz (1971) proposed that Si/Mg > 0.88 and Mg/(Mg + Fe) < 0.85 could be used as criteria for recognising crustal contamination. Fesq *et al.* (1975) further suggested that since the highest Si/Mg ratio of any mineral crystallising from kimberlite magmas should be that of phlogopite (Si/Mg ~1.2), then ratios higher than this threshold probably indicated contamination. The most commonly used measure at the present time is the Contamination Index (CI) proposed by Clement (1982). This is calculated as:

$$CI = (SiO_2 + Al_2O_3 + Na_2O) / (MgO + 2K_2O)$$

The numerator of this expression represents the elements likely to be enriched by incorporation of crustal material and the products of weathering and other alteration processes, i.e. clay minerals, while the denominator represents the original olivine and phlogopite considered to constitute the bulk of a 'typical' unaltered, uncontaminated kimberlite.

Group I kimberlites uncontaminated by crust should have a CI of around unity. Group II kimberlites normally contain greater modal abundances of phlogopite and consequently the CI for an uncontaminated example should be <1.5 (Mitchell, 1995). Exceptions to these criteria do exist. Clement (1982) reports that some Group I kimberlites which, on the basis of petrography, are fresh and uncontaminated have a CI of up to 1.5; similarly, supposedly uncontaminated Group II rocks analysed by Dawson (1987) have CIs between 1.5 and 2.6, and Clement (1982) found others with CIs of up to 5.

Although it has been almost universally adopted as a convenient expression of crustal contamination, the CI has a number of limitations. The most serious of these is its sensitivity to variation in MgO and SiO_2, which dominate the CI due to their abundance relative to Al_2O_3, Na_2O and K_2O. Consequently, modal abundance of olivine, which consists almost entirely of MgO and SiO_2, is by far the most important control on the CI. Given the potential for variation of modal mineralogy and thus bulk composition on both an inter- and intra-kimberlite scale, inconsistencies can easily occur between the CIs of samples that are contaminated to the same degree.

Sensitivity analysis (Figure 5.5) demonstrates the responsiveness of the CI to changes in each of its component variables. The starting composition used in this model is an aphanitic hypabyssal sample from Wesselton, South Africa (Shee, 1986; Edgar *et al.*, 1988). It is assumed that the major elements and volatiles constitute the entirety of the sample (i.e. trace elements are ignored), and that as one component is increased or decreased, the others decrease/increase in proportion to their abundance to retain the original sum total. This simple model clearly shows that the CI is extremely sensitive to variations in MgO and SiO_2 content, and comparatively insensitive to variations in Al_2O_3, Na_2O and K_2O.

In reality the situation is more complex, because addition (by lithospheric contamination) or removal (by fractionation) of olivine will affect all five components of the index simultaneously. Olivine is not only very enriched in MgO and SiO_2 relative to a typical primary whole rock kimberlite composition, but also deficient in Al_2O_3, Na_2O and K_2O. Figure 5.6 illustrates the effects of mixing peridotitic mantle olivine with the Wesselton aphanitic composition. It is important to note that both MgO and SiO_2 content increases on addition of olivine, but the net effect is a reduction in the CI. Using SiO_2 in isolation as an indicator of crustal contamination is therefore inadvisable.
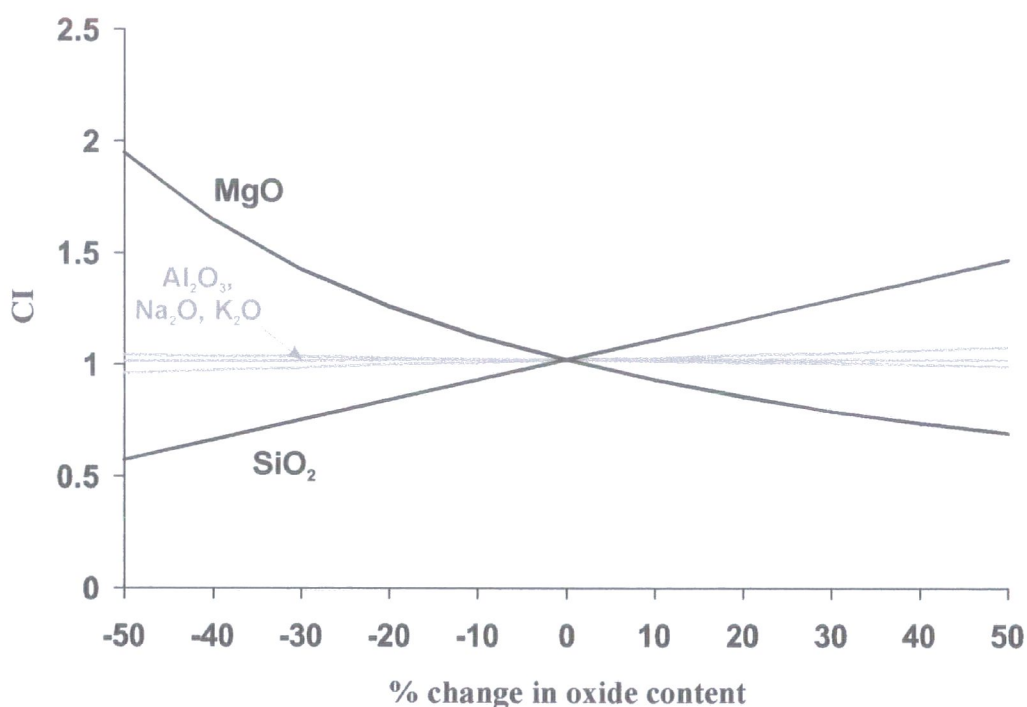
Figure 5.5 Effect on contamination index (CI: Clement, 1982) of independent variations in its five component major element oxide abundances. Starting composition (at 0%) is Wesselton aphanitic kimberlite (Edgar *et al.*, 1988).
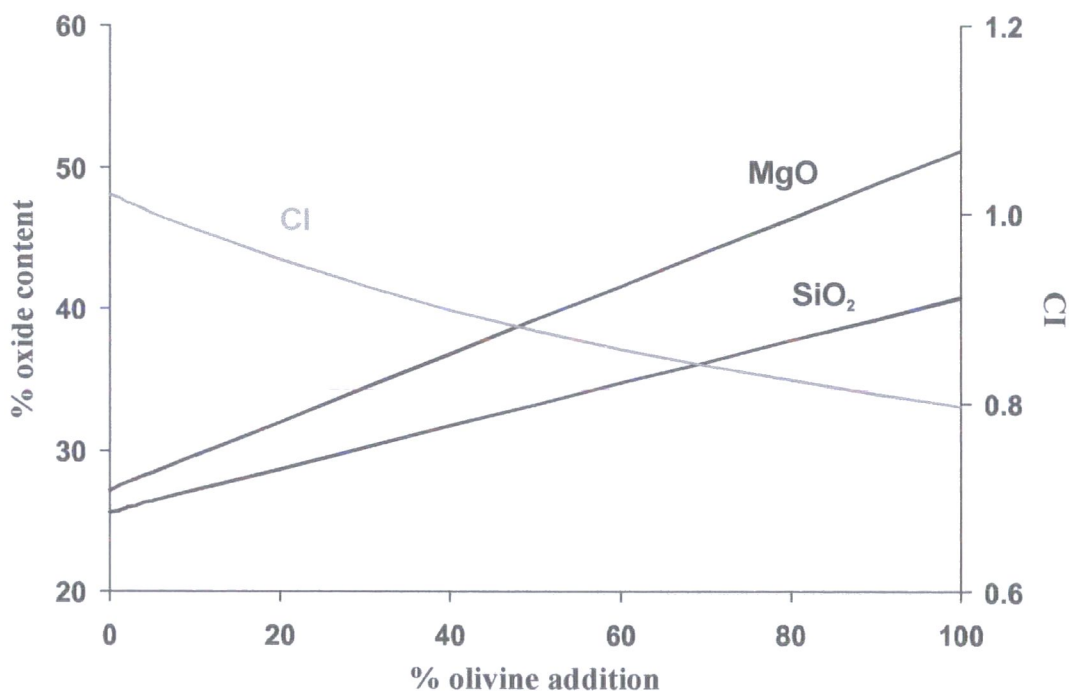
Figure 5.6 Effect on MgO, SiO$_2$ and contamination index (CI: Clement, 1982) of mixing a hypothetical 'primary' kimberlite magma composition (Wesselton aphanitic: Edgar *et al.*, 1988) with average composition of peridotitic olivine from the Slave mantle xenoliths (Pearson *et al.*, 1999).

In this model the CI tends to that of peridotitic olivine (~0.80) at 100% olivine addition; several LDG kimberlites known to have high modal olivine contents (e.g. Leslie, Grizzly, Mark) have CIs in the range of 0.80-0.90, which corresponds to a minimum of 40% olivine entrainment. This, of course, is subject to how closely the Wesselton composition corresponds to that of primary magmas at LDG, and similarly whether the olivine composition used here corresponds to that entrained by LDG kimberlites. Regardless, it is clear that entrainment of olivine has a significant effect on the CI that is not normally taken into account. Moreover, the tendency of olivine addition to lower the CI could easily offset any increase in the CI through assimilation of crustal material.

Another limitation of the CI is that it does not clearly discriminate between crustal contamination and the effects of post-emplacement alteration. Both of these processes will tend to increase the SiO_2/MgO ratio and Al_2O_3 content of the bulk rock. The Na_2O content of crustal rocks is usually much greater than that of the clays typically produced by weathering of olivine and phlogopite, but as previously demonstrated very large increases in Na_2O are required to produce significant increases in the CI. Some of the altered samples analysed by Spriggs (1988) actually have CIs that are comparable to or lower than those of the fresh hypabyssal rocks from the same study. The average CI of 14 highly weathered volcaniclastic kimberlites from Liberia (Taylor *et al.*, 1994) is 1.04, in comparison to an average of 1.03 for 13 relatively fresh hypabyssal samples from Sierra Leone. Although most Group I kimberlites do not contain large modal abundances of phlogopite, this mineral can have a misleading effect on the CI. The fresh and altered kimberlites of Spriggs (1988) with the highest

CIs are particularly micaceous, although none of these rocks can be classed as Group II from an isotopic perspective.

A third problem with the CI is that different contaminant materials produce different degrees of change in the index. The composition of continental crust is well known to be extremely variable, both between and within crustal rock types (Taylor and McLennan, 1985). Figure 5.7 shows the effect on CI of mixing a variety of different crustal end-members with the Wesselton aphanitic kimberlite composition. While the majority of these end-members produce similar effects on the CI at up to 10-20% mixing, admixtures containing 20% or more crust exhibit distinct effects. In the case of some end-members, such as felsic volcanics and carbonates there is a clear difference in the effect on CI. Because chemical sediments lack high concentrations of many or all of the CI components, mixing with these materials can produce severe dilution effects and depression of the CI. Accurate placement of constraints on the extent of crustal contamination therefore requires some knowledge of the nature of the contaminant.

Finally, it should be noted that all these simple mixing models assume complete assimilation of all entrained material into the bulk chemistry. In reality, several studies have indicated that crustal xenoliths appear largely undigested by the kimberlite
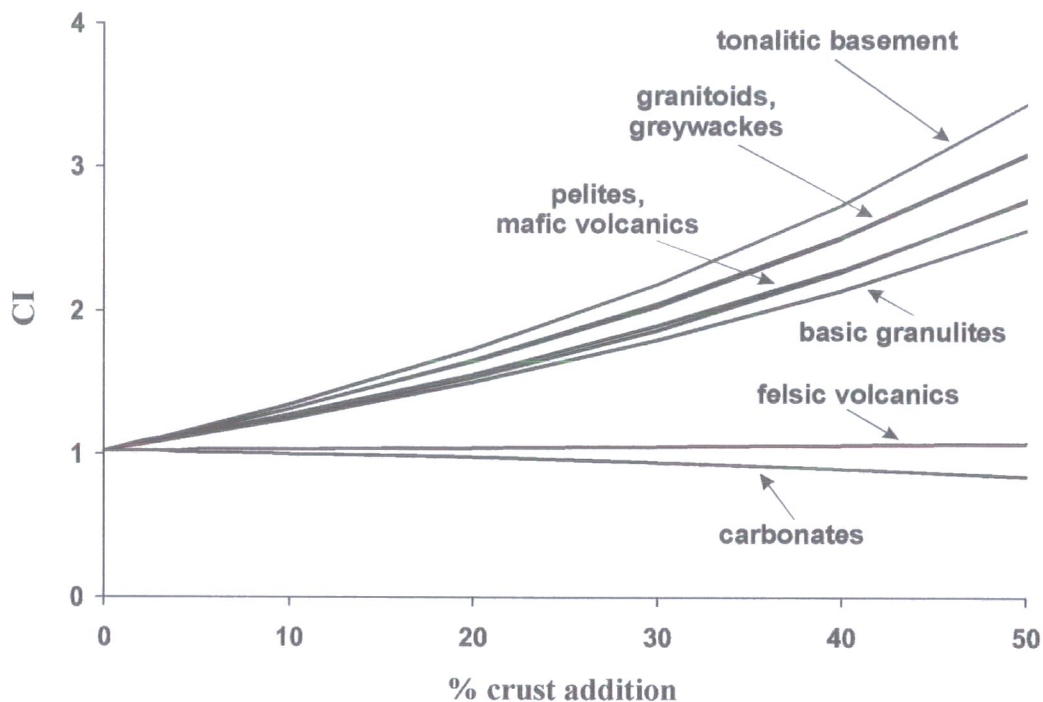
Figure 5.7 Effect on contamination index (CI: Clement, 1982) of mixing a hypothetical 'primary' kimberlite magma composition (Wesselton aphanitic: Edgar *et al.*, 1988) with average composition of various components of Slave continental crust (Yamashita *et al.*, 2000; this study).

magma, although reaction rims around xenoliths are quite common (Fesq *et al.*, 1975; Spriggs, 1988; Tainton, 1992). Fesq *et al.* (1975) suggested that higher Si/Mg ratios but lower abundance of extant crustal material in the Premier Brown kimberlite compared to the Premier Grey intrusion phase could be due to higher emplacement temperatures and greater degrees of assimilation in the Premier Brown phase. Dissolution is not, however, the only mechanism of contamination: crustal material may be finely comminuted and disseminated by attrition and other physical processes in the rapidly ascending magma. It is common practice in geochemical studies of kimberlites to remove by hand as much material of obvious crustal origin as possible,

in order to obtain an analysis that is as representative as possible of the uncontaminated magma. Nevertheless, it is inevitable that some finely disaggregated material will remain in the sample.

5.4.3 An alternative major element quantification scheme

Variation in major element content and contamination index across a range of fresh, altered and contaminated kimberlites from southern Africa (Gurney and Ebrahim, 1973; Fesq *et al.*, 1975) is shown in Figure 5.8. This clearly demonstrates that the CI cannot unequivocally distinguish between altered and contaminated material. Furthermore, altered samples may take a range of CI values and as a result the attribution of some samples as 'fresh' may be questionable. MgO, Al_2O_3 and Na_2O provide the clearest distinction between fresh and contaminated material in terms of major oxides. This is not surprising since these components form the basis of the CI. The distinction between 'fresh' and 'contaminated' in terms of SiO_2 and K_2O is, however, much less obvious – there is a large degree of overlap of these oxide abundances between fresh, altered and contaminated samples. In the case of K_2O this is almost certainly controlled by variable phlogopite content, even though all of these kimberlites are isotopically classified as Group I. The overlap in SiO_2 is largely due to the altered samples, while for the most part fresh kimberlites have lower SiO_2 contents than contaminated samples.

Given the limitations of the contamination index of Clement (1982) and the lack of discrimination provided by Fe_2O_3 $_T$, CaO, TiO_2, MnO and P_2O_5, it would seem most sensible to attempt to base a major element discriminator of crustal contamination on Al_2O_3 and Na_2O alone.

144
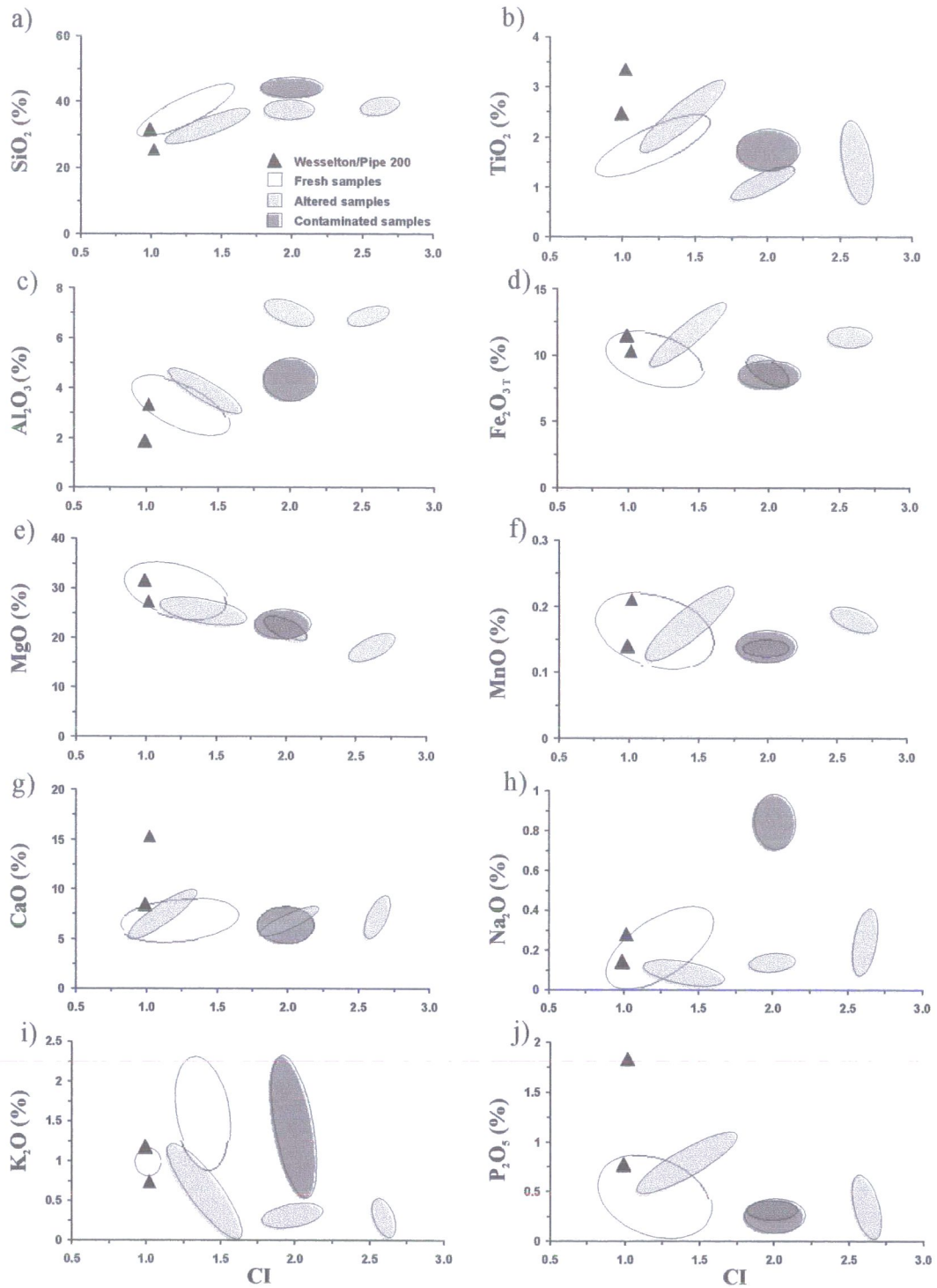
Figure 5.8 Variation of major oxide content of fresh, altered and contaminated southern African kimberlites with contamination index, CI (Clement, 1982). Data from Gurney and Ebrahim (1973) and Fesq *et al.* (1975).

Experimentation with data from LDG and southern Africa (Gurney and Ebrahim, 1973; Fesq *et al.*, 1975), using different combinations of major element log-ratio pairs, suggests that the variation of Al_2O_3/MnO with Na_2O/P_2O_5 (or the equivalent elemental ratios, Al/Mn-Na/P) best separates the fresh and altered material from contaminated material (Figure 5.9). Mn and P are utilised here as denominators on the basis of their apparent lack of sensitivity to contamination or alteration. A crustal contamination trend is evident towards higher values of Al/Mn and Na/P in both data sets. This trend corresponds to progressive contamination in the southern African data (Figure 5.9a), from the uncontaminated, aphanitic kimberlite from Wesselton (Edgar *et al.*, 1988), through the minimally contaminated Premier Black kimberlite to the samples from the Brown and Grey intrusions at Premier, which are known to be the most contaminated (Fesq *et al.*, 1975). Altered samples from Lemphane define a broadly parallel trend that is offset to higher Al/Mn and lower Na/P values. The altered and contaminated kimberlites from Koffiefontein and Ebenhaezer (Fesq *et al.*, 1975) are situated towards the upper end of this trend. This indicates that contaminated samples may be moved towards, or on to, the alteration trend by a net increase in Al/Na, which is consistent with the development of clay minerals during alteration. In the LDG data (Figure 5.9b) there are similar trends towards elevated Al/Mn and Na/P, consistent with the average compositions of typical crustal materials from the area. Volcaniclastic kimberlites from LDG, which are likely to have experienced more crustal assimilation on average than the hypabyssal facies rocks, also form clear trends towards higher Al/Mn and Na/P (not shown). The sample from the Fox kimberlite is known from visual examination to be highly contaminated, and this corresponds with Al/Mn and Na/P that is much higher than any of the other LDG kimberlites.

146
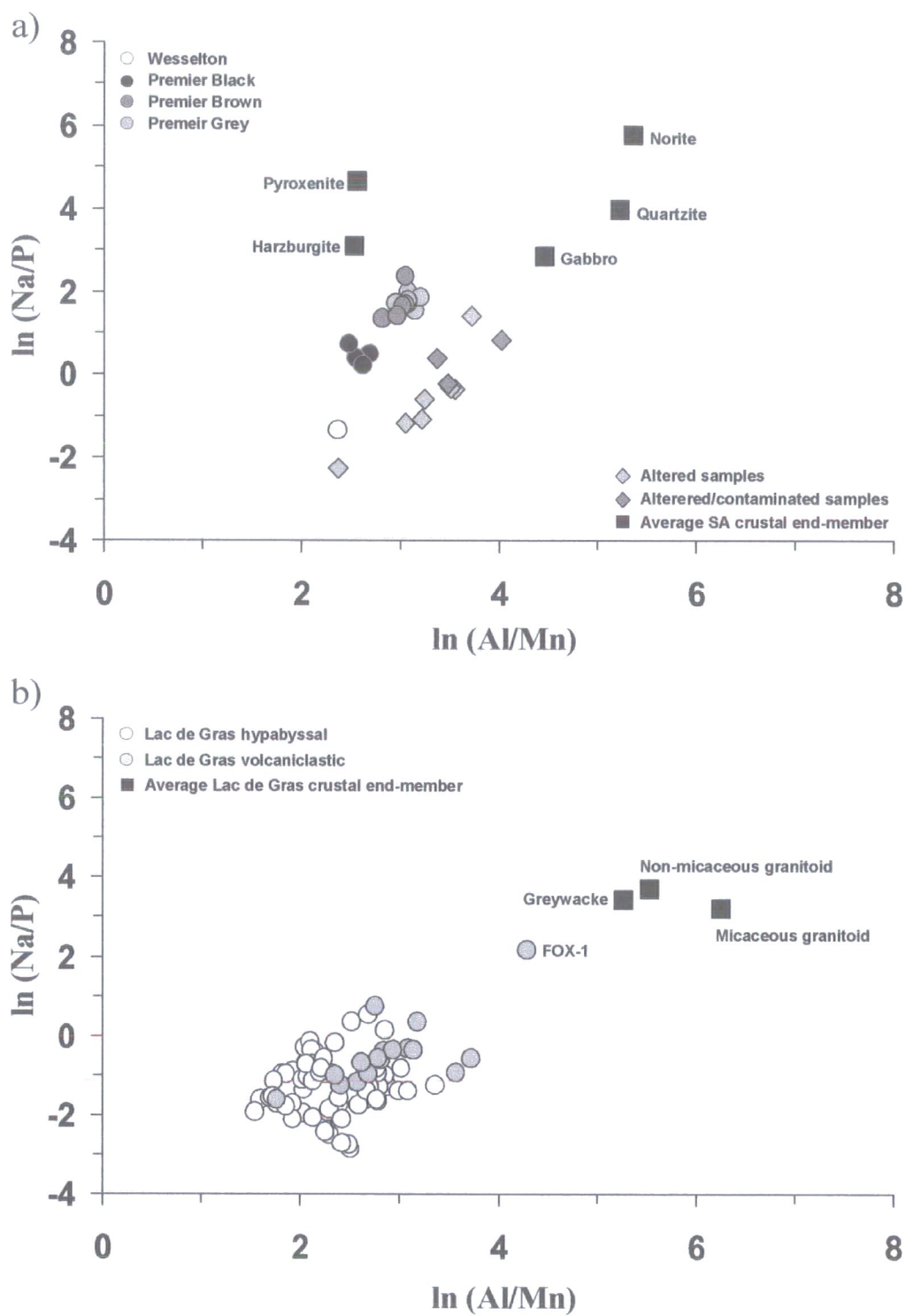
Figure 5.9 ln (Al/Mn) and ln (Na/P) variation in fresh, altered and contaminated kimberlites: a) southern Africa (Premier, Ebenhaezer, Koffiefontein); b) Lac de Gras. Data for SA samples from Gurney and Ebrahim (1973), Fesq *et al.* (1975), Cox *et al.* (1979), Wronkiewicz and Condie (1990), Eales and Cawthorn (1996).

147

5.4.4 Trace element signatures of crustal contamination

There is some uncertainty over the extent to which continental crust is capable of modifying the trace element geochemistry of kimberlites. Unlike most other mantle-derived magmas, kimberlites are enriched in both compatible and incompatible trace elements. Crustal materials tend to be poor in compatible and enriched in incompatible elements, but not – in most cases – enriched to equal or greater concentrations than those observed in kimberlites. Based on a consideration of elemental ratios (e.g. Zr/Y, Nb/Y Ta/Yb) as well as abundances, Fraser (1987) and Tainton (1992) concluded from their studies of South African Group II kimberlites that crustal contamination could not explain the observed trends in trace element enrichment or compositional scatter. Kable *et al.* (1975) previously suggested that the effect of crustal assimilation would be either negligible or a means of diluting, rather than enriching, trace element abundances in kimberlite magmas.

Figure 5.10 shows typical relative abundances of minor and trace elements between kimberlites and average crust from LDG. The kimberlite selected as a reference point in this analysis is sample RTL-1 from the Rattler body. This sample has similar MgO, SiO_2 and Al_2O_3 abundances to the hypothetical primary composition utilised in section 5.3. The natural logarithm of the ratio of average elemental abundance between kimberlite and crust is positive when an element is more abundant in the kimberlite and negative when more abundant in the crust. The majority of trace elements thus appear to be more abundant in LDG kimberlites than in the crust. Elements for which the difference in abundance is largest (e.g. Na, Lu, Ni, Cr) are likely to be most sensitive to crustal assimilation.

148
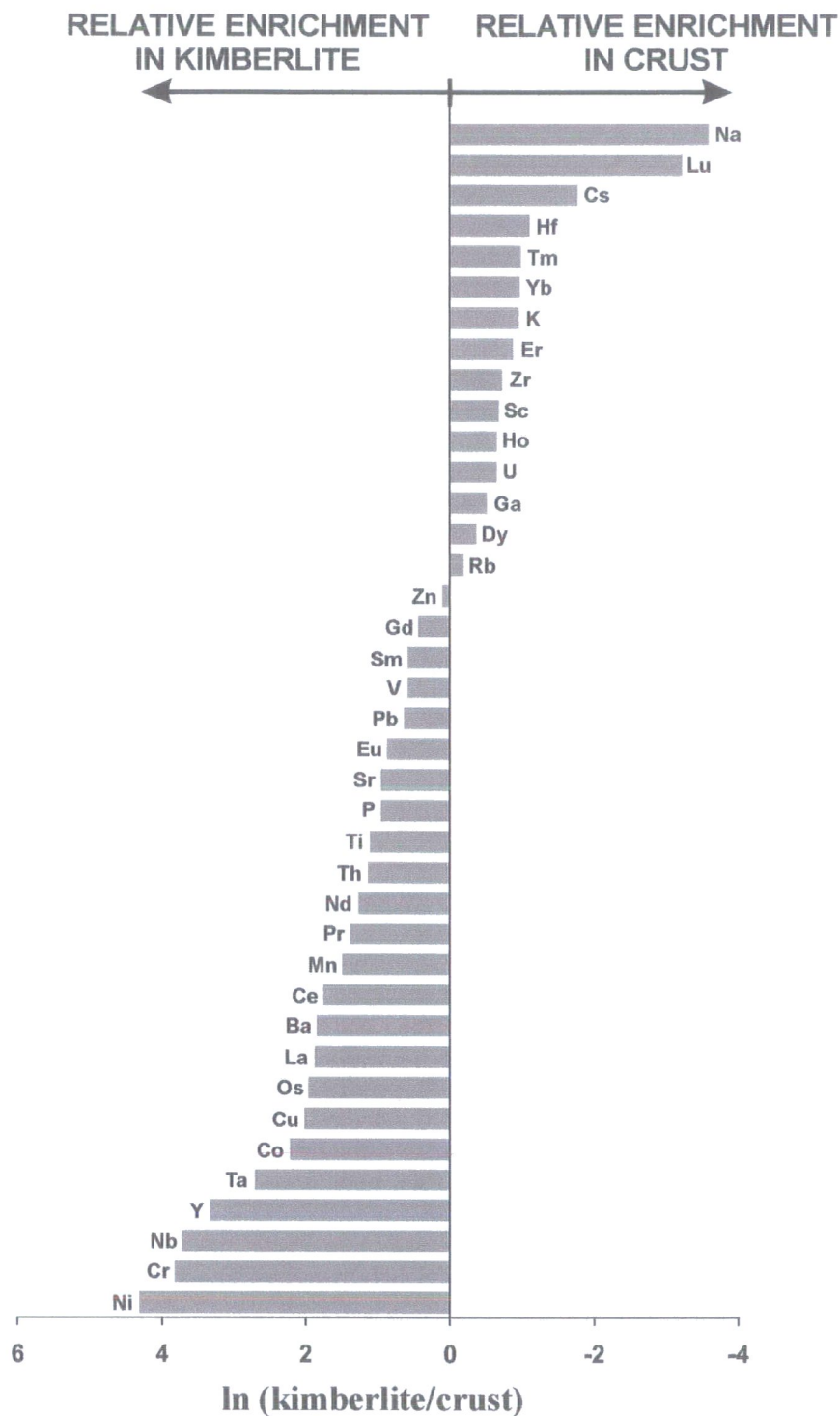
Figure 5.10 Relative abundance of minor and trace elements between Lac de Gras kimberlite representative of 'primary' composition (Rattler, sample RTL-1) and average composition of crustal material (greywackes and granitoids) from Lac de Gras region. All data from this study.

Table 5.2 summarises the differences in kimberlite-crust relative average abundances for different categories of trace elements. Kimberlite is enriched to some degree in almost all compatible and high field strength elements relative to LDG crust; only Sc, U, Hf and Ga are depleted relative to the LDG crustal components, and then only weakly. These kimberlites similarly show strong enrichment in the LREEs, and weak to moderate enrichment in the MREEs. Only the HREEs are more abundant in the LDG crust. The LILE are the only group of incompatible elements that show any consistent depletion in the LDG kimberlite relative to crust. The exceptions to this are Ba and Pb, which show strong relative enrichment in the kimberlites, and Sr, which does so to a lesser extent.

The analysis presented so far is based on averages of trace element abundances in the crust. These abundances can be extremely variable, both between and within different types of crustal material (Figure 5.11), but the general trends in enrichment/depletion relative to kimberlite identified in Figure 5.10 and Table 5.2 are still supported. The greatest variability is seen between the members of the Yellowknife Supergroup (YKSG). The basement tonalities and granitoids of the Lac de Gras area are depleted in most trace elements except LILEs, relative to the YKSG lithologies. Na (not shown) is the only element in which the granitoids are notably enriched relative to the YKSG greywackes. Although only biotite granites are shown in Figure 5.11, a number of trends are evident within the granitoids themselves. Where any variability in elemental concentrations exist it is generally the trondjhemites and hornblende tonalites that are more enriched than the micaceous granites, e.g. Cs, Sr, Zr, Cu and Zn; the micaceous granites are, unsurprisingly, more enriched in Rb and, in the case of the biotite granite, K.

Status in kimberlite relative to crust	COMPATIBLE		INCOMPATIBLE	
	First transition series elements	High field strength elements	Large ion lithophile elements	Rare earth elements
Moderate to strong enrichment	Ni Cr Co Cu Mn	Y Nb Ta	Ba	La Ce Pr Nd
Weak enrichment/ depletion	V Ti Zn Sc	Th P Zr U Hf Ga	Pb Sr Rb K	Eu Sm Gd Dy Ho Er Yb Tm
Moderate to strong depletion			Cs Na	Lu

Table 5.2 Summary of average enrichment and depletion of minor and trace elements between Jericho aphanitic kimberlite and crustal material from Lac de Gras. Moderate to strong enrichment defined as ln (kimberlite/crust) > 1.0; moderate to strong depletion defined as ln (kimberlite/crust) < -1.0. Distinction between high field strength and low field strength (large ion lithophile) elements defined as ionic potential > 2.0 for HFSE, where ionic potential = ionic charge/ionic radius (Å).

REEs are also useful trace elements for assessing the contribution of crust to the chemical composition of a kimberlite. Crustal materials are typically enriched in HREEs and depleted in LREEs relative to kimberlites. Progressive crustal contamination thus tends to reduce La/Yb ratios in kimberlite, and can produce a 'flattening' effect on the sloping chondrite-normalised REE patterns characteristic of kimberlite. This flattening is usually particularly pronounced in the MREEs to HREEs, and consequently ratios such as Sm/Yb are efficient indicators of crustal assimilation (Figure 5.12). REE patterns are almost parallel for samples from Rattler and Mark, which have variable macrocrystal olivine contents but are crustally uncontaminated. The pattern for the volcaniclastic sample from Fox is relatively flat in the HREEs, and the Sm/Yb ratio of this sample is much lower.
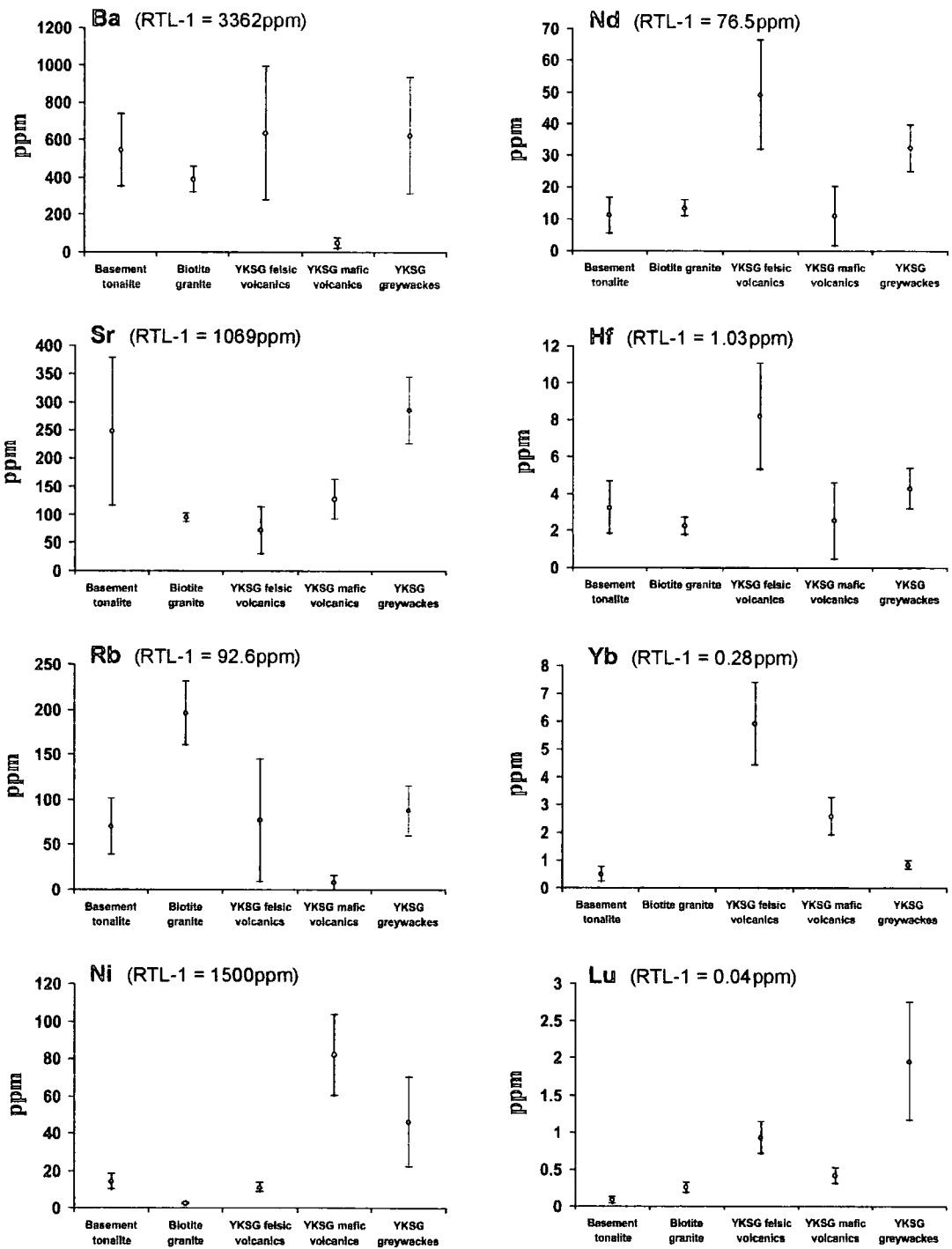
Figure 5.11 Distribution of average minor and trace element concentrations in various crustal rock types from the Lac de Gras area, compared to analysis of sample RTL-1 (Rattler) kimberlite. Error bars denote 1 standard deviation from the mean. Data from Yamashita *et al.* (2000) and this study.
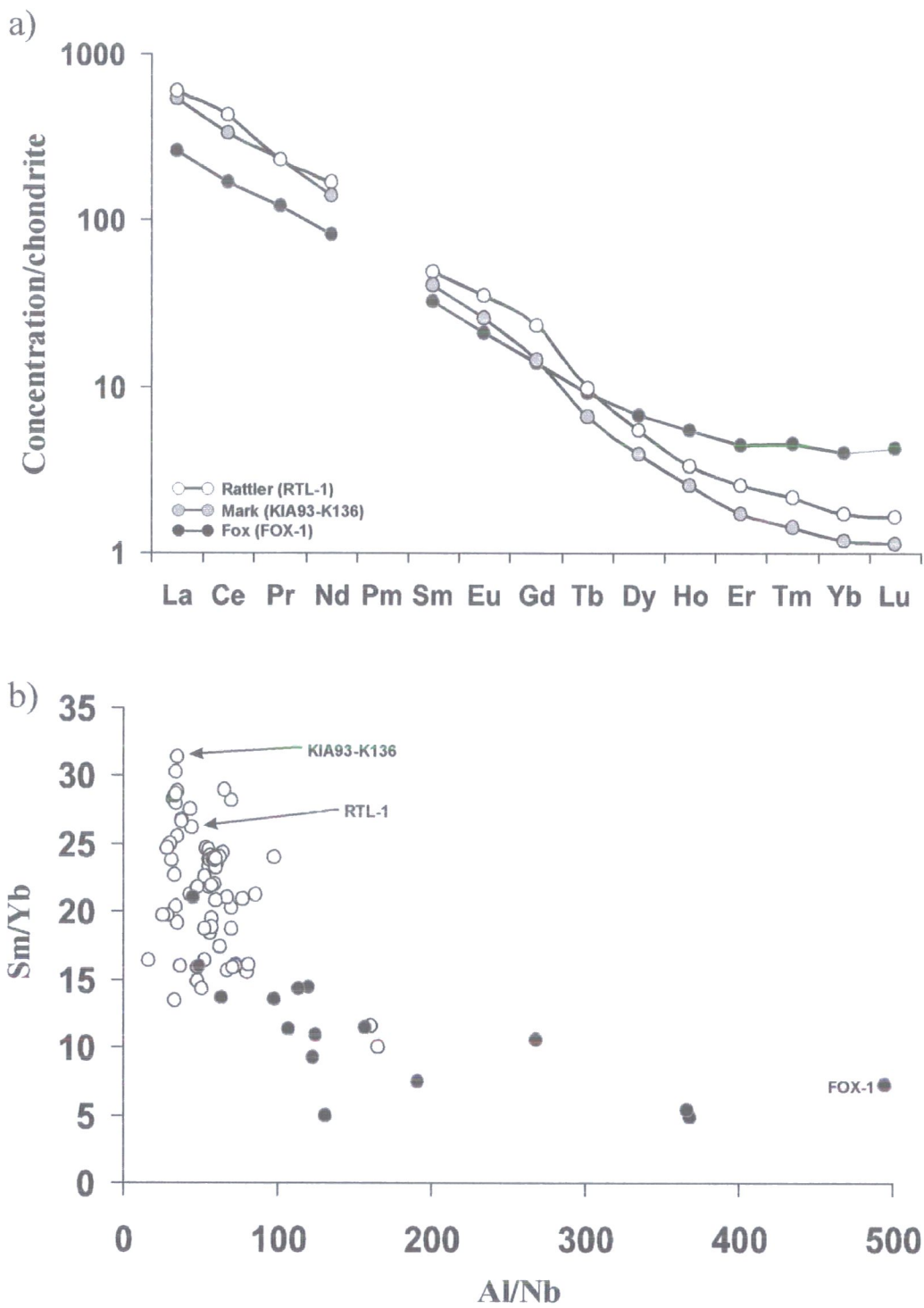
Figure 5.12 Use of REEs as indicators of crustal assimilation: a) chondrite-normalised REE patterns for crustally contaminated (Fox) and uncontaminated (Rattler, Mark) kimberlites; b) variation in Al/Nb and Sm/Yb for hypabyssal and volcaniclastic kimberlites. All data from this study. Chondritic values for normalisation from McDonough and Sun (1995).

5.4.5 Summary

All kimberlites come into contact with crustal materials during their ascent and emplacement, and incorporate this material to varying extents. It is important to be able to assess the amount of crust that a sample has assimilated if the composition of the primary kimberlite magma is to be successfully identified. Although the major element contamination index of Clement (1982) is a useful guide to the amount of crust incorporated by a kimberlite magma, there are a number of problems with its current formulation. Trace elements can be used in conjunction with major element data to help detect input from crustal contamination in the LDG kimberlites. Al/Mn, Na/P and Sm/Yb are useful indiactors of relative levels of crustal contamination in kimberlite samples. Other parameters are introduced in the next section, where crustal contamination is considered in association with assimilation of lithospheric material by the kimberlite magma.

5.5 CONTAMINATION BY LITHOSPHERIC MANTLE MATERIAL

5.5.1 Entrainment and assimilation of lithospheric mantle material

Xenoliths of mantle origin and macrocrystal olivine grains are common constituents of kimberlites. Although there are difficulties associated with discrimination of xenocrystal from cognate olivine on a petrographic basis (the 'olivine macrocryst problem' of Mitchell, 1986), there can be little doubt that a large proportion of the macrocrystal olivine grains observed in thin section are derived by disaggregation of entrained mantle peridotites.

The incorporation of material from mantle xenoliths can modify the chemistry of the kimberlite magma in a variety of ways. Olivine is the predominant component phase in

most mantle materials; consequently, addition of peridotitic material will produce enrichment in MgO and compatible elements such as Ni and Cr. There will also be a 'dilution' effect on other elements in which the peridotite is depleted relative to kimberlite. A distinction should be made between entrainment of xenoliths (i.e. the physical addition of mantle material into the magma body) and their assimilation (the digestion of solid material by the magma, with consequent changes to the magma chemistry defined as contamination). Resolving how much modification of a magma is due to chemical assimilation of peridotite, and how much is simple physical entrainment is problematic. This is because in practice it is very difficult to remove all – or even a significant proportion – of material derived by disaggregation of mantle xenoliths from the crushed sample, as it is similar in appearance to the kimberlite groundmass. Consequently, major and trace element analyses of the kimberlite whole rock will reflect the input of all incorporated peridotitic material, rather than merely the fraction that has been assimilated. The amount of entrained material in a sample may still be a useful measure of the amount of lithosphere with which the kimberlite has interacted during its ascent, although xenocrysts may be fractionated from the magma by processes such as flow differentiation in dykes, which could render samples unrepresentative of the kimberlite magma as a whole.

Theoretical studies of the effects on magmas of assimilated wallrock material dating back to the work of Bowen (1928) suggest that the capacity of magma to chemically incorporate such material is actually very limited. This is due to the large latent heat of melting that must be overcome to assimilate xenolithic material that is much cooler than the magma itself, compared to the limited amount of thermal energy that the magma can provide. This assumes that the magma is not a superheated liquid,

following the arguments of Bowen (1928). During assimilation of lithospheric mantle by a kimberlite magma, however, the temperature gradient between the magma and the contaminant is likely to be smaller than in the case of crustal assimilation. This, together with the considerable volatile contents of a typical kimberlite magma, may make it much more capable of assimilating its wallrocks.

Petrographic evidence of entrainment of lithospheric material is found in the vast majority of kimberlites. Olivine is ubiquitous as a xenocrystal phase. Additional minerals typical of mantle material, such as Cr-diopside and Cr-pyrope garnet are also commonly found, but enstatite, which constitutes up to 40% of both fertile and depleted lithospheric mantle, is very rarely observed (e.g. Mitchell, 1986; Arndt, 2003). Unless this orthopyroxene is selectively excluded from the magma in an extremely efficient manner, it appears that it is selectively and comprehensively assimilated. Some support for this is provided by experimental studies of phase equilibria in volatile-rich synthetic kimberlite systems (e.g. Eggler and Wendlandt, 1979), which indicate that across a range of pressures orthopyroxene will melt prior to olivine or clinopyroxene. A further observation of interest from these studies is that garnet will melt well before orthopyroxene, except at very high pressures (> 55 kbar).

5.5.2 Identification of a primary magma composition

As previously noted in section 5.3.4, in order to properly assess the extent of any compositional modification of kimberlite magmas by entrained lithospheric mantle, it is first necessary to place some constraints on the likely initial chemistry of the magma. Estimates of this can be made by reference to aphanitic kimberlites such as those from Wesselton in South Africa (Edgar *et al.*, 1988). These macrocryst-free rocks are

believed to be the closest available approximation to the kimberlite magmatic liquid, but are rare and may have been subject to crystal fractionation. Le Roex *et al.* (2003) use inflections between aphanitic and macrocrystal samples on binary element variation diagrams to constrain the composition of magmas parental to kimberlites from the Kimberley region of South Africa. A comparison of some key major and minor element data from Edgar *et al.* (1988) and Le Roex *et al.* (2003) are shown in Table 5.3.

	Wesselton aphanitic	Inferred primary magma of Le Roex *et al.* (2003)
SiO2 (wt%)	25.6	27-28
MgO (wt%)	27.2	28-29
Al2O3 (wt%)	3.31	~2
CaO (wt%)	15.3	
Ni (ppm)	810	~1100
Cr (ppm)	2410	

Table 5.3 A comparison of selected major and minor element abundances in the aphanitic kimberlite from Wesselton, Kaapvaal craton, SA (Edgar *et al.*, 1988) and inferred primary magma characteristics from the study of aphanitic and macrocrystal kimberlites from Kimberley, Kaapvaal craton, SA (Le Roex *et al.*, 2003).

The 28-29wt% MgO estimate of Le Roex *et al.* (2003) is slightly higher than that of the Wesselton aphanitic kimberlite, but is in broad agreement with the 30wt% estimate made in section 5.3.4 for the MgO content of a hypothetical 'primary' kimberlite composition for fractionation modelling. This value, and the associated values of 30wt% SiO_2, 8.5wt% Fe_2O_3 T, 15wt% CaO, 2.5wt% Al_2O_3, 1200ppm Ni and 1500ppm Cr are retained for the following discussion of lithospheric contamination.

5.5.3 Relative composition of kimberlite and lithospheric peridotite

The relative abundances of selected major and minor elements in a hypothetical primary kimberlite magma and common xenocryst mineral phases from LDG (Figure 5.13) demonstrate several important themes of compositional control by lithosphere. Admixing with any of the featured xenocryst phases will increase the SiO_2 content of the magma, but only olivine and orthopyroxene are able to enrich the magma to any extent in MgO; addition of clinopyroxene or garnet from peridotites or eclogites results in dilution of MgO in the magma. Fe_2O_3 T is largely insensitive to addition of olivine or garnet, whereas addition of pyroxene produces dilution of this oxide. Clinopyroxene is the only potential contaminant which could produce even marginal enrichment in CaO, whereas Cr-pyrope garnet and, in particular, olivine and orthopyroxene addition results in significant dilution of CaO. Olivine and orthopyroxene also produce substantial dilution of Al_2O_3, while peridotitic/eclogitic garnet and eclogitic clinopyroxene may enrich the magma in Al_2O_3. The overall major element signature of eclogite assimilation is broadly similar to that of mixing with continental crust, e.g. SiO_2 and Al_2O_3 enrichment, MgO and Ni dilution. An important observation from Figure 5.10 is that orthopyroxene is the only xenocryst phase that can enrich the magma simultaneously in MgO and Cr; while peridotitic clinopyroxene and garnet are much more Cr-rich, they are depleted in MgO relative to the hypothetical primary magma. Any enrichment in Ni must be entirely due to incorporation of olivine; this will, however, produce dilution of Cr. Addition of Cr-spinel can rapidly increase the Cr content of the magma.

Pdt ol

SiO₂

Al₂O₃

Fe₂O₃ₜ

MgO

CaO

Cr

Ni

6   4   2   0   -2   -4

Pdt opx

SiO₂

Al₂O₃

Fe₂O₃ₜ

MgO

CaO

Cr

Ni

6   4   2   0   -2   -4

Pdt cpx

SiO₂

Al₂O₃

Fe₂O₃ₜ

MgO

CaO

Cr

Ni

6   4   2   0   -2   -4

Pdt grt

SiO₂

Al₂O₃

Fe₂O₃ₜ

MgO

CaO

Cr

Ni

6   4   2   0   -2   -4

Ecl cpx

SiO₂

Al₂O₃

Fe₂O₃ₜ

MgO

CaO

Cr

Ni

6   4   2   0   -2   -4

Ecl grt

SiO₂

Al₂O₃

Fe₂O₃ₜ

MgO

CaO

Cr

Ni

6   4   2   0   -2   -4

ln (kimberlite/xenocryst)

SiO₂

Pdt spl

Al₂O₃

Fe₂O₃ₜ

MgO

CaO

Cr

Ni

8   6   4   2   0   -2   -4   -6

ln (kimberlite/xenocryst)
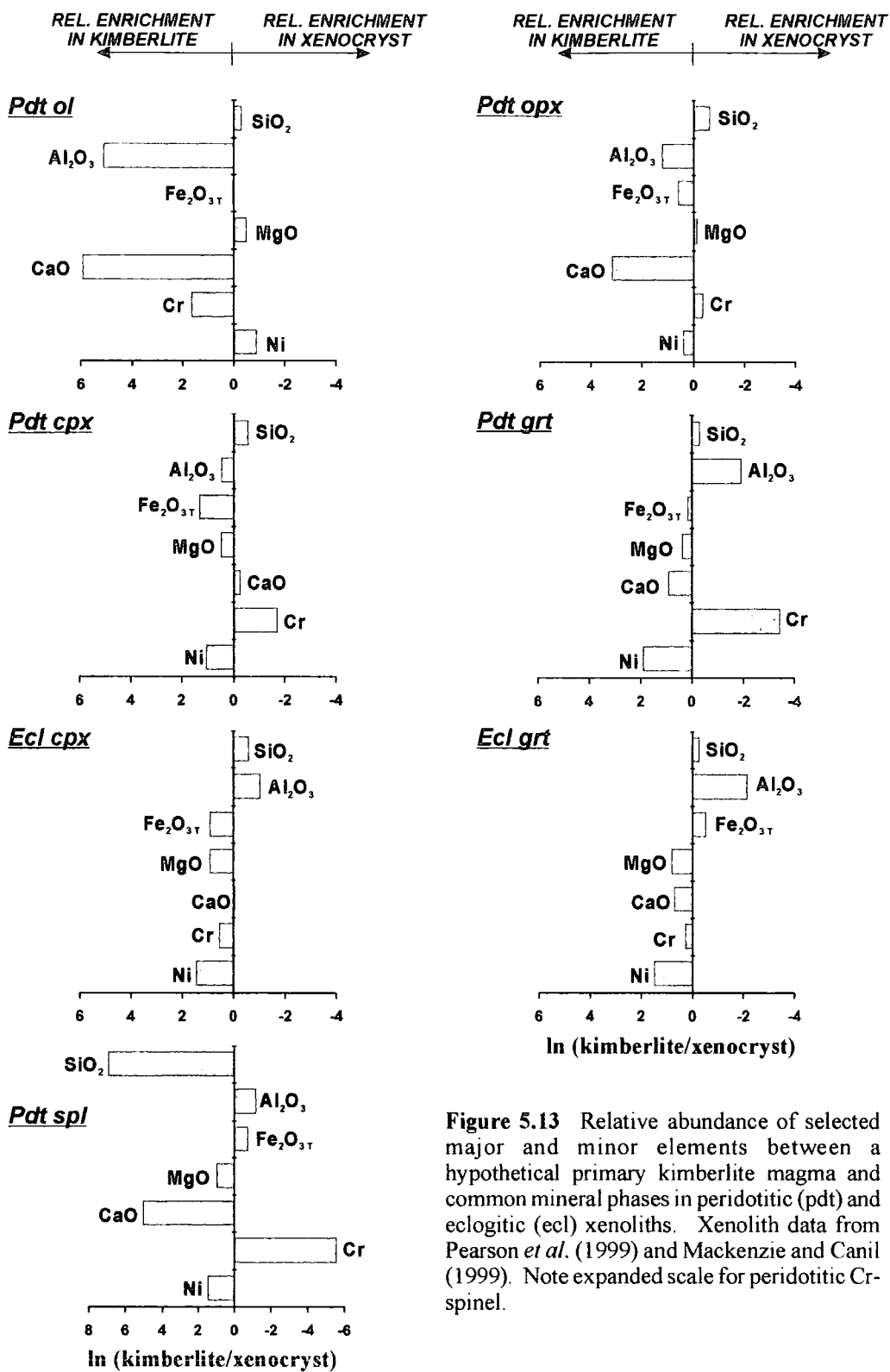
Figure 5.13 Relative abundance of selected major and minor elements between a hypothetical primary kimberlite magma and common mineral phases in peridotitic (pdt) and eclogitic (ecl) xenoliths. Xenolith data from Pearson *et al.* (1999) and Mackenzie and Canil (1999). Note expanded scale for peridotitic Cr-spinel.

159

If substantial quantities of lithospheric mantle are entrained and assimilated by kimberlite magmas then this should have a measurable effect on the bulk chemistry of the kimberlite. By comparing the major and minor element chemistry of hypabyssal kimberlites from LDG with the mantle xenoliths recovered from them, it is possible to determine whether lithospheric contamination exerts any control on the bulk composition (Figure 5.14).

Several major element oxides (TiO_2, MnO, Na_2O, K_2O, P_2O_5 – not shown) display a large degree of scatter when plotted against MgO, and thus do not provide conclusive evidence for compositional control by any of the phases present in the mantle xenocryst suite. In the case of some elements, though, the LDG kimberlites do form well-defined arrays, which could be interpreted as resulting from compositional control by specific phases (Figure 5.14). Where such trends exist, they are in most cases oriented, with increasing MgO, towards compositions that are strongly influenced by peridotitic olivine, such as the 'whole rock' peridotite compositions calculated from average mineral separate compositions and modal abundances. Cr is the only element shown in Figure 5.14 that does not demonstrate a significant degree of compositional control by peridotitic olivine in isolation; mixing with orthopyroxene or a combination of olivine and Cr-spinel can more easily account for the Cr content of LDG kimberlites with high MgO. Overall, mixing with olivine ± orthopyroxene ± Cr-spinel can account for a large amount of the observed variation of the LDG kimberlites with >30wt% MgO, in $MgO-SiO_2$, MgO-CaO, MgO-Ni and MgO-Cr space. This is strong evidence for material with a dunitic to harzburgitic composition exerting a control on the major and trace element composition of the kimberlite magma.
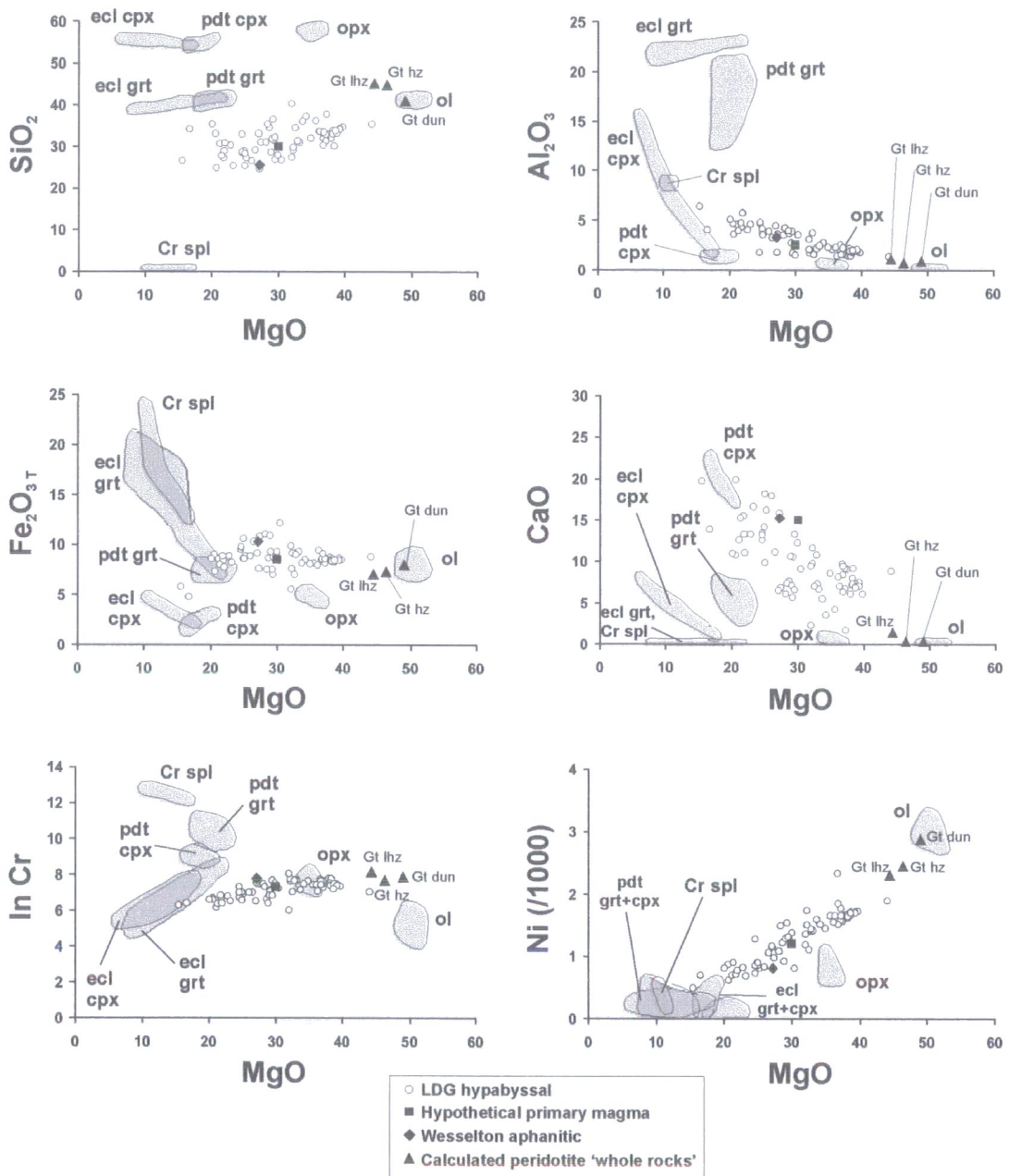
Figure 5.14 Location of Lac de Gras hypabyssal kimberlites relative to component phases of common LDG mantle xenoliths on major/minor element binary variation diagrams. Note different scales for Cr and Ni. Mineral data from Pearson *et al.* (1999), Mackenzie and Canil (1999). Modal abundances used to calculate 'whole rock' peridotite compositions: grt dunite = 95% ol, 5% grt; grt lherz = 70% ol, 20% opx, 5% cpx, 5% grt; grt harz = 75% ol, 22% opx; 3% grt.

Other phases present in the xenolith suite, such as garnet and Cr-spinel from peridotites or eclogites, may exert small degrees of compositional control on the magma and cause minor deviations from the main, olivine-orthopyroxene control trends. Small amounts of crustal contamination may also contribute towards scatter around these trends. Extension of the kimberlite array to MgO values well below the 30wt% of the hypothetical primary magma may be explained either in terms of MgO dilution by crustal addition (section 5.3), or by fractionation of olivine ± Cr-spinel from the magma (section 5.4). Samples with low MgO but high SiO_2 and Al_2O_3 strongly indicate the presence of crust.

5.5.4 Models of kimberlite-xenocryst mixing

Figure 5.15 shows models of binary mixing between the hypothetical LDG primary kimberlite magma composition and various xenocryst phases characteristically found in peridotite xenoliths. In addition, mixing trends are shown between the 'primary' kimberlite composition and 'whole rock' peridotite compositions based on typical modal abundances in peridotites recovered from LDG kimberlites (Pearson *et al.*, 1999). Actual whole rock compositions are commonly subject to infiltration and contamination by the host kimberlite liquid.

The model trends support peridotitic olivine as being a principal compositional control on LDG kimberlites that have experienced minimal or no crustal contamination. This relationship is most clearly seen in MgO-Ni space, where the amount of scatter in the data is minimal. Where deviations from the olivine-orthopyroxene control trend occur,

they can mostly be accounted for by incorporation of clinopyroxene, garnet, Cr-spinel or some combination of these phases.

As previously observed, Cr is the only element displaying compositional variation that cannot be modelled in terms of olivine control. In MgO-Cr space the general trend of increasing Cr with MgO is parallel to the mixing line between the hypothetical primary magma and orthopyroxene. Addition of olivine on this diagram could explain the cluster of analyses at high MgO which appear to have constant or slightly declining Cr contents.

Since orthopyroxene seems to be an important compositional control in addition to olivine in kimberlite magmas, an explanation is required for why orthopyroxene is invariably absent from the macrocryst assemblage. The most likely reason, as suggested by Arndt (2003), is that all of the orthopyroxene is fully assimilated into the kimberlite magma, while disaggregated olivine grains are more refractory and are able to remain within the magma in a largely unresorbed state. In some very MgO-rich kimberlites, where olivine control appears to be particularly strong (e.g. Mark, Aaron, Leslie) it is possible that the lithospheric material being incorporated is dunitic in nature and thus deficient in orthopyroxene. Microxenoliths of garnet dunite are common in the Mark and Arnie kimberlites, and depleted dunitic layers within the mantle have been advocated as a potential source of highly diamondiferous layers within the mantle (e.g. Grütter et al., 1999).
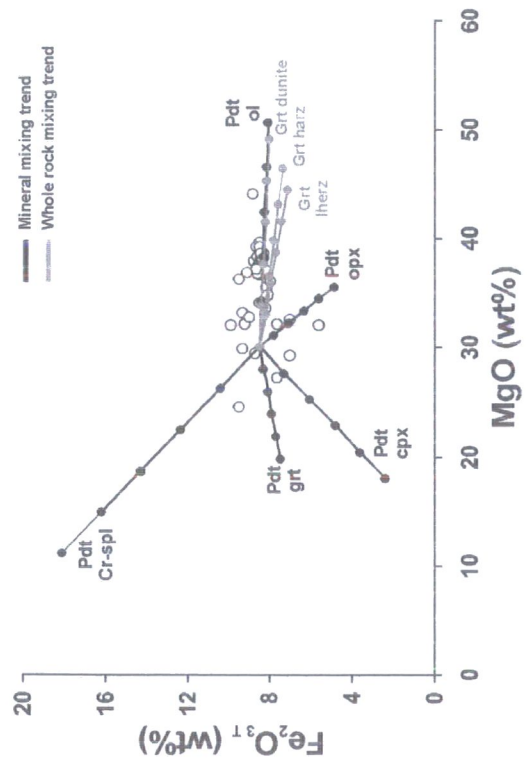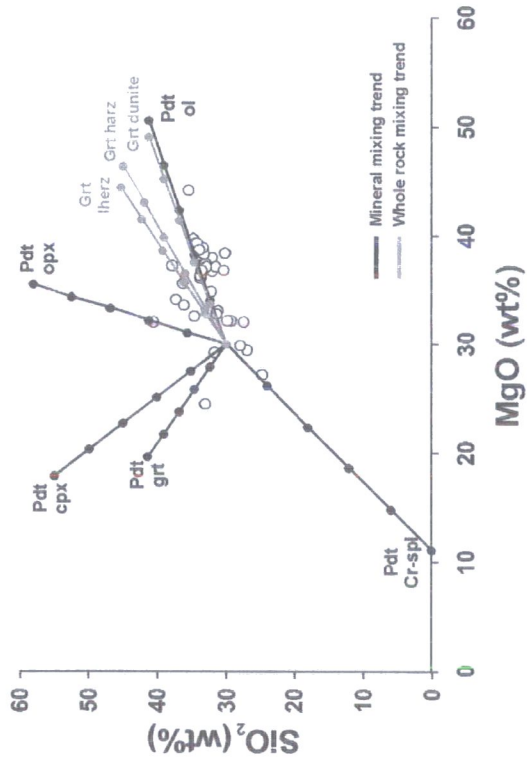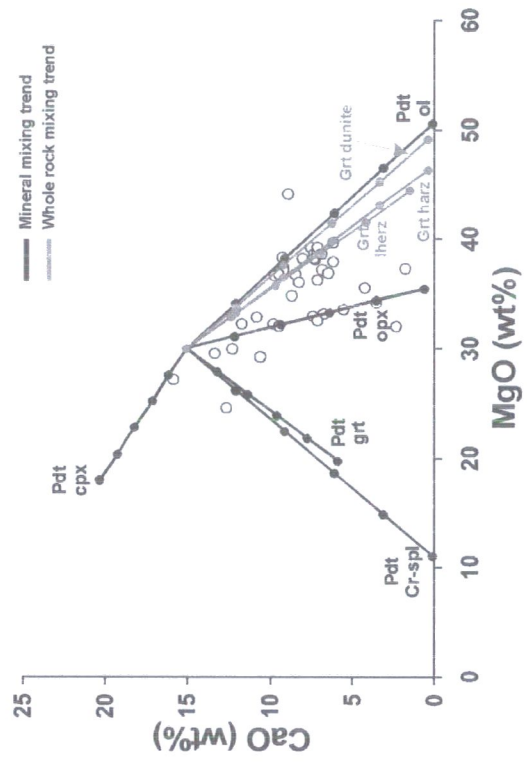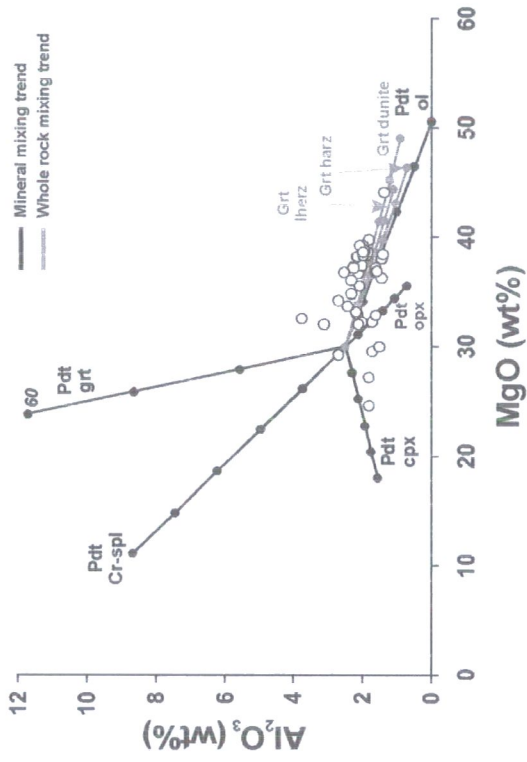
Continued - figure caption on next page.

164
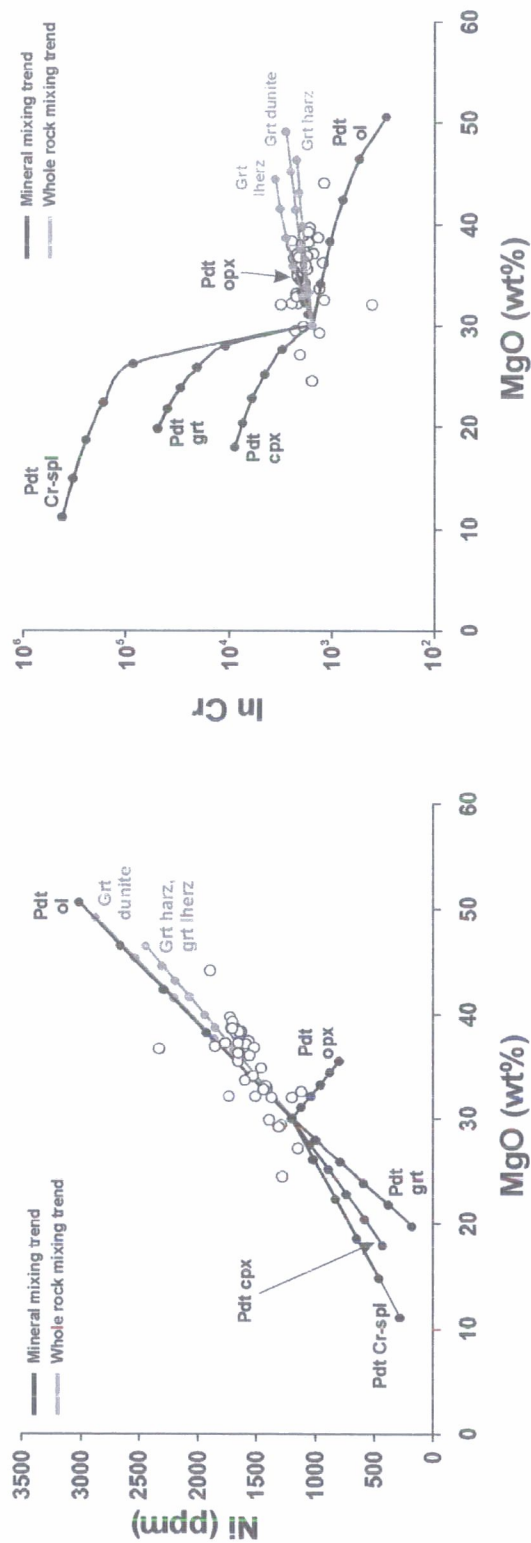
Figure 5.15 Location of LDG kimberlites with minimal crustal contamination, and modelled mixing trajectories for selected major and minor element abundances during addition of common component phases from mantle xenoliths. Tick marks are shown in 20% mixing increments; up to 100% unless stated. Xenolith data from Pearson *et al.* (1999), Mackenzie and Canil (1999). Starting composition of kimberlite magma: 30wt% MgO, 30wt% SiO_2, 8.5wt% Fe_2O_3, 2.5% Al_2O_3, 15% CaO, 1200ppm Ni, 1500ppm Cr. Modal abundances for calculated 'whole rocks': grt dunite = 95% ol, 5% grt; grt harzburgite = 75% ol, 22% opx, 3% grt; grt lherzolite = 70% ol, 20% opx, 5% cpx, 5% grt.

165

5.5.5 Models of kimberlite-lithosphere-crust mixing

The major and minor elements used in Figures 5.13-5.15 as indicators of lithospheric input can be combined to form a variety of ratios, such as Mg/Al, Mg/Fe, Ni/Cr, Al/Ni, which can be used to discriminate between the effects of contaminating kimberlite magmas with different types of lithospheric mantle and crust. The most powerful framework for analysing the relative effects of contamination by crust and lithosphere is provided by the parameters Si/Al and Mg/Yb.

It was noted in section 5.4.2 above that use of variables such as SiO_2 in isolation is an unsatisfactory means of detecting input of crust into a kimberlite, because other processes, such as addition of olivine, will also increase the SiO_2 content. The Si/Al ratio is a more appropriate variable, because it tends to decrease on addition of silicate crust, but increases on addition of olivine-rich, peridotitic mantle material. It can therefore form the basis of a model that characterises admixing of both crust and lithospheric mantle into a kimberlite magma. The distribution of the parameter *ln (Si/Al)* in the hypabyssal LDG kimberlites has a distinct first order bimodality (Figure 5.16). Since there is essentially a continuous range in Si content in these samples, the hiatus in *ln (Si/Al)* between approximately 2.1 and 2.3 must correspond to a subdivision of the data into a low-Al and a high-Al groups. This probably represents Al addition by crustal assimilation, Al dilution by entrainment of peridotitic material, or a combination of both processes.
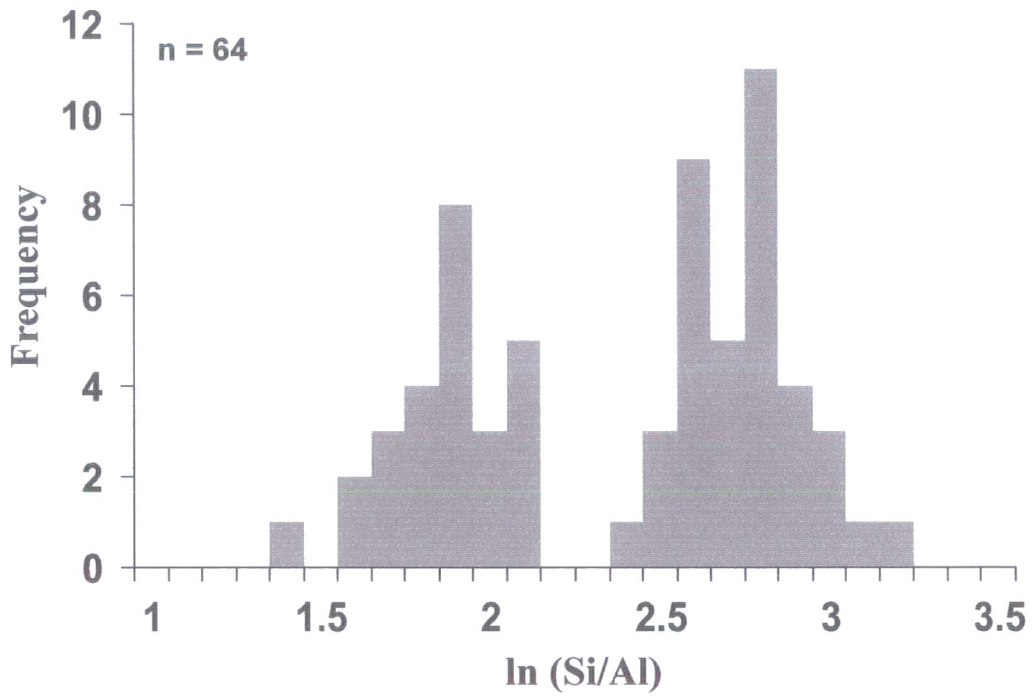
Figure 5.16 Histogram of *ln (Si/Al)* in hypabyssal facies kimberlites from Lac de Gras. The data is clearly divided into two separate high-Al (low Si/Al) and low Al (high Si/Al) groups.
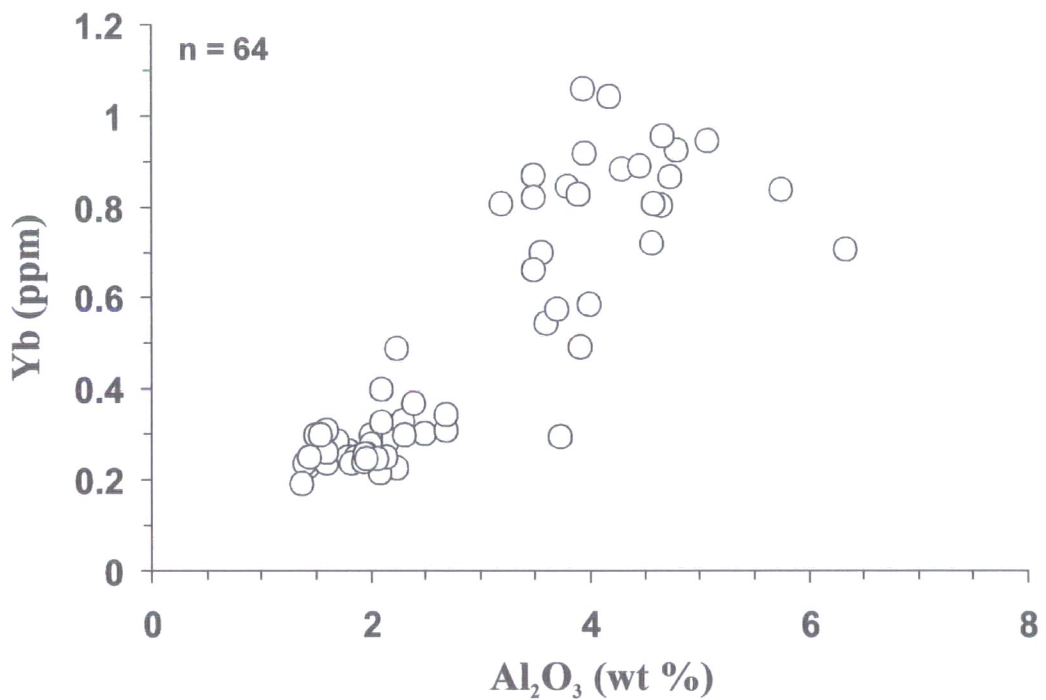
Figure 5.17 Al-Yb variation diagram for hypabyssal facies Lac de Gras kimberlites. Scatter of data increases at high Al, high Yb values.

Figure 5.17 demonstrates that there is a positive correlation between Al_2O_3 and Yb abundance, both within the LDG data as a whole, and within the low-Al and high-Al sub-groups (Figure 5.17). The increased scatter in the data at high Al_2O_3 and high Yb values could reflect compositional control exerted by a random process, such as the entrainment and assimilation of crust into the kimberlite magma. Mg/Yb and Ni/Yb ratios can be used to discriminate between contamination by crust and peridotitic material in a similar manner to Si/Al; although only Mg/Yb is illustrated in the following analysis the behaviour of these two variables is completely analogous.

Figure 5.18a demonstrates the sub-division of the LDG hypabyssal kimberlites in Si/Al-Mg/Yb space, into a low *ln (Si/Al)* group dominated by addition of crust, and a high *ln (Si/Al)* group, dominated by addition of lithospheric peridotite. In this diagram the initial composition of the magma is assumed to have the hypothetical primary magma composition used in previous models, i.e. 30wt% MgO, 30wt% SiO_2, 2.5wt% Al_2O_3 and 0.25ppm Yb. Clearly the position of these mixing trajectories depends on the location of the primary magma composition that is selected. In Figure 5.18 a range of likely compositions is indicated, based on analysis of this data and the conclusions of other recent reviews of kimberlite major element geochemistry (Arndt, 2003; Le Roex, 2003). The range shown corresponds to 25-30wt% MgO, 27-30wt% SiO_2, 2-3wt% Al_2O_3 and 0.2-0.3ppm Yb.
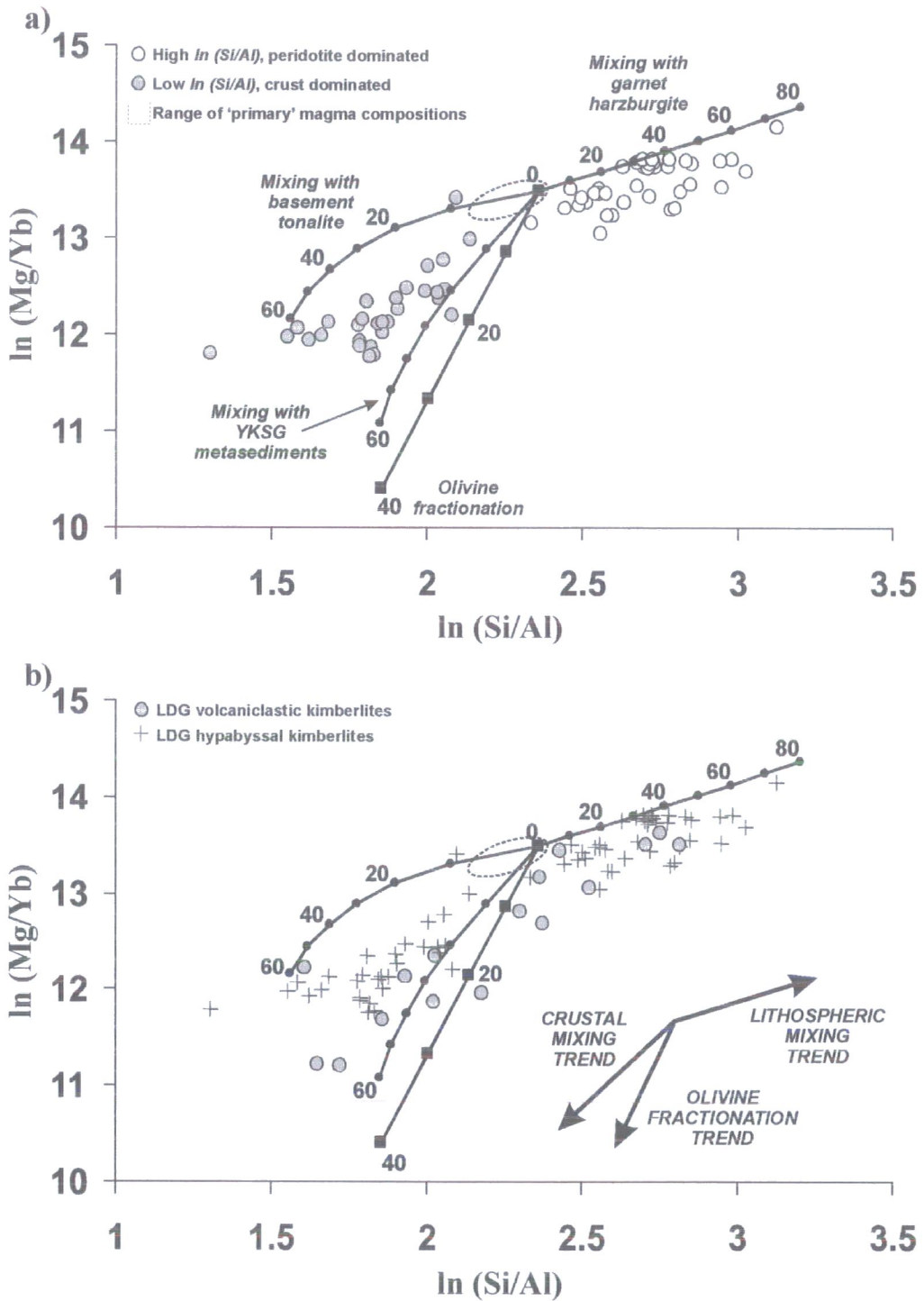
Figure 5.18 Variation of *ln (Si/Al)* and *ln (Mg/Yb)* in LDG kimberlites, and control lines for mixing with crustal and lithospheric end-members, and fractionation of olivine from a hypothetical primary magma composition: a) hypabyssal kimberlites; b) hypabyssal and volcaniclastic kimberlites. Composition for garnet harzburgite calculated from data of Pearson *et al.* (1999). Annotations to lines indicate increments of mixing and fractionation.

5.5.5.1 Fractionation trends

It was shown in section 5.3 that trends in kimberlites with MgO contents lower than that envisaged for the parental magma (e.g. <25-30wt% MgO) can be at least partially explained by fractionation of olivine ± small amounts Cr-spinel. The effects of olivine fractionation on Si/Al-Mg/Yb variations must, therefore, be taken into account. A possible trend representing the evolution of a residual liquid during fractionation of olivine is shown in Figure 5.18. This trend is based on typical K_D values for Mg, Al and Yb for basaltic systems (e.g. Henderson, 1982; Rollinson, 1993), and assuming a K_D of 1 for Si in olivine. The orientation of this fractionation trend is broadly similar to that of crustal contamination, but rapidly evolves to very low *ln (Mg/Yb)*; kimberlites with low *ln (Si/Al)* and moderate *ln (Mg/Yb)* are thus more likely to be recording signatures of crustal contamination, rather than olivine fractionation. Conversely, very low *ln (Mg/Yb)* without very low *ln (Si/Al)* could indicate evolution of the magma by fractionation either before, during or after contamination by lithopshere and crust.

5.5.5.2 Crustal contamination trends

Mixing lines to basement tonalities and Yellowkife Supergroup (YKSG) metasediments (greywackes) bracket the compositional range of low *ln (Si/Al)* kimberlites from the LDG area. On this basis, almost all low *ln (Si/Al)* kimberlites have >10% crustal contamination, and some have up to 60%. These samples correspond almost exactly to the highly contaminated kimberlites identified on the basis of Al/Mn, Na/P and Sm/Yb ratios (section 5.4).

Volcaniclastic facies kimberlites from LDG, including the sample from the Fox pipe, which is known to be heavily contaminated with crust, plot along similar contamination

vectors to those defined in Figure 5.18b, over a range of *ln (Si/Al)*. The hypabyssal facies samples from the T-146 pipe, which are also known to be heavily contaminated, have the lowest *ln (Si/Al)*, and some of the lowest *ln (Mg/Yb)* values recorded in the entire dataset. This provides a useful check on the general validity of the model.

It is difficult to make accurate quantitative estimates of the amount of crust that may have been assimilated by a kimberlite without knowing what types of material, and in what proportions, have been entrained. This would require a detailed study of samples of a kimberlite and its xenoliths from diamond drill core, but would provide a more robust test of the model presented in Figure 5.18. A further complication may arise if partial melting of country rocks produces incongruent melt compositions, making the contaminant end-members very difficult to define. It is, nevertheless, important to attempt to establish whether these samples can really assimilate 20-40%, or in some cases more, crust and yet still appear largely uncontaminated during petrographic examination. If this is genuinely the case it implies that the majority of assimilated material must be extremely finely disseminated and/or entirely chemically digested within the ascending magma. Clearly, these model estimates of crustal assimilation are also dependent on the composition assumed for the primary magma. If the Mg/Yb and Si/Al ratios of the magma are initially lower than suggested here, then the values indicated above are overestimates. In addition, the tendency for olivine fractionation to produce similar trends to assimilation of crustal material could also result in the amount of crustal contamination being overestimated. The values presented here should, therefore, be treated as maximum estimates.

5.5.5.3 Lithospheric mantle contamination trends

Mixing with a calculated garnet harzburgite 'whole rock' composition broadly defines the upper limit of variation within the LDG kimberlite data at high *ln (Si/Al)*. Using calculated garnet dunite and garnet lherzolite 'whole rock' compositions as end-members produces peridotite mixing lines of very similar length and orientation. Mixing with typical eclogitic compositions produces a very different trend, similar to that of crustal contamination (not shown in Figure 5.18); eclogite xenoliths are, however, rare relative to peridotites in LDG kimberlites (B. A. Kjarsgaard, pers. comm.), although E-type diamonds have been recovered from some bodies. It seems probable that any lithospheric contamination effects will be dominated by assimilation of peridotite, rather than eclogite.

On the basis of mixing with peridotite alone, most of the high *ln (Si/Al)* compositions can be explained by assimilation of 10-50% material with a harzburgitic composition. These values agree closely with estimates based on Os isotope studies on Slave kimberlites (Pearson *et al.*, 2003). The kimberlite with the highest *ln (Si/Al)* corresponds to ~70% peridotite incorporation; this sample is from the Mark kimberlite, which is known to contain abundant peridotite micro-xenoliths. The majority of the high *ln (Si/Al)* samples are located below the garnet harzburgite mixing line, with variable *ln (Mg/Yb)*. These offsets could be explained by small amounts of crustal contamination taking place after assimilation of lithospheric material into a kimberlite. In most cases this requires <<10% crust, and thus these samples can be considered to be minimally contaminated by crust.

5.5.6 Identification of crustal and lithospheric signatures in LDG kimberlites

Figure 5.19 shows the variation in $\ln(Si/Al)$ and $\ln(Mg/Yb)$ for all Canadian hypabyssal kimberlites analysed during this study. Nine of the fourteen samples analysed from Grizzly cluster together close to the mixing line between the 'primary' magma composition and the calculated garnet harzburgite lithospheric end-member. The location of these points corresponds to 20-40% mixing between these components. This is again in agreement with estimates based on Os isotopes (Pearson *et al.*, 2003). The other five samples from Grizzly have lower $\ln(Mg/Yb)$ across a range of $\ln(Si/Al)$. Those situated further away from the garnet harzburgite mixing line may have assimilated some crustal material, or could have experienced more fractionation of olivine than the majority of the Grizzly samples. This provides an indication of the amount of compositional variability that can be introduced by fractionation and contamination acting to variable extents on samples from a common parental magma.

Other kimberlites located in the immediate vicinity of Grizzly display a wide range of inter-kimberlite variation in $\ln(Si/Al)$ and $\ln(Mg/Yb)$, with more limited intra-kimberlite variation in these parameters. Samples from Roger, Koala West and Pigeon have compositions indicative of crustal contamination and/or olivine fractionation. Those from Leslie, Rat, Aaron, Mark and Arnie have signatures that appear to be dominated by lithospheric contamination, with variable amounts of fractionation/crustal contamination.

GROUP A1:
GRIZZLY

CRUSTAL MIXING TREND

LITHOSPHERIC MIXING TREND

OLIVINE FRACTIONATION TREND

GROUP A2:
GRIZZLY 'NEIGHBOURS'

Roger
Koala West
Leslie
Pigeon
Rat
Aaron
Mark
Arnie

GROUP B:
OTHERS NORTH OF LDG

Anne (HL-10)
Finlay (HL-11)
Don (HL-12)
Anaconda
Rattler
Porpoise

GROUP C:
SOUTH AND EAST OF LDG

T-19
T-21
T-34
T-35
T-36
T-237
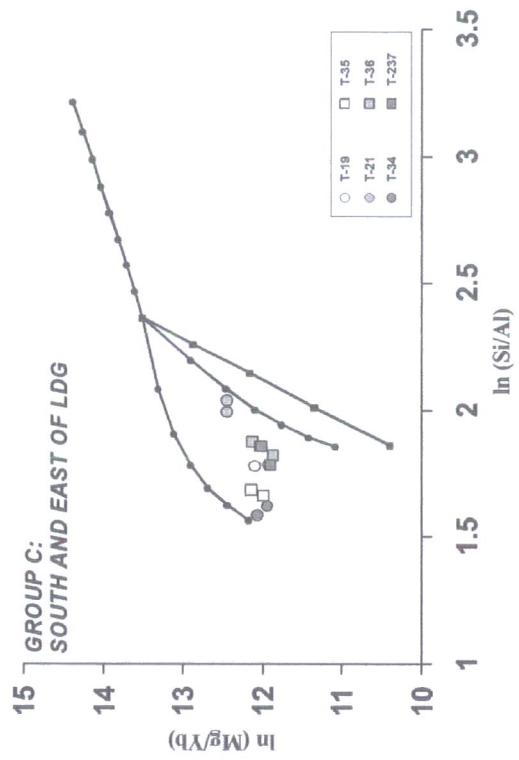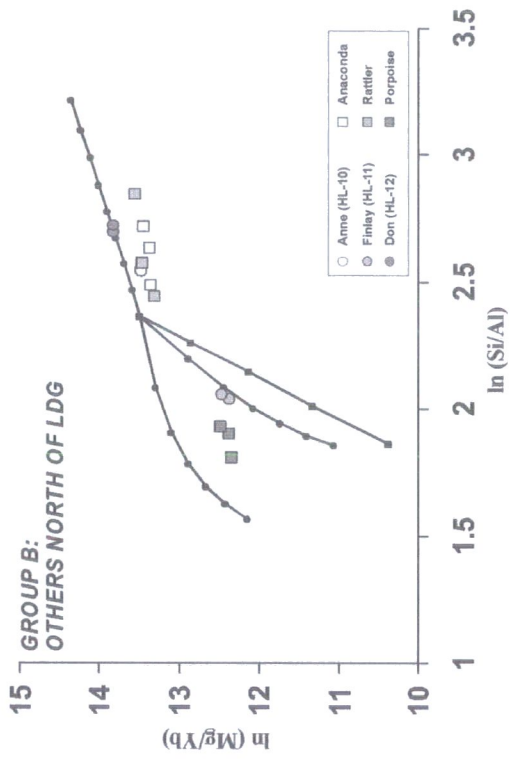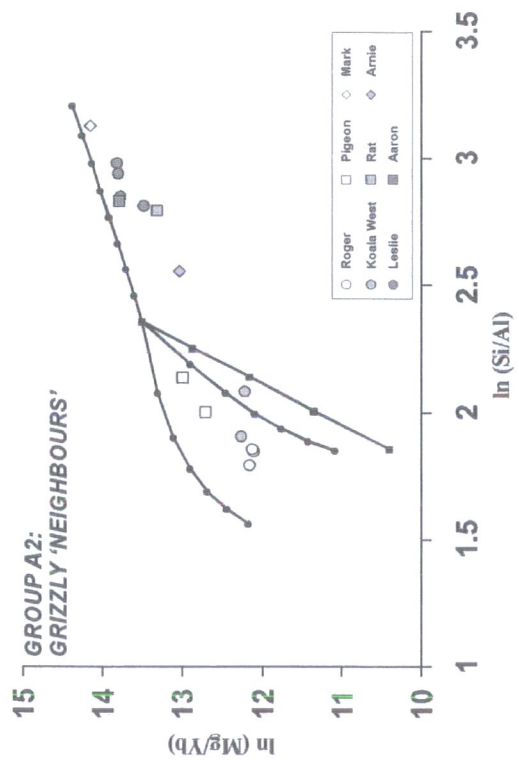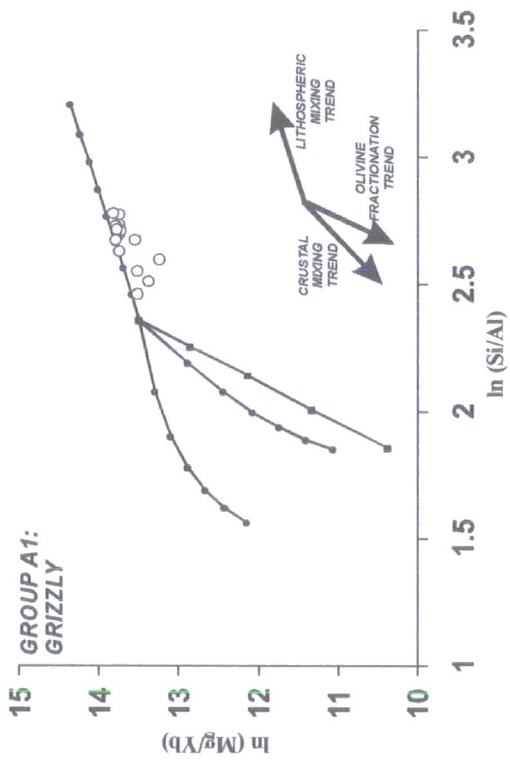
(Continued on next page)

174
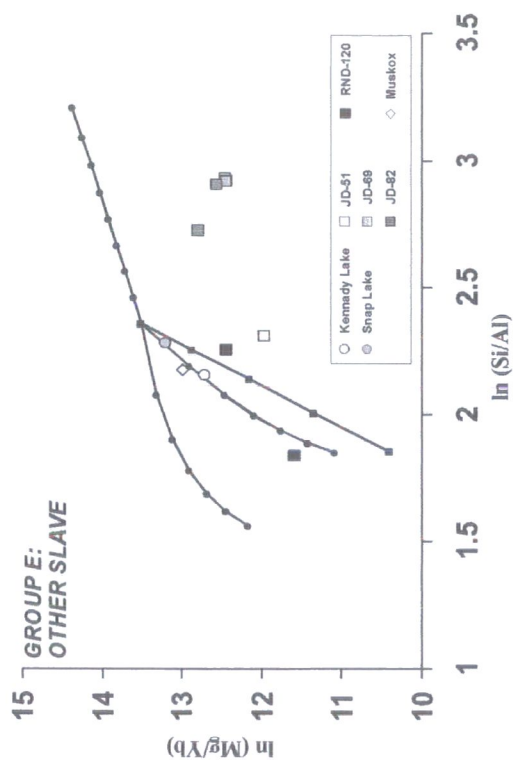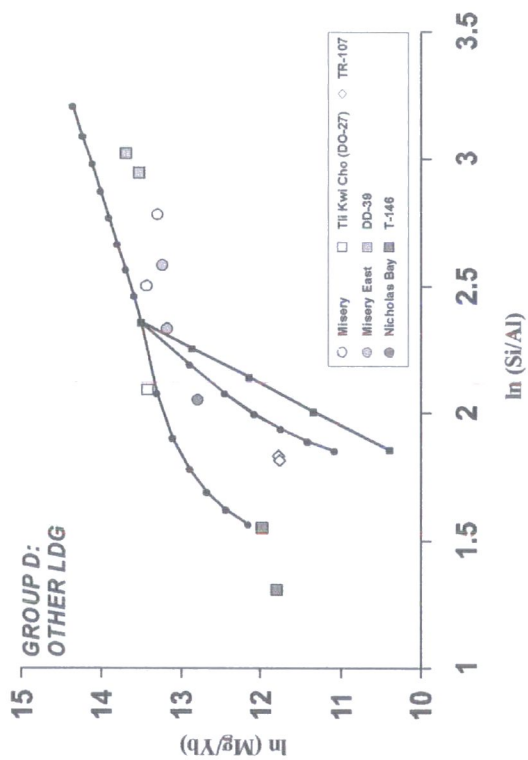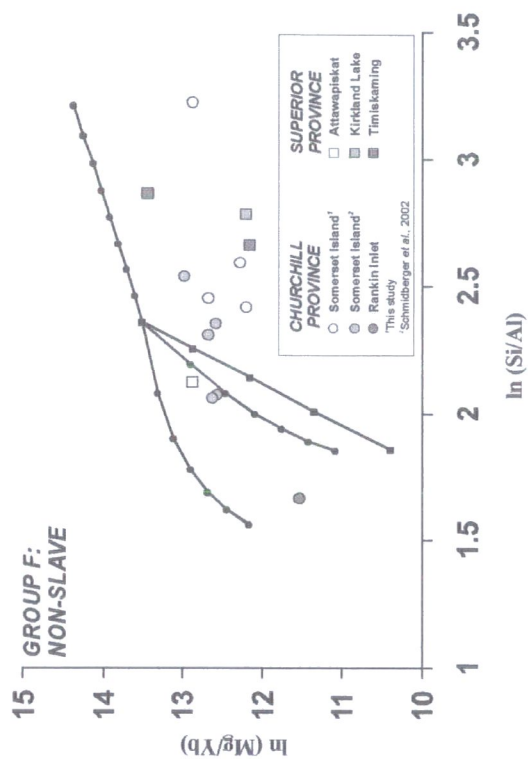
Figure 5.19 Location of all Canadian samples in *ln (Si/Al)*-*ln (Mg/Yb)* space. Samples are divided into geographically-based groups identified in Chapter 1.

A similar range of compositions is evident in other kimberlites from the north side of Lac de Gras: those from Finlay and Porpoise have low *ln (Si/Al)* and *ln (Mg/Yb)* suggesting predominant control by crustal contamination; samples from Anne and Don, and in particular Anaconda and Rattler, have signatures of variable (10-50%) lithospheric contamination and minimal (0-5%) crustal contamination.

All kimberlites analysed from the group located south and east of Lac de Gras display strong signatures of crustal contamination, plotting at a range of low *ln (Si/Al)* and *ln (Mg/Yb)* between the two bounding mixing lines to tonalite and greywacke compositions. On the basis of the model parameters presented here, T-21 is the least contaminated of this group, incorporating 20-30% crust, while the others (T-19, T-34, T-35, T-36 and T-237) contain 40-60% crust. These values may appear high, considering that there is little visible contamination, but can only be overestimates if, as noted earlier, the true composition of the magma prior to contamination has lower *ln (Si/Al)* and *ln (Mg/Yb)* than used in this model, or has been subject to olivine fractionation.

The remaining LDG hypabyssal kimberlites are also divided between signatures of crustal contamination/olivine fractionation and lithospheric assimilation. The two samples from T-146 have the lowest *ln (Si/Al)* in the entire dataset and appear to be dominated by crustal material. DO-27 (Tli Kwi Cho) and Nicholas Bay are also significantly affected by crust. Misery, Misery East and DD-39 record 0-70% lithospheric assimilation, based on the hypothetical primary composition, and ~0-10%

crustal contamination. Both Misery and Misery East display considerable intra-kimberlite variation.

Beyond Lac de Gras, samples from the Contwoyto field in the northern Slave Province, plus those from the Churchill and Superior provinces, have a similar range of *In (Si/Al)* to the LDG kimberlites, but in general have lower *In (Mg/Yb)* values. If the primary magmas in these regions were similar to those at LDG, then this would suggest that these kimberlites have assimilated up to 60% lithospheric peridotite, and subsequently up to 40% crust. Alternatively, the composition of the primary magma may have been different in these regions, so that the initial *In (Mg/Yb)* value of the magma was lower.

Many of the kimberlites from these regions have elevated CaO contents, which in some instances are coupled with MgO that is much lower than the LDG average. This is not true in all cases, but Yb contents are almost without exception comparable to those of the crustally dominated low *In (Al/Si)* group from LDG. The low *In (Mg/Yb)* therefore appears to be due to high Yb, rather than low Mg. Unlike at LDG, this elevated Yb does not in general correlate with high Al. As a result, the kimberlites from the north Slave, Churchill and Superior provinces have *In (Si/Al)* that is comparable to LDG 'lithosphere dominated' samples, but have *In (Mg/Yb)* that is more like LDG 'crust dominated' samples.

The consistently high Yb contents of these kimberlites, without associated high Al, may indicate that the lower *In (Mg/Yb)* values reflect a different composition in the primary magma, rather than modification by extensive assimilation of crust. A more extensive geochemical study of samples from these regions, ideally coupled with

petrography and information on olivine populations, would help to resolve whether these kimberlites could be fitted satisfactorily into the LDG model. Kimberlites from South Africa, Finland and China also tend towards lower *ln (Mg/Yb)*, largely as a result of high Yb levels relative to many LDG samples; unless kimberlites from these regions are consistently more contaminated than LDG samples, this would appear to support variations in Mg/Yb of the primary magma between kimberlite fields and provinces.

5.5.7 Summary

There is clear evidence for the major and trace element content of kimberlites being influenced by the addition of lithospheric mantle material into the magma. It is difficult to determine how much of this signature is due to material that has been fully assimilated into the magma, and how much results from physically entrained material that remains visible as xenoliths and xenocrysts. Olivine is probably more refractory and resistant to assimilation than phases such as orthopyroxene and garnet. In addition, olivine has the lowest Si activity of silicate phases occurring in peridotite xenoliths, and consequently will be least reactive with the SiO_2-poor kimberlite magma. Olivine and orthopyroxene are the most dominant xenocryst phases in terms of modifiying the composition of the magma, but other phases such as Cr-spinel, clinopyroxene and garnet may be responsible for some of the small deviations observed from olivine-orthopyroxene control trends.

Variations in Si/Al-Mg/Yb space are very useful for resolving the relative inputs of lithospheric mantle and crustal contamination in the LDG hypabyssal kimberlites. High Si/Al samples have a signature that is controlled by assimilation of lithospheric peridotite, with small deviations in Mg/Yb indicating variable subsequent input from

crustal components. Low Si/Al samples are controlled primarily by crustal assimilation, and appear to have experienced minimal addition, or even net removal, of macrocrystal olivine. The effects of mixing a hypothetical primary magma with peridotite or eclogite are very different on such a diagram; eclogite is capable of modifying the magma chemistry in a similar way to continental crust, and may be responsible for some of the low ln (Si/Al) signatures previously attributed solely to crustal control. The bulk of lithospheric material incorporated by LDG kimberlites is, however, likely to be peridotitic. Most or all of the LDG samples have some detectable, though often minimal, component of crustal contamination. Olivine fractionation may also produce detectable variations in Si/Al-Mg/Yb space from trends of lithospheric or crustal contamination. On the basis of the Si/Al-Mg/Yb model presented here, approximately half of the LDG hypabyssal kimberlites have compositions that are significantly influenced by crustal contamination. This signature is particularly prevalent in the kimberlites from the southern side of LDG.

Canadian kimberlites from beyond the LDG field do not appear to be directly comparable with the LDG dataset on these Si/Al-Mg/Yb diagrams. This is largely due to lower Mg/Yb values, which result primarily from much higher Yb content than is typical for LDG samples. This may reflect compositional differences between primary kimberlite magmas in different fields, rather than consistently higher degrees of crustal contamination in non-LDG kimberlites. Samples from southern Africa also plot consistently at lower Mg/Yb than LDG samples on these diagrams, across a range of Si/Al.

179

While the model proposed here is subject to some of the same limitations as the contamination index, it offers some distinct advantages. Firstly, the separate influences of crustal and peridotitic mantle material are directly addressed and can be discriminated. Secondly, the graphical presentation of the model provides better visualisation of relative contamination between samples. Thirdly, binary mixing trajectories to constrain the amount of contamination may easily be constructed using the model parameters, provided that reasonable estimates of the primary magma and contaminant compositions are available. Conversely, a detailed study of the modal abundance and composition of different contaminants within a kimberlite body could be used in conjunction with the model to constrain the composition of the primary kimberlite magma. The ability to obtain realistic estimates of the amount of contamination in a kimberlite is essential to the construction of isotopic and other petrogenetic models presented in chapter 6 and 7.

Chapter 6

Isotope geochemistry

6.1 CHAPTER OVERVIEW

This chapter provides a description of the isotopic data acquired for kimberlites from Lac de Gras and other Canadian localities during this study, and investigates the processes that may be responsible for generating the observed variation in Hf, Nd and Sr isotope signatures. The isotopic character of kimberlites from the Slave craton and elsewhere in Canada is compared throughout with the well-characterised Group I and II kimberlites from southern Africa. The possible effects of crustal contamination on isotopic compositions is carefully examined, in association with trace element constraints from Chapter 5, to ensure that all subsequent consideration of kimberlite petrogenesis (Chapter 7) is based on uncontaminated material that is representative of mantle sources and/or processes.

6.2 INTRODUCTION

6.2.1 Previous studies of kimberlite isotope geochemistry

6.2.1.1 Early work

The vast majority of studies concerning the isotopic character of kimberlites have concentrated on the Rb-Sr, Sm-Nd and U-Th-Pb systems due to contemporary limitations on analytical techniques. It is only during the last decade that the Lu-Hf and Re-Os isotope systems have become viable as tools for investigating kimberlite petrogenesis. In the 1970s isotopic work on kimberlites focussed on explaining the large observed variations in $^{87}Sr/^{86}Sr$ ratios. It was realised (Mitchell and Crockett,

1971; Barrett and Berg, 1975) that, due to the high abundance of Sr in kimberlites, very large quantitites of crustal assimilation would be required for contamination to be a plausible cause of high $^{87}Sr/^{86}Sr$ values. Berg and Allsopp (1972) and Barrett and Berg (1975) concluded that values in excess of ~0.704 were indicative of post-emplacement alteration. Results of Sr isotope determinations on kimberlites from India (Paul, 1979) and Central Africa (Demaiffe and Fieremans, 1981) were at odds with this conclusion and Mitchell (1986) has cast doubt on the criteria used to judge 'freshness' of material in these early studies.

6.2.1.2 The Group I/Group II classification

The work of Smith (1983) provided a new paradigm for kimberlite geochemistry. Building on work by Kramers (1977), Basu and Tatsumoto (1980) and Kramers *et al.* (1981), this study demonstrated that kimberlites from southern Africa could be subdivided into two groups on the basis of their Nd and Sr isotope composition. These Group I and Group II kimberlites are defined solely on the basis of their isotopic character, although there are also broad elemental and mineralogical distinctions between the groups. The conventional interpretation of this subdivision is that Group I and Group II magmas are derived from different sources within the mantle and are thus petrogenetically distinct. These sources are considered to be the convecting asthenospheric mantle and metasomatically-enriched sub-continental lithospheric mantle, respectively. This interpretation prevails up to the present day, although alternative models – mainly invoking mixing of magmas from the asthenosphere into the depleted lithosphere – have been proposed (Anderson, 1982; McCulloch *et al.*, 1983; Vollmer *et al.*, 1984).

During the last 25 years Nd, Sr and Pb isotopic data have been obtained on kimberlites from many other cratonic regions, such as Greenland (Nelson, 1989), West Africa (Taylor *et al.*, 1994), Siberia (Agashev *et al.*, 2000; 2001a), Arkhangelsk (Mahotkin *et al.*, 2000), Finland (O'Brien and Tyni, 1999), Brazil (Bizzi *et al.*, 1994; Araujo *et al.*, 2001), China (Tompkins *et al.*, 1999) and Australia (Edwards *et al.*, 1992). To date no kimberlites with Group II isotopic signatures have been found outside South Africa. Detailed studies of the South African occurrences (Fraser, 1987; Tainton, 1992) support the hypothesis of discrete mantle sources for Group I and Group II rocks. The only exceptions to the Group I/Group II model are a small number of kimberlites from the marginal region of the Kaapvaal craton, and some kimberlites from Brazil (Bizzi *et al.*, 1994) and Arkhangelsk (Mahotkin *et al.*, 2000), which have Sr and Nd isotope signatures that are transitional between Group I and Group II (Skinner *et al.*, 1994). The elemental geochemistry of these samples was also found to be transitional in some respects, but with more overall similarity to Group II than Group I kimberlites.

6.2.1.3 Hf isotope studies

Until recently, difficulties with chemical pre-concentration of Hf from kimberlites, as discussed in Chapter 2, have prevented extensive investigations of their Hf isotope composition. The first such detailed study (Nowell *et al.*, 1999; in press) demonstrated that a set of kimberlites from South Africa, including many of the samples originally analysed for Nd and Sr by Smith (1983), have very unusual Hf isotope characteristics. Lamproites, which are also derived from depth within the mantle, are the only other magmatic rocks in which these kinds of signatures have so far been observed (Nowell *et al.*, 1998b). The Lu-Hf system offers the additional advantage of particular

sensitivity to processes that take place in the presence of garnet, e.g. formation of magmas by melting at depth in the mantle, within the garnet stability zone.

Improvements to the Hf separation chemistry made during the course of this study have enabled a much larger number of kimberlites from Canada to be analysed for Hf, in addition to other isotopes. Consequently, the isotopic database presented here is an excellent basis for both further testing of the Group I/Group II paradigm, and investigation of anomalous Hf isotope signatures in kimberlites from beyond South Africa.

6.2.2 Features of the current study

For this study new, high-precision Sr, Nd and Hf isotope analyses have been made on 123 kimberlite samples. These are primarily hypabyssal facies rocks obtained from the recently discovered LDG kimberlite field (Carlson *et al.*, 1999) and other localities within the Slave province of northern Canada. All are well characterised for major and trace elements (Chapters 4 and 5). To our knowledge it is the largest and best-characterised isotopic database for a single kimberlite province, and is the most comprehensive collection of Hf isotope variations in kimberlites.

A subset of 14 analyses of separate samples from the Grizzly pipe is used to investigate intra-kimberlite variations, to attempt to further understand the processes affecting the isotopic compositions of kimberlites. Previously, the only kimberlite to have been analysed this extensively is the Finsch intrusion of South Africa (Fraser, 1987). Samples from a further 25 individual hypabyssal bodies provide constraints on inter-kimberlite isotopic variations within the LDG field. These isotopic characteristics are

then compared to those of kimberlites from other fields within the Slave province, and other kimberlite provinces beyond the Slave, including the Kaapvaal province of southern Africa.

In addition to its size, the dataset is also notable for the freshness of the samples. This is in contrast to the levels of alteration found in samples typical of the Kaapvaal kimberlites. Samples have been screened for visible signs of alteration and contamination, both before and after crushing. It is therefore an ideal basis for investigating the isotopic composition of an unmodified, 'primary' kimberlite magma and also that of the mantle source. The freshness of these samples is also beneficial to the investigation of unusual Hf-Nd isotope characteristics, as identified by Nowell *et al.* (in press) for South African kimberlites, in these rocks.

6.2.3 Parameters used for isotopic modelling

Throughout this chapter isotopic data is presented in terms of initial ratios and epsilon notation (Papanastassiou and Wasserburg, 1970; DePaolo and Wasserburg, 1976). This notation expresses isotopic signatures in terms of enrichment or depletion relative to the composition of Bulk Silicate Earth (BSE). It also enables comparison between samples of different age, and accounts for the various mass bias corrections applied to measured data during instrumental determinations by different laboratories. The parameters used in these calculations for the Rb-Sr, Sm-Nd and Lu-Hf systems are shown in Table 6.1. Unless otherwise stated, all epsilon values are calculated from initial isotopic ratios. These values are represented by the notation $\varepsilon_{Sr\,i}$, $\varepsilon_{Nd\,i}$ and $\varepsilon_{Hf\,i}$.

Rb-Sr			Sm-Nd			Lu-Hf		
PARAMETER	*VALUE*	*REF*	*PARAMETER*	*VALUE*	*REF*	*PARAMETER*	*VALUE*	*REF*

Parent-daughter decay constants

$^{87}Rb \rightarrow {}^{87}Sr$: λ	1.419×10^{-11}	[1]	$^{147}Sm \rightarrow {}^{143}Nd$: λ	6.54×10^{-12}	[3]	$^{176}Lu \rightarrow {}^{176}Hf$: λ	1.876×10^{-11}	[5]

Chondritic Uniform Reservoir (CHUR)

$^{87}Sr/^{86}Sr_{[present]}$	0.7045	[2]	$^{143}Nd/^{144}Nd_{[present]}$	0.512638	[4]	$^{176}Hf/^{177}Hf_{[present]}$	0.282772	[6]
$^{87}Rb/^{86}Sr_{[present]}$	0.0827	[2]	$^{147}Sm/^{144}Nd_{[present]}$	0.1966	[4]	$^{176}Hf/^{177}Hf_{[present]}$	0.0332	[6]

Table 6.1 Parameters used in this study for calculation of epsilon values (ε_{Sr}, ε_{Nd} and ε_{Hf}). References for parameter values: [1] Davis *et al.* (1977); [2] DePaolo (1988); [3] Lugmair and Marti (1978); [4] Goldstein *et al.* (1984); [5] Albarède *et al.* (2000); [6] Blichert-Toft and Albarède (1997).

6.3 DATA REPRESENTATION

6.3.1 Framework for representing Hf-Nd and Nd-Sr variations

6.3.1.1 Hf-Nd-Sr isotope variations and the mantle array

Observed variations in the Hf and Nd isotope compositions of most terrestrial rocks constitute a broad array relative to BSE, as summarised by Vervoort *et al.* (1999). This absence of large-scale decoupling, especially for mantle samples, is surprising given the strong potential for various minerals, such as garnet or perovskite, to fractionate parent and daughter elements to varying extents in the Lu-Hf and Sm-Nd systems. The few exceptions to this behaviour so far identified are magmas that originate from deep within the mantle, such as kimberlites (Nowell *et al.*, 1999; in press) and lamproites (Nowell *et al.*, 1998b), and some carbonatites (Bizimis, 2001).

The coherency of Hf and Nd isotope variations was first identified, and remains most striking, among oceanic basalts (Patchett and Tatsumoto, 1980), as shown in Figure 6.1a. The field of N-MORB is located entirely within the top right quadrant of the diagram (positive $\varepsilon_{Hf\ i}$, positive $\varepsilon_{Nd\ i}$), indicating derivation of these basalts from a source that is depleted relative to BSE (i.e. Lu/Hf and Sm/Nd higher in magma source than in BSE). The range of OIB compositions extends from the MORB field into the opposite, enriched quadrant (negative $\varepsilon_{Hf\ i}$, negative $\varepsilon_{Nd\ i}$). OIB magmas may therefore be variably enriched or depleted relative to BSE, depending on the exact nature of their source. HIMU (high $^{238}U/^{204}Pb$) OIB, which is characteristic of a small number of ocean islands (e.g. St Helena, Tubaii), is located at the lower margin of the mantle array, with positive $\varepsilon_{Hf\ i}$ and $\varepsilon_{Nd\ i}$.
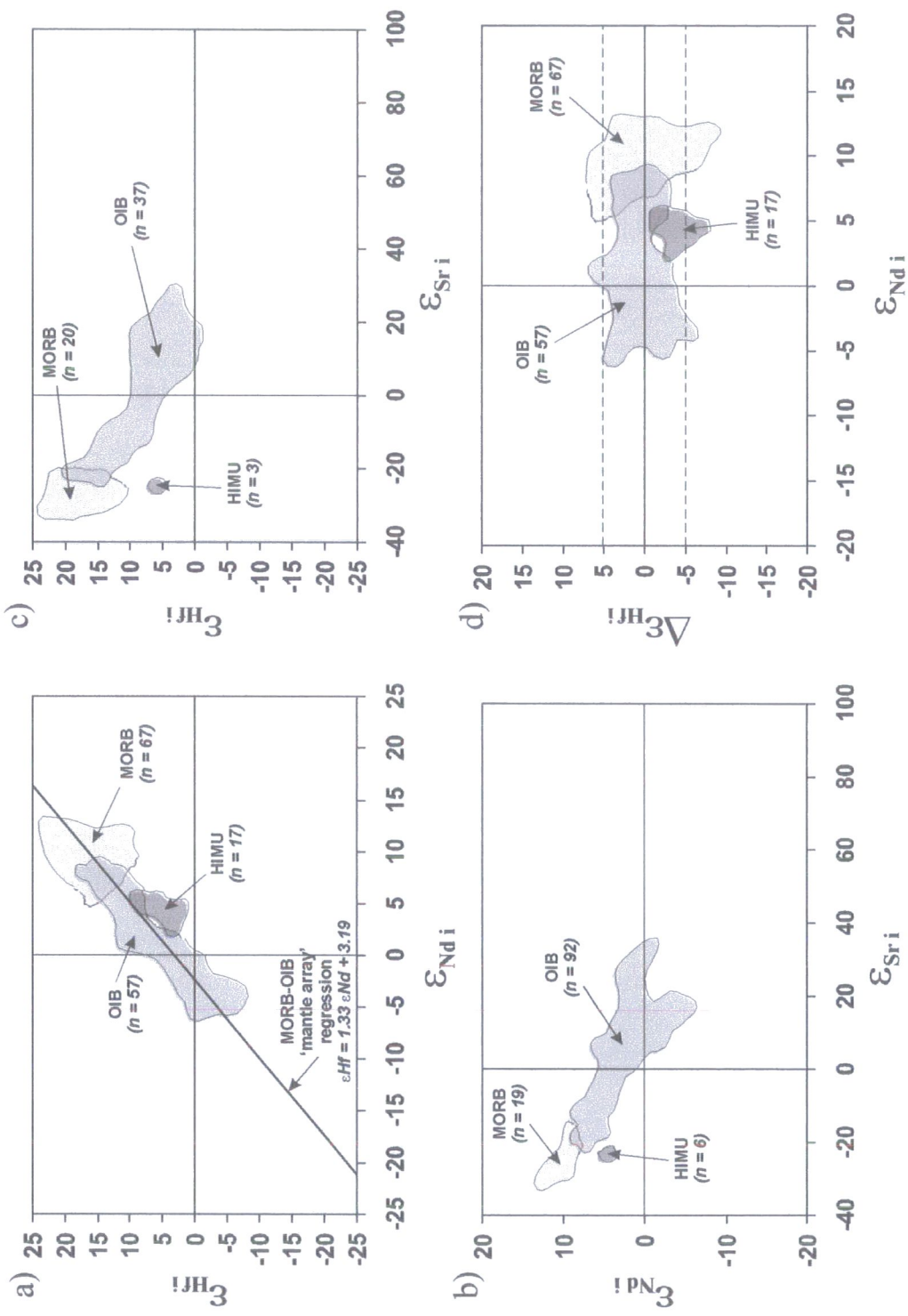
Figure 6.1 Location of MORB and OIB fields in Hf-Nd-Sr isotope space: a) $\varepsilon_{Hf\,i}$-$\varepsilon_{Nd\,i}$; b) $\varepsilon_{Nd\,i}$-$\varepsilon_{Sr\,i}$; c) $\varepsilon_{Hf\,i}$-$\varepsilon_{Sr\,i}$; d) $\Delta\varepsilon_{Hf\,i}$-$\varepsilon_{Nd\,i}$. Data from O'Nions *et al.* (1977), Dosso and Murthy (1980), Patchett and Tatsumoto (1980), White and Hofmann (1982), Patchett (1983), Stille *et al.* (1986), Salters and Hart (1991), Chauvel *et al.* (1992), Salters and White (1998), Nowell *et al.* (1998).

Similar diagrams can be constructed for Nd-Sr and Hf-Sr isotope variations in these oceanic basalts (Figures 6.1b-c). In both projections the range of OIB extends from the 'depleted' field of MORB (positive ε_{Ndi}, negative ε_{Sri}) into the 'enriched' field characterised by negative ε_{Ndi}, positive ε_{Sri}. This range in Hf-Sr isotope composition is likely to extend further, to more radiogenic Sr and unradiogenic Hf than that shown in Figure 6.1c, which is based only on samples for which both Hf and Sr isotope data are available. Consequently, the array is biased in favour of Hawaii in relation to islands with more enriched signatures, such as Kerguelen. Variations in Sr isotope composition within the mantle array are in general negatively correlated with variations in Hf and Nd isotope composition.

6.3.1.2 Quantifying deviations from the mantle array

The location of any sample relative to the mantle array on a ε_{Hfi}-ε_{Ndi} isotope diagram can be expressed by the parameter $\Delta\varepsilon_{Hfi}$ (Johnson and Beard, 1993). This quantity is simply the difference between the actual ε_{Hfi} of the sample and the value predicted from a regression line through the Hf-Nd mantle array, based on the ε_{Ndi} of the sample. It is, therefore, a measure of the displacement of a sample above or below the mantle array. In this study, the equation of the regression line through the mantle array,

$$\varepsilon_{Hfi} = 1.33\ \varepsilon_{Ndi} + 3.19$$

from Vervoort et al. (1999), is used to calculate the expected value of ε_{Hfi}:

$$\Delta\varepsilon_{Hfi} = \varepsilon_{Hfi} - (1.33\ \varepsilon_{Ndi} + 3.19).$$

Samples located above the mantle array regression line have positive $\Delta\varepsilon_{Hfi}$, while those located below the regression line have negative $\Delta\varepsilon_{Hfi}$. The location of the MORB, OIB and HIMU fields in terms of $\Delta\varepsilon_{Hfi}$ are shown in Figure 6.1d. The range of MORB and OIB variations scatter both above and below the abscissa, while HIMU OIB is located exclusively at negative $\Delta\varepsilon_{Hfi}$ values.

It should be noted that the extent of the MORB/OIB variation around the mantle array regression line is quite broad; values of up to ± 5 $\Delta\varepsilon_{Hfi}$ (indicated by dashed lines in Figure 6.1d) are still within the range of the mantle array. Kimberlites and lamproites are the only terrestrial magmatic rocks in which $\Delta\varepsilon_{Hfi}$ signatures significantly more negative than this have been measured consistently to date (Nowell *et al.*, 1998b, 1999; in press). A major aim of the current study is to attempt to identify, quantify and interpret the presence or absence of this signature within the well-characterised dataset of kimberlites from the Slave province.

6.3.2 Location of South African kimberlites in Hf-Nd-Sr space

6.3.2.1 Hf-Nd isotope characteristics

The location of Group I, Group II and Transitional kimberlites from South Africa, relative to the Hf-Nd mantle array is shown in Figure 6.2a. Each of these three groups has a range of ε_{Ndi} values that is distinct from the others (Group I = -0.2 to +4.6, mean = +2.5; Transitional = -4.9 to -2.6, mean = -3.7; Group II = -11.4 to -6.2, mean = -8.3). This is in agreement with the observations of Smith (1983) and Skinner *et al.* (1994).

The same degree of distinction is not observed in ε_{Hfi}, although Group I values (-5.2 to +3.7, mean = -0.7) are generally more radiogenic than those of Group II (-14.6 to –3.8,
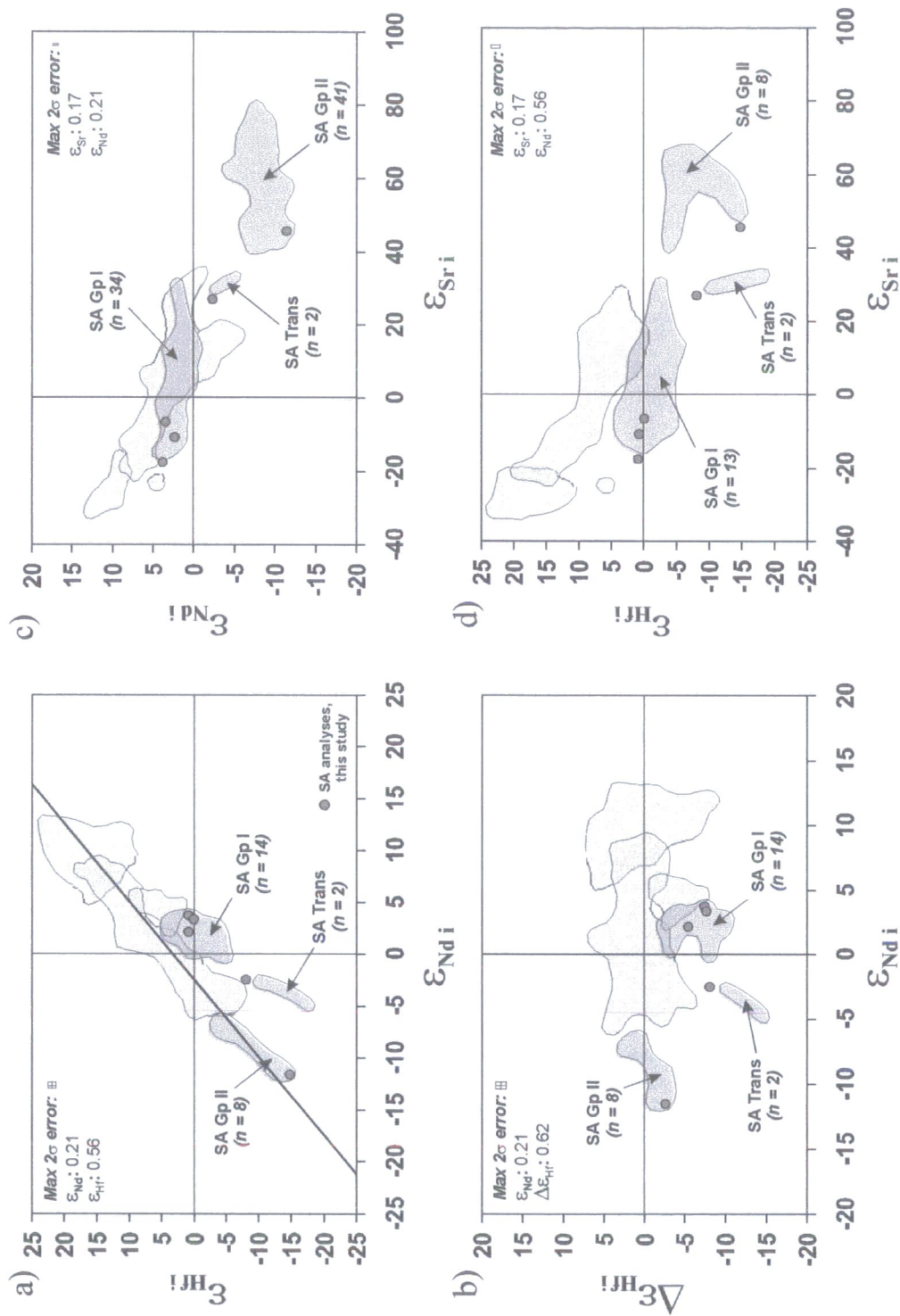
Figure 6.2 Location of fields of South African Group I, Group II and Transitional kimberlites, relative to MORB and OIB in Hf-Nd-Sr isotope space: a) $\varepsilon_{Hf\,i}$-$\varepsilon_{Nd\,i}$; b) $\Delta\varepsilon_{Hf\,i}$-$\varepsilon_{Nd\,i}$; c) $\varepsilon_{Nd\,i}$-$\varepsilon_{Sr\,i}$; d) $\varepsilon_{Hf\,i}$-$\varepsilon_{Sr\,i}$. Data from Smith (1983), Fraser (1987), Spriggs (1988), Tainton (1992), Nowell *et al.* (in press, and unpublished), this study.

mean = -8.0). The range of $\varepsilon_{Hf\,i}$ (-10.3 to -17.9, mean = -14.1) for Transitional kimberlites, although based on only two analyses, is mostly coincident with that of Group II and clearly displaced to less radiogenic values than Group I. This suggests that, in terms of Hf isotope composition, Transitional kimberlites have a greater affinity with Group II kimberlites than Group I. This agrees with the conclusions drawn by Skinner *et al.* (1994) from major and trace element data. Alternatively, it could be argued that the range of Hf-Nd isotope compositions displayed by Transitional kimberlites is part of an extension of the Group I field to more unradiogenic Hf and Nd compositions (Nowell *et al.*, in press).

This latter interpretation is to some extent supported by the range of $\Delta\varepsilon_{Hf\,i}$ across the three groups (Figure 6.2b). Transitional values (-14.6 to -10.1, mean = -12.3) are clearly closer to those of Group I (-10.4 to -2.2, mean = -6.7) than Group II (-3.2 to +2.5, mean = -0.1). Large negative deviations in $\Delta\varepsilon_{Hf\,i}$ below the mantle array regression line are, therefore, characteristic of South African Group I and Transitional magmas. The South African Group II kimberlites analysed by Nowell *et al.* (in press) do not demonstrate deviations in $\Delta\varepsilon_{Hf\,i}$ from the mantle array regression beyond the range of those observed in OIB. If magmas representative of each of these groups are sampling the same source of the negative $\Delta\varepsilon_{Hf\,i}$ signature, then either Group II magmas sample it to a lesser extent than Group I/Transitional magmas, or the source component becomes more diluted in Group II samples as a result of differential magmatic evolution. Alternatively, Group II kimberlites may be derived from, or are dominated by a different source that does not contain the negative $\Delta\varepsilon_{Hf\,i}$ signature.

6.3.2.2 Nd-Sr and Hf-Sr isotope characteristics

Group I and II kimberlites are also distinct in terms of Sr isotopes. The 'tail' of ε_{Sri} values in excess of +20 within the Group I field on Nd-Sr and Hf-Sr isotope diagrams (Figures 6.2c-d), which produces an overlap with Transitional kimberlites, may be indicative of samples that have experienced some alteration or crustal contamination. ε_{Sri} values for Group I kimberlites typically lie within the range characteristic of OIB.

Variability in Nd-Sr isotope composition for the majority of all kimberlites is contained within the boundaries of the mantle array or, in the case of Group II kimberlites, an extrapolation of the array to suitably radiogenic values of ε_{Sri}. The average ε_{Sri} value for Group I samples is close to that of BSE, insofar as an accurate value for BSE is known. This is consistent with the BSE-like signature observed in the Hf, and to some extent Nd, isotope composition of Group I kimberlites. The location of Group II kimberlites at more radiogenic ε_{Sri} values is similarly consistent with the less radiogenic Hf and Nd isotope composition of Group II kimberlites; this is a signature that is representative of an enriched mantle source. The field of Group I kimberlites only partially overlaps the Hf-Sr isotope variability of the mantle array, due to their tendency towards more unradiogenic ε_{Hfi}. Group II kimberlites are again coincident with an extension of the mantle array.

The chondritic to slightly depleted character of South African Group I kimberlites is typically interpreted (Smith, 1983) as evidence of derivation from a source such as the asthenospheric mantle. The clearly enriched nature of South African Group II samples is considered to represent a magma that either originated from, or extensively interacted with, an enriched reservoir such as metasomatised lithospheric mantle.

6.3.2.3 Analyses of southern African kimberlites for this study

The chemical procedure for pre-concentration of Hf used in this project (Chapter 2) differs from that used in Nowell *et al.* (1999). To ensure that this modified chemistry produced data that was comparable to that obtained by Nowell *et al.* (1999; in press), five new Hf-Nd-Sr analyses of kimberlites from South Africa and Lesotho were acquired at the beginning of the current project. This sample set consisted of three Group I kimberlites (Liqhobong, Pipe 200 and Gansfontein), one Group II kimberlite (Roberts Victor) and one Transitional kimberlite (Melton Wold). All samples were unaltered hypabyssal facies material, and displayed minimal evidence of crustal contamination. The Hf-Nd-Sr isotope compositions of these samples are shown on Figure 6.2, superimposed on the established fields of Group I, Group II and Transitional kimberlites; each sample plots within or adjacent to its appropriate field. This both supports the functionality of the modified pre-concentration chemistry and, together with the data of Nowell *et al.* (1999; in press), extends the compositional ranges for Group I, Group II and Transitional kimberlites defined by Smith (1983) and Skinner *et al.* (1994).

6.3.3 Data from LDG and other Canadian kimberlites

For the purposes of representing the large volume of isotopic data from the LDG kimberlite field, the dataset is first considered as a single entity and then sub-divided into the geographically based groupings introduced in Chapter 1 and used for describing major and trace element variations in Chapter 4. As in Chapter 4, no genetic association between kimberlites in each group is assumed. This is of particular importance in groups E and F, where the greater age range and geographic separation

between samples suggests a smaller likelihood of individual magmas sharing a common source.

6.3.3.1 Relative composition of kimberlites from LDG and South Africa

68 hypabyssal samples from LDG, which on the basis of visual and petrographic inspection and trace element characterisation (Section 5.2) appear to be unaltered, form well-defined arrays in terms of both Hf-Nd and Nd-Sr isotope variations (Figure 6.3).

a) Hf-Nd isotopes The range of ϵ_{Ndi} values (-4.2 to 0.1, mean = -1.9) falls between the ranges of Group I and Group II kimberlites from South Africa, but is very similar to that observed in the three Transitional samples that have been analysed (Figure 6.3a). The range in ϵ_{Hfi} of the LDG kimberlites (-10.2 to +10.5, mean = -1.1) extends to both more positive and more negative values than those observed in South African Group I kimberlites, but is similarly centred close to the BSE composition of ϵ_{Hfi} = 0. This range also partially overlaps that of South African Group II kimberlites. The large (20.7 unit) range in ϵ_{Hfi} over a small (4.3 unit) corresponding range in ϵ_{Ndi} imparts a sub-vertical trend to the LDG data, which is highly inclined to the mantle array regression line (Figure 6.3a). The field of South African Transitional kimberlites is situated directly on the trend of the LDG data.

The orientation of the LDG Hf-Nd isotope array is also very steep on a ϵ_{Ndi}-$\Delta\epsilon_{Hfi}$ diagram (Figure 6.3b), and again is coincident with the trend of the three South African Transitional data points. Some care is required in the interpretation of this array, because a sample set with any variation in ϵ_{Hfi} over a narrow range in ϵ_{Ndi} will form a steep array in ϵ_{Ndi}-$\Delta\epsilon_{Hfi}$ space. Nevertheless, the range in $\Delta\epsilon_{Hfi}$ exhibited by the LDG

195
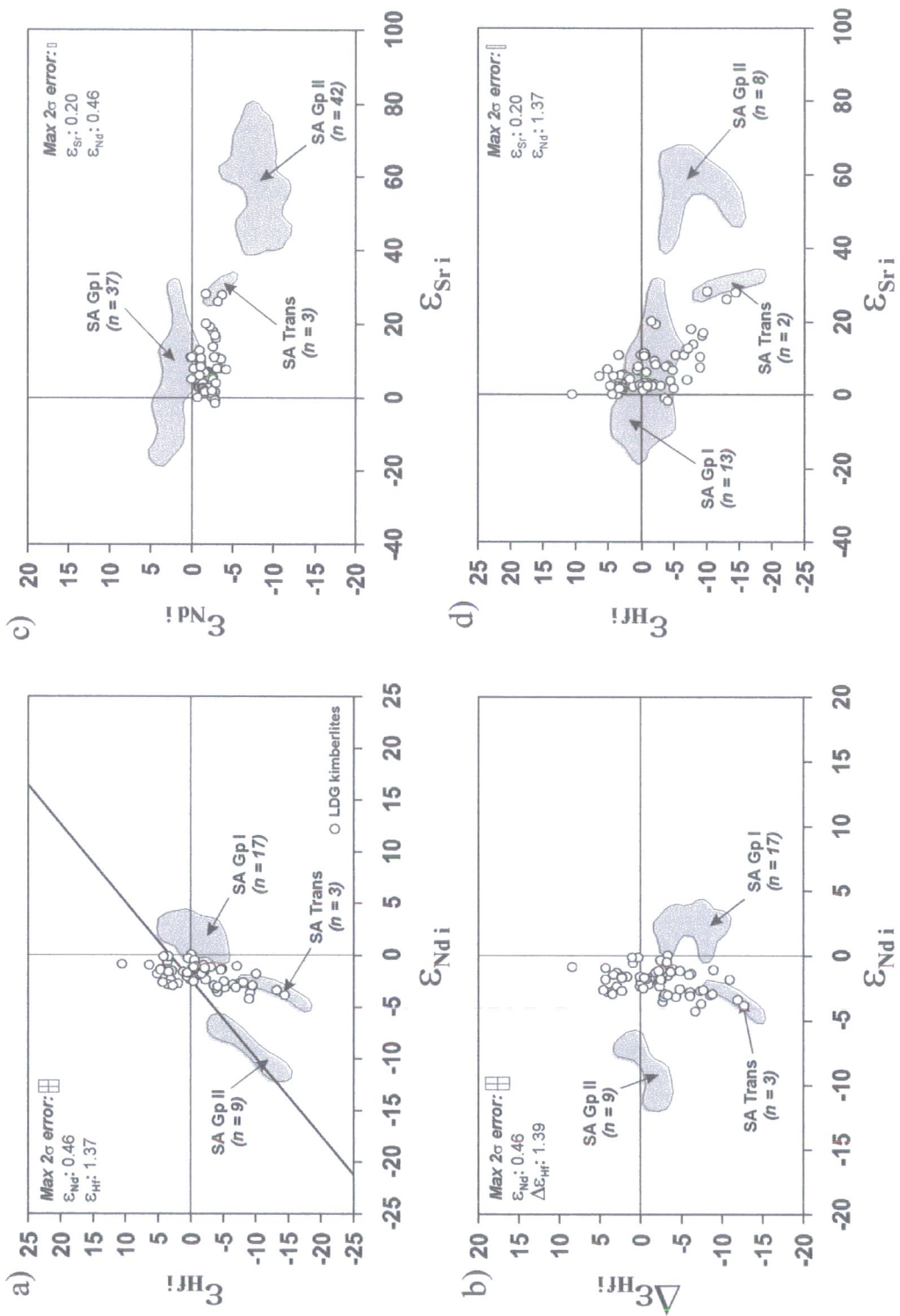
Figure 6.3 Location of unaltered Lac de Gras hypabyssal kimberlites, relative to South African Group I, Group II and Transitional fields in Hf-Nd-Sr isotope space: a) $\varepsilon_{Hf i}$-$\varepsilon_{Nd i}$; b) $\Delta\varepsilon_{Hf i}$-$\varepsilon_{Nd i}$; c) $\varepsilon_{Nd i}$-$\varepsilon_{Sr i}$; d) $\varepsilon_{Hf i}$-$\varepsilon_{Sr i}$.

samples spans the entire combined range of the South African Group I and II data. In summary, the Hf isotope character of the LDG encompasses both Group I and II signatures, while the Nd isotope signature is intermediate between that of Group I and Group II. Consequently, it is not possible to unequivocally attribute either a Group I or Group II character to the LDG samples.

b) Nd-Sr isotopes The initial Sr isotope composition of the unaltered LDG kimberlites (ε_{Sri} = -1.5 to 28.4, mean = 6.4) falls within the range of South African Group I kimberlites (Figure 6.3c). There are no examples among the unaltered samples of the more radiogenic values characteristic of South African Group II kimberlites. Three samples, from the Pigeon and Tli Kwi Cho (DO-27) kimberlites, have ε_{Sri} values that are comparable to those of South African Transitional kimberlites; these samples also have the three most negative values of ε_{Hfi} and $\Delta\varepsilon_{Hfi}$.

It should be noted that the unaltered LDG rocks featured here include both the low *ln (Si/Al)* group, which is potentially affected by continental crust, and mantle dominated high *ln (Si/Al)* samples identified in section 5.5. Some of the variation observed in Sr, and indeed Hf and Nd isotope compositions, may therefore be due to differential content of crustal and lithospheric mantle contamination. This is explored more fully in section 6.4 and Chapter 7.

c) Hf-Sr isotopes The range of Hf-Sr isotope variation in the LDG data defines a broad sub-vertical array (Figure 6.3d) that bisects the field of South African Group I kimberlites. The apparent shape of this array is largely artificial due to the scale of the diagram. The ~25 unit range in ε_{Hfi} of the LDG samples is, in fact, comparable to the

range of ε_{Sri}. The three samples from Pigeon and Tli Kwi Cho in this projection are again situated within error of the Transitional kimberlite field.

6.3.3.2 Group A1: Intra-kimberlite variation in Grizzly

a) Hf-Nd isotopes Variation in Hf-Nd isotope composition of the 14 samples from the Grizzly kimberlite is very limited (ε_{Hfi}: -4.7 to 0.1, mean = -1.6; ε_{Ndi}: -2.1 to -0.9, mean = -1.6); it forms a cluster with a small 'tail' to less radiogenic ε_{Hfi}. The centre of the cluster is situated at a composition that is slightly enriched relative to chondritic values. The total range in ε_{Hfi} of 4.8 units, with an associated range in ε_{Ndi} of just 1.2 units, suggests that the intra-kimberlite Hf-Nd isotope variation at Grizzly strongly resembles the inter-kimberlite variability of the LDG dataset as a whole. This implies that the processes affecting the isotopic composition of a single kimberlite are the same as those affecting kimberlites throughout the LDG field.

ε_{Ndi}-$\Delta\varepsilon_{Hfi}$ variations (Figure 6.4b) emphasise this similarity: the Grizzly data defines an array that starts just below the mantle array regression line ($\Delta\varepsilon_{Hfi}$ = -0.8) and trends steeply towards more negative $\Delta\varepsilon_{Hfi}$ (minimum = -6.0, mean = -2.6). The trend of the data based on these 14 samples extrapolates to positive ε_{Ndi} values, however, while the overall data trend is oriented to negative ε_{Ndi} at increasingly negative $\Delta\varepsilon_{Hfi}$.

b) Nd-Sr isotopes The Grizzly data displays a very narrow range in initial Sr isotope composition (ε_{Sri} = 2.1 to 4.0, mean = 2.9) compared to the dataset as a whole, and consequently the data cluster tightly on a Nd-Sr isotope diagram (Figure 6.4c). These slightly radiogenic values correspond well with the moderately unradiogenic ε_{Hfi} and ε_{Ndi} data. The range in Nd and Sr isotope composition displayed by Grizzly is much

smaller than that seen in a similar study of intra-kimberlite variation at Finsch (Fraser, 1987). 17 samples from Finsch show a range in ε_{Ndi} (-6.1 to -9.6, mean = -7.4) and ε_{Sri} (+48.5 to +77.7, mean = +64.0). Finsch is known to consist of several different phases of kimberlite intrusion and this may explain the greater range in isotopic values.

Although there is also evidence for multiple phases of kimberlite emplacement in many of the pipes on the northern side of LDG (D. Dyck, *pers. comm.*), all of the Grizzly samples analysed here were obtained from a single diamond drill core. It is possible, therefore, that the full extent of compositional variation in hypabyssal kimberlite from Grizzly has not been analysed. This is, of course, true for all other kimberlites considered in this study.

c) Hf-Sr isotopes Like the LDG data as a whole, the samples from Grizzly appear to form a sub-vertical array on a Hf-Sr isotope diagram (Figure 6.4d), due to the unequal scales on either axis. Nevertheless, the range in $\varepsilon_{Hf\,i}$ is over double that of ε_{Sri}. All of the Grizzly samples are situated within the field of South African Group I kimberlites in this projection.

6.3.3.3 Group A2: Neighbouring kimberlites to Grizzly

a) Hf-Nd isotopes None of the eight kimberlites that are located in the immediate vicinity of the Grizzly pipe have Hf isotope signatures that are coincident with Grizzly (Figure 6.5a). The two samples from Pigeon have very negative ε_{Hfi} that locates them at the least radiogenic end of the entire LDG array. These samples also have less radiogenic ε_{Ndi} than other kimberlites in this group. All other samples have positive ε_{Hfi} values which locate them above the Grizzly samples on the Hf-Nd isotope diagram.

199

The single analysis from the Mark kimberlite has the highest ε_{Hfi} of all those recorded in this study. This kimberlite, along with the adjacent Arnie and Aaron bodies, are known to contain abundant microxenoliths of garnet dunite (B. A. Kjarsgaard, *pers. comm.*). Four samples from the Leslie kimberlite have a range in ε_{Hfi} of +1.1 to +4.4 with a narrow associated range in ε_{Ndi} (-1.3 to −1.6). This again defines a sub-vertical trend on the Hf-Nd diagram as observed at Grizzly and in the LDG dataset as a whole. A similar trend is also apparent in samples from the Roger kimberlite; these points are largely obscured in Figures 6.5a-b due to almost exact coincidence with data from Leslie. All of these trends are also reflected in the variation of $\Delta\varepsilon_{Hfi}$ values (Figure 6.5b).

b) Nd-Sr isotopes With the exception of the data from Pigeon, the variation in Nd-Sr isotope composition displayed by these samples is within the range of the Grizzly kimberlite (Figure 6.5c). The olivine-rich samples from Mark and Leslie display some of the lowest ε_{Sri} values in this group. The highest ε_{Sri} values among these samples are seen in Koala West, which has a trace element signature indicative of compositional control predominantly by eclogite or crust, rather than peridotite.

c) Hf-Sr isotopes Most samples in this group are located at, or within error of, the upper (more radiogenic) limit of the Group I kimberlite field on the Hf-Sr isotope diagram (Figure 6.5d). Notable exceptions are Mark, which has very radiogenic Hf, and Pigeon, which has a near Transitional signature. Samples from Roger, Koala West and Leslie display a considerable range in ε_{Hfi} over a very narrow range in ε_{Sri}.
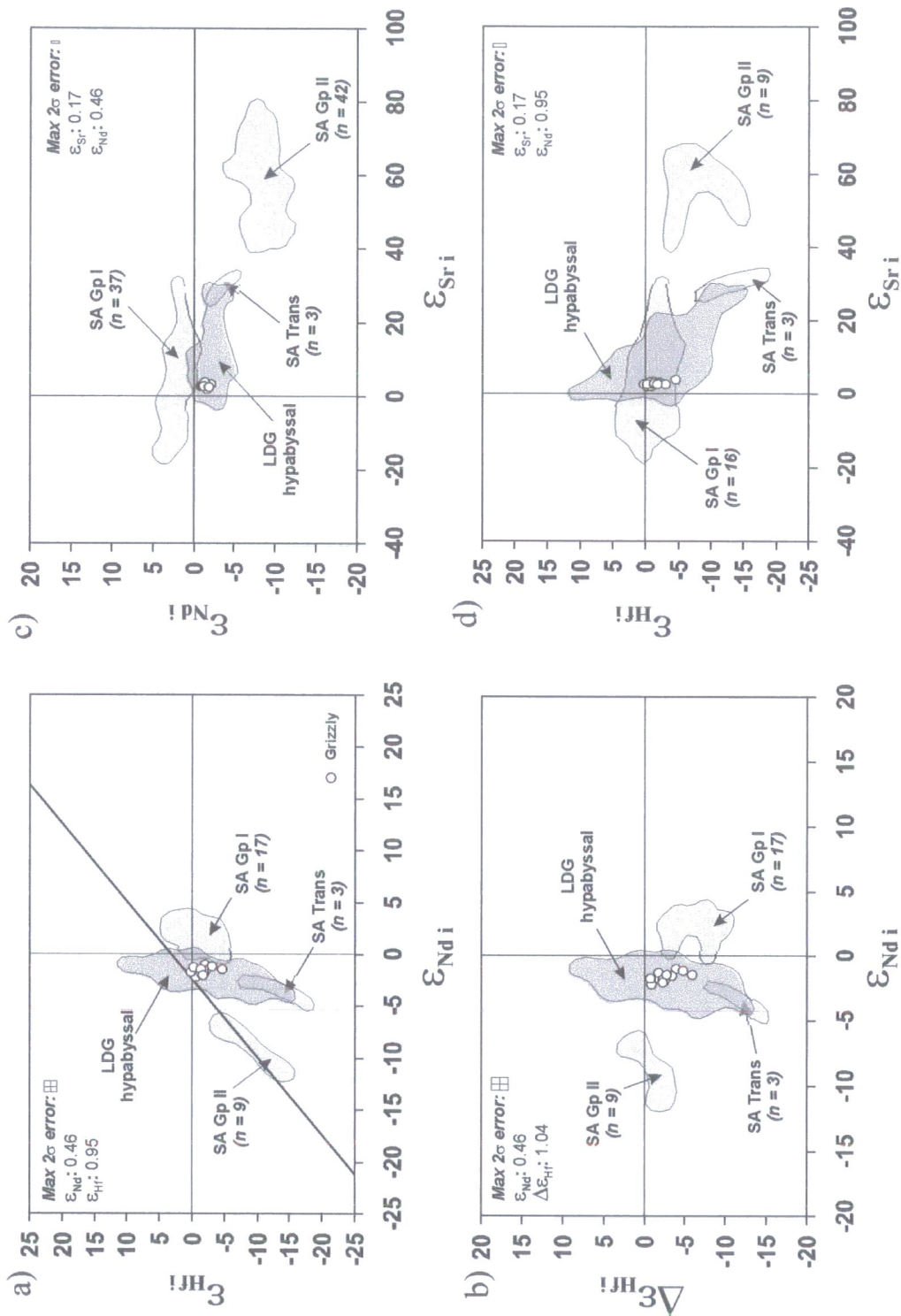
Figure 6.4 Location of samples from the Grizzly pipe relative to other hypabyssal kimberlites from Lac de Gras and South Africa in Hf-Nd-Sr isotope space: a) ε_{Hfi}-ε_{Ndi}; b) $\Delta\varepsilon_{Hfi}$-ε_{Ndi}; c) ε_{Ndi}-ε_{Sri}; d) ε_{Hfi}-ε_{Sri}.
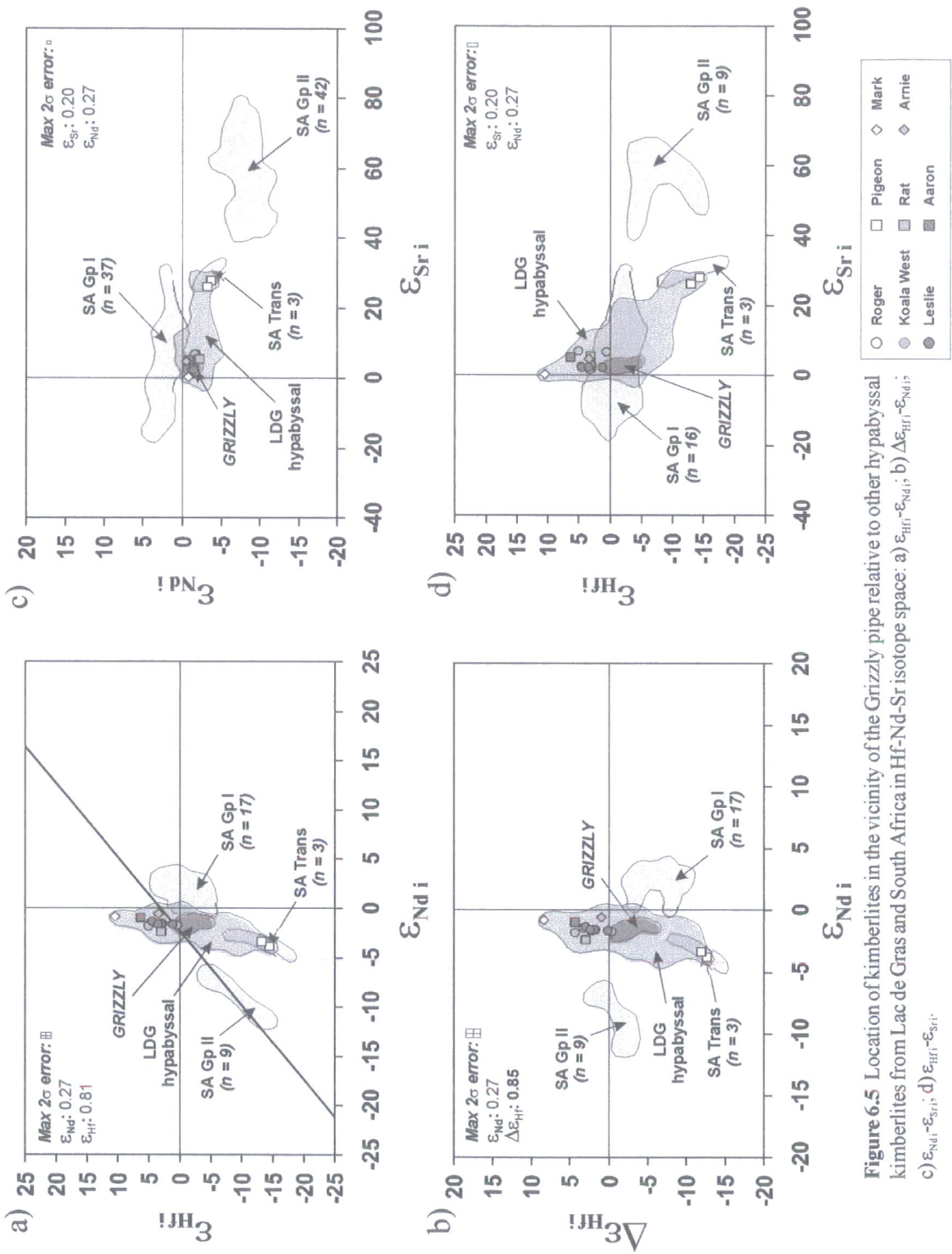
Figure 6.5 Location of kimberlites in the vicinity of the Grizzly pipe relative to other hypabyssal kimberlites from Lac de Gras and South Africa in Hf-Nd-Sr isotope space: a) $\epsilon_{Hf\,i}$-$\epsilon_{Nd\,i}$; b) $\Delta\epsilon_{Hf\,i}$-$\epsilon_{Nd\,i}$; c) $\epsilon_{Nd\,i}$-$\epsilon_{Sr\,i}$; d) $\epsilon_{Hf\,i}$-$\epsilon_{Sr\,i}$.
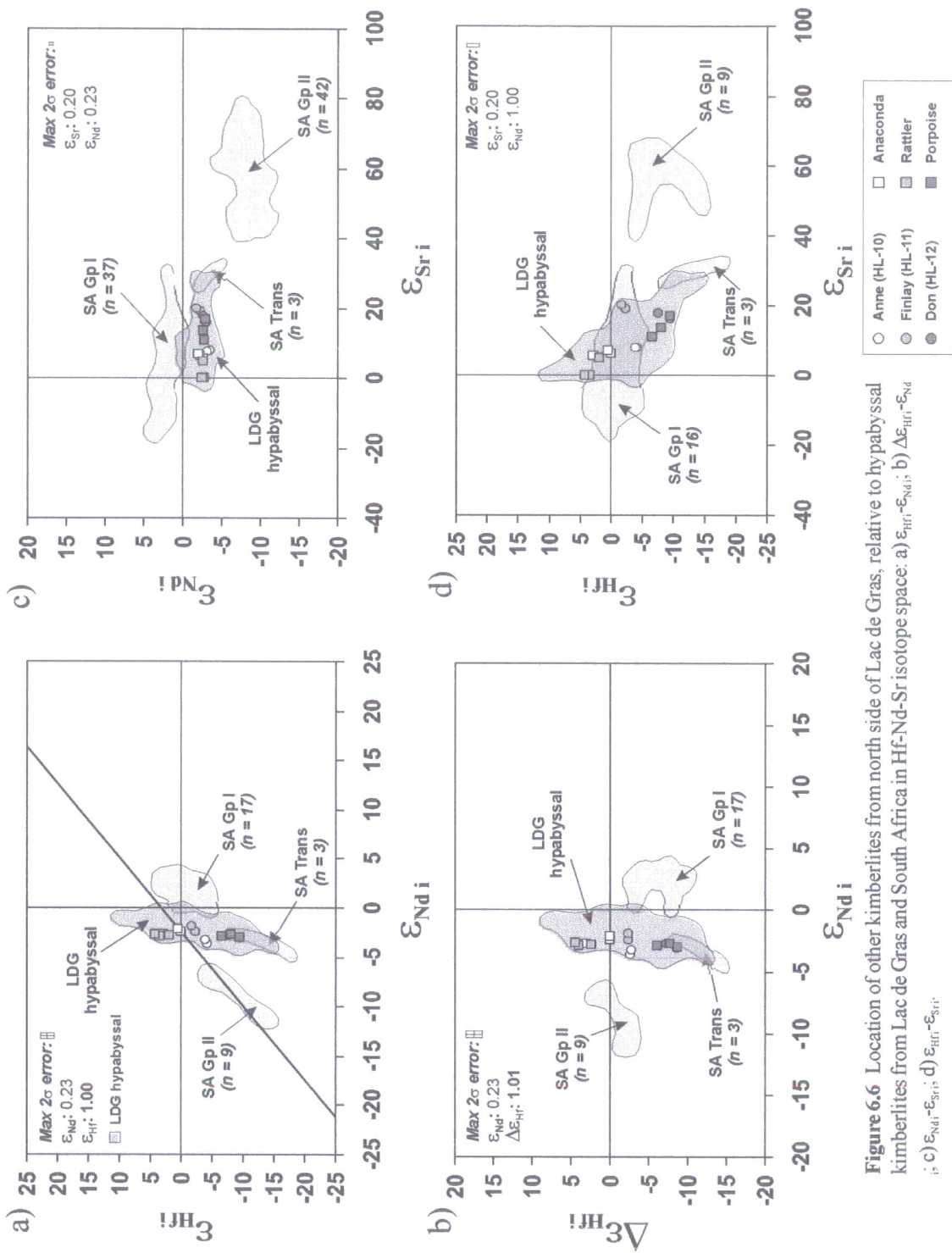
Figure 6.6 Location of other kimberlites from north side of Lac de Gras, relative to hypabyssal kimberlites from Lac de Gras and South Africa in Hf-Nd-Sr isotope space: a) ε_{Hfi}-ε_{Ndi}; b) $\Delta\varepsilon_{Hfi}$-ε_{Nd}; c) ε_{Ndi}-ε_{Sri}; d) ε_{Hfi}-ε_{Sri}.

6.3.3.4 Group B: Other kimberlites north of LDG

a) Hf-Nd isotopes As a group, these kimberlites demonstrate a much greater range in ε_{Hfi}, to both positive and negative values, than observed in Grizzly or its immediate neighbours (Figure 6.6a). Both the Rattler and Porpoise bodies again demonstrate a large intra-kimberlite range in ε_{Hfi} (up to 2.9 units) over a small (0.3 unit) range in ε_{Ndi}, resulting in near vertical arrays that are sub-parallel to the trend of the LDG data. This is the same trend as observed in the majority of pipes where multiple analyses have been acquired.

The older (71Ma) kimberlites from Hardy Lake (Anne, Finlay and Don) have a smaller range of ε_{Hfi} than the younger (53-60Ma) kimberlites from Porpoise and Rattler. The range of ε_{Ndi} across all samples is again very narrow (-3.5 to -1.8, mean = -2.7) and is on average less radiogenic than observed in the vicinity of Grizzly. The analyses from Don and Porpoise are located in a position that is almost exactly intermediate to South African Group I and II Nd isotope compositions.

b) Nd-Sr isotopes The group as a whole describes a large range in Sr isotope composition (Figure 6.6c) compared to the analyses from Grizzly and its neighbouring kimberlites. Coupled with the very limited range in ε_{Ndi} shown by these samples, this produces an array that trends parallel to the *x*-axis and the overall variation in Nd-Sr isotope composition seen at LDG. The most radiogenic values of ε_{Sri} are from Finlay, Don and Porpoise.

c) Hf-Sr isotopes The range of intra-kimberlite Hf-Sr isotope variation of some kimberlites from this group again parallels that of the entire dataset. This is clearly

demonstrated in Porpoise, where three samples define a trend of increasingly more radiogenic Sr with progressively less radiogenic Hf. This trend is not so evident in the kimberlites from Hardy Lake (Anne, Finlay and Don).

6.3.3.5 Group C: Kimberlites south and east of LDG

a) Hf-Nd isotopes The six kimberlites from the central part of the region between LDG and Aylmer Lake display a large range in ε_{Hfi} and ε_{Ndi} as a group, but again there is a considerable degree of intra-kimberlite isotopic homogeneity (Figure 6.7a). Samples from the T-19, T-21 and T-36 bodies cluster together, at close to chondritic values of ε_{Hfi}. T-34 and T-25 plot close together at less radiogenic ε_{Hfi} and ε_{Ndi} values. In ε_{Ndi}-$\Delta\varepsilon_{Hfi}$ space (Figure 6.7b) T-237 is located close to the mantle array reference line, with slightly positive $\Delta\varepsilon_{Hfi}$, while the other samples plot below the mantle array to varying degrees ($\Delta\varepsilon_{Hfi}$ = -2.5 to -6.2). The near bulk Earth Nd isotope composition of T-19 locates it just within the field of South African Group I kimberlites, but all other samples in this group have unradiogenic Nd, which is uncharacteristic of South African Group I kimberlites.

b) Nd-Sr isotopes Variations in Nd-Sr isotope composition (Figure 6.7c) define the same two broad groupings as observed above. T-34 and T-35 behave anomalously by having the most unradiogenic Sr as well as the most unradiogenic Nd and Hf compositions. All of the samples in this group have trace element signatures indicative of small to moderate amounts of crustal contamination. Considering this, their Sr isotope compositions are not excessively radiogenic (ε_{Sri} = -1.5 to +11) and are well within the range of South African Group I kimberlites.

6.3.3.6 Group D: Other LDG kimberlites

a) Hf-Nd isotopes These samples show less consistent inter- and intra-kimberlite variations in Hf-Nd isotope character (Figure 6.8a) than are observed in other groups within the LDG field. Samples from Misery are distinct from those of its satellite, Misery East, in terms of ε_{Ndi}. On average, the two samples from Misery East also have less radiogenic Hf than Misery, indicating a more enriched character in general. The single sample from Nicholas Bay, which is the most easterly-situated kimberlite in this study, has the least radiogenic ε_{Ndi} of this group and of the dataset as a whole. It also has one of the least radiogenic Hf isotope signatures in the entire dataset, placing it at the most enriched edge of the LDG field on the Hf-Nd isotope diagram. DD-39 is the only kimberlite in this group to have positive ε_{Hfi}, and this is only the case for one sample from this body.

Pairs of analyses from individual intrusions again display variation in Hf isotope composition with virtually no associated variation in ε_{Ndi} (Figure 6.8b). Although this observation is based on only two analyses for the kimberlites in this group, it agrees with the style of variation observed in other bodies with larger numbers of analyses, such as Leslie and, in particular, Grizzly. This orientation of variation in Hf-Nd isotope composition at an oblique angle to the mantle array appears to be very characteristic of most samples from the LDG field.
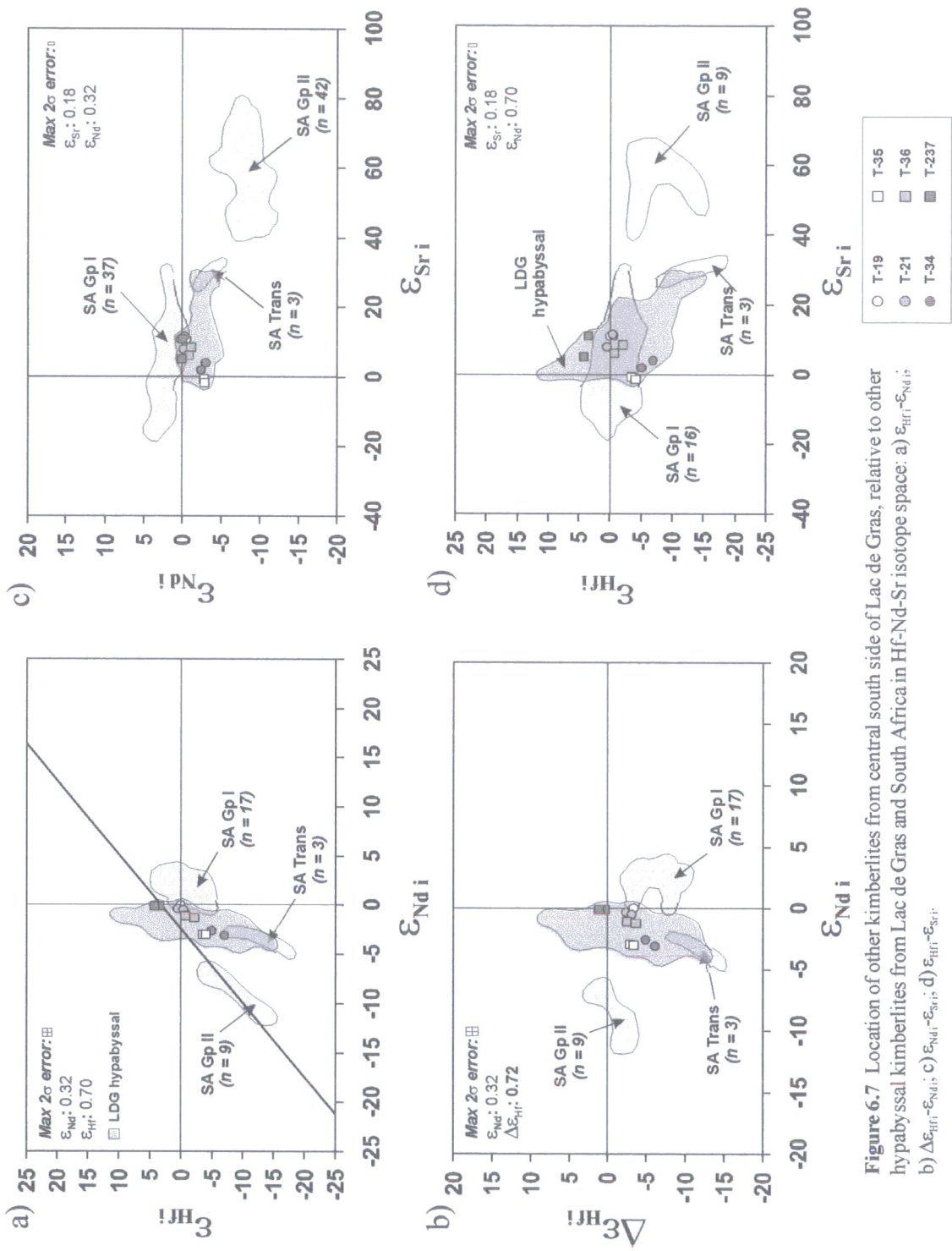
Figure 6.7 Location of other kimberlites from central south side of Lac de Gras, relative to other hypabyssal kimberlites from Lac de Gras and South Africa in Hf-Nd-Sr isotope space: a) $\varepsilon_{Hf\,i}$-$\varepsilon_{Nd\,i}$; b) $\Delta\varepsilon_{Hf\,i}$-$\varepsilon_{Nd\,i}$; c) $\varepsilon_{Nd\,i}$-$\varepsilon_{Sr\,i}$; d) $\varepsilon_{Hf\,i}$-$\varepsilon_{Sr\,i}$.

207

b)   *Nd-Sr isotopes*   Samples from each body show greater consistency of intra-kimberlite Nd-Sr isotope character (Figure 6.8c).   Trace element modelling indicates that Nicholas Bay, DO-27, T-146 and TR-107 contain significant components of crustal contamination.   In T-146 the contamination is visually discernable (B. A. Kjarsgard, pers. comm.).   Despite this, the only sample that has very radiogenic Sr is DO-27; this sample has a contamination index (Clement, 1982) of just 1.08, compared to ~1.25 at T-146.   This kimberlite has a typical SA Group I Sr isotope signature.

Trace element evidence suggests that the sample from DO-27 is as unaltered as most of the other LDG kimberlites analysed.

6.3.3.7   Group E: Slave kimberlites outside the LDG area

a) Hf-Nd isotopes Kimberlites from further north and south within the Slave province appear to have very different Hf-Nd isotope characteristics to those found at LDG (Figure 6.9a).   A sample from the Cambrian Kennady Lake body, situated south of LDG, has unradiogenic ε_{Ndi} similar to that characteristic of LDG.   All other samples analysed from this group have positive, radiogenic ε_{Ndi} that places them within the range of South African Group I kimberlites.   The Cambrian kimberlite from Snap Lake has a near chondritic Hf-Nd isotope composition that places it within the South African Group I field, and is isotopically unlike the sample from Kennady Lake.

The other kimberlite bodies in this group are Jurassic in age (172Ma: Heaman *et al.*, 1997) and are located north of LDG in the vicinity of Contwoyto Lake.   All samples from the Jericho kimberlite (JD-51, JD-69, JD-82 and RND-120) have radiogenic Nd and Hf isotope compositions located at, and just beyond, the upper end of the South African Group I field.   The Muskox kimberlite also falls within this field, at its lower

edge, having unradiogenic Hf and slightly radiogenic Nd. Overall, the Slave kimberlites studied from beyond LDG are much more akin to South African Group I kimberlites in terms of Hf-Nd isotope composition. All kimberlites in this group have negative $\Delta\varepsilon_{Hfi}$ signatures (Figure 6.9b), although most of the samples from Jericho are within 5 $\Delta\varepsilon_{Hfi}$ units of the mantle array regression line.

b) Nd-Sr isotopes The unradiogenic ε_{Ndi} signature of the sample from Kennady Lake causes it to plot within the range of LDG kimberlites on a Nd-Sr isotope diagram (Figure 6.9c). All other samples in this group plot within the range of South African Group I kimberlites, although samples from Snap Lake and Muskox are marginal to the field of LDG kimberlites. One sample from the RND-120 body at Jericho has very radiogenic ε_{Sri} of +58.9. This particular body was intruded into granite and may have incorporated a considerable amount of radiogenic Sr from this source. If this is the case, then the effect in the other RND-120 sample is much less pronounced.

c) Hf-Sr isotopes Some of the kimberlites from the South-East Slave and Contwoyto fields (Snap Lake, Muskox, JD-51 and one sample from each of JD-69 and JD-82) are located within the range of Hf-Sr isotope variations in LDG kimberlites. In JD-69, JD-82 and RND-120 there is a very large range in ε_{Sri} over a narrow range in ε_{Hfi}.

6.3.3.8 Group F: Canadian kimberlites beyond the Slave Province

a) Hf-Nd isotopes Samples from the Churchill and Superior provinces of Canada diaplay a wide range of Hf-Nd isotope variation (Figure 6.10a). Four samples from Somerset Island analysed during this study have radiogenic Hf (+1.7 to +3.9, mean =

2.9) and Nd (+0.7 to +2.0, mean = +1.2) which locate them at the upper edge of the South African Group I field and just beyond the range of the LDG data.

Also shown are four samples from the Nikos intrusion on Somerset Island analysed by Schmidberger *et al.* (2002). A very large range in ε_{Hfi} (21.1 units) is observed over a small range in ε_{Ndi} (0.5 units) in these samples. This amount of Hf isotope variation has not been recorded in any other kimberlite to date, and it is difficult to explain how it arises in this instance. It is highly probable that Nikos is synonymous with the JP South intrusion, which has been analysed during this study, and one of these four Nikos analyses is situated within error of the JP South analysis on both Hf-Nd and Nd-Sr isotope diagrams. Since one sample is in close agreement, it seems possible that the two higher ε_{Hfi} values obtained for Nikos are spurious, possibly as a result of Yb interferences which have not been fully corrected during the analysis. Although these two samples lie on an extension of the LDG Hf-Nd isotope array, they are not considered with the rest of the data until repeat analyses are available to confirm their accuracy.

A single analysis from Rankin Inlet has more radiogenic Nd and slightly more radiogenic Hf than the Somerset Island samples of this study, and in terms of Nd isotope character is more akin to the Cambrian samples from TR-107. The Rankin Inlet kimberlite (~200Ma: Heaman and Kjarsgaard, 2000) is older than those from Somerset Island (~100Ma: Smith *et al.*, 1989) and is situated approximately 1200km further south. This may provide some indication of temporal and/or geographic provinciality among kimberlites, although further analyses would be desirable to test this hypothesis.
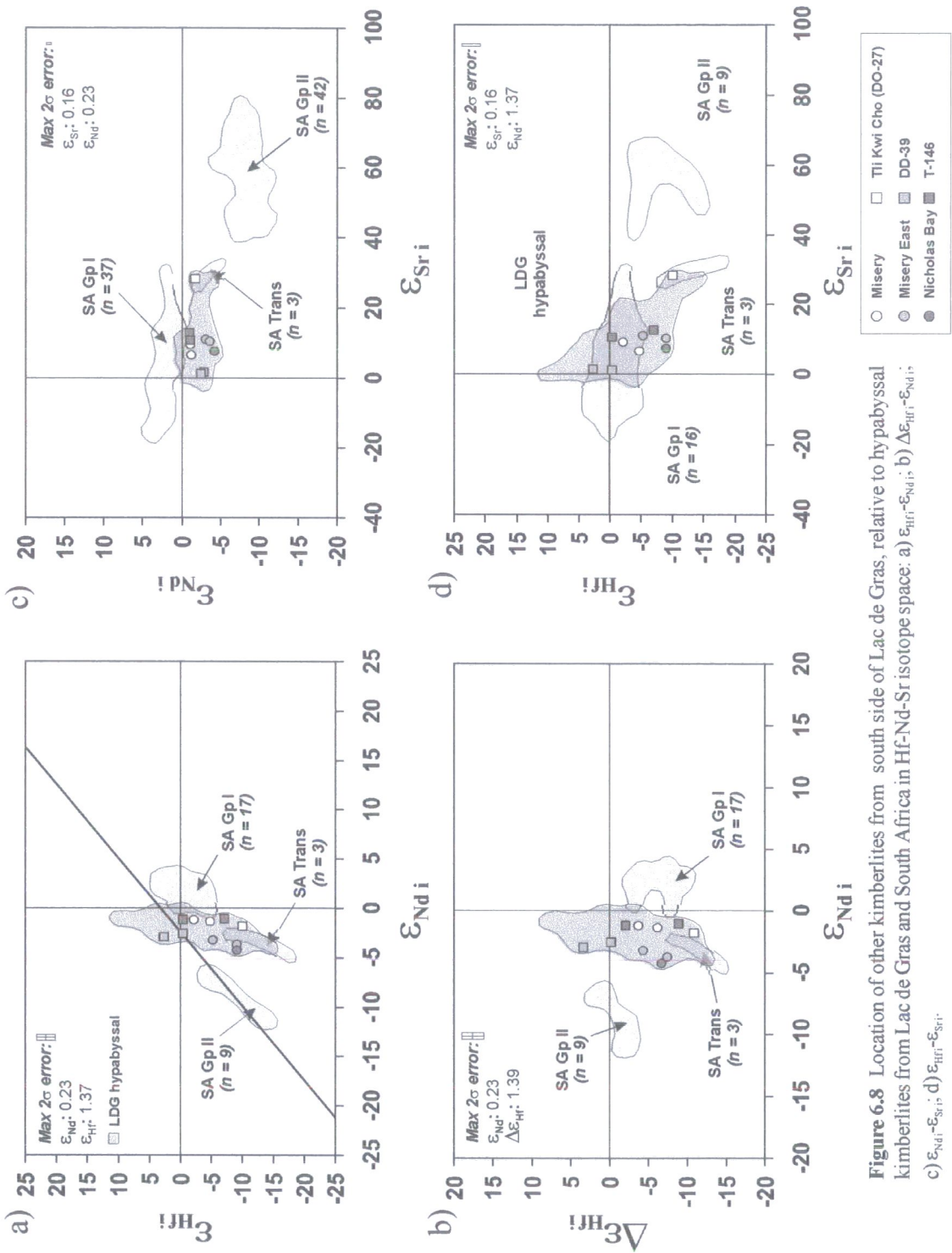
Figure 6.8 Location of other kimberlites from south side of Lac de Gras, relative to hypabyssal kimberlites from Lac de Gras and South Africa in Hf-Nd-Sr isotope space: a) $\varepsilon_{Hf\,i}$-$\varepsilon_{Nd\,i}$; b) $\Delta\varepsilon_{Hf\,i}$-$\varepsilon_{Nd\,i}$; c) $\varepsilon_{Nd\,i}$-$\varepsilon_{Sr\,i}$; d) $\varepsilon_{Hf\,i}$-$\varepsilon_{Sr\,i}$.
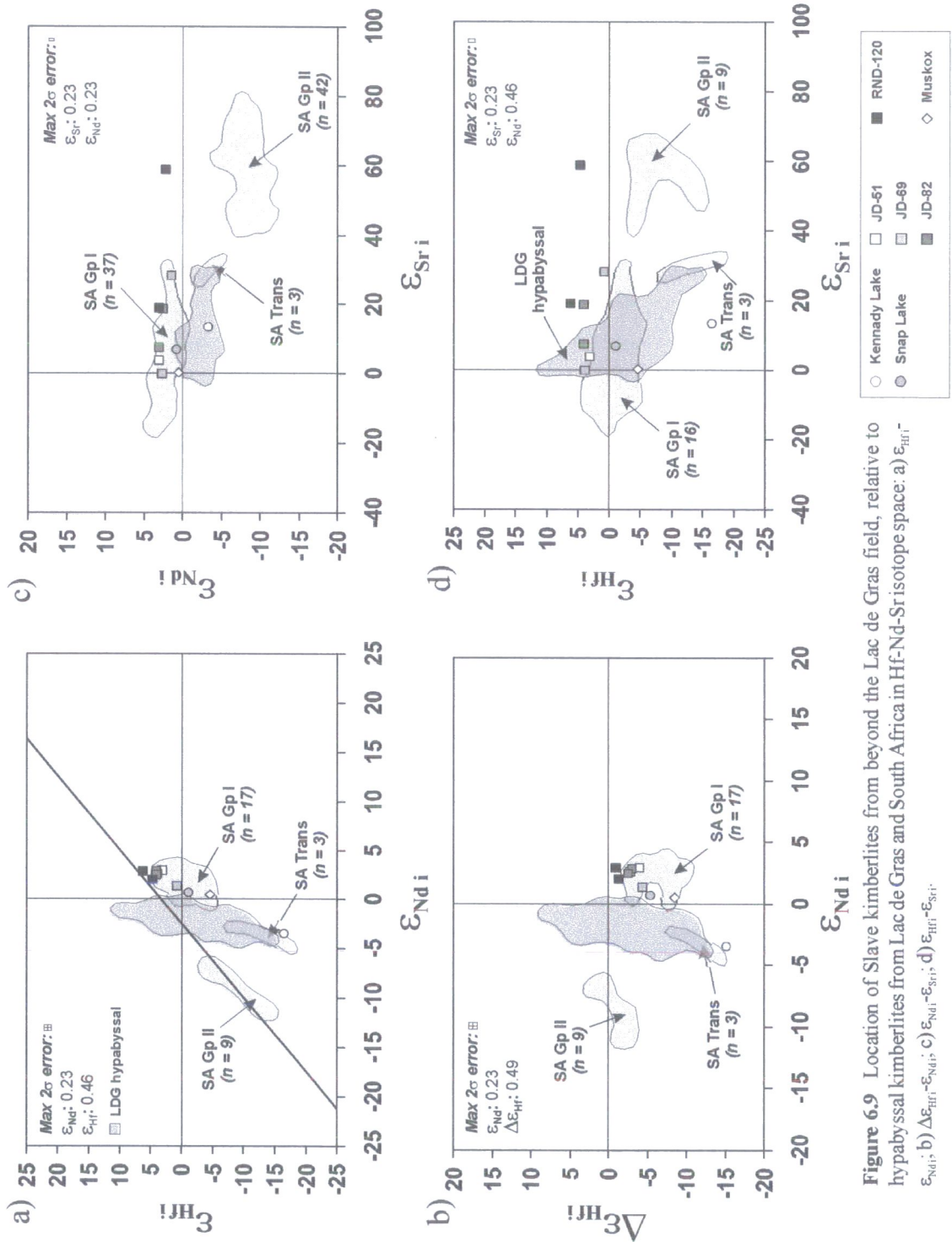
Figure 6.9 Location of Slave kimberlites from beyond the Lac de Gras field, relative to hypabyssal kimberlites from Lac de Gras and South Africa in Hf-Nd-Sr isotope space: a) $\varepsilon_{Hf\,i}$-$\varepsilon_{Nd\,i}$; b) $\Delta\varepsilon_{Hf\,i}$-$\varepsilon_{Nd\,i}$; c) $\varepsilon_{Nd\,i}$-$\varepsilon_{Sr\,i}$; d) $\varepsilon_{Hf\,i}$-$\varepsilon_{Sr\,i}$.

212
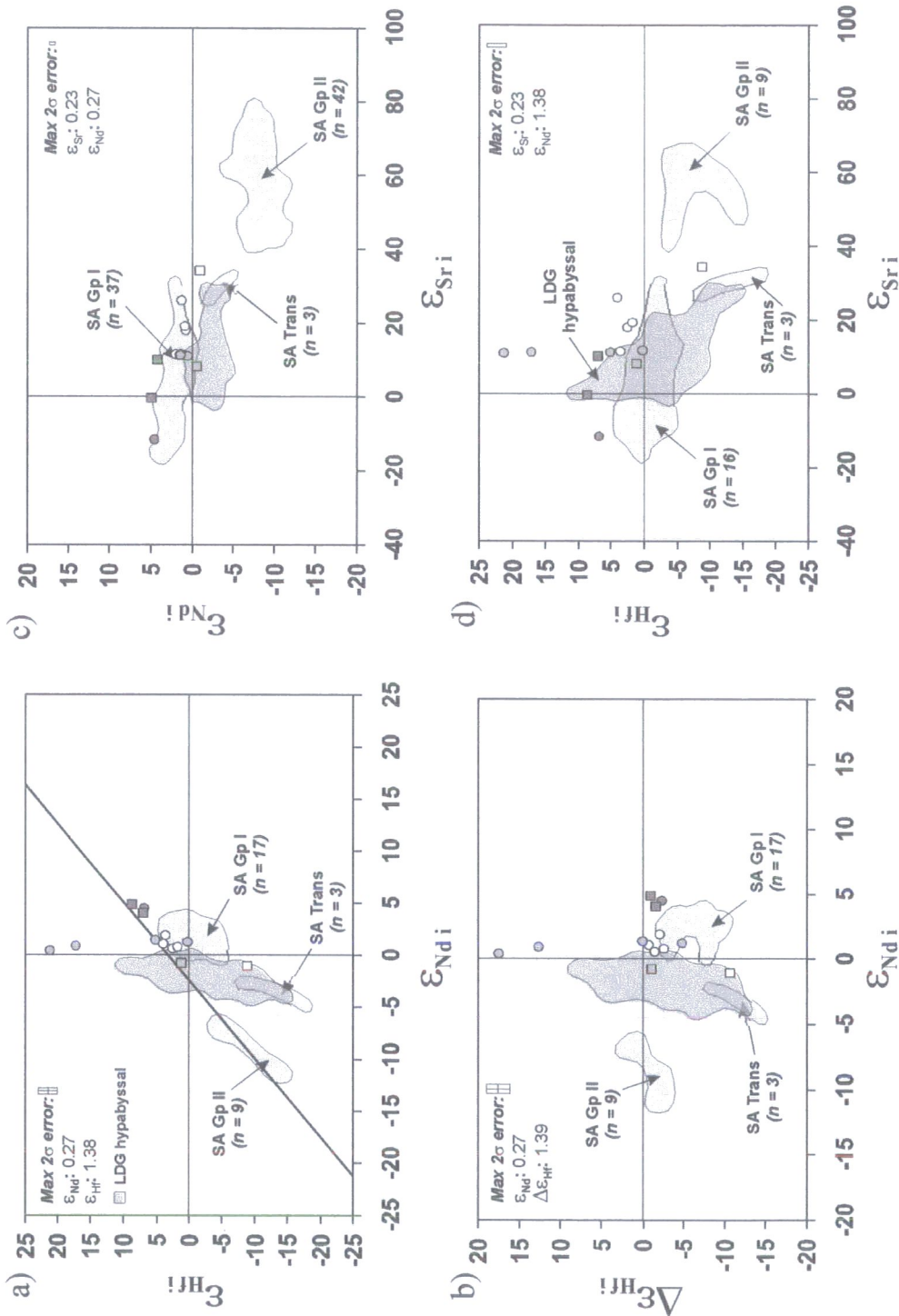
Figure 6.10 Location of Canadian kimberlites from beyond the Slave province, relative to hypabyssal kimberlites from Lac de Gras and South Africa in Hf-Nd-Sr isotope space: a) ε_{Hfi}-ε_{Ndi}; b) $\Delta\varepsilon_{Hfi}$-ε_{Ndi}; c) ε_{Ndi}-ε_{Sri}; d) ε_{Hfi}-ε_{Sri}.

The Guigues and Peddie kimberlites of the Timiskaming field have very similar Nd isotope characteristics to Rankin Inlet. These are also closer in age (Guigues ~142Ma and Peddie ~154Ma: Heaman and Kjarsgaard, 2000) to Rankin Inlet despite being situated approximately 2000km to the SE. Two other samples from the Superior Province, taken from the Attawapiskat and Kirkland Lake fields, have slightly unradiogenic ε_{Ndi}. Despite the apparent disparity in Nd isotope composition of these samples, all are located within or marginal to the range observed in South African Group I kimberlites. The Hf isotope characteristics of these samples are also broadly consistent with Group I characteristics, with only Timiskaming and Rankin Inlet being more radiogenic, and Attawapiskat more unradiogenic.

The Hf-Nd isotope variation demonstrated by the majority of these samples is within the range of the mantle array, (Figure 6.10b). Ignoring the extremely radiogenic values from Nikos, only the sample from Attawapiskat plots significantly off the mantle array, with a $\Delta\varepsilon_{Hfi}$ value of -10.8.

b) Nd-Sr isotopes Most of the samples in this group have Nd-Sr isotope variations that are located within or at the margins of the range of South African Group I compositions (Figure 6.10c). The only exception to this is the sample from Attawapiskat, which has a slightly unradiogenic Nd and very radiogenic Sr placing it just beyond the range of the fields of South African Group I and LDG data. Individual kimberlites and sub-groups do not show the same internal consistency as observed with Hf-Nd variations. The samples from Rankin Inlet and Timiskaming, for example, span a range in ε_{Sri} from -11.5 to $+10.2$. The value from Rankin Inlet is much less radiogenic than any value recorded in the LDG field. In general, the isotopic characteristics of kimberlites from

outside the Slave province are generally consistent with those of South African Group I kimberlites.

c) Hf-Sr isotopes The kimberlites in this group have a very wide range of both Hf and Sr isotope compositions. The four analyses of Somerset Island kimberlites conducted during this study range across ~20 units in ε_{Sri}, with relatively little associated variation in ε_{Hfi}. A similar, smaller offset is seen between two kimberlites from the Timiskaming field of the Superior province. The actual values of ε_{Sri} in this latter case are much less radiogenic and are thus less likely to result from alteration or crustal contamination. The effects of such processes on the isotopic composition of kimberlites are investigated in the following sections.

6.3.4 Summary of the isotopic character of Canadian kimberlites

The Hf-Nd-Sr isotope characteristics of kimberlites from LDG and other Canadian localitites analysed during this study are conveniently summarised in Table 6.2. The range of isotopic signatures from each group is compared to that of an aphanitic kimberlite from Wesselton, South Africa, which should be representative of unaltered, minimally contaminated, hypabyssal facies Group I kimberlite.

In all cases the kimberlites from LDG have unradiogenic Nd isotope signatures, in comparison to the slightly positive ε_{Ndi} of the Wesselton sample. This corresponds to a lower time integrated Sm/Nd ratio in the LDG kimberlites, which is indicative of a more enriched character to their mantle source. This characteristic is less pronounced in other Canadian kimberlites from beyond LDG, both within the Slave and other provinces. The kimberlites from the Contwoyto field (north Slave) and Somerset

Island (Churchill) have Nd isotope signatures that are more closely comparable to that of Wesselton. The kimberlites from Rankin Inlet (Churchill) and Timiskaming (Superior) have Nd isotope signatures that are clearly more radiogenic than Wesselton, indicating a higher time integrated Sm/Nd ratio in their source.

The range of Hf isotope compositions from each kimberlite field and sub-grouping within the Slave province extends to both more radiogenic and less radiogenic values than the ε_{Hfi} for Wesselton. This corresponds to both higher and lower time integrated Lu/Hf ratios in the LDG magmas than at Wesselton. This very wide range in ε_{Hfi} over a very narrow range in ε_{Ndi} produces a pronounced sub-vertical array in Hf-Nd isotope space that is strongly suggestive of mixing between two (or possibly more) mantle sources with distinct isotopic characteristics. In almost all other Canadian fields from which kimberlites have been analysed, the time integrated Lu/Hf ratio of the source must have been higher than at Wesselton, producing a more depleted signature. The only exception to this is the single analysis from Attawapiskat.

Sr isotope compositions in almost all Canadian kimberlites are more radiogenic than that of Wesselton, which has one of the least radiogenic values of ε_{Sri} known in South African Group I kimberlites. Only Rankin Inlet has a lower time integrated Rb/Sr ratio and thus more depleted signature. The Rb-Sr isotope system is typically considered to be the most sensitive to the effects of modification by crustal contamination and post-emplacement alteration. It is important to characterise these effects on Hf and Nd, as well as Sr, isotope signatures, before we can begin to interpret the kimberlite data in terms of recognising and quantifying different mantle processes.

Slave Province

Region	Number of samples	Range of $\varepsilon_{Sr\,i}$	Time integrated Rb/Sr relative to Wesselton	Range of $\varepsilon_{Nd\,i}$	Time integrated Sm/Nd relative to Wesselton	Range of $\varepsilon_{Hf\,i}$	Time integrated Lu/Hf relative to Wesselton
Grizzly ~51Ma	14	+2.1 to +4.0	Higher ⇒ more enriched signature	-2.1 to -0.9	Lower ⇒ more enriched signature	-4.7 to +0.1	Lower to higher ⇒ variably enriched to depleted signature
Central LDG (incl. Grizzly) 45-72Ma	44	+0.2 to +28.0	Higher ⇒ more enriched signature (+ contam/alteration?)	-3.8 to -0.5	Lower ⇒ more enriched signature	-14.6 to +10.5	Lower to higher ⇒ variably enriched to depleted signature
South LDG 53-74Ma	22	-1.5 to +28.4	Higher ⇒ more enriched signature (+ contam/alteration?)	-4.2 to +0.1	Lower ⇒ more enriched signature	-10.2 to +4.1	Lower to higher ⇒ variably enriched to depleted signature
South-East Slave (Snap Lake, Kennady Lake) 525-545Ma	2	+7.1 to +13.5	Higher ⇒ more enriched signature	-3.4 to +0.8	Lower ⇒ more enriched signature	-16.5 to -1.2	Lower to higher ⇒ variably enriched to depleted signature
North Slave (Jericho, Muskox) ~173Ma	8	-0.1 to +59.0	Higher ⇒ more enriched signature (+ contam/alteration?)	+0.5 to +3.0	Lower to higher ⇒ variably enriched to depleted signature	-4.6 to +6.1	Lower to higher ⇒ variably enriched to depleted signature

(cont'd)

Region	Number of samples	Range of $\varepsilon_{Sr\,i}$	Time integrated Rb/Sr relative to SA Group I	Range of $\varepsilon_{Nd\,i}$	Time integrated Sm/Nd relative to SA Group I	Range of $\varepsilon_{Hf\,i}$	Time integrated Lu/Hf relative to SA Group I
Churchill Province							
Somerset Island ~97.5Ma	4	+11.6 to +26.1	Higher ⟹ more enriched signature (+ contam/alteration?)	+0.7 to +2.0	Lower to higher ⟹ variably enriched to depleted signature	+1.7 to +3.9	Higher ⟹ more depleted signature
Rankin Inlet ~196Ma	1	-11.5	Lower ⟹ more depleted signature	+4.5	Higher ⟹ more depleted signature	+6.8	Higher ⟹ more depleted signature
Superior Province							
Attawapiskat ~175Ma	1	+34.3	Higher ⟹ more enriched signature (+ contam/alteration?)	-1.0	Lower ⟹ more enriched signature	-8.9	Lower ⟹ more enriched signature
Kirkland Lake ~155Ma	1	+8.2	Higher ⟹ more enriched signature	-0.7	Lower ⟹ more enriched signature	+1.1	Higher ⟹ more depleted signature
Timiskaming 135-155Ma	2	-0.2 to +10.2	Higher ⟹ more enriched signature	+4.1 to +4.9	Higher ⟹ more depleted signature	+7.0 to +8.7	Higher ⟹ more depleted signature

Table 6.2 Summary of the range of Sr, Nd and Hf isotopic compositions of Canadian kimberlites from this study, and comparison with the South African Group I Wesselton aphanitic kimberlite (sample = Wess 423 from Nowell *et al.*, in press; $\varepsilon_{Sr\,i}$ = -8.4, $\varepsilon_{Nd\,i}$ = 1.8, $\varepsilon_{Hf\,i}$ = -4.1) in terms of relative time integrated parent-daughter ratios required to develop these isotopic signatures. For further details on ages see AppendixA

6.4 ISOTOPIC EFFECTS OF CRUSTAL CONTAMINATION

20 samples of volcaniclastic kimberlite, including 16 from the LDG field, have been analysed for Hf, Nd and Sr isotope composition during the course of this study. Volcaniclastic kimberlites are much more commonly affected by crustal contamination than hypabyssal facies rocks, due to the nature of the kimberlite eruption process. This is confirmed by the abundance of macroscopic fragments of crustal material found in volcaniclastic samples. Consequently, these samples provide an opportunity to study the characteristic effects of crustal contamination on trace element and isotope systematics.

Combined major and trace element models (Figure 6.11) indicate that the volcaniclastic kimberlites contain a significant contribution from crustal signatures, comparable to or in excess of that seen in crustally contaminated hypabyssal kimberlites. The general characteristics that indicate the presence of contamination in these rocks are high Al and Yb, low Mg/Yb and variable Si/Al. Samples with high *ln (Si/Al)* but low *ln (Mg/Yb)* are likely to have incorporated significant lithospheric mantle material prior to interacting with crust. Al/Nb is used in Figure 6.11 as a proxy variable for Al, to account for the effects of variable volatile content in the volcaniclastic samples.

The range in Hf-Nd-Sr isotope composition shown by the 16 volcaniclastic kimberlites from Lac de Gras (Figure 6.12) demonstrates that these samples plot within and beyond the fields of 'crustally dominated', low *ln (Si/Al)* hypabyssal kimberlites. In all cases the volcaniclastic kimberlites appear to trend towards more isotopically enriched compositions.

Samples of both hypabyssal and volcaniclastic kimberlite have been analysed from the Rat and DO-27 (Tli Kwi Cho) bodies. In both cases the volcaniclastic samples have more radiogenic Sr and less radiogenic Hf and Nd, causing them to plot well outside the range of high *ln (Si/Al)* hypabyssal kimberlites (Figure 6.13). These relationships are consistent with trends of crustal assimilation in simple isotopic mixing models (Figure 6.14).

Despite careful visual screening of samples for potential crustal contamination, major and trace element models (Figure 6.11) indicate that many of the hypabyssal kimberlites from LDG have incorporated significant amounts of crustal material. Although there is a considerable amount of overlap between the range of Hf-Nd-Sr isotope for the low *ln (Si/Al)* and high *ln (Si/Al)* groups, the 'crustally dominated', low *ln (Si/Al)* group is offset to less radiogenic Hf and more radiogenic Sr isotope signatures. The volcaniclastic kimberlites and low *ln (Si/Al)* hypabyssal kimberlites from LDG thus have very similar major/trace element aNd isotope characteristics, and together define the most 'enriched' ends of observed Hf-Nd-Sr isotope arrays (Figure 6.12).

These general isotopic trends identified for volcaniclastic kimberlites and low *ln (Si/Al)* hypabyssal kimberlites are oriented sub-parallel to the trend in Hf-Nd-Sr isotope variation observed for the high *ln (Si/Al)* group. This raises the question of whether the consistent slope of the low and high *ln (Si/Al)* arrays could be a function of crustal contamination. Several lines of evidence indicate that this is not, in fact, the case.

Firstly, the Si/Al-Mg/Yb model of lithospheric and crustal assimilation (Figure 6.11a) shows that while samples with high *ln (Si/Al)* may have assimilated some crust, this is

in almost all cases <<10% and minimal compared to the amounts of crust evident in low *In (Si/Al)* hypabyssal and volcaniclastic kimberlites. Consequently, Si/Al and Mg/Yb are highly correlated in the high *In (Si/Al)* samples, and correspond closely to a mixing trend between model 'primary' kimberlite magma and lithospheric peridotite.

Secondly, to generate the observed range of Hf-Nd-Sr isotope variation in the high *In (Si/Al)* hypabyssal kimberlites, simple isotopic mixing models (Figure 6.14) require a minimum of 20-30% with any of the variety of different crustal end-member components found in the LDG area. This estimate is well in excess of the amount of possible crustal assimilation supported by major and trace element evidence. It also requires that the parental composition is located at the most radiogenic Hf and Nd compositions and least radiogenic Sr compositions of those observed. Even if the uncontaminated parental composition were located closer to the centre of the observed kimberlite arrays, a similar amount of crustal assimilation would be required. It would then also be difficult to envisage how crustal contamination could account for the development of more isotopically depleted compositions within the kimberlite array, since all crustal end-members are located at more isotopically enriched compositions.
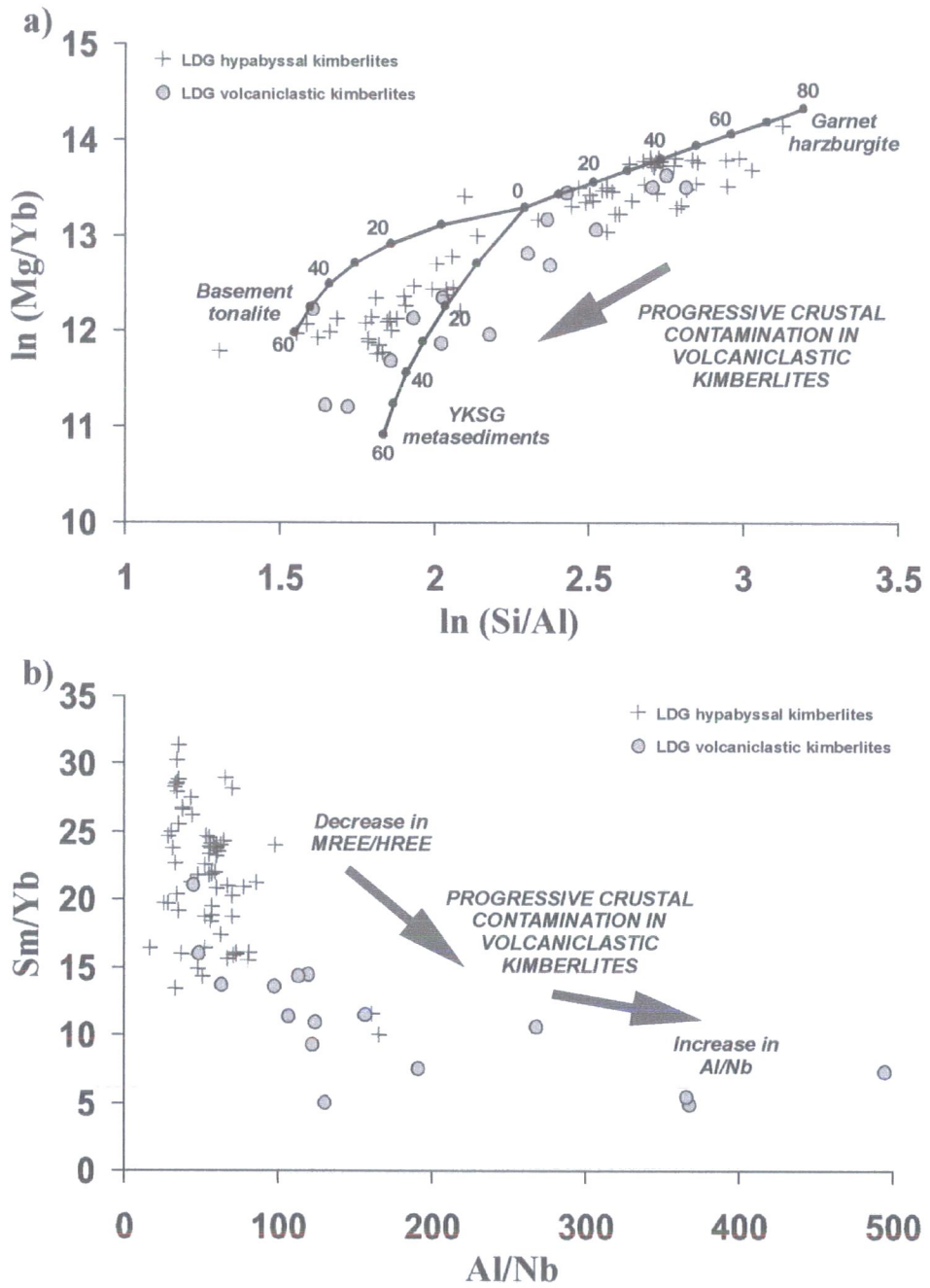
Figure 6.11 Discrimination of LDG volcaniclastic and hypabyssal kimberlites using major and trace element parameters of crustal contamination, a) ln (Si/Al) and ln (Mg/Yb); b) Al/Nb and Sm/Yb. All data from this study..
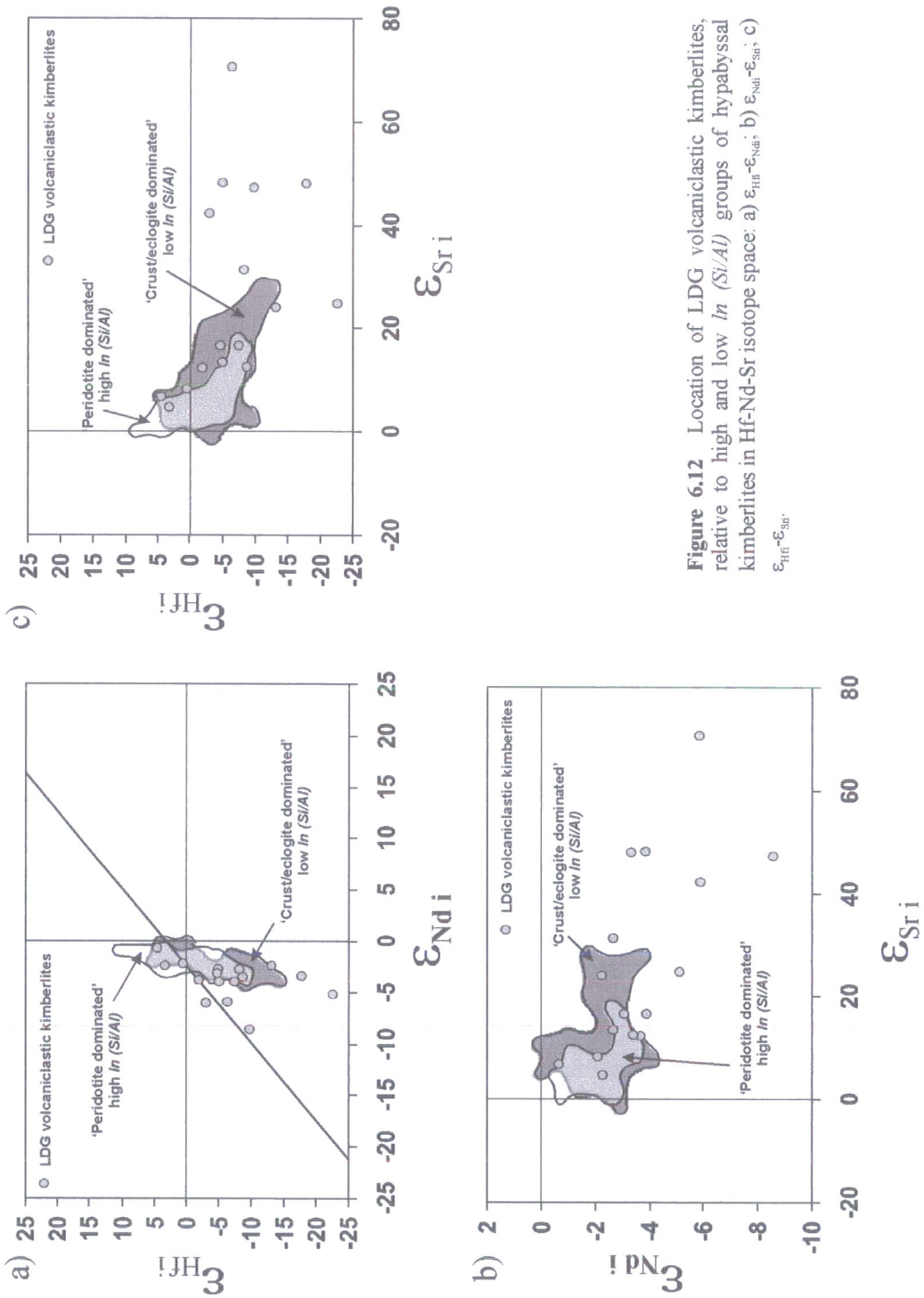
Figure 6.12 Location of LDG volcaniclastic kimberlites, relative to high and low *ln (Si/Al)* groups of hypabyssal kimberlites in Hf-Nd-Sr isotope space: a) $\varepsilon_{Hf i}$-$\varepsilon_{Nd i}$; b) $\varepsilon_{Nd i}$-$\varepsilon_{Sr i}$; c) $\varepsilon_{Hf i}$-$\varepsilon_{Sr i}$.

223
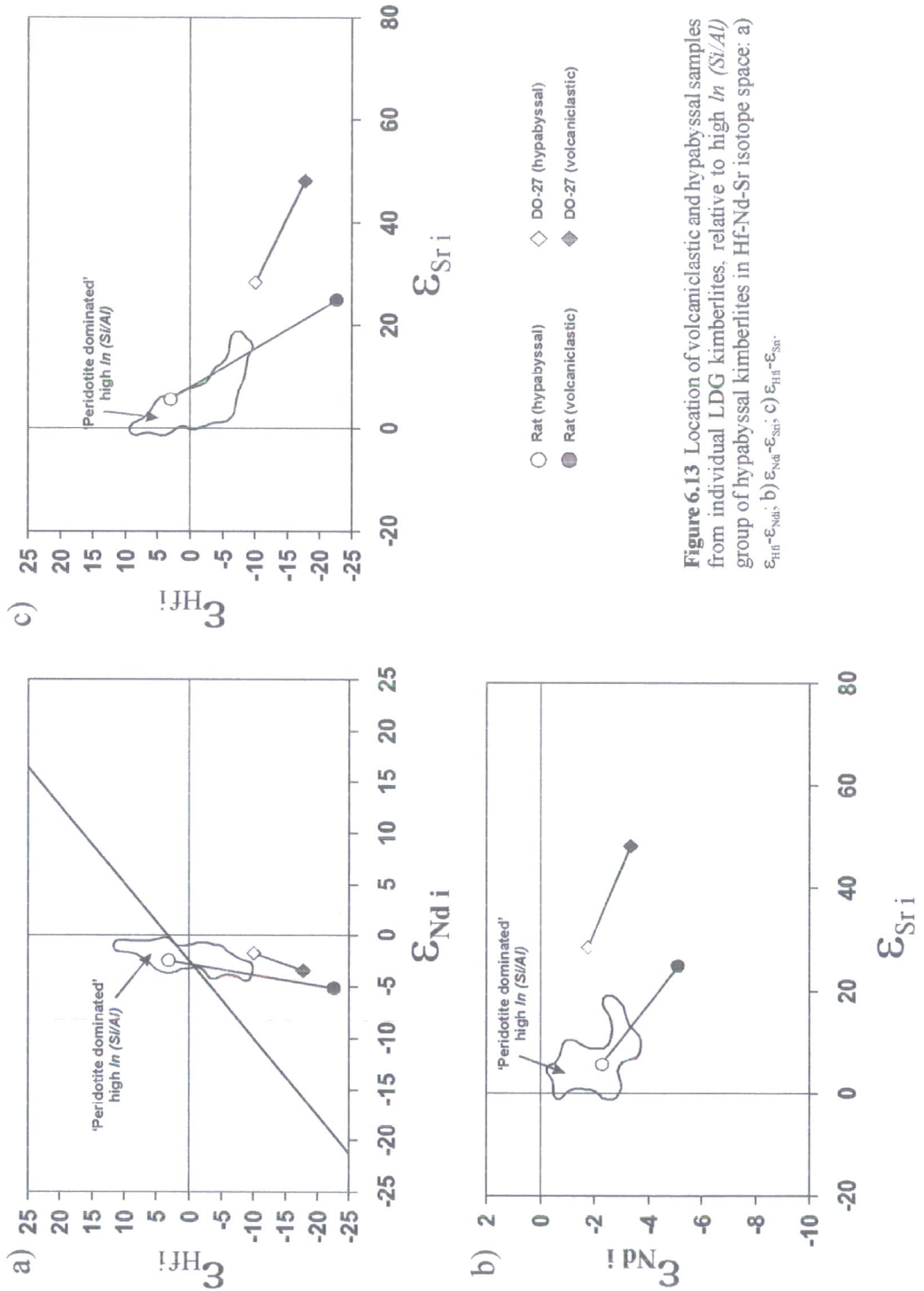
Figure 6.13 Location of volcaniclastic and hypabyssal samples from individual LDG kimberlites, relative to high ln (Si/Al) group of hypabyssal kimberlites in Hf-Nd-Sr isotope space: a) $\varepsilon_{Hfi}-\varepsilon_{Ndi}$; b) $\varepsilon_{Ndi}-\varepsilon_{Sri}$; c) $\varepsilon_{Hfi}-\varepsilon_{Sri}$.

224

Thirdly, within the high *In (Si/Al)* group of hypabyssal kimberlites, no correlation is observed between isotopic parameters, such as ε_{Hfi} and ε_{Sri}, and elemental parameters of crustal contamination, such as Al and Yb content, or La/Yb and Sm/Yb ratios (Figure 6.15). If the kimberlite array were generated by assimilation of large quantities of crust, then these isotopic and elemental parameters should be much more strongly correlated.

Finally, the trend in Hf-Nd isotope variation displayed by the LDG data (towards negative $\Delta\varepsilon_{Hfi}$ values, with an array oriented at a high angle to the Hf-Nd 'mantle array regression') is very similar to that observed in South African kimberlites by Nowell *et al.* (1999; in press). These authors have also analysed members of the low-Cr megacryst suite (e.g. garnet, clinopyroxene, ilmenite) that is commonly found in association with kimberlites in southern Africa. Megacrysts crystallise at depth within the lithospheric mantle and thus remain unaffected by crustal contamination as they ascend in the rising kimberlite magma. Consequently their isotopic signatures cannot be a function of crustal interaction, and must instead by derived from the mantle. The ranges of Hf and Nd isotope compositions observed in low-Cr megacrysts define elongate arrays, parallel to and overlapping exactly the Hf-Nd isotope variation in their host kimberlites (Nowell *et al.*, in press). This provides strong support for the isotope composition of carefully selected kimberlites being derived from sources and/or processes below the continental crust. These compositions should thus faithfully reflect those of the kimberlite source within the mantle.
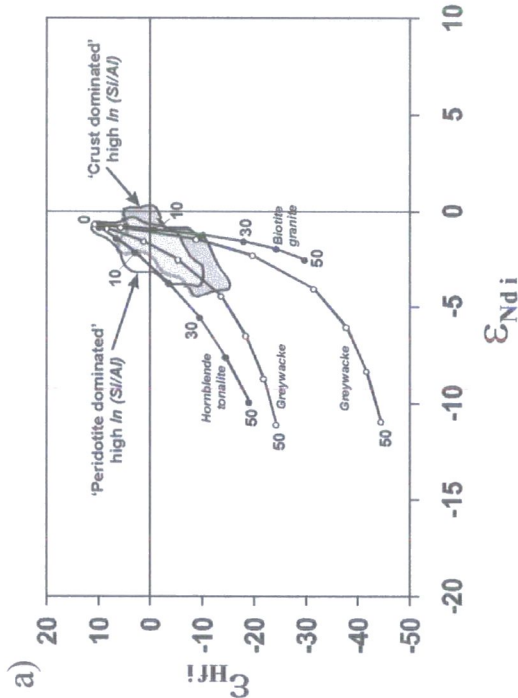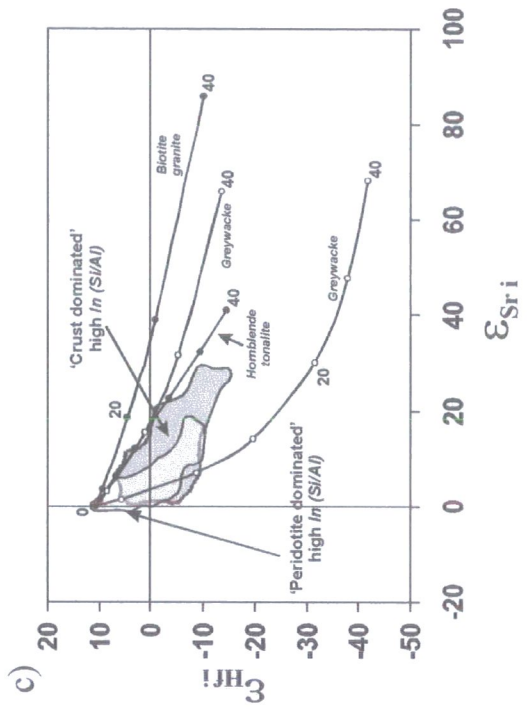
Figure 6.14 Trajectories of mixing trends between most radiogenic LDG hypabyssal kimberlite composition and selected LDG crustal materials, in Hf-Nd-Sr isotope space: a) $\varepsilon_{Hf\,i}$-$\varepsilon_{Nd\,i}$; b) $\varepsilon_{Nd\,i}$-$\varepsilon_{Sr\,i}$; c) $\varepsilon_{Hf\,i}$-$\varepsilon_{Sr\,i}$. Tick marks on mixing lines indicate increments of mixing (annotated on selected trajectories). All data from this study. Mixing trends are shown relative to orientation of high and low ln (Si/Al) groups of LDG hypabyssal kimberlites.

226
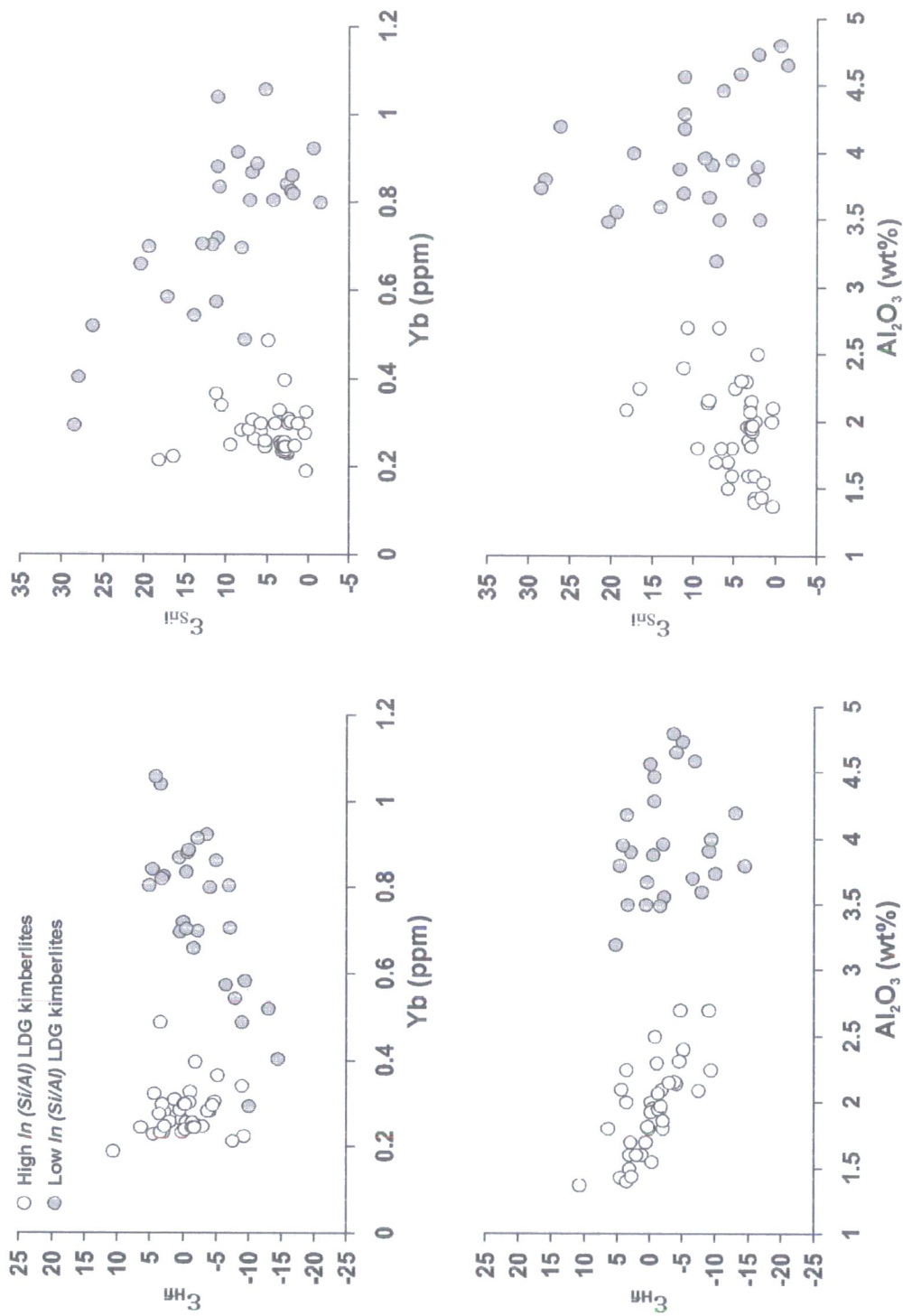
Figure 6.15 Scatter plots demonstrating lack of correlation between isotopic (ϵ_{Hf}, ϵ_{Sn}) and elemental (Yb, Al) parameters of crustal contamination across high and low *In (Al/Si)* groups of LDG hypabyssal kimberlites. All data from this study.

6.5 CAUSES OF VARIABILITY IN Hf-Nd-Sr ISOTOPE COMPOSITIONS OF LDG KIMBERLITES

6.5.1 Constraints on possible mantle components

In the following discussion, the subset of minimally contaminated LDG kimberlites, with high *ln (Si/Al)*, is used to identify isotopic components within the mantle that could interact to generate the observed LDG kimberlite array. It is possible that all the isotopic variation observed in the array could be derived from a single, heterogeneous mantle source, melting to produce magmas that do not undergo further modification en route to the surface. The orientation and linear nature of the array is, however, strongly suggestive of mixing between two components. Consequently, this analysis concentrates on identifying possible two-component mixing scenarios.

The orientation of the LDG kimberlite Hf-Nd-Sr isotope array provides some immediate constraints on the possible location of mixing end-members (Figure 6.16). The thick black line in each cartoon represents the approximate trend through the LDG kimberlite data, to which some portion of any mixing line is required to fit. In Figure 6.16a the positive gradient of the array requires that mixing end-members must be offset to more radiogenic Nd at increasingly positive ε_{Hfi}, and less radiogenic Nd at increasingly negative $\varepsilon_{Hf\,i}$, as indicated by the shaded regions on Figure 6.16a. Similar relationships for variations in Nd-Sr and Hf-Sr isotope composition are shown in Figures 6.16b-c.
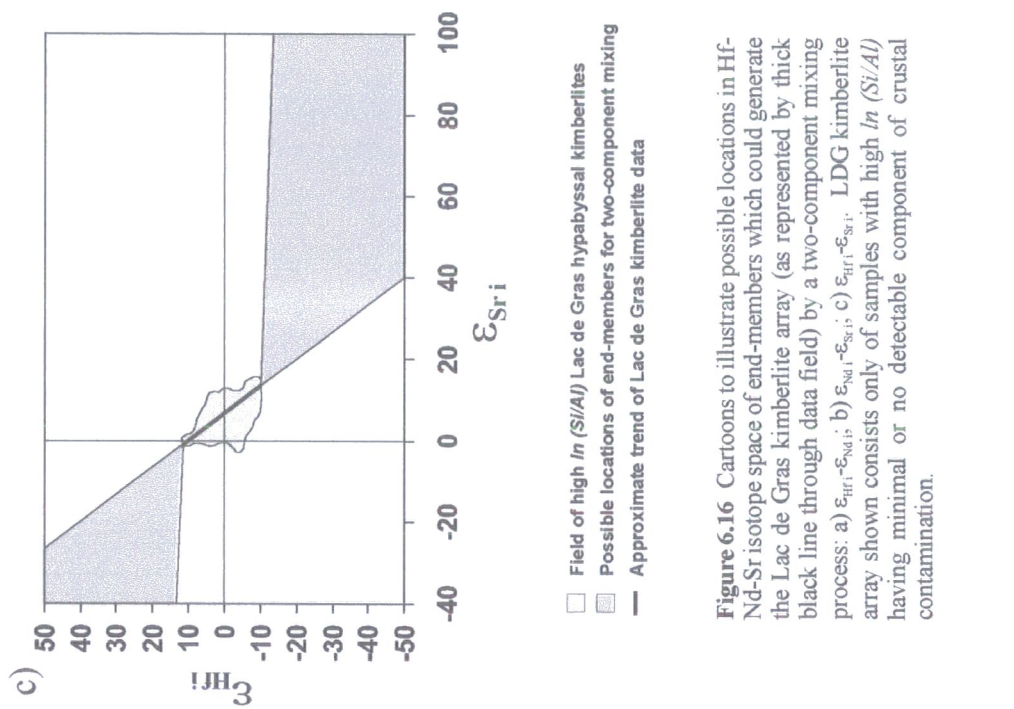
Figure 6.16 Cartoons to illustrate possible locations in Hf-Nd-Sr isotope space of end-members which could generate the Lac de Gras kimberlite array (as represented by thick black line through data field) by a two-component mixing process: a) $\varepsilon_{Hf\,i}$-$\varepsilon_{Nd\,i}$; b) $\varepsilon_{Nd\,i}$-$\varepsilon_{Sr\,i}$; c) $\varepsilon_{Hf\,i}$-$\varepsilon_{Sr\,i}$. LDG kimberlite array shown consists only of samples with high $ln\,(Si/Al)$ having minimal or no detectable component of crustal contamination.

☐ Field of high $ln\,(Si/Al)$ Lac de Gras hypabyssal kimberlites

▨ Possible locations of end-members for two-component mixing

— Approximate trend of Lac de Gras kimberlite data

229

The mixing line between the two end-members can have a range of geometries, from a straight line, to a curve that approaches a right angle at its point of inflection. The bounding lines to the shaded areas in Figure 6.16 represent these extreme cases. The curvature of the Hf-Nd isotope mixing line is controlled by the ratio:

$$(Hf/Nd)_{component\ A}\ /\ (Hf/Nd)_{component\ B}$$

Another important constraint is the position of hypothetical mixing components relative to the Hf-Nd isotope mantle array regression line. It is evident from the shaded fields in Figure 6.16 that either component may be situated above, below, or on the mantle array regression. Because the LDG kimberlite array is oriented at an oblique angle to the mantle array, however, it is not possible for *both* components to be situated on the mantle array in the same mixing scenario. No mixing line between two such components would be able to generate the kimberlite data array, regardless of the relative Hf/Nd ratios. This is important, because it rules out mixing between two obvious mantle components – the depleted MORB reservoir and the relatively enriched OIB reservoir – as a means of generating the observed isotopic variation in kimberlites.

6.5.2 Possible mixing end-members

Six mantle reservoirs/components that could contribute to the generation of the array defined by LDG hypabyssal kimberlites, and possible mixing relationships between them, are identified in Figure 6.17. These are:

Reservoirs:

1) Depleted sub-continental lithospheric mantle (SCLM)

2) MORB magma

3) EMI OIB magma

4) Metasomatised SCLM

Components:

5) Lamproitic magma

6) Enriched mantle component with negative $\Delta\varepsilon_{Hf}$ signature

The key isotopic and elemental characteristics of these reservoirs and components required for modelling their interactions are listed in Table 6.3. Variably depleted sub-continental lithospheric mantle (SCLM), represented by xenoliths of harzburgite and lherzolite, is located almost exclusively above the Hf-Nd isotope mantle array regression line (Ionov and Weiss, 2002; Schmidberger *et al.*, 2002; Simon *et al.*, 2002; Nowell *et al.*, in press) and is the most likely source of a mixing end-member with positive ε_{Hf}, which is required by the LDG data (Figure 6.17a). A source of unradiogenic Hf and Nd isotope compositions could correspond either to enriched SCLM material, such as phlogopite peridotites (PPs) or phlogopite/K-richterite peridotites (PKPs) (Harte *et al.*, 1987; Grégoire *et al.*, 2002), or to some as yet unidentified component within the mantle having an OIB-like Nd isotope character, but unradiogenic Hf and a distinctive negative $\Delta\varepsilon_{Hf}$ signature. Since almost all lithospheric mantle material analysed to date is located on or above the mantle array (Figure 7.2), it is most likely that such a reservoir would have to reside somewhere within the convecting mantle (Nowell *et al.*, in press). This unusual signature would require time to develop, and it has been suggested that a negative $\Delta\varepsilon_{Hf}$ component could reside in relative isolation from the convecting mantle at some boundary layer (e.g. the 670km

discontinuity or the D'' layer, as suggested by Nowell *et al.*, 1999). Nowell *et al.* (1999; in press) also suggest that this component could correspond to subducted E-MORB (or a combination of N-MORB and sediment), and hence elemental abundances typical of E-MORB (Sun and McDonough, 1989) are used in Table 6.3.

All possible binary Hf-Nd isotope mixing interactions between these six possible components are shown in Figure 6.17b. Several combinations can be immediately discounted because mixing lines between them either do not intersect the LDG kimberlite array, or intersect it but do not replicate the orientation of the array. Binary combinations involving reservoir 3 (the EMI OIB composition) can only generate half of the observed array, either to more or less radiogenic compositions, because this reservoir is situated within the LDG kimberlite array, near its mid-point. A two-component mixing line can only be fitted to the array in four scenarios:

A) Reservoir 2 (MORB magma) and component 6 (isotopically enriched mantle with negative $\Delta\varepsilon_{Hfi}$ signature)

B) Reservoir 1 (depleted SCLM) and reservoir 4 (metasomatised SCLM)

C) Reservoir 1 and component 5 (lamproitic magma)

D) Reservoir 1 and component 6
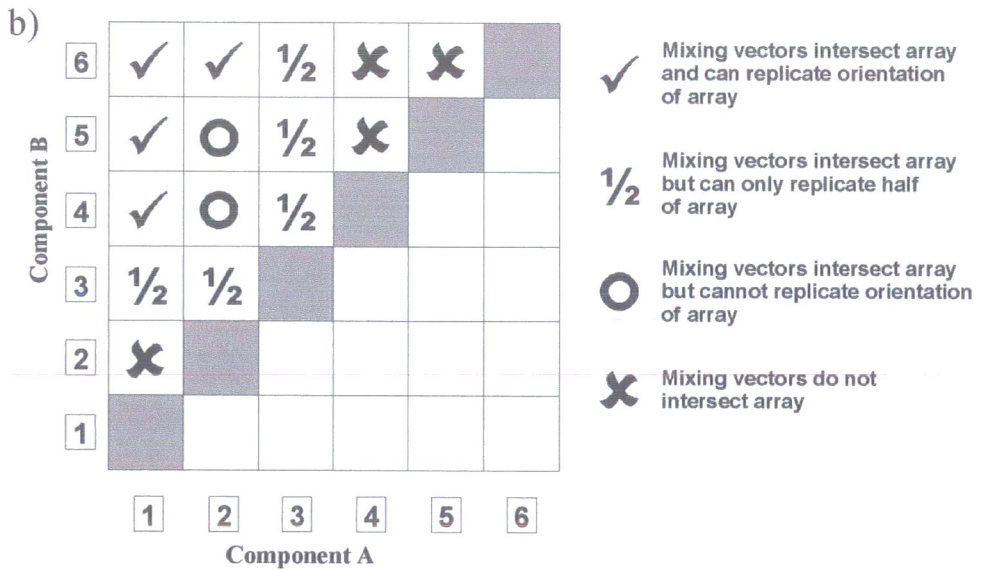
Figure 6.17 Hypothetical Hf-Nd isotopic mixing relationships between mantle reservoirs: a) cartoon demonstrating relative position of reservoirs and Lac de Gras kimberlite array in terms of Hf and Nd isotopic composition. Kimberlite array based on high *ln (Al/Si)* data with minimal crustal contamination; b) contingency table indicating outcome of binary mixing between reservoirs.

Component	Description	Isotopic/elemental characteristics	References for compositional values	Initial parameters selected for model
1	Depleted sub-continental lithospheric mantle	$\varepsilon_{Hf} \sim 0$ to $+150$, $\varepsilon_{Nd} \sim -10$ to $+15$, $\varepsilon_{Sr} < 0$, Hf = 0.01 to 0.16ppm, Nd = 0.06 to 0.5ppm, Sr = 0.02 to 0.24ppm	Isotopes: Nowell et al. (in press). Elements: Pearson and Nowell (2002 and unpubl.)	$\varepsilon_{Hf} = +30$, $\varepsilon_{Nd} = +5$, $\varepsilon_{Sr} = -20$, Hf = 0.06ppm, Nd = 0.3ppm, Sr = 0.15ppm, Hf/Nd = 0.2, Nd/Sr = 2, Hf/Sr = 0.4
2	MORB	$\varepsilon_{Hf} \sim +8$ to $+13$, $\varepsilon_{Nd} \sim +10$ to $+20$, $\varepsilon_{Sr} \sim -15$ to -30, Hf $\sim$ 2ppm, Nd $\sim$ 7ppm, Sr $\sim$ 90ppm	Isotopes: Nowell et al. (1998a). Elements: Sun and McDonough (1989)	$\varepsilon_{Hf} = +15$, $\varepsilon_{Nd} = +10$, $\varepsilon_{Sr} = -20$, Hf = 2ppm, Nd = 7ppm, Sr = 90ppm, Hf/Nd = 0.29, Nd/Sr = 0.08, Hf/Sr = 0.02
3	EMI OIB	$\varepsilon_{Hf} \sim -5$, $\varepsilon_{Nd} \sim -5$, $\varepsilon_{Sr} \sim +10$, Hf $\sim$ 8ppm, Nd $\sim$ 40ppm, Sr $\sim$ 660ppm	Isotopes: Zindler and Hart (1986); Salters and Hart (1991). Elements: Sun and McDonough (1989).	$\varepsilon_{Hf} = -5$, $\varepsilon_{Nd} = -5$, $\varepsilon_{Sr} = +10$, Hf = 8ppm, Nd = 40ppm, Sr = 660ppm, Hf/Nd = 0.2, Nd/Sr = 0.06, Hf/Sr = 0.01
4	Metasomatised sub-continental lithospheric mantle	$\varepsilon_{Hf} \sim -10$, $\varepsilon_{Nd} \sim -10$, $\varepsilon_{Sr} \sim +60$, Hf $\sim$ 0.2 to 0.8ppm, Nd $\sim$ 3 to 20ppm, Sr $\sim$ 50 to 150ppm	Isotopes: typical values for SA Group II kimberlites (Nowell et al., in press). Elements: Pearson and Nowell (2002).	$\varepsilon_{Hf} = -10$, $\varepsilon_{Nd} = -10$, $\varepsilon_{Sr} = +60$, Hf = 0.6ppm, Nd = 10ppm, Sr = 100ppm, Hf/Nd = 0.06, Nd/Sr = 0.1, Hf/Sr = 0.006
5	Lamproite	$\varepsilon_{Hf} \sim -35$, $\varepsilon_{Nd} \sim -28$, $\varepsilon_{Sr} \sim +20$, Hf $\sim$ 50ppm, Nd $\sim$ 320ppm, Sr $\sim$ 2700ppm	Isotopes and elements: typical values for Smoky Butte lamproite (Fraser, 1987; Nowell et al., 1998b)	$\varepsilon_{Hf} = -35$, $\varepsilon_{Nd} = -28$, $\varepsilon_{Sr} = +20$, Hf = 50ppm, Nd = 320ppm, Sr = 2700ppm, Hf/Nd = 0.16, Nd/Sr = 0.12, Hf/Sr = 0.02
6	Unknown mantle component with negative $\Delta\varepsilon_{Hfi}$	$\varepsilon_{Hf} <= -10$, $\varepsilon_{Nd} = 0$ to -10, $\varepsilon_{Sr} > 0$, Hf $\sim$ 2ppm, Nd $\sim$ 9ppm, Sr $\sim$ 150ppm	Isotopes: ranges estimated from Figure 6.17. Elements: Based on E-MORB values of Sun and McDonough (1989)	$\varepsilon_{Hf} = -15$, $\varepsilon_{Nd} = -5$, $\varepsilon_{Sr} = +20$, Hf = 2ppm, Nd = 9ppm, Sr = 150ppm, Hf/Nd = 0.22, Nd/Sr = 0.06, Hf/Sr = 0.01

Table 6.3 Hf-Nd-Sr isotope and elemental mixing parameters for various mantle components. Initial parameters selected for mixing model are based on typical values from references cited above. Components include both solid (e.g. 1 and 4) and melt (e.g. 2 and 3) compositions. Lamproite composition (5) may represent a melt of extremely isotopically enriched (i.e. highly metasomatised) sub-continental lithospheric mantle.

6.5.3 Testing Hf-Nd isotope mixing scenarios

Mixing lines between the mantle components identified in the four scenarios above are shown in Figure 6.18, and discussed below.

A) MORB magma and component with negative $\Delta\varepsilon_{Hfi}$

Because the initial model Hf/Nd ratios in both components are very similar, the mixing trajectory produced is a near-straight line, which touches but does not pass through the LDG kimberlite array. The trajectory can, however, be modified by adjusting the Hf/Nd ratio in one or both components. Hf-Nd isotope and elemental parameters are well constrained in MORB to the values shown in Table 6.3. It is, therefore, more appropriate to vary the Hf/Nd ratio in the negative $\Delta\varepsilon_{Hfi}$ component, the characteristics of which are relatively unknown. To produce a mixing line that passes through the LDG kimberlite array, Hf/Nd in this component would have to be between 0.22 and ~0.02, as shown by the 'alternative' mixing line. This alternative Hf/Nd ratio is an order of magnitude lower than Hf/Nd typical of an E-MORB composition. If the composition of this component is at all like that of an oceanic basaltic magma, then such a Hf/Nd ratio seems unlikely.

B) Depleted SCLM and metasomatised SCLM

In this scenario, a mixing line can only be successfully fitted through the LDG kimberlite Hf-Nd array if the isotopic signatures of the two components are carefully chosen. Because the Nd isotope composition of the metasomatised SCLM is less
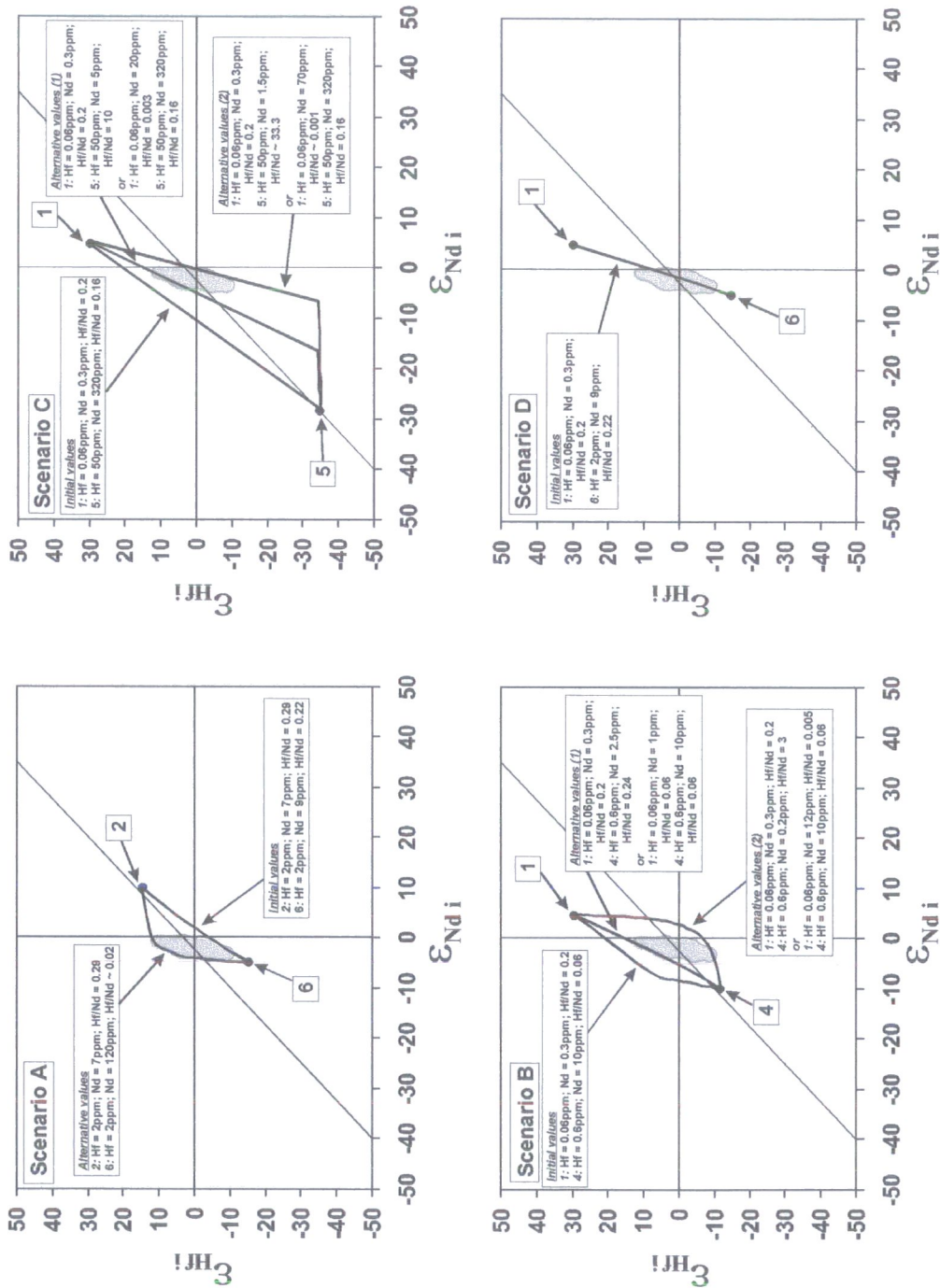
Figure 6.18 Hf-Nd isotopic mixing lines generated between representative end-members of different mantle components. Lines are shown for initial mixing parameters as listed in Table 6.3 and, where necessary, for alternative parameters adjusted to allow mixing lines to pass through field of LDG high *ln (Si/Al)* kimberlites.

236

radiogenic than the range typical of the kimberlite array, the curvature of any mixing line fitting the array dictates that the depleted SCLM component must have a near chondritic ε_{Ndi} signature. Nevertheless, since this should be an isotopically depleted reservoir, it seems likely that its Nd isotope signature will be slightly radiogenic. The metasomatised SCLM reservoir has been assigned a Hf-Nd isotope composition typical of SA Group II kimberlites, because Group II magmas are often envisaged as being derived from such a reservoir (e.g. Smith, 1983). The ε_{Hfi} signature of the metasomatised SCLM must, however, be less radiogenic than the most isotopically enriched end of the array, which rules out some SA Group II-like compositions. The mixing line generated using the initial model parameters does not pass through the LDG kimberlite array.

Mixing lines between the two reservoirs will pass through at least some part of the array, if Hf/Nd of the metasomatised SCLM is ~0.2-3.0 for initial depleted SCLM values, or if the depleted SCLM has Hf/Nd of 0.005-0.06 for initial metasomatised SCLM values. Although some SCLM lithologies may correspond with these criteria, the tightly clustered and linear nature of the Hf-Nd isotope array for LDG kimberlites indicates that both SCLM end-members would have to be isotopically very homogeneous. This seems unlikely considering the isotopic analyses of these materials that have been conducted to date (e.g. Ionov and Weiss, 2002; Schmidberger *et al.*, 2002; Simon *et al.*, 2002).

C) Depleted SCLM and lamproitic magma

A magma with a lamproitic composition has extremely unradiogenic ε_{Ndi} and ε_{Hfi}, but also has extremely high abundances of Hf, Nd and Sr. Consequently, the mixing

relationship with depleted SCLM is totally dominated by the lamproitic composition. Hf/Nd ratios are similar in both components, so the mixing line generated from the initial model parameters is straight, and does not intersect the LDG kimberlite array. Any mixing line passing through the array must have very extreme curvature, which requires that either Hf/Nd is unreasonably high ($>>1$) in the lamproitic component, or very low ($<<0.1$) in the depleted SCLM. Neither of these possibilities is realistic.

.

D) Depleted SCLM and *component with negative $\Delta\varepsilon_{Hfi}$*

Initial model parameters for these components produce a mixing line that is consistent with the orientation of the LDG kimberlite array. This fit can be improved further by small adjustments to either the isotopic composition or the Hf/Nd ratios in either end-member. A major advantage of this model is that there is much more scope for variation of the mixing parameters, while still being able to replicate the orientation of the kimberlite array. Consequently, heterogeneity in either the depleted SCLM reservoir or the negative $\Delta\varepsilon_{Hfi}$ component can be accommodated.

The Nd-Sr and Hf-Sr isotope mixing lines based on initial parameters do not fit quite as well as the Hf-Nd mixing line to the LDG kimberlite array. The agreement between mixing lines and the observed Nd-Sr and Hf-Sr isotope variation can be improved by increasing Sr abundance in the depleted SCLM to 5ppm, so that Nd/Sr = 0.06 and Hf/Sr
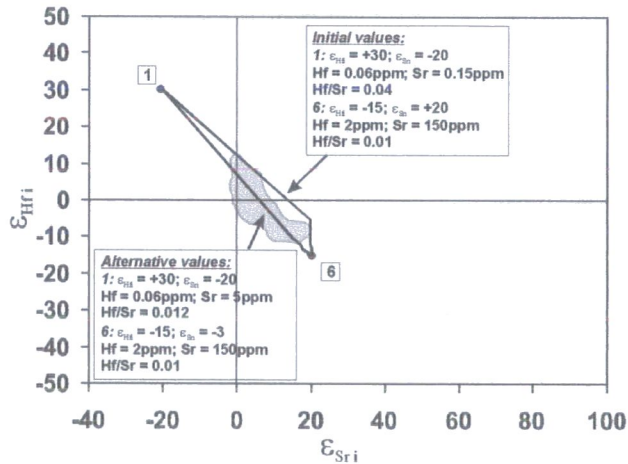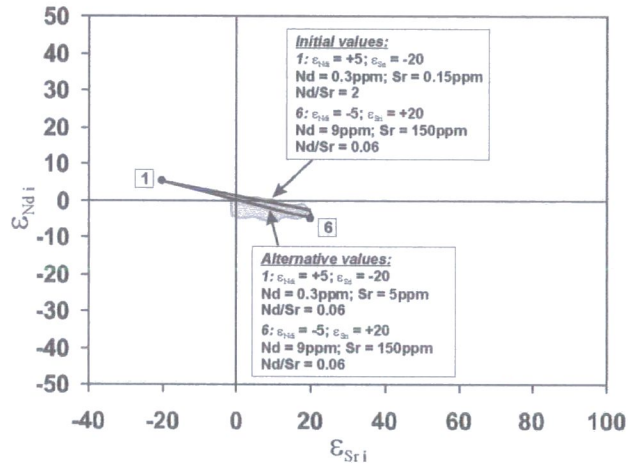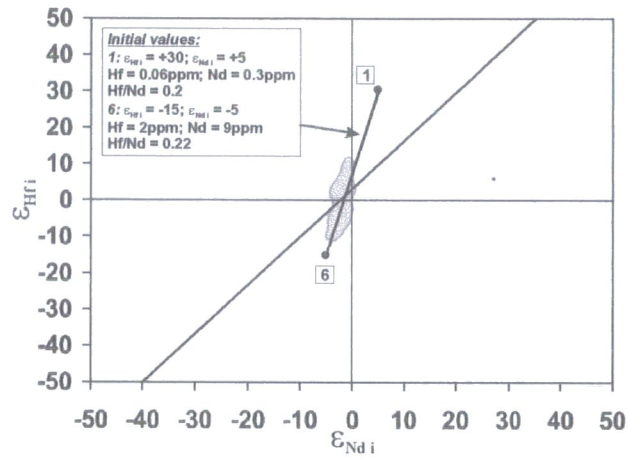
Figure 6.19 Model Hf-Nd, Nd-Sr and Hf-Sr isotopic mixing trajectories between depleted SCLM reservoir and mantle component with negative $\Delta\varepsilon_{Hf}$.

The LDG kimberlite array can also be successfully modelled by mixing a depleted SCLM component with more radiogenic ε_{Ndi}, and the negative $\Delta\varepsilon_{Hfi}$ component. This requires a Hf/Nd>1, and Hf and Nd abundances that are >1ppm. The Sr abundance must also be increased such that Nd/Sr and Hf/Sr are an order of magnitude lower than their initial values in Table 6.3. Alternatively, if the depleted SCLM elemental abundances are kept at more realistic values, then the concentration of Hf and Nd in the negative $\Delta\varepsilon_{Hfi}$ component must be reduced to around an order of magnitude lower than values that are typical of OIB or E-MORB.

6.5.4 Summary

The isotopic compositions of the LDG kimberlites differ from those of South African Group I and II kimberlites. The main difference is observed in their Nd isotope signatures, which are intermediate between those characteristic of South African Group I and Group II rocks, and correspond most closely with the Nd isotope composition of the few 'transitional' kimberlites from South Africa that have been analysed. Canadian kimberlites from beyond Lac de Gras (e.g. Contwoyto, Timiskaming) do, however, have Nd isotope signatures similar to those of South Group I kimberlites. The range of Hf isotope compositions observed in the Lac de Gras kimberlites spans the range of both Group I and Group II compositions. Consequently, these analyses constitute a trend of Hf-Nd isotope variation that extends well below, and also to some extent above, the mantle array. This provides further evidence of the existence of a negative $\Delta\varepsilon_{Hf}$ signature within kimberlites beyond southern Africa.

Hf-Nd, Nd-Sr and Hf-Sr isotope mixing lines can be constructed between various mantle reservoirs to replicate the LDG kimberlite array, by adjustment of Hf/Nd, Nd/Sr

240

and Hf/Sr values from the initial values shown in Table 6.3. In most cases, however, the elemental parameters required to force mixing lines through the kimberlite array are unrealistic for the mantle component or reservoir to which they refer. The most geologically plausible combination that fits the data involves mixing between depleted SCLM and some as yet unidentified component within the mantle having a moderately enriched elemental (e.g. similar to E-MORB), and isotopic composition, but with a distinctive negative $\Delta\varepsilon_{Hfi}$ signature, i.e. a time-integrated Lu/Hf ratio that is lower than that of Bulk Silicate Earth.

Analyses of depleted SCLM material made to date (Ionov and Weiss, 2002; Schmidberger et al., 2002; Simon et al., 2002) indicate that this component could have a range of ε_{Hfi} (0 to +160) and ε_{Ndi} (-10 to >>+50) compositions. SCLM with a near chondritic Nd isotope composition is most easy to accommodate within the models presented here. The nature of this mixing could be assimilation or physical incorporation of depleted lithosphere into an ascending magma derived from sub-lithospheric depth; trace element models (Chapter 4) and field/petrographic studies do not, however, tend to support such large amounts of incorporation of SCLM. Chapter 7 attempts to further constrain the role of these components/reservoirs in the genesis of the Lac de Gras kimberlites, on the basis of isotopic mass balances and elemental correlations.

Chapter 7

Petrogenetic summary and conclusions

7.1 CONTAMINATION OF KIMBERLITE MAGMAS

7.1.1 Major/trace element evidence

It was shown in chapter 5 that assimilation of both crust and lithospheric mantle could modify the major and trace element composition of kimberlite magma. The crustal contamination index (CI) introduced by Clement (1982) is commonly used to assess input of silica-rich crustal lithologies within kimberlites, but is unable to satisfactorily resolve the competing effects of crustal and lithospheric mantle incorporation on magma composition. Consequently, over-reliance on this parameter can result in misidentification of contaminated samples and misinterpretation of data.

While a variety of major and trace element parameters (e.g. Al/Mn, Na/P, Sm/Yb) can be used to identify relative levels of crustal contamination in the LDG hypabyssal kimberlites, the most effective means of discriminating the effects of both crustal and lithospheric peridotite assimilation into the kimberlite is using ln (Si/Al) and ln (Mg/Yb). Models based on these two parameters indicate that the LDG hypabyssal kimberlites have experienced a range of contamination by crust and lithospheric peridotite. The samples can be divided into two groups: one with signatures of 'significant crustal contamination', characterised by ln (Si/Al) <2.1, and a 'minimal crustal contamination' group, with ln (Si/Al) >2.3. Within the high ln (Si/Al) group there is a range of compositions that correspond to progressive incorporation of peridotitic material. In addition, variation in ln (Mg/Yb) within this group suggests that

many of these samples do contain small (<10%) contributions from crustal material. It appears, therefore, that very few of the samples analysed remain completely unaffected by crustal contamination. This seems plausible given the thickness of crust that all kimberlite magmas must traverse in cratonic regions such as the Slave province.

7.1.2 Possible primary composition of Lac de Gras kimberlite magma

A principal aim of this study has been to constrain the elemental and isotopic signatures of the magmas parental to the LDG kimberlites. The primary magma composition is a major control on the geometry of mixing trends between magma and crustal or lithospheric peridotite end-members in contamination models. Conversely, the primary magma composition can be inferred by fitting mixing trends to the observed scatter of the LDG kimberlite data in such models. In the LDG hypabyssal kimberlite data, there is a break in the otherwise near-continuous distribution of the variable *ln (Si/Al)*. This could correspond to the composition of kimberlite magma with no crust or peridotite incorporated. This 'compositional gap' spans a range in *ln (Si/Al)* of ~2.2-2.4, and is defined primarily by an absence of samples with 2.5-3wt% Al_2O_3. The high and low *ln (Si/Al)* groups display a considerable amount of overlap in SiO_2 content, and by varying Al_2O_3 contents the 'compositional gap' of 2.2-2.4 can be generated with a relatively constant SiO_2 content of ~30wt%. Similarly, these values equate to MgO of ~30-32wt% and Yb of ~0.30-0.35.

These values for elemental abundances in the primary magma are compared with similar estimates from other studies in Table 7.1. Values reported for kimberlites from Wesselton (Edgar *et al.*, 1988) and Jericho (Price *et al.*, 2000) are based on analyses of aphanitic hypabyssal kimberlite, which is considered to be most representative of any

243

primary kimberlite liquid, whereas the values of Le Roex *et al.* (2003) are based on points of inflection between aphanitic and macrocrystal kimberlite compositional trends. The two samples from Jericho represent the range of compositions reported for several aphanitic samples by Price *et al.* (2000). With the exception of JD-51, all of the compositions in Table 7.1 agree to within 4-5wt% MgO or SiO_2, and 1-2wt% Al_2O_3. JD-51 is relatively poor in MgO and SiO_2, and it is difficult to see how both JD-51 and JD-82-3 could be representative of primary magmas in the same kimberlite locality; they may, instead, have experienced olivine fractionation or crustal contamination relative to each other. The estimates for MgO and SiO_2 content of the primary magma in this study are higher than, but still broadly similar to, those determined by Edgar *et al.* (1988) and Le Roex *et al.* (2003). This may reflect mineralogical differences, such as modal abundance of microphenocrystal olivine, between kimberlite magmas from different regions.

	Wesselton aphanitic[1]	Jericho JD-51[2]	Jericho JD-82-3[2]	Kimberley pool[3]	This study
MgO (wt%)	27.2	16.7	25.1	28-29	30-32
SiO_2 (wt%)	25.6	20.8	30.3	27-28	~30
Al_2O_3 (wt%)	3.3	1.8	1.8	~2.0	2.5-3.0
Yb (ppm)	-	0.64	0.43	-	0.30-0.35

Table 7.1 Comparison of estimates for abundance of selected elements in primary kimberlite magmas from this study and: (1) Edgar *et al.* (1988); (2) Price *et al.* (2000); (3) Le Roex *et al.* (2003).

The composition selected for the uncontaminated, 'primary' magma will clearly also influence any quantitative estimates of the amount of crust or lithospheric peridotite incorporated in contamination models. Using a hypothetical, 'primary' composition of

30wt% MgO, 30wt% SiO_2, 2.5wt% Al_2O_3 and 0.3ppm Yb, the majority of high *ln (Si/Al)* samples record between 10-50% incorporation of peridotite with a harzburgitic composition. This is in close agreement with the estimates of Pearson *et al.* (2003) based on Os isotopes. One sample from the Mark kimberlite, which is known to contain well in excess of 50% peridotite micro-xenoliths, records a signature of ~70% harzburgite incorporation on the basis of the *ln (Si/Al)-ln (Mg/Yb)* model. The majority of the low *ln (Si/Al)* samples record between 10-50% assimilation of crustal material of varying composition, with a small number of samples being indicative of >50% crustal contamination. This may appear difficult to reconcile with the low-contamination character of these samples suggested by petrographic studies, but it is quite possible that during disaggregation and assimilation of country rock xenoliths, much of this contaminant material becomes finely disseminated throughout the kimberlite matrix. In addition, these estimates of crustal contamination are likely to be maximum figures, because any incorporation of eclogitic material or fractionation of olivine will produce similar compositional trends to those of crustal assimilation.

Quantitative estimates of crustal and lithospheric peridotite contamination will be affected if the primary kimberlite magma has lower SiO_2 and MgO contents than those suggested above. For example, if the primary magma contained 25wt% SiO_2 and 25wt% MgO, then this primary composition would be located closer to those of the crustally contaminated samples in *ln (Si/Al)-ln (Mg/Yb)* space. At higher degrees of mixing, however, the location of points on mixing trajectories are more strongly controlled by the composition of the crustal/lithospheric end-member, and consequently are less sensitive to variation in the primary composition. As a result, the majority of high *ln (Si/Al)* LDG kimberlites still have signatures characteristic of

10-50% addition of lithospheric peridotite. The majority of low *ln (Si/Al)* samples correspond to a slightly narrower range of 10-40% addition of crustal material when using lower estimates of SiO_2 and MgO for the primary magma.

7.1.3 Group I-Group II-Transitional characteristics

In chapter 4 it was noted that the Canadian kimberlite dataset, which is dominated by the samples from Lac de Gras, has several elemental characteristics that are transitional to, or unlike those of South African Group I and II kimberlites. Some of these characteristics, such as their location in K_2O-TiO_2 and SiO_2-Pb space (after Smith *et al.*, 1985a), and La/Nb-Ba/Nb space (after Le Roex, 1986), can now be re-evaluated with the benefit of information from contamination modelling. Figure 7.1 shows the relative locations of high *ln (Si/Al)* and low *ln (Si/Al)* samples according to the constructions of Smith *et al.* (1985) and Le Roex (1986), and also indicates the orientation of mixing trends between a minimally contaminated LDG kimberlite (ANA-1) and average compositions of crustal greywackes and granitoids from the vicinity of Lac de Gras. This analysis suggests that indicates that some of the more 'transitional' or 'Group II-like' characteristics, such as elevated K_2O and Ba/Nb in the overall LDG dataset, could be explained by progressive addition of crust into low *ln (Si/Al)* samples. Contamination of this nature cannot, however, account for the elevated, 'Group II-like' Pb content displayed by some of the low *ln (Si/Al)* samples. Transitional to Group II signatures are not, therefore, directly synonymous with 'Group I plus crustal contamination'. Some, but not all, of the tendency for LDG kimberlites to have pseudo-'Transitional' signatures can be attributed to such contamination. Samples with and without crustal signatures are in some cases coincident in Figure 7.1a and 7.1b, and all LDG samples are located within the SA Group I range of La/Nb in

Figure 7.1c. The predominant elemental character of the LDG hypabyssal kimberlites is thus most consistent with SA Group I.

7.1.4 Isotopic evidence

It was demonstrated in chapter 6 that contamination by crustal material does not significantly modify the isotopic composition of the kimberlite magma until levels of assimilation become very high, e.g. >50-60%. In the case of most of the LDG hypabyssal kimberlites this exceeds the maximum estimates of crustal incorporation in the samples studied. The effect on isotope characteristics is, therefore, negligible in samples known from major and trace elements to be minimally contaminated by crust.

The high *ln (Si/Al)* group of LDG kimberlites containing minimal contributions from crust is consistently offset to slightly higher values of ε_{Hfi}, and does not show the same extension to very radiogenic ε_{Sri} that is evident among the more highly contaminated, low *ln (Si/Al)* group. These LDG kimberlites also extend to consistently higher values of ε_{Hfi} than is observed in South African Group 1 kimberlites (Nowell *et al.*, 1999; in press). Depleted SCLM is the only terrestrial reservoir that consistently has highly radiogenic Hf isotope compositions (Figure 7.2), and hence it seems possible that interaction of kimberlite magmas with this reservoir could produce the extension towards radiogenic ε_{Hfi} observed in the LDG kimberlites. This is investigated using the binary mixing model shown in Figure 7.3.
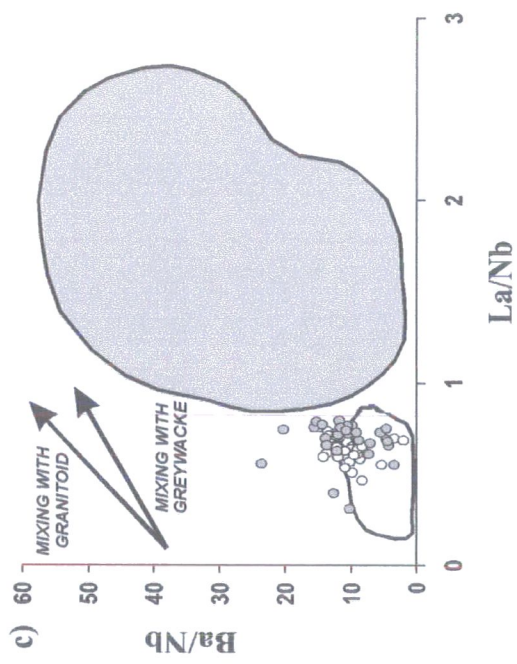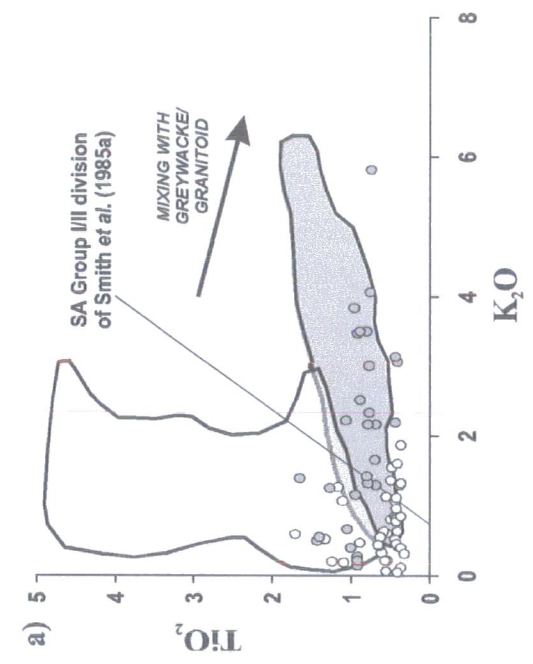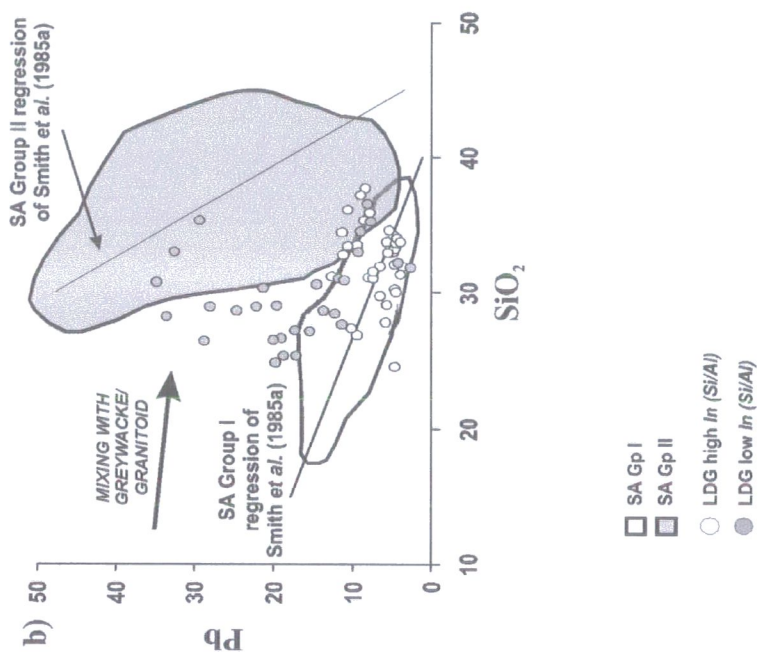
Figure 7.1 Location of high and low *ln (Si/Al)* hypabyssal kimberlites from Lac de Gras relative to fields of South African Group I and II kimberlites in the elemental classification schemes of Smith *et al.* (1985a) and Le Roex (1986). Vectors illustrate general orientation of mixing trends with typical LDG greywacke and granitoid contaminant end-members.

The lithospheric end-member compositions utilised are based on material from peridotite xenoliths obtained from kimberlites from Somerset Island in then Churchill province (Schmidberger *et al.*, 2002). The age of the Churchill lithosphere beneath Somerset Island (2.7Ga) is slightly younger than the 3.1Ga Slave lithosphere (Irvine, 2002), but is the closest analogue with available Hf data. Mineral separate, rather than whole rock, isotopic data is used to represent lithospheric compositions, because of the likelihood of infiltration and contamination of xenolith samples by the host kimberlite liquid. Olivine is the modally dominant phase in the majority of mantle peridotites, but the contribution it makes to the Sr-Nd-Hf isotope composition of the whole rock is negligible, because typical abundances of these elements in olivine are Sr <0.1ppm, Nd <0.01ppm and Hf <0.01ppm (Pearson *et al.*, 2003). Orthopyroxene is approximately an order of magnitude richer in Nd and Hf than olivine (Pearson *et al.*, 2003). Garnet and clinopyroxene are one to three orders of magnitude richer in Sr, Nd and Hf, than olivine or orthopyroxene, and consequently exert the main control on the budget of these elements and their isotopic characteristics within peridotites. The model of the isotopic effect of lithospheric material on kimberlites presented here is based on garnet alone, due to a comparative lack of isotopic data on clinopyroxene separates within the literature. Clearly the model must take account of the typical modal abundance of garnet in peridotite. In the scenarios presented here the modal abundance of garnet in the assimilated peridotite is assumed to be 10%.

Calculated mixing lines between a representative LDG hypabyssal kimberlite (ANA-2, Anaconda) and 'garnet peridotite' compositions in Hf-Nd isotope space (Figure 7.3) indicate that contamination by lithospheric material has very little effect on the isotopic composition of the kimberlite until very high degrees of mixing are reached.
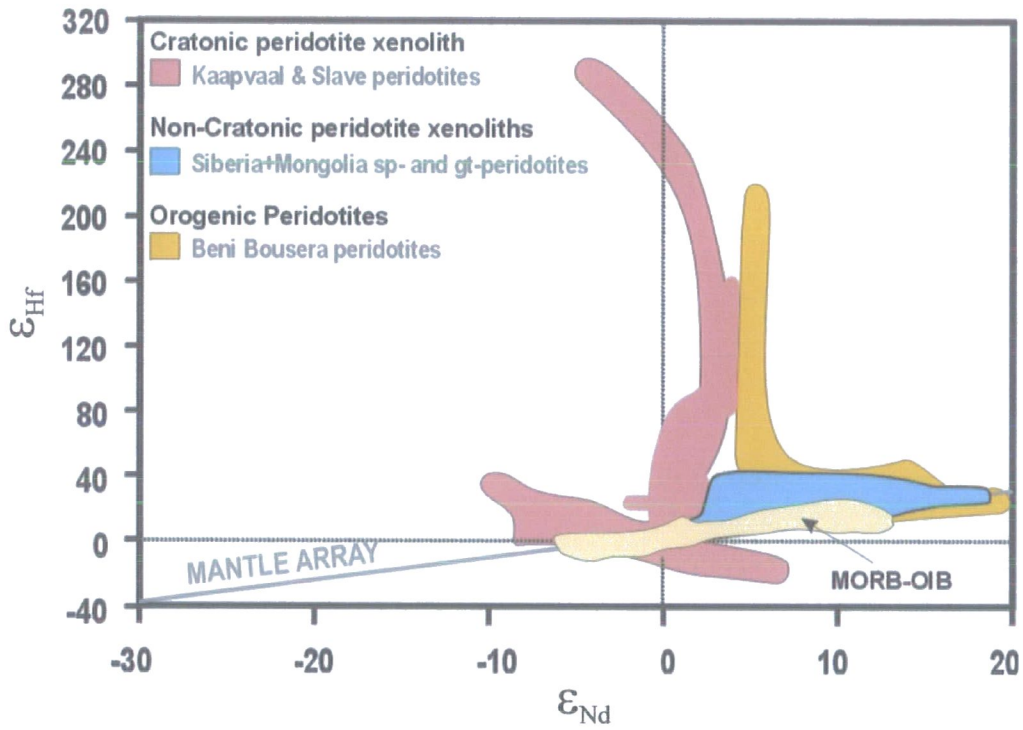
Figure 7.2 Range of Hf and Nd isotope compositions measured in garnet and clinopyroxene from lithospheric mantle peridotites. Kaapvaal peridotite data (grt + cpx) from Simon *et al.* (2002). Slave peridotite data (grt) from Schmidberger *et al.* (2002). Siberian and Mongolian peridotite field from Ionov and Weiss (2002). Beni Bousera peridotite data from Pearson (unpubl.).

In Figure 7.3a, 80% admixing of a lithospheric peridotite composition from Somerset Island produces an offset of only 9 units in ε_{Hfi}, with no associated offset in ε_{Ndi}. This is due to the Nd content of the mixture being dominated by the kimberlite ($Nd_{kimb}/Nd_{garnet} \sim 1500$), whereas the Hf content of the garnet forms a larger part of the total Hf budget for a given degree of mixing ($Hf_{kimb}/Hf_{garnet} \sim 65$). Unless the isotopic composition of the garnet is very extreme, or its Nd content is unusually high, mixing with a kimberlite composition will not produce significant offsets in ε_{Ndi} until the degree of mixing is well in excess of 90%. The Sr isotope composition of the kimberlite is even less sensitive to contamination by garnet of lithospheric origin in this manner (not shown). Consequently, the offset in Hf isotopic composition on mixing is far greater than the offset in Nd or Sr isotopic composition.

The modelled vertical Hf-Nd isotopic mixing trend for lithospheric contamination corresponds well to the sub-vertical trend of the LDG kimberlite array (Figure 7.3a), although it is clear that very large degrees of lithospheric contamination by peridotitic material are required to produce even a small proportion of the total range in ε_{Hfi} exhibited by the high *ln (Si/Al)* kimberlites. It therefore seems unlikely that contamination by lithospheric peridotite can, in isolation, be a primary control on the orientation of the kimberlite array. Differential contamination of kimberlite magmas by peridotitic material may, however, be able to account for some of the intra-kimberlite isotopic variation that is observed within the LDG dataset, as shown in Figure 7.3b for kimberlites from which three or more samples have been analysed during this study.
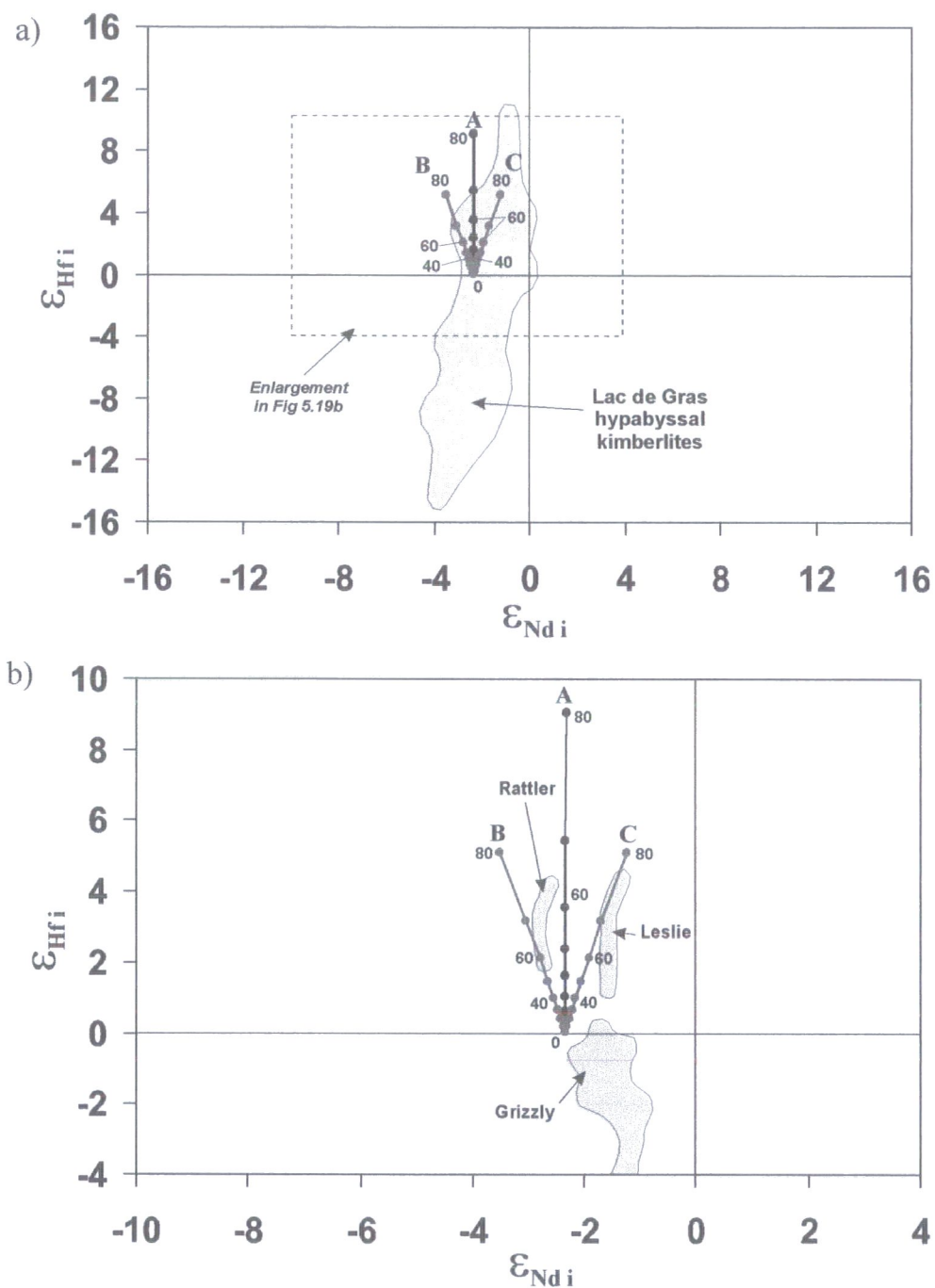
Figure 7.3 Mixing lines in Hf-Nd space between a typical Lac de Gras hypabyssal kimberlite (ANA-2) and representative and hypothetical lithospheric end-members. A = mixing with material containing 10% garnet having composition from Schmidberger *et al.* (2002), i.e. 0.027ppm Lu, 0.016ppm Hf, $^{176}Hf/^{177}Hf = 0.287403$ ($\varepsilon_{Hf} \sim 160$); 0.04ppm Sm, 0.05ppm Nd, $^{143}Nd/^{144}Nd = 0.513049$ ($\varepsilon_{Nd} \sim 6$). B, C = hypothetical mixing lines towards less and more radiogenic Nd isotope compositions. There is no distortion of scale between (a) and its enlargement, (b).

There is a general absence of strong correlations between isotopic and major/trace element indicators of lithospheric contamination in the LDG kimberlite dataset. Despite the general lack of clear trace element indicators of lithospheric input, individual cases do support the hypothesis that Hf isotope compositions of LDG hypabyssal kimberlites can be modified by interaction with SCLM. The Mark kimberlite, for example, has the highest values of *ln (Si/Al)* and *ln (Mg/Yb)*, high Mg/Nb and Ni/Nb, and low La/Nb and Yb/Nb. These are all indicators of SCLM peridotite input, and this kimberlite has the most radiogenic Hf isotope composition within the entire dataset. In general, however, trace elements do not support levels of peridotite assimilation in excess of 80% as a means of generating the variation in ε_{Hfi} within the LDG kimberlite array.

Although the high *ln (Si/Al)* LDG kimberlites, with minimal contributions from crustal contamination, show some tendency to extend above the Hf-Nd mantle array, they also extend to negative $\Delta\varepsilon_{Hfi}$ values, below the mantle array, as observed in the South African Group I kimberlites (Nowell *et al.*, 1999; in press). This indicates that, like the South African kimberlites, they could contain a signature that is derived from an unusual, rarely sampled source within the mantle.

7.2 TWO-COMPONENT MIXING SCENARIOS

In chapter 6 a detailed analysis was presented of possible binary mixing interactions between known isotopic reservoirs (e.g. depleted and enriched SCLM) and postulated isotopic components (e.g. a negative $\Delta\varepsilon_{Hfi}$ component) within the mantle that could generate the observed trend of the minimally contaminated LDG kimberlites in Hf-Nd-

Sr isotope space. It was concluded that the kimberlite array could be most satisfactorily replicated by mixing between depleted SCLM (with radiogenic Hf and a range of possible Nd isotope compositions) and a component with elemental and Nd-Sr isotope characteristics comparable to those of an OIB-type source, but also a pronounced negative $\Delta\varepsilon_{Hfi}$ character. This could correspond to rising kimberlite magma with OIB affinities, originating below the lithosphere in a source region having a negative $\Delta\varepsilon_{Hfi}$ character, which has its isotopic composition progressively modified by assimilation of garnet-bearing peridotite.

The modelling presented in Figure 7.3, however, strongly suggests that very large (>80-90%) amounts of SCLM peridotite assimilation would be required to produce offsets in ε_{Hfi} on the scale of the LDG kimberlite array. Major/trace element and Os isotope evidence does not support such large amounts of SCLM peridotite assimilation taking place in the LDG kimberlites, instead indicating that 10-50% incorporation of this type of material is more commonplace. The model of Figure 7.3 indicates that these levels of assimilation will not produce significant offsets in ε_{Hfi} on the scale of the LDG kimberlite array. In addition, the well-constrained, linear nature of the LDG kimberlite Hf-Nd array is also difficult to explain if it is generated by large amounts of interaction with, or even sourced from, depleted SCLM, which is a reservoir known to be isotopically very heterogeneous (Figure 7.2).

7.3 SINGLE COMPONENT ORIGIN FOR LDG KIMBERLITES

7.3.1 Extent of the negative $\Delta\varepsilon_{Hfi}$ signature

The linear nature of the LDG kimberlite Hf-Nd array strongly suggests that it results from variable mixing between two isotopically distinct reservoirs or components within

the mantle. Despite this, no two-component mixing scenario appears able to adequately account for both the orientation and extent of the LDG kimberlite array. An alternative explanation is that the observed Hf-Nd-Sr isotopic variation is characteristic of a single kimberlite mantle source region. The isotopic heterogeneity of such a source would dominate any subsequent contributions from small amounts of contamination by crust or lithospheric mantle peridotite. In this scenario, assimilation of crust or SCLM could only result in significant modification of kimberlite isotopic compositions, over and above the variation inherited from the source, if levels of assimilation are extremely high (i.e. >50-60% crust, >80-90% peridotite). This may account for the most extreme Hf-Nd isotope signatures observed in the LDG dataset, such as Mark, which has the most radiogenic ε_{Hfi} and trace element signatures indicative of the most extreme peridotite assimilation, and certain volcaniclastic kimberlites, which are known to have incorporated large amounts of crustal material, and are observed to have the least radiogenic Hf and Nd isotope compositions.

Figure 7.4 demonstrates that over half (58%) of the high ln (Si/Al) LDG hypabyssal kimberlites have $\Delta\varepsilon_{Hfi}$ signatures that are within the range of the majority of measured OIB compositions (-3 to +3). 16% have $\Delta\varepsilon_{Hfi}$ in excess of +3, and 26% have $\Delta\varepsilon_{Hfi}$ lower than –3, placing them beyond the range of the majority of OIB analyses forming the Hf-Nd mantle array. This is a very different situation to the South African Group I kimberlites shown in Figure 7.4d, where over 90% of samples have $\Delta\varepsilon_{Hfi}$ lower than -3. This is more comparable to the distribution of HIMU OIB shown in Figure 7.4b.
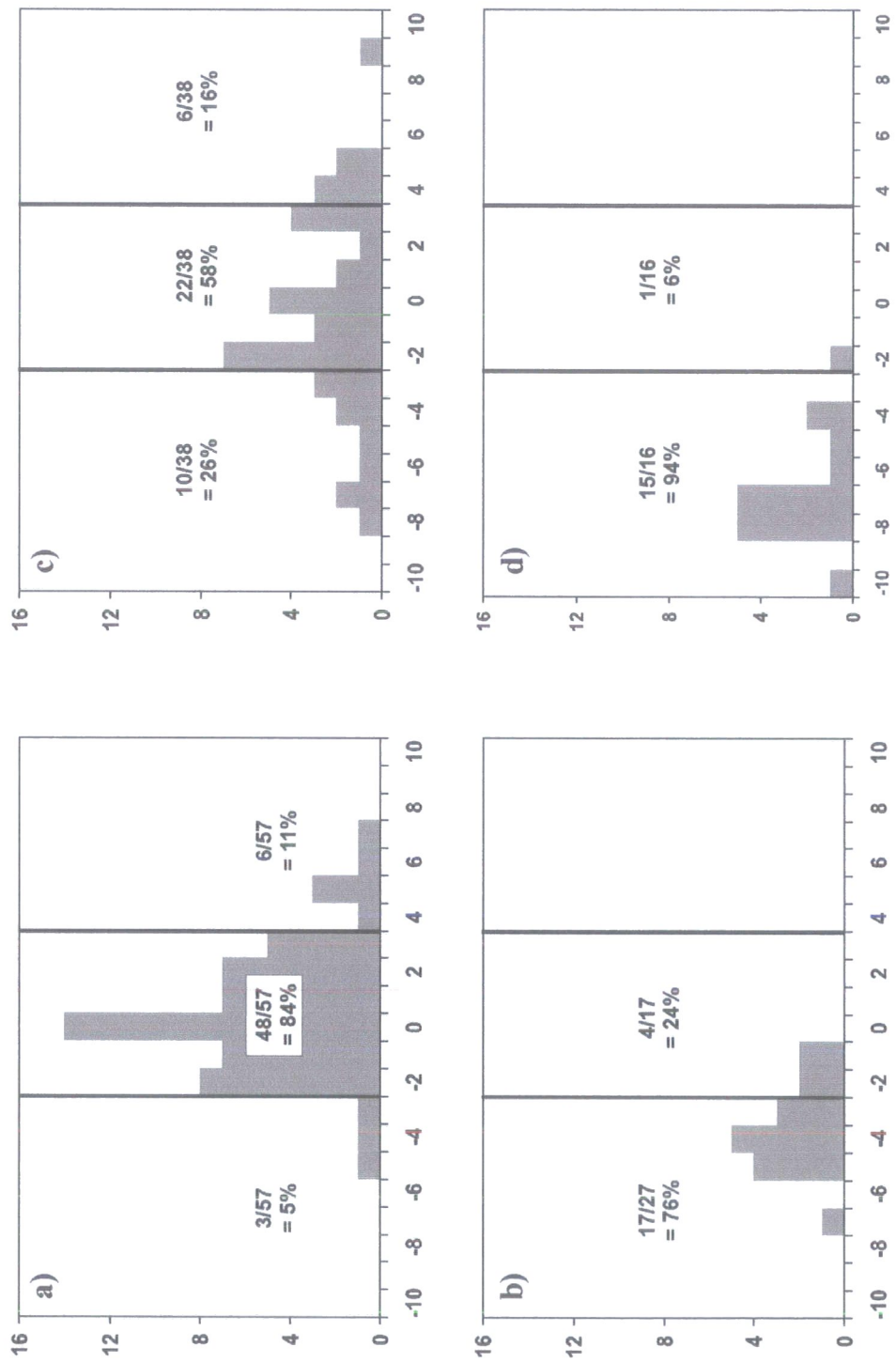
Figure 7.4 Distribution of $\Delta\varepsilon_{Hf}$ parameter across different sample sets in Hf-Nd isotope space: a) non-HIMU OIB; b) HIMU OIB; c) high *ln (Si/Al)* LDG hypabyssal kimberlites; d) SA Group I kimberlites (Nowell *et al.*, 1999; in press). Solid lines indicate shoulders of OIB distribtuion between $\Delta\varepsilon_{Hf}$ = +3 and -3.

Nevertheless, there is a clear negative $\Delta\varepsilon_{Hf\,i}$ character in the LDG kimberlites (63% have negative $\Delta\varepsilon_{Hf\,i}$ signatures), which must be a characteristic of the source, since it is unlikely to be derived from the SCLM (>80% of samples analysed so far have $\varepsilon_{Hf} > 0$), or the crust. A possible candidate for the source could thus be an OIB-like component, with a (possibly HIMU-like) negative $\Delta\varepsilon_{Hf\,i}$ character, which interacts variably with SCLM to produce kimberlite magmas that are located on and below the Hf-Nd mantle array.

7.3.2 Origins of the negative $\Delta\varepsilon_{Hf\,i}$ signature and kimberlite source regions

The analysis presented so far in chapters 6 and 7 indicates that it is unlikely that either the crust or the lithospheric mantle are a possible source of the negative $\Delta\varepsilon_{Hf\,i}$ signature observed in kimberlites from the Kaapvaal and Slave provinces. It seems most likely, therefore, that this signature must originate from some component located within the sub-lithospheric mantle. Nowell *et al.* (in press) propose two possible mechanisms for generating negative $\Delta\varepsilon_{Hf\,i}$ characteristics: fractionation of Mg-perovskite and recycling of subducted oceanic crust within the mantle.

A Mg-perovskite bearing lithology, envisaged to be either a melt residue (Blichert-Toft and Albarède, 1997) or a cumulate crystallised from a primordial magma ocean (Salters and White, 1998), will evolve to very unradiogenic $\varepsilon_{Hf\,i}$ but very radiogenic $\varepsilon_{Nd\,i}$ compositions over time (Nowell *et al.*, in press). Consequently, it is impossible for such a component to be the source of the negative $\Delta\varepsilon_{Hf\,i}$ signature observed in the LDG kimberlites, because the orientation of the LDG kimberlite Hf-Nd array requires that the negative $\Delta\varepsilon_{Hf\,i}$ component must have unradiogenic Hf and Nd. While this mechanism is more tenable as a source of negative $\Delta\varepsilon_{Hf\,i}$ in the southern African Group

257

I kimberlites, which do have radiogenic $\varepsilon_{Nd\,i}$, Nowell *et al.* (in press) do not consider it to be a likely explanation, on the grounds of Bulk Earth Lu-Hf isotope systematics not supporting Mg-perovskite fractionation in the early Earth (Blichert-Toft and Albarède, 1997).

The fractionation of Lu/Hf and Sm/Nd during generation of basaltic oceanic crust by melting of garnet-bearing peridotite, and subsequent isotopic evolution over long timescales (e.g. >1Gyr), results in negative $\Delta\varepsilon_{Hf}$ signatures in the melt product (i.e. MORB), as demonstrated by Chauvel *et al.* (1994), Salters and Zindler (1995), and Ballentine *et al.* (1997). Conversely, the solid residuum of this melting process evolves isotopically over time to have positive $\Delta\varepsilon_{Hf}$ characteristics, as demonstrated by lithospheric mantle (Nowell *et al.*, in press). On subduction, it is likely that Lu/Hf and Sm/Nd become fractionated, to some unknown extent. The model of Nowell *et al.* (in press) acknowledges this, but for simplicity assumes that Lu/Hf and Sm/Nd in MORB compositions retain their sub-chondritic or supra-chondritic character during the subduction process. Consequently, N-MORB, which at the present day has sub-chondritic Lu/Hf and supra-chondritic Sm/Nd, evolves to negative $\Delta\varepsilon_{Hf}$ with a radiogenic ε_{Nd} composition. E-MORB, which has present day sub-chondritic Lu/Hf and Sm/Nd, evolves to negative $\Delta\varepsilon_{Hf}$ with an unradiogenic ε_{Nd} composition. Incorporation of ancient, isotopically evolved N-MORB into the kimberlite source region can thus account for the Hf-Nd isotopic signatures observed in southern African kimberlites (Nowell *et al.*, in press), while incorporation of E-MORB into the source of the LDG kimberlites could explain their Hf-Nd isotope compositions.

A problem with this argument is that E-MORB is scarce relative to N-MORB in present-day settings. It is possible, though difficult to test, that E-MORB was more common in the early part of earth history, when oceanic basalts would have been generated from a less depleted mantle source. Consequently, a larger proportion of oceanic crust being subducted during the Precambrian could have been E-MORB rather than N-MORB, compared to the present day. Alternatively, E-MORB-like compositions could be recycled into the mantle by subduction of N-MORB with its accompanying cover of pelagic sediment.

Because the negative $\Delta\varepsilon_{Hf_i}$ signature is not generally observed in other mantle-derived magmas – with the exception of HIMU OIB (e.g. Chauvel et al., 1992; Ballentine et al., 1997) – it has been suggested (Nowell et al., 1999; in press) that the source of the signature, such as subducted oceanic crust, must remain isolated from the homogenising effects of mantle convection at some sub-lithospheric boundary layer. This material is then periodically entrained into upwellings within the mantle, such as plume-related activity, and rapidly transported to the base of the lithosphere, from where its chemical composition may begin to be modified by interaction with SCLM and crust. This mechanism is consistent with the connections between kimberlites and mantle plumes advocated by Le Roex (1986) and Heaman and Kjarsgaard (2000), and the association with hotspot volcanism is supported by the close agreement in Os isotope compositions between uncontaminated kimberlites and OIB compositions (e.g. Pearson et al., 1995; 2003), in samples from both the Kaapvaal and Slave provinces.

In summary, subduction of ancient N-MORB and E-MORB/N-MORB + sediment and subsequent storage for >1Ga time periods in isolation within the sub-lithospheric

mantle could produce a source region that, when periodically melted at low degrees, generates small-volume liquids with negative $\Delta\varepsilon_{Hf}$ and a range of ε_{Nd} signatures that overlap those observed in southern African Group I and LDG kimberlites. These melts are probably separated from the source and transported upwards through the mantle in a similar manner to OIB magmas, i.e. in association with plume/hotspot volcanism. Subsequent interaction of the ascending magma with SCLM peridotite and crustal lithologies can modify its elemental chemistry but has little effect on its isotopic composition unless the amount of contaminant being assimilated is very large. In these circumstances, incorporation of depleted SCLM can produce offsets towards more radiogenic $\varepsilon_{Hf\,i}$ at essentially constant ε_{Ndi} and ε_{Sri}, while assimilation of crust tends to produce offsets towards less radiogenic ε_{Hfi} and ε_{Ndi}, and more radiogenic ε_{Sri}.

7.3.3 Integration with existing petrogenetic models

The interpretation presented above is in agreement with aspects of several existing models of kimberlite petrogenesis. Many authors during the last two decades have favoured a sub-lithospheric origin for the primary kimberlite magma, including Le Roex (1986), Haggerty (1989), Nelson (1989), Ringwood *et al.* (1992), Taylor *et al.* (1994), Mahotkin *et al.* (2000), Price *et al.* (2000) and Janney *et al.* (2002). The majority of studies that propose a lithospheric origin for kimberlite magmas are those that are partly or wholly concerned with Group II rocks as encountered in South Africa (e.g. Fraser, 1987; Tainton, 1992; Mitchell, 1996). Some models, such as those of Le Roex (1986) and Haggerty (1989), suggest that all kimberlite magmas originate below the SCLM. On the basis of data acquired to date from peridotites, Hf isotopes indicate that a lithospheric origin is unlikely for any magma that consistently exhibits negative $\Delta\varepsilon_{Hfi}$ signatures.

The concept of ancient subducted basaltic oceanic crust at great depth within the mantle as a major contributor to the source of kimberlite magmas has several parallels with the transition zone melting geodynamic models of Ringwood *et al.* (1992) and Taylor *et al.* (1994), and also the conclusions of the experimental study on natural kimberlite of Edgar and Charbonneau (1993). The notion that a range of relative enrichment in these magmas (such as a possible continuum between Group I- and II-like magmas with a common source), may relate to differences in the exact nature of the subducted material being sampled, and/or to subsequent interaction with chemically and isotopically heterogeneous SCLM, agrees with many of the arguments proposed by Le Roex (1986) and Haggerty (1989), respectively. The conclusions of this multi-isotopic and elemental study of the Lac de Gras kimberlites are thus consistent with several of the central existing themes within research into kimberlite petrogenesis.

7.4 CONCLUSIONS

- The elemental geochemistry of LDG hypabyssal kimberlites has characteristics similar to both South African Group I and II rocks, and in some respects is transitional to both. Some, but not all, aspects of this transitional character (e.g. Pb content) are attributable to crustal contamination.

- Despite their apparent contamination-free nature on the basis of petrography, the LDG hypabyssal kimberlites have elemental signatures indicative of variable (in most cases 0-50%) assimilation of lithospheric mantle peridotite and crustal material. Fractionation of olivine ± Cr-spinel may also act to modify the kimberlite magma chemistry, producing similar compositional trends to crustal contamination.

261

o The location of the LDG hypabyssal kimberlites in *ln (Si/Al)-ln (Mg/Yb)* space relative to crustal and lithospheric contamination vectors suggests that an appropriate 'primary', uncontaminated magma to these samples would contain 30-32wt% MgO, ~30wt% SiO_2, 2.5-3.0wt% Al_2O_3 and 0.30-0.35ppm Yb.

o Contamination of the kimberlite magma with crustal or lithospheric mantle material has a minimal effect on its Hf-Nd isotope composition, until very high levels of incorporation are reached (>50-60% for crust, >80-90% for lithospheric peridotites). Sr isotope compositions are more sensitive to crustal input, but are highly insensitive to addition of peridotitic material.

o Although the highly linear nature of the Hf-Nd isotope array formed by minimally contaminated LDG hypabyssal kimberlites suggests that the magmas are generated by two-component mixing within the mantle, the only combination of mantle isotopic reservoirs and components that can plausibly explain the orientation of the array is depleted sub-continental lithospheric mantle and an isotopically enriched component with an OIB-like Nd-Sr isotope composition and a distinctive negative $\Delta\varepsilon_{Hf\,i}$ signature.

o In a scenario where a rising magma from below the lithosphere with negative $\Delta\varepsilon_{Hf\,i}$ interacts with depleted SCLM peridotites, the amount of peridotitic material that would have to be assimilated to generate the range of the Hf-Nd LDG kimberlite array is preclusively high (>>90%). A more likely scenario is that the majority of the observed Hf-Nd isotopic variation in the LDG kimberlites is a characteristic of a

single, heterogeneous mantle source. Only the most radiogenic Hf isotope compositions observed in kimberlites located well above the Hf-Nd mantle array are likely to record any additional interaction with large ($>>$50%) amounts of SCLM material.

- The difference in Nd isotope composition between South African Group I and LDG kimberlites can be explained by differences in the nature of the subducted oceanic crust that is sampled in the kimberlite magma. N-MORB compositions will evolve over time to radiogenic $\varepsilon_{Nd\,i}$ (as seen in SA Group I kimberlites), whereas E-MORB or N-MORB + sediment will evolve over time to unradiogenic $\varepsilon_{Nd\,i}$ (LDG kimberlites).

- Storage of the negative $\Delta\varepsilon_{Hf\,i}$ source at a deep boundary layer within the mantle could explain its absence from the majority of mantle-derived magmas. Periodic sampling of this component during deep-mantle upwellings, possibly in association with plume/hotspot activity, and subsequent transmission as an OIB-like magma through the sub-continental lithosphere and crust, produces a rock with the elemental and isotopic signatures observed in both South African Group I and LDG kimberlites.

Appendix A

Data catalogue

CONTENTS OF THE CATALOGUE

This appendix lists all the samples for which new major, trace and isotopic analyses have been acquired as part of this study. Most samples are Canadian kimberlites, but some additional analyses of South African and Siberian samples were undertaken. Table A.1 shows the breakdown of these analyses by country and region.

Country	Region	On/Off craton	Number of samples
Canada	Slave	On	98
	Churchill	On	5
	Superior	On	4
	Trans Hudson	Off	2
United States	Yapavai	Off	3
South Africa	Kaapvaal	On	7
Russia	Siberia	On	4
Total			**123**

Table A.1 Division of new analyses by country and region.

The information contained in this sample listing is as follows:

Country — within which the kimberlite is located.

Region — usually equivalent to the setting – cratonic or otherwise – setting of the body.

Field — the kimberlite field within which the body is situated.

On/Off craton — tectonic setting.

265

Locality — name of kimberlite body.

Sample ID — as assigned during this study, and as reported in Appendix D and F.

Alternative ID — other ID (e.g. company ID) by which sample may be known.

Age — quoted with 2σ error and source where a documented age refers *specifically* to the body in question. Where specific documented age is not available for Canadian kimberlites, age quoted (shown in *italics*) is the average of known ages on geographically proximal kimberlites (e.g. 53Ma for the central LDG cluster).

Non-specific ages for South African and Siberian kimberlites are allocated by close association with the following dated bodies: *(a)* Uintjesberg (Smith *et al.*, 1985b); *(b)* Monastery (Allsopp and Barrett, 1975); *(c)* median of emplacement age range for major Siberian diamondiferous kimberlites (Kinny *et al.*, 1997).

All ages listed are used throughout this study for calculation of initial isotope ratios, epsilon values, etc.

Age ref — reference for age, where documented age exists, including details of method where known (Table A.2).

Reference number	Reference	Method
1	Heaman *et al.* (2002)	Rb-Sr phl
2	Creaser *et al.* (2003)	Rb-Sr phl
3	Davis and Kjarsgaard (1997)	Rb-Sr phl
4	Scott Smith and McKinlay (2002)	Ar-Ar phl
5	Berg and Carlson (1998)	Rb-Sr phl
6	Graham *et al.* (1999)	Rb-Sr phl
7	Heaman *et al.* (2003)	U-Pb pvk, zrc
8	Agashev *et al.* (2001b)	Rb-Sr phl
9	Heaman and Kjarsgaard (2000)	U-Pb pvk
10	Smith *et al.* (1985b)	Rb-Sr phl
11	Allsopp and Barrett (1975)	Rb-Sr phl
12	Skinner *et al.* (1994)	U-Pb pvk
13	Smith *et al.* (1994)	U-Pb pvk

Table A.2 Kimberlite age references. Phl = phlogopite; pvk = perovskite; zrc = zircon.

Facies — HYP = hypabyssal facies; VOLC = volcaniclastic (diatreme or crater facies).

266

Country	Region	Field	On/Off craton	Locality	Sample ID	Alternative ID	Age (Ma)	Age ref	Facies
Canada	Slave	Contwoyto	On	Jericho	JD-51	-	*173.1 ± 1.3*	*1*	HYP
					JD-69-1	-	*173.1 ± 1.3*	*1*	HYP
					JD-69-3	-	*173.1 ± 1.3*	*1*	HYP
					JD-82-1	-	*173.1 ± 1.3*	*1*	HYP
					JD-82-3	-	*173.1 ± 1.3*	*1*	HYP
					RND-120-4S	-	*173.1 ± 1.3*	*1*	HYP
					RND-120-4SA	-	*173.1 ± 1.3*	*1*	HYP
				Muskox	RHL-11-1	KIA96-RHL-11-1	*173.1 ± 1.3*	*1*	HYP
		Lac de Gras	On	Aaron	AAR-1	DDH97-57 at 63.3	45.2 ± 1.3	2	HYP
					AAR-2	DDH97-57 at 91.1	45.2 ± 1.3	2	HYP
				Anaconda	ANA-1	DDH96-17 at 162.65	*53*		HYP
					ANA-2	DDH96-17 at 170.4	*53*		HYP
					ANA-3	DDH96-17 at 170.9	*53*		HYP
				Arnie	KPL-21	KIA92-KPL-21	47.5 ± 0.5	3	HYP
				Fox	FOX-1	KIA94-F-1	*53*		VOLC
				Grizzly	GRZ-1	DDH92-02 at 306.75	50.8 ± 4.8	2	HYP
					GRZ-2	DDH92-02 at 312.34	50.8 ± 4.8	2	HYP
					GRZ-3	DDH92-02 at 320.55	50.8 ± 4.8	2	HYP
					GRZ-4	DDH92-02 at 327.75	50.8 ± 4.8	2	HYP
					GRZ-5	92-02-X3	50.8 ± 4.8	2	HYP
					GRZ-6	92-02-X4	50.8 ± 4.8	2	HYP
					GRZ-7	92-02-X5	50.8 ± 4.8	2	HYP
					GRZ-8	92-02-X6	50.8 ± 4.8	2	HYP
					GRZ-9	92-02-X8	50.8 ± 4.8	2	HYP
					GRZ-10	92-02-X10	50.8 ± 4.8	2	HYP

Country	Region	Field	On/Off craton	Locality	Sample ID	Alternative ID	Age (Ma)	Age ref	Facies
Canada	Slave	Lac de Gras	On	Grizzly	GRZ-11	92-02-X12	50.8 ± 4.8	2	HYP
					GRZ-12	92-02-X16	50.8 ± 4.8	2	HYP
					GRZ-13	92-02-X21	50.8 ± 4.8	2	HYP
					GRZ-14	92-02-X26	50.8 ± 4.8	2	HYP
				Hardy Lake	HL-10-2	KIA96-HL-10-2	72 ± 2	4	HYP
					HL-10-3	KIA-96-HL-10-3	72 ± 2	4	HYP
					HL-11-1	KIA96-HL-11-1	71		HYP
					HL-11-2	KIA96-HL-11-2	71		HYP
					HL-12-1	KIA96-HL-12-1	71		HYP
					HL-12-3	KIA96-HL-12-3	71		HYP
				Koala West	KOW-1	KWDC-01 at 81.5	53		HYP
					KOW-2	KWDC-01 at 100.5	53		HYP
				Leslie	LES-1	LDC-09 at 15.0	53.9 ± 2.0	5	HYP
					LES-2	LDC-09 at 21.35	53.9 ± 2.0	5	HYP
					LES-3	LDC-09 at 26.45	53.9 ± 2.0	5	HYP
					LES-B1	KIA96-LES-B1	53.9 ± 2.0	5	HYP
				Mark	KIA93-K136	-	47.5		HYP
				Misery	MIS-1	MDC-1 at 43.59	53		HYP
					MIS-2	MDC-1 at 50.35	53		HYP
				Misery East	MSE-1	DDH93-13 at 14.9	53		HYP
					MSE-2	DDH93-13 at 25.75	53		HYP
				Nicholas Bay	NCB-1	KIA00-NB	53		HYP
				Pigeon	PDG-1	DDH97-54 at 311.82	53		HYP
					PDG-2	DDH97-54 at 312.12	53		HYP
				Porpoise	PRP-1	DDH94-11 at 81.1	53		HYP
					PRP-2	DDH94-11 at 87.7	53		HYP

Country	Region	Field	On/Off craton	Locality	Sample ID	Alternative ID	Age (Ma)	Age ref	Facies
Canada	Slave	Lac de Gras	On	Porpoise	PRP-3	DDH94-11 at 106.8	53		HYP
				Rat	RAT-1	DDH94-08 at 269.4B	53		VOLC
					RAT-2	DDH94-08 at 271.5	53		VOLC
					RAT-3	DDH94-08 at 257.75	53		HYP
					RAT-4	DDH-94-08 at 260.15	53		HYP
				Rattler	RTL-1	DDH96-13 at 233.25	59.7 ± 1.5	2	HYP
					RTL-2	DDH96-13 at 237.3	59.7 ± 1.5	2	HYP
					RTL-3	DDH96-13 at 238.6	59.7 ± 1.5	2	HYP
				Roger	ROG-1	DDH94-17 at 131.9	53		HYP
					ROG-2	DDH94-17 at 134.1	53		HYP
					ROG-3	DDH94-17 at 139.7	53		HYP
				Wolverine	WOL-1	-	53		VOLC
				A21	A21-1-1	-	55.7 ± 2.1	6	VOLC
					A21-1-2	-	55.7 ± 2.1	6	VOLC
				A25	A25-3-1	A25-3 at 90.0	71		VOLC
					A25-3-2	A25-3 at 117.2	71		VOLC
				A154	A154-11-1	-	54.8 ± 0.3,		VOLC
					A154-11-2	-	55.5 ± 0.5,	6	VOLC
					A154-11-3	-	56.0 ± 0.7		VOLC
				ABZ-7A	ABZ-7a-1	ABZ-7a at 160.0	53		VOLC
					ABZ-7a-2	ABZ-7a at 233.0	53		VOLC
				C13	C13-7-1	C13-7 at 60.5	73.7 ± 3.2	7	VOLC
					C13-7-2	C13-7 at 64.0	73.7 ± 3.2	7	VOLC
				DD39	DD39-5-1	DD39-5 at 44.2	53		HYP
					DD39-5-2	DD39-5 at 47.5	53		HYP
				Tli Kwi Cho (DO-27)	DO27-23-1	DO27-23 at 49.0	53		VOLC

Country	Region	Field	On/Off craton	Locality	Sample ID	Alternative ID	Age (Ma)	Age ref	Facies
Canada	Slave	Lac de Gras	On	Tli Kwi Cho (DO-27)	DO27-23-2	DO27-23 at 78.0	53		HYP
				T19	T19-1-1	T19-1 at 250.7	71		HYP
					T19-1-2	T19-1 at 272.0	71		HYP
				T21	T21-1-1	T21-1 at 105.8	71		HYP
					T21-1-2	T21-1 at 114.9	71		HYP
				T34	T34-1-1	T34-1 at 25.0	71		HYP
					T34-1-2	T34-1 at 28.5	71		HYP
				T35	T35-1-1	T35-1 at 81.5	71		HYP
					T35-1-2	T35-1 at 83.7	71		HYP
				T36	T36-1-1	T36-1 at 20.1	71		HYP
					T36-2-1	T36-2 at 21.0	71		HYP
				T146	T146-1-1	T146-1 at 26.1	71		HYP
					T146-1-2	T146-1 at 82.0	71		HYP
				T237	T237-1-1	T237-1 at 61.3	71		HYP
					T237-1-2	T237-1 at 89.3	71		HYP
				TR107	TR107-3-1	TR107-3 at 68.4	520		HYP
					TR107-3-2	TR107-3 at 75.0	520		HYP
		South-West Slave	On	Drybones	DRY-1	-	441.4 ± 0.8	7	VOLC
		South-East Slave	On	Gahcho Kue	KDY-1	96BAK 020 KIM5	540		VOLC
					KDY-2	BAK 003 Au 4	540		HYP
				Snap Lake	SNP-1	-	535 ± 11	8	HYP
	Churchill	Somerset Island	On	JP South	JPS-1	KIA99-JPS-1	97.5		HYP
				Batty Bay	BAT-1	-	97.5		HYP

Country	Region	Field	On/Off craton	Locality	Sample ID	Alternative ID	Age (Ma)	Age ref	Facies
Canada	Churchill	Somerset Island	On	Elwin Bay	ELB-1	-	*97.5*		HYP
			On	Jos	JOS-1	-	*97.5*		HYP
		Rankin Inlet	On	Rankin Inlet	RNK-1	-	196.2 ± 2.8	9	HYP
	Superior	Attawapiskat	On	James Bay Lowlands	JBL-1	-	*175*		HYP
		Kirkland Lake	On	Upper Canada Mine	UCM-1	-	155.3 ± 1.3	9	HYP
		Timiskaming	On	Guigues	GUI-1	-	142.3 ± 6.6	9	HYP
				Peddie	PED-1	-	153.6 ± 2.4	9	HYP
	Trans Hudson	Fort a la Corne	Off	Fort a la Corne	FLC-1	-	*100*		VOLC
			Off	Sturgeon Lake	STL-1	-	*98*		VOLC
United States	Yapavai	State Line	Off	Chicken Park	CHK-1	-	614.5 ± 2.1	7	HYP
				Nix	NIX-1	-			HYP
				Sloan	SLN-1	-	*400*		VOLC
South Africa	Kaapvaal	Barkly West	On	Frank Smith	FSM-2	-	113.6 ± 1.8	10	HYP
				Roberts Victor	ROVIC-1	-	127 ± 3	11	HYP
		Central Cape	Off	Gansfontein	GNS-1	-	*100 (a)*		HYP
				Melton Wold	MW-3	-	145 ± 13	12, 13	HYP

Country	Region	Field	On/Off craton	Locality	Sample ID	Alternative ID	Age (Ma)	Age ref	Facies
South Africa	Kaapvaal	North Lesotho	On	Liqhobong	LQ-7	-	90 (b)		HYP
					LQ-SAT	-	90 (b)		HYP
				Pipe 200	P200	-	90 (b)		HYP
Russia	Siberia	Malo-Botuobinsk	On	Mir	MIR-M3	-	360 (c)		HYP
				Internationalaya	INT-I2	-	360 (c)		HYP
		Daldyn-Alakit	On	Jubilee	JUB-1	-	360 (c)		HYP
				Udachnaya	UDC-1	-	360 (c)		HYP

272

Appendix B

Kimberlite petrography

Table B.1 provides a summary of the mineralogical characteristics of selected kimberlites from the Lac de Gras field, based on the work of Armstrong *et al.* (in press) and B. A. Kjarsgaard (unpublished).

The general nature of each kimberlite is described in terms of **descriptive phases**, following the system introduced by Skinner and Clement (1979), whereby kimberlites are classified according to their modally dominant minerals. Note that olivine content is not taken into account by this classification.

Legend for Table B.1 is as follows:

✗ = phase present in minor quantities

✗ = phase common throughout

✖ = phase present in abundance

Mineral name abbreviations: ol = olivine; phl = phlogopite; ksh = kinoshitalite; spl = spinel; mont = monticellite; pvk = perovskite; ap = apatite

Other abbreviations: carb = carbonate; silc = silicate; phenos = phenocrysts; gmass = groundmass

Lac de Gras samples (unpublished petrography by B. A. Kjarsgaard):

Body	Sample ID	Descriptive phases	Macrocrysts		Phenocrysts, microphenocrysts, groundmass (Mineralogy)										
			Olivine	Phlogopite	Olivine phenocrysts	Phlogopite-kinoshitalite	Spinel (A = atoll texture)	Monticellite (F = fresh)	Perovskite	Apatite	Serpentine	Carbonate microphenocrysts	Carbonate-only pockets	Carbonate + silicate pockets	Carbonate groundmass
Anaconda	DDH96-17 at 170.9	Carbonate spinel	X		X	X	X_A	X	X	X	X		X		X
Grizzly	DDH92-02 at 306.75	Serpentine spinel carbonate	X	X	X	X	X	X_F	X	X	X	X	X	X	X
Koala West	KWDC-01 at 100.5	Phlogopite spinel	X		X	X	X_A	X_F	X	X	X		X	X	X
Leslie	LDC-09 at 28.9	Spinel monticellite	X	X	X	X	X	X_F	X	X	X	X	X	X	X
Misery East	DDH93-13 at 17	Phlogopite calcite spinel	X		X	X	X	X_F	X	X	X	X	X	X	X
Porpoise	DDH94-11 at 87.7	Carbonate serpentine	X		X	X	X_A	X_F	X	X	X		X		X

(continued)

Body	Sample ID	Descriptive phases	Mineralogy												
			Macrocrysts		Phenocrysts, microphenocrysts, groundmass										
			Ol	Phl	Ol phenos	Phl-ksh	Spl ($A = atoll$)	Mont ($F = fresh$)	Pvk	Ap	Serp	Carb microphenos	Carb-only pockets	Carb + silc pockets	Carb gmass
Rat	DDH94-08 at 257.75	Monticellite carbonate	X		X	X	X$_A$	X		X	X		X		X
Rattler	DDH96-13 at 233.25	Spinel carbonate	X		X	X	X$_A$	X	X	X	X		X		X

Lac de Gras samples (petrography after Masun, 1999)

DD39

o Minimally altered macrocrystal olivine; minor serpentinisation along cracks and fractures.
o Microphenocrytal olivine is variably altered to serpophite.
o Groundmass contains abundant spinel, apatite and magnetite; perovskite and phlogopite common.
o Calcite-serpentine segregations common throughout groundmass.
o Mesostasis calcite, serpentine and barian phlogopite.
o Microxenoliths of lherzolite and lithic fragments are present but very rare.

T-19

o Olivine macrocrysts completely replaced by calcite, mantled by serpentine.
o Most olivine occurs as microphenocrysts, also replaced by calcite and serpentine.
o Spinel, apatite and magnetite common in groundmass of calcite, serpentine and phlogopite; perovskite rare.
o Calcite segregations common in groundmass.

T-34

o Rare olivine macrocrysts, altered to serpentine only at margins.
o Most olivine occurs as variable alteration to serpentine, serpophite; calcite confined to cracks.
o Groundmass consists of abundant spinel, magnetite; apatite, phlogopite, serpentine, calcite, dolomite; perovskite is common.
o Calcite segregations are common within groundmass.

T-35

• Rare calcite and serpophite pseudomorphs after macrocrystal olivine.
o Majority of olivine occured as microphenocrysts, now completely altered to calcite.
o Spinel, magnetite, perovskite and apatite common throughout groundmass.
o Calcite segregations common throughout groundmass.
o Mesostasis of calcite, serpentine and phlogopite.

T-36

o Generally fresh, fractured olivine macrocrysts; partially altered along cracks and margins to serpophite.
o Chloritised serpophite pseudomorphs after microphenocrystal olivine.
o Spinel and apatite common in groundmass.

276

o Mesostasis of calcite, serpentine and phlogopite with scattered discrete apatite crystals.

o Altered, partially resorbed xenoliths of country rock are present but rare.

T-237

o General lack of macrocrystal olivine; may appear locally aphanitic.

o Abundant, mostly fresh microphenocrystal olivine; flow alignment of olivine crystals commonly observed.

o Spinel, magnetite and apatite common within groundmass.

o Calcite-serpentine segregations are common throughout groundmass.

o Mesostasis of calcite, serpentine, fresh-altered monticellite, and partially altered barian phlogopite.

Lac de Gras samples (unpublished petrography by B. H. Scott Smith)

Anne

• Very fresh macrocrystal olivine.

• Spinel and monticellite most common groundmass phases.

• Groundmass carbonate rare to absent.

• Xenolith-poor.

Finlay

• Very fresh macrocrystal olivine.

• Monticellite predominant in groundmass.

• Carbonate segregations common in samples from this kimberlite.

• Variable amounts of xenoliths present.

Don

• Rare macrocrysts; olivine is generally fresh, only minor serpentinisation.

• Groundmass consists of spinel, perovskite, monticellite, carbonate.

• Some small, partially-resorbed xenoliths of country rock.

Appendix C

Sample preparation procedures

C.1   PREPARATION OF WHOLE-ROCK POWDERS

C.1.1   Powders produced at Durham University

All kimberlites obtained for this study were received as powders from Dr B. A. Kjarsgaard (Geological Survey of Canada) and Dr M. G. Kopylova (University of British Columbia), with the exception of the samples listed in Table C.1, which were received as hand specimens and powdered at Durham University.

Country	Region	Field	Locality	Sample
Canada	Slave	Lac de Gras	Anaconda	ANA-3
			Fox	FOX-1
			Grizzly	GRZ-2
			Rat	RAT-2
			Wolverine	WOL-1
		South-West Slave	Drybones	DRY-1
		South-East Slave	Kennady Lake	KDY-1
				KDY-2
			Snap Lake	SNP-2
	Churchill	Somerset Island	JP South	JPS-1
			Batty Bay	BAT-1
			Elwin Bay	ELB-1
			Jos	JOS-1
		Rankin Inlet	Rankin Inlet	RNK-1
	Superior	Attawapiskat	James Bay Lowlands	JBL-1
		Kirkland Lake	Upper Canada Mine	UCM-1
		Timiskaming	Guigues	GUI-1
(continued)			Peddie	PED-1

Country	Region	Field	Locality	Sample
Canada	Trans Hudson	Fort a la Corne	Fort a la Corne	FLC-1
			Sturgeon Lake	STL-1
United States	Yapavai	State Line	Chicken Park	CHK-1
			Nix	NIX-1
			Sloan	SLN-1
South Africa	Kaapvaal	Barkly West	Frank Smith	FSM-1
			Robert Victor	ROVIC-1
		Central Cape	Gansfontein	GNS-1
			Melton Wold	MW-3
		North Lesotho	Liqhobong	LQ-7
				LQ-SAT
			Pipe 200	P200

Table C.1 Samples powdered using Durham University procedures.

C.1.2 Powdering procedure

Wherever specimen size permitted, external surfaces were removed using a Clipper rock saw. Saw marks were removed from the sawn faces using a diamond lap, and the specimens were thoroughly cleaned with de-ionised water. The specimen was then crushed to a maximum chip size of ~10mm using a Fritsch stainless steel jaw crusher. The crusher was cleaned thoroughly after processing each specimen. Rock chips were washed several times with de-ionised water to float off the majority of the adherent rock dust and then dried in an oven.

Each sample crush was picked through by hand to remove any visible xenolithic or xenocrystic material (e.g. fragments of crustal material or megacrysts). In reality it is impossible to remove all contamination in this way, as some foreign material will be too fine-grained to distinguish from the kimberlite groundmass. Fresh macrocrysts of

olivine and phlogopite were for these purposes treated as part of the kimberlite magma itself, although many olivine macrocrysts are in fact likely to be derived from peridotite xenoliths (Mitchell, 1986).

An ideal powder for chemical analysis should be sufficiently fine that it can be considered to be homogeneous. This ensures that any aliquot taken from this powder should be, within analytical error, chemically the same as any other; thus no bias is introduced by sampling of the powder. Kleeman (1967) recommends comminution of powders to less than 120 mesh to ensure homogeneity is attained. Grinding to this kind of flour-like consistency can take 20-30 minutes, depending on the hardness of the minerals in the sample, although Fitton and Gill (1970) showed that considerable oxidation of Fe^{2+} to Fe^{3+} can take place if samples are mechanically ground for longer than about 1 minute. Clearly, this is not sufficient time to adequately powder the material, so the FeO and Fe_2O_3 analyses of the samples should be viewed with the effects of oxidation during grinding in mind. Specific consideration of relative FeO and Fe_2O_3 content of kimberlites does not form a part of this study.

A Fritsch rotary agate ball mill was used to grind the rock chips to a powder. Each agate mill was cleaned thoroughly between each sample by washing with de-ionised water, running the mill with clean, high-purity silica sand, and then re-rinsing in de-ionised water. Excess moisture was removed from the ground powders by drying in an oven at 110°C for 24 to 48 hours. The powder is then ready for chemical pre-treatment prior to analysis.

C.2 MAJOR ELEMENT PROCEDURES

All major element analyses were obtained courtesy of the Geological Survey of Canada (GSC), through Dr B. A. Kjarsgaard. Analyses were performed at the GSC (Ottawa), and also by Lakefield Research Ltd (Lakefield, Ontario) and Acme Analytical Laboratories Ltd (Vancouver, British Columbia). All major element data was obtained by X-ray fluorescence (XRF) techniques on fused discs of sample material. Ni and Cr concentration data obtained by XRF was also used in preference to ICP-MS data. H_2O, CO_2 and S were determined by infrared spectroscopy on combusted samples, using a LECO C-O-N-S analyser. Where only loss on ignition is recorded, this was measured by gravimetric analysis at 900°C.

C.3 TRACE ELEMENT PROCEDURES

C.3.1 Introduction

All trace element data for this study, with the exception of Ni and Cr, were obtained using the Perkin-Elmer Sciex Elan 6000 quadrupole inductively coupled plasma mass spectrometer (ICP-MS) at Durham University. A detailed description of pre-concentration chemistry, instrument operating conditions and data reduction considerations for this technique is contained in Ottley *et al.* (2003). A summary is provided below.

C.3.2 Sample digestion, spiking and dilution

Samples are usually processed in batches of 20-30, including 3-4 blanks in each batch. All acids used are SpA grade or equivalent. $0.1 \pm 0.001g$ of each sample powder are weighed into a 15mL or 22mL Savillex PFA beaker. 1mL of 16N HNO_3 is carefully added to each beaker, allowing any reaction with carbonate which may evolve CO_2 to

281

go to completion. The beaker is gently agitated by hand to produce a slurry, ensuring the powder is fully wetted. 4mL of 29N is added to each beaker. The beakers are sealed and placed on a hotplate and allowed to reflux at ~150°C for 48 hours. After this initial digestion step, the samples are dried down to a moist residue in a clean-air environment. It is important to ensure that the samples do not dry out completely, at which point they will start to oxidise. A further 1mL of 16N HNO_3 is then added to each beaker and allowed to dry down on the hotplate. This procedure is repeated a second time, to ensure that all HF has been driven off. 2.5mL of 16N HNO_3 is then added to each beaker, diluted to approximately 10mL with 18.2MΩ de-ionised water. The beakers are sealed and returned to the hotplate for a few hours at 100-120°C.

Once cool, each beaker is spiked with 1mL of a 1ppm Re-1ppm Rh solution. The sample is then diluted to 50mL in 18.2MΩ MQ, using a volumetric flask. 1mL of this sample solution is then further diluted into a polypropylene test-tube at a 1:10 ratio, to produce a convenient 11mL volume for analysis.

C.3.3 Instrumental parameters

The sample solution is introduced into the plasma using a cross-flow nebuliser assembly and a Scott double-pass spray chamber. Nebuliser argon flow rate is typically set at 0.8-0.9L per minute to optimise signal intensity. A daily check solution is run before each analysis session to ensure that instrument sensitivity and molecular interferences are at acceptable levels. During each analysis session the response of the instrument is calibrated using a set of solutions prepared from international rock standards.

The typical solution uptake rate is ~1mL per minute, with analysis for a full suite of trace elements requiring ~3 minutes for completion. Data is acquired by peak hopping, with a dwell time of approximately 10-60ms, depending on individual elemental detection limits (Ottley *et al.*, 2003). The mass spectrum is swept 25 times for each reading, and two replicate readings are obtained for each analysis. Each sample is allowed to wash in for 50 seconds prior to the analysis commencing, and the instrument is allowed to aspirate a 3% HNO_3 wash solution for 3 minutes between samples.

C.3.4 Checks on data quality

The quality of the trace element analyses produced using this procedure is monitored in a number of ways:

1. Analysis of total procedural blanks provides a check on levels of contamination introduced into the sample during the chemical procedure.

2. Inclusion of the Re-Rh internal standard allows sample loss during dilution and variability in instrument sensitivity during analysis to be corrected for.

3. Use of international rock standards during the analysis session permits accurate calibration of the machine response during each individual session.

4. Multiple analyses of blanks and standards during a session (e.g. at start, mid-way, and end of run) allow any drift in the instrument calibration to be detected. Reproducibility of elemental concentrations in standards run in this manner is almost always better than 5% (relative standard deviation), and often <3% (Ottley, 2003).

C.4 FUSION PROCEDURE FOR SAMPLE DIGESTION

C.4.1 Introduction

Certain mineral phases, such as zircon, are resistant to digestion by conventional acid-attack procedures, such as those described in Chapter 2. Because zircon is a major host for Hf, failure to properly dissolve this phase could result in inaccurate determinations of Hf isotope compositions. This factor becomes more significant when dealing with samples containing large amounts of zircon, such as sandstones or granites. Consequently, the LDG crustal rock powders analysed during this project were fused prior to dissolution, to break down the refractory phases. Two sets of isotopic determinations were then made on the crustal rocks: one based on dissolutions of the fused powders, and one based on a conventional acid-attack dissolution without prior fusion. This enabled comparison to be made between results obtained by either technique, and ensured that good data could be acquired for Sr, which can become contaminated by the flux used in the fusion procedure.

C.4.2 Fusion procedure

0.45g of sample powder and 2.25g of lithium tetraborate flux (± 0.001g) are weighed out, giving a sample:flux ratio of 1:5. The combined powder is mixed thoroughly in an agate ball mill, and then transferred to a platinum crucible. Samples are fused in an oven at 1050°C for 20 minutes. Immediately after removal from the oven, the molten sample is poured into cylindrical graphite moulds that are kept on a hotplate to reduce the temperature gradient. After pouring the molten sample is then compressed within the mould using an aluminium piston. Samples are left to cool slowly on the hotplate. On removal from the mould, the sample is in the form of a glass disc, which can be

ground to a powder using an agate pestle and mortar. This powder dissolves easily

using the procedure described in Chapter 2.

Appendix D

Whole rock major and trace element data

CONTENTS OF THE MAJOR/TRACE ELEMENT DATABASE

The following pages contain details of all major and trace element analyses of whole rock kimberlites and Lac de Gras crustal material obtained during the course of this study. Sources of data are as follows:

- All major element data was obtained by XRF analysis courtesy of Dr B. A. Kjarsgaard and the Geological Survey of Canada, with the exception of data for Jericho kimberlites (JD-51, JD-69-1, JD-69-3, JD-82-1 and JD-82-3), which is taken from Price *et al.* (2000).

- All kimberlite trace element data was obtained by ICP-MS at Durham University (see Appendix C for details of procedures and instrumentation), with the exception of Cr and Ni analyses marked with asterisks (* = XRF data, ** = ICP-OES data), which are taken from data of Dr B. A. Kjarsgaard. Comparisons between XRF and ICP-MS determinations for Ni and Cr are shown in Figure D.1, for samples with both datasets are available. For both Ni and Cr the XRF and ICP-MS data correlate strongly, although ICP-MS consistently measures a higher abundance of the element of interest.

- All trace elements for Lac de Gras crustal rocks are taken from the data of Dr B. A. Kjarsgaard. All of this data was obtained by ICP-MS with the exception of U, Yb, Lu and Y (INAA), and Sc, Cr, Ni, Cu, Zn (ICP-OES).
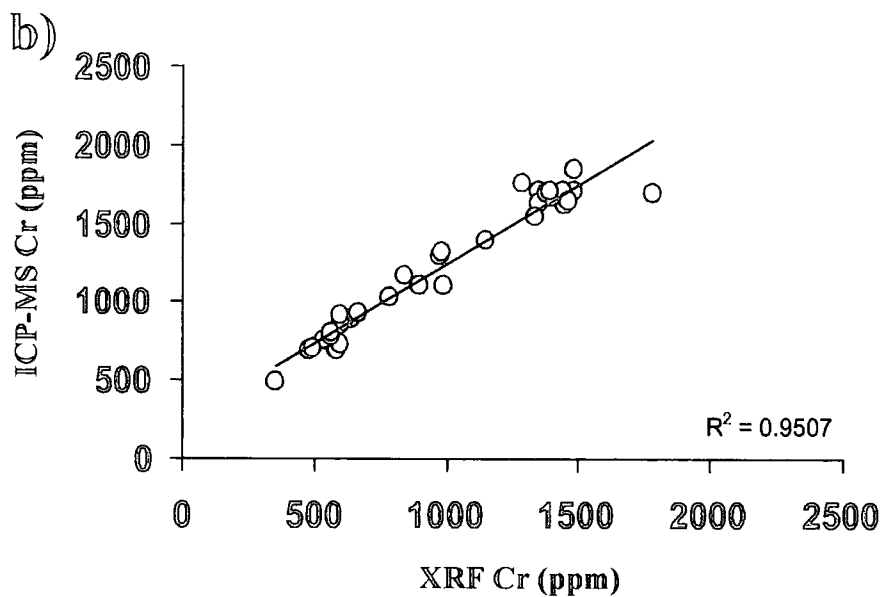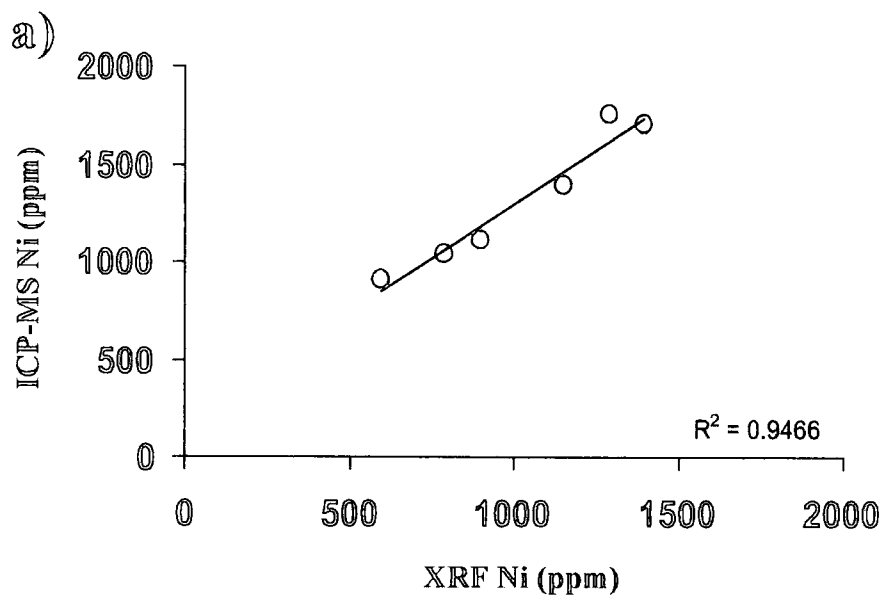
Figure D.1 Comparison between trace element determinations by XRF and ICP-MS methods on Canadian kimberlites: a) Ni; b) Cr. XRF data acquired by Geological Survey of Canada, courtesy of Dr B. A. Kjarsgaard; ICP-MS acquired using Perkin-Elmer ELAN 6000 at Durham University, for this study.

FIELD	CANADA, Slave Province							
LOCALITY	Contwoyto	Contwoyto	Contwoyto	Contwoyto	Contwoyto	Contwoyto	Contwoyto	Contwoyto
SAMPLE	Jericho	Jericho	Jericho	Jericho	Jericho	Jericho	Jericho	Muskox
(%)	JD-51	JD-69-1	JD-69-3	JD-82-1	JD-82-3	RND-120-4S	RND-120-4SA	RHL-11-2
SiO_2	20.77	24.15	29.06	28.83	30.31	34.56	33.49	29.80
TiO_2	0.89	0.51	0.49	0.57	0.77	2.96	4.31	1.85
Al_2O_3	1.82	1.14	1.38	1.39	1.75	3.19	4.69	2.99
FeO	0.57	3.58	3.79	1.51	4.64	5.67		4.70
Fe_2O_3	6.47	2.23	2.13	5.27	2.95	5.55		4.08
Total Fe as Fe_2O_3	7.04	5.81	5.92	6.78	7.59	11.22	16.84	9.30
MnO	0.19	0.16	0.14	0.16	0.15	0.32	0.46	0.17
MgO	16.65	19.71	23.69	23.25	25.14	37.06	24.06	30.70
CaO	25.45	22.25	16.69	16.86	13.32	2.03	2.88	8.69
Na_2O	0.10	0.14	0.13	0.12	0.24	0.24	0.15	0.24
K_2O	0.17	0.33	0.45	0.43	0.42	0.51	0.69	0.59
P_2O_5	0.85	0.67	0.56	0.71	0.75	0.59	0.62	0.42
H_2O+	5.30	6.40	6.40	6.00	7.50	5.80		6.90
CO_2	18.82	16.91	12.97	12.39	9.80	0.65		7.25
S								0.07
LOI	25.45			20.40	18.54		9.89	13.90
TOTAL	99.38	98.18	97.88	99.50	98.98	99.13	98.08	98.65
CCI	1.34	1.25	1.24	1.26	1.24	1.00	1.51	1.04

FIELD	Lac de Gras	Lac de Gras	Lac de Gras	Lac de Gras	Lac de Gras	Lac de Gras	Lac de Gras	Lac de Gras
LOCALITY	Aaron	Aaron	Anaconda	Anaconda	Anaconda	Arnie	Fox	Grizzly
SAMPLE	AAR-1	AAR-2	ANA-1	ANA-2	ANA-3	KPL-21	FOX-1	GRZ-1
(%)								
SiO_2	34.70	40.40	26.90	24.60	29.20	32.88	42.93	32.10
TiO_2	0.36	0.20	1.23	1.09	0.88	0.40	0.34	0.48
Al_2O_3	1.80	3.10	1.70	1.80	1.70	2.25	7.57	2.30
FeO								
Fe_2O_3								
Total Fe as Fe_2O_3	8.50	5.60	8.70	7.60	7.60	8.63	6.48	8.10
MnO	0.16	0.08	0.17	0.16	0.17	0.14	0.07	0.16
MgO	39.75	32.08	29.55	27.24	32.24	37.22	22.04	34.88
CaO	6.10	2.30	13.29	15.83	11.66	6.76	4.44	8.60
Na_2O	0.00	0.00	0.00	0.00	0.00	0.07	1.03	0.00
K_2O	0.40	1.37	0.21	0.20	0.48	0.05	1.32	1.56
P_2O_5	0.33	0.21	0.61	0.61	0.47	0.67	0.20	0.58
H_2O+	5.20	12.80	5.00	4.70	3.80			6.20
CO_2	3.60	1.20	12.30	15.20	10.80			5.30
S								
LOI			15.20	17.10	12.40	9.82	13.18	
TOTAL	100.90	99.34	97.56	96.23	96.80	98.89	99.60	100.26
CCI	0.90	1.25	0.95	0.96	0.93	0.94	2.09	0.91

FIELD	Lac de Gras	Lac de Gras	Lac de Gras	Lac de Gras	Lac de Gras	Lac de Gras	Lac de Gras	Lac de Gras
LOCALITY	Grizzly	Grizzly	Grizzly	Grizzly	Grizzly	Grizzly	Grizzly	Grizzly
SAMPLE	GRZ-2	GRZ-3	GRZ-4	GRZ-5	GRZ-6	GRZ-7	GRZ-8	GRZ-9
(%)								
SiO_2	32.00	33.00	33.30	34.30	33.80	33.80	33.30	33.50
TiO_2	0.54	0.50	0.55	0.44	0.43	0.43	0.39	0.42
Al_2O_3	2.10	2.00	2.50	1.96	1.86	2.15	1.82	1.93
FeO								
Fe_2O_3								
Total Fe as Fe_2O_3	8.50	8.60	8.60	8.67	8.32	8.44	8.28	8.33
MnO	0.17	0.17	0.17	0.17	0.15	0.17	0.16	0.16
MgO	36.75	37.47	36.81	39.30	38.30	38.20	38.70	38.70
CaO	9.72	9.10	8.42	7.47	7.99	7.21	7.30	7.06
Na_2O	0.00	0.10	0.00	0.14	0.08	0.16	0.19	0.21
K_2O	0.62	0.81	1.13	0.54	0.85	1.08	0.42	0.46
P_2O_5	0.68	0.49	0.54	0.48	0.43	0.42	0.43	0.41
H_2O+	4.90	4.40	4.70					
CO_2	4.80	4.10	4.00					
S				0.04	0.02			0.02
LOI				6.54	7.82	6.92	7.77	7.74
TOTAL	100.78	100.74	100.72	100.01	100.03	98.98	98.76	98.92
CCI	0.90	0.90	0.92	0.90	0.89	0.89	0.89	0.90

FIELD	Lac de Gras	Lac de Gras	Lac de Gras	Lac de Gras	Lac de Gras	Lac de Gras	Lac de Gras	Lac de Gras
LOCALITY	Grizzly	Grizzly	Grizzly	Grizzly	Grizzly	Anne	Anne	Finlay
SAMPLE	GRZ-10	GRZ-11	GRZ-12	GRZ-13	GRZ-14	HL-10-2	HL-10-3	HL-11-1
(%)								
SiO_2	33.10	33.30	33.70	34.10	33.80	31.20	31.10	31.10
TiO_2	0.41	0.42	0.42	0.42	0.42	0.64	0.66	1.43
Al_2O_3	1.96	1.95	2.31	2.07	1.97	2.14	2.16	3.56
FeO						3.70	3.70	6.80
Fe_2O_3						5.10	5.20	3.60
Total Fe as Fe_2O_3	8.35	8.39	7.95	8.47	8.44	9.21	9.31	10.80
MnO	0.16	0.16	0.15	0.15	0.17	0.17	0.18	0.27
MgO	38.30	38.90	36.10	39.30	38.70	33.00	33.20	27.40
CaO	7.25	7.06	8.16	7.03	6.85	7.31	6.66	6.85
Na_2O	0.18	0.13	0.27	0.14	0.12	0.11	0.10	0.14
K_2O	0.64	0.83	1.12	0.78	0.97	0.44	0.45	0.50
P_2O_5	0.45	0.45	0.56	0.42	0.42	0.50	0.51	0.60
H_2O+						8.40	8.20	8.40
CO_2						5.81	5.38	4.44
S				0.02		0.01	0.01	0.05
LOI	8.07	7.04	7.08	6.33	6.90	14.80	14.70	16.80
TOTAL	98.87	98.63	97.82	99.21	98.76	99.52	99.03	99.45
CCI	0.89	0.87	0.95	0.89	0.88	0.99	0.98	1.23

FIELD	Lac de Gras	Lac de Gras	Lac de Gras	Lac de Gras	Lac de Gras	Lac de Gras	Lac de Gras	Lac de Gras
LOCALITY	Finlay	Don	Don	Koala West	Koala West	Leslie	Leslie	Leslie
SAMPLE	HL-11-2	HL-12-1	HL-12-3	KOW-1	KOW-2	LES-B1	LES-1	LES-2
(%)								
SiO_2	31.00	37.80	36.20	29.10	26.70	32.00	31.40	30.30
TiO_2	1.39	0.38	0.36	1.27	1.64	0.54	0.58	0.62
Al_2O_3	3.49	2.25	2.09	3.20	3.50	1.43	1.60	1.60
FeO	4.00	4.30	4.40			4.40		
Fe_2O_3	6.55	3.71	3.27			3.88		
Total Fe as Fe_2O_3	11.00	8.49	8.16	10.30	12.20	8.77	8.20	8.60
MnO	0.26	0.15	0.15	0.22	0.25	0.16	0.16	0.17
MgO	28.20	37.30	35.60	26.59	30.45	38.00	37.20	36.83
CaO	6.07	1.70	4.21	11.12	9.11	6.10	9.14	9.40
Na_2O	0.19	0.09	0.09	0.00	0.00	0.09	0.10	0.10
K_2O	0.56	1.31	1.33	1.26	1.41	0.23	0.64	0.56
P_2O_5	0.74	0.41	0.41	1.03	0.96	0.41	0.42	0.45
H_2O+	8.00	6.50	5.80	7.60	7.80	6.10	5.90	7.80
CO_2	3.72	1.11	3.35	7.30	5.60	4.73	5.00	4.10
S	0.05	0.02	0.02			0.04		
LOI	16.60	9.30	10.10			11.00		
TOTAL	99.50	99.18	98.70	98.99	99.62	98.73	100.34	100.53
CCI	1.18	1.01	1.00	1.11	0.91	0.87	0.86	0.84

FIELD	Lac de Gras	Lac de Gras	Lac de Gras	Lac de Gras	Lac de Gras	Lac de Gras	Lac de Gras	Lac de Gras
LOCALITY	Leslie	Mark	Misery	Misery	Misery East	Misery East	Nicholas Bay	Pigeon
SAMPLE	LES-3	KIA93-K136	MIS-1	MIS-2	MSE-1	MSE-2	NCB-1	PDG-1
(%)								
SiO_2	30.10	35.40	37.30	33.00	36.00	31.60	34.56	36.60
TiO_2	0.61	0.37	0.36	0.32	0.40	0.36	0.43	0.41
Al_2O_3	1.40	1.37	2.70	1.80	2.40	2.70	3.91	3.80
FeO								
Fe_2O_3								
Total Fe as Fe_2O_3	8.60	8.84	8.50	9.50	8.20	7.00	8.65	7.50
MnO	0.17	0.16	0.17	0.25	0.15	0.13	0.15	0.13
MgO	38.41	44.16	34.20	24.59	33.67	29.32	28.71	29.25
CaO	9.16	8.81	3.48	12.58	5.48	10.57	7.61	5.70
Na_2O	0.10	0.00	0.00	0.00	0.00	0.10	0.12	0.00
K_2O	0.33	0.12	0.86	0.32	1.61	1.88	2.21	3.07
P_2O_5	0.54	0.47	0.65	0.43	0.66	0.48	0.74	0.35
H_2O+	7.40		10.00	7.70	8.00	8.80		9.30
CO_2	3.10		2.00	9.60	3.50	7.60		3.70
S		0.05						
LOI		6.76					10.27	
TOTAL	99.92	106.46	100.22	100.09	100.07	100.54	97.36	99.81
CCI	0.81	0.83	1.11	1.38	1.04	1.04	1.16	1.14

293

FIELD	Lac de Gras	Lac de Gras	Lac de Gras	Lac de Gras	Lac de Gras	Lac de Gras	Lac de Gras	Lac de Gras
LOCALITY	Pigeon	Porpoise	Porpoise	Porpoise	Rat	Rat	Rat	Rat
SAMPLE	PDG-2	PRP-1	PRP-2	PRP-3	RAT-1	RAT-2	RAT-3	RAT-4
(%)								
SiO_2	35.30	24.90	30.40	29.00	28.80	38.52	27.90	34.20
TiO_2	0.43	0.89	1.06	0.94	1.51	0.75	1.32	0.65
Al_2O_3	4.20	3.60	4.00	3.70	1.70	3.85	1.50	4.00
FeO								
Fe_2O_3								
Total Fe as Fe_2O_3	7.50	7.30	8.90	8.60	9.60	5.96	9.30	4.80
MnO	0.13	0.17	0.19	0.19	0.20	0.11	0.19	0.15
MgO	28.38	20.67	22.81	24.93	31.12	25.03	29.99	16.63
CaO	7.33	19.92	13.31	14.11	11.61	6.54	12.22	13.85
Na_2O	0.00	0.10	0.10	0.10	0.00	0.20	0.00	0.00
K_2O	3.15	2.52	2.23	1.16	0.46	2.63	0.53	1.68
P_2O_5	0.35	0.72	0.86	1.00	0.43	0.24	0.41	0.08
H_2O+	8.80	6.10	8.70	8.50	4.00		3.70	6.30
CO_2	4.80	14.00	7.60	7.60	11.50		13.30	18.20
S								
LOI						14.93		
TOTAL	100.37	100.89	100.16	99.83	100.93	98.76	100.36	100.54
CCI	1.14	1.11	1.27	1.20	0.95	1.41	0.95	1.91

FIELD	Lac de Gras	Lac de Gras	Lac de Gras	Lac de Gras	Lac de Gras	Lac de Gras	Lac de Gras	Lac de Gras
LOCALITY	Rattler	Rattler	Rattler	Roger	Roger	Roger	Wolverine	A21
SAMPLE	RTL-1	RTL-2	RTL-3	ROG-1	ROG-2	ROG-3	WOL-1	A21-1-1
(%)								
SiO_2	29.80	27.40	31.30	27.30	26.60	25.40	36.66	41.10
TiO_2	1.17	1.70	1.10	0.91	0.91	0.92	0.57	0.41
Al_2O_3	2.00	2.10	1.60	3.80	3.90	3.50	3.04	5.26
FeO								
Fe_2O_3								6.45
Total Fe as Fe_2O_3	9.20	9.90	9.00	8.90	8.90	8.60	7.86	6.45
MnO	0.18	0.21	0.17	0.21	0.22	0.21	0.12	0.10
MgO	32.26	32.09	32.88	25.27	26.03	25.03	31.74	24.10
CaO	9.74	9.42	10.79	16.19	17.93	18.16	5.37	2.45
Na_2O	0.10	0.00	0.00	0.00	0.00	0.00	0.11	0.00
K_2O	1.28	0.61	1.08	0.28	0.16	0.22	1.29	0.70
P_2O_5	0.52	0.71	0.51	1.50	1.32	1.28	0.28	0.22
H_2O+	5.90	8.60	4.00	8.20	8.70	8.60		
CO_2	8.20	7.80	8.00	6.50	4.60	7.00		
S								
LOI							12.08	17.50
TOTAL	100.35	100.54	100.43	99.06	99.27	98.92	99.12	98.29
CCI	0.92	0.89	0.94	1.20	1.16	1.13	1.16	1.82

FIELD	Lac de Gras	Lac de Gras	Lac de Gras	Lac de Gras	Lac de Gras	Lac de Gras	Lac de Gras	Lac de Gras
LOCALITY	A21	A25	A25	A154	A154	A154	ABZ	ABZ
SAMPLE	A21-1-2	A25-3-1	A25-3-2	A154-11-1	A154-11-2	A154-11-3	ABZ-7a-1	ABZ-7a-2
(%)								
SiO_2	41.90	27.20	31.70	36.80	37.90	37.90	37.20	40.60
TiO_2	0.42	0.96	0.81	0.36	0.42	0.42	1.04	0.88
Al_2O_3	4.87	4.61	4.99	2.60	2.13	2.00	5.12	4.74
FeO								
Fe_2O_3	6.65			7.10	7.71	7.53		
Total Fe as Fe_2O_3	6.65	10.30	8.93	7.10	7.71	7.53	7.22	6.46
MnO	0.08	0.24	0.23	0.13	0.13	0.13	0.16	0.14
MgO	25.10	14.60	14.70	30.20	34.80	32.20	18.40	21.70
CaO	1.90	17.30	14.90	3.90	2.28	4.35	10.90	5.46
Na_2O	0.00	0.23	0.24	0.00	0.00	0.00	0.27	0.21
K_2O	0.57	2.24	3.50	0.24	1.42	0.54	2.76	1.65
P_2O_5	0.15	1.29	1.07	0.17	0.30	0.23	0.65	0.51
H_2O+								
CO_2								
S		0.05	0.10				0.08	0.10
LOI	16.50	18.80	17.20	17.20	11.40	13.40	15.00	17.10
TOTAL	98.14	97.77	98.27	98.70	98.49	98.70	98.72	99.45
CCI	1.78	1.68	1.70	1.28	1.06	1.20	1.78	1.82

FIELD	Lac de Gras	Lac de Gras	Lac de Gras	Lac de Gras	Lac de Gras	Lac de Gras	Lac de Gras	Lac de Gras
LOCALITY	C13	C13	DD39	DD39	Tli Kwi Cho	Tli Kwi Cho	T19	T19
SAMPLE	C13-7-1	C13-7-2	DD39-5-1	DD39-5-2	DO27-23-1	DO27-23-2	T19-1-1	T19-1-2
(%)								
SiO_2	37.30	37.60	33.50	33.60	38.90	34.50	30.70	29.00
TiO_2	0.33	0.33	0.57	0.55	0.22	0.50	0.75	0.80
Al_2O_3	3.30	3.09	1.55	1.44	3.02	3.74	4.57	4.29
FeO								
Fe_2O_3								
Total Fe as Fe_2O_3	6.86	6.99	9.08	9.47	5.93	7.02	8.61	8.45
MnO	0.12	0.13	0.19	0.21	0.13	0.16	0.18	0.18
MgO	25.30	27.70	36.90	36.30	27.90	32.60	21.20	21.90
CaO	6.93	4.77	6.38	7.03	4.41	7.05	12.60	13.30
Na_2O	0.17	0.12	0.07	0.05	0.17	0.11	0.20	0.11
K_2O	2.13	1.91	0.22	0.07	0.79	1.38	4.07	3.51
P_2O_5	0.42	0.37	0.55	0.59	0.14	0.56	0.93	0.99
H_2O+								
CO_2								
S	0.08	0.07	0.05	0.03	0.27	0.02	0.03	
LOI	16.70	16.00	10.90	10.80	16.40	11.90	15.10	15.20
TOTAL	99.56	99.01	99.91	100.11	98.01	99.52	98.91	97.73
CCI	1.38	1.29	0.94	0.96	1.43	1.08	1.21	1.15

FIELD	Lac de Gras	Lac de Gras	Lac de Gras	Lac de Gras	Lac de Gras	Lac de Gras	Lac de Gras	Lac de Gras
LOCALITY	T21	T21	T34	T34	T35	T35	T36	T36
SAMPLE	T21-1-1	T21-1-2	T34-1-1	T34-1-2	T35-1-1	T35-1-2	T36-1-1	T36-2-1
(%)								
SiO_2	31.90	32.30	25.40	27.20	28.70	28.50	33.10	27.70
TiO_2	0.69	0.70	0.68	0.77	0.79	0.80	0.96	0.92
Al_2O_3	3.67	3.88	4.59	4.74	4.80	4.66	4.47	3.96
FeO								
Fe_2O_3								
Total Fe as Fe_2O_3	9.29	8.71	8.26	8.90	9.84	9.73	9.16	8.05
MnO	0.20	0.18	0.19	0.20	0.22	0.22	0.19	0.17
MgO	29.10	29.50	23.20	21.80	24.60	24.60	27.10	21.40
CaO	7.10	6.61	16.60	15.50	13.20	13.50	6.54	15.30
Na_2O	0.19	0.24	0.14	0.22	0.17	0.14	0.13	0.07
K_2O	1.31	1.67	2.18	2.35	1.34	1.43	3.85	3.48
P_2O_5	0.23	0.24	0.88	0.95	1.07	0.95	0.50	0.59
H_2O+								
CO_2								
S	0.02	0.02	0.03		0.02	0.02	0.03	0.03
LOI	14.40	14.10	16.70	16.50	14.30	15.00	13.00	17.50
TOTAL	98.08	98.13	98.82	99.13	99.03	99.53	99.00	99.14
CCI	1.13	1.11	1.09	1.21	1.23	1.21	1.08	1.12

FIELD	Lac de Gras	Lac de Gras	Lac de Gras	Lac de Gras	Lac de Gras	Lac de Gras	South-West Slave	South-East Slave
LOCALITY	T146	T146	T237	T237	TR107	TR107	Drybones	Gahcho Kue
SAMPLE	T146-1-1	T146-1-2	T237-1-1	T237-1-2	TR107-3-1	TR107-3-2	DRY-1	KDY-1
(%)								
SiO_2	26.50	30.80	28.30	28.70	33.10	35.40	41.38	42.06
TiO_2	0.74	0.88	1.01	1.04	0.79	0.77	1.31	0.64
Al_2O_3	6.34	5.75	4.18	3.95	4.67	5.08	3.62	3.32
FeO								
Fe_2O_3								7.40
Total Fe as Fe_2O_3	5.83	7.74	10.60	10.90	9.01	8.63	8.44	7.40
MnO	0.15	0.19	0.26	0.24	0.19	0.20	0.10	0.12
MgO	15.50	22.00	25.00	28.90	20.60	20.10	28.76	25.99
CaO	19.70	11.10	9.88	10.60	10.80	11.00	1.62	6.13
Na_2O	0.17	0.28	0.15	0.08	0.30	0.55	0.44	0.93
K_2O	5.83	3.51	0.40	0.67	2.17	3.02	0.53	1.39
P_2O_5	1.01	1.08	1.23	1.13	0.93	0.82	0.24	0.29
H_2O+								
CO_2								
S		0.03	0.02	0.03	0.05	0.05		
LOI	16.50	14.10	15.60	13.00	15.90	13.10	12.93	10.80
TOTAL	98.27	97.43	96.61	99.21	98.46	98.67	99.37	99.07
CCI	1.22	1.27	1.26	1.08	1.53	1.57	1.52	1.61

CANADA, Churchill Province

FIELD	South-East Slave	South-East Slave	Somerset Island	Somerset Island	Somerset Island	Somerset Island	Rankin Inlet
LOCALITY	Gahcho Kue	Snap Lake	JP South	Batty Bay	Elwin Bay	Jos	Rankin Inlet
SAMPLE	KDY-2	SNP-1	JPS-1	BAT-1	ELB-1	JOS-1	RNK-1
(%)							
SiO_2	43.49	34.70	24.26	20.90	27.30	23.10	23.30
TiO_2	0.68	0.84	1.41	1.63	1.16	1.12	3.54
Al_2O_3	4.45	3.12	1.60	1.64	2.07	0.81	3.87
FeO	6.69						
Fe_2O_3	6.69	8.24					
Total Fe as Fe_2O_3		8.24	8.03	7.62	7.77	7.79	13.60
MnO	0.09	0.21	0.10	0.15	0.15	0.15	0.26
MgO	26.58	30.50	26.39	21.60	28.30	27.00	18.70
CaO	2.83	3.91	18.06	21.50	11.80	21.80	16.20
Na_2O	0.11	0.00	0.05	0.12	0.09	0.10	0.31
K_2O	2.19	0.88	0.46	0.11	1.22	0.30	0.46
P_2O_5	0.50	0.42	0.74	0.65	0.59	0.48	0.28
H_2O+							
CO_2							
S							
LOI	11.60	15.10	17.75	22.90	18.90	17.50	19.50
TOTAL	99.21	97.92	98.85	98.82	99.35	100.15	100.02
CCI	1.55	1.17	0.95	1.04	0.96	0.87	1.40

300

FIELD		CANADA, Superior Province				CANADA, Trans-Hudson Domain	
		Attawapiskat	Kirkland Lake	Timiskaming	Timiskaming	Fort a la Corne	Fort a la Corne
LOCALITY		James Bay Lowlands	Upper Canada Mine	Guiges	Peddie	Fort a la Corne	Sturgeon Lake
SAMPLE		JBL-1	UCM-2	GUI-1	PED-1	FLC-1	STL-1
(%)							
SiO_2		29.01	32.44	32.30	25.70	30.31	22.94
TiO_2		0.89	1.51	1.06	2.37	2.62	0.75
Al_2O_3		3.06	1.77	1.62	1.58	1.47	0.40
FeO							
Fe_2O_3							
Total Fe as Fe_2O_3		7.17	8.47	8.18	8.43	8.83	6.33
MnO		0.12	0.13	0.13	0.18	0.15	0.12
MgO		24.88	31.45	33.60	30.90	36.82	18.21
CaO		13.38	5.66	4.94	13.80	4.03	22.72
Na_2O		0.06	1.85	0.26	0.01	0.02	0.02
K_2O		0.10	2.73	1.18	0.42	0.05	0.10
P_2O_5		0.28	0.42	0.37	1.14	0.67	0.16
H_2O+							
CO_2							
S							
LOI		21.29	12.17	14.90	14.40	15.08	26.96
TOTAL		100.24	98.60	98.54	98.93	100.05	98.71
CCI		1.28	0.98	0.95	0.86	0.86	1.27

FIELD	USA, Yapavai Domain			South Africa, Kaapvaal Province			
	State Line	State Line	State Line	Barkly West	Barkly West	Central Cape	Central Cape
LOCALITY	Nix	Chicken Park	Sloan	Frank Smith	Roberts Victor	Gansfontein	Melton Wold
SAMPLE	NIX-1	CHK-1	SLN-1	FSM-2	ROVIC-1	GNS-13	MW-3
(%)							
SiO_2	26.00	28.07	41.76	39.63	31.32	26.29	34.90
TiO_2	1.29	3.85	1.08	1.02	1.00	4.82	1.08
Al_2O_3	1.90	2.42	4.50	6.96	2.72	3.86	2.80
FeO							
Fe_2O_3							
Total Fe as Fe_2O_3	8.51	12.80	7.00	9.00	8.07	16.96	8.30
MnO	0.18	0.15	0.16	0.11	0.12	0.18	0.10
MgO	30.00	28.61	24.62	19.78	28.10	25.11	30.56
CaO	12.80	7.97	9.94	7.44	9.31	9.10	5.65
Na_2O	0.13	0.04	0.21	2.00	0.28	0.66	0.03
K_2O	0.13	1.05	2.74	1.40	1.61	0.77	2.05
P_2O_5	0.66	0.43	0.41	0.43	2.90	1.12	0.14
H_2O+							
CO_2							
S							
LOI	17.50	13.73	6.55	11.69	12.72	10.64	13.14
TOTAL	99.10	99.12	98.97	99.46	98.15	99.51	98.75
CCI	0.93	0.99	1.54	2.15	1.10	1.16	1.09

FIELD	North Lesotho	North Lesotho	North Lesotho
LOCALITY	Liqhobong	Liqhobong	Pipe 200
SAMPLE	LQ-7	LQ-SAT	P200
(%)			
SiO_2	30.07	39.61	31.57
TiO_2	1.89	0.93	2.47
Al_2O_3	4.36	10.89	1.85
FeO			
Fe_2O_3			
Total Fe as Fe_2O_3	9.75	11.23	11.47
MnO	0.14	0.18	0.14
MgO	26.25	19.12	31.57
CaO	8.60	8.10	8.43
Na_2O	0.11	0.36	0.14
K_2O	1.01	0.01	1.14
P_2O_5	0.60	0.15	0.77
H_2O+			
CO_2			
S			
LOI	16.67	9.13	9.76
TOTAL	99.45	99.71	99.31
CCI	1.22	2.66	0.99

FIELD	RUSSIA, Siberian Province				
LOCALITY	Malo-Botuobinsk	Malo-Botuobinsk	Daldyn-Alakit	Daldyn-Alakit	
	Mir	Internationalaya	Jubilee	Udachnaya	
SAMPLE	MIR-M3	INT-I2	JUB-1	UDC-1	
(%)					
SiO_2	33.70	30.50	26.10	30.10	
TiO_2	1.50	0.48	1.00	1.43	
Al_2O_3	2.20	1.95	1.10	2.11	
FeO					
Fe_2O_3					
Total Fe as Fe_2O_3	9.20	5.07	6.13	9.23	
MnO	0.10	0.12	0.05	0.16	
MgO	29.90	27.00	19.10	32.50	
CaO	5.16	12.30	19.80	8.67	
Na_2O	0.17	0.16	0.08	0.12	
K_2O	0.57	0.59	0.19	0.48	
P_2O_5	0.21	0.64	0.33	0.41	
H_2O+					
CO_2					
S					
LOI	15.80	20.60	25.90	14.80	
TOTAL	98.51	99.41	99.78	100.01	
CCI	1.16	1.16	1.40	0.97	

LAC DE GRAS Crustal rocks								
ROCK TYPE	Greywacke	Greywacke	Greywacke	Greywacke	Greywacke	Greywacke	Tronjhemite	Trondjhemite
SAMPLE	KIA92-K075	KIA92-K089	KIA92-K096	KIA92-K152	KIA92-K153	KIA92-P067	KIA92-K069	KIA92-K078
(%)								
SiO_2	73.20	65.10	61.70	70.10	57.60	48.20	61.80	58.60
TiO_2	0.47	0.62	0.69	0.53	0.72	0.95	0.46	0.47
Al_2O_3	12.60	16.40	18.70	14.10	23.50	27.80	18.90	20.50
FeO	2.40	4.70	5.50	3.10	5.20	6.20	3.00	3.10
Fe_2O_3	0.70	1.20	1.30	1.30	1.00	1.60	0.90	1.00
Total Fe as Fe_2O_3	3.10	5.90	6.80	4.40	6.20	7.80	3.90	4.10
MnO	1.80	2.30	3.60	2.07	3.39	4.36	2.73	2.24
MgO	0.03	0.13	0.07	0.03	0.06	0.07	0.05	0.05
CaO	1.56	3.02	1.11	1.29	0.81	1.71	4.99	4.75
Na_2O	3.00	3.20	2.30	2.90	1.20	2.50	4.00	4.50
K_2O	1.92	2.25	2.49	1.95	3.32	3.89	2.06	2.47
P_2O_6	0.08	0.22	0.11	0.11	0.17	0.15	0.19	0.16
H_2O+	1.10	1.30	2.20	1.60	2.60	2.50	1.10	1.30
CO_2			0.10			0.20	0.20	0.10
S	0.14		0.11	0.10	0.07	0.12	0.03	0.10
TOTAL	99.00	100.44	99.98	99.18	99.64	100.25	100.41	99.34

305

ROCK TYPE	Trondhjemite	Quartz diorite	Hornblende tonalite	Hornblende tonalite	Hornblende tonalite	Hornblende tonalite	Hornblende tonalite	Hornblende tonalite
SAMPLE	KIA92-K145	KIA92-K053	KIA92-K003	KIA92-K049	KIA92-K058A	KIA92-K131	KIA92-K134	KIA92-K136
(%)								
SiO_2	61.90	63.70	74.00	59.00	63.60	62.00	65.50	62.70
TiO_2	0.39	0.44	0.18	0.54	0.42	0.45	0.40	0.38
Al_2O_3	18.80	17.20	14.70	17.10	16.70	17.20	16.70	18.60
FeO	2.80	1.20	0.90	3.30	2.70	2.80	2.70	2.80
Fe_2O_3	0.70	2.60	0.30	1.90	1.00	1.10	0.80	0.60
Total Fe as Fe_2O_3	3.50	3.80	1.20	5.20	3.70	3.90	3.50	3.40
MnO	0.04	0.05	0.01	0.07	0.06	0.05	0.04	0.05
MgO	2.28	2.83	0.60	3.27	2.71	2.76	2.35	2.01
CaO	4.39	4.13	0.37	5.32	3.80	3.95	3.75	3.52
Na_2O	3.70	3.30	3.70	7.00	3.10	3.50	3.70	4.80
K_2O	2.37	3.26	4.87	1.68	4.01	3.06	1.90	2.29
P_2O_5	0.12	0.18	0.15	0.30	0.16	0.16	0.09	0.24
H_2O+	1.30	1.20	0.80	0.60	1.30	1.60	1.10	1.00
CO_2	0.10	0.40	0.10	0.20	0.10	0.40	0.10	0.10
S	0.04			0.02				
TOTAL	98.93	100.49	100.68	100.30	99.66	99.03	99.13	99.09

306

ROCK TYPE	Hornblende tonalite	Hornblende tonalite	Hornblende tonalite	Hornblende tonalite	Hornblende tonalite	Hornblende tonalite	Phlogopite granite	Phlogopite granite
SAMPLE	KIA92-K177A	KIA92-K177B	KIA92-P26B	KIA92-P55B-1	KIA92-P55B-2	KIA92-L128-1	KIA92-K106	KIA92-K141
(%)								
SiO_2	60.20	73.40	59.60	72.10	75.00	58.90	74.20	71.40
TiO_2	0.52	0.04	0.48	0.12		0.73	0.10	0.14
Al_2O_3	17.30	15.00	18.60	15.50	14.40	21.90	13.80	15.10
FeO	3.10		4.00	0.70	0.80	6.40	0.60	0.70
Fe_2O_3	1.40		0.90	0.20	0.30	1.50	0.50	0.40
Total Fe as Fe_2O_3	4.50	0.00	4.90	0.90	1.10	7.90	1.10	1.10
MnO	3.25	0.36	2.79	0.43	0.18	3.71	0.46	0.47
MgO	0.05	0.01	0.08	0.01	0.28	0.06	0.01	0.01
CaO	4.77	2.54	6.22	1.90	0.39	0.57	0.50	0.57
Na_2O	3.70	4.00	3.60	5.20	4.80	1.10	2.90	3.20
K_2O	2.58	1.86	1.59	2.34	1.88	2.88	5.24	5.78
P_2O_5	0.21	0.51	0.24	0.04	0.20	0.09	0.31	0.35
H_2O+	1.40	0.90	1.30	0.50	0.80	2.10	0.70	0.90
CO_2	0.20		0.10		0.10		0.10	0.20
S	0.02		0.04			0.09		
TOTAL	98.70	98.62	99.54	99.04	99.13	100.03	99.42	99.22

ROCK TYPE	Phlogopite granite	Phlogopite granite	2 mica granite	2 mica granite	2 mica granite	2 mica granite	2 mica granite	2 mica granite	2 mica granite
SAMPLE	KIA92-K142	KIA92-K143	KIA92-K042	KIA92-K102	KIA92-K139	KIA92-K140	KIA92-K159	KIA92-P10a
(%)									
SiO_2	71.10	72.20	70.10	70.90	72.50	72.20	73.80	58.50
TiO_2	0.12	0.17	0.21	0.12	0.11	0.13	0.07	0.56
Al_2O_3	15.50	15.10	16.80	15.50	14.90	14.80	14.60	17.80
FeO	0.80	1.00	1.00	0.50	0.50	0.80	0.40	3.40
Fe_2O_3	0.40		0.40	0.20	0.20	0.40		1.70
Total Fe as Fe_2O_3	1.20	1.00	1.40	0.70	0.70	1.20	0.40	5.10
MnO	0.49	0.47	0.71	0.37	0.32	0.40	0.26	2.83
MgO	0.01	0.01	0.02		0.01	0.01	0.01	0.06
CaO	0.61	0.55	2.70	0.57	0.65	0.59	0.32	5.02
Na_2O	3.60	3.30	5.80	3.30	3.60	3.50	2.50	6.80
K_2O	5.23	5.54	1.05	5.92	4.80	5.02	5.19	1.59
P_2O_5	0.36	0.29	0.09	0.23	0.23	0.33	0.23	0.29
H_2O^+	1.00	0.70	0.50	0.70	0.70	0.70	1.00	0.80
CO_2	0.10		0.10	0.10	0.10	0.10		
S								
TOTAL	99.32	99.33	99.48	98.41	98.62	98.98	98.38	99.35

ROCK TYPE	2 mica granite	2 mica granite
SAMPLE	KIA92-L070	KIA92-L124
(%)		
SiO_2	70.20	55.30
TiO_2	0.15	0.66
Al_2O_3	16.10	18.80
FeO	0.70	4.50
Fe_2O_3	0.30	1.10
Total Fe as Fe_2O_3	1.00	5.60
MnO	0.47	4.27
MgO	0.01	0.08
CaO	0.55	7.68
Na_2O	2.90	5.00
K_2O	6.37	1.07
P_2O_5	0.29	0.24
H_2O+	1.10	1.20
CO_2	0.20	
S		
TOTAL	99.34	99.90

309

FIELD	CANADA, Slave Province												
	Contwoyto		Contwoyto		Contwoyto		Contwoyto		Contwoyto		Contwoyto		
LOCALITY	Jericho		Jericho		Jericho		Jericho		Jericho		Jericho		
SAMPLE	JD-51	+/- 2σ	JD-69-1	+/- 2σ	JD-69-3	+/- 2σ	JD-82-1	+/- 2σ	JD-82-3	+/- 2σ	RND-120-4S	+/- 2σ
(ppm)												
Sc	23.0	0.2	14.4	0.3	22.6	1.1	15.9	0.2	18.7	2.2	35.5	0.6
V	140	0	99	2	83	3	102	2	77	5	256	1
Cr	2013*		1301*		1570*		1513*		1891*		6557	41
Co	89.2	0.1	62.1	1.4	78.5	3.0	100.7	2.1	94.9	4.0	127.1	0.6
Ni	598*		789*		1151*		1291*		1396*		1844	7
Cu	109.9	0.7	68.6	2.3	56.1	2.2	81.2	2.8	84.1	5.3	253.9	1.2
Zn	31.4	4.0			51.1	3.6			61.9	10.9	56.2	5.5
Ga	7.00	0.00	3.94	0.05	3.75	0.07	4.64	0.02	5.29	0.08	11.20	0.15
Rb	14.8	0.1	28.4	1.1	30.5	0.6	32.2	0.1	28.0	1.8	48.9	0.0
Sr	661	1	1289	40	625	17	679	7	339	26	188	1
Y	14.88	0.21	10.97	0.48	10.39	0.11	11.03	0.31	9.60	0.28	20.43	0.07
Zr	167.3	0.9	89.0	2.3	70.8	1.4	93.1	1.1	112.1	4.1	176.0	0.1
Nb	351	1	216	6	142	1	234	3	246	7	499	1
Cs	2.61	0.02	1.22	0.02	2.62	0.01	3.20	0.06	2.99	0.02	6.20	0.12
Ba	870	7	3366	76	7169	155	3912	46	3245	4	1533	51
Hf	3.86	0.02	2.00	0.04	1.57	0.06	2.08	0.03	2.56	0.15	4.57	0.06
Ta	16.9	0.2	8.7	0.0	6.3	0.1	10.6	0.1	11.5	0.2	29.1	0.4
Pb	27.92	0.25	17.73	0.13	14.91	0.25	19.48	0.22	16.93	0.37	18.99	0.43
Th	42.6	0.1	22.1	0.0	16.0	0.6	26.6	0.2	30.2	0.7	52.6	1.0
U	9.05	0.06	4.47	0.01	2.74	0.16	5.49	0.08	4.32	0.08	131.90	2.76
La	259	1	179	3	174	7	188	1	168	1	285	12
Ce	411	8	266	3	261	16	275	0	272	0	488	19
Pr	46.0	0.1	28.4	0.3	24.4	1.6	30.2	0.4	28.2	0.0	55.4	1.9
Nd	146.1	0.7	89.9	1.0	77.6	4.4	95.4	0.8	92.6	1.2	179.2	8.7
Pm												
Sm	16.61	0.16	10.45	0.17	9.42	0.12	11.08	0.26	10.85	0.12	20.83	0.90
Eu	3.83	0.06	2.64	0.04	2.51	0.09	2.77	0.01	2.85	0.12	4.98	0.11
Gd	8.88	0.00	6.09	0.14	6.94	0.01	6.29	0.09	6.75	0.28	11.17	0.14
Tb	0.90	0.00	0.62	0.01	0.63	0.01	0.64	0.02	0.63	0.02	1.15	0.05
Dy	3.64	0.02	2.56	0.05	2.55	0.05	2.61	0.04	2.49	0.08	4.67	0.14
Ho	0.53	0.01	0.38	0.00	0.37	0.01	0.39	0.01	0.34	0.02	0.67	0.03
Er	1.01	0.03	0.74	0.02	0.78	0.03	0.73	0.01	0.69	0.01	1.31	0.02
Tm	0.124	0.000	0.089	0.002	0.102	0.002	0.091	0.002	0.084	0.000	0.169	0.004
Yb	0.64	0.02	0.46	0.02	0.56	0.02	0.50	0.01	0.43	0.01	0.89	0.02
Lu	0.091	0.002	0.065	0.002	0.082	0.002	0.070	0.002	0.059	0.004	0.129	0.004

FIELD	Contwoyto		Contwoyto		Lac de Gras		Lac de Gras		Lac de Gras		Lac de Gras	
LOCALITY	Jericho		Muskox		Aaron		Aaron		Anaconda		Anaconda	
SAMPLE	RND-120-4SA	+/- 2σ	RHL-11-2	+/- 2σ	AAR-1	+/- 2σ	AAR-2	+/- 2σ	ANA-1	+/- 2σ	ANA-2	+/- 2σ
(ppm)												
Sc	42.2	1.7	12.4	0.1	12.1	0.1	5.8	0.1	12.8	0.3	11.3	0.1
V	245	2	135	3	63	1	77	2	130	0	153	0
Cr	8737	54	1916*		2300**		730**		2100**		1800**	
Co	166.4	4.0	83.5	1.0	87.6	1.3	60.8	3.2	78.4	0.4	68.9	0.5
Ni	1775	44	900*		1720**		1180**		1230**		1100**	
Cu	264.7	7.2			49.5	1.7	20.2	1.2	88.2	0.7	85.3	0.2
Zn	141.5	8.4							49.9	0.6	37.5	0.4
Ga	14.83	0.66	5.63	0.12	3.52	0.05	4.09	0.18	4.44	0.11	3.95	0.04
Rb	49.2	0.7	40.2	0.4	104.1	0.7	65.0	2.0	25.5	0.5	18.8	0.2
Sr	187	3	1059	2	621	4	83	2	1451	1	1947	2
Y	21.69	0.13	7.35	0.26	4.42	0.07	7.36	0.19	5.71	0.06	5.40	0.04
Zr	206.7	4.1	70.0	0.9	32.7	0.7	28.8	0.4	52.3	0.2	48.1	0.3
Nb	577	3	162	2	171	1	54	1	277	1	281	0
Cs	3.83	0.14	0.40	0.00	1.75	0.06	1.36	0.03	0.78	0.01	0.62	0.04
Ba	2897	62	2699	49	1317	36	326	2	1469	36	2839	5
Hf	5.34	0.10	1.64	0.04	0.95	0.09	0.83	0.04	1.14	0.03	1.05	0.03
Ta	33.5	0.5	10.8	0.1	10.9	0.2	2.6	0.0	15.9	0.1	13.8	0.1
Pb	21.73	0.41	13.22	0.16	5.37	0.09	6.97	0.11	9.46	0.03	4.68	0.10
Th	61.4	1.0	17.7	0.0	20.3	0.4	6.3	0.1	17.7	0.1	16.5	0.2
U	39.88	0.05	3.16	0.01	3.21	0.07	2.82	0.06	3.99	0.06	4.56	0.06
La	326	10	118	2	106	2	42	0	153	2	161	1
Ce	676	29	188	3	178	3	69	0	274	1	288	2
Pr	60.6	1.1	19.9	0.3	19.2	0.3	7.4	0.1	22.7	0.3	25.6	0.0
Nd	200.4	7.2	64.8	1.2	58.9	0.3	23.8	0.1	81.5	0.2	76.5	0.6
Pm												
Sm	23.78	0.57	7.56	0.19	5.71	0.11	2.81	0.04	7.93	0.20	7.35	0.07
Eu	5.81	0.26	2.04	0.03	1.37	0.02	0.62	0.01	1.91	0.02	1.90	0.02
Gd	14.25	0.11	5.31	0.17	3.02	0.16	1.93	0.09	4.78	0.04	3.59	0.02
Tb	1.45	0.02	0.47	0.01	0.25	0.00	0.24	0.00	0.40	0.01	0.33	0.00
Dy	6.03	0.21	1.81	0.01	1.01	0.04	1.25	0.01	1.47	0.02	1.28	0.02
Ho	0.89	0.06	0.27	0.01	0.15	0.01	0.23	0.00	0.20	0.01	0.18	0.00
Er	1.94	0.05	0.58	0.03	0.31	0.02	0.59	0.01	0.43	0.01	0.36	0.02
Tm	0.257	0.012	0.075	0.002	0.040	0.002	0.093	0.004	0.051	0.004	0.046	0.000
Yb	1.36	0.04	0.42	0.01	0.25	0.01	0.55	0.02	0.28	0.01	0.26	0.00
Lu	0.196	0.000	0.061	0.006	0.036	0.004	0.090	0.002	0.041	0.002	0.038	0.000

FIELD	Lac de Gras		Lac de Gras		Lac de Gras		Lac de Gras		Lac de Gras		Lac de Gras	
LOCALITY	Anaconda		Arnie		Fox		Grizzly		Grizzly		Grizzly	
SAMPLE	ANA-3	+/-2σ	KPL-21	+/-2σ	FOX-1	+/-2σ	GRZ-1	+/-2σ	GRZ-2	+/-2σ	GRZ-3	+/-2σ
(ppm)												
Sc	12.7	0.5	15.6	0.6	10.6	0.7	13.0	0.7	17.0	0.4	12.6	0.1
V	159	2	92	1	83	1	62	1	99	0	78	0
Cr	1700**	0.9	2326**	0.3	571**	1.3	2300**	1.2	2300**	0.3	2200**	1.6
Co	97.0		97.6		70.0		80.0		120.7		83.4	
Ni	1240**	0.4	1100**		1090**		1390**		1490**		1550**	0.9
Cu	85.3	7.1			32.3	0.5	47.0	0.3	59.4	0.3	41.6	0.9
Zn	26.0				22.5	13.8	42.9	0.8	33.6	11.4		
Ga	4.56	0.11	5.44	0.16	11.29	0.01	4.24	0.05	4.67	0.11	3.92	0.01
Rb	38.2	0.0	12.5	0.1	85.3	0.3	107.6	0.4	84.1	0.4	90.3	1.6
Sr	1781	1	1356	8	745	7	1195	14	1169	1	837	1
Y	5.91	0.05	9.09	0.02	8.75	0.17	5.61	0.13	6.79	0.11	5.50	0.01
Zr	51.4	0.4	69.4	0.4	37.1	0.1	41.0	1.1	53.7	0.3	45.7	0.1
Nb	270	1	362	0	81	0	214	4	320	4	202	2
Cs	1.09	0.02	0.66	0.03	1.77	0.02	1.36	0.02	0.97	0.02	1.39	0.04
Ba	2922	29	4905	30	729	7	2091	5	2600	23	2187	2
Hf	1.07	0.02	1.55	0.03	0.91	0.01	0.95	0.02	1.23	0.06	1.14	0.02
Ta	14.6	0.1	17.3	0.0	3.7	0.0	10.5	0.2	13.0	0.3	11.2	0.0
Pb	5.60	0.05	11.19	0.32	7.44	0.21	4.57	0.02	6.54	0.23	5.42	0.08
Th	16.7	0.1	38.8	0.3	7.3	0.0	18.0	0.2	22.5	0.1	20.2	0.0
U	4.36	0.00	6.34	0.03	1.96	0.01	3.23	0.11	4.45	0.00	3.18	0.01
La	169	0	223	1	62	1	109	0	149	0	121	0
Ce	256	18	350	4	103	1	177	3	240	0	201	2
Pr	27.7	0.2	35.9	0.1	11.3	0.2	16.3	0.2	25.8	0.1	21.7	0.1
Nd	83.4	0.9	110.1	1.8	37.3	0.6	60.4	1.7	79.6	0.7	67.5	0.6
Pm												
Sm	8.11	0.13	11.04	0.07	4.74	0.03	6.38	0.10	8.07	0.09	6.75	0.08
Eu	1.84	0.03	2.77	0.02	1.17	0.01	1.67	0.04	1.82	0.01	1.67	0.01
Gd	3.83	0.18	7.79	0.12	2.75	0.00	3.98	0.02	3.81	0.01	3.43	0.13
Tb	0.36	0.00	0.61	0.01	0.33	0.01	0.34	0.01	0.37	0.01	0.31	0.01
Dy	1.39	0.01	2.32	0.02	1.63	0.05	1.32	0.05	1.57	0.01	1.29	0.03
Ho	0.20	0.00	0.33	0.00	0.30	0.00	0.19	0.00	0.24	0.01	0.19	0.00
Er	0.39	0.01	0.71	0.02	0.71	0.02	0.43	0.01	0.51	0.02	0.40	0.02
Tm	0.052	0.002	0.084	0.004	0.111	0.002	0.056	0.002	0.068	0.004	0.052	0.000
Yb	0.28	0.01	0.49	0.02	0.65	0.02	0.33	0.01	0.40	0.00	0.30	0.01
Lu	0.042	0.004	0.072	0.002	0.105	0.014	0.046	0.000	0.061	0.004	0.045	0.000

FIELD	Lac de Gras		Lac de Gras		Lac de Gras		Lac de Gras		Lac de Gras		Lac de Gras	
LOCALITY	Grizzly		Grizzly		Grizzly		Grizzly		Grizzly		Grizzly	
SAMPLE	GRZ-4	+/-2σ	GRZ-5	+/-2σ	GRZ-6	+/-2σ	GRZ-7	+/-2σ	GRZ-8	+/-2σ	GRZ-9	+/-2σ
(ppm)												
Sc	14.0	0.2	11.8	0.7	10.8	0.0	11.3	0.3	10.5	0.2	11.1	0.2
V	89	1	68	1	73	1	58	1	62	2	64	0
Cr	2300**		1885*		1760*		1760*		1760*		1822*	
Co	82.7	0.8	87.7	0.3	83.5	1.3	84.2	2.1	84.3	1.7	86.9	1.8
Ni	1490**		1484**		1451**		1387**		1397**		1348**	
Cu	64.2	1.6	41.1	0.9	31.1	0.6	66.5	0.6	37.8	0.4	38.1	0.1
Zn	44.4	1.2	46.8	1.3	44.3	2.2	46.5	0.9	45.8	1.9	45.4	1.1
Ga	4.38	0.04	3.49	0.01	3.21	0.04	3.62	0.15	2.98	0.19	3.14	0.00
Rb	117.1	3.5	73.0	1.0	91.3	0.6	90.0	0.1	39.0	0.4	45.6	0.0
Sr	868	18	620	7	1205	31	704	2	835	4	736	19
Y	5.50	0.20	4.76	0.03	4.60	0.10	4.52	0.08	4.25	0.01	4.43	0.03
Zr	47.4	0.8	39.5	0.0	37.8	0.9	40.5	0.4	34.4	0.0	35.2	1.0
Nb	218	2	186	0	175	6	176	3	172	1	174	2
Cs	1.78	0.02	1.25	0.02	1.41	0.05	1.36	0.09	0.77	0.02	1.21	0.02
Ba	2045	13	1656	34	2218	192	1462	47	2003	42	1543	18
Hf	1.08	0.07	0.90	0.02	0.87	0.03	0.92	0.03	0.80	0.01	0.82	0.01
Ta	11.9	0.0	9.5	0.0	9.1	0.0	9.3	0.1	8.7	0.1	8.9	0.1
Pb	5.19	0.10	4.75	0.06	5.59	0.03	3.98	0.02	4.81	0.05	4.49	0.02
Th	20.3	0.2	16.6	0.1	15.8	0.3	16.4	0.1	15.3	0.2	15.6	0.2
U	3.32	0.02	3.10	0.03	2.72	0.08	2.62	0.06	2.59	0.02	2.60	0.03
La	134	3	117	4	115	3	112	3	107	2	108	1
Ce	238	3	191	4	186	5	185	6	176	3	179	1
Pr	23.6	0.2	20.4	0.3	19.6	0.6	19.9	0.6	18.5	0.3	18.9	0.2
Nd	72.9	1.4	62.3	1.0	60.2	1.1	60.8	2.3	56.6	1.0	58.0	0.3
Pm												
Sm	7.14	0.15	6.14	0.20	6.05	0.11	6.03	0.17	5.58	0.05	5.74	0.03
Eu	1.63	0.02	1.50	0.03	1.52	0.02	1.45	0.01	1.43	0.02	1.41	0.01
Gd	4.44	0.18	3.06	0.08	3.03	0.08	2.91	0.22	2.92	0.19	2.87	0.08
Tb	0.37	0.01	0.27	0.02	0.27	0.00	0.27	0.01	0.26	0.00	0.26	0.00
Dy	1.40	0.02	1.13	0.02	1.08	0.01	1.08	0.07	1.02	0.04	1.05	0.03
Ho	0.20	0.01	0.17	0.01	0.16	0.00	0.17	0.00	0.15	0.00	0.16	0.00
Er	0.43	0.00	0.34	0.02	0.33	0.01	0.33	0.01	0.32	0.00	0.33	0.02
Tm	0.055	0.002	0.049	0.004	0.044	0.002	0.047	0.006	0.043	0.002	0.045	0.004
Yb	0.30	0.01	0.26	0.00	0.25	0.01	0.25	0.01	0.24	0.01	0.24	0.01
Lu	0.046	0.002	0.040	0.000	0.038	0.002	0.038	0.000	0.036	0.002	0.037	0.002

313

FIELD	Lac de Gras		Lac de Gras		Lac de Gras		Lac de Gras		Lac de Gras		Lac de Gras	
LOCALITY	Grizzly		Grizzly		Grizzly		Grizzly		Grizzly		Anne	
SAMPLE	GRZ-10	+/- 2σ	GRZ-11	+/- 2σ	GRZ-12	+/- 2σ	GRZ-13	+/- 2σ	GRZ-14	+/- 2σ	HL-10-2	+/- 2σ
(ppm)												
Sc	10.4	0.6	10.5	0.5	11.1	0.3	10.6	0.4	11.1	0.1	12.9	0.1
V	68	2	66	2	61	2	59	2	53	2	122	1
Cr	1697*	1.7	1760*	1.4	1508*	1.0	1697*	3.3	1760*	2.6	1847**	
Co	85.4		89.0		78.7		87.3		86.3		91.8	0.1
Ni	1353**		1442**		1337**		1784**		1379**		1100**	
Cu	36.2	0.0	15.1	0.2	52.1	0.4	31.6	0.2	58.0	0.2		
Zn	45.8	1.0	47.5	0.2	44.8	0.5	45.7	1.3	63.7	0.1		
Ga	3.32	0.01	3.29	0.05	3.76	0.05	3.26	0.04	3.31	0.12	4.73	0.10
Rb	50.5	1.0	81.3	0.8	105.8	0.7	78.6	2.7	75.8	1.0	91.6	0.6
Sr	825	14	694	1	888	1	708	15	714	11	1484	3
Y	4.52	0.14	4.71	0.05	4.99	0.00	4.46	0.18	4.44	0.01	5.02	0.17
Zr	36.8	0.3	38.0	0.5	39.1	0.0	37.3	0.8	39.6	0.4	46.6	0.4
Nb	173	0	173	2	181	0	175	2	172	0	212	0
Cs	0.88	0.01	1.23	0.01	1.31	0.04	1.25	0.02	1.09	0.00	1.46	0.09
Ba	2031	53	1666	39	2111	13	1725	64	1546	23	2585	15
Hf	0.85	0.03	0.89	0.01	0.93	0.03	0.86	0.02	0.89	0.03	1.11	0.05
Ta	9.0	0.1	9.3	0.2	8.7	0.1	9.2	0.0	9.3	0.2	11.5	0.1
Pb	4.79	0.02	4.64	0.04	4.47	0.15	4.37	0.06	3.95	0.03	7.99	0.10
Th	16.0	0.3	16.2	0.2	15.8	0.2	16.1	0.0	16.1	0.1	18.9	0.1
U	2.76	0.01	2.45	0.04	3.04	0.05	2.73	0.03	2.49	0.03	48.27	0.12
La	103	3	113	2	128	1	112	3	108	3	153	0
Ce	168	2	187	1	203	0	184	2	180	3	250	1
Pr	17.9	0.2	19.9	0.2	21.2	0.0	19.5	0.2	19.2	0.1	25.7	0.2
Nd	55.8	0.1	60.7	0.8	64.3	0.9	59.5	0.8	59.1	0.1	76.7	0.4
Pm												
Sm	5.75	0.09	6.11	0.05	6.25	0.09	5.88	0.16	5.87	0.05	6.95	0.06
Eu	1.47	0.02	1.49	0.02	1.59	0.01	1.47	0.04	1.44	0.01	1.64	0.03
Gd	2.96	0.02	2.99	0.17	3.24	0.30	2.94	0.17	2.94	0.06	4.71	0.02
Tb	0.27	0.01	0.27	0.01	0.28	0.01	0.27	0.02	0.26	0.01	0.37	0.00
Dy	1.10	0.04	1.12	0.01	1.18	0.03	1.07	0.03	1.07	0.02	1.32	0.05
Ho	0.16	0.00	0.17	0.01	0.18	0.00	0.16	0.01	0.16	0.01	0.18	0.01
Er	0.33	0.02	0.35	0.02	0.38	0.01	0.33	0.01	0.32	0.02	0.41	0.01
Tm	0.047	0.002	0.046	0.002	0.053	0.002	0.045	0.002	0.045	0.004	0.052	0.006
Yb	0.25	0.01	0.26	0.00	0.30	0.01	0.25	0.01	0.25	0.02	0.28	0.01
Lu	0.038	0.000	0.039	0.000	0.045	0.006	0.037	0.002	0.038	0.004	0.041	0.000

FIELD	Lac de Gras		Lac de Gras		Lac de Gras		Lac de Gras		Lac de Gras		Lac de Gras	
LOCALITY	Anne		Finlay		Finlay		Don		Don		Koala West	
SAMPLE	HL-10-3	+/- 2σ	HL-11-1	+/- 2σ	HL-11-2	+/- 2σ	HL-12-1	+/- 2σ	HL-12-3	+/- 2σ	KOW-1	+/- 2σ
(ppm)												
Sc	12.8	0.1	18.6	0.6	17.9	0.9	11.9	0.6	11.1	0.5	19.0	0.2
V	115	3	102	3	58	0	69	0	62	0	115	1
Cr	1916**	0.1	1642**	2.2	1574**	0.6	2258**	1.4	2053**	1.1	1600**	1.1
Co	92.1		83.9		88.7		98.7		93.8		76.7	
Ni	1000**		700**		700**		1200**		1100**		980**	
Cu											90.7	0.1
Zn												
Ga	4.80	0.06	7.99	0.13	7.65	0.01	4.46	0.15	4.13	0.15	10.09	0.00
Rb	95.1	0.1	49.4	0.5	39.7	0.4	92.8	0.7	85.2	0.1	150.9	1.1
Sr	1540	17	1763	30	1605	9	409	2	614	1	1550	11
Y	5.05	0.02	12.02	0.22	11.59	0.14	4.44	0.05	4.24	0.16	15.46	0.19
Zr	45.8	0.4	105.0	0.6	101.8	0.8	43.8	0.2	42.5	0.5	133.5	0.5
Nb	207	1	332	0	320	2	169	1	167	2	584	3
Cs	1.55	0.00	2.07	0.01	2.15	0.02	1.99	0.01	1.92	0.10	2.73	0.01
Ba	2764	62	3034	10	2830	3	1468	54	1475	4	4127	6
Hf	1.10	0.02	2.45	0.07	2.36	0.01	1.04	0.01	1.02	0.02	3.07	0.12
Ta	11.9	0.1	17.2	0.1	16.3	0.1	8.7	0.1	8.7	0.0	27.4	0.1
Pb	7.46	0.24	11.74	0.30	10.98	0.21	8.41	0.34	10.60	0.13	19.56	0.04
Th	19.5	0.1	29.8	0.5	28.2	0.2	15.8	0.2	16.2	0.0	56.6	0.1
U	3.58	0.03	12.31	0.26	6.98	0.07	4.22	0.11	3.92	0.03	7.22	0.03
La	152	2	232	1	220	1	116	3	114	1	357	1
Ce	250	3	385	4	367	0	195	6	193	0	588	1
Pr	25.9	0.3	41.1	0.6	39.6	0.1	20.5	0.4	20.4	0.1	53.4	0.7
Nd	77.3	0.7	128.8	1.1	123.4	0.4	63.7	2.0	63.1	0.2	161.5	0.4
Pm												
Sm	6.96	0.27	12.90	0.34	12.44	0.11	6.32	0.20	6.22	0.06	15.86	0.18
Eu	1.63	0.01	3.09	0.07	2.98	0.03	1.37	0.04	1.38	0.03	3.86	0.08
Gd	4.49	0.17	8.62	0.00	8.25	0.25	4.04	0.11	4.05	0.14	8.59	0.23
Tb	0.36	0.00	0.76	0.00	0.72	0.05	0.32	0.00	0.31	0.01	0.82	0.00
Dy	1.33	0.01	2.97	0.06	2.87	0.10	1.17	0.01	1.16	0.08	3.42	0.04
Ho	0.18	0.01	0.44	0.01	0.43	0.00	0.16	0.01	0.15	0.01	0.52	0.01
Er	0.42	0.01	0.96	0.04	0.94	0.02	0.34	0.02	0.33	0.02	1.08	0.03
Tm	0.052	0.000	0.122	0.002	0.119	0.006	0.040	0.002	0.037	0.002	0.143	0.002
Yb	0.28	0.01	0.70	0.03	0.66	0.02	0.22	0.02	0.21	0.01	0.81	0.02
Lu	0.040	0.000	0.102	0.004	0.098	0.004	0.034	0.000	0.033	0.002	0.119	0.008

315

FIELD	Lac de Gras		Lac de Gras		Lac de Gras		Lac de Gras		Lac de Gras		Lac de Gras	
LOCALITY	Koala West		Leslie		Leslie		Leslie		Leslie		Mark	
SAMPLE	KOW-2	+/- 2σ	LES-B1	+/- 2σ	LES-1	+/- 2σ	LES-2	+/- 2σ	LES-3	+/- 2σ	KIA93-K136	+/- 2σ
(ppm)												
Sc	22.3	0.2	12.0	0.2	12.1	0.1	12.8	0.2	12.8	0.1	11.9	0.1
V	99	2	100	2	80	0	69	1	85	2	64	0
Cr	1900**	0.9	2326**	0.5	2200**	2.3	2200**	0.1	2300**	3.5	2545**	1.7
Co	76.2	0.3	97.8		86.2	1.5	81.4	0.7	89.1	1.9	94.5**	2.4
Ni	637**	8.0	1100**		1460**	0.1	1430**	3.5	1430**	1.8	1795**	9.0
Cu	106.6				51.5		64.4		58.9		38.7	
Zn	117.7				47.5		52.7		44.0		40.3	
Ga	10.29	0.06	3.59	0.13	3.59	0.19	3.37	0.07	3.47	0.15	2.67	0.09
Rb	80.4	1.1	68.1	0.1	102.3	1.7	103.6	1.0	66.7	1.5	8.9	0.2
Sr	1427	5	760	2	1066	3	1084	10	846	1	582	10
Y	16.63	0.04	4.38	0.21	4.70	0.03	5.51	0.04	4.79	0.03	3.94	0.01
Zr	166.8	0.7	38.9	0.7	35.8	0.2	45.2	0.3	42.3	0.2	28.0	0.3
Nb	710	10	200	1	196	0	196	2	210	1	208	1
Cs	1.49	0.03	0.72	0.04	1.50	0.00	1.40	0.06	1.00	0.07	0.24	0.01
Ba	2304	36	1697	5	2291	38	2348	46	2495	129	1501	12
Hf	3.83	0.02	0.91	0.04	0.85	0.01	1.04	0.03	0.96	0.10	0.73	0.03
Ta	35.4	0.5	10.8	0.0	10.8	0.1	10.7	0.1	11.8	0.1	10.3	0.1
Pb	19.05	0.17	3.68	0.01	3.86	0.06	4.61	0.16	4.56	0.40	8.52	0.04
Th	70.4	1.4	17.0	0.1	16.1	0.4	16.9	0.5	18.8	1.2	19.9	0.0
U	3.91	0.05	2.88	0.02	2.65	0.06	2.78	0.08	2.99	0.16	3.10	0.00
La	392	9	117	1	126	3	127	6	125	8	127	1
Ce	655	14	193	1	205	5	219	10	221	13	204	1
Pr	60.5	1.0	20.2	0.1	18.7	0.2	21.7	1.0	21.7	1.1	21.3	0.1
Nd	180.1	3.9	62.2	0.1	67.3	0.4	66.7	1.5	67.7	3.0	64.0	0.8
Pm												
Sm	17.16	0.25	6.14	0.11	6.47	0.05	6.57	0.16	6.78	0.35	5.98	0.10
Eu	3.88	0.08	1.43	0.02	1.68	0.01	1.53	0.08	1.53	0.08	1.44	0.02
Gd	9.02	0.01	3.98	0.10	4.12	0.29	4.15	0.04	4.19	0.21	2.86	0.10
Tb	0.86	0.04	0.32	0.02	0.32	0.00	0.34	0.01	0.33	0.00	0.24	0.02
Dy	3.68	0.06	1.17	0.02	1.18	0.03	1.35	0.04	1.24	0.02	0.96	0.06
Ho	0.56	0.00	0.16	0.01	0.16	0.00	0.19	0.00	0.17	0.01	0.14	0.00
Er	1.17	0.04	0.35	0.03	0.35	0.01	0.43	0.03	0.35	0.02	0.27	0.01
Tm	0.160	0.000	0.039	0.002	0.042	0.002	0.056	0.002	0.044	0.000	0.035	0.000
Yb	0.87	0.02	0.23	0.01	0.24	0.02	0.31	0.01	0.24	0.02	0.19	0.01
Lu	0.129	0.000	0.034	0.002	0.033	0.002	0.049	0.000	0.036	0.002	0.028	0.002

316

FIELD	Lac de Gras		Lac de Gras		Lac de Gras		Lac de Gras		Lac de Gras		Lac de Gras	
LOCALITY	Misery		Misery		Misery East		Misery East		Nicholas Bay		Pigeon	
SAMPLE (ppm)	MIS-1	+/- 2σ	MIS-2	+/- 2σ	MSE-1	+/- 2σ	MSE-2	+/- 2σ	NCB-1	+/- 2σ	PDG-1	+/- 2σ
Sc	11.8	0.0	9.9	0.2	12.3	0.2	11.4	0.1	14.2	0.1	10.4	0.1
V	49	0	181	3	41	1	32	0	62	0	59	1
Cr	2100**		1700**		1800**		1600**		1533**		1200**	
Co	79.9	2.2	66.4	1.2	79.3	1.0	66.2	0.1	70.9	0.4	77.9	4.2
Ni	1560**		1200**		1620**		1250**		1128**		1500**	
Cu	62.5	0.7	54.1	0.8	47.5	0.3	36.9	0.7	81.2	0.1	44.4	1.1
Zn	51.8	7.6	41.5	6.4	48.3	0.7	44.9	3.5	44.5	0.2	43.1	2.3
Ga	5.35	0.01	3.45	0.05	4.31	0.18	4.46	0.13	6.60	0.02	5.68	0.12
Rb	56.9	0.3	27.9	0.2	99.9	1.0	108.2	2.6	161.5	3.5	134.8	3.7
Sr	645	4	875	8	1072	4	877	7	1266	13	639	18
Y	5.72	0.01	4.73	0.07	6.50	0.04	5.90	0.13	7.44	0.07	5.76	0.13
Zr	43.5	0.6	36.7	0.4	58.4	0.2	52.7	0.3	54.3	0.3	40.2	1.2
Nb	165	1	171	0	216	0	202	1	282	1	125	3
Cs	1.46	0.04	0.91	0.00	1.37	0.02	1.46	0.01	2.75	0.02	2.67	0.02
Ba	556	2	1499	20	3183	8	2679	19	3849	14	1499	3
Hf	1.08	0.03	0.88	0.03	1.34	0.03	1.24	0.04	1.31	0.06	1.02	0.02
Ta	9.2	0.1	7.7	0.0	8.3	0.1	7.4	0.0	10.8	0.2	6.5	0.0
Pb	8.99	0.16	5.45	0.03	7.85	0.07	7.44	0.10	8.92	0.26	8.09	0.05
Th	17.5	0.3	14.8	0.0	18.8	0.2	17.5	0.4	23.3	0.3	11.8	0.1
U	3.21	0.06	2.55	0.01	3.38	0.07	3.14	0.08	3.41	0.00	2.27	0.02
La	115	0	104	0	163	2	144	1	197	2	88	1
Ce	187	1	165	0	304	1	265	3	332	0	142	1
Pr	20.1	0.1	17.2	0.1	27.6	0.3	24.0	0.1	26.2	0.2	12.5	0.0
Nd	62.8	0.0	53.0	0.6	84.0	0.9	72.3	1.0	89.8	1.2	45.6	0.4
Pm												
Sm	6.50	0.04	5.47	0.06	8.04	0.15	6.90	0.06	7.89	0.11	4.65	0.05
Eu	1.53	0.02	1.39	0.01	2.00	0.07	1.73	0.02	2.18	0.02	1.25	0.01
Gd	3.51	0.16	3.00	0.20	3.82	0.36	3.30	0.21	5.23	0.04	3.30	0.08
Tb	0.32	0.01	0.27	0.00	0.35	0.00	0.31	0.00	0.42	0.04	0.29	0.00
Dy	1.29	0.02	1.08	0.03	1.47	0.03	1.32	0.03	1.68	0.12	1.23	0.01
Ho	0.20	0.01	0.16	0.01	0.22	0.01	0.21	0.00	0.26	0.01	0.20	0.00
Er	0.40	0.01	0.34	0.01	0.46	0.00	0.44	0.02	0.61	0.02	0.48	0.02
Tm	0.055	0.002	0.045	0.002	0.066	0.002	0.062	0.004	0.085	0.004	0.068	0.000
Yb	0.31	0.01	0.25	0.01	0.37	0.00	0.34	0.01	0.49	0.01	0.40	0.01
Lu	0.043	0.004	0.034	0.004	0.050	0.000	0.056	0.000	0.077	0.006	0.065	0.004

317

FIELD	Lac de Gras		Lac de Gras		Lac de Gras		Lac de Gras		Lac de Gras		Lac de Gras	
LOCALITY	Pigeon		Porpoise		Porpoise		Porpoise		Rat		Rat	
SAMPLE	PDG-2	+/-2σ	PRP-1	+/-2σ	PRP-2	+/-2σ	PRP-3	+/-2σ	RAT-1	+/-2σ	RAT-2	+/-2σ
(ppm)												
Sc	11.9	0.3	14.5	0.2	15.7	0.0	15.8	0.4	11.6	0.1	10.4	0.2
V	82	2	46	0	35	1	72	1	123	2	144	4
Cr	1500**		1100**		1500**		1200**		1900**		941	21
Co	75.9	2.4	49.5	0.4	62.2	1.1	64.5	1.5	91.6	2.6	58.3	1.2
Ni	1410**		579**		770**		842**		1300**		889	15
Cu	53.1	2.6	56.5	0.9	70.6	2.7	79.0	2.6	113.1	4.0	53.9	0.9
Zn	43.1	3.2	51.8	5.0	56.1	2.8	54.3	2.2	54.0	1.1	26.4	8.6
Ga	5.59	0.20	6.70	0.10	8.11	0.20	7.78	0.10	4.24	0.15	7.08	0.05
Rb	147.6	5.6	147.6	0.3	146.0	2.5	125.0	2.2	44.3	0.7	210.5	0.6
Sr	663	19	1809	9	1542	53	1289	37	955	22	508	5
Y	6.97	0.12	10.52	0.10	10.79	0.42	10.44	0.29	4.65	0.00	11.35	0.15
Zr	51.5	1.1	89.8	1.3	91.1	3.0	98.5	2.1	36.5	0.0	138.5	5.9
Nb	134	2	270	4	368	7	408	8	199	2	155	0
Cs	2.48	0.06	1.90	0.01	2.35	0.05	3.47	0.03	0.47	0.02	2.09	0.07
Ba	1558	14	3233	13	1652	19	2868	91	2067	70	1153	15
Hf	1.25	0.05	2.11	0.03	2.36	0.09	2.20	0.04	0.90	0.02	3.65	0.03
Ta	6.7	0.0	16.4	0.2	19.1	0.3	18.1	0.1	13.2	0.1	7.6	0.1
Pb	7.62	0.13	19.64	0.05	21.25	0.46	27.98	1.16	6.26	0.13	10.26	0.16
Th	12.5	0.4	33.0	0.0	32.9	0.4	32.7	1.4	13.7	0.3	16.2	0.0
U	2.48	0.08	5.72	0.02	5.77	0.11	6.32	0.14	2.18	0.02	2.56	0.01
La	107	2	169	1	278	1	273	13	111	2	68	1
Ce	167	2	348	2	461	6	438	24	178	2	114	1
Pr	17.2	0.1	32.5	0.3	37.1	0.2	42.1	1.2	15.9	0.2	12.3	0.0
Nd	52.1	0.3	100.1	0.1	133.0	2.1	128.8	3.0	56.8	0.8	39.1	0.3
Pm												
Sm	5.22	0.07	10.15	0.16	12.82	0.25	12.51	0.25	5.43	0.09	4.78	0.12
Eu	1.26	0.03	2.56	0.02	2.95	0.03	2.83	0.02	1.42	0.02	1.00	0.03
Gd	3.46	0.17	5.35	0.19	8.24	0.23	7.78	0.14	3.37	0.09	3.13	0.02
Tb	0.33	0.01	0.54	0.01	0.68	0.02	0.66	0.01	0.29	0.01	0.41	0.00
Dy	1.45	0.04	2.28	0.06	2.60	0.07	2.53	0.05	1.12	0.04	2.09	0.04
Ho	0.24	0.01	0.35	0.01	0.37	0.01	0.36	0.03	0.16	0.00	0.39	0.01
Er	0.60	0.01	0.73	0.02	0.83	0.02	0.81	0.03	0.36	0.01	0.97	0.02
Tm	0.088	0.008	0.100	0.004	0.107	0.006	0.102	0.006	0.045	0.002	0.165	0.004
Yb	0.52	0.01	0.54	0.01	0.59	0.03	0.58	0.02	0.26	0.01	0.96	0.03
Lu	0.084	0.002	0.082	0.002	0.087	0.002	0.088	0.000	0.038	0.002	0.149	0.010

FIELD	Lac de Gras		Lac de Gras		Lac de Gras		Lac de Gras		Lac de Gras		Lac de Gras	
LOCALITY	Rat		Rat		Rattler		Rattler		Rattler		Roger	
SAMPLE	RAT-3	+/-2σ	RAT-4	+/-2σ	RTL-1	+/-2σ	RTL-2	+/-2σ	RTL-3	+/-2σ	ROG-1	+/-2σ
(ppm)												
Sc	12.1	0.5	8.7	0.3	13.7	0.0	17.1	0.9	12.3	0.3	23.1	0.1
V	125	5	103	1	95	1	156	5	94	0	62	0
Cr	1800**		660**		2300**		3000**		2100**		1400**	
Co	91.3	1.0	43.9	0.7	88.7	0.8	86.1	4.3	81.2	1.1	62.8	2.3
Ni	1250**		658**		1380**		1250**		1440**		771**	
Cu	127.0	2.6	47.9	0.0	84.6	0.3	140.1	4.8	84.4	0.4	66.4	2.4
Zn	58.3	1.9	51.7	0.2	51.5	0.2	58.7	1.5	56.8	2.2	74.3	1.6
Ga	4.31	0.16	5.79	0.05	4.33	0.17	5.64	0.24	4.08	0.06	11.30	0.24
Rb	43.6	1.0	85.0	1.3	92.6	3.4	99.8	4.1	54.9	0.4	121.9	6.7
Sr	971	27	483	6	1069	38	1388	43	1188	2	1573	0
Y	5.25	0.09	9.57	0.02	5.13	0.06	6.41	0.16	5.05	0.03	15.43	0.23
Zr	45.9	0.6	58.3	0.7	44.9	1.3	74.0	1.6	72.1	0.5	130.2	1.4
Nb	224	0	80	1	238	4	323	6	223	1	647	1
Cs	0.48	0.02	2.36	0.04	1.49	0.03	1.66	0.02	0.49	0.01	5.29	0.11
Ba	2401	100	764	11	3362	95	2845	14	2090	33	5802	139
Hf	1.12	0.03	1.53	0.04	1.03	0.02	1.46	0.05	1.22	0.01	2.89	0.06
Ta	15.1	0.4	5.1	0.1	15.7	0.3	22.8	0.4	15.5	0.1	29.5	0.8
Pb	5.84	0.09	7.05	0.03	6.55	0.11	10.21	0.07	12.57	0.07	17.25	0.28
Th	15.6	0.4	5.7	0.1	17.5	0.2	26.0	0.5	19.3	0.1	59.2	0.4
U	2.47	0.04	1.63	0.05	2.96	0.04	4.12	0.12	3.37	0.02	9.02	0.03
La	120	5	52	1	141	4	206	2	135	1	472	9
Ce	208	5	86	2	261	3	349	15	258	6	746	16
Pr	19.9	0.4	9.2	0.2	21.4	0.1	34.3	1.3	23.9	0.4	60.5	0.7
Nd	59.8	0.5	29.2	0.1	76.5	0.8	104.3	4.5	72.8	1.2	213.6	2.9
Pm												
Sm	5.71	0.05	3.58	0.10	7.28	0.08	9.82	0.37	6.91	0.08	20.03	0.40
Eu	1.33	0.02	0.76	0.01	1.98	0.05	2.18	0.14	1.65	0.02	5.03	0.07
Gd	3.76	0.12	2.77	0.05	4.58	0.03	6.04	0.34	3.19	0.14	12.56	0.53
Tb	0.32	0.01	0.33	0.00	0.35	0.02	0.47	0.00	0.30	0.01	1.02	0.01
Dy	1.25	0.02	1.69	0.06	1.34	0.01	1.72	0.04	1.20	0.01	3.85	0.06
Ho	0.18	0.00	0.32	0.00	0.18	0.01	0.23	0.01	0.17	0.00	0.54	0.01
Er	0.40	0.01	0.83	0.02	0.41	0.01	0.49	0.04	0.35	0.01	1.20	0.04
Tm	0.053	0.000	0.137	0.004	0.053	0.012	0.055	0.002	0.047	0.002	0.157	0.010
Yb	0.30	0.00	0.81	0.03	0.28	0.01	0.32	0.01	0.26	0.01	0.84	0.03
Lu	0.044	0.002	0.130	0.000	0.040	0.006	0.049	0.002	0.039	0.004	0.129	0.004

319

FIELD	Lac de Gras		Lac de Gras		Lac de Gras		Lac de Gras		Lac de Gras		Lac de Gras	
LOCALITY	Roger		Roger		Wolverine		A21		A21		A25	
SAMPLE	ROG-2	+/-2σ	ROG-3	+/-2σ	WOL-1	+/-2σ	A21-1-1	+/-2σ	A21-1-2	+/-2σ	A25-3-1	+/-2σ
(ppm)												
Sc	26.1	0.1	22.1	0.5	9.2	0.2	10.6	1.3	10.2	0.7	23.1	1.1
V	108	0	75	1	81	0	92	3	73	1	169	2
Cr	1500**		1600**		1315	12	1095*		1095*		503*	
Co	64.4	0.2	62.4	0.2	90.3	2.1	63.6	0.8	77.6	1.0	54.9	0.5
Ni	717**		734**		1622	19	1186	15	1441**	2	276**	
Cu	66.6	0.5	71.0	1.4	57.5	0.3	28.0	0.6	24.9	0.6	87.7	0.7
Zn	59.3	0.5	59.6	1.2	50.9	7.6	57.9	0.9	61.3	2.0	87.7	8.8
Ga	8.79	0.21	8.05	0.18	5.15	0.24	7.17	0.41	6.98	0.25	11.05	0.43
Rb	10.9	0.2	54.7	0.2	74.3	1.5	60.1	0.2	44.8	0.2	185.8	4.9
Sr	1868	49	1330	5	536	1	333	4	245	1	2871	49
Y	16.26	0.47	15.78	0.17	5.36	0.05	9.30	0.08	7.89	0.05	20.29	0.43
Zr	135.0	2.3	130.4	0.4	36.6	0.1	56.9	2.2	40.6	0.3	141.7	5.4
Nb	668	12	638	1	102	1	75	1	70	1	497	10
Cs	0.63	0.02	2.91	0.02	1.57	0.07	2.79	0.04	2.07	0.05	3.54	0.13
Ba	7883	132	7329	7	726	2	699	27	443	3	6229	152
Hf	2.91	0.05	2.84	0.02	0.88	0.03	1.46	0.12	1.09	0.05	3.20	0.06
Ta	29.2	0.6	29.2	0.1	6.2	0.2	4.1	0.1	3.7	0.0	24.5	0.5
Pb	19.97	0.20	18.66	0.24	5.85	0.18	11.68	0.45	8.27	0.06	29.42	0.21
Th	60.2	0.3	59.8	0.7	8.6	0.2	7.6	0.2	7.6	0.2	46.0	0.1
U	8.98	0.13	8.13	0.12	1.93	0.06	3.04	0.09	3.05	0.03	8.97	0.21
La	480	3	482	4	69	1	52	3	51	0	374	6
Ce	759	2	755	3	115	3	86	4	88	0	684	8
Pr	72.9	0.6	72.6	1.2	11.9	0.3	9.1	0.3	9.1	0.1	59.9	0.3
Nd	217.8	0.4	215.6	4.0	38.5	0.9	29.6	1.4	29.5	0.6	187.0	1.7
Pm												
Sm	20.64	0.06	20.19	0.43	4.21	0.03	3.75	0.14	3.54	0.04	18.69	0.23
Eu	4.70	0.13	4.64	0.11	0.97	0.02	0.89	0.02	0.82	0.02	4.64	0.06
Gd	12.91	1.33	13.11	0.17	2.66	0.15	3.07	0.03	2.71	0.09	10.88	0.01
Tb	1.05	0.09	1.06	0.00	0.26	0.02	0.35	0.00	0.29	0.01	1.01	0.03
Dy	3.95	0.13	3.91	0.02	1.16	0.02	1.71	0.06	1.44	0.03	4.25	0.08
Ho	0.56	0.00	0.55	0.01	0.18	0.00	0.32	0.00	0.26	0.01	0.65	0.01
Er	1.21	0.02	1.18	0.02	0.43	0.00	0.80	0.05	0.68	0.03	1.53	0.02
Tm	0.151	0.006	0.147	0.004	0.063	0.008	0.124	0.002	0.103	0.014	0.210	0.004
Yb	0.83	0.02	0.82	0.02	0.37	0.01	0.78	0.06	0.66	0.01	1.17	0.03
Lu	0.125	0.006	0.126	0.006	0.056	0.002	0.124	0.014	0.104	0.002	0.181	0.002

FIELD	Lac de Gras		Lac de Gras		Lac de Gras		Lac de Gras		Lac de Gras		Lac de Gras	
LOCALITY	A25		A164		A164		A164		ABZ		ABZ	
SAMPLE	A25-3-2	+/- 2σ	A164-11-1	+/- 2σ	A164-11-2	+/- 2σ	A164-11-3	+/- 2σ	ABZ-7a-1	+/- 2σ	ABZ-7a-2	+/- 2σ
(ppm)												
Sc	21.0	1.6	8.0	0.8	10.9	0.3	11.8	0.8	16.1	0.3	13.7	0.3
V	174	7	61	5	37	1	60	4	166	6	136	0
Cr	691*		1368*		1847*		1779*		880*		754*	
Co	51.3	1.6	78.2	2.5	89.7	0.5	84.5	2.4	57.4	0.2	57.9	0.9
Ni	333**		1481	60	1737	26	1589	32	538**		629**	
Cu	89.9	3.8	26.1	1.0	37.1	0.2	38.9	1.0	69.0	0.3	52.8	0.6
Zn	109.9	2.9	45.5	2.1	50.3	0.9	43.5	0.9	77.5	1.8	64.9	5.4
Ga	11.06	0.35	3.87	0.20	3.66	0.30	2.79	0.01	9.39	0.08	8.72	0.06
Rb	237.7	4.3	24.4	1.0	80.6	2.5	51.4	1.0	154.2	1.5	105.1	2.2
Sr	2224	17	199	7	350	14	449	5	1703	13	744	19
Y	19.39	0.19	5.17	0.08	4.03	0.11	3.92	0.08	14.46	0.51	12.81	0.30
Zr	122.1	0.1	30.6	0.6	28.5	0.8	38.1	0.3	94.7	1.6	94.1	1.9
Nb	414	8	72	0	99	2	108	0	251	2	203	5
Cs	5.66	0.01	1.38	0.03	1.31	0.06	1.20	0.03	3.26	0.06	3.52	0.06
Ba	3117	36	410	4	1036	7	1108	3	1381	14	2115	53
Hf	2.81	0.10	0.74	0.01	0.71	0.02	0.87	0.03	2.18	0.07	2.19	0.02
Ta	19.2	0.4	3.9	0.1	5.3	0.0	5.6	0.1	13.4	0.3	10.6	0.2
Pb	26.32	0.44	5.94	0.02	4.85	0.01	5.51	0.16	14.28	0.04	13.50	0.22
Th	37.2	0.2	7.2	0.2	9.1	0.2	9.3	0.1	22.7	0.2	19.0	0.2
U	8.14	0.05	2.51	0.08	1.73	0.06	2.57	0.08	3.67	0.05	4.06	0.16
La	353	7	49	0	64	1	67	0	178	4	144	3
Ce	627	17	81	1	106	4	108	1	291	7	235	8
Pr	53.8	1.3	8.2	0.0	10.8	0.5	10.9	0.3	30.3	0.6	24.5	1.3
Nd	167.7	4.1	26.2	0.5	34.3	0.7	34.7	0.2	97.5	2.2	78.9	4.0
Pm												
Sm	16.51	0.43	2.91	0.02	3.61	0.10	3.61	0.03	10.59	0.09	8.55	0.20
Eu	3.96	0.06	0.69	0.04	0.95	0.03	0.98	0.02	2.50	0.07	2.07	0.06
Gd	9.55	0.53	2.15	0.18	2.60	0.27	2.51	0.14	6.70	0.23	5.46	0.12
Tb	0.92	0.01	0.22	0.01	0.23	0.01	0.24	0.01	0.69	0.04	0.55	0.02
Dy	3.96	0.14	1.00	0.03	0.89	0.03	0.91	0.06	2.91	0.04	2.47	0.08
Ho	0.63	0.00	0.18	0.00	0.14	0.00	0.14	0.00	0.47	0.03	0.41	0.02
Er	1.47	0.02	0.43	0.01	0.31	0.01	0.31	0.01	1.13	0.08	0.98	0.02
Tm	0.209	0.006	0.061	0.002	0.044	0.002	0.042	0.004	0.167	0.008	0.153	0.014
Yb	1.21	0.03	0.39	0.00	0.25	0.01	0.27	0.02	0.94	0.01	0.92	0.00
Lu	0.190	0.006	0.061	0.002	0.040	0.006	0.038	0.004	0.142	0.002	0.146	0.000

FIELD	Lac de Gras		Lac de Gras		Lac de Gras		Lac de Gras		Lac de Gras		Lac de Gras	
LOCALITY	C13		C13		DD39		DD39		Tli Kwi Cho		Tli Kwi Cho	
SAMPLE	C13-7-1	+/- 2σ	C13-7-2	+/- 2σ	DD39-5-1	+/- 2σ	DD39-5-2	+/- 2σ	DO27-23-1	+/- 2σ	DO27-23-2	+/- 2σ
(ppm)												
Sc	12.1	0.7	11.0	0.3	15.7	0.4	11.6	0.7	5.5	0.0	10.3	0.4
V	85	3	90	5	94	1	84	6	36	0	64	2
Cr	1257*		1194*		1822*		1948*		880*		1194*	
Co	79.4	1.1	80.7	2.5	102.1	2.1	89.2	5.1	70.4	2.3	62.1	1.5
Ni	1282**		1306**		1463**		1483**		1372**		987**	
Cu	38.8	1.5	37.2	0.3	71.4	0.5	67.1	3.0	18.1	0.5	43.1	1.0
Zn	46.8	5.9	47.6	1.8	51.3	0.3	48.2	2.8	42.0	0.2	44.1	1.3
Ga	6.06	0.14	5.49	0.14	4.49	0.31	3.12	0.00	4.29	0.06	5.76	0.18
Rb	114.3	2.0	109.4	0.4	31.3	0.4	6.6	0.3	37.5	1.3	100.7	2.0
Sr	639	1	616	9	698	23	436	17	308	8	980	13
Y	6.92	0.04	6.97	0.03	5.70	0.14	4.76	0.16	3.46	0.09	5.59	0.09
Zr	49.9	0.4	54.5	0.2	55.8	0.5	41.7	1.7	22.8	0.8	46.5	1.2
Nb	146	0	131	1	232	2	222	2	60	0	202	1
Cs	1.66	0.02	1.75	0.07	0.82	0.01	0.48	0.01	1.50	0.05	1.53	0.01
Ba	600	23	616	3	1046	34	405	18	379	4	1649	9
Hf	1.11	0.03	1.31	0.03	1.14	0.02	0.89	0.02	0.60	0.02	1.16	0.02
Ta	7.3	0.0	6.6	0.0	11.7	0.1	10.3	0.1	2.7	0.0	10.6	0.2
Pb	8.64	0.16	8.79	0.08	10.61	0.25	9.48	0.20	6.69	0.04	11.30	0.12
Th	12.8	0.2	12.3	0.1	20.2	0.6	17.7	0.4	7.4	0.1	19.2	0.4
U	2.73	0.05	2.68	0.04	3.80	0.15	3.51	0.09	1.79	0.02	3.73	0.08
La	100	2	96	0	160	8	152	6	46	0	132	1
Ce	171	7	162	1	262	14	243	7	76	0	215	3
Pr	18.0	0.7	16.9	0.3	26.5	1.6	25.5	0.5	7.8	0.1	22.9	0.4
Nd	57.8	1.4	54.3	0.1	81.7	4.7	76.0	1.2	23.9	0.2	69.7	1.1
Pm												
Sm	6.01	0.15	5.66	0.16	7.62	0.26	7.11	0.29	2.59	0.02	7.04	0.16
Eu	1.35	0.05	1.24	0.02	1.73	0.10	1.56	0.06	0.59	0.01	1.65	0.03
Gd	3.41	0.10	3.32	0.05	4.19	0.16	3.43	0.23	1.49	0.10	3.68	0.21
Tb	0.33	0.01	0.33	0.02	0.37	0.03	0.29	0.02	0.16	0.01	0.34	0.01
Dy	1.38	0.01	1.43	0.04	1.38	0.04	1.22	0.04	0.71	0.05	1.35	0.05
Ho	0.21	0.01	0.23	0.01	0.19	0.00	0.17	0.01	0.12	0.00	0.20	0.00
Er	0.51	0.02	0.57	0.02	0.44	0.03	0.35	0.01	0.28	0.01	0.40	0.01
Tm	0.074	0.012	0.082	0.002	0.055	0.002	0.047	0.004	0.045	0.004	0.054	0.004
Yb	0.42	0.01	0.52	0.03	0.30	0.02	0.25	0.01	0.25	0.02	0.29	0.00
Lu	0.063	0.000	0.080	0.004	0.047	0.002	0.038	0.002	0.041	0.002	0.044	0.002

322

FIELD	Lac de Gras		Lac de Gras		Lac de Gras		Lac de Gras		Lac de Gras		Lac de Gras	
LOCALITY	T19		T19		T21		T21		T34		T34	
SAMPLE	T19-1-1	+/- 2σ	T19-1-2	+/- 2σ	T21-1-1	+/- 2σ	T21-1-2	+/- 2σ	T34-1-1	+/- 2σ	T34-1-2	+/- 2σ
(ppm)												
Sc	15.1	0.6	20.9	1.0	18.5	0.2	18.4	0.3	20.3	1.8	22.4	0.6
V	145	6	133	2	21	1	24	0	177	7	140	6
Cr	943*		880*		1257*		1320*		880*		943*	
Co	54.9	1.1	64.2	1.6	83.1	2.6	82.4	1.1	60.8	2.7	64.4	2.0
Ni	586**		539**		977**		980**		479**		495**	
Cu	77.5	0.3	66.8	0.6	53.3	1.6	203.8	2.0	78.3	1.9	85.5	4.1
Zn	57.9	0.2	62.2	2.0	124.8	1.9	53.7	1.2	73.6	3.0	62.3	4.5
Ga	7.59	0.16	9.69	0.37	7.20	0.10	7.28	0.24	8.95	0.20	9.24	0.27
Rb	225.4	2.4	271.7	1.2	126.1	3.3	130.6	3.4	161.9	2.4	149.1	4.1
Sr	1631	7	2573	57	821	19	2252	50	2462	14	2557	6
Y	12.73	0.15	15.13	0.56	11.54	0.02	11.70	0.15	12.13	0.14	13.20	0.04
Zr	79.0	0.9	99.7	3.0	75.9	0.2	81.3	3.0	89.6	2.7	104.1	1.4
Nb	358	0	467	6	381	1	624	24	301	5	342	0
Cs	4.50	0.05	4.11	0.05	2.97	0.04	1.74	0.08	1.46	0.05	1.63	0.00
Ba	3131	102	6364	143	8987	432	6276	34	4634	134	3514	47
Hf	1.95	0.01	2.27	0.09	1.78	0.07	1.83	0.07	1.96	0.13	2.18	0.05
Ta	15.8	0.0	17.7	0.2	16.4	0.2	16.4	0.0	14.6	0.4	17.0	0.4
Pb	14.49	0.07	22.19	0.35	2.64	0.13	4.20	0.10	17.09	0.29	15.35	0.52
Th	26.3	0.1	39.8	0.0	32.3	1.1	30.3	0.4	28.0	0.5	31.3	0.5
U	3.96	0.02	7.77	0.02	2.98	0.03	5.56	0.15	5.33	0.13	5.86	0.11
La	246	5	309	1	213	10	195	0	227	6	248	2
Ce	403	7	485	124	320	19	288	2	374	8	412	1
Pr	37.5	0.4	42.9	0.0	31.2	1.4	27.9	0.4	39.6	0.8	43.7	0.7
Nd	110.2	1.6	130.3	1.5	96.0	2.1	86.8	0.3	126.4	4.8	140.1	2.2
Pm												
Sm	11.25	0.22	13.13	0.13	9.97	0.48	9.44	0.12	12.47	0.47	13.81	0.13
Eu	2.90	0.07	3.58	0.10	3.15	0.18	2.80	0.08	3.16	0.11	3.42	0.10
Gd	6.44	0.32	8.44	0.93	7.02	0.35	6.43	0.42	7.29	0.45	8.18	0.03
Tb	0.65	0.01	0.79	0.04	0.62	0.00	0.59	0.02	0.66	0.03	0.71	0.01
Dy	2.88	0.10	3.34	0.04	2.55	0.06	2.55	0.05	2.69	0.08	2.87	0.09
Ho	0.45	0.02	0.50	0.00	0.39	0.00	0.39	0.01	0.42	0.01	0.45	0.02
Er	0.99	0.01	1.16	0.01	0.91	0.08	0.90	0.01	0.98	0.02	1.06	0.01
Tm	0.134	0.000	0.160	0.008	0.122	0.010	0.124	0.004	0.142	0.004	0.150	0.008
Yb	0.72	0.01	0.88	0.03	0.70	0.02	0.70	0.02	0.81	0.04	0.86	0.03
Lu	0.107	0.008	0.133	0.002	0.105	0.012	0.104	0.008	0.123	0.008	0.137	0.006

323

FIELD	Lac de Gras		Lac de Gras		Lac de Gras		Lac de Gras		Lac de Gras		Lac de Gras	
LOCALITY	T35		T35		T35		T36		T146		T146	
SAMPLE	T35-1-1	+/- 2σ	T35-1-2	+/- 2σ	T35-1-1	+/- 2σ	T36-2-1	+/- 2σ	T146-1-1	+/- 2σ	T146-1-2	+/- 2σ
(ppm)												
Sc	23.7	2.3	17.6	0.7	22.6	0.0	21.4	1.5	17.4	1.3	21.3	1.7
V	187	11	130	2	62	0	83	3	115	5	186	9
Cr	1005*		1131*		1257*		1068*		566*		628*	
Co	74.7	1.9	61.6	0.1	76.9	2.4	67.2	1.1	44.3	0.2	61.2	0.0
Ni	601**		601**		842**		643**		355**		563**	
Cu	91.5	2.0	78.5	0.7	71.3	1.1	70.9	0.7	54.0	1.4	64.2	0.4
Zn	69.6	2.0	56.7	1.2	55.3	0.7	59.2	0.6	49.6	1.9	65.5	2.3
Ga	10.55	0.62	7.29	0.16	10.48	0.22	10.08	0.32	11.58	0.00	11.94	0.32
Rb	153.2	5.6	107.4	0.8	155.5	1.8	194.5	2.3	293.0	12.0	595.5	5.5
Sr	2144	73	857	1	811	29	1463	9	3284	83	2921	17
Y	13.81	0.58	11.71	0.31	15.35	0.58	16.03	0.07	14.52	0.92	16.10	0.14
Zr	105.4	3.1	89.0	0.4	117.1	1.6	113.4	0.1	105.0	2.7	125.2	0.9
Nb	355	3	303	2	447	5	437	5	431	9	509	2
Cs	2.50	0.06	1.68	0.02	2.26	0.04	2.45	0.07	4.09	0.02	20.70	0.13
Ba	3435	82	3149	76	1884	27	2339	33	4569	93	10232	635
Hf	2.21	0.04	1.90	0.05	2.63	0.03	2.54	0.06	2.40	0.05	2.79	0.10
Ta	17.5	0.1	15.2	0.3	21.4	0.3	19.3	0.6	19.2	0.2	22.8	0.2
Pb	13.57	0.11	12.20	0.06	9.26	0.03	11.27	0.12	28.65	0.06	34.85	0.40
Th	32.7	0.1	28.9	0.1	47.8	0.1	43.9	0.2	43.3	0.2	51.2	1.3
U	6.03	0.13	4.90	0.01	3.80	0.06	4.18	0.01	8.28	0.02	8.56	0.07
La	272	3	232	3	295	5	318	5	320	5	380	15
Ce	444	3	423	6	573	9	585	8	584	18	706	26
Pr	47.0	0.2	42.6	0.3	47.8	0.8	48.7	0.0	49.4	1.6	58.8	1.4
Nd	150.0	0.8	130.7	0.2	146.3	0.5	148.2	0.5	151.9	3.6	178.7	6.2
Pm												
Sm	14.68	0.18	12.88	0.08	14.52	0.04	14.54	0.21	14.75	0.16	17.38	1.15
Eu	3.64	0.06	3.17	0.02	3.46	0.05	3.47	0.05	3.68	0.10	4.69	0.31
Gd	8.76	0.78	6.41	0.50	8.62	0.33	8.72	0.68	8.78	0.21	10.28	1.13
Tb	0.76	0.01	0.61	0.03	0.86	0.01	0.85	0.03	0.80	0.03	0.92	0.06
Dy	3.05	0.13	2.61	0.00	3.54	0.04	3.51	0.12	3.22	0.10	3.69	0.04
Ho	0.46	0.01	0.42	0.00	0.55	0.01	0.54	0.01	0.46	0.02	0.54	0.02
Er	1.12	0.04	0.95	0.03	1.22	0.04	1.23	0.03	1.03	0.03	1.19	0.02
Tm	0.155	0.002	0.141	0.002	0.167	0.010	0.160	0.002	0.131	0.006	0.155	0.012
Yb	0.92	0.03	0.80	0.01	0.89	0.01	0.92	0.02	0.71	0.03	0.84	0.03
Lu	0.140	0.000	0.125	0.006	0.134	0.010	0.135	0.004	0.103	0.002	0.125	0.004

FIELD	Lac de Gras		Lac de Gras		Lac de Gras		Lac de Gras		South-West Slave		South-East Slave	
LOCALITY	T237		T237		TR107		TR107		Drybones		Gahcho Kue	
SAMPLE	T237-1-1	+/- 2σ	T237-1-2	+/- 2σ	TR107-3-1	+/- 2σ	TR107-3-2	+/- 2σ	DRY-1	+/- 2σ	KDY-1	+/- 2σ
(ppm)												
Sc	25.7	1.2	26.8	1.6	24.0	1.4	23.4	1.3	9.6	1.1	10.2	0.7
V	171	0	189	3	146	7	130	2	58	4	46	3
Cr	943*		1257*		880*		754*		582	37	1238*	
Co	76.5	0.3	80.9	0.4	68.4	0.9	65.3	1.7	71.7	1.3	74.3	3.8
Ni	620**		666**		603**		566**		1347	28	1249**	
Cu	74.6	0.9	110.3	3.0	75.2	0.3	73.7	1.5	3.6	0.1	55.4	1.5
Zn	73.8	0.6	76.9	0.6	69.8	1.4	76.7	1.1	46.2	0.5	51.9	0.1
Ga	10.95	0.13	10.80	0.51	11.14	0.09	11.09	0.50	5.75	0.25	6.47	0.32
Rb	109.9	0.3	125.6	0.3	151.2	0.2	179.6	1.6	26.8	0.2	77.1	1.4
Sr	2989	32	2469	19	2713	38	2239	58	138	2	719	7
Y	18.90	0.45	18.84	0.06	16.59	0.43	15.71	0.11	5.09	0.02	8.34	0.10
Zr	129.6	0.9	122.9	0.9	133.1	5.1	128.7	4.1	143.8	1.1	87.5	0.8
Nb	1328	8	560	7	467	9	429	1	83	1	137	0
Cs	2.32	0.02	2.19	0.03	3.14	0.12	3.59	0.13	1.78	0.04	0.81	0.02
Ba	16562	723	2451	35	7060	160	6126	74	260	6	1610	22
Hf	2.82	0.07	2.88	0.05	2.92	0.05	2.84	0.05	3.53	0.06	2.05	0.06
Ta	25.7	0.5	24.7	0.3	17.6	0.0	16.3	0.3	6.1	0.0	7.1	0.0
Pb	33.51	0.86	24.63	0.10	32.50	0.00	29.23	0.53	2.76	0.04	10.15	0.10
Th	56.5	0.6	53.5	0.2	48.8	0.3	46.0	0.6	7.2	0.1	16.9	0.2
U	13.83	0.03	7.82	0.07	7.70	0.10	7.45	0.19	1.76	0.06	2.56	0.04
La	526	17	380	12	368	8	332	2	52	2	99	0
Ce	744	19	674	25	706	18	636	7	87	5	163	3
Pr	58.8	0.3	55.3	1.8	60.4	0.5	54.5	1.2	9.3	0.4	17.2	0.4
Nd	175.6	4.7	167.4	4.2	185.8	2.0	169.4	1.6	30.6	1.1	57.2	1.4
Pm												
Sm	17.05	0.99	16.85	0.33	17.86	0.17	16.42	0.20	3.68	0.09	7.16	0.09
Eu	5.43	0.03	4.09	0.07	4.54	0.09	4.16	0.11	0.93	0.08	1.83	0.09
Gd	11.05	0.08	10.18	0.07	10.23	0.29	9.32	0.97	2.69	0.09	5.11	0.53
Tb	1.00	0.03	1.01	0.03	0.93	0.00	0.87	0.04	0.27	0.01	0.48	0.00
Dy	4.17	0.01	4.26	0.08	3.75	0.10	3.50	0.13	1.13	0.04	1.95	0.01
Ho	0.63	0.01	0.63	0.03	0.56	0.00	0.54	0.01	0.18	0.01	0.30	0.00
Er	1.46	0.07	1.43	0.07	1.27	0.06	1.24	0.01	0.42	0.02	0.61	0.04
Tm	0.187	0.002	0.196	0.008	0.166	0.006	0.165	0.006	0.060	0.008	0.076	0.004
Yb	1.04	0.04	1.06	0.03	0.95	0.02	0.94	0.03	0.36	0.02	0.43	0.03
Lu	0.157	0.008	0.156	0.004	0.140	0.000	0.145	0.004	0.050	0.000	0.063	0.002

CANADA, Churchill Province

FIELD	South-East Slave		South-East Slave		Somerset Island		Somerset Island		Somerset Island	
LOCALITY	Gahcho Kue		Snap Lake		JP South		Batty Bay		Elwin Bay	
SAMPLE	KDY-2	+/- 2σ	SNP-1	+/- 2σ	JPS-1	+/- 2σ	BAT-1	+/- 2σ	ELB-1	+/- 2σ
(ppm)										
Sc	10.7	0.4	15.1	0.8	16.3	0.1	13.2	0.4	12.0	0.3
V	92	4	50	1	126	1	143	3	112	1
Cr	1293*		1984*		1304	11	616**		1300**	
Co	80.2	2.0	124.8	1.0	74.9	1.6	60.6	0.4	61.1	0.3
Ni	1245**		1479	47	1208	14	797**		887**	
Cu	58.0	1.3	11.6	0.9	52.6	0.7	39.6	0.2	45.0	0.4
Zn	39.0	0.6	36.9	1.1			55.9	4.6	58.9	12.6
Ga	8.17	0.03	6.92	0.14	6.00	0.15	4.85	0.00	4.73	0.12
Rb	132.6	0.3	98.3	1.6	39.2	0.9	8.2	0.0	63.7	1.2
Sr	264	3	244	1	1388	17	1372	12	901	3
Y	9.36	0.23	5.64	0.12	14.95	0.02	13.76	0.22	10.15	0.18
Zr	93.3	0.6	130.4	0.5	195.3	3.7	132.0	0.4	103.2	0.2
Nb	174	1	219	2	207	3	189	1	135	0
Cs	1.40	0.00	1.86	0.06	0.45	0.01	0.87	0.03	0.79	0.01
Ba	904	29	2812	72	2015	24	3255	98	1245	2
Hf	2.40	0.09	2.91	0.14	4.57	0.13	2.94	0.02	2.32	0.04
Ta	8.3	0.1	15.5	0.3	11.6	0.4	9.0	0.1	7.0	0.0
Pb	2.37	0.02	2.64	0.05	9.32	0.12	10.13	0.03	7.18	0.05
Th	21.5	0.7	40.3	1.7	19.1	0.4	18.0	0.2	12.2	0.1
U	3.25	0.13	2.64	0.13	3.99	0.10	3.40	0.02	2.21	0.01
La	106	4	194	6	146	1	133	2	93	1
Ce	173	8	331	11	256	4	266	8	165	3
Pr	18.0	0.8	35.0	1.5	30.1	0.4	26.8	0.8	19.4	0.3
Nd	58.6	2.2	107.5	3.2	105.0	0.6	92.2	1.5	66.7	1.1
Pm										
Sm	7.44	0.34	8.97	0.24	13.70	0.09	11.84	0.25	8.52	0.14
Eu	1.70	0.09	2.18	0.10	3.50	0.04	3.21	0.04	2.22	0.03
Gd	5.34	0.34	6.28	0.42	8.32	0.32	7.36	0.07	5.32	0.02
Tb	0.52	0.05	0.47	0.00	0.89	0.03	0.76	0.00	0.55	0.02
Dy	2.10	0.08	1.65	0.02	3.82	0.11	3.16	0.08	2.34	0.06
Ho	0.32	0.01	0.22	0.01	0.57	0.01	0.47	0.01	0.35	0.01
Er	0.68	0.06	0.49	0.02	1.13	0.01	0.95	0.01	0.73	0.04
Tm	0.083	0.008	0.055	0.008	0.141	0.014	0.124	0.004	0.096	0.000
Yb	0.48	0.00	0.34	0.01	0.75	0.04	0.66	0.02	0.54	0.00
Lu	0.070	0.000	0.050	0.002	0.099	0.000	0.093	0.002	0.079	0.000

CANADA, Superior Province

FIELD	Somerset Island		Rankin Inlet		Attawapiskat		Kirkland Lake		Timiskaming	
LOCALITY	Jos		Rankin Inlet		James Bay Lowlands		Upper Canada Mine		Gulges	
SAMPLE	JOS-1	+/- 2σ	RMK-1	+/- 2σ	JBL-1	+/- 2σ	UCM-2	+/- 2σ	GUI-1	+/- 2σ
(ppm)										
Sc	10.1	0.3	25.7	0.3	12.1	0.6	14.1	0.7	9.5	0.2
V	110	1	228	4	92	4	46	3	99	0
Cr	684**		958*		889	36	657	34	1095*	
Co	73.9	2.1	70.1	1.7	66.6	1.8	81.0	1.0	84.4	0.0
Ni	1024**		302**		842	5	1396	40	1229***	
Cu	21.4	1.0	64.3	1.6	133.3	0.1	44.4	1.4	24.2	0.2
Zn	48.3	5.6	112.5	0.3	50.6	1.3	75.6	4.1	58.3	7.4
Ga	2.80	0.15	13.32	0.08	5.21	0.03	6.61	0.08	3.71	0.07
Rb	18.9	0.0	29.2	0.3	17.0	0.1	162.1	3.4	50.8	0.7
Sr	1639	21	1636	16	349	0	933	16	308	2
Y	8.09	0.05	21.76	0.28	5.55	0.09	17.63	0.20	5.28	0.01
Zr	71.2	1.1	285.9	3.6	38.4	0.4	204.0	0.0	72.4	1.1
Nb	123	1	354	6	36	0	159	0	79	1
Cs	0.29	0.02	0.39	0.00	0.59	0.02	2.16	0.07	0.76	0.01
Ba	1621	0	1370	28	915	0	2424	11	625	10
Hf	1.55	0.02	7.13	0.07	0.98	0.01	4.04	0.03	1.76	0.03
Ta	6.0	0.0	22.1	0.1	2.4	0.0	8.8	0.1	4.8	0.1
Pb	7.79	0.17	12.06	0.09	5.51	0.04	10.76	0.02	5.37	0.09
Th	11.1	0.1	38.7	0.3	3.7	0.0	13.2	0.2	6.1	0.1
U	2.14	0.02	5.87	0.05	0.69	0.01	4.89	0.07	1.40	0.01
La	86	0	305	8	24	0	108	4	47	1
Ce	149	0	554	13	39	0	193	7	81	2
Pr	17.1	0.0	53.5	1.4	4.4	0.1	21.9	0.0	9.0	0.2
Nd	57.7	0.3	178.3	4.5	16.0	0.3	78.5	0.4	30.6	0.5
Pm										
Sm	7.20	0.02	21.25	0.46	2.38	0.01	10.98	0.30	3.99	0.10
Eu	1.93	0.05	5.17	0.05	0.76	0.03	3.01	0.02	1.04	0.00
Gd	4.32	0.02	12.00	0.30	2.00	0.14	8.26	0.16	2.55	0.06
Tb	0.44	0.01	1.27	0.02	0.23	0.00	0.90	0.05	0.27	0.01
Dy	1.88	0.00	5.42	0.06	1.08	0.02	3.94	0.10	1.18	0.00
Ho	0.28	0.00	0.82	0.01	0.19	0.00	0.64	0.00	0.18	0.00
Er	0.56	0.02	1.65	0.05	0.44	0.01	1.39	0.02	0.39	0.02
Tm	0.077	0.006	0.213	0.002	0.066	0.006	0.173	0.000	0.054	0.006
Yb	0.42	0.02	1.12	0.00	0.39	0.01	0.96	0.02	0.30	0.00
Lu	0.065	0.000	0.155	0.002	0.064	0.002	0.134	0.000	0.042	0.002

327

CANADA, Trans-Hudson Domain

FIELD	Timiskaming		Fort a la Corne		Fort a la Corne	
LOCALITY	Peddle		Fort a la Corne		Sturgeon Lake	
SAMPLE	PED-1	+/-2σ	FLC-1	+/-2σ	STL-1	+/-2σ
(ppm)						
Sc	16.4	0.1	13.4	0.8	10.0	0.8
V	144	1	166	7	35	1
Cr	1163*		2070	98	575	26
Co	73.0	1.4	109.3	6.1	78.8	4.3
Ni	880**		1587	70	1437	46
Cu	94.8	2.6	78.6	3.8	11.9	0.5
Zn	88.2	40.8	67.2	4.2	42.1	0.2
Ga	6.15	0.11	5.20	0.06	1.32	0.16
Rb	35.2	0.2	4.1	0.0	5.7	0.1
Sr	967	1	134	4	238	0
Y	20.53	0.24	6.08	0.06	3.66	0.01
Zr	196.6	1.8	102.5	1.2	33.7	0.5
Nb	354	1	129	0	83	0
Cs	0.43	0.01	0.04	0.00	0.09	0.02
Ba	4171	85	62	0	259	12
Hf	3.93	0.06	2.62	0.04	0.74	0.03
Ta	15.3	0.1	10.8	0.2	4.9	0.1
Pb	18.34	0.21	5.19	0.15	4.50	0.02
Th	36.6	0.3	11.8	0.3	10.3	0.1
U	6.88	0.05	2.51	0.08	1.12	0.02
La	260	4	69	0	54	1
Ce	442	9	124	2	88	3
Pr	42.6	0.3	13.8	0.3	9.0	0.3
Nd	143.5	3.0	47.7	0.3	28.9	1.2
Pm						
Sm	17.97	0.09	5.89	0.05	3.40	0.08
Eu	4.70	0.05	1.36	0.02	0.82	0.01
Gd	10.68	0.04	3.51	0.08	2.41	0.06
Tb	1.15	0.02	0.36	0.00	0.24	0.00
Dy	4.89	0.03	1.49	0.02	0.92	0.03
Ho	0.74	0.00	0.21	0.00	0.14	0.01
Er	1.46	0.03	0.43	0.01	0.29	0.02
Tm	0.189	0.004	0.055	0.000	0.036	0.002
Yb	0.99	0.02	0.29	0.02	0.22	0.01
Lu	0.145	0.004	0.041	0.002	0.032	0.006

328

	USA, Yapavai Domain						South Africa, Kaapvaal Province			
FIELD	State Line		State Line		State Line		Barkly West		Barkly West	
LOCALITY	Nix		Chicken Park		Sloan		Frank Smith		Roberts Victor	
SAMPLE	NIX-1	+/-2σ	CHK-1	+/-2σ	SLM-1	+/-2σ	FSM-2	+/-2σ	ROVIC-1	+/-2σ
(ppm)										
Sc	12.9	0.0	20.1	0.6	13.5	0.1	20.6	0.6	28.6	0.4
V	115	2	170	3	142	2	152	3	65	0
Cr	1437*		1651	9	1693	13	630	6	1490	10
Co	69.8	1.1	103.2	0.6	69.7	3.2	61.2	0.0	64.6	0.3
Ni	862**		1096	23	1114	64	866	3	1098	2
Cu	7.7	0.2	114.0	0.9	17.2	1.0	66.5	1.0	63.0	0.9
Zn	53.4	1.1	94.8	1.5	59.1	1.6				
Ga	5.45	0.15	9.96	0.43	10.60	0.06	10.63	0.42	8.77	0.14
Rb	24.1	0.2	60.8	1.2	164.9	6.4	64.2	0.1	75.8	0.5
Sr	1259	15	710	8	622	23	764	1	2036	2
Y	11.32	0.19	19.09	0.22	25.69	0.58	16.85	0.31	39.95	0.03
Zr	130.2	0.1	203.8	2.7	177.2	4.3	116.2	1.3	606.4	2.9
Nb	274	2	228	5	197	4	52	0	177	1
Cs	0.49	0.02	1.43	0.04	2.88	0.09	3.02	0.05	1.81	0.02
Ba	2228	31	762	23	1587	11	667	5	6873	57
Hf	2.98	0.02	5.36	0.15	4.33	0.12	2.72	0.04	13.52	0.07
Ta	13.3	0.2	16.9	0.2	10.2	0.2	3.0	0.1	7.0	0.0
Pb	6.25	0.01	4.89	0.20	13.74	0.12	6.83	0.09	65.62	0.96
Th	33.6	0.3	14.3	0.6	27.4	0.5	6.2	0.0	60.2	0.9
U	5.20	0.09	2.73	0.06	6.34	0.12	1.54	0.03	9.37	0.08
La	191	4	112	5	139	1	45	1	407	5
Ce	350	10	205	6	227	7	83	1	755	16
Pr	31.1	0.5	23.9	1.0	24.2	1.1	9.9	0.1	93.6	1.3
Nd	95.3	2.2	87.9	3.2	81.3	3.1	36.2	0.5	311.3	3.8
Pm										
Sm	10.23	0.06	12.88	0.45	10.58	0.62	5.62	0.04	33.44	0.96
Eu	2.47	0.06	3.35	0.17	2.20	0.06	1.48	0.00	7.58	0.15
Gd	5.38	0.11	8.83	0.12	7.39	0.39	4.34	0.17	17.04	0.00
Tb	0.58	0.00	1.00	0.06	0.89	0.03	0.60	0.01	1.85	0.01
Dy	2.50	0.04	4.36	0.08	4.45	0.08	3.10	0.14	8.44	0.14
Ho	0.39	0.01	0.67	0.02	0.83	0.01	0.60	0.01	1.38	0.01
Er	0.83	0.01	1.39	0.07	2.15	0.04	1.50	0.06	2.99	0.03
Tm	0.115	0.010	0.177	0.014	0.341	0.010	0.239	0.014	0.424	0.010
Yb	0.64	0.03	0.92	0.01	2.05	0.07	1.42	0.02	2.29	0.02
Lu	0.095	0.006	0.128	0.004	0.319	0.004	0.224	0.014	0.328	0.008

FIELD	Central Cape		Central Cape		North Lesotho		North Lesotho		North Lesotho	
LOCALITY	Gansfontein		Melton Wold		Liqhobong		Liqhobong		Pipe 200	
SAMPLE	GNS-13	+/-2σ	MW-3	+/-2σ	LQ-7	+/-2σ	LQ-SAT	+/-2σ	P200	+/-2σ
(ppm)										
Sc	24.0	0.7	16.5	0.2	17.2	0.1	37.2	0.4	14.7	0.4
V	197	1	88	1	165	1	265	1	163	1
Cr	611	7	1431	15	1232	5	283	3	1215	15
Co	123.8	0.1	79.2	0.9	80.7	2.2	43.5	0.1	92.2	2.0
Ni	478	6	1451	21	1078	31	91	1	1358	33
Cu	143.7	1.6	11.6	0.1	73.2	0.8	64.7	0.7	71.9	3.1
Zn										
Ga	26.77	0.20	5.99	0.06	10.45	0.18	3.69	0.02	7.49	0.06
Rb	82.9	1.0	144.7	2.3	102.9	1.6	2.8	0.0	80.3	0.7
Sr	1687	27	1147	13	937	3	769	9	745	9
Y	35.92	0.13	8.98	0.06	18.53	0.22	23.95	0.03	14.46	0.04
Zr	2013.3	18.2	156.8	0.9	220.1	2.9	93.4	0.9	381.6	2.6
Nb	416	1	163	1	150	3	7	0	149	1
Cs	1.04	0.02	1.57	0.00	1.71	0.04	0.20	0.00	0.76	0.01
Ba	1786	1	3249	22	1191	26	205	2	1011	5
Hf	54.50	0.43	3.69	0.05	5.16	0.11	2.47	0.05	9.30	0.19
Ta	29.9	0.0	9.9	0.1	10.3	0.3	0.5	0.1	9.4	0.2
Pb	14.08	0.03	17.19	0.12	4.70	0.24	2.64	0.01	4.52	0.17
Th	37.0	0.4	18.6	0.3	12.3	0.3	1.5	0.0	11.8	0.2
U	8.67	0.00	3.05	0.04	2.74	0.07	0.27	0.01	2.87	0.03
La	238	1	87	0	94	1	10	0	89	1
Ce	406	6	153	0	176	3	22	0	165	2
Pr	53.5	0.3	17.6	0.1	21.6	0.3	3.0	0.0	20.1	0.2
Nd	197.7	2.0	61.5	0.2	80.1	1.7	13.2	0.2	73.9	2.0
Pm										
Sm	28.95	0.24	7.85	0.07	12.05	0.27	3.30	0.06	10.98	0.25
Eu	7.44	0.04	1.92	0.02	3.12	0.06	1.06	0.03	2.90	0.05
Gd	19.11	0.07	4.53	0.06	8.17	0.06	4.07	0.16	7.15	0.33
Tb	2.11	0.01	0.48	0.01	0.96	0.01	0.67	0.02	0.81	0.01
Dy	9.00	0.09	2.10	0.05	4.28	0.06	4.06	0.10	3.56	0.10
Ho	1.34	0.03	0.33	0.00	0.69	0.00	0.86	0.03	0.54	0.02
Er	2.63	0.00	0.71	0.01	1.49	0.04	2.36	0.01	1.09	0.02
Tm	0.332	0.010	0.106	0.002	0.204	0.004	0.390	0.004	0.139	0.002
Yb	1.77	0.04	0.65	0.01	1.14	0.03	2.34	0.08	0.71	0.02
Lu	0.218	0.004	0.111	0.002	0.160	0.006	0.377	0.026	0.095	0.004

330

RUSSIA, Siberian Province

FIELD	Malo-Botuobinsk		Malo-Botuobinsk		Daldyn-Alakit		Daldyn-Alakit	
LOCALITY	Mir		Internationalaya		Jubilee		Udachnaya	
SAMPLE	MIR-M3	+/-2σ	INT-I2	+/-2σ	JUB-1	+/-2σ	UDC-1	+/-2σ
(ppm)								
Sc	10.8	0.3	14.5	0.5	8.4	0.0	10.2	0.3
V	107	0	59	1	68	1	100	1
Cr	699	2	1292	46	1175	18	1065	9
Co	85.2	0.2	54.1	2.0	70.1	0.8	82.0	1.3
Ni	1404	4	1474	39	1489	26	1398	39
Cu	51.4	0.2	23.9	0.1	4.9	0.2	44.0	1.5
Zn	57.1	0.1	36.8	0.5	16.2	0.2	58.3	0.7
Ga	4.18	0.09	4.65	0.14	2.74	0.06	4.82	0.39
Rb	19.7	0.1	28.1	0.5	12.9	0.1	55.8	1.9
Sr	436	3	1083	18	402	8	489	16
Y	8.78	0.05	12.38	0.29	5.57	0.00	7.58	0.04
Zr	80.8	0.4	147.3	0.4	67.2	1.0	93.7	1.8
Nb	88	0	146	2	112	1	136	2
Cs	1.02	0.00	0.36	0.00	0.17	0.01	1.00	0.05
Ba	222	5	819	11	277	6	856	43
Hf	2.01	0.07	3.21	0.09	1.61	0.02	2.28	0.14
Ta	5.7	0.1	6.6	0.1	6.3	0.1	8.9	0.1
Pb	5.69	0.05	1.36	0.03	1.03	0.09	5.19	0.11
Th	5.1	0.0	13.9	0.4	7.7	0.0	8.5	0.2
U	1.35	0.00	2.33	0.05	1.24	0.02	1.96	0.04
La	41	0	106	3	64	1	71	2
Ce	76	0	182	6	95	1	121	4
Pr	8.9	0.1	21.1	0.4	10.2	0.1	13.5	0.8
Nd	31.0	1.0	72.4	0.6	33.9	0.2	46.1	2.2
Pm								
Sm	4.41	0.05	9.68	0.07	4.36	0.05	6.03	0.13
Eu	1.18	0.01	2.47	0.04	1.59	0.01	1.56	0.10
Gd	3.36	0.08	6.85	0.23	3.13	0.12	4.31	0.27
Tb	0.39	0.00	0.71	0.02	0.31	0.02	0.44	0.02
Dy	1.77	0.02	2.94	0.03	1.24	0.01	1.90	0.05
Ho	0.30	0.00	0.45	0.00	0.18	0.01	0.29	0.00
Er	0.71	0.01	0.94	0.05	0.38	0.01	0.60	0.01
Tm	0.106	0.010	0.121	0.002	0.049	0.000	0.077	0.004
Yb	0.59	0.02	0.65	0.03	0.27	0.01	0.42	0.01
Lu	0.089	0.004	0.094	0.004	0.040	0.002	0.061	0.006

LAC DE GRAS Crustal rocks

ROCK TYPE	Greywacke	Greywacke	Greywacke	Greywacke	Greywacke	Greywacke	Trondjhemite	Trondjhemite	Trondjhemite	Quartz diorite	Hornblende tonalite	Hornblende tonalite
SAMPLE	KIA92-K075	KIA92-K089	KIA92-K098	KIA92-K152	KIA92-K153	KIA92-P067	KIA92-K089	KIA92-K078	KIA92-K145	KIA92-K053	KIA92-K003	KIA92-K049
Sc		22									35	
V	118	71	90	156	80	201	59	60	57	65	6	86
Cr	57	81	130	76	150	180	52	46	48	60	5	73
Co	15.9	6.6	17.8	20.4	9.9	25.1	14.1	10	11.9	14.2	2	23.3
Ni	47.2	15.2	57.2	52.1	24.6	81.1	29.4	17.3	26.7	33.2	3	32.3
Cu	12.8	17.3	1	35.8	29.8	40.9	17.2	33	14.9	11.7	1.1	29.8
Zn	73	56	49	78	58	118	56	64	57	51	27	52
Ga	7	6	6	4	6	6	5	10	7	8	9	10
Rb	84.9	58.7	64.3	116.5	74.6	127	65.5	72.8	104.3	93.5	166.6	81.5
Sr	277	263	365	238	221	351	647	613	613	564	112	937
Y	0.22	0.18	0.43	0.3	0.17	0.43	0.06	0.09	0.08	0.15		0.1
Zr	125.4	222.1	144.5	117	138.9	131.7	88.9	121.1	99.3	113.9	110.8	39.1
Nb	6.8	6.3	6.4	7.4	5.6	10.3	4.4	6	4.3	6.2	7.3	3.3
Cs	5.2	18.2	4.4	12.4	18.3	9.5	14.8	23.8	13.8	9.7	1.5	17.3
Ba	698	465	145	979	533	916	575	669	633	699	608	743
Hf	3.9	6.4	3.7	3.4	4.1	4.2	2.9	3.9	3.3	4	3.8	1.3
Ta	0.5	0.5	0.6	3.6	2.1	11.8	0.4	0.4	0.3	0.6	0.5	0.1
Pb	3.5	4.4	5	4.5	2.5	3.7	2.9	3.1	2.7	2.9	8.2	2.3
Th	5.9	11	7.2	8.9	8.1	10.8	3.4	5.1	2.7	2	18.3	1.4
U	6.4	11	6.2	7.8	6.9	11	4	5	3	2	18	1.5
La	30.4	40.9	32.3	39	31	43.1	27.6	8.5	14.8	28.7	23	29.3
Ce	58.5	74.4	67.7	79	58.5	88.8	55.8	18.4	31.7	54.3	52.4	60.7
Pr	6.75	8.07	8.1	9.08	6.18	10.25	6.8	2.23	3.79	6.95	5.79	7.04
Nd	25.2	29.4	34.2	36.8	24.4	43.1	25.7	8.9	15.5	28.9	22.3	29.2
Pm												
Sm	4.7	4.6	7.2	6.9	4	8	4.2	1.5	2.6	5	5	4.5
Eu	1.06	1.27	1.77	1.18	0.91	1.55	1.04	0.81	0.69	0.97	0.34	1.2
Gd	3.33	2.82	6.69	5.37	3	6.87	2.15	1.29	1.65	3.88	3.67	2.99
Tb												
Dy	2.79	2.3	5.36	4.2	2.19	4.99	1.23	1.01	1.1	2.29	1.58	1.7
Ho	0.51	0.42	1.16	0.78	0.4	1.05	0.22	0.24	0.2	0.47	0.2	0.27
Er	1.72	1.11	3.3	2.06	1.2	3.01	0.57	0.6	0.62	1.17	0.47	0.87
Tm	0.22	0.16	0.53	0.33	0.18	0.49	0.06	0.07	0.09	0.15	0.06	0.12
Yb	1.5	1.2	2.8	2	1.2	3	0.5	0.5	0.5	1	0.4	0.7
Lu			0.8	0.7		1						

332

ROCK TYPE	Hornblende tonalite	Hornblende tonalite	Hornblende tonalite	Hornblende tonalite	Hornblende tonalite	Hornblende tonalite	Hornblende tonalite	Hornblende tonalite	Hornblende tonalite	Hornblende tonalite	Phlogopite granite	Phlogopite granite
SAMPLE	KIA92-K050A	KIA92-K131	KIA92-K134	KIA92-K136	KIA92-K177A	KIA92-K177B	KIA92-P26B	KIA92-P55B-1	KIA92-P55B-2	KIA92-L129-1	KIA92-K106	KIA92-K141
Sc	22					23					25	28
V	62	70	63	42	74	79	88	77	12	96	6	1.5
Cr	58	59	54	37	67	5	61	5	5	150	5	5
Co	11.9	14.1	10	8.9	16.4	17	19.2	16.1	1.4	20.6	1.9	1.8
Ni	25.4	30.9	28.1	15.4	40.3	48.7	16.1	21.8	2.5	27.5	2.5	2.4
Cu	6.4	9.4	21.2	13.7	7.4	18	12	11.9	1.1	21	0.5	0.4
Zn	42	50	59	62	45	60	31	58	23	38	27	41
Ga	11	8	7	7	3	14	9	9	5	6	7	7
Rb	103.8	115.1	66.7	117.8	54.1	77.8	46.9	50.9	34.7	30.2	153.9	237.9
Sr	468	517	724	646	639	699	1114	766	464	1105	96	104
Y	0.3	0.17	0.07	0.1	0.14	0.13	0.06	0.15	0.06	0.2		
Zr	137.1	127.4	158.6	92.4	141.4	132.5	10.6	113.9	57.7	129.1	36.9	58
Nb	5.1	6.9	5.3	5.2	6.6	6.4	3.2	5	1.5	6.5	3.5	5.8
Cs	7.4	12.3	12.6	11	1.1	4.3	5.8	8.4	4	5	6.8	9.3
Ba	764	586	622	593	852	612	878	470	1075	549	422	465
Hf	4.9	3.9	5.1	2.9	4.6	4.2	0.7	3	2.4	3.8	1.6	2.7
Ta	0.5	0.5	0.4	0.3	0.4	0.4	0.3	0.5	0.1	0.2	0.4	0.8
Pb	7.2	6.3	4.1	1.5	5.3	4.8	1.1	2.9	4.1	1.3	2.1	3.1
Th	6.3	5.7	5.6	3.7	8.1	6.8	0.3	4.6	1.5	0.7	5	9.4
U	7.4	6	6.5	3.9	5.9	7	0.3	3.7	1.7	1.3	4.7	9.9
La	30.9	30.2	27	26.8	39.7	46.6	23	30.6	8.9	30.6	9.2	13.6
Ce	63.8	62.9	50.6	55.4	82.1	92	45.9	59.2	16.4	68.6	20.2	32.7
Pr	8.13	7.51	5.63	6.59	9.72	10.26	5.53	7.29	1.8	8.97	2.47	4
Nd	34.2	29.9	20	26.7	37.4	38.5	23.1	29.1	6.7	40.5	10.4	15.8
Pm												
Sm	6.9	5.4	2.2	3.9	6.4	5.9	3.7	5.3	1.4	6.8	2.5	3.9
Eu	0.96	0.91	0.82	0.97	1.17	1.22	1.05	1.32	0.22	1.85	0.22	0.26
Gd	5.1	3.35	1.13	2.45	4.05	3.34	2.32	3.72	1.08	5.03	2.39	2.82
Tb												
Dy	3.72	2.36	0.8	1.34	2.2	2.09	1.3	2.65	0.67	3.12	1.19	1.22
Ho	0.65	0.46	0.14	0.24	0.49	0.33	0.2	0.45	0.1	0.54	0.13	0.16
Er	2.08	1.31	0.45	0.65	1.13	1.01	0.5	1.28	0.29	1.47	0.33	0.34
Tm	0.32	0.18	0.07	0.09	0.14	0.11	0.08	0.16	0.02	0.18	0.02	0.02
Yb										0.5	0.2	
Lu	2.1	1.3	0.5	0.4	1.1	0.9	0.4	1		1.3		

ROCK TYPE	Phlogopite granite	Phlogopite granite	2 mica granite	2 mica granite	2 mica granite	2 mica granite	2 mica granite	2 mica granite	2 mica granite	2 mica granite
SAMPLE	KIA92-K142	KIA92-K143	KIA92-K042	KIA92-K102	KIA92-K139	KIA92-K140	KIA92-K159	KIA92-P10a	KIA92-L070	KIA92-L124
Sc	24	21	17	29	28				34	
V	5	2.3	9	1.4	1.4	2.7	2.3	7	1.9	10
Cr	5	5	9	5	5	5	5	74	5	80
Co	1.4	1.9	3.8	1.4	1.3	1.2	0.8	1.5	1.7	0.2
Ni	2.3	2.2	3.5	1.9	1.5	1.9	1.1	3	1.8	1
Cu	0.8	0.1	0.05	0.4	1.6	0.1	0.4	8.2	0.3	1.4
Zn	43	50	31	21	31	53	13	4	45	1
Ga	10	5	8							
Rb	184.5	205.8	49.9	152.8	198.1	230.8	176.2	16.7	206.2	94.4
Sr	91	87	545	118	134	82	56	422	139	182
Y							0.13	0.28		
Zr	52.4	58.9	87.4	39.1	59.7	52	31.4	13.3	83	14
Nb	5.9	8.5	3.6	3.1	5.1	9.6	4.6	0.8	6.9	9.5
Cs	6.7	8.3	6.3	2.8	3.7	10.1	5.7	0.5	8.3	2.6
Ba	357	307	134	495	524	272	186	348	461	230
Hf	2.1	2.5	2.5	2	2.7	2.2	1.5	0.7	3.5	1.6
Ta	0.7	0.8	0.3	0.2	0.5	0.9	0.3	0.05	0.8	3.1
Pb	3.7	2.9	2.1	4.1	4.7	2.1	1.6	2.3	5.3	1.5
Th	5.3	8.6	1.6	3.8	6.8	6.1	3.3	0.4	11.8	0.2
U	5.9	8.3	1.9	3.2	6.9	6.2	3.2	0.3	12	0.6
La	10.6	12	11.1	8.6	11.1	9.3	3.9	5.1	20.1	1.7
Ce	25.5	29.1	21.4	19.3	23.6	22.4	9.1	12.7	42	2.2
Pr	3.13	3.66	2.31	2.47	2.77	2.82	1.17	1.75	5.14	0.21
Nd	11.9	15.1	8.6	9.4	11	10.7	5	8.2	20.4	0.9
Pm										
Sm	3.3	3.6	1.4	2.2	2	2.9	1.1	2.3	4.7	0.3
Eu	0.14	0.23	0.61	0.26	0.14	0.17	0.12	1.59	0.33	0.52
Gd	2.47	2.78	0.75	1.17	1.29	1.95	1.52	2.86	2.73	0.13
Tb										
Dy	1.45	1.15	0.37	0.52	0.62	1.15	1.55	3.73	0.91	0.25
Ho	0.22	0.14	0.09	0.02	0.07	0.16	0.29	0.73	0.1	0.05
Er	0.49	0.28	0.24	0.16	0.17	0.36	0.79	2.34	0.21	0.21
Tm	0.06	0.2	0.02	0.02	0.02	0.02	0.12	0.34	0.02	0.02
Yb		0.8						0.6		
Lu	0.3		0.3			0.3	0.9	2.1	0.3	0.4

Appendix E

Additional elemental abundance variation diagrams

This appendix contains box-plots and histograms of selected elemental abundances in kimberlites from Canada, southern Africa and other cratonic areas worldwide, to complement those presented for the principal major and trace elements in Chapter 4. As previously noted, samples from Greenland (Scott, 1979) have been reclassified as ultramafic lamprophyres, but are included here for comparative purposes.

Sources of data are as listed in Table E.1 below:

Region	References
Canada	This study
Southern Africa	Smith *et al.* (1985); Fraser (1987); Spriggs (1989); Tainton (1992); Nowell (unpublished data)
West Africa	Taylor *et al.* (1994)
East European Platform	O'Brien and Tyni (1999); Mahotkin *et al.* (2000)
Greenland	Scott (1979)
China	Tompkins *et al.* (1999)

Table E.1 Sources of data used for compilation of elemental abundance diagrams in presented in Appendix E.
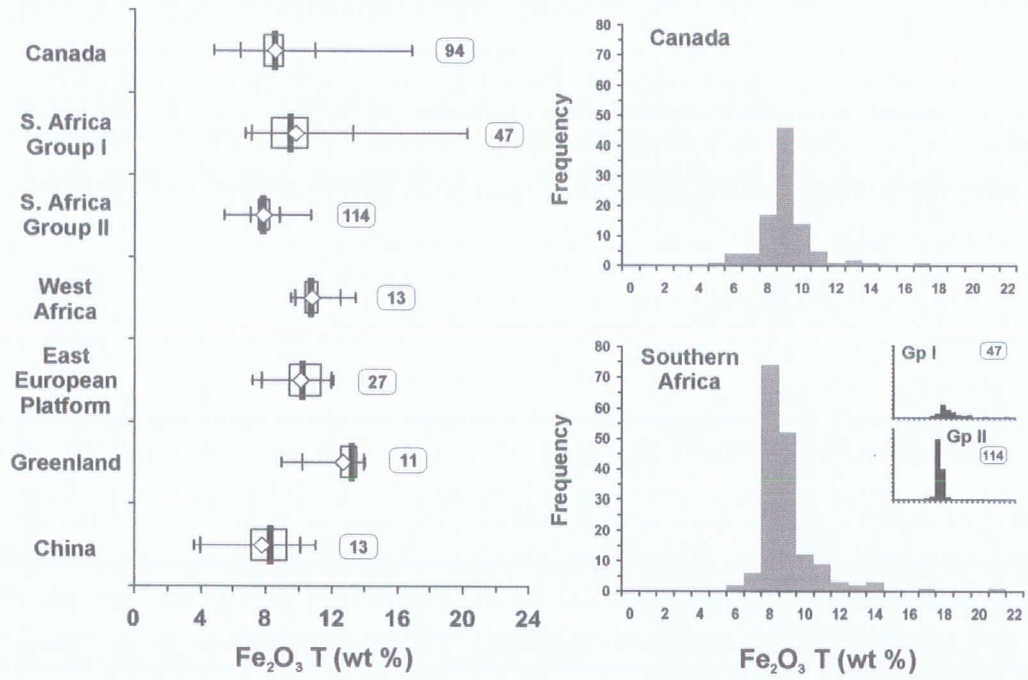
Figure E.1 Dispersion and distribution of Fe_2O_3 T in selected global hypabyssal kimberlite occurrences.
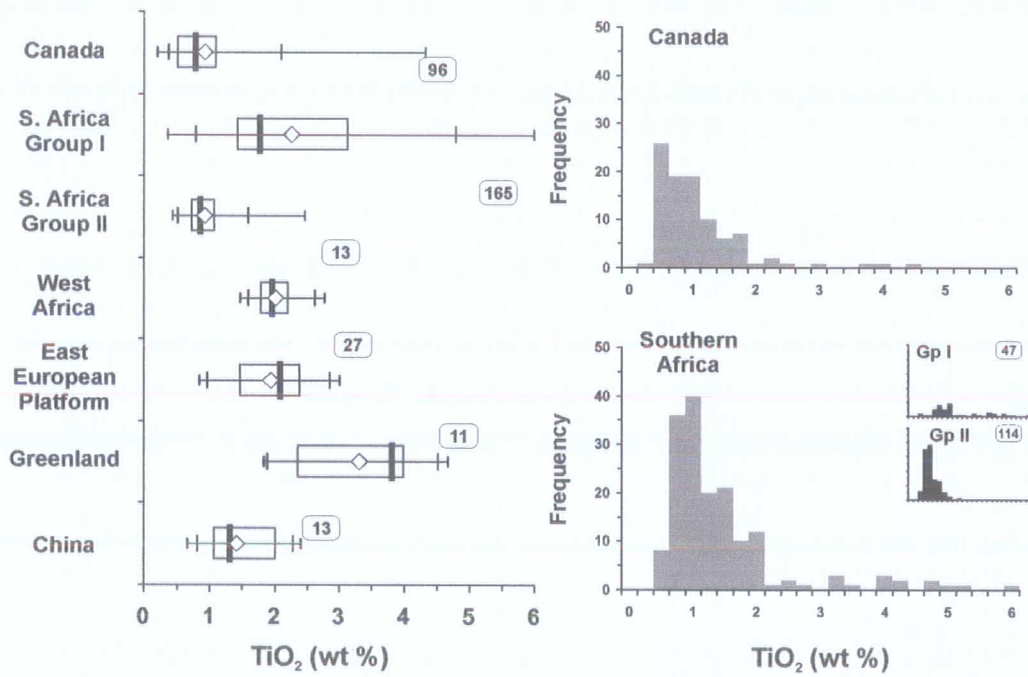

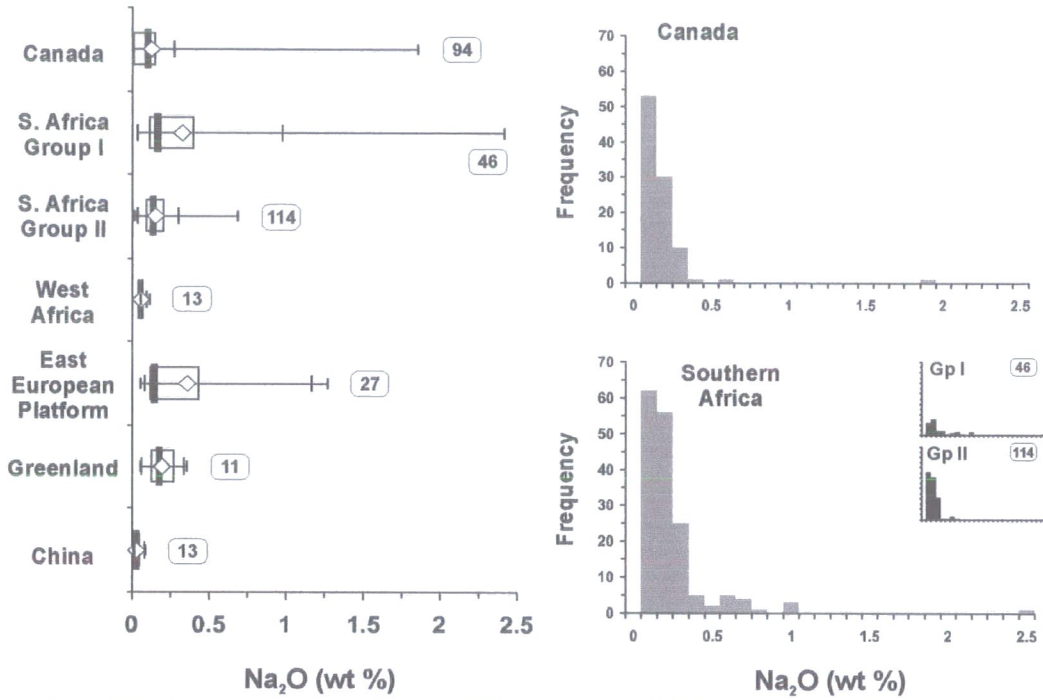**Figure E.2** Dispersion and distribution of TiO_2 in selected global hypabyssal kimberlite occurrences.

Figure E.3 Dispersion and distribution of Na_2O in selected global hypabyssal kimberlite occurrences.
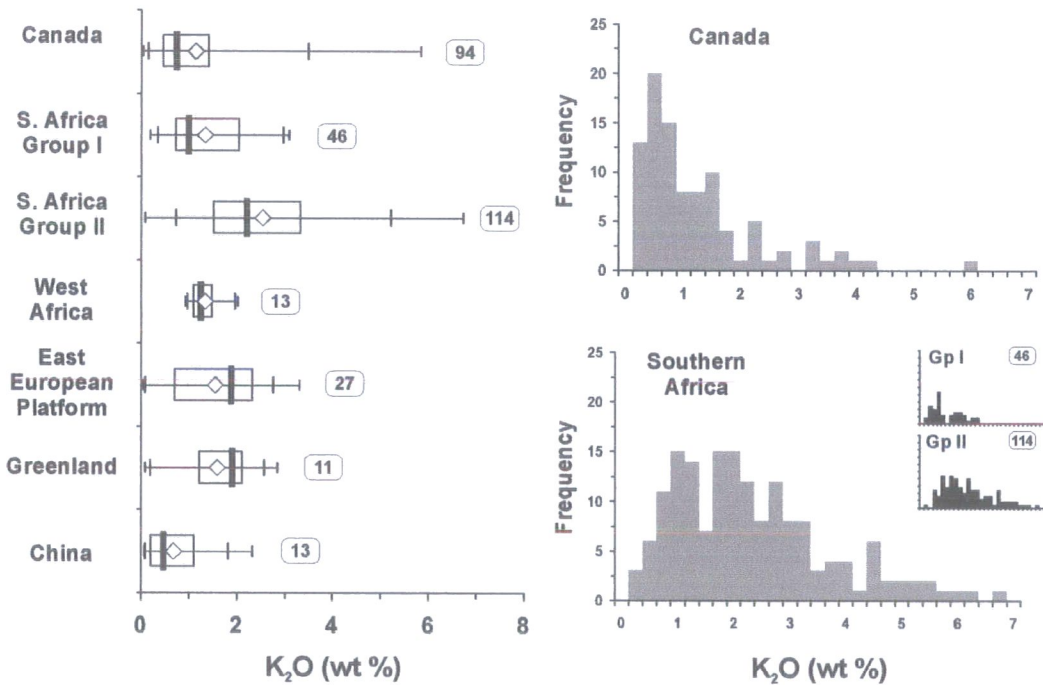

Figure E.4 Dispersion and distribution of K_2O in selected global hypabyssal kimberlite occurrences.
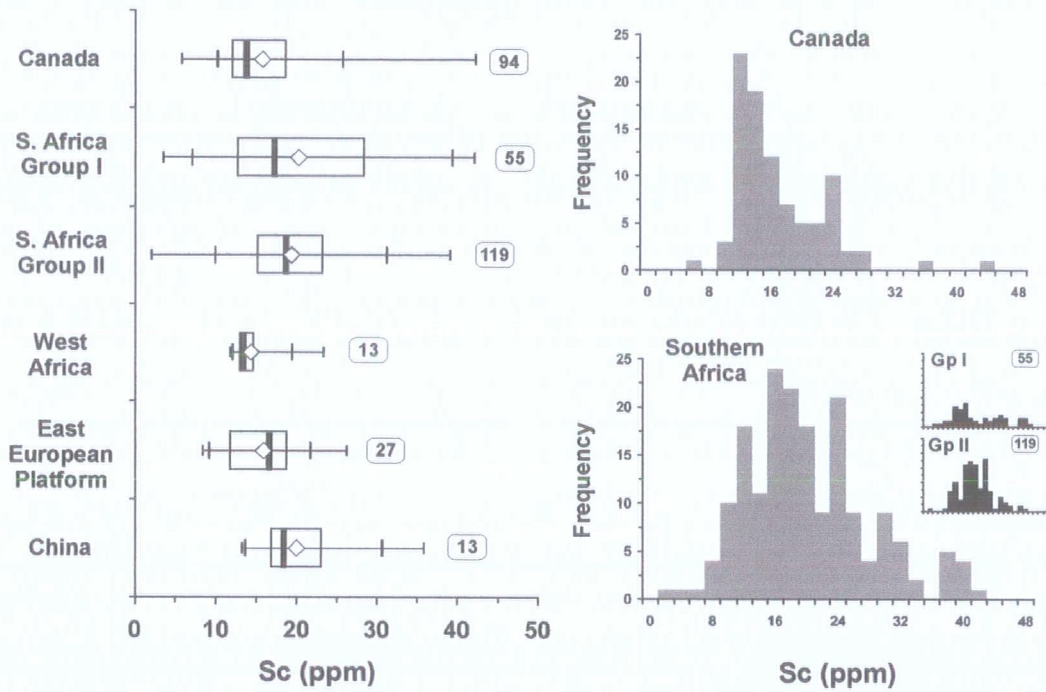
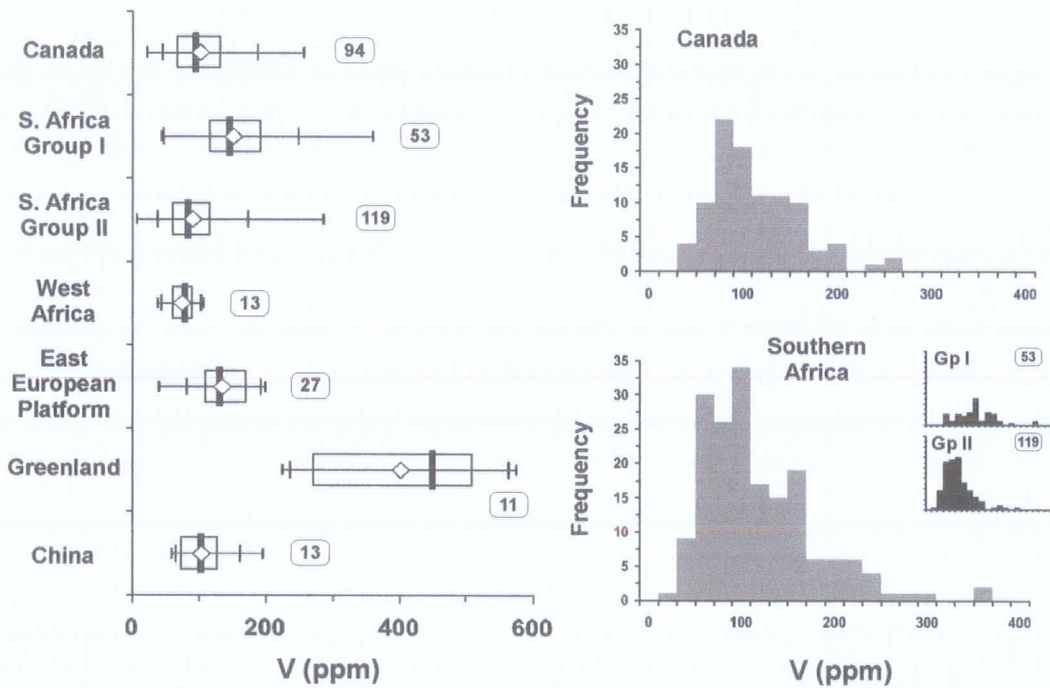**Figure E.5** Dispersion and distribution of Sc in selected global hypabyssal kimberlite occurrences.

Figure E.6 Dispersion and distribution of V in selected global hypabyssal kimberlite occurrences.

Figure E.7 Dispersion and distribution of Rb in selected global hypabyssal kimberlite occurrences.

Figure E.8 Dispersion and distribution of Pb in selected global hypabyssal kimberlite occurrences.

Figure E.9 Dispersion and distribution of Ba in selected global hypabyssal kimberlite occurrences.

Figure E.10 Dispersion and distribution of Hf in selected global hypabyssal kimberlite occurrences.
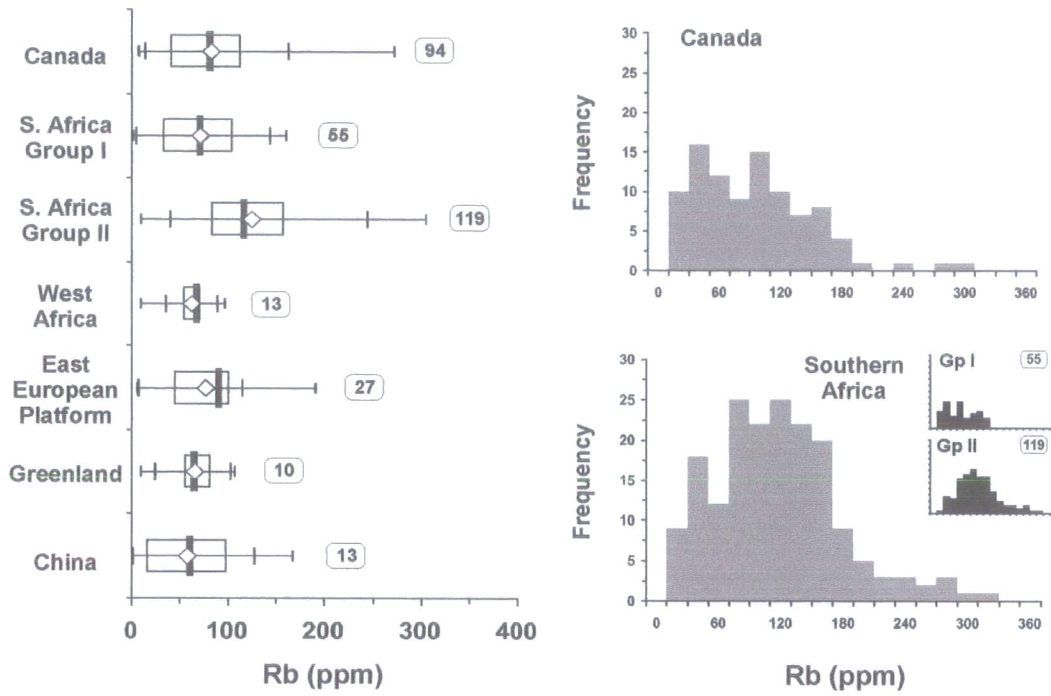
340

Figure E.11 Dispersion and distribution of Zr in selected global hypabyssal kimberlite occurrences.
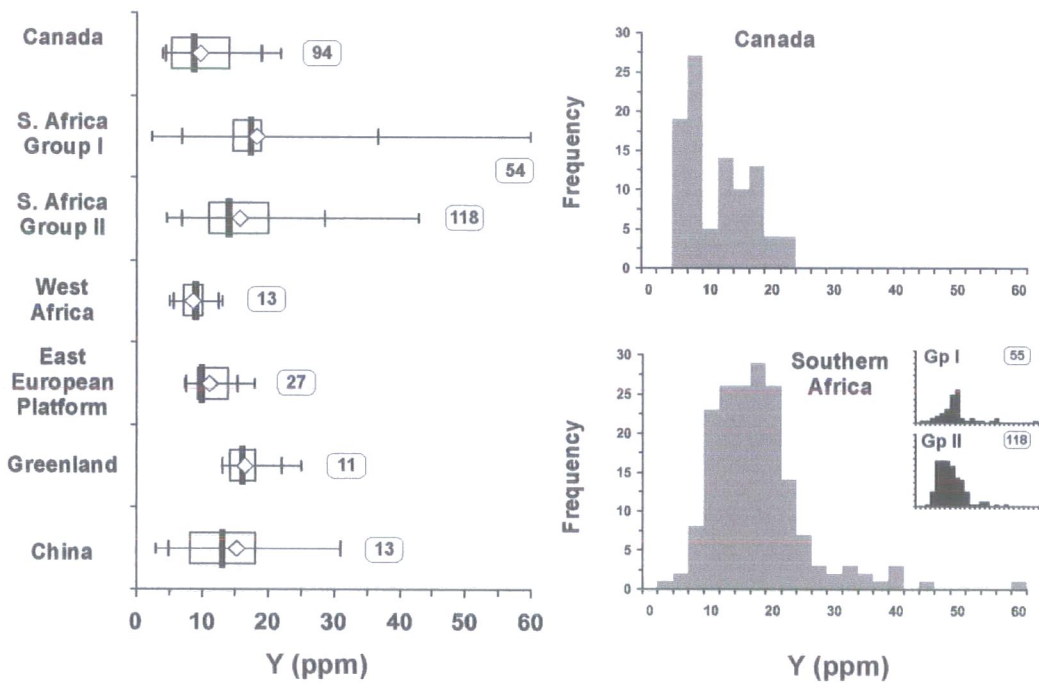
Figure E.12 Dispersion and distribution of Y in selected global hypabyssal kimberlite occurrences.
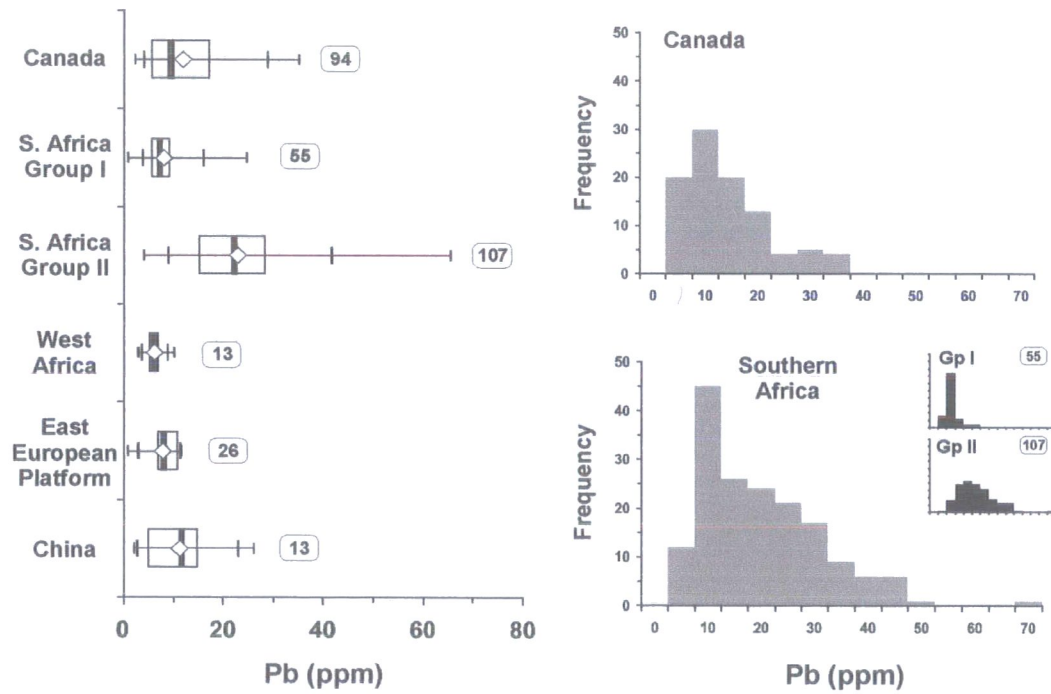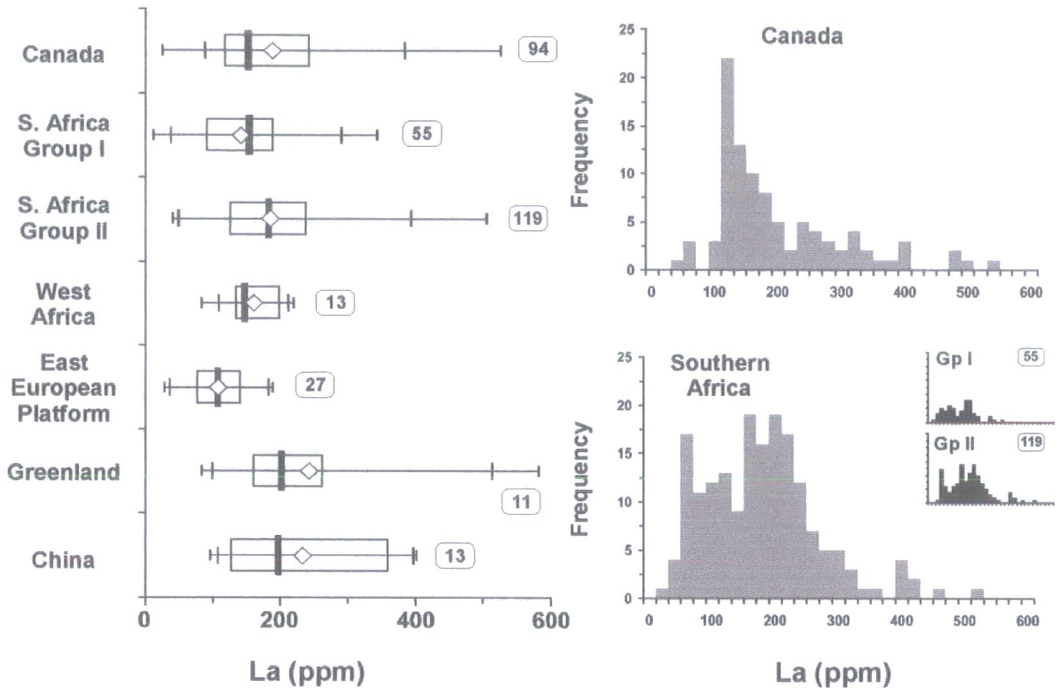
Figure E.13 Dispersion and distribution of La in selected global hypabyssal kimberlite occurrences.
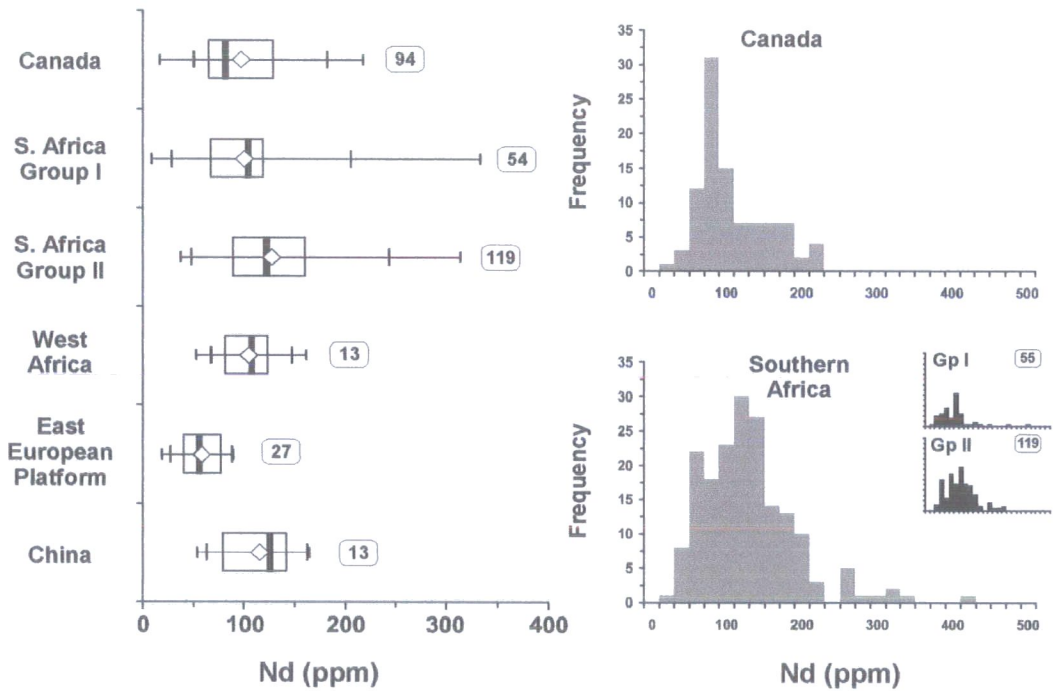
Figure E.14 Dispersion and distribution of Nd in selected global hypabyssal kimberlite occurrences.
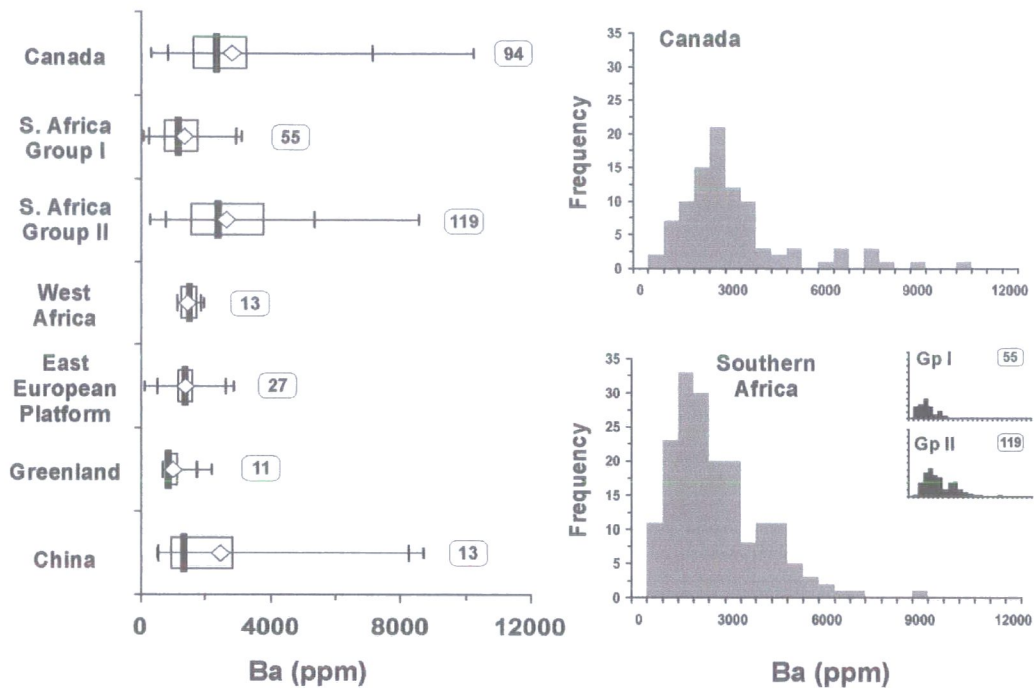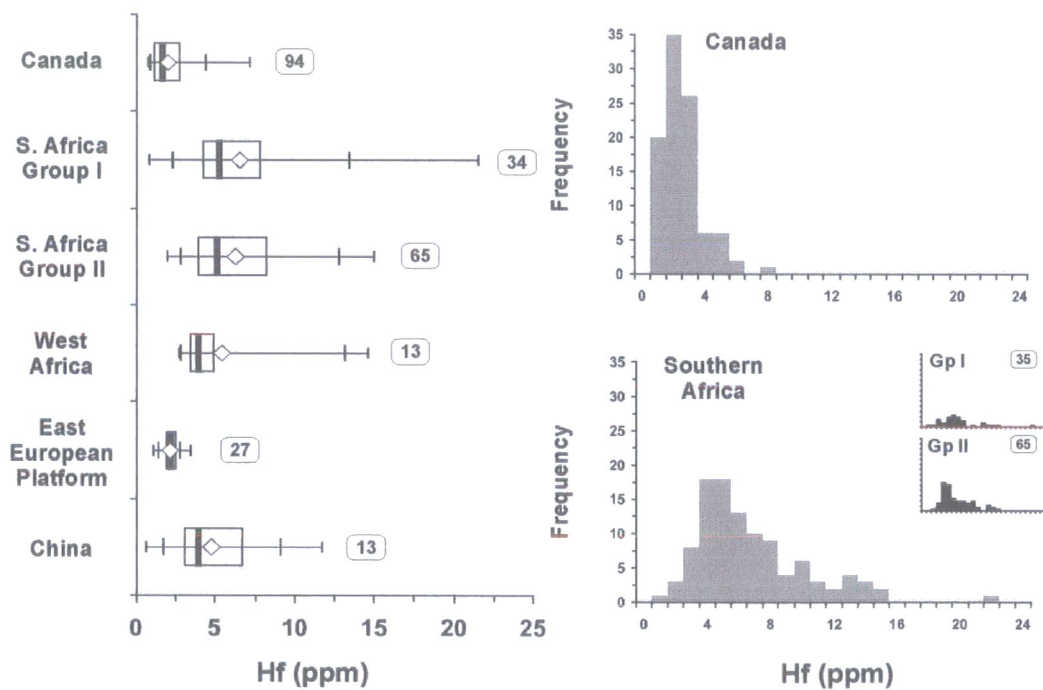
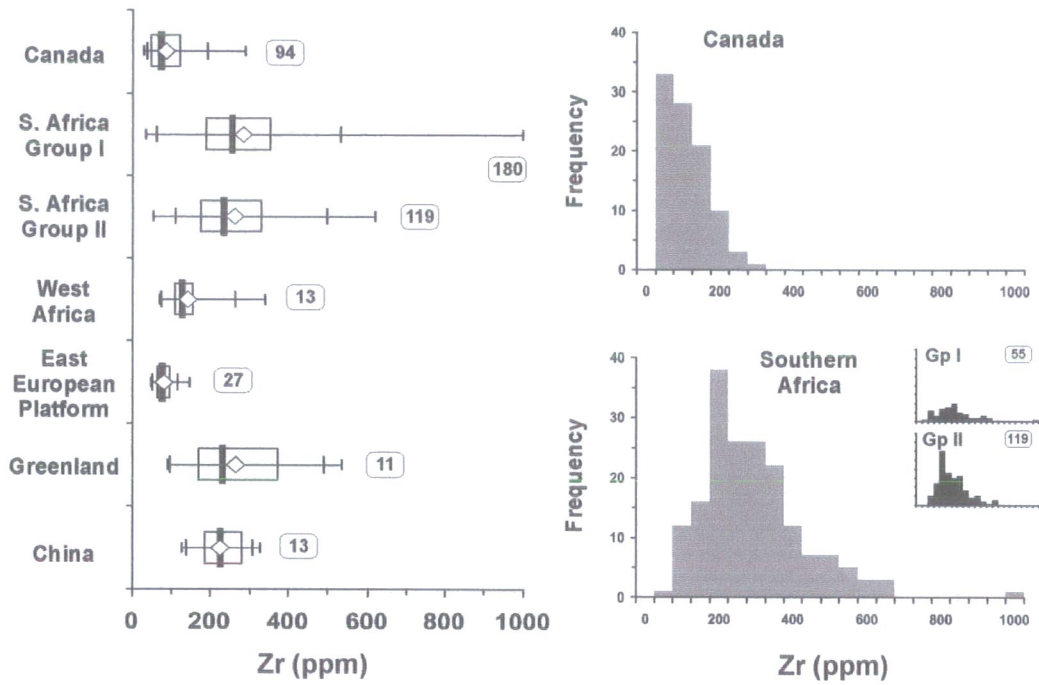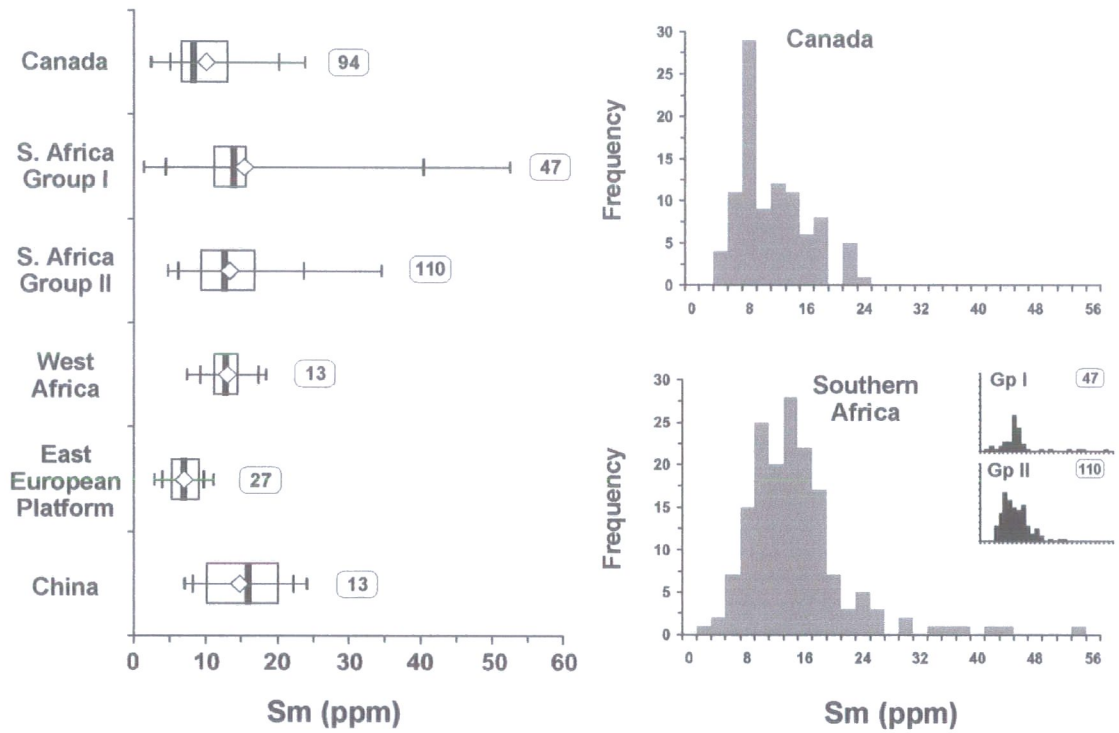**Figure E.15** Dispersion and distribution of Sm in selected global hypabyssal kimberlite
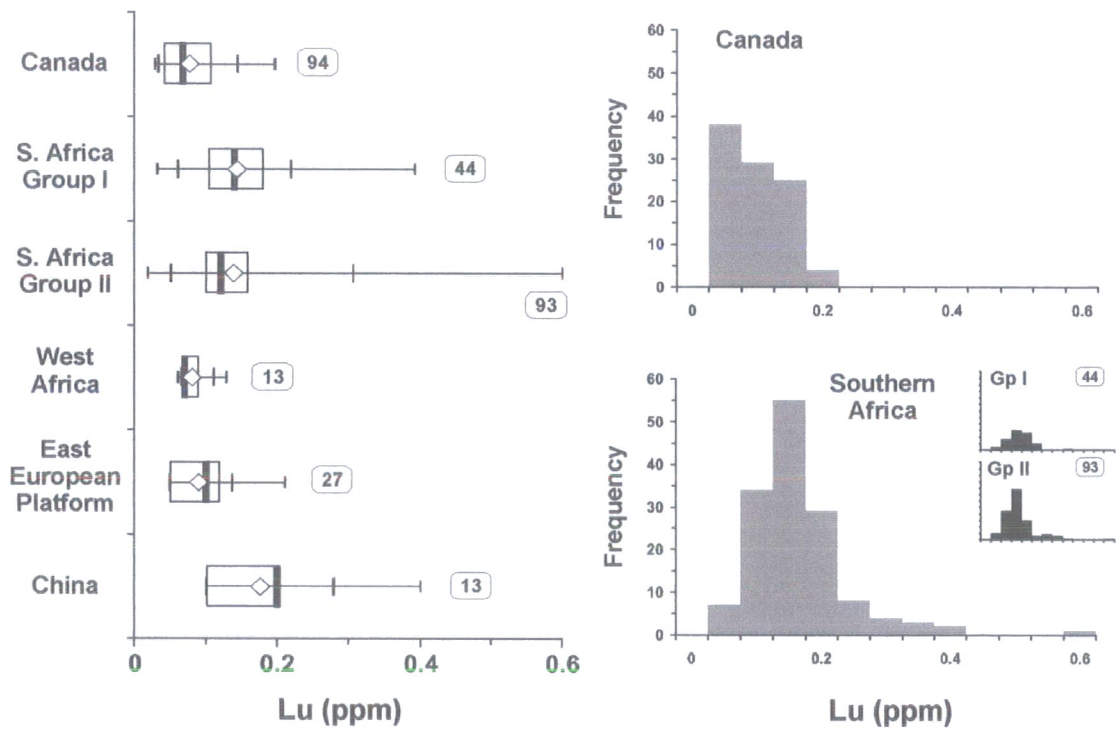
Figure E.16 Dispersion and distribution of Lu in selected global hypabyssal kimberlite

343
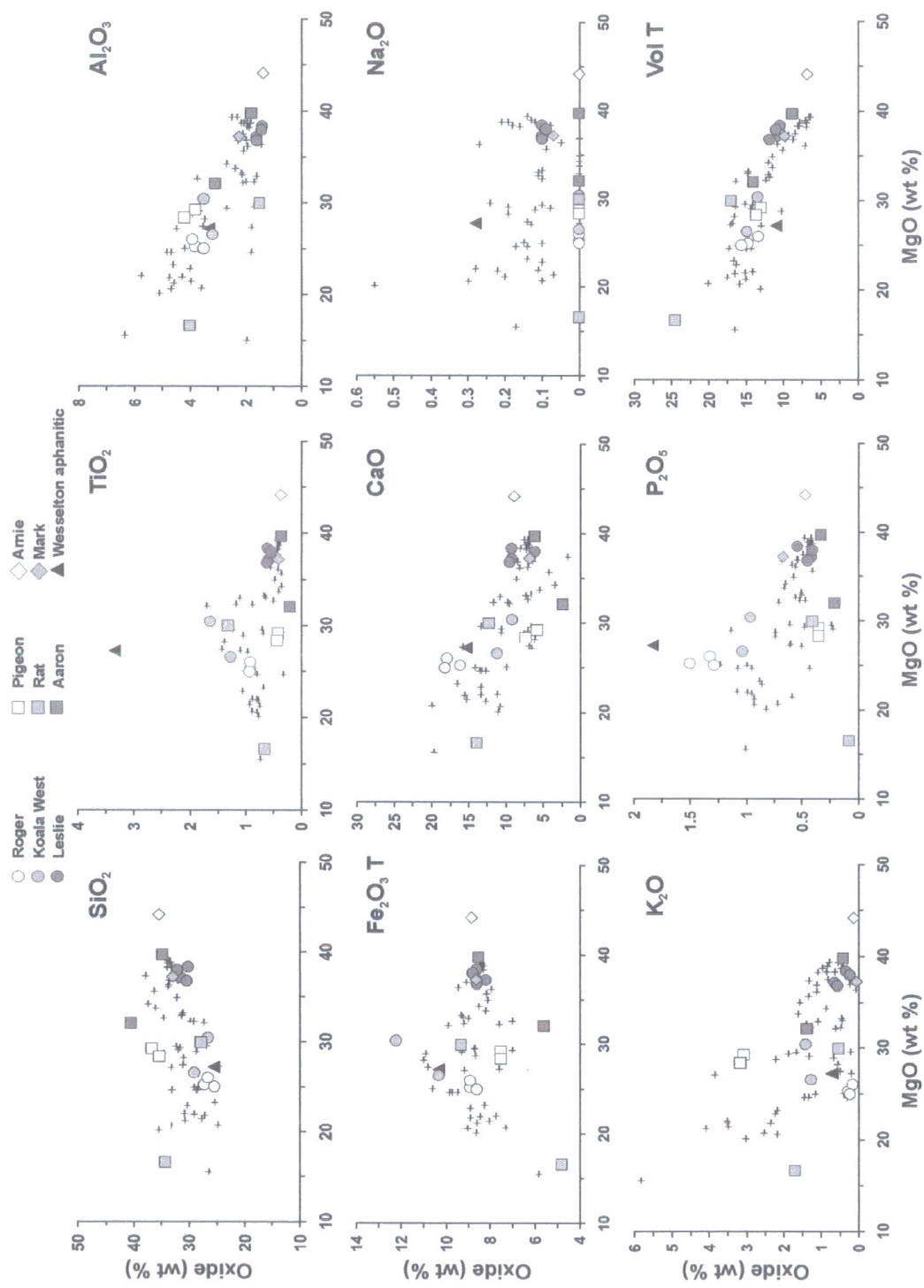
Figure E.17 Major element compositional variation in hypabyssal kimberlite from bodies adjacent to Grizzly, relative to other Lac de Gras intrusions and Wesselton aphanitic kimberlite.

344
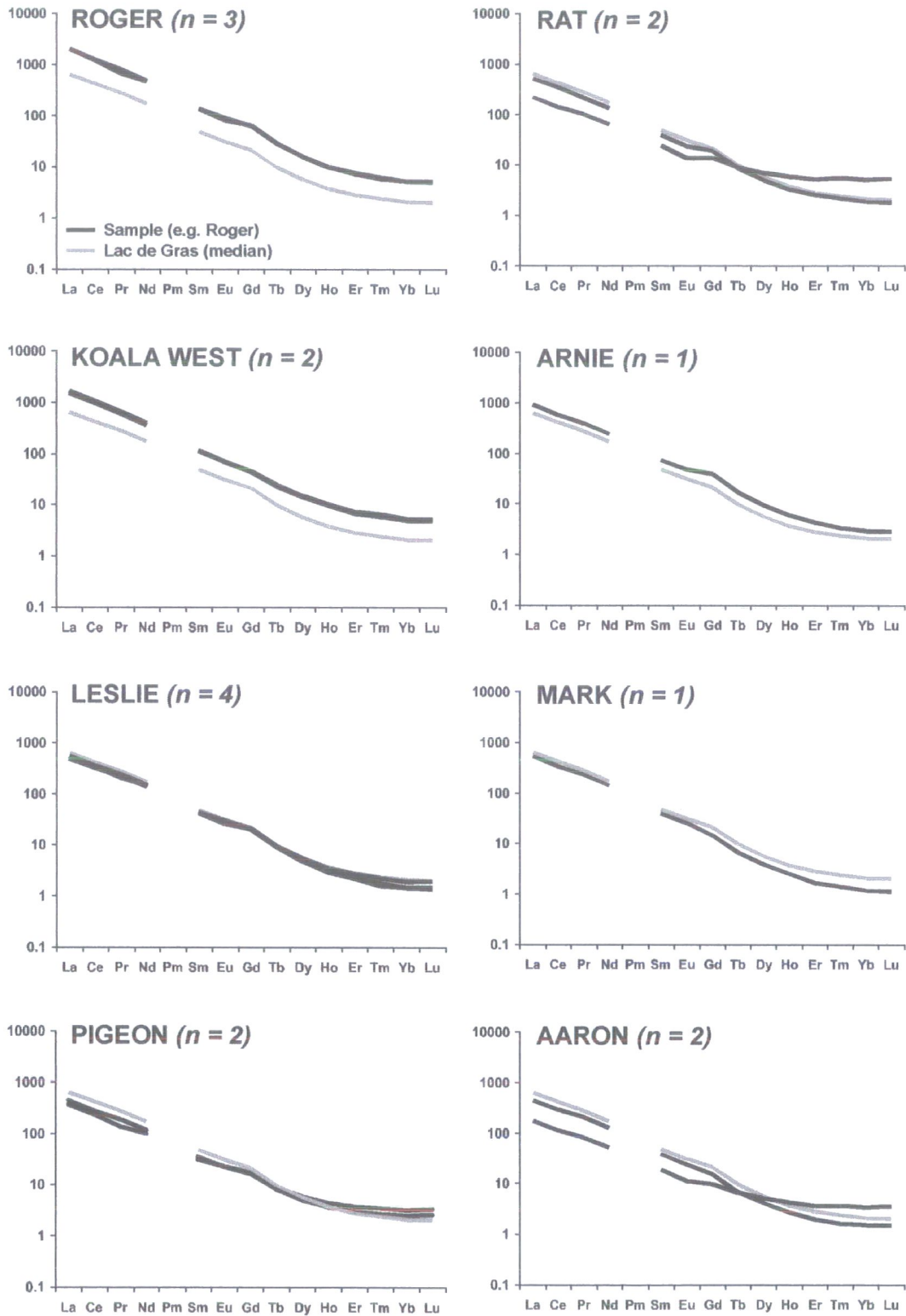
Figure E.18 Chondrite-normalised rare earth element patterns for kimberlites in the vicinity of Grizzly, compared to Lac de Gras median.
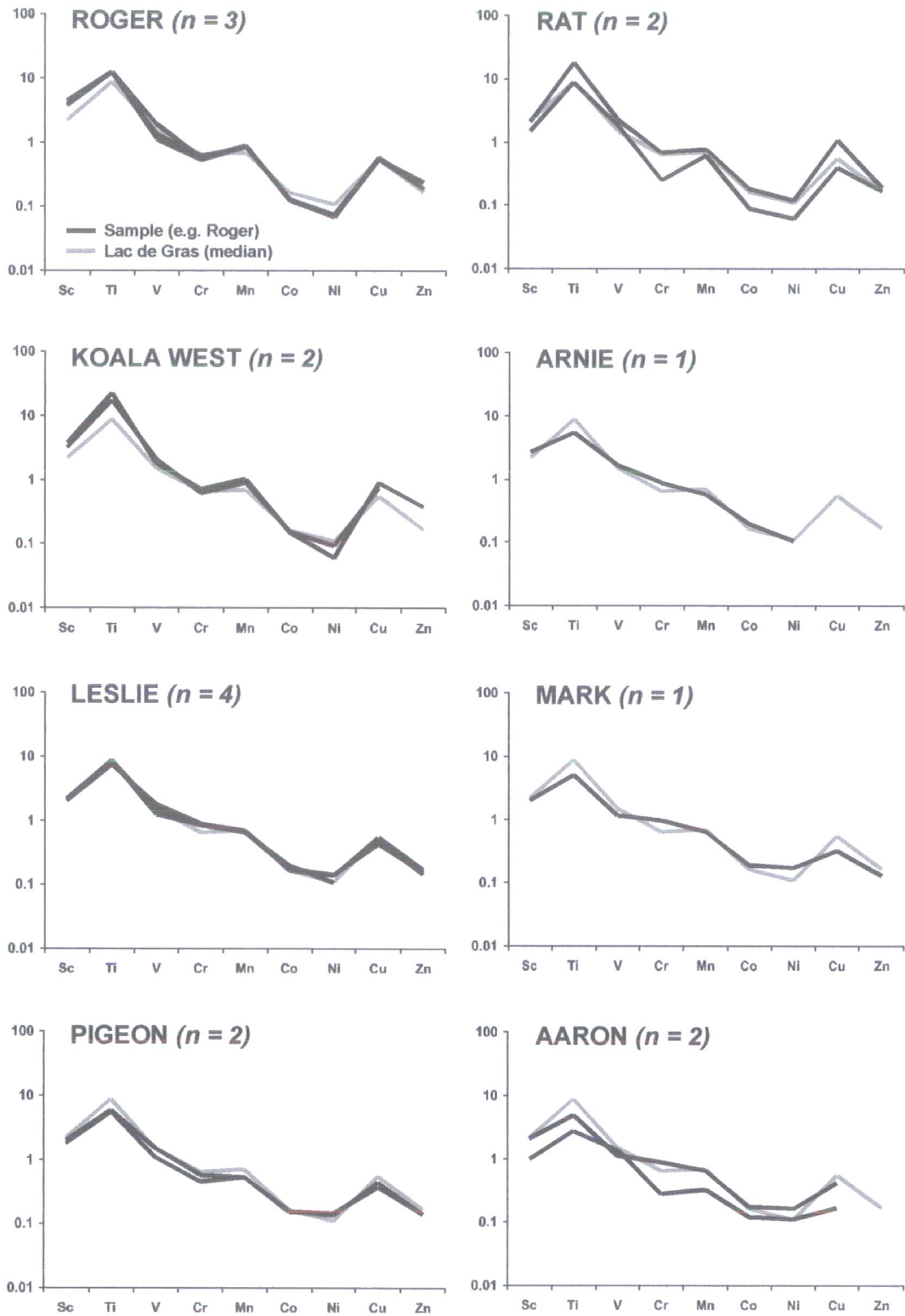
Figure E.19 Chondrite-normalised compatible element patterns for kimberlites in the vicinity of Grizzly, compared to Lac de Gras median.
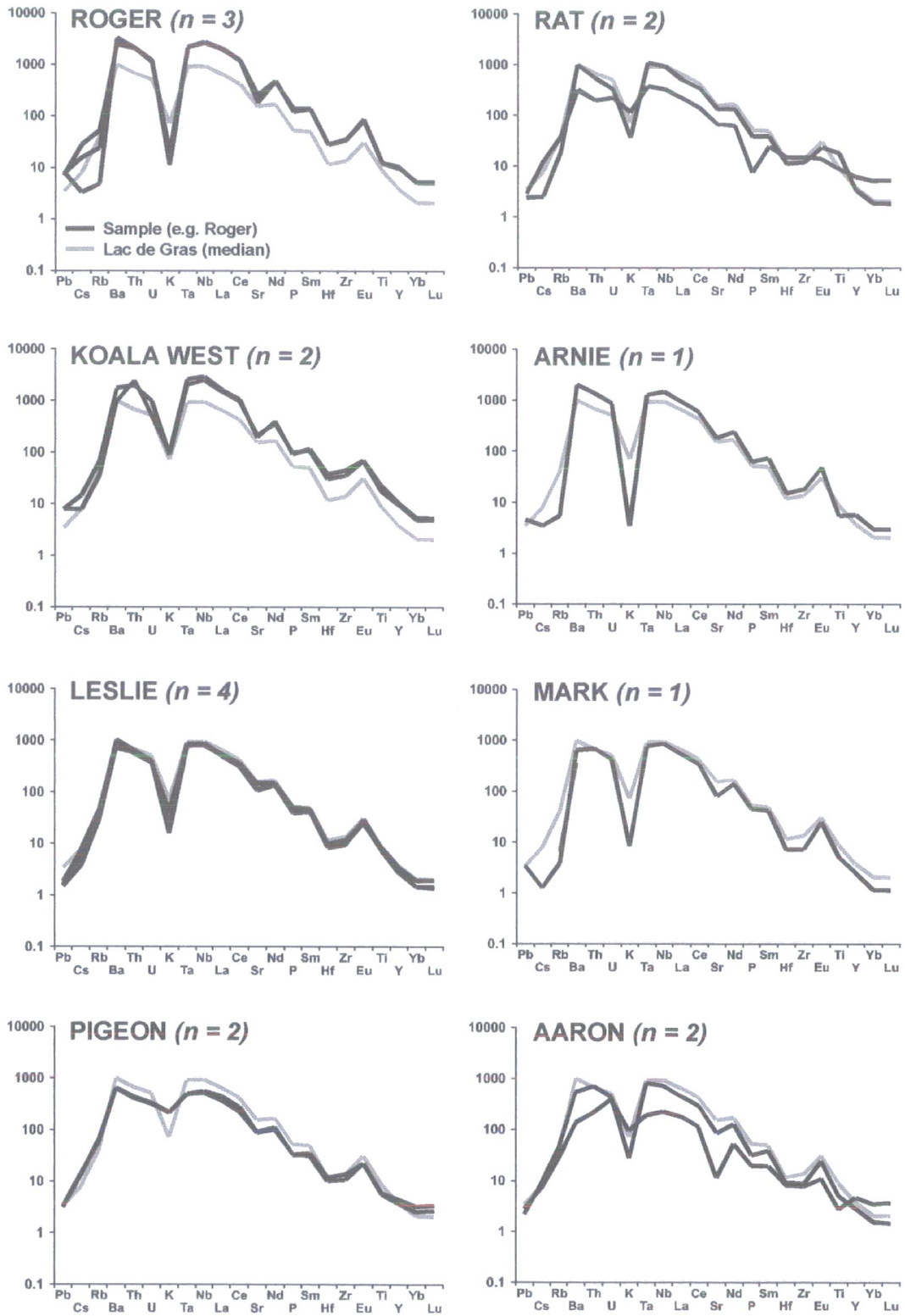
Figure E.20 Chondrite-normalised incompatible element patterns for kimberlites in the vicinity of Grizzly, compared Lac de Gras median.

347
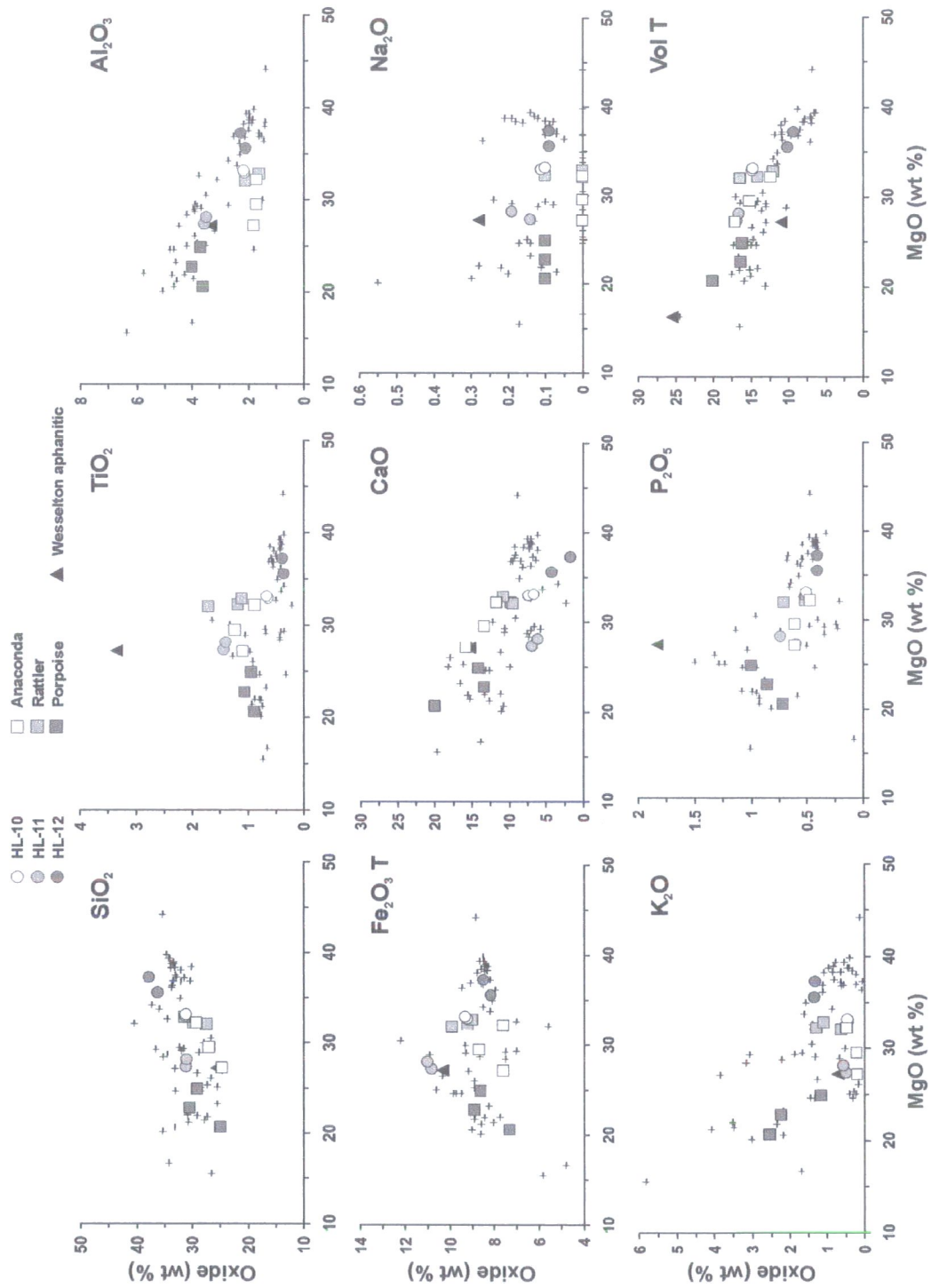
Figure E.21 Major element compositional variation of hypabyssal kimberlite from northern Lac de Gras bodies beyond immediate vicinity of Grizzly, relative to other Lac de Gras intrusions and Wesselton aphanitic kimberlite.
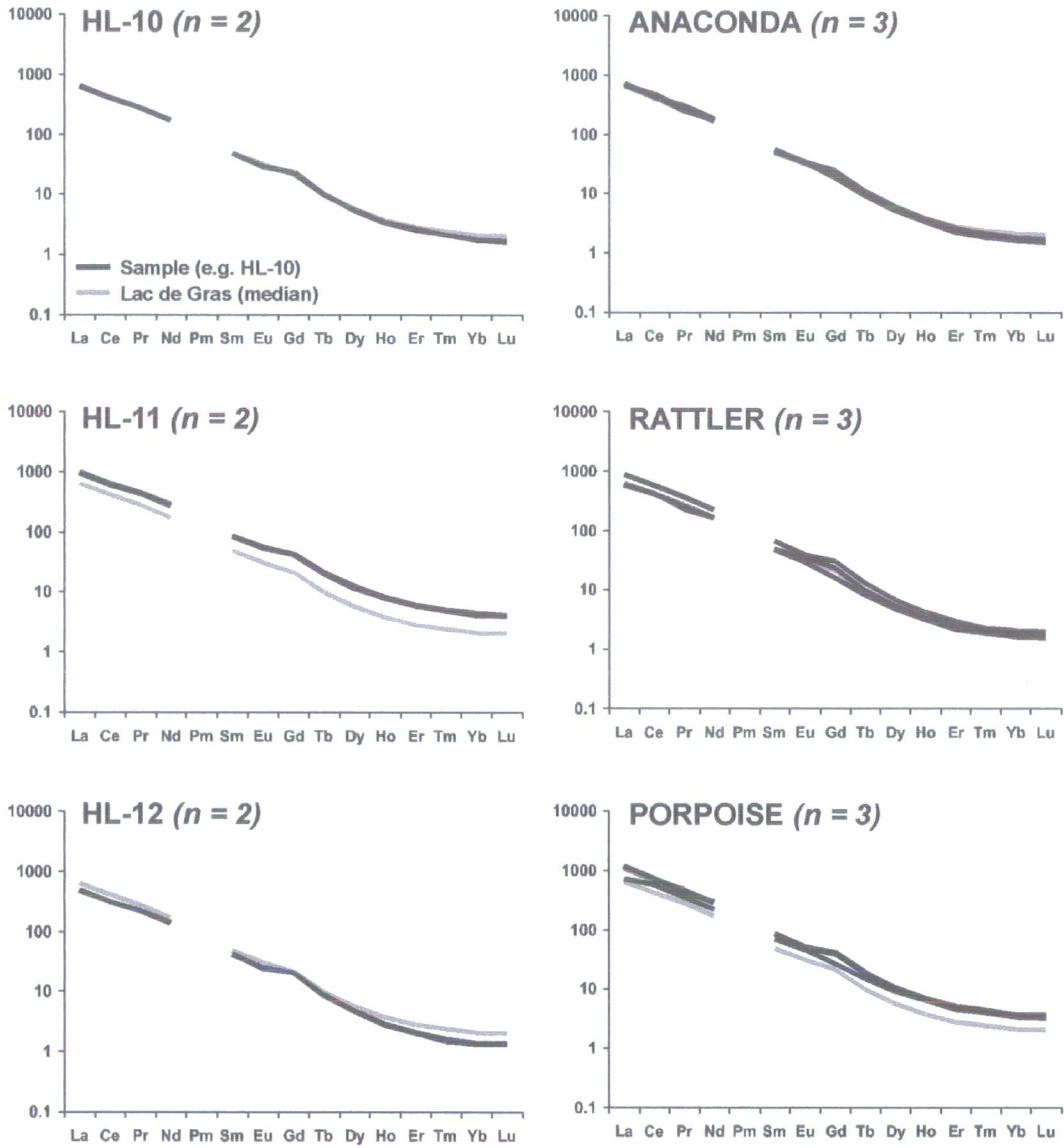
Figure E.22 Chondrite-normalised rare earth element patterns for kimberlites on north side of Lac de Gras, compared to Lac de Gras median.
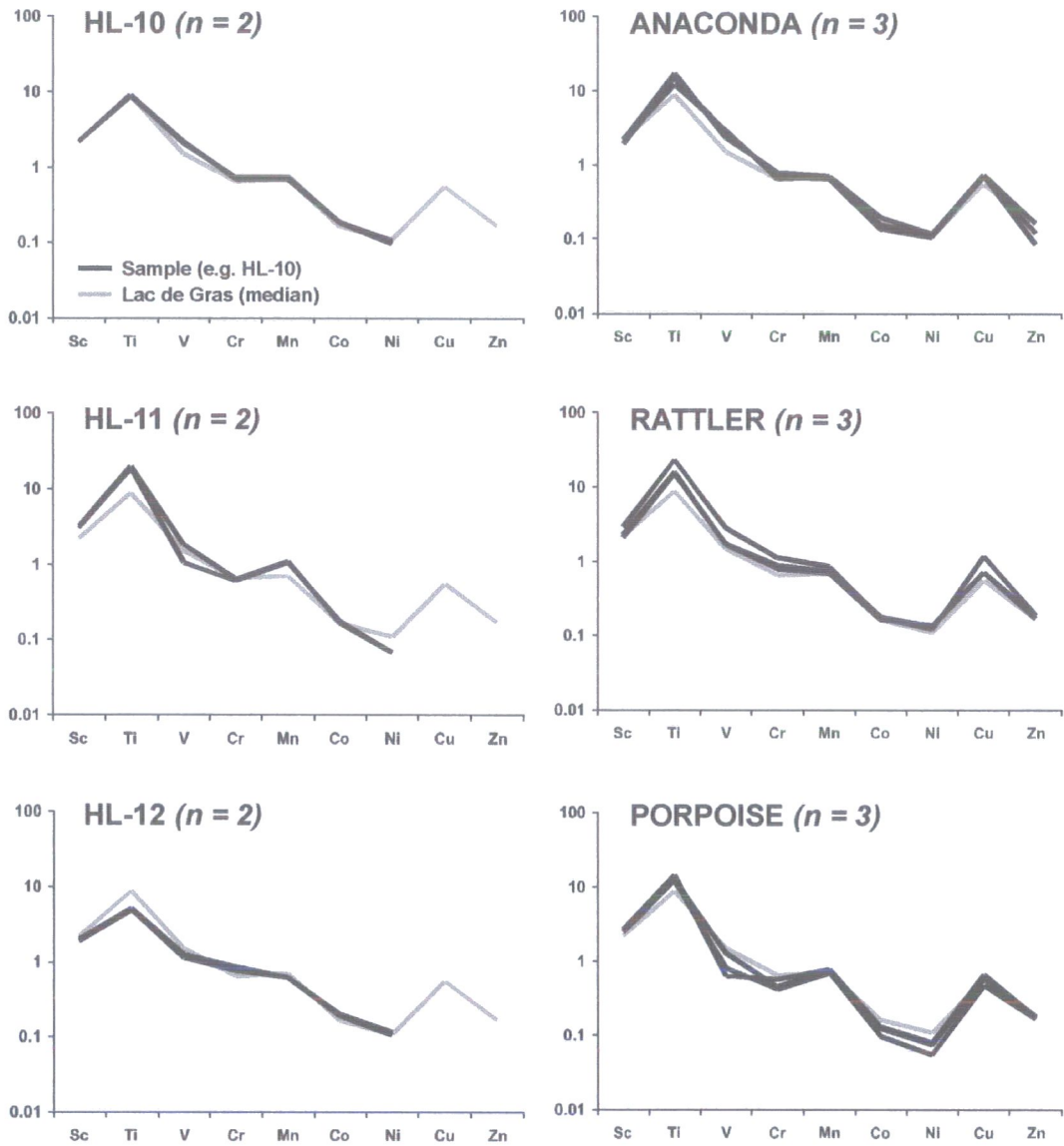
Figure E.23 Chondrite-normalised compatible element patterns for kimberlites on north side of Lac de Gras, compared to Lac de Gras median.
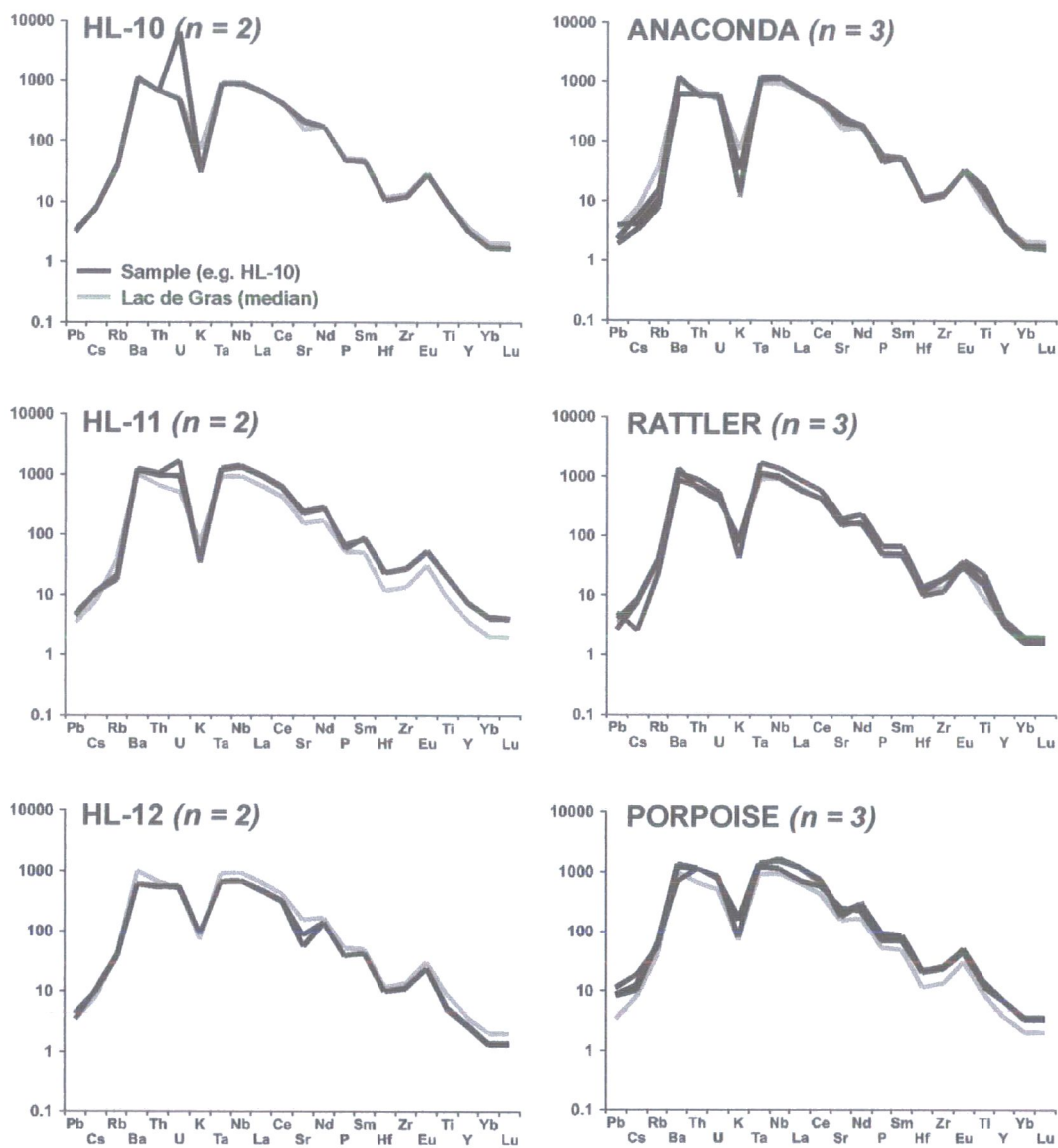
Figure E.24 Chondrite-normalised incompatible element patterns for kimberlites on north side of Lac de Gras, compared to Lac de Gras median.
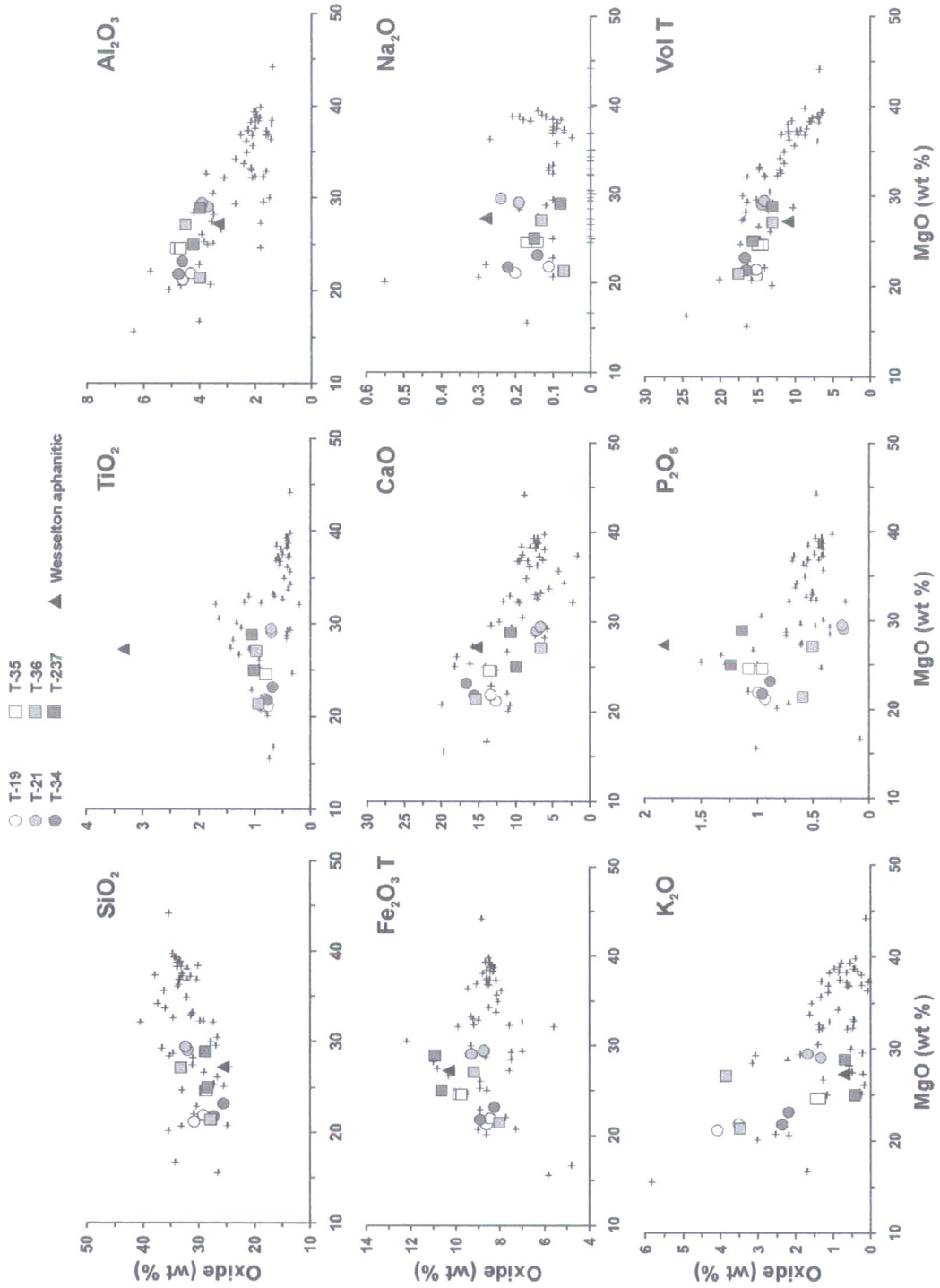
Figure E.25 Major element compositional variation of hypabyssal kimberlite from south and east of Lac de Gras, relative to other Lac de Gras intrusions and aphanitic kimberlite.

352
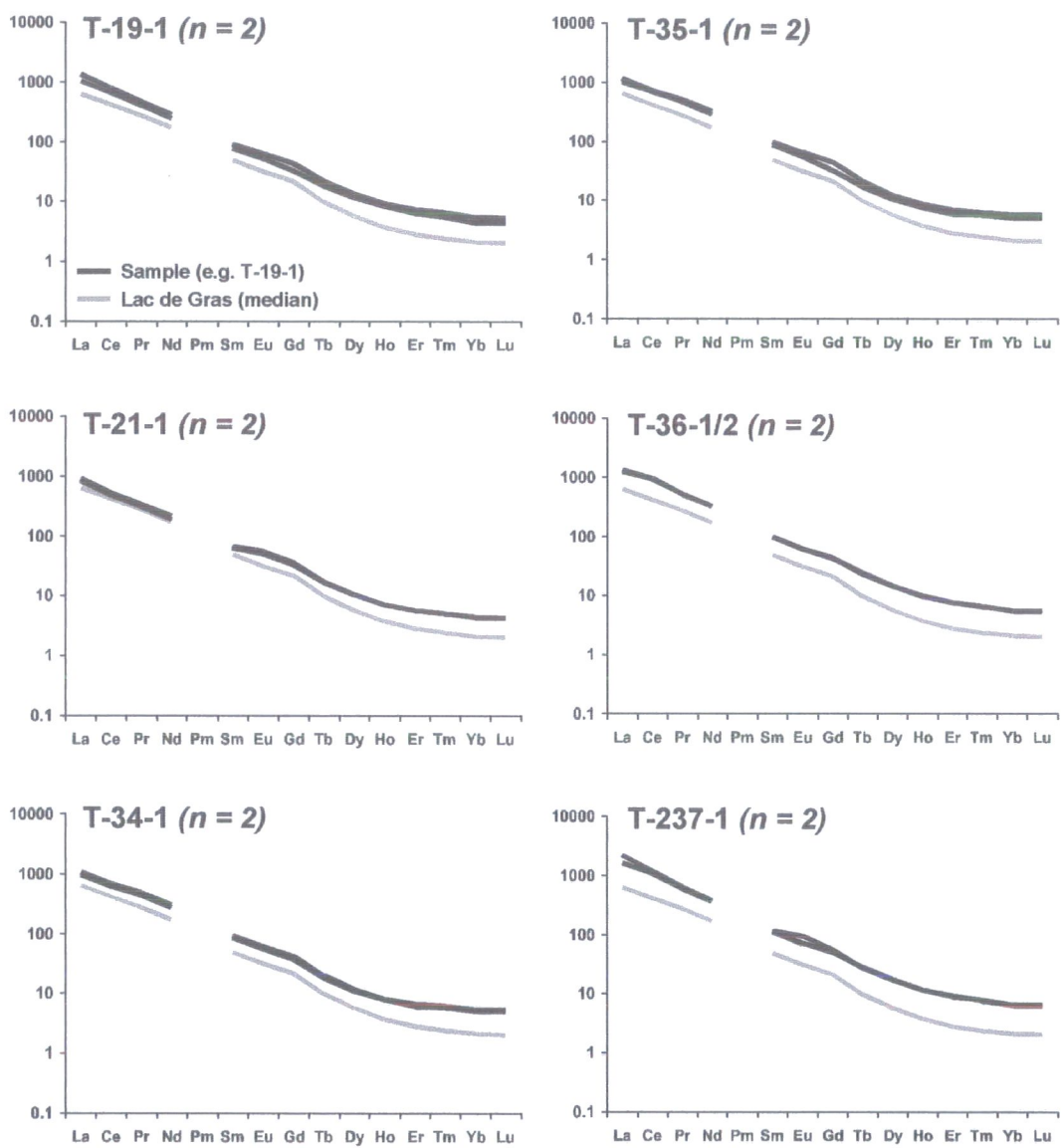
Figure E.26 Chondrite-normalised rare earth element patterns for kimberlites south and east of Lac de Gras, compared to Lac de Gras median.
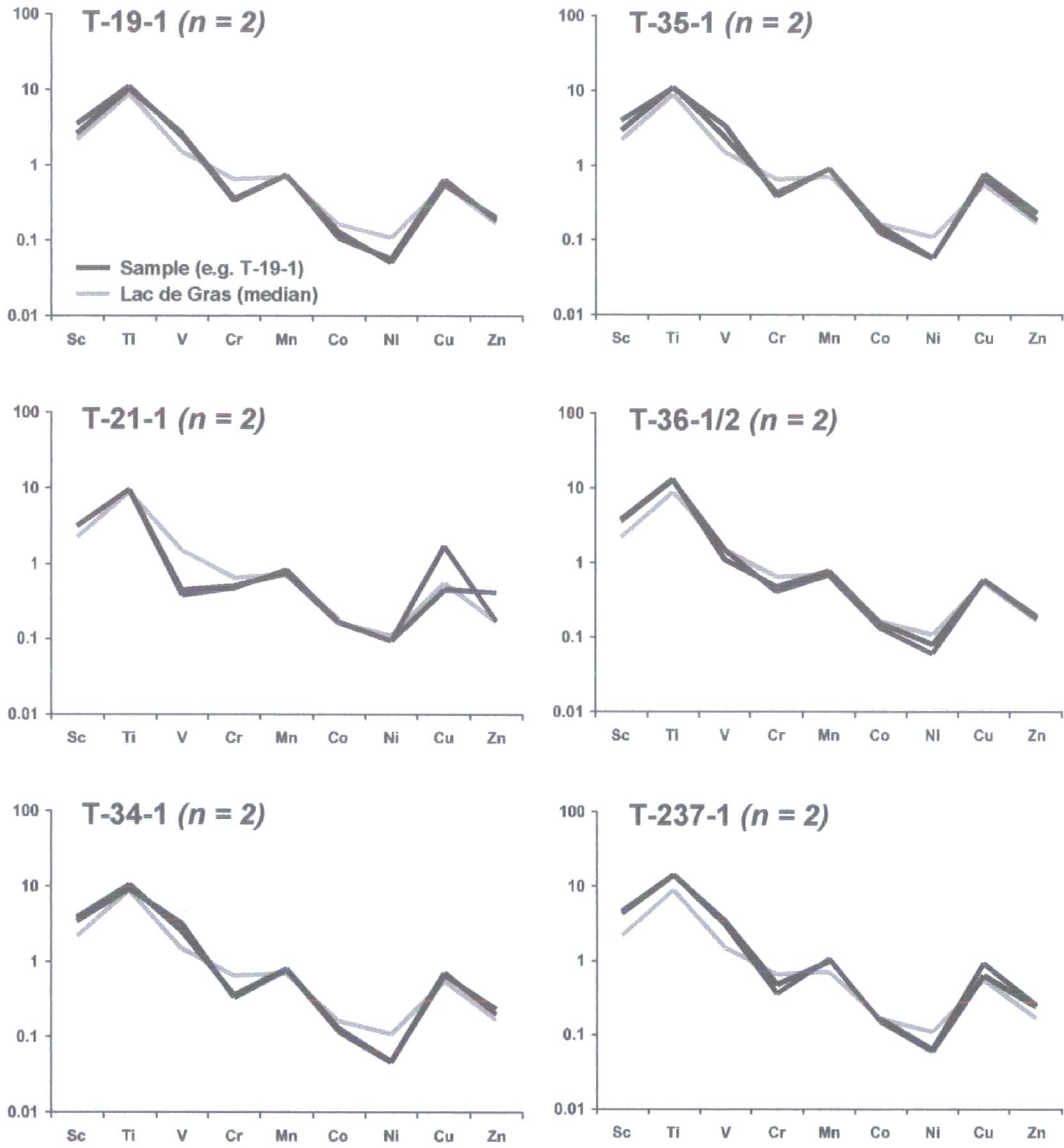
Figure E.27 Chondrite-normalised compatible element patterns for kimberlites south and east Lac de Gras, compared to Lac de Gras median.
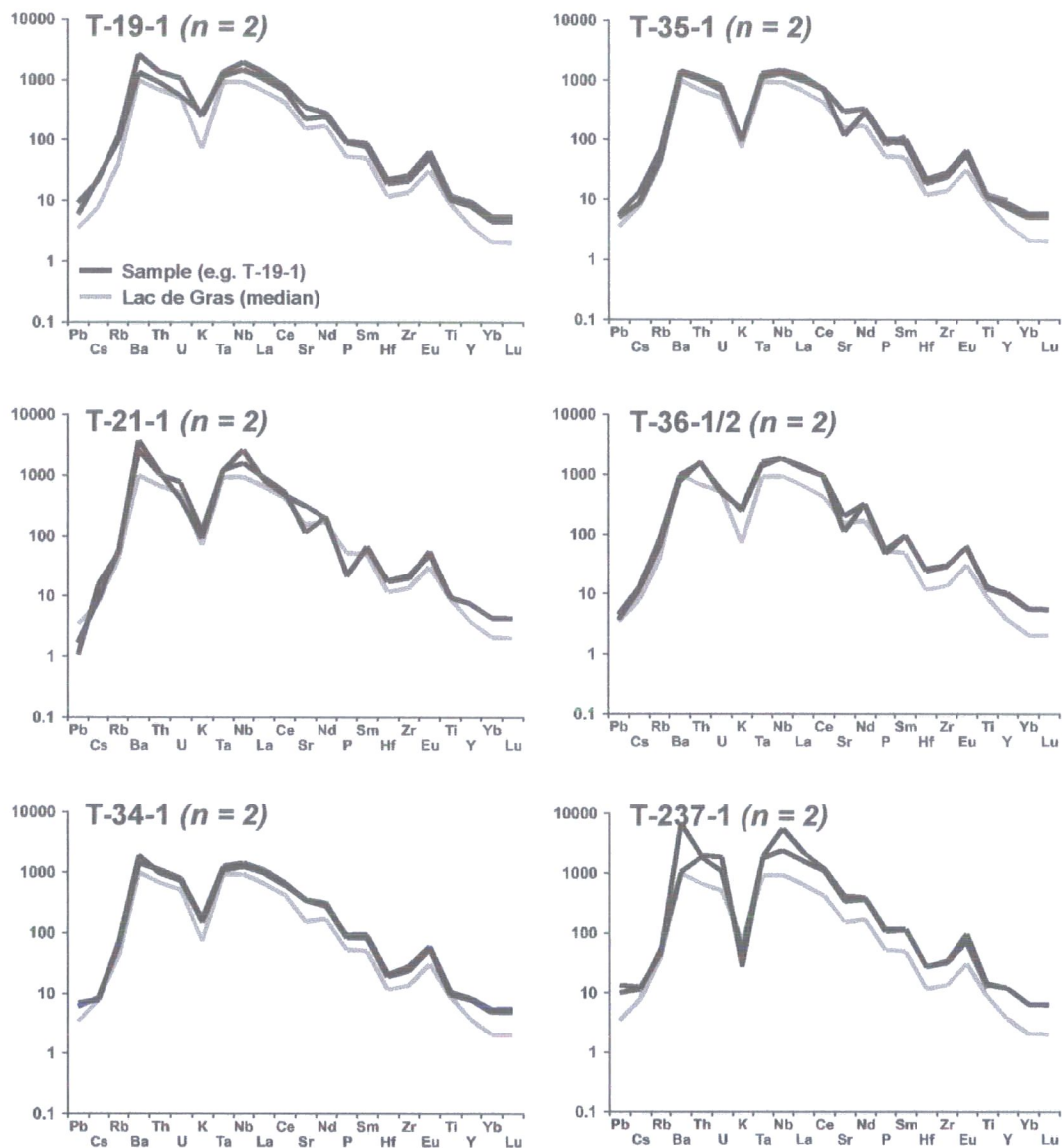
Figure E.28 Chondrite-normalised incompatible element patterns for kimberlites south and east of Lac de Gras, compared to Lac de Gras median.
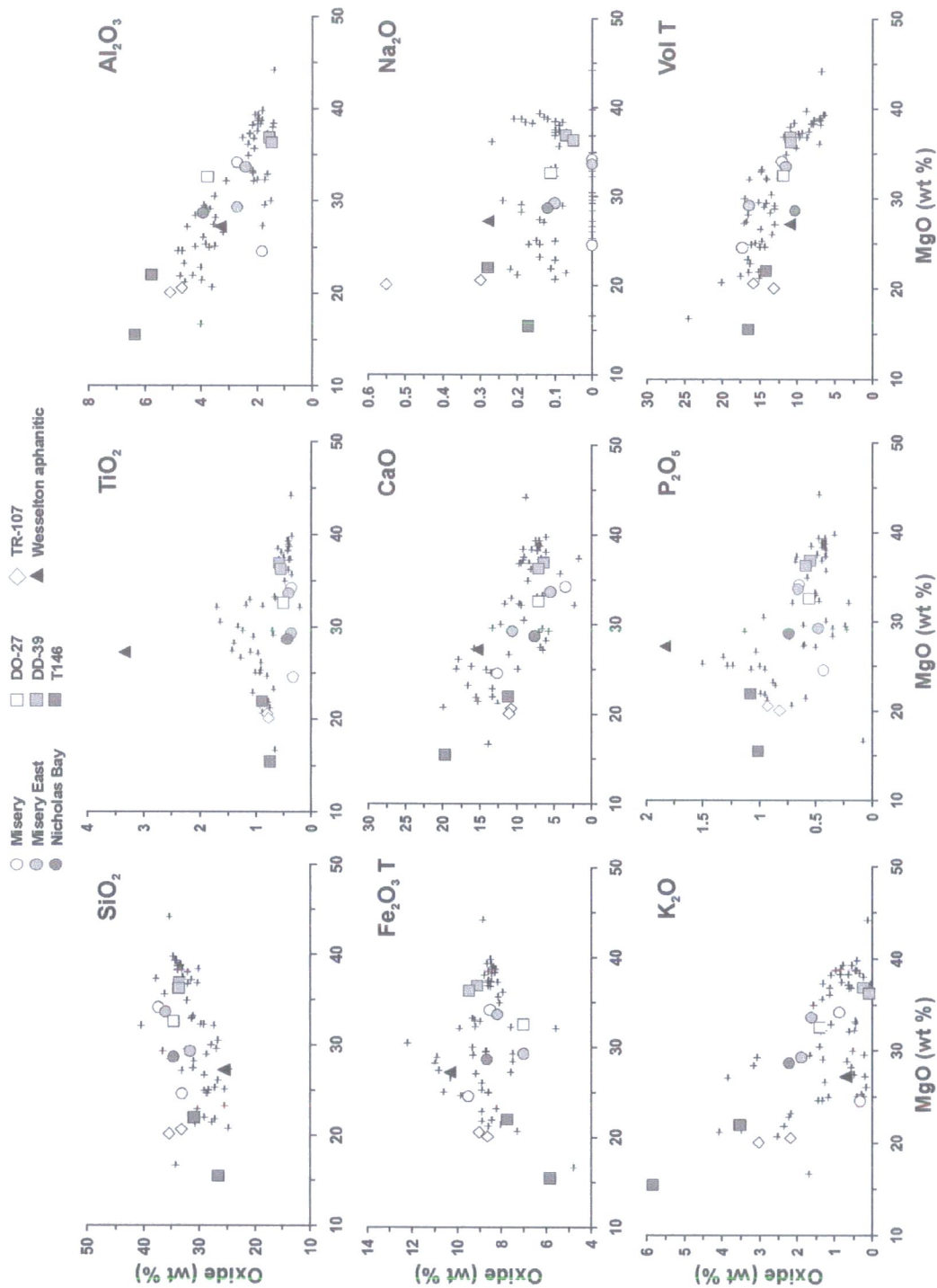
Figure E.29 Major element compositional variation of hypabyssal kimberlite from outlying bodies in southern Lac de Gras, relative to other Lac de Gras intrusions and aphanitic kimberlite.

356
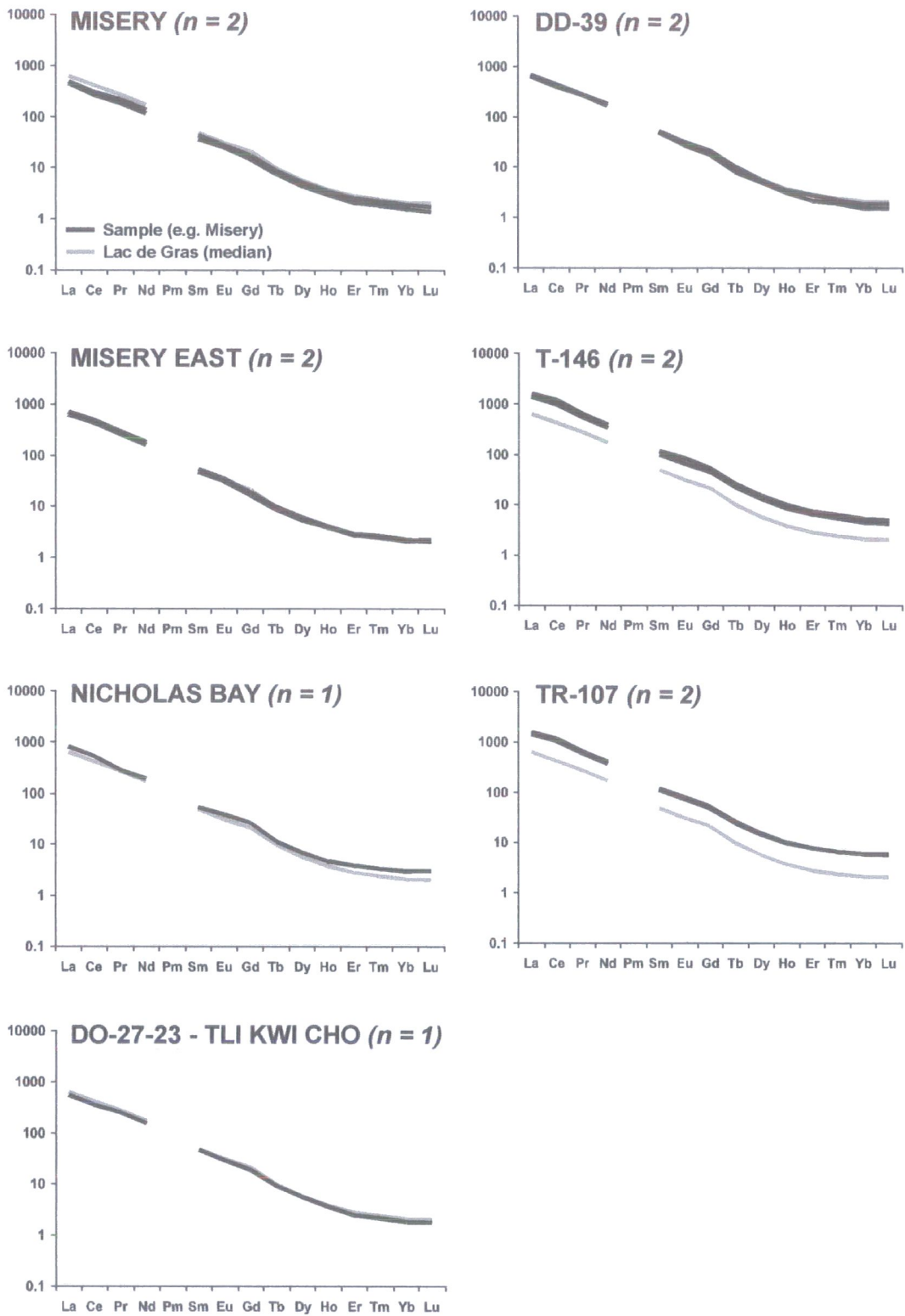
Figure E.30 Chondrite-normalised rare earth element patterns for kimberlites situated south of Lac de Gras, compared to Lac de Gras median.
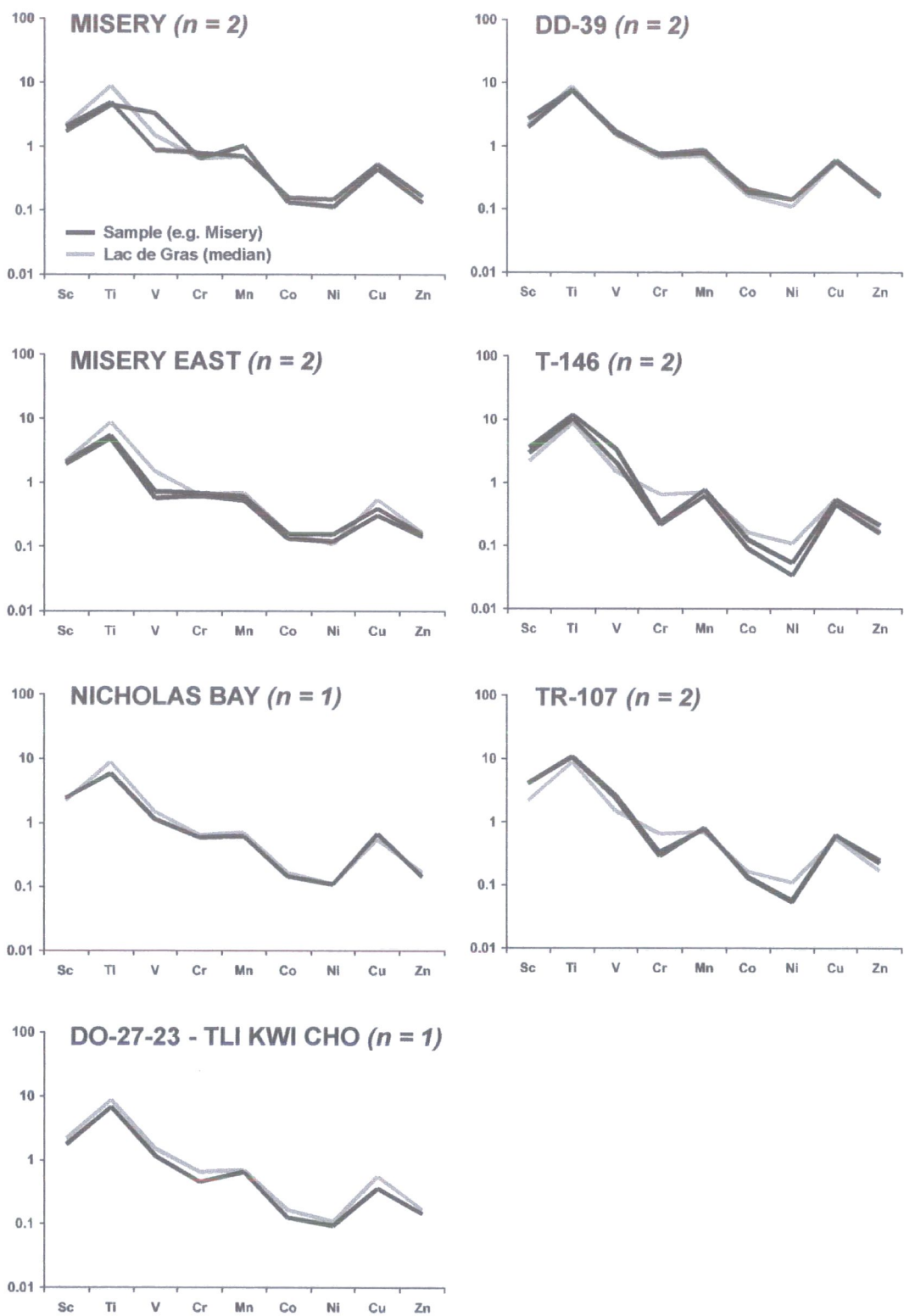
Figure E.31 Chondrite-normalised compatible element patterns for kimberlites situated south of Lac de Gras, compared to Lac de Gras median.
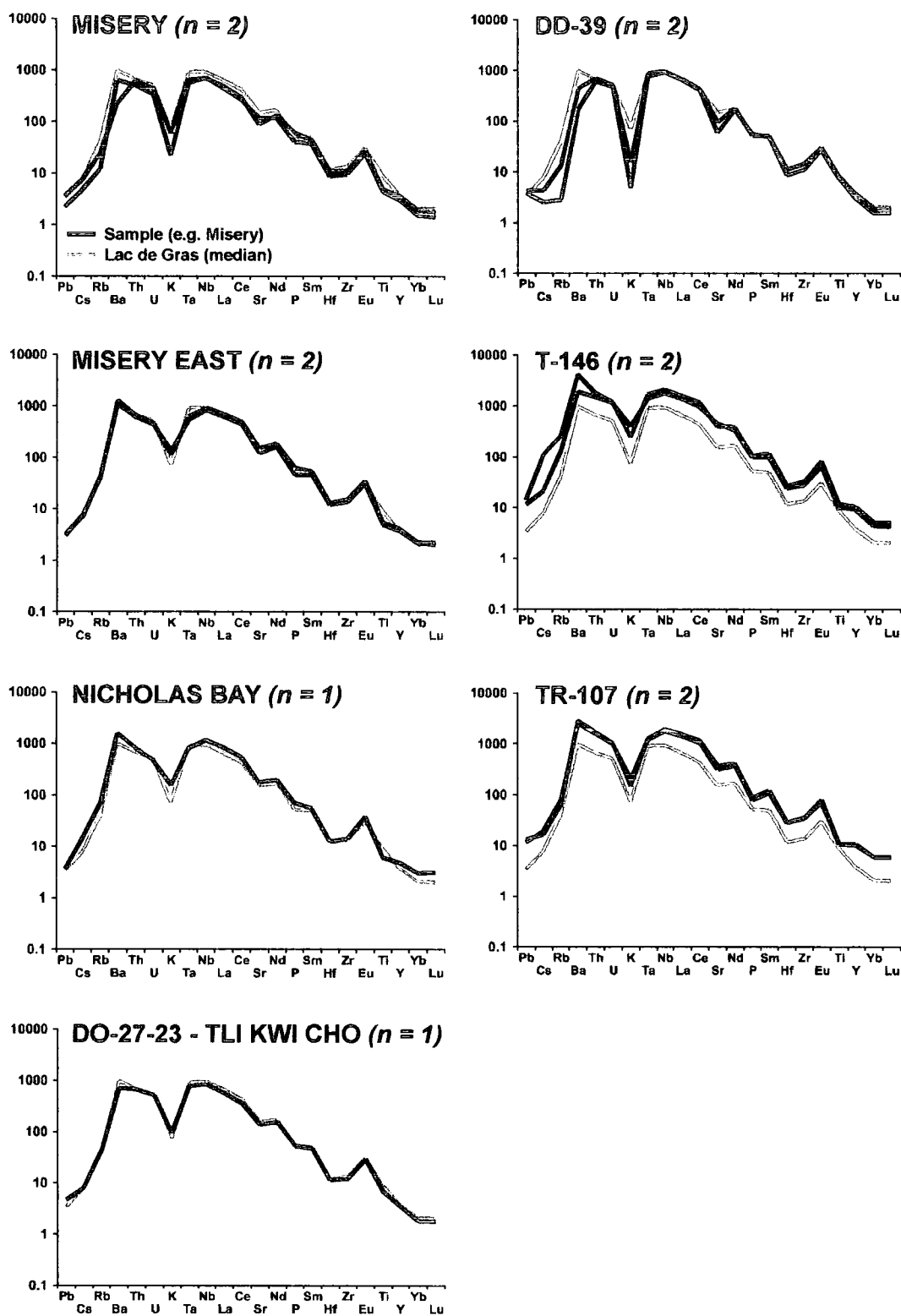
Figure E.32 Chondrite-normalised incompatible element patterns for kimberlites situated south of Lac de Gras, compared to JD-51 (Contwoyto) and Lac de Gras median.
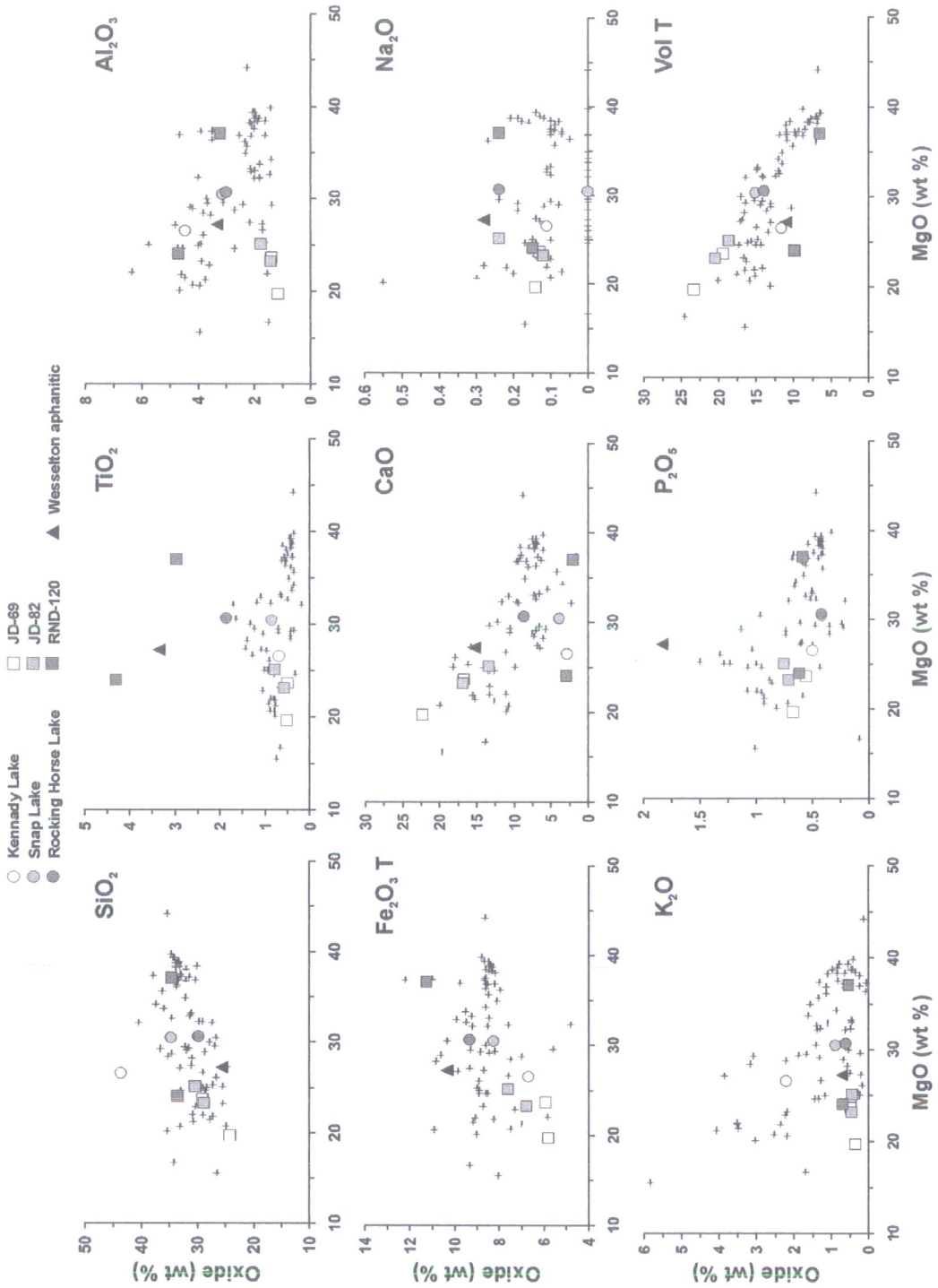
Figure E.33 Major element compositional variation of Slave hypabyssal kimberlite from beyond the Lac de Gras field, relative to Lac de Gras intrusions and Wesselton aphanitic kimberlite.
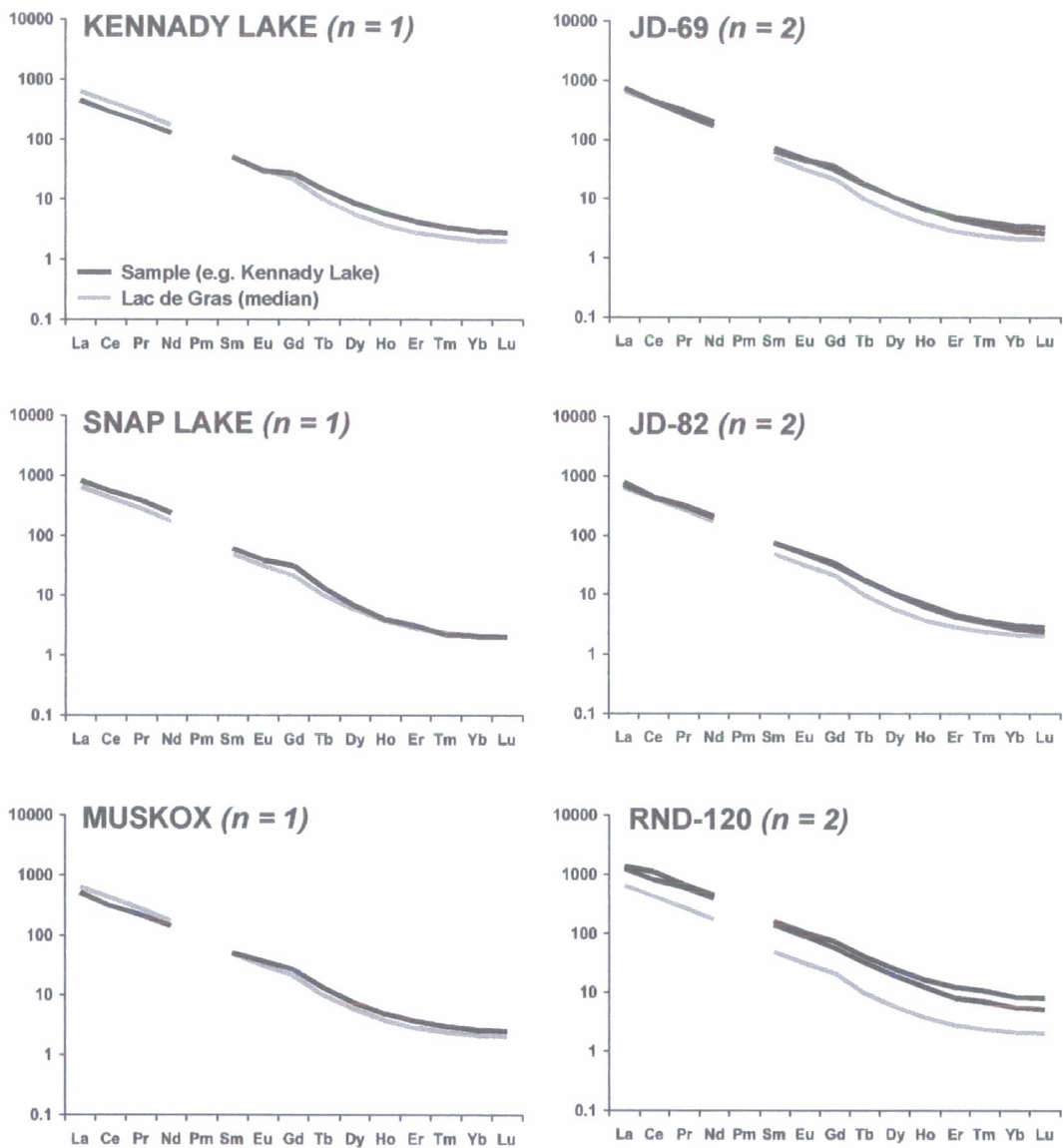
Figure E.34 Chondrite-normalised rare earth element patterns for Slave kimberlites beyond Lac de Gras, compared to Lac de Gras median.
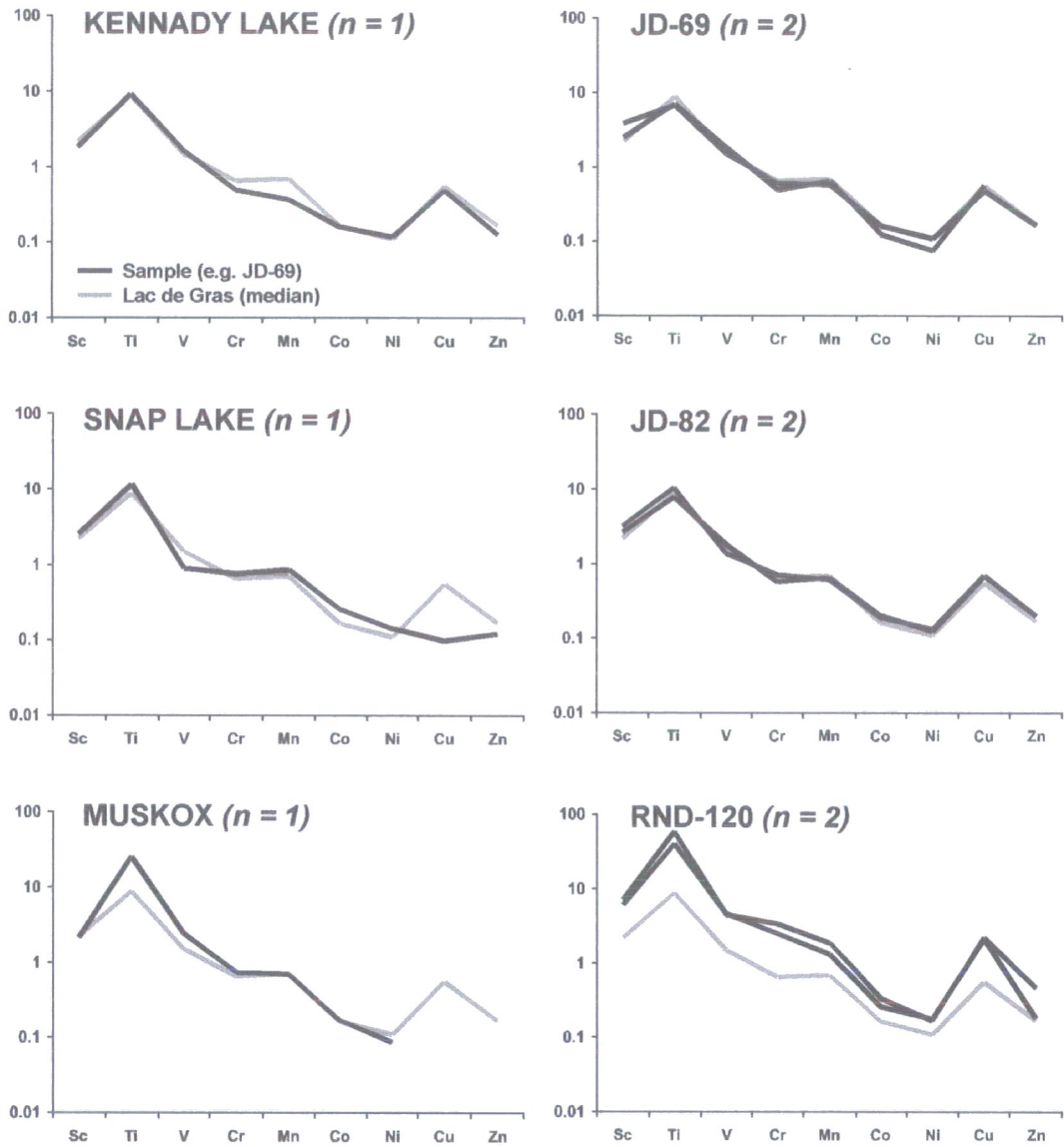
Figure E.35 Chondrite-normalised compatible element patterns for Slave kimberlites beyond Lac de Gras, compared to Lac de Gras median.
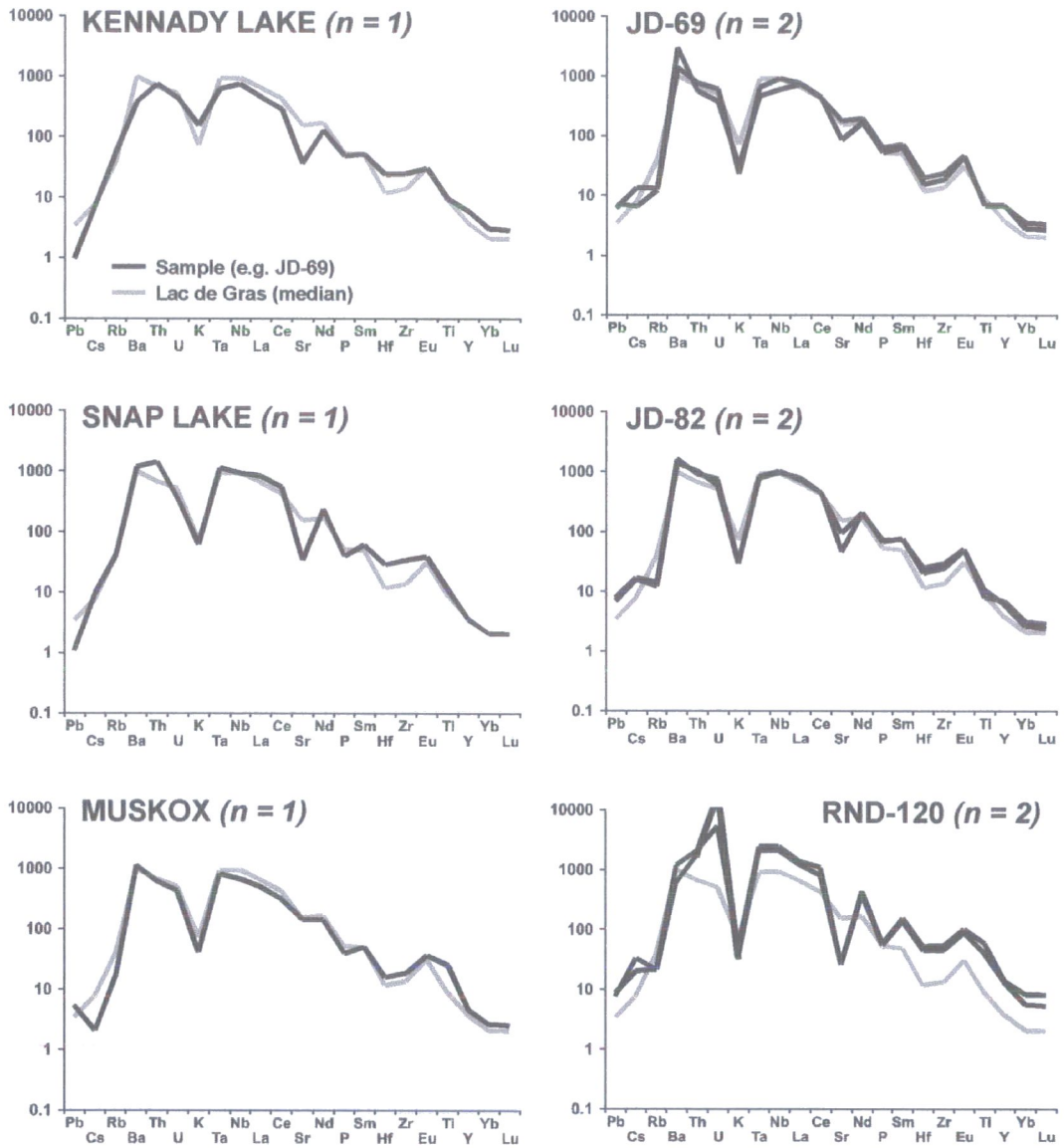
Figure E.36 Chondrite-normalised incompatible element patterns for Slave kimberlites beyond Lac de Gras, compared to Lac de Gras median.
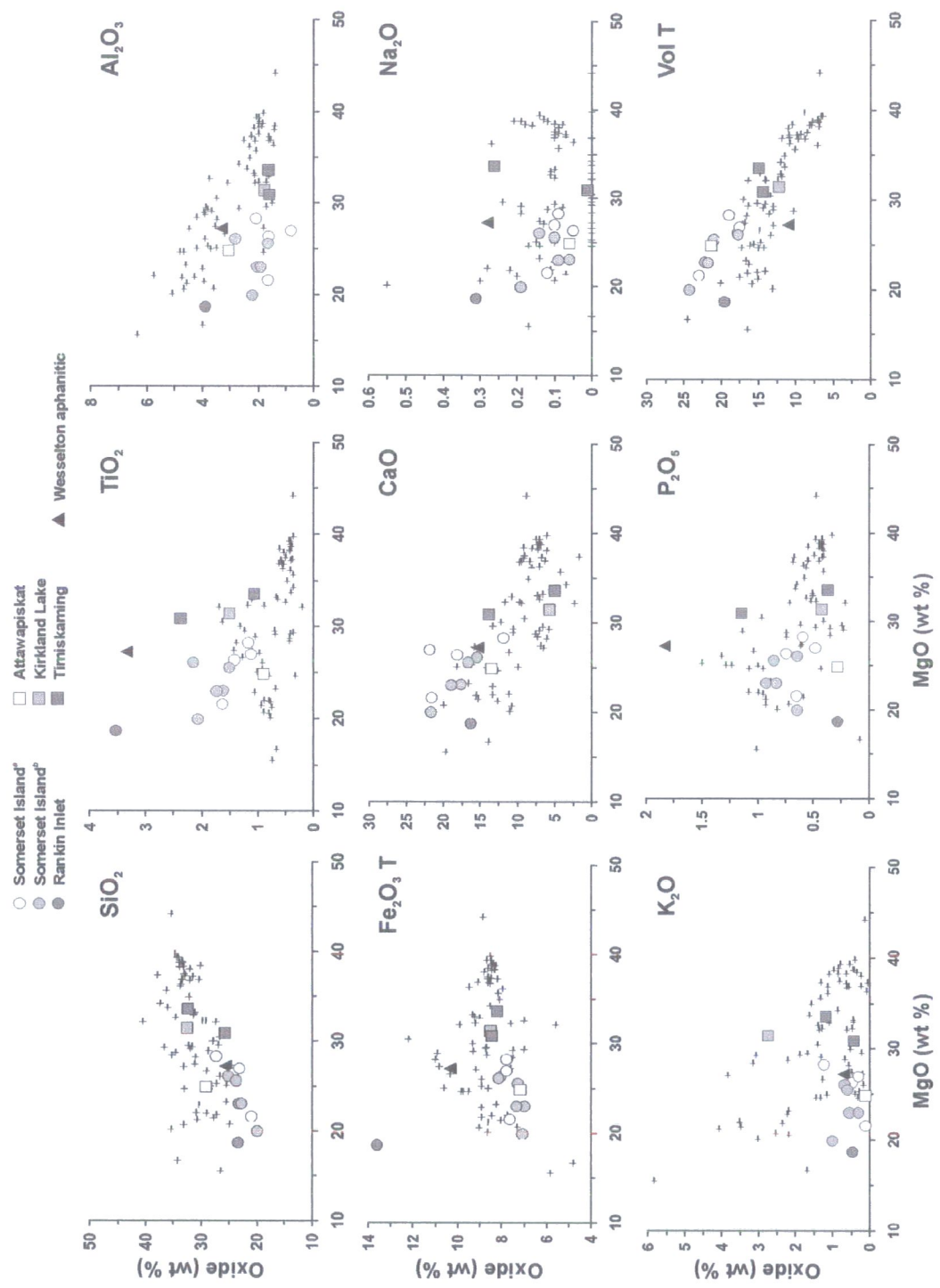
Figure E.37 Major element compositional variation of Canadian hypabyssal kimberlites from beyond the Slave province, relative to Lac de Gras intrusions and aphanitic kimberlite. a = Somerset Island (this study); b = Somerset Island (Schmidberger *et al.*, 2002).
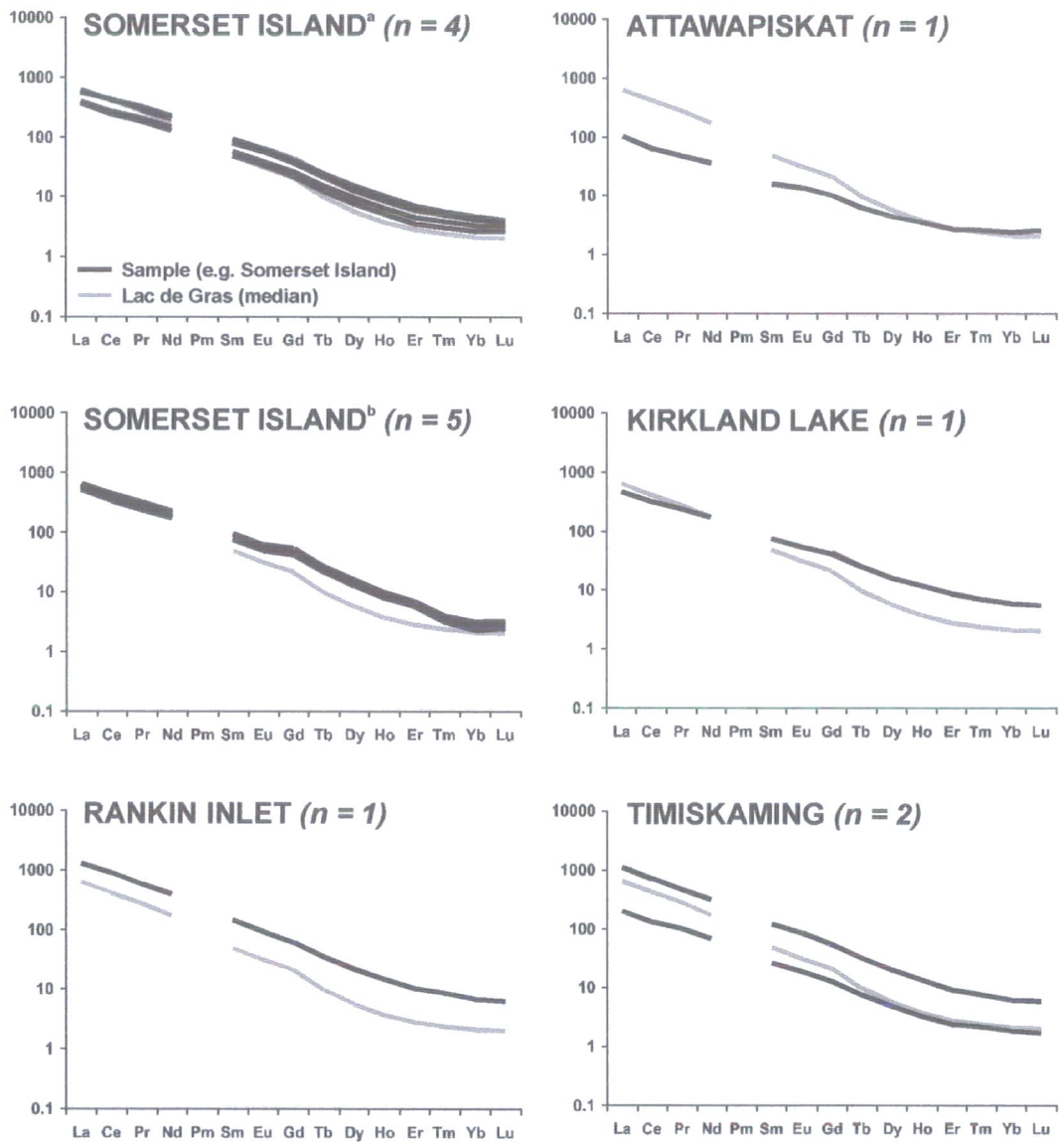
Figure E.38 Chondrite-normalised rare earth element patterns for Canadian kimberlites beyond the Slave province, compared to Lac de Gras median. a = Somerset Island (this study); b = Somerset Island (Schmidberger *et al.*, 2002).
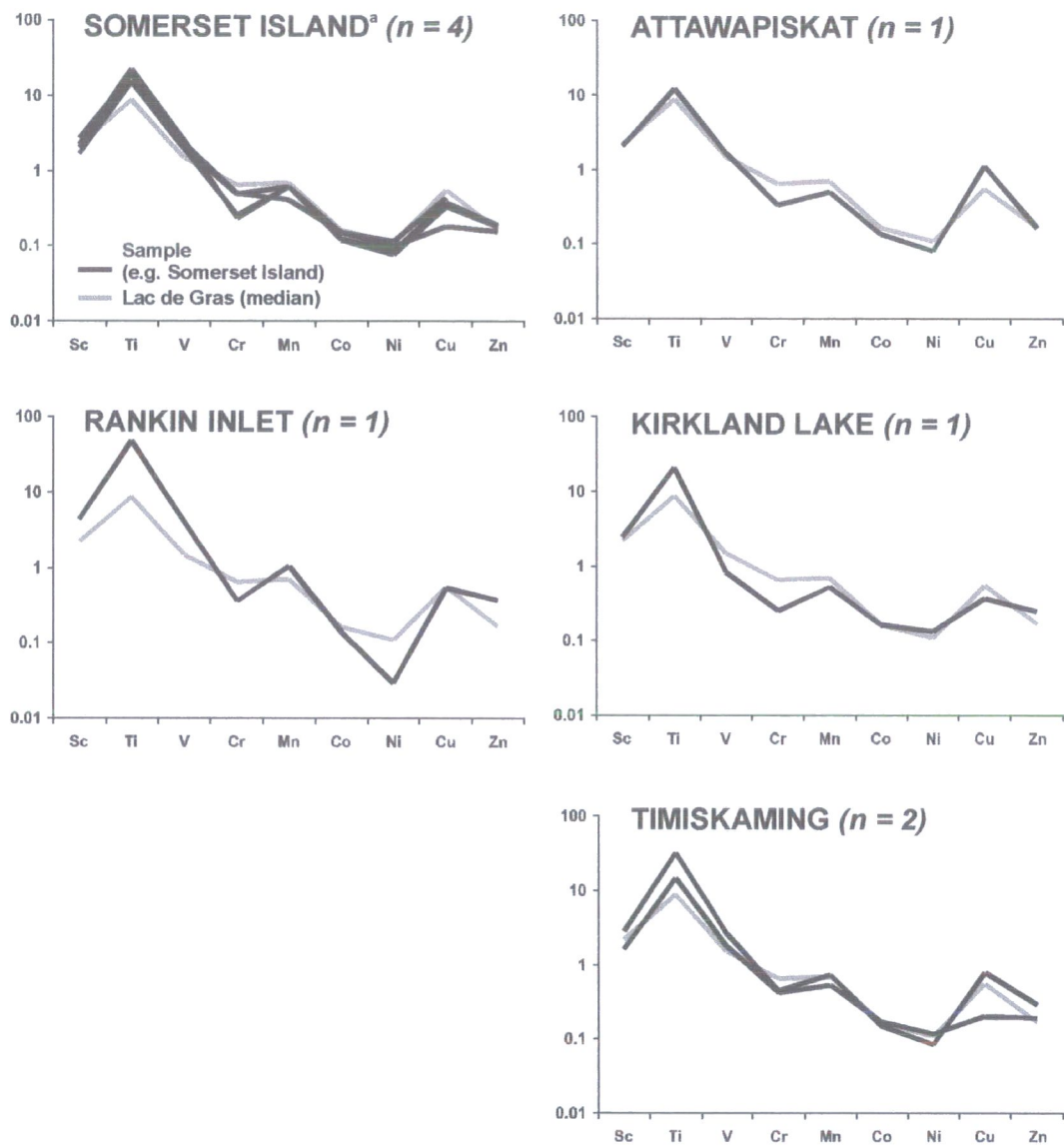
Figure E.39 Chondrite-normalised compatible element patterns for Canadian kimberlites beyond the Slave province, compared to Lac de Gras median. a = Somerset Island (this study); insufficient data available for Somerset Island kimberlites from Schmidberger *et al*. (2002).
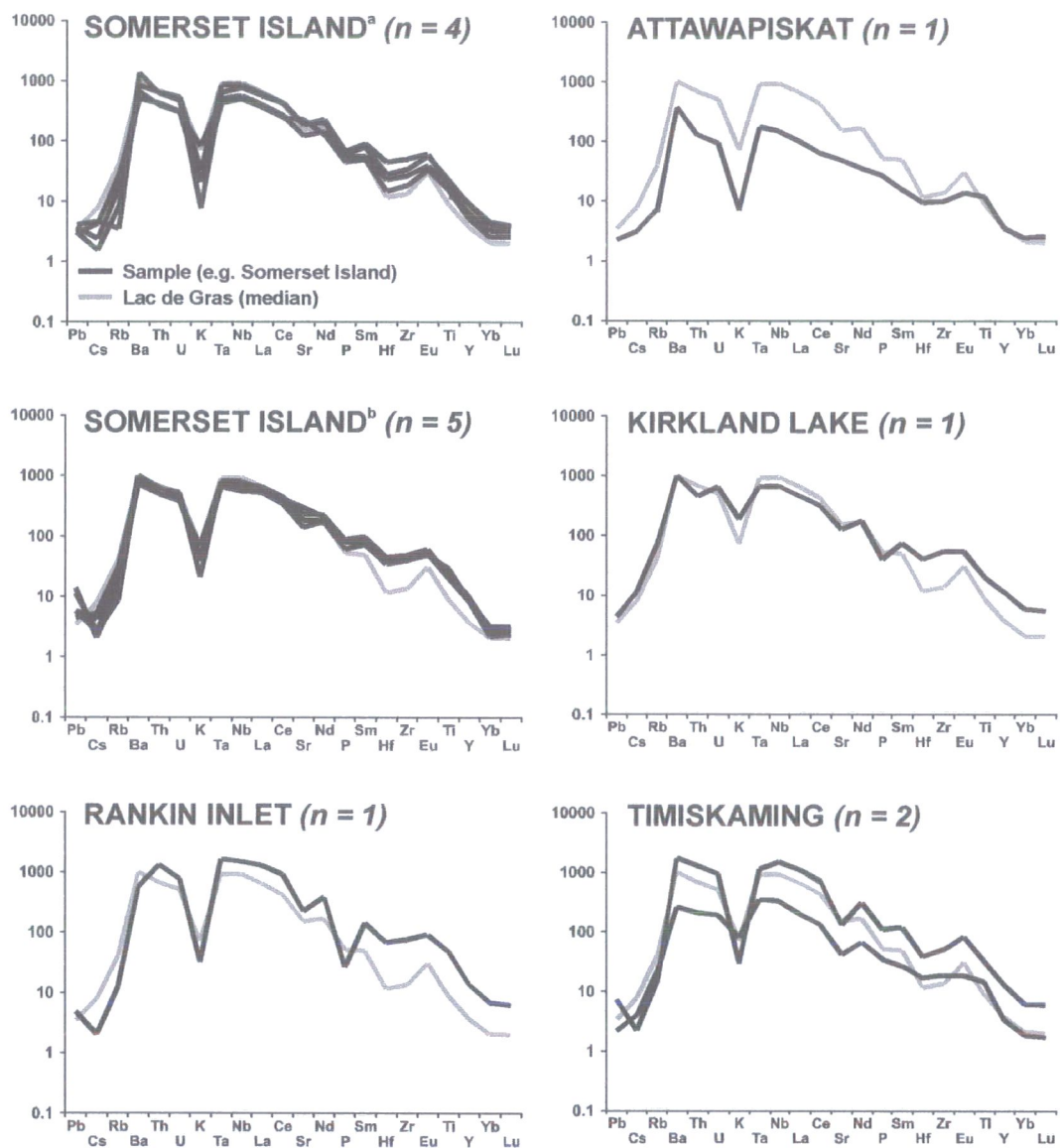
Figure E.40 Chondrite-normalised incompatible element patterns for Canadian kimberlites beyond the Slave province, compared to Lac de Gras median. a = Somerset Island (this study); b = Somerset Island (Schmidberger *et al.*, 2002).

Appendix F

Whole rock isotope data

CONTENTS OF THE ISOTOPIC DATABASE

The following pages contain details of all Sr, Nd and Hf isotopic analyses of whole rock kimberlites and Lac de Gras crustal material obtained during the course of this study. The data was acquired in 35 analytical sessions between April 2000 and January 2003. A summary of the standard data for each of these sessions is presented in Appendix G.

For each isotopic system, elemental concentrations of parent and daughter elements (i.e. Rb, Sr, Sm, Nd, Lu and Hf) were determined by quadrupole ICP-MS (Appendix D). Parent-daughter isotopic ratios (^{87}Rb/^{86}Sr, ^{147}Sm/^{144}Nd and ^{176}Lu/^{177}Hf) were calculated from the elemental ratios (Rb/Sr, Sm/Nd and Lu/Hf) using the relationship (example for Rb/Sr):

$$^{87}\text{Rb}/^{86}\text{Sr} = \text{Rb/Sr} \times \underbrace{(IA^{87}\text{Rb} \times AW\text{Sr}) / (IA^{86}\text{Sr} \times AW\text{Rb})}_{\text{'conversion factor'}}$$

where IA^{87}Rb and IA^{86}Sr are the isotopic abundances of ^{87}Rb and ^{86}Sr, and AWRb and AWSr are the atomic weights of Rb and Sr (Table F.1). A constant value of the 'conversion factor' for each isotopic system, calculated from the International Union of Pure and Applied Chemistry (IUPAC) accepted values for isotopic abundances and atomic weights (Rosman and Taylor, 1998; Vocke, 1999) has been applied to each

sample. This is an approximation, because the relative abundance of isotopes, and thus the atomic weights of elements, will vary slightly between samples (Faure, 1986).

Rb-Sr		Sm-Nd		Lu-Hf	
Isotopic abundances (IA) – as proportions (10% = 0.1)					
^{87}Rb	0.2783 ± 2	^{147}Sm	0.1499 ± 18	^{176}Lu	0.0259 ± 2
^{86}Sr	0.0986 ± 1	^{144}Nd	0.238 ± 3	^{177}Hf	0.1860 ± 2
Atomic weights (AW)					
Rb	85.4678 ± 3	Sm	150.36 ± 3	Lu	174.967 ± 1
Sr	87.62 ± 1	Nd	144.24 ± 3	Hf	178.49 ± 2
Conversion factors					
$\frac{Rb/Sr \Rightarrow}{^{87}Rb/^{86}Sr}$	2.8936 ± 21	$\frac{Sm/Nd \Rightarrow}{^{147}Sm/^{144}Nd}$	0.6042 ± 73	$\frac{Lu/Hf \Rightarrow}{^{176}Lu/^{177}Hf}$	0.1421 ± 11

Table F.1 Conversion factors for determining parent-daughter isotopic ratios from parent-daughter elemental ratios. Isotopic abundances from Rosman and Taylor (1998); atomic weights from Vocke (1999).

The other isotopic data reported in this section (again using Rb-Sr as an example) are:

^{87}Sr/^{86}Sr$_N$: The measured isotopic ratio, normalised to the accepted value for the standard (see Appendix G). Errors are expressed as $\pm$ 2 standard errors of the mean ($\pm$2SE).

^{87}Sr/^{86}Sr$_i$: The initial isotopic ratios, calculated from the normalised measured ratio, the parent-daughter isotopic ratio, the sample age (t) and the parent daughter decay constant (λ):

$$^{87}Sr/^{86}Sr_i = {}^{87}Sr/^{86}Sr_N - {}^{87}Rb/^{86}Sr \times (e^{\lambda t}-1)$$

$\varepsilon_{Sr\,i}$: The initial epsilon value, calculated from the initial isotopic ratio of the sample and the corresponding isotopic composition of the chondritic uniform reservoir (CHUR), back-corrected to the age of the sample:

$$\varepsilon_{Sr\,i} = 10,000 \times (({}^{87}Sr/^{86}Sr_i \div {}^{87}Sr/^{86}Sr_{CHUR(t)}) - 1)$$

Corresponding isotopic parameters for Nd and Hf are calculated in the same manner. In the case of Hf, the parameter $\Delta\varepsilon_{Hf\,i}$ (see section 6.3.1.2) is also calculated according to the relationship:

$$\Delta\varepsilon_{Hf\,i} = \varepsilon_{Hf\,i} - (1.33\ \varepsilon_{Nd\,i} + 3.19).$$

FIELD	Contwoyto	Contwoyto	Contwoyto	Contwoyto	Contwoyto	Contwoyto	Contwoyto	Contwoyto	Lac de Gras	Lac de Gras	Lac de Gras	Lac de Gras
LOCALITY	Jericho	Jericho	Jericho	Jericho	Jericho	Jericho	Jericho	Muskox	Aaron	Aaron	Anaconda	Anaconda
SAMPLE	JD-61	JD-69-1	JD-69-3	JD-82-1	JD-82-3	RND-120-4S	RND-120-4SA	RHL-11-2	AAR-1	AAR-2	ANA-1	ANA-2
Rb-Sr												
Analysis date	25/26-Dec-00	25/26-Dec-00	18-Oct-01	25/26-Dec-00	05-Jun-02	25/26-Dec-00	05-Jun-02	30-Oct-02	18-Oct-01	18-Oct-01	25-Jul-01	30-Oct-02
Analysis method	TIMS - 262	TIMS - 262	PIMMS - Nept	TIMS - 262	PIMMS - Nept	TIMS - 262	PIMMS - Nept	PIMMS - Nept	PIMMS - Nept	PIMMS - Nept	PIMMS - Nept	PIMMS - Nept
Standard average	0.710263	0.710263	0.710261	0.710263	0.710268	0.710263	0.710268	0.710254	0.710261	0.710261	0.710282	0.710254
+/- 2σ	38	38	13	38	11	38	11	20	13	13	10	20
Rb (ppm)	14.8	28.4	30.5	32.2	28.0	48.9	49.2	40.2	104.1	65.0	25.5	18.8
Sr (ppm)	661	1289	625	679	339	188	187	1059	621	83	1451	1947
^{87}Rb/^{86}Sr	0.0649	0.0638	0.1412	0.1372	0.2387	0.7540	0.7629	0.1098	0.4845	2.2606	0.0509	0.0279
^{87}Sr/^{86}Sr$_N$	0.704709	0.704427	0.706637	0.705142	0.706215	0.707465	0.710311	0.704585	0.705169	0.710755	0.704875	0.704916
+/- 2SE	08	08	10	08	08	08	16	12	10	10	08	12
^{87}Sr/^{86}Sr$_i$	0.704551	0.704271	0.706292	0.704807	0.705632	0.705622	0.708447	0.704317	0.704858	0.709305	0.704837	0.704895
$\varepsilon_{Sr\,i}$	3.59	-0.38	28.31	7.23	18.94	18.81	58.91	0.27	5.84	68.96	5.66	6.49
Sm-Nd												
Analysis date	25/26-Dec-00	25/26-Dec-00	26-Oct-01	25/26-Dec-00	17-Jul-02	25/26-Dec-00	20-May-02	31-Oct-02	26-Oct-01	26-Oct-01	19-Jul-01	31-Oct-02
Analysis method	TIMS - 262	TIMS - 262	PIMMS - Nept	TIMS - 262	PIMMS - Nept	TIMS - 262	PIMMS - Nept	PIMMS - Nept	PIMMS - Nept	PIMMS - Nept	PIMMS - Nept	PIMMS - Nept
Standard average	0.511930	0.511930	0.511118	0.511930	0.511109	0.511930	0.511097	0.511109	0.511118	0.511118	0.511100	0.511109
+/- 2σ	19	19	15	19	18	19	18	12	15	15	14	12
Sm (ppm)	16.6	10.4	9.4	11.1	10.9	20.8	23.8	7.6	5.7	2.8	7.9	7.4
Nd (ppm)	146	90	78	95	93	179	200	65	59	24	82	77
^{147}Sm/^{144}Nd	0.0687	0.0702	0.0733	0.0702	0.0708	0.0702	0.0717	0.0705	0.0585	0.0713	0.0588	0.0580
^{143}Nd/^{144}Nd$_N$	0.512648	0.512632	0.512570	0.512646	0.512624	0.512648	0.512603	0.512520	0.512542	0.512348	0.512454	0.512469
+/- 2SE	10	10	12	08	05	06	09	10	12	14	06	05
^{143}Nd/^{144}Nd$_i$	0.512571	0.512553	0.512487	0.512567	0.512544	0.512569	0.512522	0.512441	0.512525	0.512327	0.512434	0.512449
$\varepsilon_{Nd\,i}$	3.00	2.66	1.38	2.93	2.49	2.97	2.06	0.47	-1.08	-4.94	-2.66	-2.36
Lu-Hf												
Analysis date	Dec-00	Dec-00	24-Oct-01	Dec-00	12-Jun-02	Dec-00	12-Jun-02	18-Dec-02	24-Oct-01	24-Oct-01	6-Jun-01	18-Dec-02
Analysis method	PIMMS - P54	PIMMS - P54	PIMMS - Nept	PIMMS - P54	PIMMS - Nept	PIMMS - P54	PIMMS - Nept	PIMMS - Nept	PIMMS - Nept	PIMMS - Nept	PIMMS - P54	PIMMS - Nept
Standard average	0.282178	0.282178	0.282160	0.282178	0.282156	0.282178	0.282156	0.282163	0.282160	0.282160	0.282218	0.282163
+/- 2σ	12	12	10	12	09	12	09	05	10	10	10	05
Lu (ppm)	0.09	0.07	0.08	0.07	0.06	0.13	0.20	0.06	0.04	0.09	0.04	0.04
Hf (ppm)	3.86	2.00	1.57	2.08	2.56	4.57	5.34	1.64	0.95	0.83	1.14	1.05
^{176}Lu/^{177}Hf	0.0034	0.0046	0.0074	0.0048	0.0033	0.0040	0.0052	0.0053	0.0054	0.0154	0.0051	0.0051
^{176}Hf/^{177}Hf$_N$	0.282762	0.282788	0.282707	0.282793	0.282787	0.282850	0.282810	0.282551	0.282921	0.282480	0.282822	0.282745
+/- 2SE	11	09	09	10	09	12	08	09	16	16	06	28
^{176}Hf/^{177}Hf$_i$	0.282751	0.282773	0.282683	0.282778	0.282776	0.282837	0.282793	0.282534	0.282916	0.282467	0.282817	0.282740
$\varepsilon_{Hf\,i}$	3.06	3.83	0.65	3.99	3.95	6.10	4.54	-4.63	6.10	-9.79	2.75	0.03
$\Delta\varepsilon_{Hf\,i}$	-4.10	-2.87	-4.38	-3.07	-2.55	-1.02	-1.39	-8.44	4.35	-6.42	3.10	-0.02

FIELD	Lac de Gras	Lac de Gras	Lac de Gras	Lac de Gras	Lac de Gras	Lac de Gras	Lac de Gras	Lac de Gras	Lac de Gras	Lac de Gras	Lac de Gras	Lac de Gras
LOCALITY	Anaconda	Amie	Fox	Grizzly	Grizzly	Grizzly	Grizzly	Grizzly	Grizzly	Grizzly	Grizzly	Grizzly
SAMPLE	ANA-3	KPL-21	FOX-1	GRZ-1	GRZ-2	GRZ-3	GRZ-4	GRZ-5	GRZ-6	GRZ-7	GRZ-8	GRZ-9
Rb-Sr												
Analysis date	25/26-Dec-00	18-Oct-01	25/26-Dec-00	24-Jul-01	25/26-Dec-00	18-Oct-01	18-Oct-01	06-Jun-02	06-Jun-02	06-Jun-02	06-Jun-02	06-Jun-02
Analysis method	TIMS - 262	PIMMS - Nept	TIMS - 262	PIMMS - Nept	TIMS - 262	PIMMS - Nept	PIMMS - Nept	PIMMS - Nept	PIMMS - Nept	PIMMS - Nept	PIMMS - Nept	PIMMS - Nept
Standard average	0.710263	0.710261	0.710263	0.710273	0.710263	0.710261	0.710261	0.710272	0.710272	0.710272	0.710272	0.710272
+/- 2σ	38	13	38	16	38	13	13	09	09	09	09	09
Rb (ppm)	38.2	12.5	85.3	107.6	84.1	90.3	117.1	73.0	91.3	90.0	39.0	45.6
Sr (ppm)	1781	1356	745	1195	1169	837	868	620	1205	704	835	736
$^{87}Rb/^{86}Sr$	0.0620	0.0267	0.3313	0.2607	0.2083	0.3122	0.3904	0.3406	0.2192	0.3698	0.1350	0.1792
$^{87}Sr/^{86}Sr_N$	0.704966	0.704797	0.708002	0.704875	0.704775	0.704836	0.704879	0.704929	0.704825	0.704910	0.704739	0.704762
+/- 2SE	08	07	08	09	06	08	07	11	09	08	08	09
$^{87}Sr/^{86}Sr_i$	0.704919	0.704779	0.707753	0.704687	0.704625	0.704611	0.704597	0.704683	0.704667	0.704643	0.704642	0.704633
$\varepsilon_{Sr\,i}$	6.84	4.75	47.06	3.50	2.62	2.42	2.23	3.45	3.22	2.88	2.86	2.73
Sm-Nd												
Analysis date	25/26-Dec-00	27-Oct-01	25/26-Dec-00	19-Jul-01	25/26-Dec-00	27-Oct-01	27-Oct-01	20-May-02	20-May-02	20-May-02	20-May-02	20-May-02
Analysis method	TIMS - 262	PIMMS - Nept	TIMS - 262	PIMMS - Nept	TIMS - 262	PIMMS - Nept	PIMMS - Nept	PIMMS - Nept	PIMMS - Nept	PIMMS - Nept	PIMMS - Nept	PIMMS - Nept
Standard average	0.511930	0.511112	0.511930	0.511100	0.511930	0.511112	0.511112	0.511097	0.511097	0.511097	0.511097	0.511097
+/- 2σ	19	14	19	14	19	14	14	18	18	18	18	18
Sm (ppm)	8.1	11.0	4.7	6.4	8.1	6.7	7.1	6.1	6.0	6.0	5.6	5.7
Nd (ppm)	83	110	37	60	80	68	73	62	60	61	57	58
$^{147}Sm/^{144}Nd$	0.0588	0.0606	0.0768	0.0639	0.0613	0.0604	0.0591	0.0595	0.0607	0.0599	0.0596	0.0597
$^{143}Nd/^{144}Nd_N$	0.512487	0.512568	0.512158	0.512502	0.512544	0.512505	0.512501	0.512480	0.512515	0.512533	0.512502	0.512526
+/- 2SE	08	12	08	05	10	12	12	24	17	17	16	14
$^{143}Nd/^{144}Nd_i$	0.512467	0.512549	0.512131	0.512481	0.512524	0.512485	0.512481	0.512460	0.512495	0.512513	0.512482	0.512506
$\varepsilon_{Nd\,i}$	-2.02	-0.54	-8.55	-1.79	-0.96	-1.71	-1.78	-2.19	-1.52	-1.16	-1.76	-1.30
Lu-Hf												
Analysis date	Dec-00	24-Oct-01	Dec-00	6-Jun-01	Dec-00	24-Oct-01	24-Oct-01	12-Jun-02	12-Jun-02	14-Jun-02	12-Jun-02	12-Jun-02
Analysis method	PIMMS - P54	PIMMS - Nept	PIMMS - P54	PIMMS - P54	PIMMS - P54	PIMMS - Nept	PIMMS - Nept	PIMMS - Nept	PIMMS - Nept	PIMMS - Nept	PIMMS - Nept	PIMMS - Nept
Standard average	0.282178	0.282160	0.282178	0.282218	0.282178	0.282160	0.282160	0.282156	0.282156	0.282152	0.282156	0.282156
+/- 2σ	12	10	12	10	12	10	10	09	09	09	09	09
Lu (ppm)	0.04	0.07	0.11	0.05	0.06	0.05	0.05	0.04	0.04	0.04	0.04	0.04
Hf (ppm)	1.07	1.55	0.91	0.95	1.23	1.14	1.08	0.90	0.87	0.92	0.80	0.82
$^{176}Lu/^{177}Hf$	0.0056	0.0066	0.0164	0.0069	0.0071	0.0056	0.0060	0.0063	0.0062	0.0059	0.0064	0.0064
$^{176}Hf/^{177}Hf_N$	0.282756	0.282845	0.282479	0.282712	0.282689	0.282737	0.282717	0.282728	0.282684	0.282657	0.282749	0.282736
+/- 2SE	16	17	09	08	10	17	14	21	18	14	27	24
$^{176}Hf/^{177}Hf_i$	0.282750	0.282839	0.282463	0.282705	0.282682	0.282732	0.282711	0.282722	0.282678	0.282651	0.282743	0.282730
$\varepsilon_{Hf\,i}$	0.40	3.42	-9.77	-1.24	-2.05	-0.31	-1.03	-0.65	-2.20	-3.14	0.09	-0.37
$\Delta\varepsilon_{Hf\,i}$	-0.08	0.95	-1.56	-2.04	-3.94	-1.22	-1.85	-0.92	-3.37	-4.79	-0.75	-1.83

FIELD	Lac de Gras	Lac de Gras	Lac de Gras	Lac de Gras	Lac de Gras	Lac de Gras	Lac de Gras	Lac de Gras	Lac de Gras	Lac de Gras	Lac de Gras	Lac de Gras
LOCALITY	Grizzly	Grizzly	Grizzly	Grizzly	Grizzly	Anne	Anne	Finley	Finley	Don	Don	Koala West
SAMPLE	GRZ-10	GRZ-11	GRZ-12	GRZ-13	GRZ-14	HL-10-2	HL-10-3	HL-11-1	HL-11-2	HL-12-1	HL-12-3	KOW-1
Rb-Sr												
Analysis date	06-Jun-02	06-Jun-02	06-Jun-02	06-Jun-02	06-Jun-02	08-Apr-00	18-Oct-01	08-Apr-00	08-Apr-00	08-Apr-00	18-Oct-01	18-Oct-01
Analysis method	PIMMS - Nept	PIMMS - Nept	PIMMS - Nept	PIMMS - Nept	PIMMS - Nept	TIMS - 262	PIMMS - Nept	TIMS - 262	TIMS - 262	TIMS - 262	PIMMS - Nept	PIMMS - Nept
Standard average	0.710272	0.710272	0.710272	0.710272	0.710272	0.710243	0.710261	0.710243	0.710243	0.710243	0.710261	0.710261
+/- 2σ	09	09	09	09	09	05	13	05	05	05	13	13
Rb (ppm)	50.5	81.3	105.8	78.6	75.8	91.6	95.1	49.4	39.7	92.8	85.2	150.9
Sr (ppm)	825	694	888	708	714	1484	1540	1763	1605	409	614	1550
$^{87}Rb/^{86}Sr$	0.1772	0.3393	0.3448	0.3209	0.3072	0.1787	0.1787	0.0811	0.0716	0.6568	0.4012	0.2817
$^{87}Sr/^{86}Sr_N$	0.704778	0.704892	0.704978	0.704881	0.704857	0.705166	0.705161	0.705860	0.705919	0.706232	0.706095	0.705150
+/- 2SE	12	09	08	10	10	10	10	10	08	08	09	10
$^{87}Sr/^{86}Sr_i$	0.704650	0.704647	0.704729	0.704650	0.704636	0.704983	0.704978	0.705778	0.705847	0.705570	0.705691	0.704938
$\varepsilon_{Sr\,i}$	2.98	2.94	4.10	2.97	2.77	8.06	7.99	19.33	20.30	16.37	18.09	7.10
Sm-Nd												
Analysis date	20-May-02	20-May-02	20-May-02	20-May-02	20-May-02	15-Apr-00	27-Oct-01	15-Apr-00	15-Apr-00	15-Apr-00	27-Oct-01	26-Oct-01
Analysis method	PIMMS - Nept	PIMMS - Nept	PIMMS - Nept	PIMMS - Nept	PIMMS - Nept	TIMS - 262	PIMMS - Nept	TIMS - 262	TIMS - 262	TIMS - 262	PIMMS - Nept	PIMMS - Nept
Standard average	0.511097	0.511097	0.511097	0.511097	0.511097	0.511164	0.511112	0.511164	0.511164	0.511164	0.511112	0.511118
+/- 2σ	18	18	18	18	18	16	14	16	16	16	14	15
Sm (ppm)	5.7	6.1	6.2	5.9	5.9	7.0	7.0	12.9	12.4	6.3	6.2	15.9
Nd (ppm)	56	61	64	60	59	77	77	129	123	64	63	162
$^{147}Sm/^{144}Nd$	0.0623	0.0608	0.0587	0.0597	0.0600	0.0548	0.0544	0.0605	0.0609	0.0599	0.0595	0.0593
$^{143}Nd/^{144}Nd_N$	0.512497	0.512498	0.512517	0.512519	0.512488	0.512390	0.512409	0.512455	0.512482	0.512420	0.512437	0.512498
+/- 2SE	16	16	20	19	16	08	12	08	08	06	12	12
$^{143}Nd/^{144}Nd_i$	0.512476	0.512478	0.512498	0.512499	0.512468	0.512364	0.512383	0.512427	0.512454	0.512392	0.512409	0.512477
$\varepsilon_{Nd\,i}$	-1.88	-1.85	-1.47	-1.43	-2.04	-3.54	-3.16	-2.34	-1.82	-3.02	-2.68	-1.80
Lu-Hf												
Analysis date	12-Jun-02	14-Jun-02	14-Jun-02	12-Jun-02	14-Jun-02	18-Dec-02	24-Oct-01	15-Apr-00	16-Apr-00	15-Apr-00	24-Oct-01	24-Oct-01
Analysis method	PIMMS - Nept	PIMMS - Nept	PIMMS - Nept	PIMMS - Nept	PIMMS - Nept	PIMMS - Nept	PIMMS - Nept	PIMMS (P54)	PIMMS (P54)	PIMMS (P54)	PIMMS - Nept	PIMMS - Nept
Standard average	0.282156	0.282152	0.282152	0.282156	0.282152	0.282163	0.282160	0.282154	0.282161	0.282154	0.282160	0.282160
+/- 2σ	09	09	09	09	09	05	10	09	11	09	10	10
Lu (ppm)	0.04	0.04	0.05	0.04	0.04	0.04	0.04	0.10	0.10	0.03	0.03	0.12
Hf (ppm)	0.85	0.89	0.93	0.86	0.89	1.11	1.10	2.45	2.36	1.04	1.02	3.07
$^{176}Lu/^{177}Hf$	0.0063	0.0062	0.0069	0.0061	0.0061	0.0053	0.0052	0.0059	0.0059	0.0046	0.0046	0.0055
$^{176}Hf/^{177}Hf_M$	0.282694	0.282704	0.282614	0.282705	0.282694	0.282616	0.282626	0.282672	0.282690	0.282467	0.282517	0.282888
+/- 2SE	23	23	23	24	19	13	18	04	04	12	19	08
$^{176}Hf/^{177}Hf_i$	0.282688	0.282698	0.282607	0.282699	0.282688	0.282609	0.282619	0.282664	0.282682	0.282461	0.282511	0.282883
$\varepsilon_{Hf\,i}$	-1.85	-1.49	-4.70	-1.46	-1.84	-4.18	-3.82	-2.25	-1.61	-9.44	-7.67	5.08
$\Delta\varepsilon_{Hf\,i}$	-2.54	-2.22	-5.94	-2.74	-2.32	-2.67	-2.81	-2.33	-2.39	-8.62	-7.30	4.29

FIELD	Lac de Gras	Lac de Gras	Lac de Gras	Lac de Gras	Lac de Gras	Lac de Gras	Lac de Gras	Lac de Gras	Lac de Gras	Lac de Gras	Lac de Gras	Lac de Gras
LOCALITY	Koala West	Leslie	Leslie	Leslie	Leslie	Mark	Misery	Misery	Misery East	Misery East	Nicholas Bay	Pigeon
SAMPLE	KOW-2	LES-B1	LES-1	LES-2	LES-3	KIA93-K136	MIS-1	MIS-2	MSE-1	MSE-2	NCB-1	PDG-1
Rb-Sr												
Analysis date	18-Oct-01	25/26-Dec-00	24-Jul-01	25-Jul-01	18-Oct-01	23-Oct-01	18-Oct-01	18-Oct-01	18-Oct-01	18-Oct-01	25-Jul-01	23-Oct-01
Analysis method	PIMMS - Nept	TIMS - 262	PIMMS - Nept	PIMMS - Nept	PIMMS - Nept	PIMMS - Nept	PIMMS - Nept	PIMMS - Nept	PIMMS - Nept	PIMMS - Nept	PIMMS - Nept	PIMMS - Nept
Standard average	0.710261	0.710263	0.710273	0.710282	0.710261	0.710256	0.710261	0.710261	0.710261	0.710261	0.710282	0.710256
+/- 2σ	13	38	16	10	13	25	13	13	13	13	10	25
Rb (ppm)	80.4	68.1	102.3	103.6	66.7	8.9	56.9	27.9	99.9	108.2	161.5	134.8
Sr (ppm)	1427	760	1066	1084	846	582	645	875	1072	877	1266	639
$^{87}Rb/^{86}Sr$	0.1632	0.2593	0.2775	0.2765	0.2283	0.0444	0.2550	0.0924	0.2697	0.3567	0.3691	0.6104
$^{87}Sr/^{86}Sr_N$	0.705040	0.704782	0.704866	0.704813	0.704782	0.704488	0.705104	0.705170	0.705425	0.705450	0.705257	0.706868
+/- 2SE	08	08	08	09	10	14	08	07	08	07	08	13
$^{87}Sr/^{86}Sr_i$	0.704917	0.704584	0.704654	0.704602	0.704607	0.704458	0.704912	0.705101	0.705222	0.705182	0.704979	0.706409
$\varepsilon_{Sr\,i}$	6.81	2.09	3.08	2.34	2.42	0.20	6.73	9.41	11.13	10.56	7.69	27.98
Sm-Nd												
Analysis date	26-Oct-01	25/26-Dec-00	19-Jul-01	19-Jul-01	27-Oct-01	27-Oct-01	27-Oct-01	27-Oct-01	27-Oct-01	27-Oct-01	19-Jul-01	27-Oct-01
Analysis method	PIMMS - Nept	TIMS - 262	PIMMS - Nept	PIMMS - Nept	PIMMS - Nept	PIMMS - Nept	PIMMS - Nept	PIMMS - Nept	PIMMS - Nept	PIMMS - Nept	PIMMS - Nept	PIMMS - Nept
Standard average	0.511118	0.511930	0.511100	0.511100	0.511112	0.511112	0.511112	0.511112	0.511112	0.511112	0.511100	0.511112
+/- 2σ	15	19	14	14	14	14	14	14	14	14	14	14
Sm (ppm)	17.2	6.1	6.5	6.6	6.8	6.0	6.5	5.5	8.0	6.9	7.9	4.7
Nd (ppm)	180	62	67	67	68	64	63	53	84	72	90	46
$^{147}Sm/^{144}Nd$	0.0575	0.0597	0.0581	0.0595	0.0606	0.0565	0.0625	0.0623	0.0579	0.0577	0.0531	0.0617
$^{143}Nd/^{144}Nd_N$	0.512504	0.512525	0.512510	0.512509	0.512510	0.512552	0.512523	0.512531	0.512429	0.512402	0.512371	0.512396
+/- 2SE	12	10	08	07	10	10	12	12	12	10	08	12
$^{143}Nd/^{144}Nd_i$	0.512484	0.512504	0.512490	0.512488	0.512489	0.512534	0.512501	0.512509	0.512409	0.512382	0.512353	0.512375
$\varepsilon_{Nd\,i}$	-1.67	-1.26	-1.54	-1.57	-1.56	-0.83	-1.34	-1.18	-3.14	-3.66	-4.24	-3.81
Lu-Hf												
Analysis date	24-Oct-01	Dec-00	6-Jun-01	7-Jun-01	24-Oct-01	25-Oct-01	24-Oct-01	24-Oct-01	24-Oct-01	24-Oct-01	7-Jun-01	25-Oct-01
Analysis method	PIMMS - Nept	PIMMS - P54	PIMMS - P54	PIMMS - P54	PIMMS - Nept	PIMMS - Nept	PIMMS - Nept	PIMMS - Nept	PIMMS - Nept	PIMMS - Nept	PIMMS - P54	PIMMS - Nept
Standard average	0.282160	0.282178	0.282218	0.282213	0.282160	0.282156	0.282160	0.282160	0.282160	0.282160	0.282213	0.282156
+/- 2σ	10	12	10	09	10	05	10	10	10	10	09	05
Lu (ppm)	0.13	0.03	0.03	0.05	0.04	0.03	0.04	0.03	0.05	0.06	0.08	0.07
Hf (ppm)	3.83	0.91	0.85	1.04	0.96	0.73	1.08	0.88	1.34	1.24	1.31	1.02
$^{176}Lu/^{177}Hf$	0.0048	0.0053	0.0055	0.0067	0.0053	0.0055	0.0057	0.0055	0.0053	0.0064	0.0083	0.0090
$^{176}Hf/^{177}Hf_N$	0.282758	0.282868	0.282827	0.282778	0.282840	0.283044	0.282608	0.282683	0.282593	0.282486	0.282489	0.282336
+/- 2SE	06	12	07	07	23	15	19	20	18	14	12	11
$^{176}Hf/^{177}Hf_i$	0.282753	0.282863	0.282821	0.282771	0.282835	0.283039	0.282602	0.282678	0.282588	0.282480	0.282481	0.282327
$\varepsilon_{Hf\,i}$	0.50	4.39	2.93	1.16	3.40	10.49	-4.83	-2.17	-5.35	-9.17	-9.14	-14.57
$\Delta\varepsilon_{Hf\,i}$	-0.46	2.91	1.79	0.06	2.29	8.41	-6.24	-3.79	-4.36	-7.49	-6.69	-12.69

374

FIELD	Lac de Gras	Lac de Gras	Lac de Gras	Lac de Gras	Lac de Gras	Lac de Gras	Lac de Gras	Lac de Gras	Lac de Gras	Lac de Gras	Lac de Gras	Lac de Gras
LOCALITY	Pigeon	Porpoise	Porpoise	Porpoise	Rat	Rat	Rat	Rat	Rattler	Rattler	Rattler	Roger
SAMPLE	PDG-2	PRP-1	PRP-2	PRP-3	RAT-1	RAT-2	RAT-3	RAT-4	RTL-1	RTL-2	RTL-3	ROG-1
Rb-Sr												
Analysis date	25-Jul-01	23-Oct-01	23-Oct-01	25-Jul-01	24-Jul-01	23-Oct-01	23-Oct-01	23-Oct-01	24-Jul-01	25-Jul-01	23-Oct-01	23-Oct-01
Analysis method	PIMMS - Nept	PIMMS - Nept	PIMMS - Nept	PIMMS - Nept	PIMMS - Nept	PIMMS - Nept	PIMMS - Nept	PIMMS - Nept	PIMMS - Nept	PIMMS - Nept	PIMMS - Nept	PIMMS - Nept
Standard average	0.710282	0.710256	0.710256	0.710282	0.710273	0.710256	0.710256	0.710256	0.710273	0.710282	0.710256	0.710256
+/- 2σ	10	25	25	10	16	25	25	25	16	10	25	25
Rb (ppm)	147.6	147.6	146.0	125.0	44.3	210.5	43.6	85.0	92.6	99.8	54.9	121.9
Sr (ppm)	663	1809	1542	1289	955	508	971	483	1069	1388	1188	1573
$^{87}Rb/^{86}Sr$	0.6444	0.2361	0.2740	0.2807	0.1342	1.1992	0.1298	0.5092	0.2507	0.2081	0.1337	0.2243
$^{87}Sr/^{86}Sr_N$	0.706763	0.705596	0.705852	0.705433	0.704883	0.707100	0.704932	0.706425	0.704646	0.704609	0.704900	0.704786
+/- 2SE	08	14	10	07	09	12	11	14	09	08	12	13
$^{87}Sr/^{86}Sr_i$	0.706278	0.705418	0.705646	0.705222	0.704782	0.706198	0.704834	0.706042	0.704434	0.704433	0.704787	0.704617
$\varepsilon_{Sr\,i}$	26.13	13.92	17.15	11.13	4.89	24.98	5.63	22.77	0.05	0.04	5.06	2.55
Sm-Nd												
Analysis date	19-Jul-01	27-Oct-01	27-Oct-01	19-Jul-01	19-Jul-01	27-Oct-01	27-Oct-01	27-Oct-01	19-Jul-01	19-Jul-01	27-Oct-01	27-Oct-01
Analysis method	PIMMS - Nept	PIMMS - Nept	PIMMS - Nept	PIMMS - Nept	PIMMS - Nept	PIMMS - Nept	PIMMS - Nept	PIMMS - Nept	PIMMS - Nept	PIMMS - Nept	PIMMS - Nept	PIMMS - Nept
Standard average	0.511100	0.511112	0.511112	0.511100	0.511100	0.511112	0.511112	0.511112	0.511100	0.511100	0.511112	0.511112
+/- 2σ	14	14	14	14	14	14	14	14	14	14	14	14
Sm (ppm)	5.2	10.2	12.8	12.5	5.4	4.8	5.7	3.6	7.3	9.8	6.9	20.0
Nd (ppm)	52	100	133	129	57	39	60	29	77	104	73	214
$^{147}Sm/^{144}Nd$	0.0605	0.0613	0.0583	0.0587	0.0578	0.0739	0.0576	0.0741	0.0574	0.0569	0.0573	0.0566
$^{143}Nd/^{144}Nd_N$	0.512419	0.512455	0.512439	0.512447	0.512470	0.512332	0.512469	0.512346	0.512447	0.512456	0.512450	0.512516
+/- 2SE	06	10	12	07	07	10	12	12	05	07	12	14
$^{143}Nd/^{144}Nd_i$	0.512398	0.512434	0.512419	0.512427	0.512450	0.512306	0.512449	0.512320	0.512425	0.512434	0.512428	0.512496
$\varepsilon_{Nd\,i}$	-3.35	-2.66	-2.95	-2.79	-2.34	-5.14	-2.36	-4.87	-2.67	-2.49	-2.61	-1.43
Lu-Hf												
Analysis date	6-Jun-01	25-Oct-01	25-Oct-01	7-Jun-01	6-Jun-01	25-Oct-01	25-Oct-01	25-Oct-01	6-Jun-01	7-Jun-01	25-Oct-01	25-Oct-01
Analysis method	PIMMS - P54	PIMMS - Nept	PIMMS - Nept	PIMMS - P54	PIMMS - P54	PIMMS - Nept	PIMMS - Nept	PIMMS - Nept	PIMMS - P54	PIMMS - P54	PIMMS - Nept	PIMMS - Nept
Standard average	0.282218	0.282156	0.282156	0.282213	0.282218	0.282156	0.282156	0.282156	0.282218	0.282213	0.282156	0.282156
+/- 2σ	10	05	05	09	10	05	05	05	10	09	05	05
Lu (ppm)	0.08	0.08	0.09	0.09	0.04	0.15	0.04	0.13	0.04	0.05	0.04	0.13
Hf (ppm)	1.25	2.11	2.36	2.20	0.90	3.65	1.12	1.53	1.03	1.46	1.22	2.89
$^{175}Lu/^{177}Hf$	0.0095	0.0055	0.0052	0.0057	0.0060	0.0058	0.0056	0.0121	0.0055	0.0048	0.0046	0.0063
$^{175}Hf/^{177}Hf_N$	0.282375	0.282516	0.282475	0.282557	0.282837	0.282105	0.282829	0.282522	0.282843	0.282863	0.282797	0.282873
+/- 2SE	07	07	07	04	06	06	18	07	06	05	10	07
$^{175}Hf/^{177}Hf_i$	0.282365	0.282511	0.282470	0.282551	0.282831	0.282099	0.282823	0.282510	0.282837	0.282858	0.282792	0.282867
$\varepsilon_{Hf\,i}$	-13.21	-8.08	-9.52	-6.64	3.25	-22.63	2.99	-8.10	3.60	4.34	2.02	4.52
$\Delta\varepsilon_{Hf\,i}$	-11.94	-7.74	-8.79	-6.11	3.17	-18.98	2.93	-4.81	3.96	4.46	2.30	3.23

FIELD	Lac de Gras	Lac de Gras	Lac de Gras	Lac de Gras	Lac de Gras	Lac de Gras	Lac de Gras	Lac de Gras	Lac de Gras	Lac de Gras	Lac de Gras	Lac de Gras
LOCALITY	Roger	Roger	Wolverine	A21	A21	A25	A26	A154	A154	A154	ABZ	ABZ
SAMPLE	ROG-2	ROG-3	WOL-1	A21-1-1	A21-1-2	A25-3-1	A25-3-2	A154-11-1	A154-11-2	A154-11-3	ABZ-7a-1	ABZ-7a-2
Rb-Sr												
Analysis date	25-Jul-01	23-Oct-01	05-Jun-02	30-Oct-02	30-Oct-02	05-Jun-02	05-Jun-02	30-Oct-02	30-Oct-02	30-Oct-02	05-Jun-02	06-Jun-02
Analysis method	PIMMS - Nept	PIMMS - Nept	PIMMS - Nept	PIMMS - Nept	PIMMS - Nept	PIMMS - Nept	PIMMS - Nept	PIMMS - Nept	PIMMS - Nept	PIMMS - Nept	PIMMS - Nept	PIMMS - Nept
Standard average	0.710282	0.710256	0.710268	0.710254	0.710254	0.710268	0.710268	0.710254	0.710254	0.710254	0.710268	0.710272
+/- 2σ	10	25	11	20	20	11	11	20	20	20	11	09
Rb (ppm)	10.9	54.7	74.3	60.1	44.8	185.8	237.7	24.4	80.6	51.4	154.2	105.1
Sr (ppm)	1868	1330	536	333	245	2871	2224	199	350	449	1703	744
$^{87}Rb/^{86}Sr$	0.0168	0.1190	0.4007	0.5229	0.5301	0.1872	0.3093	0.3539	0.6660	0.3309	0.2620	0.4088
$^{87}Sr/^{86}Sr_N$	0.704594	0.704656	0.705618	0.707481	0.709477	0.705085	0.705322	0.707905	0.706706	0.706207	0.705585	0.705924
+/- 2SE	07	06	09	12	17	08	07	11	14	12	07	07
$^{87}Sr/^{86}Sr_i$	0.704582	0.704566	0.705317	0.707068	0.709058	0.704896	0.705010	0.707626	0.706181	0.705946	0.705388	0.705617
$\varepsilon_{Sr\,i}$	2.04	1.83	12.48	37.38	65.63	6.81	8.43	45.30	24.79	21.46	13.49	16.73
Sm-Nd												
Analysis date	19-Jul-01	27-Oct-01	20-May-02	31-Oct-02	31-Oct-02	8-Jun-02	20-May-02	31-Oct-02	31-Oct-02	31-Oct-02	20-May-02	20-May-02
Analysis method	PIMMS - Nept	PIMMS - Nept	PIMMS - Nept	PIMMS - Nept	PIMMS - Nept	PIMMS - Nept	PIMMS - Nept	PIMMS - Nept	PIMMS - Nept	PIMMS - Nept	PIMMS - Nept	PIMMS - Nept
Standard average	0.511100	0.511112	0.511097	0.511109	0.511109	0.511104	0.511097	0.511109	0.511109	0.511109	0.511097	0.511097
+/- 2σ	14	14	18	12	12	18	18	12	12	12	18	18
Sm (ppm)	20.6	20.2	4.2	3.7	3.5	18.7	16.5	2.9	3.6	3.6	10.6	8.5
Nd (ppm)	218	216	39	30	29	187	168	26	34	35	97	79
$^{147}Sm/^{144}Nd$	0.0573	0.0566	0.0660	0.0766	0.0724	0.0604	0.0595	0.0672	0.0636	0.0629	0.0656	0.0655
$^{143}Nd/^{144}Nd_N$	0.512510	0.512505	0.512402	0.512333	0.512336	0.512540	0.512464	0.512438	0.512500	0.512520	0.512455	0.512433
+/- 2SE	06	12	11	12	09	09	18	09	13	13	21	10
$^{143}Nd/^{144}Nd_i$	0.512490	0.512485	0.512379	0.512305	0.512310	0.512512	0.512436	0.512414	0.512477	0.512497	0.512432	0.512410
$\varepsilon_{Nd\,i}$	-1.55	-1.65	-3.72	-5.10	-5.01	-0.68	-2.15	-2.99	-1.75	-1.35	-2.68	-3.11
Lu-Hf												
Analysis date	7-Jun-01	25-Oct-01	12-Jun-02	18-Dec-02	18-Dec-02	12-Jun-02	12-Jun-02	18-Dec-02	18-Dec-02	18-Dec-02	12-Jun-02	12-Jun-02
Analysis method	PIMMS - P54	PIMMS - Nept	PIMMS - Nept	PIMMS - Nept	PIMMS - Nept	PIMMS - Nept	PIMMS - Nept	PIMMS - Nept	PIMMS - Nept	PIMMS - Nept	PIMMS - Nept	PIMMS - Nept
Standard average	0.282213	0.282156	0.282156	0.282163	0.282163	0.282156	0.282156	0.282163	0.282163	0.282163	0.282156	0.282156
+/- 2σ	09	05	09	05	05	09	09	05	05	05	09	09
Lu (ppm)	0.13	0.13	0.06	0.12	0.10	0.18	0.19	0.06	0.04	0.04	0.14	0.15
Hf (ppm)	2.91	2.84	0.88	1.46	1.09	3.20	2.81	0.74	0.71	0.87	2.18	2.19
$^{175}Lu/^{177}Hf$	0.0061	0.0063	0.0090	0.0120	0.0136	0.0080	0.0096	0.0117	0.0081	0.0062	0.0092	0.0095
$^{176}Hf/^{177}Hf_N$	0.282825	0.282837	0.282693	0.282686	0.282592	0.282865	0.282753	0.282628	0.282538	0.282398	0.282608	0.282614
+/- 2SE	03	07	18	11	19	35	12	26	16	12	14	08
$^{176}Hf/^{177}Hf_i$	0.282819	0.282831	0.282684	0.282673	0.282578	0.282854	0.282740	0.282616	0.282530	0.282392	0.282599	0.282605
$\varepsilon_{Hf\,i}$	2.82	3.25	-1.94	-2.26	-5.64	4.48	0.44	-4.30	-7.35	-12.23	-4.96	-4.75
$\Delta\varepsilon_{Hf\,i}$	1.70	2.25	-0.18	1.33	-2.17	2.19	0.11	-3.52	-8.21	-13.62	-4.58	-3.80

376

	Lac de Gras	Lac de Gras	Lac de Gras	Lac de Gras	Lac de Gras	Lac de Gras	Lac de Gras	Lac de Gras	Lac de Gras	Lac de Gras	Lac de Gras	Lac de Gras
FIELD	Lac de Gras	Lac de Gras	Lac de Gras	Lac de Gras	Lac de Gras	Lac de Gras	Lac de Gras	Lac de Gras	Lac de Gras	Lac de Gras	Lac de Gras	Lac de Gras
LOCALITY	C13	C13	DD39	DD39	Til Kwi Cho	Til Kwi Cho	T19	T19	T21	T21	T34	T34
SAMPLE	C13-7-1	C13-7-2	DD39-6-1	DD39-6-2	DO27-23-1	DO27-23-2	T19-1-1	T19-1-2	T21-1-1	T21-1-2	T34-1-1	T34-1-2
Rb-Sr												
Analysis date	06-Jun-02	06-Jun-02	06-Jun-02	06-Jun-02	06-Jun-02	06-Jun-02	06-Jun-02	06-Jun-02	06-Jun-02	06-Jun-02	06-Jun-02	06-Jun-02
Analysis method	PIMMS - Nept	PIMMS - Nept	PIMMS - Nept	PIMMS - Nept	PIMMS - Nept	PIMMS - Nept	PIMMS - Nept	PIMMS - Nept	PIMMS - Nept	PIMMS - Nept	PIMMS - Nept	PIMMS - Nept
Standard average	0.710272	0.710272	0.710272	0.710272	0.710272	0.710272	0.710272	0.710272	0.710272	0.710272	0.710272	0.710272
+/- 2σ	09	09	09	09	09	09	09	09	09	09	09	09
Rb (ppm)	114.3	109.4	31.3	6.6	37.5	100.7	225.4	271.7	126.1	130.6	161.9	149.1
Sr (ppm)	639	616	698	436	308	980	1631	2573	821	2252	2462	2557
$^{87}Rb/^{86}Sr$	0.5174	0.5135	0.1298	0.0438	0.3521	0.2975	0.3998	0.3055	0.4447	0.1678	0.1904	0.1687
$^{87}Sr/^{86}Sr_N$	0.706139	0.705842	0.704624	0.704585	0.708096	0.706663	0.705597	0.705498	0.705428	0.705405	0.704903	0.704727
+/- 2SE	08	10	08	09	09	07	07	08	07	08	09	09
$^{87}Sr/^{86}Sr_i$	0.705598	0.705305	0.704526	0.704552	0.707831	0.706439	0.705194	0.705190	0.704980	0.705236	0.704711	0.704557
$\varepsilon_{Sr\,i}$	16.81	12.65	1.26	1.62	48.17	28.41	11.04	10.98	8.00	11.63	4.18	1.99
Sm-Nd												
Analysis date	20-May-02	20-May-02	8-Jun-02	8-Jun-02	8-Jun-02	8-Jun-02	8-Jun-02	8-Jun-02	8-Jun-02	8-Jun-02	8-Jun-02	8-Jun-02
Analysis method	PIMMS - Nept	PIMMS - Nept	PIMMS - Nept	PIMMS - Nept	PIMMS - Nept	PIMMS - Nept	PIMMS - Nept	PIMMS - Nept	PIMMS - Nept	PIMMS - Nept	PIMMS - Nept	PIMMS - Nept
Standard average	0.511097	0.511097	0.511104	0.511104	0.511104	0.511104	0.511104	0.511104	0.511104	0.511104	0.511104	0.511104
+/- 2σ	18	18	18	18	18	18	18	18	18	18	18	18
Sm (ppm)	6.0	5.7	7.6	7.1	2.6	7.0	11.3	13.1	10.0	9.4	12.5	13.8
Nd (ppm)	58	54	82	76	24	70	110	130	96	87	126	140
$^{147}Sm/^{144}Nd$	0.0628	0.0629	0.0563	0.0565	0.0656	0.0610	0.0617	0.0609	0.0627	0.0657	0.0596	0.0596
$^{143}Nd/^{144}Nd_N$	0.512372	0.512397	0.512461	0.512440	0.512419	0.512500	0.512578	0.512540	0.512560	0.512554	0.512417	0.512443
+/- 2SE	17	19	08	10	05	11	16	12	05	09	08	16
$^{143}Nd/^{144}Nd_i$	0.512342	0.512367	0.512441	0.512420	0.512396	0.512479	0.512549	0.512512	0.512531	0.512524	0.512389	0.512415
$\varepsilon_{Nd\,i}$	-3.93	-3.44	-2.50	-2.91	-3.39	-1.77	0.05	-0.68	-0.31	-0.45	-3.07	-2.56
Lu-Hf												
Analysis date	14-Jun-02	12-Jun-02	14-Jun-02	14-Jun-02	14-Jun-02	14-Jun-02	14-Jun-02	14-Jun-02	14-Jun-02	14-Jun-02	14-Jun-02	18-Dec-02
Analysis method	PIMMS - Nept	PIMMS - Nept	PIMMS - Nept	PIMMS - Nept	PIMMS - Nept	PIMMS - Nept	PIMMS - Nept	PIMMS - Nept	PIMMS - Nept	PIMMS - Nept	PIMMS - Nept	PIMMS - Nept
Standard average	0.282152	0.282156	0.282152	0.282152	0.282152	0.282152	0.282152	0.282152	0.282152	0.282152	0.282152	0.282163
+/- 2σ	09	09	09	09	09	09	09	09	09	09	09	05
Lu (ppm)	0.06	0.08	0.05	0.04	0.04	0.04	0.11	0.13	0.11	0.10	0.12	0.14
Hf (ppm)	1.11	1.31	1.14	0.89	0.60	1.16	1.95	2.27	1.78	1.83	1.96	2.18
$^{175}Lu/^{177}Hf$	0.0081	0.0087	0.0058	0.0061	0.0097	0.0054	0.0078	0.0083	0.0084	0.0081	0.0089	0.0089
$^{176}Hf/^{177}Hf_N$	0.282527	0.282491	0.282732	0.282820	0.282245	0.282457	0.282734	0.282719	0.282749	0.282722	0.282541	0.282595
+/- 2SE	13	20	39	31	25	28	11	12	16	14	17	10
$^{176}Hf/^{177}Hf_i$	0.282516	0.282479	0.282726	0.282814	0.282235	0.282452	0.282724	0.282708	0.282738	0.282711	0.282529	0.282583
$\varepsilon_{Hf\,i}$	-7.44	-8.74	-0.45	2.65	-17.81	-10.16	-0.15	-0.70	0.36	-0.58	-7.02	-5.12
$\Delta\varepsilon_{Hf\,i}$	-5.40	-7.35	-0.31	3.34	-16.50	-10.99	-3.41	-2.98	-2.42	-3.17	-6.13	-4.90

FIELD	Lac de Gras	Lac de Gras	Lac de Gras	Lac de Gras	Lac de Gras	Lac de Gras	Lac de Gras	Lac de Gras	Lac de Gras	Lac de Gras	South-West Slave	South-East Slave
LOCALITY	T35	T35	T36	T36	T146	T146	T237	T237	TR107	TR107	Drybones	Gahcho Kue
SAMPLE	T35-1-1	T35-1-2	T36-1-1	T36-2-1	T146-1-1	T146-1-2	T237-1-1	T237-1-2	TR107-3-1	TR107-3-2	DRY-1	KDY-1
Rb-Sr												
Analysis date	22-Sep-02	22-Sep-02	22-Sep-02	22-Sep-02	22-Sep-02	22-Sep-02	22-Sep-02	22-Sep-02	22-Sep-02	22-Sep-02	30-Oct-02	10-Jan-03
Analysis method	PIMMS - Nept	PIMMS - Nept	PIMMS - Nept	PIMMS - Nept	PIMMS - Nept	PIMMS - Nept	PIMMS - Nept	PIMMS - Nept	PIMMS - Nept	PIMMS - Nept	PIMMS - Nept	PIMMS - Nept
Standard average	0.710268	0.710268	0.710268	0.710268	0.710268	0.710268	0.710268	0.710268	0.710268	0.710268	0.710254	0.710285
+/- 2σ	12	12	12	12	12	12	12	12	12	12	20	13
Rb (ppm)	153.2	107.4	155.5	194.5	293.0	595.5	109.9	125.6	151.2	179.6	26.8	77.1
Sr (ppm)	2144	857	811	1463	3284	2921	2989	2469	2713	2239	138	719
$^{87}Rb/^{86}Sr$	0.2068	0.3625	0.5548	0.3845	0.2582	0.5899	0.1064	0.1472	0.1613	0.2321	0.5600	0.3106
$^{87}Sr/^{86}Sr_N$	0.704578	0.704678	0.705415	0.705402	0.705585	0.705773	0.705298	0.704931	0.705390	0.705796	0.713156	0.707396
+/- 2SE	09	10	10	10	10	11	13	12	10	11	14	11
$^{87}Sr/^{86}Sr_i$	0.704370	0.704313	0.704856	0.705014	0.705325	0.705178	0.705191	0.704783	0.704196	0.704077	0.709637	0.705007
$\varepsilon_{Sr\,i}$	-0.67	-1.48	6.23	8.49	12.89	10.82	10.99	5.20	4.38	2.69	80.35	16.24
Sm-Nd												
Analysis date	17-Jul-02	17-Jul-02	17-Jul-02	17-Jul-02	17-Jul-02	17-Jul-02	17-Jul-02	17-Jul-02	17-Jul-02	17-Jul-02	31-Oct-02	11-Jan-03
Analysis method	PIMMS - Nept	PIMMS - Nept	PIMMS - Nept	PIMMS - Nept	PIMMS - Nept	PIMMS - Nept	PIMMS - Nept	PIMMS - Nept	PIMMS - Nept	PIMMS - Nept	PIMMS - Nept	PIMMS - Nept
Standard average	0.511109	0.511109	0.511109	0.511109	0.511109	0.511109	0.511109	0.511109	0.511109	0.511109	0.511109	0.511103
+/- 2σ	18	18	18	18	18	18	18	18	18	18	12	15
Sm (ppm)	14.7	12.9	14.5	14.5	14.7	17.4	17.1	16.8	17.9	16.4	3.7	7.2
Nd (ppm)	150	131	146	148	152	179	176	167	186	169	31	57
$^{147}Sm/^{144}Nd$	0.0591	0.0595	0.0600	0.0593	0.0586	0.0588	0.0587	0.0608	0.0581	0.0586	0.0728	0.0756
$^{143}Nd/^{144}Nd_N$	0.512425	0.512421	0.512520	0.512511	0.512520	0.512515	0.512569	0.512571	0.512391	0.512379	0.512354	0.512160
+/- 2SE	04	05	04	06	05	04	04	05	05	05	13	08
$^{143}Nd/^{144}Nd_i$	0.512398	0.512393	0.512492	0.512483	0.512493	0.512488	0.512542	0.512543	0.512193	0.512179	0.512143	0.511893
$\varepsilon_{Nd\,i}$	-2.91	-2.99	-1.06	-1.23	-1.05	-1.15	-0.10	-0.08	4.39	4.13	1.44	-0.97
Lu-Hf												
Analysis date	18-Jul-02	18-Jul-02	18-Jul-02	18-Jul-02	18-Jul-02	18-Jul-02	18-Jul-02	18-Jul-02	18-Jul-02	18-Jul-02	18-Dec-02	19-Dec-02
Analysis method	PIMMS - Nept	PIMMS - Nept	PIMMS - Nept	PIMMS - Nept	PIMMS - Nept	PIMMS - Nept	PIMMS - Nept	PIMMS - Nept	PIMMS - Nept	PIMMS - Nept	PIMMS - Nept	PIMMS - Nept
Standard average	0.282156	0.282156	0.282156	0.282156	0.282156	0.282156	0.282156	0.282156	0.282156	0.282156	0.282163	0.282158
+/- 2σ	10	10	10	10	10	10	10	10	10	10	05	12
Lu (ppm)	0.14	0.13	0.13	0.14	0.10	0.13	0.16	0.16	0.14	0.15	0.05	0.06
Hf (ppm)	2.21	1.90	2.63	2.54	2.40	2.79	2.82	2.88	2.92	2.84	3.53	2.05
$^{176}Lu/^{177}Hf$	0.0090	0.0093	0.0072	0.0075	0.0061	0.0064	0.0079	0.0077	0.0068	0.0073	0.0020	0.0044
$^{176}Hf/^{177}Hf_N$	0.282636	0.282622	0.282715	0.282676	0.282533	0.282721	0.282833	0.282854	0.282560	0.282488	0.282417	0.282059
+/- 2SE	08	08	08	20	34	08	09	08	06	05	07	11
$^{176}Hf/^{177}Hf_i$	0.282624	0.282610	0.282705	0.282666	0.282525	0.282713	0.282822	0.282844	0.282493	0.282417	0.282400	0.282015
$\varepsilon_{Hf\,i}$	-3.67	-4.18	-0.79	-2.19	-7.18	-0.54	3.35	4.10	1.65	-1.05	-3.38	-14.85
$\Delta\varepsilon_{Hf\,i}$	-2.99	-3.39	-2.57	-3.74	-8.97	-2.20	0.29	1.01	-7.38	-9.73	-8.49	-16.74

	CANADA, Churchill Province							CANADA, Superior Province			
FIELD	South-East Slave	South-East Slave	Somerset Island	Somerset Island	Somerset Island	Somerset Island	Rankin Inlet	Attawapiskat	Kirkland Lake	Timiskaming
LOCALITY	Gahcho Kue	Snap Lake	JP South	Batty Bay	Elwin Bay	Jos	Rankin Inlet	James Bay Lowlands	Upper Canada Mine	Gulges
SAMPLE	KDY-2	SNP-1	JPS-1	BAT-1	ELB-1	JOS-1	RNK-1	JBL-1	UCM-2	GUI-1
Rb-Sr										
Analysis date	10-Jan-03	10-Jan-03	Dec-00	18-Oct-01	18-Oct-01	18-Oct-01	22-Sep-02	22-Sep-02	22-Sep-02	22-Sep-02
Analysis method	PIMMS - Nept	PIMMS - Nept	TIMS - 262	PIMMS - Nept	PIMMS - Nept	PIMMS - Nept	PIMMS - Nept	PIMMS - Nept	PIMMS - Nept	PIMMS - Nept
Standard average	0.710285	0.710285	0.710240	0.710261	0.710261	0.710261	0.710268	0.710268	0.710268	0.710268
+/- 2σ	13	13	04	13	13	13	12	12	12	12
Rb (ppm)	132.6	98.3	39.2	8.2	63.7	18.9	29.2	17.0	162.1	50.8
Sr (ppm)	264	244	1388	1372	901	1639	1636	349	933	308
$^{87}Rb/^{86}Sr$	1.4533	1.1643	0.0818	0.0173	0.2048	0.0333	0.0517	0.1410	0.5029	0.4776
$^{87}Sr/^{86}Sr_N$	0.715992	0.713163	0.705318	0.705691	0.706030	0.706272	0.703600	0.707061	0.706005	0.705291
+/- 2SE	11	11	12	09	09	15	11	09	09	11
$^{87}Sr/^{86}Sr_i$	0.704813	0.704290	0.705205	0.705667	0.705746	0.706226	0.703456	0.706711	0.704896	0.704326
$\varepsilon Sr\,i$	13.48	5.98	11.63	18.19	19.32	26.13	-11.55	34.31	8.21	-0.10
Sm-Nd										
Analysis date	11-Jan-03	11-Jan-03	Dec-00	26-Oct-01	26-Oct-01	26-Oct-01	17-Jul-02	17-Jul-02	17-Jul-02	17-Jul-02
Analysis method	PIMMS - Nept	PIMMS - Nept	TIMS - 262	PIMMS - Nept	PIMMS - Nept	PIMMS - Nept	PIMMS - Nept	PIMMS - Nept	PIMMS - Nept	PIMMS - Nept
Standard average	0.511103	0.511103	0.511931	0.511118	0.511118	0.511118	0.511109	0.511109	0.511109	0.511109
+/- 2σ	15	15	21	15	15	15	18	18	18	18
Sm (ppm)	7.4	9.0	13.7	11.8	8.5	7.2	21.2	2.4	11.0	4.0
Nd (ppm)	59	108	105	92	67	58	178	16	78	31
$^{147}Sm/^{144}Nd$	0.0767	0.0504	0.0788	0.0776	0.0772	0.0754	0.0720	0.0895	0.0845	0.0787
$^{143}Nd/^{144}Nd_N$	0.512039	0.512168	0.512663	0.512595	0.512605	0.512618	0.512706	0.512463	0.512487	0.512777
+/- 2SE	08	07	08	14	12	10	05	07	04	04
$^{143}Nd/^{144}Nd_i$	0.511768	0.511991	0.512613	0.512545	0.512556	0.512570	0.512614	0.512360	0.512401	0.512704
$\varepsilon Nd\,i$	-3.41	0.83	1.95	0.64	0.84	1.12	4.45	-1.02	-0.72	4.86
Lu-Hf										
Analysis date	19-Dec-02	19-Dec-02	Dec-00	24-Oct-01	24-Oct-01	24-Oct-01	18-Jul-02	18-Jul-02	18-Jul-02	18-Jul-02
Analysis method	PIMMS - Nept	PIMMS - Nept	PIMMS - P54	PIMMS - Nept	PIMMS - Nept	PIMMS - Nept	PIMMS - Nept	PIMMS - Nept	PIMMS - Nept	PIMMS - Nept
Standard average	0.282158	0.282158	0.282178	0.282160	0.282160	0.282160	0.282156	0.282156	0.282156	0.282156
+/- 2σ	12	12	12	10	10	10	10	10	10	10
Lu (ppm)	0.07	0.05	0.10	0.09	0.08	0.07	0.16	0.06	0.13	0.04
Hf (ppm)	2.40	2.91	4.57	2.94	2.32	1.55	7.13	0.98	4.04	1.76
$^{176}Lu/^{177}Hf$	0.0041	0.0024	0.0031	0.0045	0.0048	0.0060	0.0031	0.0093	0.0047	0.0034
$^{176}Hf/^{177}Hf_N$	0.282010	0.282430	0.282818	0.282790	0.282768	0.282833	0.282850	0.282441	0.282720	0.282936
+/- 2SE	09	13	10	07	07	10	06	31	05	10
$^{176}Hf/^{177}Hf_i$	0.281968	0.282405	0.282812	0.282782	0.282759	0.282822	0.282839	0.282411	0.282706	0.282927
$\varepsilon Hf\,i$	-16.50	-1.12	3.58	2.50	1.70	3.92	6.69	-8.92	1.10	8.62
$\Delta\varepsilon Hf\,i$	-15.15	-5.42	-2.21	-1.55	-2.61	-0.76	-2.42	-10.75	-1.13	-1.03

FIELD	CANADA, Trans-Hudson Domain			USA, Yapavai Domain			South Africa, Kaapvaal Province		
	Timiskaming	Fort a la Corne	Fort a la Corne	State Line	State Line	State Line	Barkly West	Barkly West	Central Cape
LOCALITY	Peddie	Fort a la Corne	Sturgeon Lake	Nix	Chicken Park	Sloan	Frank Smith	Roberts Victor	Gansfontein
SAMPLE	PED-1	FLC-1	STL-1	NIX-1	CHK-1	SLN-1	FSM-2	ROVIC-1	GNS-13

Rb-Sr

	PED-1	FLC-1	STL-1	NIX-1	CHK-1	SLN-1	FSM-2	ROVIC-1	GNS-13
Analysis date	22-Sep-02	06-Jun-02	30-Oct-02	22-Sep-02	22-Sep-02	22-Sep-02	30-Oct-02	Dec-00	Dec-00
Analysis method	PIMMS - Nept	PIMMS - Nept	PIMMS - Nept	PIMMS - Nept	PIMMS - Nept	PIMMS - Nept	PIMMS - Nept	TIMS - 262	TIMS - 262
Standard average	0.710268	0.710272	0.710254	0.710268	0.710268	0.710268	0.710254	0.710240	0.710240
+/- 2σ	12	09	20	12	12	12	20	04	04
Rb (ppm)	35.2	4.1	5.7	24.1	60.8	164.9	64.2	75.8	82.9
Sr (ppm)	967	134	238	1259	710	622	764	2036	1687
$^{87}Rb/^{86}Sr$	0.1053	0.0890	0.0689	0.0553	0.2476	0.7670	0.2435	0.1077	0.1422
$^{87}Sr/^{86}Sr_N$	0.705268	0.705800	0.706784	0.703967	0.704880	0.709606	0.708060	0.707772	0.704124
+/- 2SE	10	06	12	08	10	11	13	08	12
$^{87}Sr/^{86}Sr_i$	0.705038	0.705674	0.706688	0.703652	0.702712	0.705240	0.707667	0.707578	0.703922
$\varepsilon_{Sr\,i}$	10.21	18.33	32.70	-5.35	-15.12	17.20	46.86	45.81	-6.54

Sm-Nd

	PED-1	FLC-1	STL-1	NIX-1	CHK-1	SLN-1	FSM-2	ROVIC-1	GNS-13
Analysis date	17-Jul-02	20-May-02	31-Oct-02	17-Jul-02	17-Jul-02	17-Jul-02	31-Oct-02	Dec-00	Dec-00
Analysis method	PIMMS - Nept	PIMMS - Nept	PIMMS - Nept	PIMMS - Nept	PIMMS - Nept	PIMMS - Nept	PIMMS - Nept	TIMS - 262	TIMS - 262
Standard average	0.511109	0.511097	0.511109	0.511109	0.511109	0.511109	0.511109	0.511931	0.511931
+/- 2σ	18	18	12	18	18	18	12	21	21
Sm (ppm)	18.0	5.9	3.4	10.2	12.9	10.6	5.6	33.4	28.9
Nd (ppm)	144	48	29	95	88	81	36	311	198
$^{147}Sm/^{144}Nd$	0.0757	0.0746	0.0711	0.0649	0.0885	0.0786	0.0936	0.0649	0.0885
$^{143}Nd/^{144}Nd_N$	0.512727	0.512566	0.512624	0.512412	0.512358	0.512363	0.512535	0.511938	0.512740
+/- 2SE	06	07	12	04	05	04	11	06	10
$^{143}Nd/^{144}Nd_i$	0.512651	0.512517	0.512578	0.512242	0.512002	0.512157	0.512465	0.511884	0.512682
$\varepsilon_{Nd\,i}$	4.11	0.15	1.30	2.32	3.04	0.66	-0.52	-11.52	3.37

Lu-Hf

	PED-1	FLC-1	STL-1	NIX-1	CHK-1	SLN-1	FSM-2	ROVIC-1	GNS-13
Analysis date	18-Jul-02	12-Jun-02	18-Dec-02	19-Jul-02	19-Jul-02	19-Jul-02	18-Dec-02	Dec-00	Dec-00
Analysis method	PIMMS - Nept	PIMMS - Nept	PIMMS - Nept	PIMMS - Nept	PIMMS - Nept	PIMMS - Nept	PIMMS - Nept	PIMMS - P54	PIMMS - P54
Standard average	0.282156	0.282156	0.282163	0.282153	0.282153	0.282153	0.282163	0.282178	0.282178
+/- 2σ	10	09	05	11	11	11	05	12	12
Lu (ppm)	0.15	0.04	0.03	0.10	0.13	0.32	0.22	0.33	0.22
Hf (ppm)	3.93	2.62	0.74	2.98	5.36	4.33	2.72	13.52	54.50
$^{176}Lu/^{177}Hf$	0.0052	0.0022	0.0061	0.0045	0.0034	0.0105	0.0117	0.0034	0.0006
$^{176}Hf/^{177}Hf_N$	0.282889	0.282714	0.282748	0.282627	0.282532	0.282548	0.282625	0.282283	0.282708
+/- 2SE	14	09	29	07	04	05	07	07	05
$^{176}Hf/^{177}Hf_i$	0.282874	0.282710	0.282737	0.282593	0.282493	0.282469	0.282600	0.282275	0.282707
$\varepsilon_{Hf\,i}$	6.99	0.01	0.91	2.51	3.74	-1.86	-3.58	-14.79	-0.10
$\Delta\varepsilon_{Hf\,i}$	-1.66	-3.39	-4.00	-3.77	-3.49	-5.94	-6.08	-2.65	-7.77

380

	Central Cape	North Lesotho	North Lesotho	RUSSIA, Siberian Province			
FIELD				Malo-Botuobinsk	Malo-Botuobinsk	Daldyn-Alakit	Daldyn-Alakit
LOCALITY	Melton Wold	Liqhobong	Pipe 200	Mir	Internationalaya	Jubilee	Udachnaya
SAMPLE	MW-3	LQ-7	P200	MIR-M3	INT-I2	JUB-1	UDC-1
Rb-Sr							
Analysis date	Dec-00	Dec-00	30-Oct-02	25-Jul-01	25-Jul-01	25-Jul-01	25-Jul-01
Analysis method	TIMS - 262	TIMS - 262	PIMMS - Nept	PIMMS - Nept	PIMMS - Nept	PIMMS - Nept	PIMMS - Nept
Standard average	0.710240	0.710240	0.710254	0.710282	0.710282	0.710282	0.710282
+/- 2σ	04	04	20	10	10	10	10
Rb (ppm)	144.7	102.9	80.3	19.7	28.1	12.9	55.8
Sr (ppm)	1147	937	745	436	1083	402	489
$^{87}Rb/^{86}Sr$	0.3653	0.3179	0.3119	0.1308	0.0751	0.0930	0.3302
$^{87}Sr/^{86}Sr_N$	0.706996	0.704048	0.703564	0.705825	0.705425	0.707606	0.706170
+/- 2SE	10	08	09	08	08	08	07
$^{87}Sr/^{86}Sr_i$	0.706244	0.703642	0.703165	0.705155	0.705041	0.707130	0.704479
$\varepsilon_{Sr\,i}$	27.17	-10.69	-17.45	15.32	13.69	43.37	5.72
Sm-Nd							
Analysis date	Dec-00	Dec-00	31-Oct-02	19-Jul-01	19-Jul-01	19-Jul-01	19-Jul-01
Analysis method	TIMS - 262	TIMS - 262	PIMMS - Nept	PIMMS - Nept	PIMMS - Nept	PIMMS - Nept	PIMMS - Nept
Standard average	0.511931	0.511931	0.511109	0.511100	0.511100	0.511100	0.511100
+/- 2σ	21	21	12	14	14	14	14
Sm (ppm)	7.8	12.0	11.0	4.4	9.7	4.4	6.0
Nd (ppm)	62	80	74	31	72	34	46
$^{147}Sm/^{144}Nd$	0.0771	0.0909	0.0898	0.0860	0.0808	0.0778	0.0791
$^{143}Nd/^{144}Nd_N$	0.512402	0.512690	0.512767	0.512594	0.512605	0.512560	0.512556
+/- 2SE	10	08	07	07	08	06	07
$^{143}Nd/^{144}Nd_i$	0.512329	0.512636	0.512714	0.512391	0.512415	0.512377	0.512370
$\varepsilon_{Nd\,i}$	-2.39	2.23	3.74	4.23	4.69	3.94	3.81
Lu-Hf							
Analysis date	Dec-00	Dec-00	18-Dec-02	7-Jun-01	7-Jun-01	7-Jun-01	7-Jun-01
Analysis method	PIMMS - P54	PIMMS - P54	PIMMS - Nept	PIMMS - P54	PIMMS - P54	PIMMS - P54	PIMMS - P54
Standard average	0.282178	0.282178	0.282163	0.282213	0.282213	0.282213	0.282213
+/- 2σ	12	12	05	09	09	09	09
Lu (ppm)	0.11	0.16	0.10	0.09	0.09	0.04	0.06
Hf (ppm)	3.69	5.16	9.30	2.01	3.21	1.61	2.28
$^{176}Lu/^{177}Hf$	0.0043	0.0044	0.0015	0.0063	0.0042	0.0035	0.0038
$^{176}Hf/^{177}Hf_N$	0.282463	0.282742	0.282740	0.282737	0.282781	0.282728	0.282701
+/- 2SE	16	09	05	06	09	07	07
$^{176}Hf/^{177}Hf_i$	0.282451	0.282735	0.282738	0.282694	0.282753	0.282704	0.282675
$\varepsilon_{Hf\,i}$	-8.14	0.66	0.77	5.21	7.28	5.55	4.54
$\Delta\varepsilon_{Hf\,i}$	-8.15	-5.49	-7.40	-3.61	-2.15	-2.88	-3.72

CANADA, Slave Province

	Greywacke	Greywacke	Greywacke	Greywacke (rep)	Greywacke	Greywacke	Greywacke	Greywacke	Greywacke	Trondhjemite	Trondhjemite
LITHOLOGY											
FUSED/UNFUSED	Fused	Unfused	Fused	Fused (rep)	Unfused	Fused	Unfused	Fused	Unfused	Fused	Unfused
SAMPLE	KIA92-K076	KIA82-K075	KIA92-K089	KIA92-K089	KIA92-K089	KIA92-K152	KIA92-K152	KIA92-P067	KIA92-P067	KIA92-K078	KIA92-K078
Rb-Sr											
Analysis date	10-Jan-03	10-Jan-03	10-Jan-03	10-Jan-03	10-Jan-03	10-Jan-03	10-Jan-03	10-Jan-03	10-Jan-03	10-Jan-03	10-Jan-03
Analysis method	PIMMS - Nept	PIMMS - Nept	PIMMS - Nept	PIMMS - Nept	PIMMS - Nept	PIMMS - Nept	PIMMS - Nept	PIMMS - Nept	PIMMS - Nept	PIMMS - Nept	PIMMS - Nept
Standard average	0.710285	0.710285	0.710285	0.710285	0.710285	0.710285	0.710285	0.710285	0.710285	0.710285	0.710285
+/- 2σ	13	13	13	13	13	13	13	13	13	13	13
Rb (ppm)	84.9	84.9	58.7	58.7	58.7	116.5	116.5	127.0	127.0	72.8	72.8
Sr (ppm)	277	277	263	263	263	238	238	351	351	613	613
$^{87}Rb/^{86}Sr$	0.8869	0.8869	0.6458	0.6458	0.6458	1.4164	1.4164	1.0470	1.0470	0.3436	0.3436
$^{87}Sr/^{86}Sr_N$	0.734243	0.734158	0.725682	0.725763	0.725901	0.753099	0.754155	0.740636	0.741403	0.713411	0.713409
+/- 2SE	15	17	14	13	21	10	11	12	08	11	10
$^{87}Sr/^{86}Sr_i$	0.700520	0.700435	0.701125	0.701206	0.701344	0.699241	0.700297	0.700825	0.701592	0.700344	0.700342
$\varepsilon_{Sr\,i}$	-11.91	-13.13	-3.29	-2.13	-0.16	-30.14	-15.09	-7.56	3.38	-14.42	-14.45
Sm-Nd											
Analysis date	11-Jan-03	11-Jan-03	11-Jan-03	11-Jan-03	11-Jan-03	11-Jan-03	11-Jan-03	11-Jan-03	11-Jan-03	11-Jan-03	11-Jan-03
Analysis method	PIMMS - Nept	PIMMS - Nept	PIMMS - Nept	PIMMS - Nept	PIMMS - Nept	PIMMS - Nept	PIMMS - Nept	PIMMS - Nept	PIMMS - Nept	PIMMS - Nept	PIMMS - Nept
Standard average	0.511103	0.511103	0.511103	0.511103	0.511103	0.511103	0.511103	0.511103	0.511103	0.511103	0.511103
+/- 2σ	15	15	15	15	15	15	15	15	15	15	15
Sm (ppm)	4.7	4.7	4.6	4.6	4.6	6.9	6.9	8.0	8.0	1.5	1.5
Nd (ppm)	25	25	29	29	29	37	37	43	43	9	9
$^{147}Sm/^{144}Nd$	0.1127	0.1127	0.0945	0.0945	0.0945	0.1133	0.1133	0.1121	0.1121	0.1018	0.1018
$^{143}Nd/^{144}Nd_N$	0.511078	0.511063	0.510904	0.510893	0.510881	0.511182	0.511149	0.511248	0.511227	0.511178	0.511166
+/- 2SE	15	06	08	08	07	05	06	06	06	09	11
$^{143}Nd/^{144}Nd_i$	0.509123	0.509108	0.509264	0.509253	0.509241	0.509217	0.509184	0.509302	0.509281	0.509411	0.509399
$\varepsilon_{Nd\,i}$	-2.05	-2.34	0.72	0.51	0.27	-0.21	-0.86	1.48	1.06	3.62	3.38
Lu-Hf											
Analysis date	09-Jan-03	19-Dec-02	09-Jan-03	09-Jan-03	19-Dec-02	09-Jan-03	19-Dec-02	09-Jan-03	19-Dec-02	09-Jan-03	19-Dec-02
Analysis method	PIMMS - Nept	PIMMS - Nept	PIMMS - Nept	PIMMS - Nept	PIMMS - Nept	PIMMS - Nept	PIMMS - Nept	PIMMS - Nept	PIMMS - Nept	PIMMS - Nept	PIMMS - Nept
Standard average	0.282144	0.282158	0.282144	0.282144	0.282158	0.282144	0.282158	0.282144	0.282158	0.282144	0.282158
+/- 2σ	03	12	03	03	12	03	12	03	12	03	12
Lu (ppm)	1.50	1.50	1.20	1.20	1.20	2.00	2.00	3.00	3.00	0.50	0.50
Hf (ppm)	3.90	3.90	6.40	6.40	6.40	3.40	3.40	4.20	4.20	3.90	3.90
$^{176}Lu/^{177}Hf$	0.0546	0.0546	0.0266	0.0266	0.0266	0.0836	0.0836	0.1015	0.1015	0.0182	0.0182
$^{176}Hf/^{177}Hf_N$	0.281651	0.281446	0.281330	0.281346	0.281308	0.281798	0.281597	0.281982	0.281651	0.281365	0.281406
+/- 2SE	112	14	29	20	11	34	17	31	22	95	20
$^{176}Hf/^{177}Hf_i$	0.278888	0.278683	0.279983	0.279999	0.279961	0.277572	0.277371	0.276850	0.276519	0.280444	0.280485
$\varepsilon_{Hf\,i}$	-78.45	-85.74	-39.49	-38.92	-40.27	-125.26	-132.41	-150.93	-162.71	-23.09	-21.63
$\Delta\varepsilon_{Hf\,i}$	-78.92	-85.82	-43.64	-42.78	-43.82	-128.17	-134.46	-156.08	-167.31	-31.09	-29.31

LITHOLOGY	Hbl tonalite	Hbl tonalite	Hbl tonalite	Hbl tonalite	Biotite granite	Biotite granite (rep)	Biotite granite	2 mica granite	2 mica granite
FUSED/UNFUSED	Fused	Unfused	Fused	Unfused	Fused	Fused (rep)	Unfused	Fused	Unfused
SAMPLE	KIA92-K049	KIA92-K049	KIA92-K177A	KIA92-K177A	KIA92-K106	KIA92-K106	KIA92-K106	KIA92-K139	KIA92-K139
Rb-Sr									
Analysis date	10-Jan-03	10-Jan-03	10-Jan-03	10-Jan-03	10-Jan-03	10-Jan-03	10-Jan-03	10-Jan-03	10-Jan-03
Analysis method	PIMMS - Nept	PIMMS - Nept	PIMMS - Nept	PIMMS - Nept	PIMMS - Nept	PIMMS - Nept	PIMMS - Nept	PIMMS - Nept	PIMMS - Nept
Standard average	0.710285	0.710285	0.710285	0.710285	0.710285	0.710285	0.710285	0.710285	0.710285
+/- 2σ	13	13	13	13	13	13	13	13	13
Rb (ppm)	81.5	81.5	54.1	54.1	153.9	153.9	153.9	198.1	198.1
Sr (ppm)	937	937	639	639	96	96	96	134	134
$^{87}Rb/^{86}Sr$	0.2517	0.2517	0.2450	0.2450	4.6388	4.6388	4.6388	4.2778	4.2778
$^{87}Sr/^{86}Sr_N$	0.710214	0.710239	0.711756	0.711748	0.860725	0.862471	0.864316	0.860917	0.863176
+/- 2SE	11	11	11	11	16	14	74	14	43
$^{87}Sr/^{86}Sr_i$	0.700644	0.700669	0.702441	0.702433	0.687068	0.688814	0.690659	0.700775	0.703034
$\varepsilon_{Sr\,i}$	-10.15	-9.79	15.47	15.36	-204.39	-179.50	-153.20	-8.97	23.24
Sm-Nd									
Analysis date	11-Jan-03	11-Jan-03	11-Jan-03	11-Jan-03	11-Jan-03	11-Jan-03	11-Jan-03	11-Jan-03	11-Jan-03
Analysis method	PIMMS - Nept	PIMMS - Nept	PIMMS - Nept	PIMMS - Nept	PIMMS - Nept	PIMMS - Nept	PIMMS - Nept	PIMMS - Nept	PIMMS - Nept
Standard average	0.511103	0.511103	0.511103	0.511103	0.511103	0.511103	0.511103	0.511103	0.511103
+/- 2σ	15	15	15	15	15	15	15	15	15
Sm (ppm)	4.5	4.5	6.4	6.4	2.5	2.5	2.5	2.0	2.0
Nd (ppm)	29	29	27	27	10	10	10	11	11
$^{147}Sm/^{144}Nd$	0.0931	0.0931	0.1411	0.1411	0.1452	0.1452	0.1452	0.1099	0.1099
$^{143}Nd/^{144}Nd_N$	0.511056	0.511045	0.511033	0.511021	0.511913	0.511944	0.511932	0.511341	0.511335
+/- 2SE	06	07	08	06	55	16	08	10	09
$^{143}Nd/^{144}Nd_i$	0.509441	0.509430	0.508585	0.508573	0.509432	0.509463	0.509451	0.509464	0.509458
$\varepsilon_{Nd\,i}$	4.19	3.97	-12.62	-12.85	2.99	3.60	3.37	3.63	3.51
Lu-Hf									
Analysis date	09-Jan-03	19-Dec-02	09-Jan-03	19-Dec-02	09-Jan-03		19-Dec-02	09-Jan-03	19-Dec-02
Analysis method	PIMMS - Nept	PIMMS - Nept	PIMMS - Nept	PIMMS - Nept	PIMMS - Nept		PIMMS - Nept	PIMMS - Nept	PIMMS - Nept
Standard average	0.282144	0.282158	0.282144	0.282158	0.282144		0.282158	0.282144	0.282158
+/- 2σ	03	12	03	12	03		12	03	12
Lu (ppm)	0.70	0.70	1.10	1.10	0.20	0.20	0.20	-	-
Hf (ppm)	1.30	1.30	4.60	4.60	1.60	1.60	1.60	2.70	2.70
$^{176}Lu/^{177}Hf$	0.0765	0.0765	0.0340	0.0340	0.0178	0.0178	0.0178	-	-
$^{176}Hf/^{177}Hf_N$	0.281805	0.281779	0.281491	0.281535	0.281393	0.281278	-	0.281354	0.281244
+/- 2SE	128	42	49	20	87	66	-	89	30
$^{176}Hf/^{177}Hf_i$	0.277936	0.277910	0.279773	0.279817	0.280509	0.280394	-	0.281354	0.281244
$\varepsilon_{Hf\,i}$	-112.29	-113.21	-46.96	-45.39	-21.70	-25.79	-	8.36	4.45
$\Delta\varepsilon_{Hf\,i}$	-121.05	-121.69	-33.36	-31.48	-28.87	-33.46	-	0.34	-3.42

Appendix G

Summary of isotope standard data

The tables presented below summarise all isotopic standard data obtained during the course of this study. Accepted values for the isotopic standards used are listed in Table 2.11.

G.1 Sr STANDARD DATA

Date	Instrument	Standard	No. stds run	Average ± 2σ (abs)	Rel. 2σ error (ppm)
8 Apr 00	TIMS - 262	NBS-987	3	0.710243 ± 05	7.0
25/26 Dec 00	TIMS - 262	NBS-987	7	0.710263 ± 38	53.5
24 Jul 01	PIMMS - Neptune	200ppb NBS-987	4	0.710273 ± 16	22.5
25 Jul 01	PIMMS - Neptune	200ppb NBS-987	8	0.710282 ± 10	14.1
18 Oct 01	PIMMS - Neptune	200ppb NBS-987	11	0.710261 ± 13	18.3
23 Oct 01	PIMMS - Neptune	200ppb NBS-987	15	0.710256 ± 25	35.2
5 Jun 02	PIMMS - Neptune	1ppm NBS-987	5	0.710268 ± 11	15.5
6 Jun 02	PIMMS - Neptune	1ppm NBS-987	16	0.710272 ± 09	12.7
22 Sept 02	PIMMS - Neptune	750ppb NBS-987	14	0.710268 ± 12	16.9
30 Oct 02	PIMMS - Neptune	750ppb NBS-987	11	0.710254 ± 20	28.2
10 Jan 03	PIMMS - Neptune	750ppb NBS-987	14	0.710285 ± 13	18.3

G.2 Nd STANDARD DATA

Date	Instrument	Standard	No. stds run	Average ± 2σ (abs)	Rel. 2σ error (ppm)
15 Apr 00	TIMS - 262	J&M	3	0.511164 ± 16	31.3
25/26 Dec 00	TIMS - 262	NIGL La Jolla	8	0.511930 ± 19	37.1
19 Jul 01	PIMMS - Neptune	200ppb J&M	18	0.511100 ± 14	27.4
26 Oct 01	PIMMS - Neptune	200ppb J&M	11	0.511118 ± 15	29.3
27 Oct 01	PIMMS - Neptune	200ppb J&M	17	0.511112 ± 14	27.4
20 May 02	PIMMS - Neptune	200 ppb J&M	19	0.511097 ± 18	35.2
8 Jun 02	PIMMS - Neptune	200ppb J&M	14	0.511104 ± 18	35.2
17 Jul 02	PIMMS - Neptune	200ppb J&M	22	0.511109 ± 18	35.2
31 Oct 02	PIMMS - Neptune	140ppb J&M	12	0.511109 ± 12	23.5
11 Jan 03	PIMMS - Neptune	200ppb J&M	14	0.511103 ± 15	29.3

G.3 Hf STANDARD DATA

Date	Instrument	Standard	No. stds run	Average ± 2σ (abs)	Rel. 2σ error (ppm)
15 Apr 00	PIMMS – P54	100ppb JMC-475	6	0.282154 ± 09	31.9
16 Apr 00	PIMMS – P54	100ppb JMC-475	7	0.282161 ± 11	39.0
25/26 Dec 00	PIMMS – P54	100ppb JMC-475	12	0.282178 ± 12	42.5
6 Jun 01	PIMMS – P54	100ppb JMC-475	6	0.282218 ± 10	35.4
7 Jun 01	PIMMS – P54	100ppb JMC-475	8	0.282213 ± 09	31.9
24 Oct 01	PIMMS - Neptune	200ppb JMC-475	15	0.282160 ± 10	35.4
25 Oct 01	PIMMS - Neptune	200ppb JMC-475	8	0.282156 ± 05	17.7
12 Jun 02	PIMMS - Neptune	200ppb JMC-475	11	0.282156 ± 09	31.9
14 Jun 02	PIMMS - Neptune	200ppb JMC-475	11	0.282152 ± 09	31.9
18 Jul 02	PIMMS - Neptune	200ppb JMC-475	12	0.282156 ± 10	35.4

(cont/d)

Date	Instrument	Standard	No. stds run	Average ± 2σ (abs)	Rel. 2σ error (ppm)
19 Jul 02	PIMMS – Neptune	200ppb JMC-475	11	0.282153 ± 11	39.0
18 Dec 02	PIMMS – Neptune	200ppb JMC-475*	12	0.282163 ± 05	17.7
19 Dec 02	PIMMS – Neptune	200ppb JMC-475*	12	0.282158 ± 12	42.5
9 Dec 03	PIMMS - Neptune	200ppb JMC-475*	7	0.282144 ± 03	10.6

*Using Cetac Aridus desolvating nebuliser.

References

Agashev, A. M., Orihashi, Y., Watanabe, T., Pokhilenko, N. P., Serenko, V. P. (2000) Sr and Nd isotope and geochemical features of Siberian Platform kimberlites. *Russ. Geol. Geophys.*, **41**, 92-101.

Agashev, A. M., Watanabe, T., Bydaev, D. A., Pokhilenko, N. P., Fomin, A. S., Maehara, K., Maeda, J. (2001a) Geochemistry of kimberlites from the Nakyn field, Siberia: evidence for unique source composition. *Geology*, **29**, 267-270.

Agashev, A. M., Pokhilenko, N. P., McDonald, J. A., Takazawa, E., Vavilov, M. A., Sobolev, N. V., Watanabe, T. (2001b) A unique kimberlite-carbonatite primary association in the Snap Lake dyke system, Slave Craton: evidence from geochemical and isotopic studies. *Slave-Kaapvaal Workshop, Merrickville, Ontario, Extended Abstracts.*

Aitchison, J. (1986) *The statistical analysis of compositional data.* Chapman and Hall, London. 416pp.

Albarède, F., Blichert-Toft, J., Vervoort, J. D., Gleason, J. G., Rosing, M. (2000) Hf-Nd evidence for for a transient dynamic regime in early terrestrial mantle. *Nature*, **404**, 488-490.

Allsopp, H. L., Barrett, D. R. (1975) Rb-Sr age determinations of South African kimberlites. *Phys. Chem. Earth*, **9**, 605-617.

Anderson, D. L. (1982) Isotopic evolution of the mantle: the role of magma mixing. *Earth Planet. Sci. Lett.*, **57**, 1-12.

Araujo, A. L. N., Carlson, R. W., Gaspar, J. C., Bizzi, L. A. (2001) Petrology of kamafugites and kimberlites from the Alto Paranaíba alkaline province, Minas Gerais, Brazil. *Contrib. Mineral. Petrol.*, **142**, 163-177.

Armstrong, J. P., Wilson, M., Barnett, R. L., Nowicki, T., Kjarsgaard, B. A. (in press) Paragenesis of calcite, calcite-dolomite solid solution and dolomite in ultrafresh hypabyssal kimberlite, Lac de Gras, NWT. *Procs. 8th Int. Kimb. Conf.*

Arndt, N. (2003) Komatiites, kimberlites, and boninites. *J. Geophys. Res.*, 108, B6-2293, ECV 5.

Ballentine, C. J., Lee, D. C., Halliday, A. N. (1997) Hafnium isotope studies of the Cameroon Line and new Hf paradoxes. *Chem. Geol.*, 139, 111-124.

Barrett, D. R., Berg, G. W. (1975) Complementary petrographic and strontium isotope ratio studies of South African kimberlites. *Phys. Chem. Earth*, 9, 619-636.

Barovich, K. M., Beard, B. L., Cappel, J. B., Johnson, C. M., Kyser, T. K., Morgan, B. E. (1995) A chemical method for hafnium separation from high-Ti whole-rock and zircon samples. *Chem. Geol.*, 121, 303-308.

Bassett, H. (1954) The Igwisi craters and lavas. *Rec. Geol. Surv. Tanganyika*, 4, 81-92.

Basu, A. R., Tatsumoto, M. (1980) Nd-isotopes in mantle-derived rocks and minerals and their implications for mantle evolution. *Contrib. Mineral. Petrol.*, 75, 43-54.

Beakhouse, G. P., McNutt, R. H., Krogh, T. E. (1988) Comparative Rb-Sr and U-Pb zircon geochronology of late- to post-tectonic plutons in the Winnipeg River belt, northwestern Ontario, Canada. *Chem. Geol.*, 72, 337-351.

Berg, G. W., Allsopp, H. L. (1972) Low ^{87}Sr/^{86}Sr ratios in fresh South African kimberlites. *Earth Planet. Sci. Lett.*, 16, 27-30.

Berg, G. W., Carlson, J. A. (1998) The Leslie kimberlite pipe of Lac de Gras, Northwest Territories, Canada: evidence for near surface hypabyssal emplacement. 7th Int. Kimb. Conf., Extended Abstracts, 81-83.

Bhatia, M. R. (1983) Plate tectonics and geochemical composition of sandstones. *J. Geol.*, 91, 611-627.

Bickford, M. E., Collerson, K. D., Lewry, J. F. (1994) Crustal history of the Rae and Hearne provinces, southwestern Canadian shield, Saskatchewan: constraints from geochronologic and isotopic data. *Precamb. Res.*, 68, 1-21.

Bizimis, M. (2001) Geochemical processes in the upper mantle: evidence from peridotites, kimberlites and carbonatites. Unpubl. PhD thesis. Florida State University, Tallahassee, USA.

Bizzi, L. A., Smith, C. B., de Wit, M. J., Armstrong, R. A., Meyer, H. O. A. (1994) Mesozoic kimberlites and related alkalic rocks in the south-western São Francisco craton, Brazil: a case for local mantle reservoirs and their interaction. *Procs. 5th Intl. Kimb. Conf.*, 1, 156-171.

Blackadar, R. G. (1967) Precambrian geology of the Boothia Peninsula, Somerset Island and the Prince of Wales Island, District of Franklin. *Bull. Geol. Surv. Canada*, 151, 62.

Bleeker, W., Ketchum, J. W. F., Davis, W. J. (1999a) The Central Slave Basement Complex, Part II: age and tectonic significance of high-strain zones along the basement-cover contact. *Can. J. Earth Sci.*, 36, 1111-1130.

Bleeker, W., Ketchum, J. W. F., Jackson, V. A., Villeneuve, M. E. (1999b) The Central Slave Basement Complex, Part I: its structural topology and autochthonous cover. *Can. J. Earth Sci.*, 36, 1083-1109.

Blichert-Toft, J., Albarède, F. (1997) The Lu-Hf isotope geochemistry of chondrites and the evolution of the mantle-crust system. *Earth Planet. Sci. Lett.*, 148, 243-258.

Blichert-Toft, J., Chauvel, C., Albarède, F. (1997) Separation of Hf and Lu for high-precision isotope analysis of rock samples by magnetic sector-multiple collector ICP-MS. *Contrib. Mineral. Petrol.*, 127, 248-260.

Boctor, N. Z., Boyd, F. R. (1979) Distribution of the rare earth elements in perovskite from kimberlites. *Carnegie Inst. Washington, Ann. Rept. Dir. Geophys. Lab., 1978-79,* 572-574.

Boer, R. H., Beukes, G. J., Meyer, F. M., Smith, C. B. (1993) Fluoride precipitates in silicate wet-chemistry: implications on REE fractionation. *Chem. Geol.,* 104, 93-98.

Bostock, H. H. (1980) Geology of the Itchen Lake area, District of Mackenzie. Geological Survey of Canada, Memoir 391, 101pp.

Bowen, N. L. (1928) *The evolution of the igneous rocks.* Princeton University Press.

Butler, J. C. (1981) Effect of various transformations on the analysis of percentage data. *J. Math. Geol.,* 13, 53-68.

Butler, J. C. (1986) The role of spurious correlation in the development of a komatiite alteration model. *J. Geophys. Res.,* 91, E275-E280.

Card, K. D. (1990) A review of the Superior Province of the Canadian Shield, a product of Archean accretion. *Precamb. Res.,* 48, 99-156.

Carlson, J. A., Kirkley, M. B., Thomas, E. M., Hillier, W. D. (1999) *Procs. 7th Intl. Kimb. Conf.,* 1, 81-89.

Chauvel, C., Hofmann, A. W., Vidal, P. (1994) HIMU-EM: the French Polynesian connection. *Earth Planet. Sci. Lett.,* 110, 99-119.

Chayes, F. (1949) On ratio correlation in petrography. *J. Geol.,* 57, 239-254.

Chayes, F. (1960) On correlation between variables of constant sum. *J. Geophys. Res.,* 65, 4185-4193.

Chayes, F. (1971) *Ratio correlation.* Chicago University Press. 99pp.

Clement, C. R. (1979) The origin and infilling of kimberlite pipes. *Kimberlite Symposium II, Extended Abstracts.* Cambridge.

Clement, C. R. (1982) A comparative geological study of some major kimberlite pipes in the Northern Cape and Orange Free State. Unpubl. PhD thesis (2 vols.), Univ. Cape Town.

Clement, C. R., Skinner, E. M. W. (1979) A textural genetic classification of kimberlite rocks. *Kimberlite Symposium II, Extended Abstracts.* Cambridge.

Cookenboo, H. O., Daoud, D. (1996) Middle Devonian conodonts from limestone xenoliths in the Jericho kimberlite, NWT. Exploration overview. NWT Geological Mapping Division, Department of Northern Affairs and Development.

Corfu, F., Krogh, T. E., Kwok, Y. Y., Jensen, L. S. (1989) U-Pb zircon geochronology in the southwestern Abitibi greenstone belt, Superior Province. *Can. J. Earth Sci.,* 26, 1747-1763.

Cox, K. G., Bell, J. D., Pankhurst, R. J. (1979) *The interpretation of igneous rocks.* Chapman and Hall, London. 450pp.

Creaser, R., Grütter, H., Carlson, J., Crawford, B. (2003) Macrocrystal phlogopite Rb-Sr dates for the Ekati property kimberlites, Slave province, Canada: evidence for multiple intrusive episodes in the Paleocene and Eocene. 8th Int. Kimb. Conf., Extended Abstracts.

Croudace, I. W. (1980) A possible error source in silicate wet-chemistry caused by insoluble fluorides. *Chem. Geol.,* 31, 153-155.

David, K., Birck, J. L., Telouk, P., Allègre, C. J. (1999) Application of isotope dilution for precise measurement of Zr/Hf and ^{176}Hf/^{177}Hf ratios by mass spectrometry (ID-TIMS/ID-MC-ICP-MS). *Chem. Geol.,* 157, 1-12.

David, K., Frank, M., O'Nions, R. K., Belshaw, N. S., Arden, J. W. (2001) The Hf isotope composition of global seawater and the evolution of Hf isotopes in the deep Pacific Ocean from Fe-Mn crusts. *Chem. Geol.*, 178, 23-42.

Davis, D. W., Gray, J., Cumming, G. L. (1977) Determination of the [87]Sr decay constant. *Geochim. Cosmochim. Acta*, 41, 1745-1749.

Davis, J. C. (2002) *Statistics and data analysis in geology*. 3rd edition. John Wiley and Sons. 638pp.

Davis, W. J., Fryer, B. J., King, J. E. (1994) Geochemistry and evolution of Late Archean plutonism and its significance to the tectonic development of the Slave craton. *Precamb. Res.*, 67, 207-241.

Davis, W. J., Hegner, E. (1992) Neodymium isotopic evidence for the tectonic assembly of Late Archean crust in the Slave province, northwest Canada. *Contrib. Mineral. Petrol.*, 111, 493-504.

Davis, W. J., Kjarsgaard, B. A. (1997) A Rb-Sr isochron age for a kimberlite from the recently discovered Lac de Gras field, Slave province, northwest Canada. *J. Geol.*, 105, 503-509.

Dawson, J. B. (1980) *Kimberlites and their xenoliths*. Springer Verlag, New York.

Dawson, J. B. (1987) The kimberlite clan: relationship with olivine and leucite lamproites, and inferences for upper-mantle metasomatism. In: *Alkaline Igneous Rocks (eds. J. G. Fitton and B. G. J. Upton)*. Geological Society Special Publication, 30, 95-101.

Dawson, J. B., Hawthorne, J. B. (1973) Magmatic sedimentation and carbonatitic differentiation in kimberlite sills at Benfontein, South Africa. *J. Geol. Soc. London*, 129, 61-85.

Deer, W. A., Howie, R. A., Zussman, J. (1992) *An introduction to the rock-forming minerals.* 2nd ed. Longman Scientific and Technical, Harlow. 696pp.

Demaiffe, D., Fieremans, M. (1981) Strontium isotope geochemistry of the Mbuji-Mayi and Kundelungu kimberlites, Zaire, Central Africa. *Chem. Geol.*, **31**, 311-323.

DePaolo, D. J. (1981) Trace element and isotopic effects of combined wallrock assimilation and fractional crystallisation. *Earth Planet. Sci. Lett.*, **53**, 189-202.

DePaolo, D. J. (1988) *Neodymium isotope geochemistry: an introduction.* Springer Verlag, New York.

DePaolo, D. J., Wasserburg, G. J. (1976) Nd isotopic variation and petrogenetic models. *Geophys. Res. Letts.*, **3**, 249-252.

Dimroth, E., Imreh, L., Rocheleau, M., Goulet, N. (1982) Evolution of the south-central part of the Archean Abitibi Belt, Quebec. Part I: stratigraphy and paleogeographic model. *Can. J. Earth Sci.*, **19**, 1729-1758.

Dowall, D. P., Nowell, G. M., Pearson, D. G. (2003) Chemical pre-concentration procedures for high-precision analysis of Hf-Nd-Sr isotopes in geological materials by plasma ionisation multi-collector mass spectrometry (PIMMS) techniques. In: *Plasma source mass spectrometry – applications and emerging technologies* (eds. G. Holland and S. D. Tanner). Royal Society of Chemistry, Cambridge. 321-337.

Dosso, L., Murthy, V. R. (1980) A Nd isotopic study of the Kerguelen islands: inferences on enriched oceanic mantle sources. *Earth Planet. Sci. Lett.*, **48**, 268-276.

Eales, H. V., Cawthorn, R. G. (1996) The Bushveld Complex. In: *Layered intrusions (ed. R. G. Cawthorn).* Elsevier. 181-230.

Edgar, A. D., Arima, M, Baldwin, D. K., Bell, D. R., Shee, S. R., Skinner, E. M. W., Walker, E. C. (1988) High pressure-high temperature melting experiments on a SiO_2-poor aphanitic kimberlite from the Wesselton mine, Kimberley, South Africa. *Am. Mineral.*, 73, 524-533.

Edwards, D., Rock, N. M. S., Taylor, W. R., Griffin, B. J., Ramsay, R. R. (1992) Mineralogy and petrology of the Aries diamondiferous kimberlite pipe, central Kimberley Block, Western Australia. *J. Petrol.*, 33, 1157-1191.

Eggler, D. H., Wendlandt, R. F. (1979) Experimental studies on the relationship between kimberlite magmas and partial melting of peridotite. SIKC, 1, 330-338.

Fahrig, W. F. (1987) The tectonic setting of the continental mafic dyke swarms: failed arm and early passive margins. In: *Mafic dyke swarms* (eds. H. C. Halls, W. F. Fahrig). Geological Association of Canada Paper 34, 331-348.

Fairbairn, P. E., Robertson, R. H. S. (1966) Stages in the tropical weathering of kimberlite. *Clay Minerals*, 6, 351-371.

Faure, G. (1986) *Principles of isotope geology.* 2nd edition. Wiley, New York. 589pp.

Fesq, H. W., Kable, E. J. D., Gurney, J. J. (1975) Aspects of the geochemistry of kimberlites from the Premier Mine and other South African occurrences, with particular reference to the rare earth elements. *Phys. Chem. Earth*, 9, 686-707.

Field, M., Scott-Smith, B. H. (1999) Contrasting geology and near-surface emplacement of kimberlite pipes in southern Africa and Canada. *Procs. 7th Intl. Kimb. Conf.*, 1, 214-237.

Fisher, R. V. (1961) Proposed classification of volcaniclastic sediments and rocks. *Geol. Soc. Am. Bull.*, 72, 1409-1414.

Fitton, J. G., Gill, R. C. O. (1970) The oxidation of ferrous iron in rocks during mechanical grinding. *Geochim. Cosmonchim. Acta*, 34, 518-524.

Folinsbee, R. E. (1949) Lac de Gras, District of Mackenzie, Northwest Territories. Geological Survey of Canada, Map 977A.

Frantsesson, E. V. (1968) *The petrology of kimberlites.* Izdatelstvo. Nedra, Moscow. In Russian.

Frantsesson, E. V. (1970) *The petrology of kimberlites* (translated by D. A. Brown). Publ. No. 150, Dept. Geology, Australian National University, Canberra.

Fraser, K. J. (1987) Petrogenesis of kimberlites from South Africa and lamproites from Western Australia and North America. Unpublished PhD Thesis, Open University, 270pp.

Frisch, T., Digel, M. R., Williams, E. J. (1987) Precambrian shield of the Boothia uplift, southern Somerset Island and northern Boothia Peninsula, District of Franklin. *Geological Survey of Canada, Current Research Part A*, Paper **87-1A**, 429-434.

Frisch, T., Sandeman, H. A. I. (1991) Reconnaissance geology of the Precambrian shield of the Boothia uplift, northwestern Somerset Island and eastern Prince of Wales Island, District of Franklin. *Geological Survey of Canada, Current Research Part C*, Paper **91-1C**, 173-178.

Goldstein, S. L., O'Nions, R. K., Hamilton, P. J. (1984) A Sm-Nd study of atmospheric dusts and particulates from major river systems. *Earth Planet Sci. Lett.*, **70**, 221-236.

Graham, I., Burgess, J. L., Bryan, D., Ravenscroft, P. J., Thomas, E., Doyle, B. J., Hopkins, R., Armstrong, K. A. (1999) Exploration history and geology of the Diavik kimberlites, Lac de Gras, Northwest Territories, Canada. Procs. 7th Int. Kimb. Conf., 262-279.

Grégoire, M., Bell, D. R., Le Roex, A. P. (2002) Trace element geochemistry of phlogopite-rich mafic mantle xenoliths: their classification and their relationship to phlogopite-bearing peridotites and kimberlites revisited. *Contrib. Mineral. Petrol.*, 142, 603-625.

Grütter, H. S., Apter, D. B., Kong, J. (1999) Crust-mantle coupling: evidence from mantle-derived xenocrystic garnets. *Procs. 7th Intl. Kimb. Conf.*, 1, 307-313.

Gurney, J. J., Ebrahim, S. (1973) Chemical composition of Lesotho kimberlites. In: *Lesotho Kimberlites*, (ed. P. H. Nixon), 280-284.

Gurney, J. J., Moore, R. O., Otter, M. L., Kirkley, M. B., Hops, J. J., McCandless, T. E. (1991) Southern African kimberlites and their xenoliths. In: *Magmatism in extensional structural settings: the Phanerozoic African plate.* (Eds. A. B. Kampunzu, R. T. Lubala). Springer-Verlag, Berlin. 495-536.

Hamblin, A. P., Stasiuk, L. D., Sweet, A. R., Lockhart, G. D., Dyck, D. R., Jagger, K., Snowdon, L. R. (2003) Post-kimberlite Eocene strata within a crater basin, Lac de Gras, Northwest Territories, Canada. 8th Int. Kimb. Conf., Extended Abstracts.

Harte, B., Winterburn, P. A., Gurney, J. J. (1987) Metasomatic and enrichment phenomena in garnet peridotite facies mantle xenoliths from the Matsoku kimberlite pipe, Lesotho. In: *Mantle metasomatism* (Eds. M. A. Menzies, C. J. Hawkesworth). Academic Press.

Hawthorne, J. B. (1975) Model of a kimberlite pipe. *Phys. Chem. Earth*, 9, 1-15.

Heaman, L. M., Kjarsgaard, B. A. (2000) Timing of eastern North American kimberlite magmatism: continental extension of the Great Meteor hotspot track? *Earth Planet. Sci. Lett.*, 178, 253-268.

Heaman, L.M., Creaser, R.A., Cookenboo, H.O. (2002) Extreme high field strength element enrichment in Jericho eclogite xenoliths: a cryptic record of

Paleoproterozoic subduction, partial melting and metasomatism beneath the Slave craton, Canada. *Geology*, **30**, 507-510.

Heaman, L. M., Kjarsgaard, B. A., Creaser, R. A. (2003) The timing of kimberlite magmatism is North America: implications for global kimberlite genesis and diamond exploration. *Lithos*, in press.

Heaman, L. M., Kjarsgaard, B. A., Creaser, R. A., Cookenboo, H. O., Kretschmar, U. (1997) Multiple episodes of kimberlite magmatism in the Slave Province, North America. In: *Slave-Northern Cordillera Lithospheric Evolution (SNORCLE) transect and Cordilleran tectonics workshop meeting (7-9 March), University of Calgary*. LITHOPROBE Report, **56**, 14-17.

Helmstaedt, H., Gurney, J.J. (1997) Geodynamic controls of kimberlites – what are the roles of hotspots and plate tectonics? *Russ. Geol. Geophys.*, **38**, 492-508.

Henderson, J. B., James, D. T., Thompson, P. H. (1999) Geology, Healey Lake-Artillery Lake, Northwest Territories-Nunavut. Geological Survey of Canada Open File 3819, scale 1:250,000.

Henderson, P. (1982) *Inorganic geochemistry*. Pergamon, Oxford, UK. 353pp.

Hetman, C. M., Scott Smith, B. H., Paul, J. L., Winter, F. W. (2003) Geology of the Gahcho Kué kimberlite pipes, NWT, Canada: root to diatreme transition zones. 8th *Int. Kimb. Conf., Extended Abstracts*.

Hoffman, P. F. (1988) United plates of America, the birth of a continent: Early Proterozoic assembly and growth of Laurentia. *Ann. Rev. Earth Planet. Sci.*, **16**, 543-603.

Hoffman, P. F. (1990) Geological constraints on the origin of the mantle root beneath the Canadian shield. *Phil. Trans. R. Soc. London*, **A331**, 523-532.

Hornig-Kjarsgaard, I. (1998) Rare earth elements in sovitic carbonatites and their mineral phases. *J. Petrol.*, **39**, 2105-2121.

Ilupin, I. P., Lutz, B. G. (1971) The chemical composition of kimberlite and questions on the origin of kimberlite magmas. *Sovietskaya Geol.*, **6**, 61-73 (in Russian).

Ionov, D. A., Weiss, D. (2002) Hf isotope composition of mantle peridotites: first results and inferences for the age and evolution of the lithospheric mantle. *Ofioliti*, **27**.

Johnson, C. M., Beard, B. L. (1993) Evidence from hafnium isotopes for ancient sub-oceanic mantle beneath the Rio Grande rift. *Nature*, **362**, 441-444.

Jones, A. P., Wylie, P. J. (1984) Minor elements in perovskite from kimberlites and the distribution of rare earth elements: an electron microprobe study. *Earth Planet. Sci. Lett.*, **69**, 128-140.

Kable, E. J. D., Fesq, H. W., Gurney, J. J. (1975) The significance of the inter-element relationships of some minor and trace elements in South African kimberlites. *Phys. Chem. Earth*, **9**, 709-734.

King, J. E., Davis, W. J., Relf, C., Avery, R. W. (1988) Deformation and plutonism in the western Contwoyto Lake map area, central Slave province, District of Mackenzie, NWT. In: Current Research, Part C, Geological Survey of Canada, Paper **88-1C**, 161-176.

King, J. E., Davis, W. J., Relf, C. (1992) Late Archean tectono-magmatic evolution of the central Slave province, Northwest Territories. *Can. J. Earth Sci.*, **29**, 2156-2170.

King, J. E., van Nostrand, T., Bethune, K., Wingate, M. T., Relf, C. (1991) Final field report on the Contwoyto-Nose Lake map area, central Slave province, District of Mackenzie, NWT. In: Current Research, Part C, Geological Survey of Canada, Paper **91-1C**, 99-108.

Kinny, P. D., Griffin, B. J., Heaman, L. M., Brakhfogel, F. F., Spetsius, Z. V. (1997) SHRIMP U-Pb ages of perovskite from Yakutian kimberlites. *Procs. 6th Int. Kimb. Conf.*, 91-99.

Kjarsgaard, B. A. (2001) Geology of the Lac de Gras kimberlite field, central Slave province, Canada. Slave-Kaapvaal Workshop 2001, Program with abstracts.

Kjarsgaard, B. A. (2003) Volcanology of kimberlite. Mineral Deposit Research Unit, University of British Columbia, Short Course #37. Vancouver, B.C., January 25-26, unpaginated.

Kjarsgaard, B. A., Wilkinson, L., Armstrong, J. A. (2002) Geology, Lac de Gras kimberlite field, central Slave province, North West Territories-Nunavut. Geological Survey of Canada Open File 3238. Scale 1:250,000.

Kleeman, A. W. (1967) Sampling error in the chemical analysis of rocks. *J. Geol. Soc. Aust.*, 14, 43-47.

Kramers, J. D. (1977) Lead and strontium isotopes in Cretaceous kimberlites and mantle-derived xenoliths from Southern Africa. *Earth Planet. Sci. Lett.*, 34, 419-431.

Kramers, J. D., Smith, C. B., Lock, N., Harmon, R., Boyd, F. R. (1981) Can kimberlite be generated from ordinary mantle? *Nature*, 291, 53-56.

Kresten, P. (1973) Differential thermal analysis of kimberlites. In: *Lesotho Kimberlites* (ed. P. H. Nixon), 269-279.

Kusky, T. M. (1989) Accretion of the Archean Slave province. *Geology*, 17, 63-67.

Lambert, M. B. (1982) The Back River volcanic complex, District of Mackenzie, Northwest Territories. Geological Survey of Canada Open File 848. Scale 1: 50,000.

Lambert, M. B. (1996) Stratigraphy of the southern portion of an Archean stratovolcano in the Back River volcanic complex, Slave province, Northwest Territories. In: Current Research 1996-C, Geological Survey of Canada, 19-28.

Langford, F. F., Morin, M. A. (1976) The development of the Superior Province of northwestern Ontario by merging island arcs. *Am. J. Sci.*, 276, 1023-1034.

Langmyhr, F. T., Kringstad, K. (1966) An investigation of the composition of the precipitates formed by the decomposition of silicate rocks in 38-40% hydrofluoric acid. *Anal. Chim.*, 35, 131-135.

LeCheminant, A. N., Heaman, L. M. (1989) Mackenzie igneous events, Canada: middle Proterozoic hotspot magmatism associated with ocean opening. *Earth Planet. Sci. Lett.*, 96, 38-48.

LeCheminant, A. N., van Breeman, O. (1994) U-Pb ages of Proterozoic dyke swarms, Lac de Gras area, NWT: evidence for progressive break-up of an Archean supercontinent. Geological Association of Canada, Program with Abstracts, 19, A62.

LeMaitre, R. W. (1976) The chemical variability of some common igneous rocks. *J. Petrol.*, 17, 589-637.

Le Roex, A. P. (1986) Geochemical correlation between southern African kimberlites and South Atlantic hotspots. *Nature*, 324, 243-245.

Le Roex, A. P., Bell, D. R., Davis, P. (2003) Petrogenesis of Kimberley Group I hypabyssal kimberlites: evidence from bulk rock geochemistry. *Extended Abstracts, 8th International Kimberlite Conf.*

Ludden, J. N., Hubert, C., Gariépy, C. (1986) The tectonic evolution of the Abitibi greenstone belt of Canada. *Geol. Mag.*, 123, 153-166.

Lugmair, G. W., Marti, K. (1978) Lunar initial $^{143}Nd/^{144}Nd$: differential evolution of the lunar crust and mantle. *Earth Planet. Sci. Lett.*, **39**, 349-357.

Mackenzie, J. M., Canil, D. (1999) Composition and thermal evolution of cratonic mantle beneath the central Archean Slave province, NWT, Canada. *Contrib. Mineral. Petrol.*, **134**, 313-324.

MacLachlan, K., Relf, C., Cairns, S., Renaud, J., Mills, A. (2002) New bedrock mapping and preliminary U-Pb geochronology in the Walmsley Lake area, southeatern Slave province, NWT. In: Current Research, Geological Survey of Canada.

Mahotkin, I. L., Gibson, S. A., Thompson, R. N., Zhuravlev, D. Z., Zherdev, P. U. (2000) Late Devonian diamondiferous kimberlite and alkaline picrite (proto-kimberlite?) magmatism in the Arkhangelsk Region, NW Russia. *J. Petrol.*, **41**, 201-227.

Masun, K. M. (1999) The petrology and mineralogy of the Lac de Gras kimberlite field, Slave province, Northwest Territories: a comparative study. Unpublished MSc thesis, Lakehead University, Thunder Bay. 324pp.

McCulloch, M. T., Jaques, A. L., Nelson, D. R., Lewis, J. D. (1983) Nd and Sr isotopes in kimberlites and lamproites from Western Australia: an enriched mantle origin. *Nature*, **302**, 400-403.

McDonough, W. F., Sun, S.-S. (1995) The composition of the Earth. *Chem. Geol.*, **120**, 223-253.

McGlynn, J. C. (1977) Geology of the Slave province. Geological Survey of Canada Open File 445. Scale 1:1,000,000.

Mitchell, R. H. (1986) *Kimberlites: Mineralogy, geochemistry and petrology.* Plenum Press, New York. 442pp.

Mitchell, R. H. (1995) *Kimberlites, orangeites and related rocks.* Plenum Press, New York. 410pp.

Mitchell, R. H. (1997) *Kimberlites, orangeites, lamproites, melilitites and minettes: a petrographic atlas.* Almaz Press, Thunder Bay. 243pp.

Mitchell, R. H., Brunfelt, A. O. (1975) Rare earth element geochemistry of kimberlite. *Phys. Chem. Earth*, 9, 671-686.

Mitchell, R. H., Clarke, D. B. (1976) Oxide and sulphide mineralogy of the Peuyuk kimberlite, Somerset Island, NWT, Canada. *Contrib. Mineral. Petrol.*, 56, 157-172.

Mitchell, R. H., Crocket, J. H. (1971) The isotopic composition of strontium in some South African kimberlites. *Contrib. Mineral. Petrol.*, 30, 277-290.

Mitchell, R. H., Fritz, P. (1973) Kimberlite from Somerset Island, district of Franklin, N.W.T., Canada. *Can. J. Earth Sci.*, 10, 384-393.

Mitchell, R. H., Scott Smith, B. H., Larsen, L. M. (1999) Mineralogy of ultramafic dikes from the Sarfartoq, Sisimiut and Maniitsoq areas, West Greenland. *Procs. 7th Int. Kimb. Conf.*, 2, 574-583.

Mogg, T., Kopylova, M., Scott Smith, B., Kirkley, M. (2003) Petrology of the Snap Lake kimberlite, NWT, Canada. *8th Int. Kimb. Conf., Extended Abstracts.*

Moore, J. C. G. (1956) Courageous-Matthews Lakes area, District of Mackenzie, Northwest Territories. Geological Survey of Canada, Memoir 283. 52pp.

Mortenson, J. K., Thorpe, R. I., Padgham, W. A., King, J. E., Davis, W. J. (1988) U-Pb zircon ages for felsic volcanism in Slave province, NWT. In: *Radiogenic age and isotopic studies*, Report 2, Geological Survey of Canada, Paper 88-2, 85-96.

Moser, D. (1988) Structures of the Wawa gneiss terrain near Chapleau, Ontario. *Geol. Surv. Can. Pap.*, 88-1C, 93-99.

Moser, D., Krogh, T. E., Herman, L. M., Hanes, J. A., Helmstaedt, H. (1991) Evidence for 2920Ma gneisses and the timing of mid-crustal extension in the Wawa gneiss domain, Superior Province, Ontario. GAC-MAC-SEG, Program with abstracts, **16**, A86.

Nelson, D. R. (1989) Isotopic characteristics and petrogenesis of the lamproites and kimberlites of central West Greenland. *Lithos*, **22**, 265-274.

Nesbitt, H. W., Markovics, G., Price, R. C. (1980) Chemical processes affecting alkalis and alkaline earths during continental weathering. *Geochim. Cosmochim. Acta*, **44**, 1659-1666.

Nixon, P. H. (1973, ed.) *Lesotho kimberlites.* Lesotho National Development Corporation, Maseru. 350pp.

Nowell, G. M., Kempton, P. D., Noble, S. R., Fitton, J. G., Saunders, A. D., Mahoney, J. J., Taylor, R. N. (1998a) High precision Hf isotope measurements of MORB and OIB by thermal ionisation mass spectrometry: insights into the depleted mantle. *Chem. Geol.*, **149**, 211-233.

Nowell, G. M., Pearson, D. G., Kempton, P. D., Irving, A. J., Turner, S. (1998b) A Hf isotope study of lamproites: implications for their origins and relationship to kimberlites. *7th Int. Kimb. Conf. Extended Abstracts.* 637-639.

Nowell, G. M., Parrish, R. R. (2001) Simultaneous acquisition of isotope compositions and parent/daughter ratios by non-isotope dilution solution-mode plasma ionisation multi-collector mass spectrometry (PIMMS). In: *Plasma source mass spectrometry: the new millennium* (eds. J. G. Holland and S. D. Tanner). Royal Society of Chemistry, Cambridge. 298-310.

Nowell, G. M., Pearson, D. G., Kempton, P. D., Noble, S. R., Smith, C. B. (1999) Origins of kimberlites: a Hf isotope perspective. *Procs. 7th Intl. Kimb. Conf.*, **2**, 616-624.

Nowell, G. M., Pearson, D. G., Bell, D. R., Carlson, R. W., Smith, C. B., Kempton, P. D., Noble, S. R. (in press) Hf isotope systematics of kimberlites and their megacrysts: new constraints on their source regions. *J. Petrol.*

Nowell, G. M., Pearson, D. G., Ottley, C. J., Schwieters, J., Dowall, D. (2003) Long-term performance characteristics of a plasma ionisation multi-collector mass spectrometer (PIMMS): the ThermoFinnigan Neptune. In: *Plasma source mass spectrometry – applications and emerging technologies* (eds. G. Holland and S. D. Tanner). Royal Society of Chemistry, Cambridge. 307-320.

Nowicki, T. E., Crawford, B., Dyck, D., Carlson, J., McElroy, R., Helmstaedt, H., Oshust, P. (2003) A review of the geology of kimberlite pipes of the Ekati property, Northwest Territories, Canada. *Extended Abstracts, 8th International Kimberlite Conf.*

O'Brien, H. E., Tyni, M. (1999) Mineralogy and geochemistry of kimberlites and related rocks from Finland. *Procs. 7th Intl. Kimb. Conf.*, 1, 625-636.

Okulitch, A. V., Packard, J. J., Zolnai, A. I. (1986) Evolution of the Boothia uplift, Arctic Canada. *Can. J. Earth. Sci.*, 23, 350-358.

O'Nions, R. K., Hamilton, P. J., Evensen, N. M. (1977) Variations in ^{143}Nd/^{144}Nd and ^{87}Sr/^{86}Sr ratios in oceanic basalts. *Earth Planet. Sci. Lett.*, 34, 13-22.

Ottley, C. J., Pearson, D. G., Irvine, G. J. (2003) A routine method for the dissolution of geological samples for the analysis of REE and trace elements via ICP-MS. In: *Plasma source mass spectrometry – applications and emerging technologies* (eds. G. Holland and S. D. Tanner). Royal Society of Chemistry, Cambridge. 221-230.

Padgham, W. A., Fyson, W. K. (1992) The Slave province: a distinct Archean craton. *Can. J. Earth Sci.*, 29, 2972-2086.

Papanastassiou, D. A., Wasserburg, G. J. (1970) Rb-Sr ages of lunar rocks from the Sea of Tranquility. *Earth Planet. Sci. Lett.*, 8, 1-19.

Patchett, P. J. (1983) Hafnium isotope results from mid-ocean ridges and Kerguelen. *Lithos*, 16, 47-51.

Patchett, P. J., Tatsumoto, M. (1980) A routine high-precision method for Lu-Hf isotope geochemistry and chronology. *Contrib. Mineral. Petrol.*, 75, 263-267.

Paul, D. K. (1979) Isotopic composition of strontium in Indian kimberlites. *Geochim. Cosmochim. Acta*, 43, 389-394.

Pearson, D. G. and Nowell, G. M. (2002) The continental lithospheric mantle: characteristics and significance as a mantle reservoir. *Phil. Trans. R. Soc. Lond.*, 360, 2383-2410.

Pearson, D. G., Nowell, G. M., Dowall, D. P., Kjarsgaard, B. A., Kopylova, M. G., Armstrong, J. A. (2003) The relative roles of lithosphere and convecting mantle in kimberlites from the Slave province, NWT: constraints from Re-Os isotopes and olivine population studies. *Extended Abstracts, 8th International Kimberlite Conf.*

Pearson, K. (1896) On a form of spurious self correlation which may arise when indices are used in the measurement of organs. *Proc. R. Soc. London*, 60, 489-502.

Pearson, N. J., Griffin, W. L., Doyle, B. J., O'Reilly, S. Y., van Achterbergh, E., Kivi, K. (1999) Xenoliths from kimberlite pipes of the Lac de Gras area, Slave craton, Canada. *Procs. 7th Int. Kimb. Conf.*, 2, 644-658.

Percival, J. A. (1996) Archean cratons. In: *Searching for diamonds in Canada* (eds. A. N. LeCheminant, D. G. Richardson, R. N. W. DiLabio, K. A. Richardson). Geological Survey of Canada Open File 3228. 161-169.

Pell, J. A. (1997) Kimberlites in the Slave craton, Northwest Territories, Canada: a preliminary review. *Russ. Geol. Geophys.*, 38, 5-16.

Peterson, T. D., Esperança, S., LeCheminant, A. N. (1994) Geochemistry and origin of the Proterozoic ultrapotassic rocks of the Churchill Province, Canada. *Mineral. Petrol.*, 51, 251-276.

Potts, P. J. (1987) *A handbook of silicate rock analysis.* 1st edition. Blackie, London. 622pp.

Price, S. E., Russell, J. K., Kopylova, M. G. (2000) Primitive magma from the Jericho pipe, NWT, Canada: constraints on primary kimberlite melt chemistry. *J. Petrol.*, 41, 789-808.

Renaud, J., MacLachlan, K., Relf, C., Duke, N. (2001) Volcanic stratigraphy and mineral potential of the Aylmer Lake dome, southeastern Slave province, NWT. In: Current Research 2001-C5, Geological Survey of Canada.

Reyment, R. A., Savazzi, E. (1999) *Aspects of multivariate statistical analysis in geology.* Elsevier, Amsterdam. 285pp, + CD.

Rollinson, H. R. (1992) Another look at the constant sum problem in geochemistry. *Mineral. Mag.*, 56, 469-475.

Rollinson, H. R. (1993) *Using geochemical data: evaluation, presentation, interpretation.* Longman, Harlow. 352pp.

Rollinson, H. R., Roberts, C. R. (1986) Ratio correlation and major element mobility in altered basalts and komatiites. *Contrib. Mineral. Petrol.*, 93, 89-97.

Rosman, K. J. R., Taylor, P. D. P. (1998) Isotopic compositions of the elements 1997. *Pure Appl. Chem.*, 70, 217-236.

Royse, K., Kempton, P. D., Darbyshire, D. P. F. (1998) NERC Isotope Geosciences Laboratory Report Series, 121.

Salters, V. J. M., Hart, S. R. (1991) The mantle sources of ocean ridges, islands and arcs: the Hf-isotope connection. *Earth Planet. Sci. Lett.*, 104, 364-380.

Salters, V. J. M., White, W. M. (1998) Hf isotope constraints on mantle evolution. *Chem. Geol.*, 145, 447-460.

Salters, V. J. M., Zindler, A. (1995) Extreme $^{176}Hf/^{177}Hf$ in the sub-oceanic mantle. *Earth Planet. Sci. Lett.*, 129, 13-30.

Schmidberger, S. S., Simonetti, A., Francis, D., Gariepy, C. (2002) Probing Archean lithosphere using the Lu-Hf isotopic systematics of peridotite xenoliths from Somerset Island kimberlites, Canada. *Earth Planet. Sci. Lett.*, 197, 245-259.

Scott, B. H. (1979) Petrogenesis of kimberlites and associated potassic lamprophyres from Central West Greenland. *Procs. 2nd Int. Kimb. Conf.*, 1, 190-205.

Scott Smith, B.H., McKinlay, T. (2002) Emplacement of the Hardy Lake kimberlites, NWT, Canada. Geological Association of Canada/ Mineralogical Association of Canada Meeting in Saskatoon, Saskatchewan, 106.

Shee, S. R. (1986) The petrogenesis of the Wesselton mine kimberlites, Kimberley, South Africa. Unpublished PhD thesis, University of Cape Town, South Africa.

Simon, N. S. C., Carlson, R. W., Pearson, D. G., Davies, G. R. (2002) The Lu-Hf isotope composition of cratonic lithosphere: disequilibrium between garnet and clinopyroxene in kimberlite xenoliths. *Geochim. Cosmochim. Acta*, 66, A717.

Skinner, E. M. W., Clement, C. R. (1979) Mineralogical classification of Southern African kimberlites. *Procs. 2nd Int. Kimb. Conf.*, 1, 129-139.

Skinner, E. M. W., Smith, C. B., Viljoen, K. S., Clark, T. C. (1994) The petrography, tectonic setting and emplacement ages of kimberlites in the south western border region of the Kaapvaal craton, Prieska area, South Africa. *Procs. 5th Int. Kimb. Conf.*, 80-97.

Smith, C. B. (1983) Pb, Sr and Nd isotopic evidence for sources of African Cretaceous kimberlites. *Nature*, 304, 51-54.

Smith, C. B., Allsopp, H. L., Garvie, O. G., Kramers, J. D., Jackson, P. F. S., Clement, C. R. (1989) Note on the U-Pb perovskite method for dating kimberlites: examples from the Wesselton and De Beers mines, South Africa, and Somerset Island, Canada. *Chem. Geol.*, 79, 137-145.

Smith, C. B., Gurney, J. J., Skinner, E. M. W., Clement, C. R., Ebrahim, N. (1985a) Geochemical character of southern African kimberlites: a new approach based on isotopic constraints. *Trans. Geol. Soc. S. Afr.*, 88, 267-280.

Smith, C. B., Allsopp, H. L., Kramers, J. D., Hutchinson, G., Roddick, J. C. (1985b) Emplacement ages of Jurassic-Cretaceous South African kimberlites by the Rb-Sr method on phlogopite and whole rock samples. *Trans. Geol. Soc. S. Afr.*, 88, 249-266.

Smith, C. B., Clark, T. C., Barton, E. S., Bristow, J. W. (1994) Emplacement ages of kimberlite occurrences in the Prieska region, southwest border of the Kaapvaal craton, South Africa. *Chem. Geol.*, 113, 149-169.

Smith , T. E., Huang, C. H., Riddle, C., Choudhry, A. G. (1985) The geochemistry of Archean igneous and meta-igneous rocks, Gamitagama area, Wawa (Shebandowan) sub-province, Ontario. *Neues. Jahrb. Miner. Abh.*, 151, 53-86.

Spriggs, A. J. (1988) An isotopic and geochemical study of kimberlites and associated alkaline rocks from Namibia. Unpublished PhD thesis, University of Leeds, UK.

Stasiuk, L. D., Sweet, A. R., Issler, D. R., Kivi, K., Lockhart, G. D., Dyck, D. R. (2003) Pre- and post-kimberlite emplacement thermal history of Cretaceous and Tertiary sediments, Lac de Gras, Northwest Territories, Canada. 8th Int. Kimb. Conf., Extended Abstracts.

Stewart, W. D. (1987) Late Proterozoic to Early Tertiary stratigraphy of Somerset Island and northern Boothia peninsula, District of Franklin. Geological Survey of Canada Paper **83-26**, 78pp.

Stille, P., Unruh, D. M., Tatsumoto, M. (1986) Pb, Sr, Nd and Hf constraints on the origin of Hawaiian basalts and evidence for a unique mantle source. *Geochim. Cosmochim. Acta*, **50**, 2303-2319.

Stubley, M. P. (2003) Spatial distribution of kimberlite in the Slave craton: a geometrical approach. 8th Int. Kimb. Conf., Extended Abstracts.

Sun, S.-S., McDonough, W. F. (1989) Chemical and isotopic systematics of oceanic basalts: implications for mantle composition and processes. In: *Magmatism in the ocean basins* (eds. A. D. Saunders and M. J. Norry). Geol. Soc. Spec. Publ., **42**, 313-346.

Sweet, A. R., Stasiuk, L. D., Nassichuk, W. W., Catunneau, O., McIntyre, D. J. (2003) Palaeontology and diamonds: geological environments associated with kimberlite emplacement, Lac de Gras, Northwest Territories, Canada. 8th Int. Kimb. Conf., Extended Abstracts.

Sylvester, P. J., Attoh, K., Schulz, K. J. (1987) Tectonic setting of late Archean bimodal volcanism in the Michipicoten (Wawa) greenstone belt, Ontario. *Can. J. Earth Sci.*, **24**, 1120-1134.

Tainton, K. M. (1992) The petrogenesis of group-2 kimberlites and lamproites from the northern Cape Province, South Africa. Unpublished PhD thesis, University of Cambridge, UK.

Taylor, S. R., McLennan, S. M. (1985) *The continental crust: its composition and evolution*. Blackwell Scientific, Oxford. 312pp.

Taylor, W. R., Tompkins, L. A., Haggerty, S. E. (1994) Comparative geochemistry of West African kimberlites: evidence for a micaceous endmember of sublithospheric origin. *Geochim. Cosmochim. Acta.*, 58, 4017-4037.

Thirlwall, M. F. (1991) Long-term reproducibility of multicollector Sr and Nd isotope ratio analysis. *Chem. Geol.*, 94, 85-104.

Thompson, P. H., Kerswill, J. A. (1994) Preliminary geology of the Winter Lake-Lac de Gras area. Geological Survey of Canada Open File 2740 (revised), scale 1:250,000.

Thompson, P. H., Ross, D., Froese, E., Kerswill, J. A., Peshko, M. (1993) Regional geology in the Winter Lake-Lac de Gras area, central Slave province. District of Mackenzie, Northwest Territories. In: *Current Research, Part C*, Geological Survey of Canada, paper 93-1C, 61-70.

Thompson, P. H., Ross, D., Davidson, A. (1994) Regional geology in the Winter Lake-Lac de Gras area, central Slave province. District of Mackenzie, Northwest Territories. In: *Current Research, 1994-C*, Geological Survey of Canada, 1-12.

Thompson, P. H., Russell, I., Paul, D., Kerswill, J. A., Froese, E. (1995) Regional geology and mineral potential of the Winter Lake-Lac de Gras area, central Slave province, Northweset Territories. In: *Current Research, 1995-C*, Geological Survey of Canada, 107-119.

Thorpe, R. I., Cumming, G. L., Mortensen, J. K. (1992) A significant Pb isotope boundary in the Slave province and its probable relation to ancient basement in the western Slave province. In: *Project summaries, Canada-Northwest Territories mineral development subsidiary agreement 1987-1991* (eds. D. G. Richardson, M. Irving). Geological Survey of Canada Open File 2484, 179.

Tompkins, L. A., Meyer, S. P., Han, Z., Hu, S., Armstrong, R., Taylor, W. R. (1999) Petrology and geochemistry of kimberlites from Shandongn and Liaoning provinces, China. *Procs. 7th Intl. Kimb. Conf.*, 1, 872-887.

Turner, C. C., Walker, R. G. (1973) Sedimentology, stratigraphy and crustal evolution of the Archean greenstone belt near Sioux Lookout, Ontario. *Can. J. Earth Sci.*, **10**, 817-845.

van Breeman, O, Davis, W. J., King, J. E. (1990) U-Pb zircon and monazite ages from plutonic rocks in the Contwoyto-Nose Lakes map area, central Slave province, District of Mackenzie, Northwest Territories. In: *Radiogenic age and isotopic studies*, Report 3, Geological Survey of Canada, Paper **89-2**, 29-37.

van Breeman, O., Davis, W. J., King. J. E. (1992) Temporal distribution of granitoid plutonic rocks in the Archean Slave province, northwest Canadian shield. *Can. J. Earth Sci.*, **29**, 2186-2199.

van Breeman, O., Henderson, J. B., Sullivan, R. W., Thompson, P. H. (1987) U-Pb zircon and monazite ages from the eastern Slave province, Healey Lake area, NWT. In: *Radiogenic age and isotopic studies*, Report 1, Geological Survey of Canada, Paper **87-2**, 101-110.

Vervoort, J. D., Patchett, P. J., Blichert-Toft, J., Albarède, F. (1999) Relationships between Lu-Hf and Sm-Nd isotopic systems in the global sedimentary system. *Earth Planet. Sci. Lett.*, **168**, 79-99.

Villeneuve, M. (1993) Preliminary geochronological results from the Winter Lake-Lac de Gras Slave province NATMAP project, Northwest Territories. In: *Radiogenic age and isotopic studies*, Report 7, Geological Survey of Canada, Paper **93-2**, 29-38.

Villeneuve, M., Henderson, J. R., Hrabi, R. B., Jackson, V. A., Relf, C. (1997) 2.70-2.58Ga plutonism and volcanism in the Slave province, District of Mackenzie, Northwest Territories. In: *Radiogenic age and isotopic studies*, Report 10, Geological Survey of Canada, Current Research 1997-F, 37-60.

Villeneuve, M., Lambert, M. B., van Breeman, O., Mortenson, J. K. (2001) Note: geochronology of the Back River Volcanic Complex, Nunavut-Northwest

Territories. In: *Radiogenic age and isotopic studies*, Report 14, Geological Survey of Canada, Current Research 2001-F2.

Vocke, Jr, R. D. (1999) Atomic weights of the elements 1997. *Pure Appl. Chem.*, 71, 1593-1607.

Vollmer, R., Ogden, P. R., Schilling, J.-G., Kingsley, R. H., Waggoner, D. D. (1984) Nd and Sr isotopes in ultrapotassic volcanic rocks from the Leucite Hills, Wyoming. *Contrib. Mineral. Petrol.*, 87, 359-368.

Wagner, P. A. (1914) *The diamond fields of Southern Africa.* Transvaal Leader, Johannesburg.

Walsh, J. N. (1980) The simultaneous determination of the major, minor and trace constituents of silicate rocks using inductively coupled plasma spectrometry. *Spectrochim. Acta*, B35, 107-111.

Wasserburg, G. J., Jacobsen, S. B., DePaolo, D. J., McCulloch, M. T., Wen, T. (1981) Precise determination of Sm/Nd ratios, Sm and Nd isotopic abundances in standard solutions. *Geochim. Cosmochim. Acta.*, 45, 2311-2323.

White, W. M., Hofmann, A. W. (1982) Sr and Nd isotope geochemistry of oceanic basalts and mantle evolution. *Nature*, 296, 821-825.

Wilkinson, L., Kjarsgaard, B. A., LeCheminant, A. N., Harris, J. (2001) Diabase dyke swarms in the Lac de Gras area, Northwest Territories, and their significance to kimberlite exploration: initial results. In: Current Research 2001-C8, Geological Survey of Canada.

Williams, A. F. (1932) *The genesis of diamond.* 2 vols. Ernest Benn Ltd., London.

Wooden, J. L., Ggoldich, S. S., Suhr, N. H. (1982) Origin of the Morton gneiss, southwestern Minnesota. 2. Geochemistry. *Geol. Soc. Am. Spec. Pap.*, 182, 57-75.

Wright, K. J. (1998) Possible structural controls of kimberlites in the Lac de Gras region, central Slave province, Northwest Territories, Canada. MSc thesis, Queen's University, Kingston. 150pp.

Wronkiewicz, D. J., Condie, K. C. (1990) Geochemistry and mineralogy of sediments from the Ventersdorp and Transvaal supergroups, South Africa; cratonic evolution during the early Proterozoic. *Geochim. Cosmochim Acta*, 54, 343-354.

Yamashita, K., Creaser, R. A., Jensen, J. E., Heaman, L. M. (2000) Origin and evolution of mid- to late-Archean crust in the Hanikahimajuk Lake area, Slave Province, Canada; evidence from U-Pb geochronological, geochemical and Nd-Pb isotope data. *Precam. Res.*, 99, 197-224.

Yokoyama, T., Makishima, A., Nakamura, E. (1999) Evaluation of the coprecipitation of incompatible trace elements with fluoride during silicate rock dissolution by acid digestion. *Chem. Geol.*, 157, 175-187.

Zindler, A., Hart, S. R. (1986) Chemical geodynamics. *Ann. Rev. Earth Planet. Sci.*, 14, 493-571.